The University Of Sheffield.

Synthesis, characterisation and reactivity of low-valent and hypercoordinate azido, triazenido and nitrato complexes of Group 14 and Group 15 elements

By:

Benjamin Peerless

A thesis submitted in fulfilment of the requirements for the degree of
Doctor of Philosophy

The University of Sheffield
Faculty of Science
Department of Chemistry

August 2017

ACKNOWLEDGEMENTS

Firstly, I would like to thank Dr Peter Portius for his expert and valuable guidance, and supervision throughout all the years I have been a member of the research group. As well as always being available for discussion and pushing me to be a better chemist. All previous members of the group, Dr Martin Davis and Dr Lara James, for their help with acclimatising to a research laboratory environment. Ben Crozier, Rory Campbell and Zoe Smallwood for making the atmosphere in the laboratory and the write-up room a positive place. The technical staff at the University of Sheffield for their support and training. Especially to Harry Adams for extensive training and help with single crystal X-ray crystallography and, Susan Bradshaw and Dr Sandra van Meurs for training on the NMR spectrometers. Finally, I would like to thank Masters students, Andy Sadler, Stephen Say, Robbie Davies, Lewis Thomas-Hargreaves and Josh Nicks who have helped with some of the work carried out in this project.

ABSTRACT

A new method using silver nitrate and $(PPN)NO_3$ as ionic nitrate transfer reagents has resulted in previously unknown polynitrato Main Group complexes, in particular, the homoleptic hexanitratosilicate as the salt $(PPN)_2Si(NO_3)_6$ (PPN = $(Ph_3P)_2N^+$). Unlike other silicon nitrates, the compound is thermally stable, with onset of decomposition at 138°C. Thermal decomposition of this compound proceeds *via* loss of NO_2 and O_2 to give SiO_2. The arsenic(III) nitrates $As(NO_3)_3$ and $(PPN)AsCl_2(NO_3)_2$ were prepared using a similar methodology. These two compounds are thermally labile and decompose within two hrs. The nitrato ligand can act as a halogen bond accepter. Strong halogen bonds are present in the solid-state structure of (1-methyl-3-bromopyridinium)$_2E(NO_3)_6$ (E = Ge, Sn). Phlegmatising cations have been used to prepare low-valent homoleptic azido germanates(1−) and stannates(1−) without the need of bulky and strong σ-donor ligands, $(PPh_4)Ge(N_3)_3$ and $(PPh_4)Sn(N_3)_3$. Both compounds represent the first homoleptic low valent germanium(II) and tin(II) azides. Formation of Lewis base adducts of binary Main Group azides is a convenient method of stabilising these shock and friction sensitive species. It has been demonstrated that (3-halopyridine)$_2Si(N_3)_4$ (halo = Br or I) form weak halogen azide interactions in the solid-state. N-heterocyclic carbene (NHC) adducts of $Si(N_3)_4$ and $P(N_3)_5$ were prepared and fully characterised. Complexes containing amidinato ligands (^{dipp}NCN) of P(III), P(V) and Si(IV) azides, and a Si(IV) hydride azide have been synthesised and characterised. These compounds are ideal precursors for the synthesis of low-valent silicon and phosphorus azides. Reduction of $(NHC)Si(N_3)_4$ with KC_8 and salt metathesis of $(NHC)SiCl_2$ with sodium azide affords the same product, thought to be $(NHC)(N_3)Si(\mu_2\text{-}N)_2Si(N_3)(NHC)$. Reduction of (^{dipp}NCN)$E(N_3)_x$ (E = Si, x = 3; E = P, x = 2 or 4) and $(NHC)Si(N_3)_4$ with magnesium(I) dimers forms (^{dipp}NCN)E and (NHC)Si, despite stoichiometry, and ^{R}NacnacMgN$_3$ as products. Dependent on the R-group, ^{R}NacnacMgN$_3$ has either a hexameric or trimeric structure in non-coordinating solvents and the solid-state. A "deazoimidation" reaction between (^{dipp}NCN)$SiH(N_3)_2$ and either NHC or $Li(N(SiMe_3)_2$ was unsuccessful giving peculiar Si(IV) hydride azides: (^{dipp}NCN)$SiH(N_3)_2$(abnormal-NHC) and (^{dipp}NCN)$SiH(N_3)(N(SiMe_3)_2)$. The N-heterocyclic carbene I^{t}Bu reduces (^{dipp}NCN)$SiH(N_3)_2$, however, the only isolable product was (I^{t}BuH)[(^{dipp}NCN)$SiH(N_3)_3$]. Three triazenides have been successfully synthesised and characterised with either sodium or (PPN) cations. 1,3-bis(*p*-methoxyphenyl)triazenide (bpat) and 1,3-bis(*p*-methoxyphenyl)triazenide (bptt)

were investigated as non-energetic ligands. Each triazenide acts as a bidentate ligand towards silicon forming $(bptt)_2SiCl_2$ and $(bpat)_2SiCl_2$ as products despite a 1:1 stoichiometry between triazenide and $SiCl_4$. The nitrogen-rich triazenide 1,3-bis(1-methyltetrazol-5-yl)triazenide (b1mtt) was prepared with sodium and (PPN) counterions. The reaction between $SnCl_4$ and (PPN)(b1mtt) gives $(b1mtt)SnCl_3$ with the triazenide acting as a terdentate ligand *via* the central nitrogen atom of the triazenide unit and a nitrogen atom from each of the tetrazoles. 1-aminotetrazole and 1-amino-5-methyltetrazole were synthesised, however, in very poor yields in a time-consuming synthesis. It was possible to prepare the 1,3-bis(5-methyltetrazol-1-yl)triazenide, however, the PPN salt of the anion was not isolated as a pure compound.

TABLE OF CONTENTS

1. Introduction ... 3

1.1 Hypercoordination and hypervalency ... 3

1.2 Low valence and the inert pair effect ... 6

1.3 Explosophoric Ligands ... 8

1.4 Characterisation methods ... 13

1.5 Ligands used for the stabilisation of low-valent coordination centres ... 16

2. Research Questions ... 20

3. Nitrato Complexes of Main Group Elements ... 21

3.1 Introduction ... 21

3.1.1 Main Group nitrates ... 21

3.1.2 Alkali and alkali earth metal nitrates ... 25

3.1.2 Group 13 polynitrato compounds ... 26

3.1.3 Group 14 polynitrato complexes ... 31

3.2 Results and Discussion ... 34

3.2.1 Group 14 nitrato complexes ... 34

3.2.2 Group 15 nitrato complexes ... 44

3.3 Conclusions ... 49

4. Halogen Bonding in Energetic Complexes ... 52

4.1 Introduction ... 52

4.2 Results and Discussion ... 56

4.2.1 Halopyridine adducts of $Si(N_3)_4$ ... 56

4.2.2 Counterions containing halogens for Group 14 nitrato complexes ... 66

4.3 Conclusions ... 74

5. Ge(II) and Sn(II) azido and nitrato complexes ... 76

5.1 Introduction ... 76

5.2 Results and discussion ... 78

5.2.1 A nitrato group on a low valent Main Group coordination centre? ... 78

5.2.2 Homoleptic azido Ge(II) and Sn(II) complexes ... 83

5.3 Conclusion ... 100

6. A Third Row Low-Valent Azido Complex? 103

6.1 Introduction 103

6.2 Results and discussion 107

6.2.1 Salt metathesis of the Si(II) halides $IPrSiX_2$ 107

6.2.2 Main Group azido complexes: Precursors for reduction reactions 108

6.2.3 Reduction reactions of Main Group polyazido complexes 132

6.2.4 Hydrido(azido)silicon compounds 147

6.2.5 Attempted 'deazoimidation' of hydrido(azido) silicon compounds 155

6.3 Conclusion 172

7. Triazenido Ligands for Main Group Centres 175

7.1 Introduction 175

7.2 Results and discussion 178

7.2.1 Group 14 triazenido complexes 178

7.2.2 Nitrogen-rich triazenides 184

7.2.3 Nitrogen-rich triazenides as ligands 197

7.3 Conclusion 199

8. Summary 202

9. Experimental 210

9.1 General procedure 210

9.2 Preparative procedures 212

10. References 244

11. Appendix 258

11.1 Abbreviations 258

11.2 Compound Numbers 259

11.3 FT-IR and NMR spectra 260

11.4 Crystal data and structure refinement tables 272

1. INTRODUCTION

Nitrogen-rich molecules have been extensively studied as candidates for energetic materials, owing to their propensity to release large amounts of dinitrogen on decomposition. Incorporation of nitrogen-rich ligands, to appropriate coordination centres, provides a convenient method of producing a molecule with a high nitrogen content. For this purpose, an excellent choice of ligand is the azide anion as an all nitrogen species. However, conventional energetic materials rely on the oxidation of organic molecules, such as nitroglycerine and trinitrotoluene. Therefore, rather than a nitrogen-rich coordination complex, an alternative would be to combine an oxygen-rich coordination complex with an organic substrate to ensure the complete combustion of organic material. Unlike the azide anion, polyoxygen ligands are difficult to handle and source, however, the nitrate anion is a suitable substitute. Ammonium nitrate is commonly added to organic explosives to increase performance by providing more oxygen for combustion. Main group coordination centres are an attractive option in the field of energetic coordination chemistry, as they are relatively cheap and potentially less sensitive to external stimuli, such as light, compared to *d*- and *f*- block elements. The Lewis acidic nature of a majority of *p*-block elements allows the synthesis of complexes with a high number of nitrogen- and oxygen-rich ligands, a hypercoordinate complex. On the other hand, low coordinate complexes are highly interesting chemical systems that have been at the forefront of modern Main Group research for the last decade. Combining energetic ligand chemistry with these *low valent* coordination centres opens up potential avenues of exciting research.

1.1 Hypercoordination and hypervalency

The nature of the bonding in complexes with *p*-block elements functioning as a coordination centre has been debated since the 1920s.[1] Lewis argued that complexes containing more than four ligands broke the octet rule. Each coordination bond described as a two-centre two-electron (2c-2e) bond. The molecule SF_6, for instance, would contain six bonding electron pairs and, thus, break the octet rule.[2] On the other side of the argument, Langmuir preferred a bonding model that upheld the octet rule and assumed an ionic component.[3] In SF_6 this leads to a number of salt-like resonance forms

of the formula $[SF_4]^{2+}(F^-)_2$. Of course, both of the arguments put forward fall short of explaining the stability of the compounds SF_6 satisfactorily from a modern perspective. If the octet rule is broken the extra bonding electrons would reside in antibonding orbitals and weakening the coordination bonds. The ionic description would lead to thermodynamically unfavourable charge separation.

Another popular theory to describe bonding in such molecules was put forward by Rundle and Pimentel in the 1940s and 1950s.[4,5] This introduced the concept of a four-centre three-electron (4c-3e) bond. A similar theory was postulated by Sugden in the 1930s involving a two-centre one-electron (2c-1e) bond. However, this theory was poorly accepted at the time.[1] The 4c-3e bond theory viewed the bonds as two linear 2c-1e bonds.

The molecules under discussion were described as *hypervalent* by Musher in 1969. He suggested that these molecules were unique in that the atom acting as a coordination centre can possess identical, monovalent ligands that bond in two different ways.[6] The term *hypervalent* has always been controversial. Its definition requires a molecule to contain more than four electron pairs around a single atom, therefore, exceeding the electron octet. In 2002, Gillespie and Silvi described the term as "not a useful concept" on the grounds that the properties of hypervalent molecules were not significantly different to Lewis octet molecules. Therefore, hypervalent molecules should be considered rather as *hypercoordinate* as they have a coordination number larger than the standard valency of a particular element.[7]

The nature of the orbitals involved in the bonding in hypercoordinate molecules has sparked debate, too. It was originally considered that *d*-orbitals of the atom at the coordination centre are involved. This idea was helped by the fact that the only hypercoordinate molecules known always contained elements belonging to the third row or lower in the periodic table. Clearly, the hybridisation of one *s*, three *p* and two *d* orbitals results in six sp^3d^2 hybrid orbitals which satisfy the octet rule and geometrical requirements around the molecule. However, the energy of the *d*-orbitals is much too high to hybridise effectively with the *p*- and *s*- orbitals. The enthalpy gain provided by bond formation involving such hybrids is not enough to account for the promotion of an electron to the sp^3d^2 hybrid. To avoid this problem, molecular orbital (MO) theory can be used in which symmetry adapted linear combinations (SALCs) can be calculated for the complexes adhering to point group, O_h. This results in six SALCs that transform with the A_{1g}, T_{1u} and E_g symmetry species. The same treatment can be easily applied to

molecules of other geometries. Figure 1.1 shows the MO diagrams of a tetrahedral, trigonal bipyramidal and an octahedral molecule with a Main Group coordination centre.

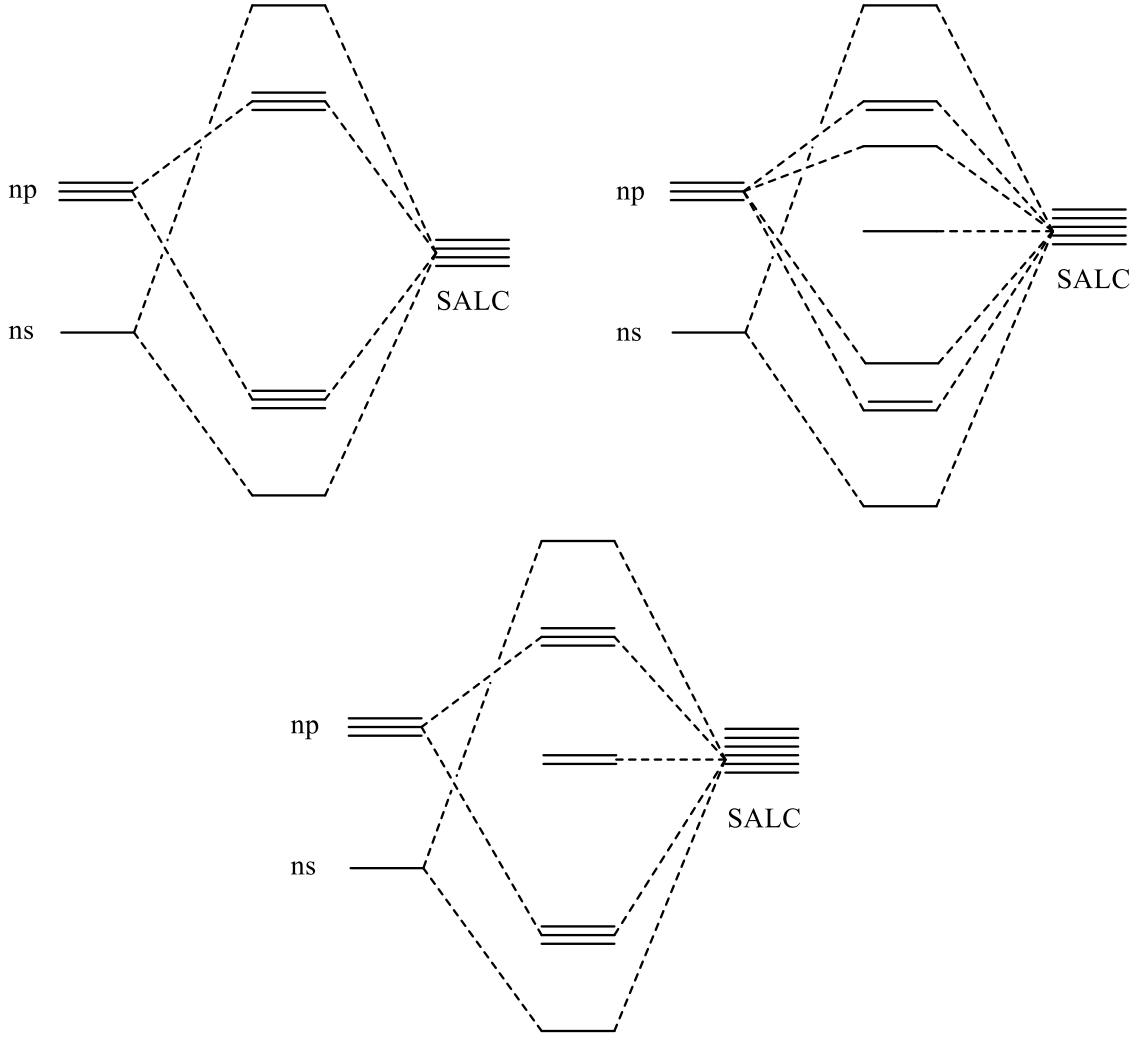

Figure 1.1. MO diagrams for Main Group tetrahedral (top left), trigonal bipyramidal (top right) and octahedral (bottom) molecules. Molecular orbital labels omitted for clarity.

From Figure 1.1, it is clear that as the coordination number exceeds four a non-bonding orbital is present in the bonding model. This leads to four bonding orbitals and a number of ligand-centred non-bonding orbitals, dependant on the geometry of the molecule, without the need of the *d*-orbitals. The overall treatment allows a valid description for the phenomenon of hypercoordination without breaking the octet rule or having an ionic component in the bonding scheme.

1.2 Low valence and the inert pair effect

If hypercoordination is the phenomenon involving a molecule appearing to contain a Main Group atom with *more than four* electron pairs, then low valence is a molecule containing an atom with *fewer than four* electron pairs. Another definition requires a molecule to have an atom which is assigned an oxidation state that is lower than its *principal oxidation state*. In reality, while there are several examples where the former definition is true, e.g. $SnCl_2$ has six electrons in the outer shell, the latter definition considers molecules that have eight electrons in the outer shell and can still be regarded as low valent, e.g. in $[SnCl_3]^-$ the coordination centre can be thought as bearing eight valence electrons.

When considering low valency it is best illustrated with an example. Methane carbon has a valency of four, whereas in the simplest carbene, CH_2, carbon only has a valency of two. Figure 1.2 shows the conventional hybridisation of the carbon atom in both cases. In methane, the carbon atom is described as sp^3 hybridised, whereas the carbon atom in a carbene is described as sp^2 hybridised. From Figure 1.2 it is clear that in the low valent case a *lone electron pair* resides in a sp^2 orbital leaving a *p*-orbital empty. On descending Group 14 and changing from carbon to silicon to germanium, tin and lead the energy gap between the *s* and *p* orbitals increases. Consequently, the electrons in the *s*-orbital become less involved in bonding and penetrate closer to the nucleus in relation to those in the outer *p* orbitals. This is the premise of the *inert pair effect*.

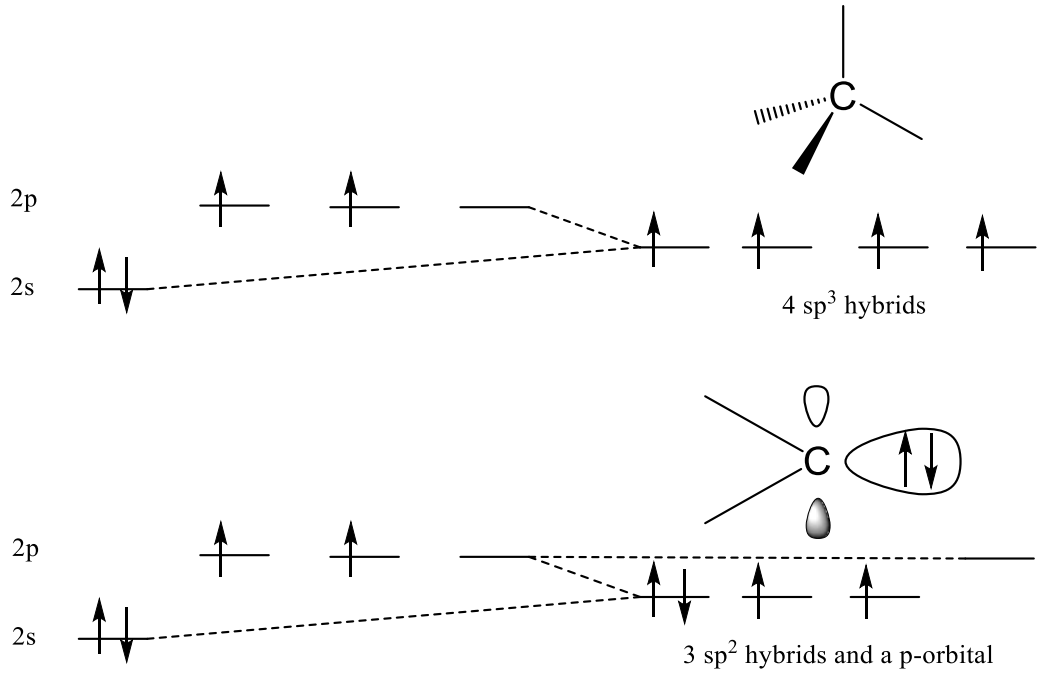

Figure 1.2. Representation of the electronic structure of the carbon atom: Top: carbon atom with a valency of four. Bottom: carbon atom with a valency of two. Electrons provided by bonded atoms are omitted.

The inert pair effect was first proposed by Nevil Sidgwick in 1927, where he described *s*-electrons in heavy Main Group elements as an "*inert pair*".[8] A simple explanation is that the energy gap between the *s*-orbital and *p*-orbital is too large, thus preventing the *s*-electrons from participating in bonding. However, this argument breaks down by simply inspecting the second and third ionisation potentials (IPs) of Group 13 elements.[9] It would be expected that these potentials should increase down the group as the electrons become more "inert".

Element	First IP	Second IP	Third IP	Second + Third IP
B	800.6	2427.1	3659.7	6086.8
Al	577.5	1816.7	2744.8	4561.5
Ga	578.8	1979.3	2963	4942.3
In	558.3	1820.6	2704	4524.6
Tl	589.4	1971	2878	4849

Table 1.1. Ionisation potentials of Group 13 elements in kJ mol^{-1}.[9]

As seen in Table 1.1, the order of the sum of second and third IPs down the group, In < Al < Tl < Ga < B, clearly shows no such trend and that there is rather a general decrease down the group as electrons lie further away from the nucleus. Relativistic

effects are responsible for the phenomenon that the IP sum is larger for thallium over indium while the *d*-block contraction explains the high IP of gallium. Drago, in 1958, attempted to evaluate the inert pair effect by looking at the thermodynamic data of the halides of Groups 13 and 14.[10] He suggested that the instabilities of Pb(IV) chloride, for instance, is related to a decrease in the degree of covalency of the E−Cl bond. The energy required to oxidise the element at the coordination centre to the oxidation state +IV is too great in comparison to any energy gained from producing four E−Cl bonds and therefore, the oxidation state +II is more stable in this case. As stated earlier, these *s*-electrons penetrate relatively close to the nucleus. A heavier nucleus results in these *s*-electrons travelling close to the speed of light and, therefore, relativistic effects begin to become significant. These effects were studied in 1992 and backed up Drago's theory that the enthalpy of formation of Pb−Cl is not a large enough factor to promote a change to the oxidation state +IV.[11]

It is clear that a comparison of the stability of different oxidation states between elements in a certain group should be made with caution. Rather, a fair comparison would be between the two oxidation states of a particular element. In Group 14, tin and lead exhibit a preference towards the oxidation state +II. Germanium and silicon show a preference for the oxidation state +IV. This makes the synthesis of Si(II) and Ge(II) compounds a preparative challenge. A number of methods have been employed to stabilise such species with the two most successful being stabilisation *via* σ donation from an N-heterocyclic carbene (NHC) or stabilisation through bulky, anionic N donor ligands. These classes of compounds have a diverse and rich chemistry. Germanium(II) centres have been synthesised without such a need for stabilising ligands, e.g. $[GeCl_3]^-$, while no such examples exist for silicon, demonstrating further the relative instability of the Si(II) oxidation state.

1.3 Explosophoric Ligands

The study of energetic materials has always remained at the forefront of scientific research and has changed dramatically over the last century from Nobel's work in the safe handling of nitroglycerine to energetic coordination polymers that have emerged in the last decade.[12–15] Unsurprisingly, with the need of such compounds in the use of explosives and propellants, a variety of different classes of energetic materials have

been prepared in attempts to improve and increase their efficiency. A conventional energetic material primarily contains a carbon-based backbone, which, on decomposition, produce various environmentally unfriendly carbon oxides depending on the appropriate oxygen balance. These unwanted products make nitrogen-based energetic materials desirable as the main product of decomposition is dinitrogen gas.

Two types of nitrogen-based energetic compounds are conceivable. These are (i) organic nitrogen-based compounds, such as 5,5'-bis(1H-tetrazolyl)amine and 5,5'-bis(1H-tetrazolyl)hydrazine, and (ii) using an endothermic ligand (explosophoric ligand) on a coordination centre.[16–18] Examples of endothermic ligands include peroxide, nitrate, azide, tetrazolate, hydrazine and others. Oxygen-based ligands act as oxidisers to organic substrates whereas nitrogen-based ligands provide a large enthalpic component through their propensity to release dinitrogen gas. The use of such ligands has resulted in novel coordination complexes from Main Group complexes such as (*cyclo*-$[P(N_3)_2]_3N_3$) to transition metal coordination polymers $[Ni(H_2NNH_2)_2]^{2+}$.[19–22]

Azide and nitrate anions are ideal candidates as ligands for Main Group coordination centres. The nitrate anion is a planar tetratomic group consisting of three oxygen atoms in a trigonal arrangement around a single nitrogen atom. Each oxygen atom is equidistant from the nitrogen atom as a result of a single, negative charge delocalised over all sites. The N−O bond is shorter than a single bond, though slightly longer than that of a double bond.[23] The azide anion is a linear arrangement of three nitrogen atoms carrying a single negative overall charge. The terminal nitrogen atoms are equidistant from the centre. The simplest known azido and nitrato compounds are the protic acids, HN_3 and HNO_3. Hydrazoic acid was first synthesised in 1890 by Curtius by the addition of sulfuric acid to sodium azide,[24] whereas nitric acid has been known for several centuries in alchemy as *aqua fortis*. The commercial synthesis of nitric acid was developed by Ostwald in 1907 by oxidising ammonia with oxygen over a platinum catalyst at 300°C.[25]

The molecular geometry of hydrazoic acid is well understood, both theoretically and experimentally. In 1940, infrared (IR) spectroscopy gave the first account on the molecular geometry of HN_3,[26] which was supplemented by electron diffraction experiments reported in 1942.[27] Both of these reports confirmed N(α)−N(β) and N(β)−N(γ) (H−N(α)−N(β)−N(γ)) bond lengths of 1.24 Å and 1.13 Å, respectively, assuming the nitrogen atoms were in a linear arrangement. Despite these results and further computational studies it was not until 2011 when the solution phase and solid

phase structures of pure HN_3 were investigated experimentally by ^{14}N nuclear magnetic resonance (NMR) spectroscopy and X-ray diffraction methods.[28] HN_3 was shown to contain an ionic azide in the solution phase by ^{14}N NMR with identical chemical shifts for N(α) and N(γ) atoms. In contrast to ethereal hydrazoic acid, which displays three signals in the NMR spectrum suggesting a covalent azide.[29] In the solid phase, HN_3 crystallises in a repeated two-layer structure with only van der Waals' interactions between the two layers.

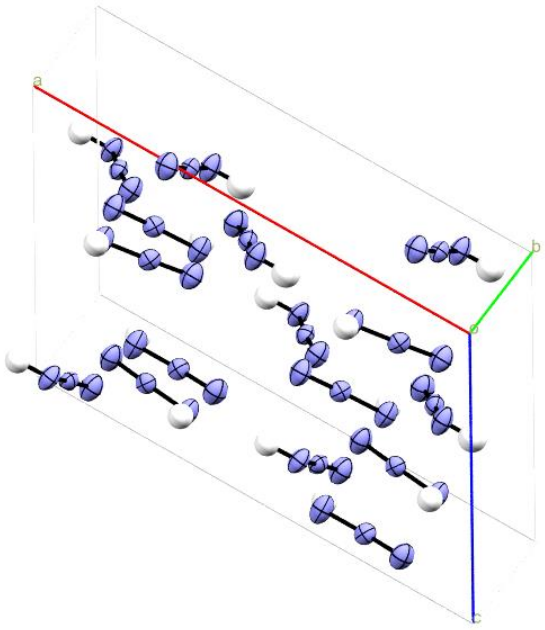

Figure 1.3. Thermal ellipsoid plot of hydrazoic acid, blue, N; white, H. Ellipsoids are set at the 50% probability level. Image generated from cif file from reference 28.

In comparison, the crystal structures of hydrated and anhydrous HNO_3 were first determined by X-ray diffraction in the 1950s.[30] Luzatti determined that HNO_3 crystallises in the space group $P2_1/c$ below the melting point of 232 K. The crystal structure is remarkably complex for such a simple molecule. In the unit cell there are four molecules that form hydrogen-bonded chains along the crystallographic *b*-axis packed in a herringbone arrangement. It was noted by Luzatti that the structure contained disorder from the presence of streaks on the Weissenberg photographs parallel to 0*kl*. The measurement was repeated in 2010 by Allan *et al* in their work on the high pressure structure of nitric acid. In their attempts at solving the structure they noticed systematic absences in the diffraction pattern that did not fit those expected for an orthorhombic or monoclinic lattice.[31] This was attributed to the fractional coordinates of the central nitrogen atom in each independent molecule having an *x*, *y* or

z value close to 0, 1/4, 1/2, 3/4, which created artificial absences not related to the presence of a symmetry operation. This same observation was made by Luzzati in the 1950s.

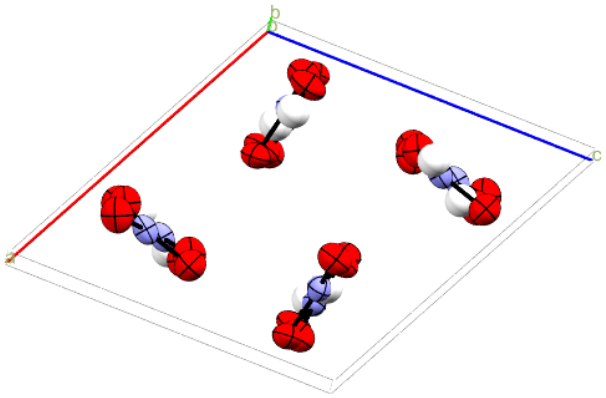

Figure 1.4. Thermal ellipsoid plot of the unit cell of HNO_3 showing the herringbone arrangement, red: oxygen. Ellipsoids are set to the 50% probability level. Image generated from cif file from reference 31.

In terms of the energetic content of azides, the introduction of an azido group to an organic molecule increases the energy released on decomposition by approximately 355 kJ mol^{-1}.[32] This increase in energy content is due to the difference in covalent bond dissociation enthalpy of N−N, N=N and N≡N bonds. As a result, there has been extensive research into inorganic azides and its use as a ligand to transition metal and Main Group coordination centres.[33,34] In the case of the nitrato ligand, transition metal nitrato complexes are known and well characterised; however, reports on nitrato Main Group complexes, except Group 13, are lacking.[35]

Besides the nitrato and azido ligands, other energtic ligands can be used for coordination complexes. However, these groups are often poor ligands. For example, charge-neutral hydrazine is a weaker Lewis base compared to an anionic ligand. As a consequence, very few endothermic ligands have been used and the only nitrogen-rich ligand commonly used is the azide anion. Attempts to prepare polynitrogen molecules with more nitrogen atoms becomes a synthetic challenge. In fact, there are only two other known polynitrogen ions, N_5^- and N_5^+. The pentazolate anion is a cyclic molecule and an ideal ligand, however, has only been detected *in situ* by mass spectrometry.[36] As a compromise, a nitrogen atom can be replaced in N_5^- with a CH group giving the tetrazolate anion, HCN_4^-. A versatile and well known ligand in coordination

chemistry.[37–40] On the other hand, the pentazonium cation, a chain, has been prepared and used as a counterion for $[AsF_6]^-$, $[P(N_3)_6]^-$, $[SbF_6]^-$ and $[B(N_3)_4]^-$.[41]

Other polynitrogen chains can act as a bridge between two organic groups (RN_xR) and a large number of compounds have been prepared including triazenes (x = 3), tetrazenes (x = 4), pentazenes (x = 5) and hexazadienes (x = 6).[42–52] All of these molecules consist of alternating single and double N−N bonds. An even number of nitrogen atoms in the chain give a charge-neutral ligand whereas an odd number of nitrogen atoms requires a proton to satisfy the valency of the nitrogen atoms. Deprotonation results in an anionic ligand.

The issue with these molecules is that they often contain aromatic R-groups. Using phenyl rings will obviously dilute any nitrogen content making the ligand considerably less endothermic. However, it is possible to increase the nitrogen content of the aromatic component by using tetrazole. Aminotetrazole, a key reagent in the synthesis of such nitrogen-rich chains, possesses different regioisomers where the amine can sit on either the carbon atom (5-aminotetrazole), the nitrogen next to the carbon (1-aminotetrazole) or the next nitrogen along (2-aminotetrazole), Figure 1.5. These could be used to prepare nitrogen-rich chains, which are candidates as potential endothermic ligands.

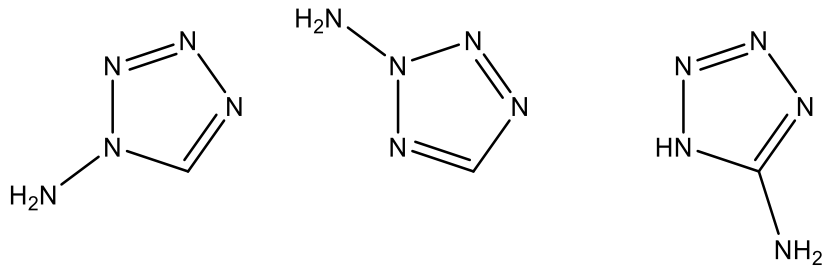

1-aminotetrazole 2-aminotetrazole 5-aminotetrazole

Figure 1.5. Regioisomers of aminotetrazole.

Recently, the sodium salt of bis(1-methyltetrazol-5-yl)-triazenide was isolated by deprotonating the corresponding triazene with sodium hydroxide.[53] An ideal candidate as an endothermic ligand.

Complexes bearing endothermic ligands become increasingly difficult to handle the more endothermic ligands present. There are two methods commonly used to aid in the study of such compounds. $Si(N_3)_4$, as an example, is a highly sensitive liquid that cannot

be isolated and must be kept as a dilute solution in benzene.[54] However, adding a weakly coordinating cation (WCC) such as PPh_4^+ or $(Ph_3P)_2N^+$ (PPN) with an azide counterion to $Si(N_3)_4$ results in the formation of $(WCC)_2Si(N_3)_6$.[55] The formation of a hypercoordinate molecule results in an increase of the ionicity of the azido ligand and the addition of the WCC dilutes the nitrogen content of the compound making it isolable and safe to handle on the gram scale. The other method is to use a Lewis base, such as 2,2'-bipyridine (bpy), to prepare a stable neutral adduct that can be isolated and studied.[54,56–58] These methods allow the study of novel endothermic coordination complexes to be completed safely.

1.4 Characterisation methods

Arguably the most common characterisation techniques in chemistry are ^1H and ^{13}C NMR spectroscopies. Endothermic ligands, ideally, have no or very little C−H functionalities limiting the use of ^1H and ^{13}C NMR spectroscopies. This leaves IR spectroscopy and, where possible, ^{14}N, ^{19}F, ^{29}Si and ^{31}P NMR spectroscopies as the main methods of *in situ* characterisation. In the cases where it is possible to grow crystals of the compounds, single crystal X-ray diffraction is a vital tool for structural characterisation.

The azido group is an excellent IR reporter. An ionic azide has one IR active vibration, the $\nu_{as}(N_3)$ vibration. On coordination, the $\nu_{sym}(N_3)$ also becomes IR active. These vibrations appear between 2200 and 2000 cm^{-1} and 1350 and 1200 cm^{-1}, respectively. Due to the spectral position of the symmetric vibration absorption band in the fingerprint region, it can sometimes be difficult to identify. However, the asymmetric vibration is in an ideal position in a quiet region of the IR spectrum. Figure 1.6 shows representations of these vibrations.

Figure 1.6. The vibrational modes of the azide anion. Left: asymmetric. Right: symmetric. Arrows indicate the paths along which the atoms move during vibration.

The range associated with the $\nu_{as}(N_3)$ vibration is dependent on the bond between the azido group and the coordination centre. Ionic azides fall closer to 2000 cm^{-1} while covalent azides vary upwards to 2200 cm^{-1}. Figure 1.7 shows the different resonance forms of a covalent azido group. The counterion to the azide anion can also influence the spectral position of the asymmetric vibration. For example, in sodium azide there are strong interactions between the sodium ions and the azide anion resulting in a permutation of the charge distribution that causes a shift of the vibrational frequency to approximately 2130 cm^{-1}. The peak also appears very broad. In contrast, the vibrational frequency of the anion in $(PPN)N_3$ is at 2000 cm^{-1} and a very sharp peak results as a consequence of very little to no *covalent* interaction between anion and cation. The other extreme of the resonance hybrids is where the E−N bond appears to have double bond character as seen in the triazidocarbonium cation, $[C(N_3)_3]^+$, which has a vibrational frequency of 2208 cm^{-1}.[59,60]

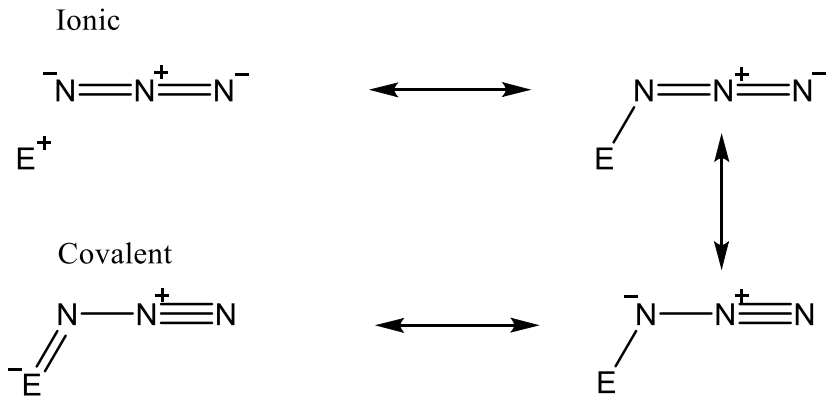

Figure 1.7. Resonance hybrids of EN_3. E denotes an atom of the Main Group elements.

IR spectroscopy can also be used to give a tentative assessment for any potential shock, friction or thermal sensitivity of the azido group. However, findings based on spectroscopic data alone must be taken with extreme caution and only be used to give an idea of the nature of the azido group in the molecule. It is clear from the resonance hybrid that the covalent form appears to have pre-formed dinitrogen and this reduces the kinetic barrier present for decomposition.

All of these reasons make IR spectroscopy a very useful tool in the study of azido compounds. Moving to other endothermic ligands, while remaining a vital form of characterisation, IR spectroscopy begins to become more difficult to interpret. A

monodentate coordinated nitrate, for example, has three characteristic absorption bands in the IR spectrum, as seen in Figure 1.8. All three lie either very close or inside the fingerprint region making assignment difficult. However, the biggest problem arises from the difference between a complex bearing one nitrato ligand or any number of nitrato ligands. Azides often have well-separated peaks and the geometry of azido compounds can be determined through the use of Group theory. With nitrates, peaks are often overlapping and it is not clear as to how many peaks are actually present in the spectrum. There is also a narrow range of frequencies observed for monodentate nitrato complexes compared with azido complexes, the $\nu_{as}(NO_2)$ appears between 1600 and 1500 cm^{-1}. Also, there has been very little work to determine how a compound that has a band at 1600 cm^{-1} is different to one with a band at 1500 cm^{-1}. However, there appears to be a general trend in which the number of nitrato groups correlates with the wavenumbers, more groups equals a higher wavenumber.[61]

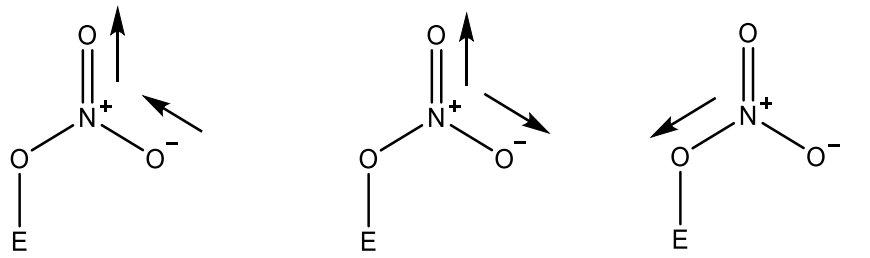

Figure 1.8. Vibrational modes of a coordinated nitrato group in a monodentate fashion. Arrows indicate the paths along which the atoms move during vibration.

IR spectroscopy of triazenides is even less understood other than that the asymmetric vibration of the chain, Figure 1.9, appears between 1500 and 1400 cm^{-1} and the anionic triazenide is observed at higher frequencies than the neutral triazene. It is also known that the bidentate coordination mode of the triazenide causes the $\nu_{as}(NNN)$ vibration to shift to lower energies between 1350 and 1200 cm^{-1}.[47,48] Triazenides often contain an organic R group that is attached at either end. In these cases ^{1}H-NMR spectroscopy is a viable technique of characterisation.

1500 - 1400 cm^{-1} 1350 - 1250 cm^{-1}

Figure 1.9. Vibrational mode of a triazenide. Arrows indicate the paths along which the atoms move during vibration.

^{14}N NMR spectroscopy is a useful tool for the characterisation of inorganic and organometallic azides.[62,63] These compounds usually display three signals for the resonances N(α), N(β) and N(γ) (E−N(α)−N(β)−N(γ)). Due to the short relaxation times, as a result of the quadrupole moment of ^{14}N, peaks are often very broad unless in a highly symmetric environment which can sometimes reduce the linewidth. The azido group often has a sharp signal for N(β) as it is the most symmetric environment, while N(α) has a very broad signal with a full width at half maximum (FWHM) of several hundreds of Hz making it difficult to observe. N(γ) is less broad, however still on the scale of hundreds of Hz. The position of these resonances follows the trend N(α) < N(γ) < N(β) between –320 and –130 ppm against $MeNO_2$ as a reference. In cases when it is possible to determine all the nitrogen environments, the difference between N(γ) and N(α) resonances can give an indication of the electronic situation of the azido group. Ionic azides have a chemical shift difference, Δ(N(α)N(γ)), of 0 ppm, e.g. $(PPN)N_3$, whereas the covalent azido compound $C(N_3)_4$ has a Δ(N(α)N(γ)) of 154 ppm.

A paper in 1975 reported on the ^{14}N NMR resonances of a variety of metal nitrato complexes.[64] The signals appeared at chemical shifts ranging from 0 ppm to 64 ppm with respect to the nitrate anion, as an external reference. It was found that the chemical shift of organic nitrates appeared at higher ppm than metal nitrates and the metalloids in between. There appeared to be very little difference whether the nitrato ligand was either coordinated in a monodentate or bidentate fashion.

1.5 Ligands used for the stabilisation of low-valent coordination centres

Low-valent coordination centres of light Main Group elements require certain types of ligands for their isolation. The thermodynamic and kinetic instability of the reduced oxidation state is relieved by strong σ-donor ligands containing bulky ancillary groups. Common classes of ligands include N-heterocylic carbenes (NHCs), doubly reduced butazadienes and amidinato type ligands, Figure 1.10.[65–85]

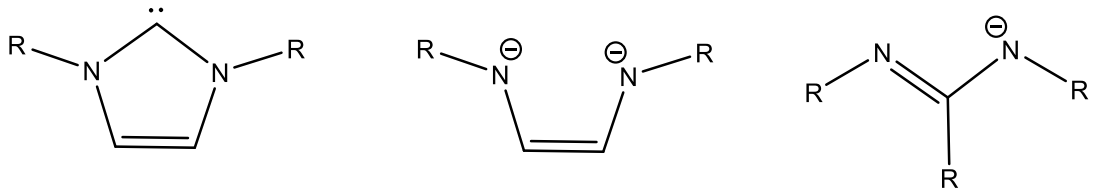

Figure 1.10. Common classes of ligands used in the isolation of low-valent Main Group compounds. R is usually a large, bulky organic group.

NHCs are molecules that contain a carbon atom that is formally divalent. Stabilised by the donation of a lone electron pair from a nitrogen atom into the empty *p*-orbital of the carbon atom reducing the electrophilicity and increasing the thermodynamic stability. The first stable and isolable NHC, reported in 1991 by Arduengo and co-workers, was 1,3-diadamantyl-imidazol-2-ylidene prepared by reducing the corresponding imidazolium chloride with NaH.[65] The structure of this NHC shows a narrow N−C−N bond angle of 102.2°, a noticeable deviation from the 108-109° seen in imidazolium rings. The C−N bond lengths are slightly longer in the NHC than the imidazolium salt suggesting a lower degree of delocalisation of π-electrons in the carbene structure. After this landmark discovery many more NHCs have been prepared varying the R group attached to the nitrogen, varying the groups attached to the carbon backbone, and as well as saturated ring systems. The strong σ-donor strength of an NHC, partnered with the steric bulk that can be included into an NHC has allowed for the preparation and isolation of several Si(0), Si(II), P(0), P(I) and many other highly reactive molecules of the Main Group elements. Substituting the carbene carbon with other Main Group elements has afforded a variety of other metalylenes of Group 13 and Group 14 elements, as recently reviewed by Asay, Jones and Driess in 2011.[86]

Amidinato type ligands differ primarily from NHCs in that they carry a single negative charge. As a result a plethora of compounds containing Si(I) or Si(II) coordination centres have been prepared.[79,85] Over the last two decades the preparation of low-valent Main Group compounds bearing these ligands has been at the forefront of Main Group chemistry research. Figure 1.11 shows some important examples of silicon.

All these low-valent silicon compounds are highly reactive compounds and their extensive and interesting chemistry has been thoroughly investigated.

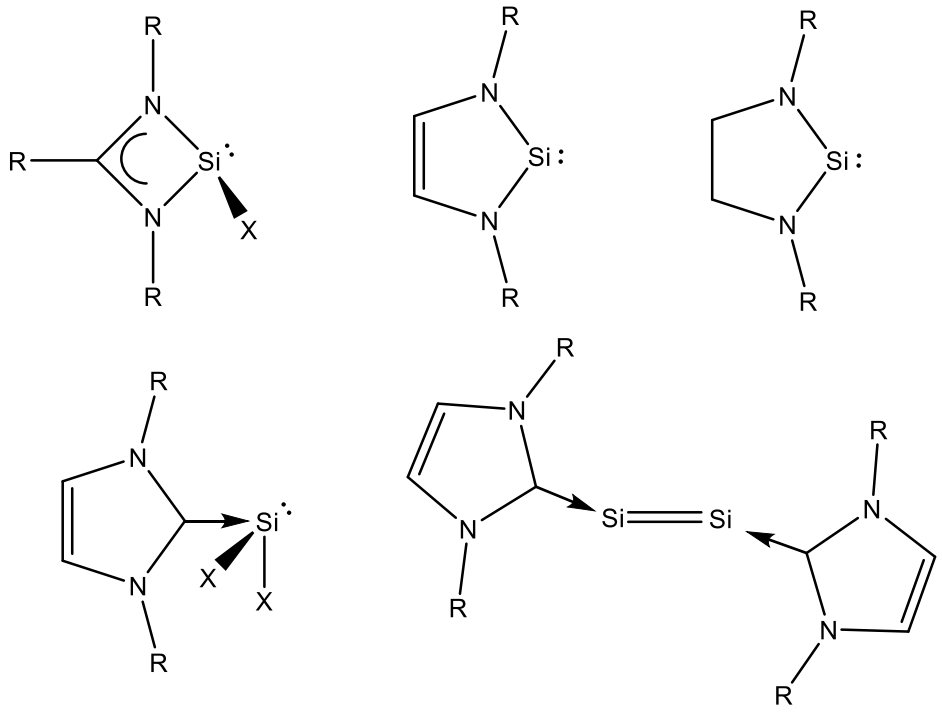

Figure 1.11. General structures of Si(II) compounds. R is often a bulky aromatic group or t-butyl and X is a halide. [73–75,79]

These ligands clearly increase the carbon content of the molecules therefore it is not possible to consider any molecule bearing these ligands as energetic. However, due to the nature of the low-valent centre, if it were possible to add an endothermic ligand it could open the possibility to new reactivity of the ligand.

The preparation of low-valent complexes was initially targeted by treatment of the corresponding Si(IV) halide with potassium metal or potassium graphite. These harsh conditions often resulted in the desired compounds however in low yields making the study of their properties and reactivity difficult. A more viable route to some of the compounds in Figure 1.11 is *via* the reductive elimination of HCl from Si(IV) hydride chloride. Complexes bearing a halide are of interest as it is possible to exchange the halide for another functional group. The silylene, $(({}^{t}BuN)_2CPh)SiCl$, can be treated with LiY (where Y= PPh_2, NPh_2, NCy_2, $N^{i}Pr_2$, NMe_2 and $N(SiMe_3)_2$) in toluene to prepare a variety of Si(II)−N bearing complexes in high yields.[87] Opening the possibility to the

preparation of a Si(II) centre bearing a nitrogen based endothermic ligand such as the azido ligand.

2. RESEARCH QUESTIONS

I. Can stable homoleptic polynitrato complexes of Group 14 and 15 elements be prepared? What factors affect the thermal stability of Main Group nitrato complexes? What inorganic products form on thermal decomposition of hexanitratosilicates, hexanitratogermanates and hexanitratostannates?

II. Can Lewis bases containing halogen atoms be used to isolate $Si(N_3)_4$ adducts in the solid state? What structural features are present in halopyridine adducts of $Si(N_3)_4$ in the solid state? Can cations containing halogen atoms stabilise $[E(NO_3)_6]^{2-}$ (E = Ge, Sn)? Does halogen bonding affect the structural properties of $[E(NO_3)_6]^{2-}$?

III. Can the formation of $[E(N_3)_3]^-$ anions stabilise germanium(II) and tin(II) azides without the need of a bulky ancillary ligand? What physical and chemical properties do these compounds have? Can the nitrato group be used as a ligand for a low valent Main Group coordination centre?

IV. What is the reactivity of different NHCs towards $Si(N_3)_4$? What other ligands, commonly used for stabilising low valent Main Group coordination centres, can be used to prepare silicon(IV) azides, silicon(IV) hydride azides, phosphorus(III) azides and phosphorus(V) azides?

V. Is it possible to prepare a silicon(II) or phosphorus(I) azide? What methods can be used to prepare such compounds?

VI. Are nitrogen-rich triazenides viable candidates as new energetic ligands for Main Group coordination centres? Is it possible to prepare triazenides from 1-aminotetrazoles to tie the current record for number of catenated nitrogen atoms?

3. NITRATO COMPLEXES OF MAIN GROUP ELEMENTS

3.1 Introduction

3.1.1 Main Group nitrates

The nitrate anion and the formation of anhydrous covalent polynitrato complexes have been extensively studied for the transition metals, Group 13 elements and tin over the past 50 years. Anhydrous covalent nitrates are of interest due to their reactivity being vastly different to that of the ionic nitrates.[61] There is considerable variability in the reactivity amongst covalent polynitrato complexes, which ranges from chemically inert to a vigorous reaction with simple hydrocarbons. The main contributions to this range of reactivity rely on the coordination of the nitrato ligand and the coordination centre.[88] Due to the structure of the anion it can coordinate in a number of ways: monodentate (κ^1*O*), bidentate (κ^2*O,O'*) and bridging ($\mu_{1,3}$-O(NO)O). Terdentate coordination has been postulated, though examples of this type of structure are yet to be determined.

In early studies of covalent nitrates the only readily available tool for determining the structure was IR spectroscopy.[89] Gatehouse, Livingstone and Nyholm compared the IR spectra of a variety of polyleptic nitrato metal complexes of Co, Pt, Pd and Ni with a number of ionic nitrates. The spectra of ten different ionic nitrates were reported by Miller and Wilkins who found that a strong band appears between 1390-1350 cm^{-1} and a less intense band between 836-815 cm^{-1}.[90] However, it is worth noting that in some examples, e.g. $Ca(NO_3)_2$, another much weaker band is present at 1050 cm^{-1}. This band, due to an IR-forbidden absorption, can be sometimes seen due to intermolecular interactions in the crystal which modify symmetry.[91] A comparison of the IR spectrum of an ionic nitrate with that of a covalent nitrato ligand, the difference is obvious. In monodentate covalent nitrato complexes three strong bands are present in the regions of 1530-1480 cm^{-1}, 1290-1250 cm^{-1} and 1030-974 cm^{-1}. The work by Gatehouse *et al* only contained complexes with monodentate nitrate coordination and so it was still unclear how bidentate coordination affected the IR absorption of the nitrato group. However, it was assumed that a N−O stretch seen above 1600 cm^{-1} (seen between 1580-1480 cm^{-1} in monodentate nitrates) was consistent with bidentate coordination.[92]

This could be proven beyond doubt when the crystal structures of $Sn(NO_3)_4$ and $Ti(NO_3)_4$ were determined.[93,94]

The coordination mode of the nitrato ligand depends highly on sterics. If there is sufficient space around the coordination centre, the nitrate will coordinate in a bidentate fashion. Even though this coordination mode should increase the complex stability resulting from a chelate effect, it is these anhydrous, covalent, nitrate compounds with bidentate nitrato ligands, which exhibit particularly high reactivity.[88] It has been suggested that a nitrato ligand in a bidentate complex must dissociate differently compared to a nitrato ligand in a monodentate complex. Table 3.1 summarises the possible products of dissociation from either bidentate or monodentate coordination.

	Dissociation products
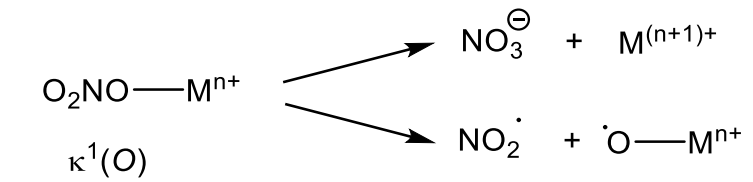	
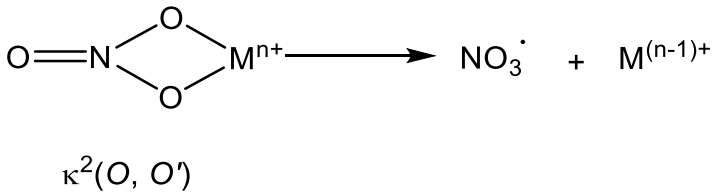	

Table 3.1. Dissociation processes of the nitrato ligand from a monodentate and bidentate coordination mode.

Addison postulated that if these nitrogen oxides are the dissociation products of a coordinated nitrate then it is clear that the main driver for the reactivity of an anhydrous covalent nitrato complex is the $NO_3^{\cdot}$ radical.[88] This leads to a number of criteria that must be met for the nitrato complex to be reactive: (i) the element acting as the coordination centre in the nitrato complex must have a lower oxidation state available; (ii) a change in the coordination mode from bidentate to monodentate leads to a loss of reactivity; (iii) the decomposition pathway cannot pass through a monodentate coordination mode. This leads to the question: how does the bidentate nitrate group dissociate from the coordination centre?

It would be easy to assume that the $NO_3^{\cdot}$ radical will dissociate in a two-step process where one oxygen ligator dissociates followed by the second; however, this mechanism would pass through a monodentate coordination which cannot happen. Therefore, it is suggested that bidentate NO_3 is not coordinated via two E−O σ bonds but rather a three-centre two-electron bond.[88] The nature of the bonding is speculative and is suggested to occur between a single electron pair spread over the sp^3 orbitals on both oxygen atoms and, in the case of a tetrahedral Main Group element, a sp^3 orbital.

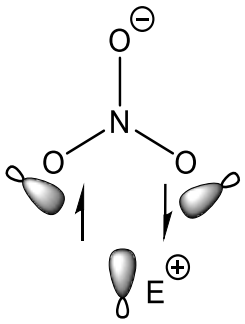

Figure 3.1. Representation of the bonding in a bidentate nitrato group. Two electrons are spread between three orbitals to give a three-centre-two-electron bond.

In early investigations of these complexes, it was found that the reativity of complexes containing bidentate nitrato groups towards organic substrates was largely based on one factor: a readily accessible lower oxidation state. This is evidenced in the examples of $Zn(NO_3)_2$ and $Sn(NO_3)_4$. On addition of diethyl ether, no reaction is observed with $Zn(NO_3)_2$,[95] whereas $Sn(NO_3)_4$ reacts vigorously.[92] This increased reactivity is due to the availability of a lower oxidation state for tin as it can be reduced from Sn(IV) to Sn(II). The dinitrato cuprate, $[Cu(NO_3)_3]^-$, is also shown to react with diethyl ether whereas $Co(NO_3)_2$ and $Ni(NO_3)_2$ are unreactive.

A number of anhydrous, homoleptic polynitrato complexes have been synthesised for transition metals but data is much less abundant on complexes with atoms of Main Group elements acting as coordination centres. In fact, the majority of characterised homoleptic polynitrato complexes belong to Group 13. Table 3.2 shows, which homoleptic Main Group nitrates have been synthesised prior to this project.

n | q	0	1–	2–	3–
1	Li, Na, K, Rb, Cs, F, Cl, Br, I	–	–	–
2	Be, Mg, Ca, Sr, Ba	–	–	–
3	Al, In, Sb	–	–	–
4	Sn	B, Al, Ga In	–	–
5	–	–	Al, In	–
6	–	Bi	Sn	Al

Table 3.2. Known homoleptic Main Group nitrates, $[E(NO_3)_n]^{q-}$. n = 1-6; q = 0, 1, 2, 3. E = Main Group element.[96–112]

Several methods have been employed in the synthesis of such compounds depending on the group and particular elements involved. Anhydrous Group 1 nitrates, besides lithium, can be isolated by crystallisation from aqueous solution after reaction of the metal or metal carbonate with nitric acid.[61] Lithium nitrate crystallises as $Li(NO_3)\cdot 3H_2O$ using this method and so removal of water is completed by heating the salt. The same method is employed with barium, strontium and calcium nitrates, however, the corresponding beryllium or magnesium nitrates decompose on heating. For the majority of anhydrous metal nitrates these methods are not feasible due to the low decomposition temperatures of these compounds so other methods have to be used. The use of silver nitrate in non-aqueous solvents has been used with the metals manganese, copper, nickel and cobalt, however, this often leads to a solvated metal nitrate.[113] The example of copper and silver nitrate in acetonitrile gives $CuNO_3\cdot 4MeCN$ and attempts to remove the solvent led to the decomposition of the nitrate.[114,115]

The most successful method and most widely used is the use of N_2O_5. Dinitrogen tetroxide, N_2O_4, has also seen a high level of success though it has been shown that N_2O_5 often gives faster reaction rates.[61] This method requires the *in situ* synthesis of N_2O_5 where HNO_3 is dehydrated using diphosphorus pentoxide. The N_2O_5 is condensed on to the reaction vessel using an ozone carrier gas.[92] The ozone also oxidises any N_2O_4 that may be present as the presence of N_2O_4 impurity has been shown to decrease reactivity. This method has seen success in Group 13 and 14 and this is where the majority of anhydrous polynitrato Main Group complexes are seen.

3.1.2 Alkali and alkali earth metal nitrates

Group 1 metals produce ionic salts with the nitrate anion and show remarkable thermal stability with respect to the nitrate anion in comparison to covalent metal nitrato complexes. Thermally induced decomposition of the ionic nitrates of sodium and potassium has been known to produce oxygen and the corresponding nitrite as early as 1774 when Scheele investigated these compounds.[116] The decomposition of these nitrates is a complex process. In 1939, Leschewski and Degenhard discovered that heating sodium nitrate and potassium nitrate to 750°C and 850°C, respectively, produces peroxides.[116] Furthermore, it was found that when potassium nitrate is heated to 550°C in an evacuated tube, nitric oxide is produced. Field and Hardy, however, demonstrated in 1963 that at a pressure of approximately 5 x 10^{-3} mmHg alkali metal nitrates, excluding lithium, distil with minimal decomposition between the temperatures 350−500°C.[117]

Among Group 2 elements, arguably the most interesting structure belongs to $Be_4(NO_3)_6O$, Figure 3.2, since it possesses the rare structural feature of a bridging nitrato ligand.[88] While the characteristics found in the IR spectrum of $Be_4(NO_3)_6O$ are compatible with the presence of a N=O bond similar to those of bidentate nitrate compounds, its reactivity is much lower. Whether this is due to the lack of a lower oxidation state available, i.e. Be(II) cannot be reduced easily, or, the more likely reason, a significant difference in bonding is unknown. The concept of the 3-centre-2-electron bond which rationalises the coordination of bidentate nitrates (*vide supra*) appears to be a less appropriate model for bridging nitrato ligands. Instead a traditional 2-centre-2-electron bond seems more reasonable. Therefore, it is more likely that the mechanism for the nitrato ligand loss will involve the consecutive cleavage of Be−O bonds.

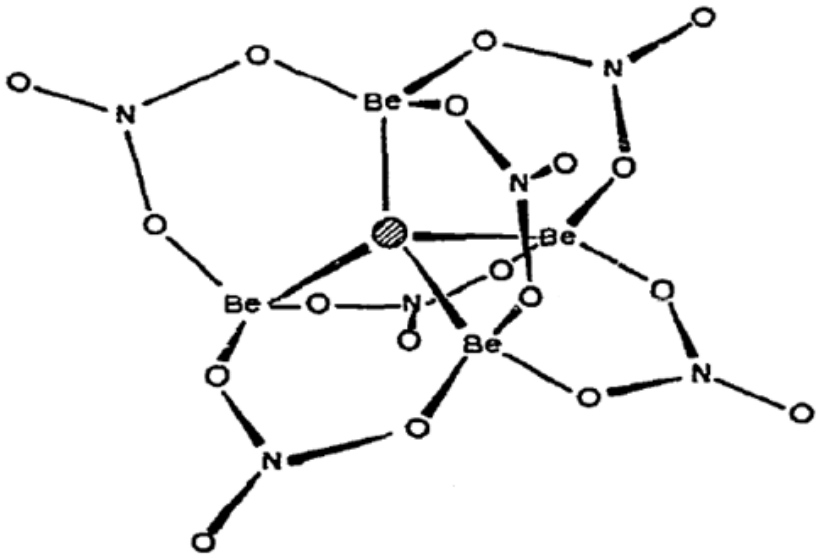

Figure 3.2. Molecular structure of basic beryllium nitrate, $Be_4(NO_3)_6O$. Reproduced from ref: 88 with permission, copyright Elsevier.

3.1.2 Group 13 polynitrato compounds

Tetranitrato borate was first synthesised in 1966 as the tetramethylammonium salt by Guibert and Marshall by reaction of N_2O_4 with $(Me_4N)[BCl_4]$. Tetramethylammonium tetranitratoborate was found to be insensitive to friction and stable at room temperature and most surprisingly showed very little water sensitivity.[100] Three years later Titova and Rosolovskii determined that on heating $(Me_4N)B(NO_3)_4$ and $(Et_4N)B(NO_3)_4$ to 75°C and 130°C, respectively, B_2O_3, NO_2, O_2 and $(R_4N)NO_3$ are obtained.[118] The authors also reported the same decomposition products for the rubidium and caesium salts starting at 40°C.[104] Decomposition of these compounds is noticeable at temperatures as low as room temperature. It was not until 1978, that the structure of the $[B(NO_3)_4]^-$ anion was determined by single crystal X-ray crystallography.[109] It was found that all nitrato ligands in $(Et_4N)B(NO_3)_4$ are bound in a monodentate fashion creating a distorted tetrahedral $[BO_4]$ coordination skeleton with O−B−O angles of 97.6° and 115.6°.

Synthesis of anhydrous aluminium nitrates was first achieved in the sixties and seventies. The first report of an anhydrous aluminium nitrate involves the attempted synthesis of anhydrous $Al(NO_3)_3$.[119] Archambault, Sisler and Ryschkewitsch combined $AlCl_3$ and N_2O_4 at −78°C in order to obtain the $Al(NO_3)_3$. The reaction mixture was then kept at room temperature over a period of seven days and a yellow crystalline solid

was obtained. Analysis of their compound suggested the formation of a mixture of $Al(NO_3)_3$ and $(NO)Al(NO_3)_4$. On heating the yellow solid at 80°C in a vacuum over a period of 4 hr a white powder was obtained which analysis suggested to be a mixture of $Al(NO_3)_3$ and a basic aluminium nitrate, such as $Al_2O(NO_3)_4$. An IR spectrum of the powder exhibits two strong bands at 1570 cm^{-1} and 1610 cm^{-1}, which is indicative of monodentate and bidentate character. Whether these bands belong to $Al(NO_3)_3$ alone or a mixture with some other aluminium oxide-nitrate(s) could not be ascertained.

In 1966, however, Addison, Boorman and Logan reported that the reaction of $AlCl_3$ and N_2O_4 only affords the aluminium oxide-nitrates: $AlO(NO_3)$ or $Al_2O(NO_3)_4$.[120] They go on to report their attempts at the synthesis of $Al(NO_3)_3$ by adding an excess of N_2O_5 to $Al(NO_3)_3{\cdot}9H_2O$. They obtained $Al(NO_3)_3{\cdot}xN_2O_5$ (where $0 < x \leq 1$) and could not fully remove N_2O_5 ($x = 0.7, 0.13, 0.07$). Addison and co-workers also attempted a method that had been previously completed by Schmeisser and Brändle, though no analytical data was provided, involving the addition of $AlBr_3$ to three equivalents of $ClNO_3$.[121] This reaction formed a pink solid, the IR spectrum of which suggested the presence of an aluminium nitrate and dinitrogen pentoxide but also showed the presence of aluminium bromide which could not be removed.[120] The first successful attempt to produce *pure* anhydrous $Al(NO_3)_3$ was completed by Shirokova, Zhuk and Rosolovskii in 1976. It was found that $Al(NO_3)_3{\cdot}N_2O_5$, which alternatively can be represented as a nitronium salt, $(NO_2)Al(NO_3)_4$, reacts with the strong Lewis acid $AlCl_3$.[112] Based on initial assumptions and the volatile nature of $Al(NO_3)_3$, it was thought that N_2O_5 would bind more strongly to the $AlCl_3$ allowing $Al(NO_3)_3$ to be distilled off, Scheme 3.1.

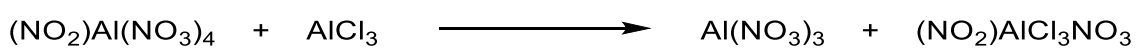

Scheme 3.1. Reaction scheme of $(NO_2)Al(NO_3)_4$ and aluminium trichloride to produce anhydrous aluminium trinitrate.

This method produces $Al(NO_3)_3$, however, not according to the equation proposed initially. It was found that $AlCl_3$ reacts with the aluminium nitrate instead to produce anhydrous $Al(NO_3)_3$ and nitronium chloride, NO_2Cl. IR data suggests the structure of $Al(NO_3)_3$ to be pseudo octahedral with three bidentate nitrato groups. Differential thermal analysis (DTA) of the compound showed two endothermic peaks between

65−100°C and 120−150°C and suggests that thermal decomposition produces $AlO(NO_3)$.[112]

The first homoleptic nitratoaluminate anion was $[Al(NO_3)_4]^-$. This complex ion was synthesised as the salt $(NO_2)Al(NO_3)_4$ in 1966 by Addison and co-workers.[120] They also reported the tetraethylammonium salt, $(Et_4N)Al(NO_3)_4$, though the complete structure of the aluminate was not fully discussed. In 1971, Shirokova and Rosolovskii synthesised pure crystalline $(NO_2)Al(NO_3)_4$ from $AlBr_3$ and dry N_2O_5 free of HNO_3.[105] Their first attempts involved an analogous method used for the corresponding caesium salt using nitric oleum (N_2O_5 dissolved in nitric acid), however, a mixture of products including aluminium nitrate and oxy nitrate adducts with N_2O_5 and N_2O_4 were formed. This method was, therefore, deemed unsuitable for the synthesis of $(NO_2)Al(NO_3)_4$. The salt was shown to sublime in the range 50-80°C at 0.01 mmHg and from IR spectroscopic measurements it suggested the structure contained two bidentate nitrates and two monodentate nitrates. Thermal properties of the salt were compared with that of the caesium analogue and showed very little difference, therefore, suggesting that any stability due to anion and cation interactions are very small.

In the synthesis of $CsAl(NO_3)_4$, the pentanitratoaluminate, $Cs_2Al(NO_3)_5$, was also obtained.[106] The authors also report that their method does not yield the hexanitratoaluminate, $Cs_3Al(NO_3)_6$. Unlike in the synthesis of $(NO_2)Al(NO_3)_4$, the reaction did not require dry N_2O_5, but a mixture of HNO_3 and N_2O_5 (1:3 by weight) after it was found that using pure HNO_3 formed $CsNO_3$ and hydrated aluminium nitrate. The reaction schemes suggested are shown in Schemes 3.2 and 3.3 for the caesium salt of tetranitratoaluminate and pentanitratoaluminate, respectively.

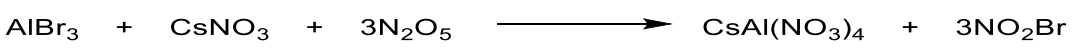

Scheme 3.2. Reaction scheme for the synthesis of $CsAl(NO_3)_4$.

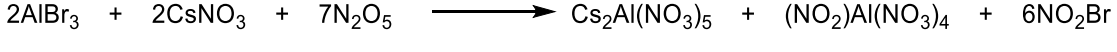

Scheme 3.3. Reaction schemes for the synthesis of $Cs_2Al(NO_3)_5$.

Scheme 3.3 is more favourable due to the lattice enthalpy gain of $Cs_2Al(NO_3)_5$. The difference in thermal stability of the pentanitratoaluminate and tetranitratoaluminate

anions is seen in the decomposition temperatures of 192-214°C and 101-125°C respectively. Decomposition of these salts release NO_2 and O_2 and the final solid products are $CsNO_3$ and aluminium oxide. Insights into the structure of $Cs_2Al(NO_3)_5$ from the IR spectrum suggested two possible structures: four monodentate nitrato groups and one bidentate nitrato group or a coordination polymer with two bridging nitrato groups per aluminium centre, Figure 3.3.[106]

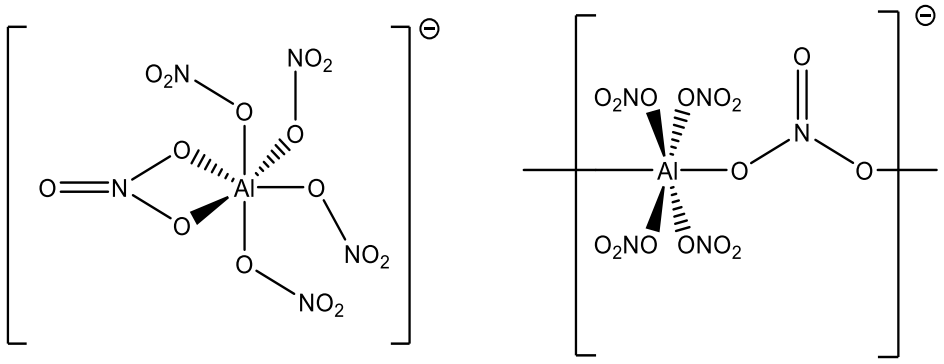

Figure 3.3. Possible structures of the $[Al(NO_3)_5]^-$ anion.

In 1973, the structure of $Cs_2Al(NO_3)_5$ was determined by X-ray crystallography, Figure 3.4.[97] Colourless crystals of $Cs_2Al(NO_3)_5$ were obtained from nitric oleum. The anion has crystallographically required C_2 symmetry and crystallises in the trigonal space group $P32I$.

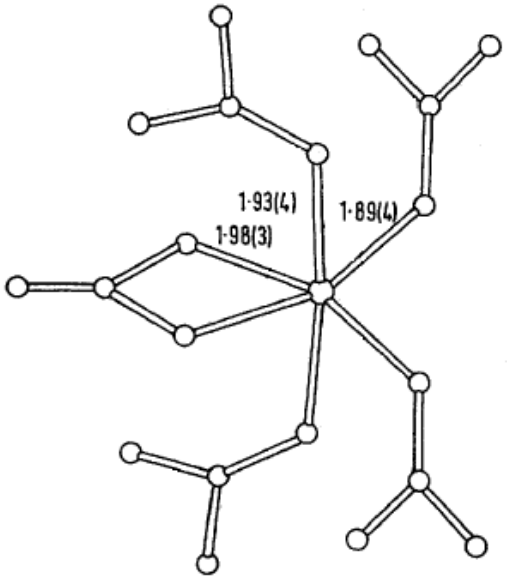

Figure 3.4. Ball-and-stick projection of the pentanitratoaluminate anion as determined by X-ray crystallography from the crystal structure of $Cs_2Al(NO_3)_5$. Reproduced from reference 97 with permission, copyright RSC.

The Al−O bond is significantly longer for the bidentate coordination mode than monodentate coordination. The bidentate nitrato ligand is shown to be symmetric, with the Al−O bonds of similar lengths. This finding contrasts with $[Co(NO_3)_4]^-$, for example, where the two Co−O bond lengths of a single bidentate nitrato group vary as much as 0.4 Å. This suggests that there is equal electron density between the aluminium centre and both oxygen atoms.

Increasing the number of nitrato ligands coordinating to aluminium to six has only been observed with K^+ as the counterion.[110] This unusual salt was synthesised combining $AlBr_3$ with KNO_3 and N_2O_5 in nitric oleum. Depending on the stoichiometry of reactants, either $K_2Al(NO_3)_5$ or $K_3Al(NO_3)_6$ is obtained. Thermal decomposition pathways of aluminium nitrates have been shown to depend on the number of coordinated nitrato ligands to the aluminium centre. Decomposition of $K_3Al(NO_3)_6$ has been shown to produce KNO_3, aluminium oxide nitrate, oxygen and nitrogen oxides.[112] The pentanitrato- and tetranitrato- aluminates, however, decompose *via* a higher coordinate nitrato complex before giving the same products mentioned previously. $K_2Al(NO_3)_5$ decomposes to aluminium oxide nitrate which undergoes simultaneous fusion with KNO_3 to produce $K_3Al(NO_3)_6$. For $KAl(NO_3)_4$ an analogous process is seen to form $K_2Al(NO_3)_5$.

It is clear that a significant amount of work has been published on aluminium nitrates, mainly their syntheses and thermal properties as studied by thermal gravimetric analysis (TGA). Similar work has been published on gallium nitrates, in particular $Ga(NO_3)_3$ and $[Ga(NO_3)_4]^-$. [108] Their structures were not discussed in terms of their IR spectra, however, on reviewing the information it appears that both species contain bidentate nitrato ligands as the wavenumbers are greater than 1610 cm^{-1} akin to their lighter congeners. Synthesis of such nitrato complexes is *via* the common method of the appropriate halide and N_2O_5. To produce the charged species $LiNO_3$ or $NaNO_3$ was added to the mixture described, similar to the nitratoaluminates. A thermogram, from TGA measurements, shows that $Ga(NO_3)_3$ sublimes at 140°C. This differs from the hydrated Ga(III) nitrate which undergoes three endothermic effects. Lithium and sodium tetranitratogallate show three endothermic steps at similar temperatures. It is suggested that the first step is decomposition to a gallium oxide nitrate and this compound decomposes in the next step to gallium oxide and ending with the formation of lithium or sodium metagallates, $MGaO_2$. Indium trinitrate has also been reported, however, some spurious elemental analysis data is provided, with both the indium and nitrate content being low by 2 percent.[101] Only an IR spectrum is provided to suggest any insight into the structure and the significant bands lie on the border between these monodentate and bidentate nitrates so there is no certainty in its true structure.

3.1.3 Group 14 polynitrato complexes

There are several examples of organopoly(nitrato) Group 14 complexes, e.g. $Me_3Sn(NO_3)$,[122] $Me_3Ge(NO_3)$ and $Me_3Si(NO_3)$.[123] However, the only known homoleptic polynitrates in this group are $Sn(NO_3)_4$,[92] $[Sn(NO_3)_6]^{2-}$,[122] and $Pb(NO_3)_2$. Efforts to prepare $[Ge(NO_3)_6]^{2-}$ and $[Pb(NO_3)_6]^{2-}$ proved unsuccessful using N_2O_5 and the corresponding elemental chloride and only GeO_2 and $Pb(NO_3)_2$ were obtained.[124] The reason provided for the lack of relevant germanium complexes was the high electronegativity of the coordination centre, even though it is possible to synthesise $Me_3Ge(NO_3)$ and $Me_2Ge(NO_3)_2$ using the corresponding organogermanium chloride and N_2O_5.[123,125] This method also enabled the synthesis of $Et_2Pb(NO_3)_2$.[126]

Silicon nitrates are scarce in the literature.[127] Only two molecular structures have been determined that possess the $Si(NO_3)$ moiety, Figure 3.5.

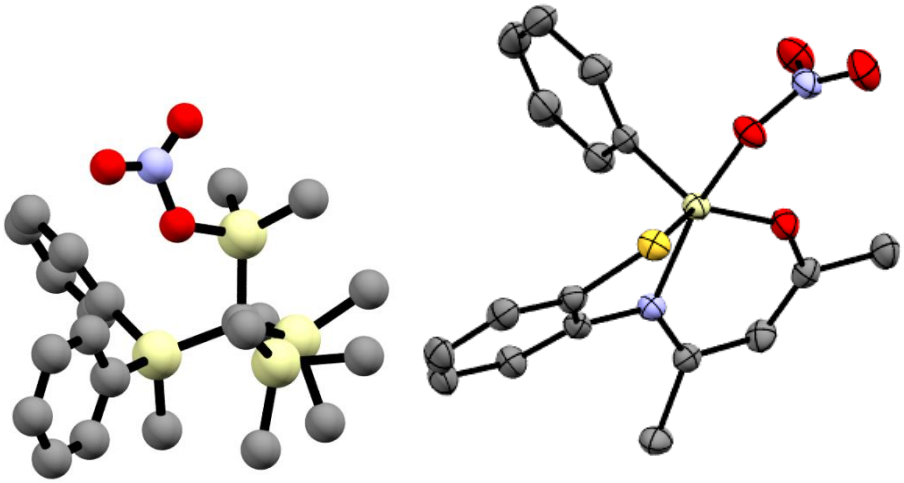

Figure 3.5. Left: ball and stick representation of $O_2NO{-}SiMe_2\{C(SiMePh_2)(SiMe_3)_2\}$. Right: thermal ellipsoid plot of $Si(NO_3\text{-}\kappa^1O)\{O{-}C(Me){=}CH{-}C(Me){=}N{-}C_6H_4{-}S\text{-}\kappa^3\textit{N},\textit{O},\textit{S})\}Ph$. Blue, N; red, O; grey, C; yellow, S; light yellow, silicon. The thermal ellipsoids are set at the 50% probability level. Images generated from cif files from reference 128 (left) and 127 (right).

The structure of the pentacoordinate silicon nitrate was the first higher coordinate nitrato silicon structure to be studied both in solution and solid state. This coordination compound was shown to be stable at −20°C as a solid over a period of a couple of months, while at a temperature of 20°C decomposition was noted over a couple of weeks. In CD_2Cl_2 solution, decomposition was noted within a few hours as monitored by NMR spectroscopy. The only decomposition products identified were 2-methyl-1,3-benzothiazole and acetone.[127]

As for a homoleptic silicon nitrate, the only mention in the literature originates from Beattie and Leigh in 1961 in their attempts to synthesise $Si(NO_3)_4{\cdot}2py$.[128] This coordination compound was prepared by combining silver nitrate and $SiCl_4$ in acetonitrile and diethyl ether at −40°C followed by an addition of pyridine at the same temperature. The only evidence for the proposed hypercoordinated species is an IR spectrum and a spurious elemental analysis. No evidence is provided for the $Si(NO_3)_4$ intermediate other than the assertion that it is thermally labile and prone to rapid decomposition at room temperature.

Though organogermanium nitrates have been synthesised previously, the majority of the work in Group 14 is concerned with compounds of tin. Several structural studies have been reported on many tin nitrates, including structures determined by single crystal X-ray diffraction of tin tetranitrate and the Mossbauer spectra of several

organotin nitrates. Tin tetranitrate is highly reactive to organic substrates and is known to react violently with diethyl ether.[92] Due to the ease at which this species sublimes, thermal gravimetric analysis was not possible. It has been reported that at 98°C decomposition occurs accompanied with brown fumes leaving a tin(IV) oxide. It was therefore suggested that decomposition does not pass through a tin oxide nitrate unlike the nitrato aluminates.

The crystal structure of tin tetranitrate was shown to be isomorphous to the titanium tetranitrate, possessing four symmetric bidentate nitrato ligands.[93] If nitrato ligands were replaced with a methyl group it would be expected the remaining nitrates would retain their bidentate coordination. However, it has been shown that that might not be the case. $MeSn(NO_3)_3$ does possess bidentate nitrato coordination as determined from the crystal structure (Figure 3.6)[99] but $Me_2Sn(NO_3)_2$ has been discussed to either be polymeric with bridging nitrato ligands or monomeric with bidentate nitrato ligands. Mossbauer spectroscopy could not distinguish between the two, only that the compound was possibly analogous to R_2SnCl_2, which does have a polymeric structure, as the isomer shift varied very little between the two compounds.[122] Raman spectroscopy also provides evidence for this structure, combined with the low volatility in comparison to tin tetranitrate and $MeSn(NO_3)_3$. As for $Me_3Sn(NO_3)$ it is not possible to be entirely confident in what the molecular structure is, though it is accepted to be polymeric. This is based on the similar isomer shift in the Mossbauer spectrum for this species and Me_3SnCl, which is known to be polymeric.[122] However, there is no X-ray diffraction data to support or disprove these claims. On addition of pyridine to these compounds the Mossbauer and IR spectra suggest disruption of any polymeric structure.

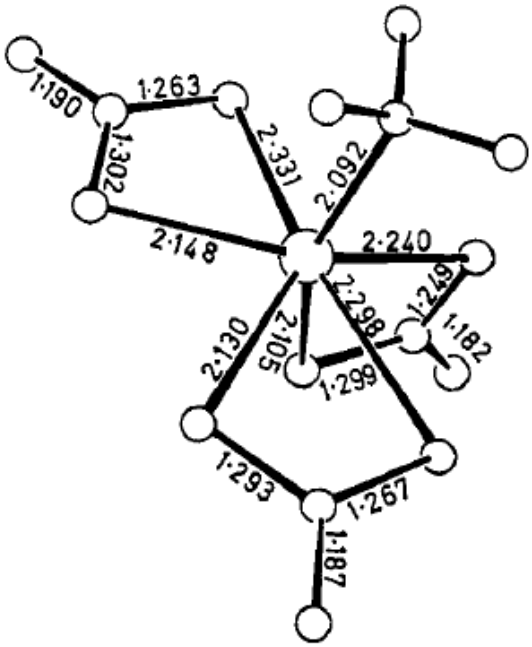

Figure 3.6. Ball and stick diagram of the molecular structure of $MeSn(NO_3)_3$ in the crystal. Reproduced from reference 99 with permission, copyright RSC.

In comparison to Main Group azido compounds, which spans across all groups in the *p*-block,[33,34] the majority of work in homoleptic polynitrato Main Group chemistry concerns either Group 13 or tin. No examples can be found for germanium and silicon. However, there are reports of polyleptic nitrato complexes of these elements. What is known about all Main Group nitrato complexes is limited to basic structural information determined by IR spectroscopy, though there are a few examples of X-ray diffraction studies to support the results from spectroscopy. As a consequence, the preparation of homoleptic silicon and germanium nitrato complexes as well as Group 15 elements was investigated.

3.2 Results and Discussion

3.2.1 Group 14 nitrato complexes

3.2.1.1 Syntheses and spectroscopy

Previous success has been made in our research group for the synthesis of the hexanitratostannate and hexanitratogermanate anions, *via* $E(NO_3)_4$ (E = Ge, Sn) in a two-step process. A modified procedure was devised for the synthesis of $(PPN)_2Si(NO_3)_6$. Addition of ECl_4 (E = Ge, Sn) to an acetonitrile solution of silver nitrate gives a stock solution of $E(NO_3)_4$. When applying the same method to silicon no

reaction occurs unless silicon tetrachloride is first dissolved in diethyl ether and the whole reaction mixture is cooled to −40°C. Removal of the silver chloride precipitate by filtration aids in the completion of the reaction. It is essential that all silver nitrate is used up before the next stage of the reaction. Any unreacted silver nitrate would react with $(PPN)NO_3$ to give $(PPN)Ag(NO_3)_2$.

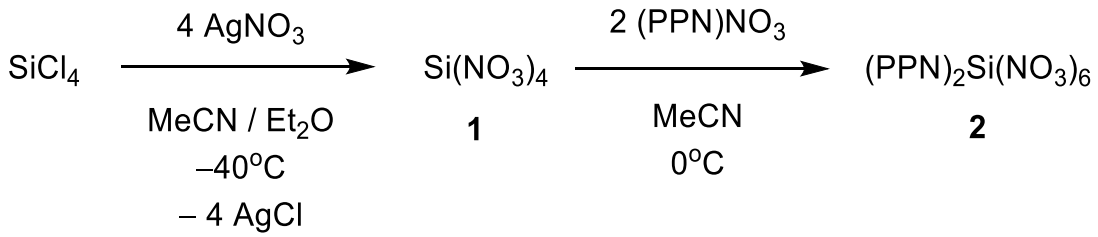

Scheme 3.4. Preparation of $(PPN)_2Si(NO_3)_6$ *via* the thermally labile $Si(NO_3)_4$.

Figure 3.7 shows the Fourier transform infrared (FT-IR) spectrum of $Si(NO_3)_4$ (**1**) in acetonitrile/diethyl ether (1:1) immediately from the reaction solution and the spectrum rerecorded over a period of twenty minutes at room temperature. The peak at 1618 cm^{-1} and shoulder at 1602 cm^{-1} have disappeared in approximately 4 minutes. The large peak at 1667 cm^{-1} can be attributed to nitric acid, most likely as the reaction solution is cold and as the volumetric pipette is taken out of the reaction vessel, and transferred to the solution cell, water will condense on the pipette and react with the sample. It is unknown what the peak at 1657 cm^{-1} corresponds to, though possibly the decomposition product, a silicon(oxy)nitrate. $Ge(NO_3)_4$ and $Sn(NO_3)_4$ in acetonitrile both show no observable changes in their IR spectra over a period of hours at room temperature.

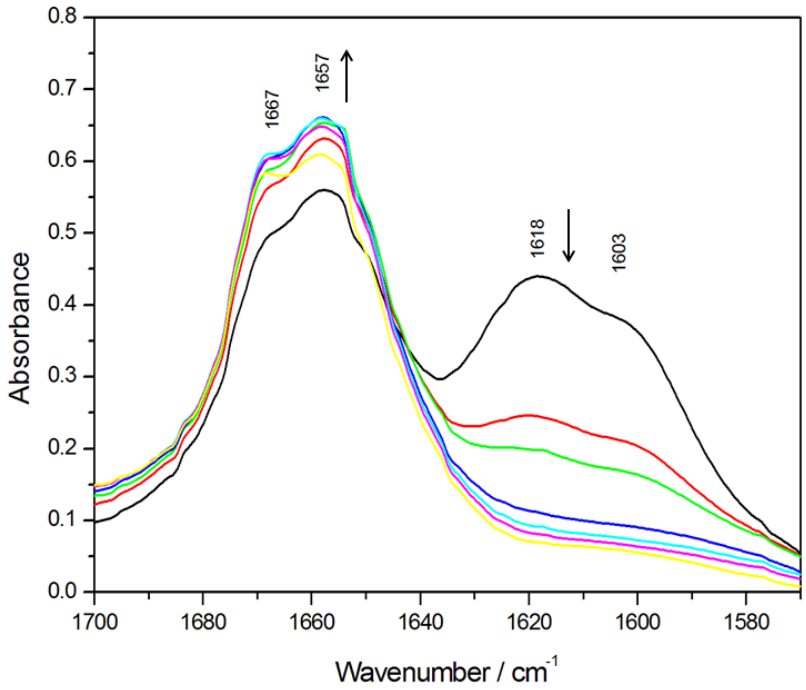

Figure 3.7. Series of FT-IR spectra of **1** in a MeCN / Et_2O (1 : 1) solution recorded over a period of 20 min. Black is t = 0 mins.

Before the addition of $(PPN)NO_3$ to **1** it is imperative the diethyl ether is first removed from the solution *in vacuo* to give a stock solution of **1** in acetonitrile. The presence of ether causes the immediate precipitation of $(PPN)NO_3$ slowing the reaction rate and increasing the likelihood of thermal decomposition of **1**. After the reaction has completed, which can be monitored by IR spectroscopy, it is possible to isolate $(PPN)_2Si(NO_3)_6$ (**2**) at room temperature as any thermal sensitivity is vastly decreased on formation of the salt. The compound crystallises as large colourless block crystals that are soluble in dichloromethane and acetonitrile, but insoluble in ethers and hydrocarbons. On exposure to air, the crystals appear to be highly hygroscopic and start to decompose within half an hour. Table 3.3 summarises the IR absorptions of the nitrato groups in $E(NO_3)_4$ and $(PPN)_2E(NO_3)_6$ (E = Si, Ge, Sn). In the solution FT-IR spectrum of **1** (*vide supra*) the $\nu_{as}(NO_2)$ vibration appears at 1618 and 1603 cm^{-1} whereas a nujol mull spectrum of **2** displays the same vibration at a lower wavenumber, 1568 cm^{-1}. The heavy congeners also follow this general trend where the $\nu_{as}(NO_2)$ is shifted to lower energy between $E(NO_3)_4$ and $[E(NO_3)_6]^{2-}$. Equally, the $\nu_{sym}(NO_2)$ vibration is also shifted to lower energy between the tetracoordinate and hexacoorinate complexes. Changing the element acting as the coordination centre results in a decrease in the spectral position of $\nu_{as}(NO_2)$ and $\nu_{sym}(NO_2)$ on descending the group. However, $\nu(ON)$ does not follow this trend, rather the order is $[Si(NO_3)_6]^{2-}$ > $[Sn(NO_3)_6]^{2-}$ >

$[Ge(NO_3)_6]^{2-}$. The silicon and germanium anions have C_{2h} symmetry, whereas hexanitratostannate has D_{3d} symmetry, as determined by single crystal X-ray crystallography (discussed in **3.2.1.3.**). The differences in symmetry may account for this discrepancy.

Compound		$\nu_{as}(NO_2)$	$\nu_{sym}(NO_2)$	$\nu(ON)$
1	$MeCN/Et_2O$ (1:1)	1618, 1603	1353	-
2	nujol	1569	1322	977
$Ge(NO_3)_4$	MeCN	1574, 1550	1323	-
$(PPN)_2Ge(NO_3)_6$	nujol	1561	1298	959
$Sn(NO_3)_4$	MeCN	1554	1285	-
$(PPN)_2Sn(NO_3)_6$	nujol	1547	1280	964

Table 3.3. IR absorptions (cm^{-1}) of the nitrato group in $E(NO_3)_4$ and $(PPN)_2E(NO_3)_6$. The $\nu(ON)$ is masked by the absorption of the CaF_2 windows and solvent for $E(NO_3)_4$.

The ^{14}N NMR spectra of the three $(PPN)_2E(NO_3)_6$ salts were recorded in CD_2Cl_2. All three spectra show a number of resonances for NO_3 groups at δ (^{14}N)/ ppm ≈ −7($\Delta\nu_{1/2}$ = 87 Hz), −44 ($\Delta\nu_{1/2}$ = 85 Hz) (**2**), −13 ($\Delta\nu_{1/2}$ = 22 Hz), −34 ($\Delta\nu_{1/2}$ = 65 Hz), −40 ($\Delta\nu_{1/2}$ = 50 Hz) ($(PPN)_2Ge(NO_3)_6$) and −13 ($\Delta\nu_{1/2}$ = 88 Hz), −29 ($\Delta\nu_{1/2}$ = 82 Hz) ($(PPN)_2Sn(NO_3)_6$, also Me*C*N at −136.0, $\Delta\nu_{1/2}$ = 90 Hz). The most deshielded signals in the spectra are accounted for by NO_3 anions. Therefore, the other signals are thought to be due to $[E(NO_3)_6]^{2-}$ and dissociation into $[E(NO_3)_{6-x}]^{(2-x)-}$ ions.

3.2.1.2. Thermal properties

Thermal decomposition pathways have been extensively investigated in the 1960s and 1970s for a variety of aluminium nitrates, where the general consensus is decomposition passes through an aluminium oxy nitrate intermediate before decomposing to aluminium oxide. More recently in 2012, the decomposition of the transition metal nitrato complexes $(NO)Au(NO_3)_4$, $(NO)_2Pd(NO_3)_4$ and $(NO)_2Pt(NO_3)_6$ was investigated via TGA and X-ray photoelectron spectroscopy (XPS) measurements. The final decomposition products for all three compounds were determined to be the elemental metal. However, different intermediates were suggested for each complex.

The palladium complex decomposes *via* $Pd(NO_3)_2$ to PdO before elemental palladium by 734°C. For $(NO)_2Pt(NO_3)_6$ the first intermediate is unknown and the second is tentatively assigned to PtO_2 followed by Pt metal at 550°C. The decomposition pathway of $(NO)Au(NO_3)_4$ is even less understood but assumed to pass through a gold oxide before producing elemental gold at a significantly lower temperature than the other two metal complexes at 240°C.

The thermal decomposition of the $(PPN)_2E(NO_3)_6$ salts was investigated by TGA measurements (Figures 3.8, 3.9 and 3.10). All three anions decompose in two steps by 350°C, any further decomposition is masked by the degradation of the PPN cation. The silicon and germanium salts decompose at similar temperatures with onset of the first step at 138°C and 145°C, respectively. The second step is again at similar temperatures for both complexes at 257°C and 260°C, respectively. In contrast, the tin complex decomposes at much higher temperatures of 204 and 303°C with an extra step observed at 93°C for the loss of acetonitrile solvate.

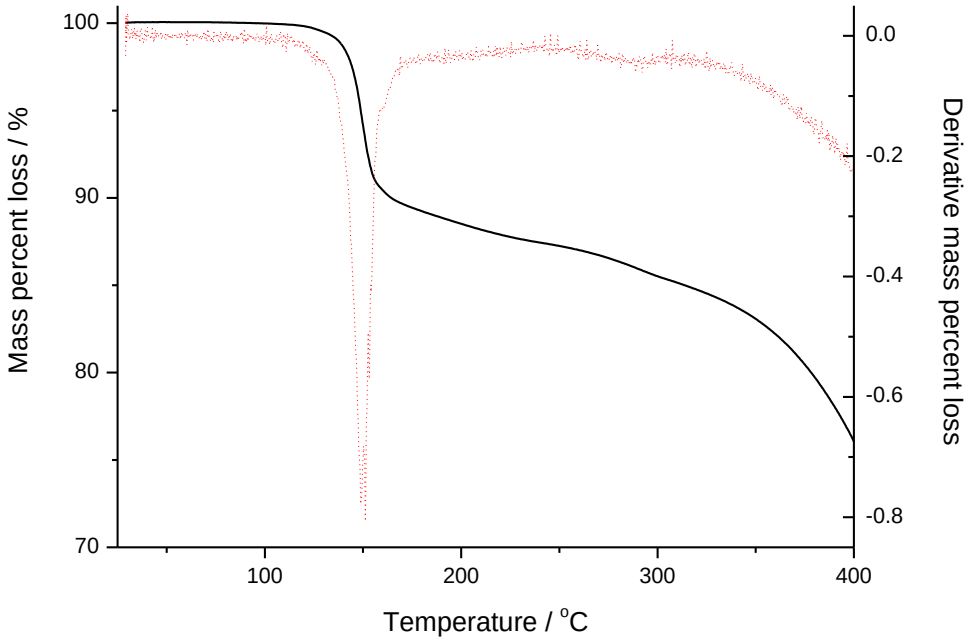

Figure 3.8. TGA thermogram of $(PPN)_2Si(NO_3)_6$; black = mass percent loss; red = derivative mass percent loss.

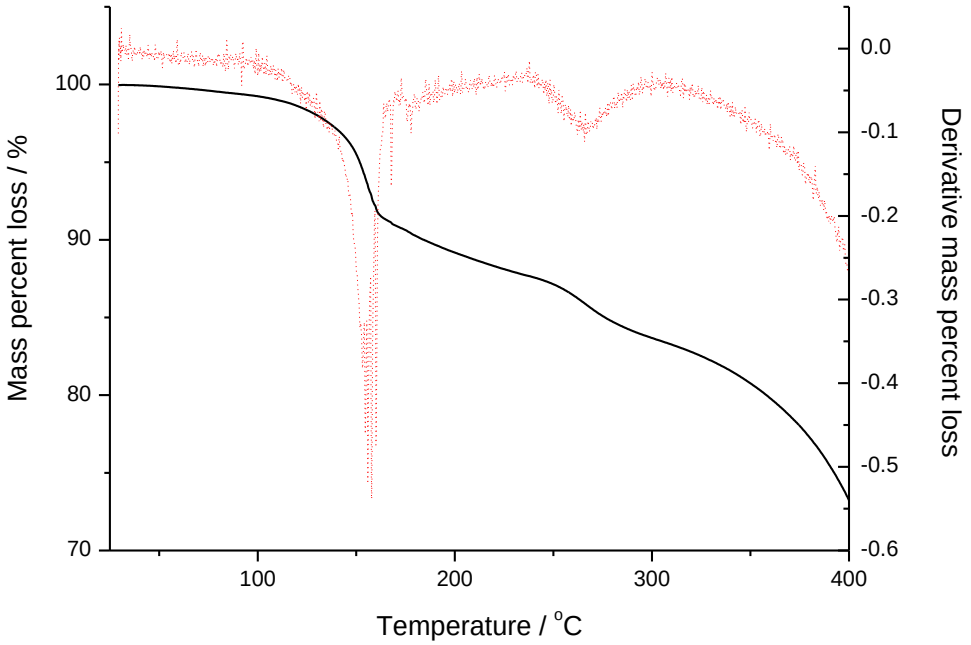

Figure 3.9. TGA thermogram of $(PPN)_2Ge(NO_3)_6$; black = mass percent loss; red = derivative mass percent loss.

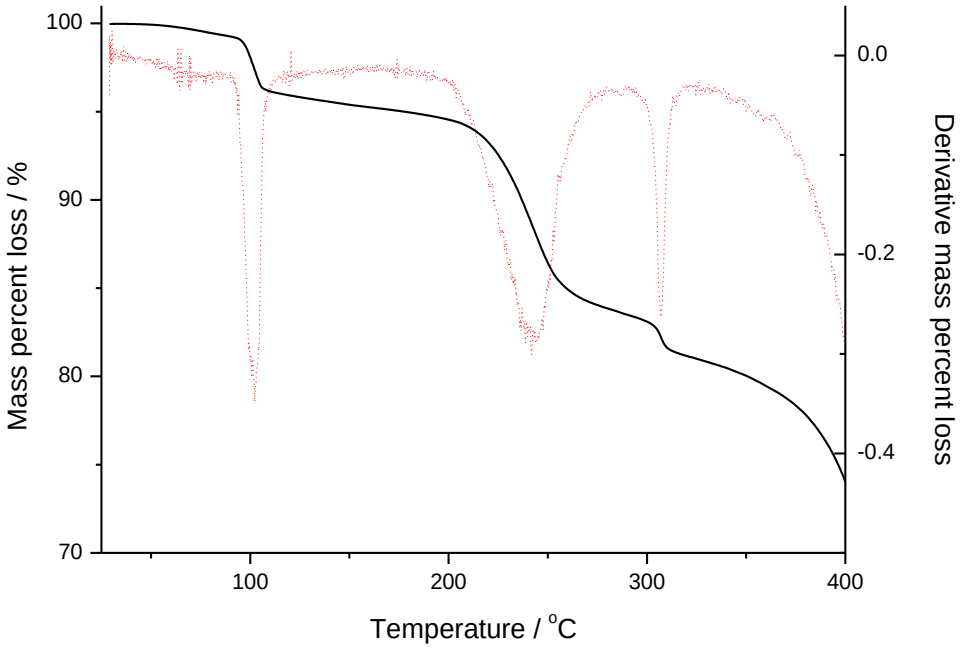

Figure 3.10. TGA thermogram of $(PPN)_2Sn(NO_3)_6 \cdot 2MeCN$; black = mass percent loss; red = derivative mass percent loss.

The TGA thermograms clearly show a significant mass loss occurs leaving material behind that is stable to a higher temperature. To investigate the product of thermal decomposition samples of crystalline $(PPN)_2Si(NO_3)_6$ and $(PPN)_2Ge(NO_3)_6$ were heated to 160°C. On decomposition, the colourless crystals turned yellow with release of brown fumes. IR analysis of the yellow solid showed the presence of $(PPN)NO_3$ and

another unidentifiable compound containing a coordinated nitrato group, most likely a silicon oxide-nitrate or germanium oxide-nitrate. Addison postulated that decomposition of a monodentate nitrato ligand occurs with loss of NO_2 to give a metal oxide. Therefore, Scheme 3.6 can be tentatively assigned for the thermal decomposition of $(PPN)_2E(NO_3)_6$. Mass losses of each stage were determined by looking at the derivative of the mass loss with respect to temperature giving the mass losses given in Table 3.4. From the combined mass losses of each step there is good correlation between the observed and theoretical values of n in Scheme 3.6. This gives SiO_2, Ge and SnO as the thermal decomposition products at 350°C of the three complex salts. (E = Si, n = 2, Δm (%) = 14.8 predicted, 14.7 observed. E = Ge, n = 0, Δm (%) = 16.3 predicted, 16.2 observed. E = Sn, n = 1, Δm (%) = 14.8 predicted, 14.5 observed.)

$$(PPN)_2E(NO_3)_6 \longrightarrow 2(PPN)NO_3 + EO_n + 4NO_2 + (2 - n/2)O_2$$

Scheme 3.6. Proposed decomposition pathway of $(PPN)_2E(NO_3)_6$.

	Mass percent loss of $(PPN)_2E(NO_3)_6$		
	Step 1	Step 2	Total
E = Si	12.7 %	2.0 %	14.7 %
E = Ge	12.0 %	4.2 %	16.2 %
E = Sn	11.7 %	2.8 %	14.5 %

Table 3.4. Percentage mass losses of $(PPN)_2E(NO_3)_6$ as determined by TGA.

3.2.1.3. Single crystal X-ray diffraction

All three compounds, **2**, $(PPN)_2Ge(NO_3)_6$ and $(PPN)_2Sn(NO_3)_6$, are easily recrystallized from acetonitrile and the crystals were investigated by single crystal X-ray diffraction. These structures are the first examples of a hexanitrato Main Group species determined by single crystal X-ray diffraction studies. The molecular structure of **2** is shown in Figure 3.11. Compound **2** crystallises in the triclinic space group $P\bar{1}$ with two formula units per unit cell. The only interaction between the cation and anions are van der Waals interactions between the hydrogen atoms of the PPN cation and the terminal oxygen atoms. The $[Si(NO_3)_6]^{2-}$ anion possesses C_{2h} symmetry with all nitrato ligands mutually *trans* to one another. The complex does not contain a C_3 axis as one of the nitrato ligands is twisted out of the plane with the E−O bond. The $[SiO_6]$ octahedron

of the coordination skeleton is noticeably distorted with O−Si−O angles between 85° and 95°. Two nitrato ligands are related by a mirror plane. Si−O(1)−N(3) and Si−O(4)−N(4) have very similar bond angles of 125.5(1)° and 128.1(1)°, respectively. The third nitrato ligand in this "C_3" group has a much larger Si−O−N bond angle of 130.6(1)°. A silicon atom is not a large enough coordination centre to accommodate six equivalent nitrato groups and, therefore, the complex is forced to C_{2h} symmetry. The average N−OSi bond length is 1.35(3) Å whereas the average terminal N−O bond length is 1.225(7) Å, slightly longer than a N−O double bond (1.14 Å), however, significantly shorter than a N−O single bond (1.43 Å).[116] In comparison to the two other known structures containing Si−ONO_2 (see **3.1.3**), the average Si−O bond length in **2** is 1.78 Å, shorter than the pentacoordinate complex (1.83 Å) and longer than the tetracoordinate complex (1.73 Å).[127,129] All N−O bonds are comparable between $[Si(NO_3)_6]^{2-}$ and $Si(NO_3\text{-}(\kappa^1O)\{O{-}C(Me){=}CH{-}C(Me){=}N{-}C_6H_4{-}S\text{-}\kappa^3\mathit{N},\mathit{O},\mathit{S})\}Ph$; however, the tetracoordinate complex has shorter terminal N−O bonds (1.22 Å vs 1.19 Å) and a longer N−OSi bond (1.35 Å vs 1.38 Å). All three O−N−O bond angles in the nitrato group of $[Si(NO_3)_6]^{2-}$ are different. The O(1)−N(3)−O(2) bond angle is close to the expected 120° while O(1)−N(3)−O(3A) has an angle of 116(14)° and O(2)−N(3)−O(3A) has an angle of 122(13)°. This is a result of a secondary interaction between the terminal oxygen of a nitrato ligand and the coordination centre. One of the oxygen atoms of the nitrato ligand is directed towards the coordination centre as a consequence of the approximate 120° bond angle of Si−O−N. The Si···O distance for the two hypercoordinate complexes are comparable, though the pentacoordinate complex is slightly shorter due to less steric hindrance around the silicon (average of 3.12 Å vs 3.07 Å). As sterics appear to the reason for a shorter distance, it is not unexpected that the tetrahedral molecule has the shortest Si···O distance of the three molecules (2.88 Å).

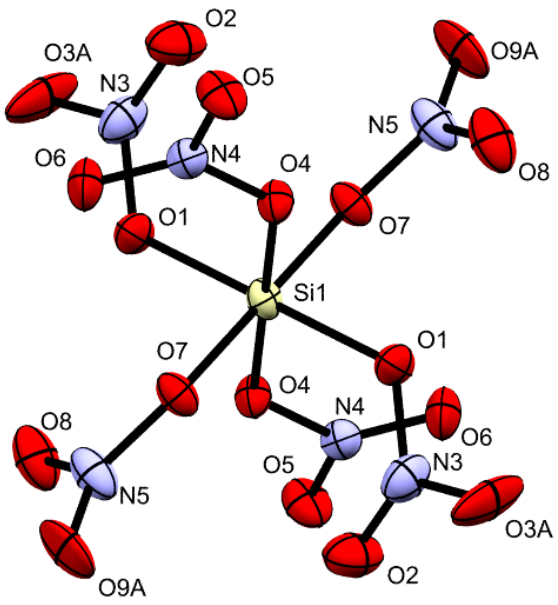

Figure 3.11. Thermal ellipsoid plot of one component of the two crystallographically independent hexa(nitrato)silicate(2−) complexes in crystals of **2** at 100 K. Ellipsoids are set to 50% probability. Selected bond lengths [Å] and angles [°]: Si1−O1 1.7875(16), Si1−O4 1.7936(14), Si1−O7 1.7689(15), N3−O2 1.213(2), N3−O3A 1.221(4), N3−O1 1.345(2), N4−O6 1.210(2), N4−O5 1.216(2), N4−O4 1.352(2), N5−O8 1.207(3), N5−O9A 1.224(4), N5−O7 1.347(2); O1−Si1−O1 180, O1−Si1−O4 96.13(7), O1−Si1−O4i 83.87(7), O4−Si1−O4 180, O1−Si1−O7 90.78(7), O1−Si1−O7i 89.22(7), O4−Si1−O7 88.19(7), O4−Si1−O7i 91.81(7), O7−Si1−O7i 180, N3−O1−Si1 125.55(14), N4−O4−Si1 128.12(14), N5−O7−Si1 130.59(14), O2−N3−O3A 122.3(13), O2−N3−O1 120.0(2), O3A−N3−O1 116.0(14), O6−N4−O5 125.6(2), O6−N4−O4 120.78(19), O5−N4−O4 113.6(2), O8−N5−O9A 121.7(14), O8−N5−O7 119.5(2), O9A−N5−O7 117.8(15).

Both $[Si(NO_3)_6]^{2-}$ and $[Ge(NO_3)_6]^{2-}$ possess C_{2h} symmetry, whereas $[Sn(NO_3)_6]^{2-}$ has D_{3d} symmetry. The secondary interactions are approximately the same length for all three complexes (3.098−3.121 Å), however, as an electrostatic interaction, and the larger van der Waals radii of tin over germanium and silicon, the interaction is stronger for the tin complex. Overall, a larger E−O−N bond angle for germanium (124.5-127.9°) and silicon (125.6-130.6°) over tin (121.9-123.0°) is observed. Therefore, the second oxygen ligator is relatively further away from the coordination centre due to crowding around the coordination sphere. The larger tin atom can accommodate an E−O−N bond angle closer to the ideal 120° and maintain secondary interactions from all nitrato ligands giving the D_{3d} symmetry.

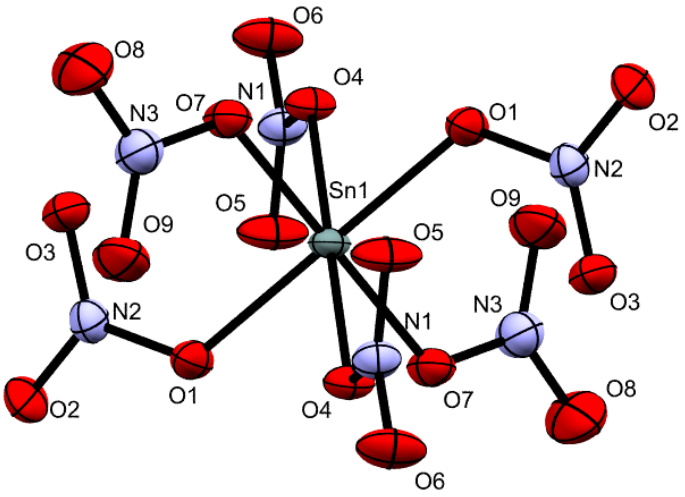

Figure 3.12. Thermal ellipsoid plot of the anion $[Sn(NO_3)_6]^{2-}$. Thermal ellipsoids are set at the 50% probability level. Selected bond lengths (Å) and angles (°): Sn1−O1 2.0624(1), Sn1−O7 2.0706(16), Sn1−O4 2.0831(16), O1−N2 1.333(2), O2−N2 1.214(2), O3−N2 1.225(2), O4−N1 1.329(2), O5−N1 1.217(2), O6−N1 1.216(2), O7−N3 1.334(3), O8−N3 1.207(3), O9−N3 1.215(3), O1−Sn1−O4 78.79(6), O1−Sn1−O4 101.21(6), O1−Sn1−O7 99.21(7), O1−Sn1−O7 80.79(7), O7−Sn1−O4 79.17(7), O7−Sn1−O4 100.83(7), N2−O1−Sn1 122.56(13), N1−O4−Sn1 121.86(13), N3−O7−Sn1 122.96(14), O6−N1−O5 125.1(2), O6−N1−O4 115.64(19), O5−N1−O4 119.23(18), O2−N2−O3 125.70(19), O2−N2−O1 115.41(19), O3−N2−O1 118.88(19), O8−N3−O9 126.1(2), O8−N3−O7 115.3(2), O9−N3−O7 118.6(2).

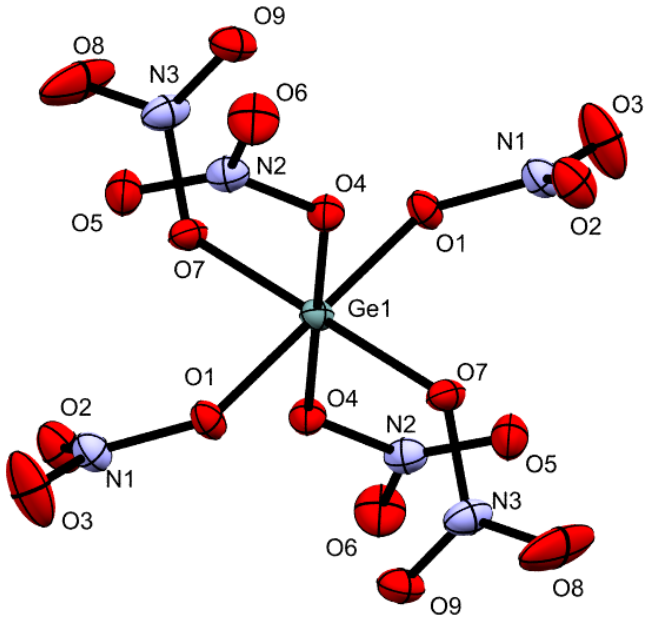

Figure 3.13. Thermal ellipsoid plot of the anion $[Ge(NO_3)_6]^{2-}$. Thermal ellipsoids are set at the 50% probability level. Selected bond lengths (Å) and angles (°): Ge1−O1 1.8947(13), Ge1−O4 1.9168(13), Ge1−O7 1.8920(13), N1−O2 1.206(2), N1−O3 1.212(2), N1−O1 1.356(2), N2−O6 1.219(2), N2−O5 1.220, N2−O4 1.345(2), N3−O8 1.201(2), N3−O9 1.212(2), N3−O7 1.347(2), O1−Ge1−O4 91.60(6), O1−Ge1−O4 88.40(6), O7−Ge1−O1 93.56(6), O7−Ge1−O1 86.44(6), O7−Ge1−O4 99.69(6), O7−Ge1−O4 80.31(6), N1−O1−Ge1 127.88(11), N2−O4−Ge1 124.48(11), N3−O7−Ge1 125.42(11), O2−N1−O3 125.80(18), O2−N1−O1 119.78(16), O3−N1−O1 114.34(16), O6−N2−O5 125.52(18), O6−N2−O4 114.26(16), O5−N2−O4 120.21(16), O8−N3−O9 125.70(18), O8−N3−O7 113.92(17), O9−N3−O7 120.37(16).

	Average bond lengths of $[E(NO_3)_6]^{2-}$		
	E−O	EO−N	Terminal N−O
E = Si	1.78(2)	1.35(3)	1.22(7)
E = Ge	1.90(1)	1.34(3)	1.21(3)
E = Sn	2.07(2)	1.33(3)	1.21(3)

Table 3.5. Average bond lengths (Å) of $[E(NO_3)_6]^{2-}$.

	Average bond angles of $[E(NO_3)_6]^{2-}$				
	O−E−O	E−O−N	O(1)−N−O(3)	O(1)−N−O(2)	O(2)−N−O(3)
E = Si	85.8(1), 94.6(1)	127.3(3)	114.9(3)	120.5(3)	124.3(3)
E = Ge	85.0(1), 94.9(1)	126.5(1)	114.9(3)	120.0(3)	125.7(3)
E = Sn	79.5(1), 100.4(1)	122.4(3)	115.4(3)	118.9(3)	125.6(3)

Table 3.6. Average bond angles (°) of $[E(NO_3)_6]^{2-}$.

The identity of the coordination centre has little bearing on the bond lengths of the N−O bond, Table 3.5. The major differences between the complexes are in the bond angles, summarised in Table 3.6, due to the two different symmetries observed, C_{2h} and D_{3d}. The average bond angle of O−E−O shows a larger distortion of the octahedral centre for tin in comparison to silicon and germanium. This value deviates as much as 10° from the ideal 90° for tin allowing the higher symmetric point group of the molecule, almost identical to the $[Pt(NO_3)_6]^{2-}$ anion.[130] As a result, the E−O−N bond angle is closer to the 120° expected from the sp^2 hybridisation of the oxygen atom.

3.2.2 Group 15 nitrato complexes

3.2.2.1 Syntheses and IR spectroscopy

The stability of arsenic(V) compounds is known to be low, $AsCl_5$ decomposes above −50°C. On the otherhand, arsenic(III) is a stable oxidation state, therefore, after the successful synthesis of **2**, the same synthetic methods were applied to arsenic(III) chloride to prepare $As(NO_3)_3$ and $(PPN)As(NO_3)_4$. Firstly, the synthesis of $As(NO_3)_3$ (**3**) was completed by addition of silver nitrate to $AsCl_3$ in acetonitrile at −40°C. After removing the silver chloride by-product by filtration, as long as the filtrate solution containing **3** is stored at −40°C it remains colourless. Addition of $(PPN)NO_3$ to **3** in acetonitrile results in no reaction and the only solid material obtained is $(PPN)NO_3$.

There are two possible reasons to why this might be the case, (i) the nitrate anion is a weaker ligand than acetonitrile, or (ii) $(PPN)NO_3$ has a larger lattice enthalpy than $(PPN)As(NO_3)_4$ resulting in dissociation of the hypercoordinate species. To prevent the possible coordination of acetonitrile, the solvent was changed from acetonitrile to dichloromethane. This results in another issue in that silver nitrate is not soluble in dichloromethane at low temperature. Nevertheless, $AsCl_3$ was added to a suspension of silver nitrate in dichloromethane at −40°C. No reaction was observed until the suspension was warmed up to 0°C at which point silver chloride began to precipitate. $(PPN)NO_3$ was added to the reaction solution and colourless crystals of $(PPN)AsCl_2(NO_3)_2$ (**5**) as identified by single crystal X-ray crystallography were obtained. The product obtained from the intial reaction between silver nitrate and $AsCl_3$ was $AsCl_2(NO_3)$ (**4**). The low solubility of silver nitrate in dichloromethane accounts for the incomplete conversion. Compounds **4** and **5** are significantly more thermally stable than **3**, but, still decompose at room temperature within a couple of hours. In the light of these results another method was attempted to prepare $(PPN)As(NO_3)_4$ *via* $(PPN)AsCl_4$. Addition of silver nitrate to $(PPN)AsCl_4$ in acetonitrile gives the silver chloride precipitate, however, IR analysis of the reaction solution shows that the product of the reaction is $As(NO_3)_3$. As it is known that $(PPN)NO_3$ reacts with silver nitrate, it can be assumed that $(PPN)As(NO_3)_4$ dissociates in acetonitrile rather than $(PPN)AsCl_4$. Scheme 3.7 summarises the syntheses of arsenic(III) nitrates. It appears that dichloromethane may be the only solvent suitable for the preparation of $(PPN)As(NO_3)_4$.

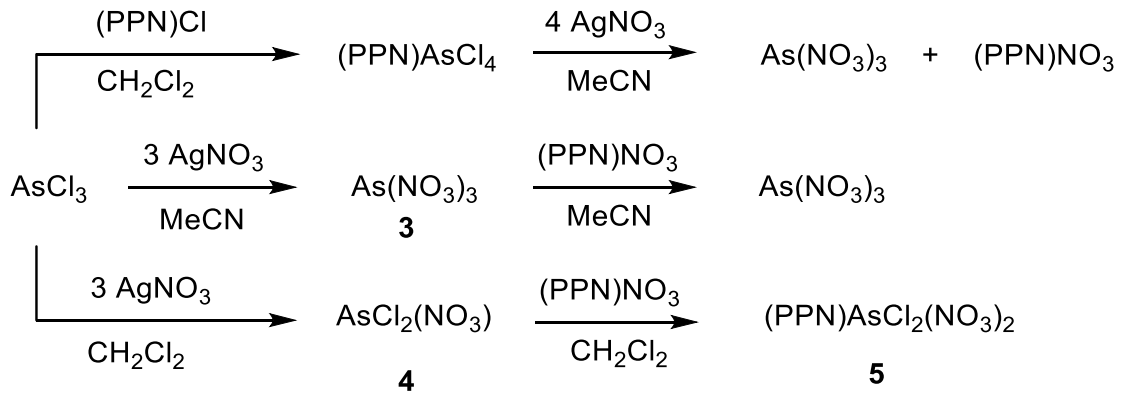

Scheme 3.7. Syntheses of arsenic(III) nitrates. By-products omitted for clarity.

Figure 3.14 shows the IR spectral series of a solution of **3** in acetonitrile at room temperature recorded several times over a period of ten minutes. Even in the initial spectrum, NO_2 is observed at 1739 cm^{-1}. A large peak at 1670 cm^{-1} is present for HNO_3, as seen in the IR spectrum of $Si(NO_3)_4$, and the $\nu_{as}(NO_2)$ of **3** appears at 1648 cm^{-1}. The spectral position of which is indicative of bidentate coordination, however, the presence of NO_2 as the decomposition product indicates monodentate coordination. Supported further by the FT-IR spectrum of **4** in dichloromethane, Figure 3.15, which shows a peak at 1680 cm^{-1} for **4** and, more significantly, a signal at 1844 cm^{-1} for NO that appears on decomposition. Formation of NO on thermal decomposition indicates bidentate coordination, therefore, it is clear that the nitrato ligands in **3** are not bound in a bidentate fashion despite such a high wavenumber for the $\nu_{as}(NO_2)$ vibration. It has not been possible to determine the structure of **3** in acetonitrile unequivocally, the IR spectroscopic evidence suggests that the nitrato ligands in **3** are in fact bridging between arsenic centres.

Another interesting difference between compounds **3** and **4** is the time taken for decomposition. From the FT-IR spectrum of **3** the IR signature of the product has almost all disappeared within 10 mins at room temperature, whilst **4** is still present even after 75 mins at room temperature. It is not possible to determine if this vast difference in sensitivity is due to the presence of more nitrato ligands in **3** or the different coordination mode of the nitrato ligand in the two complexes. Compound **5** has an absorption at 1510 cm^{-1} for $\nu_{as}(NO_2)$, undoubtedly monodentate coordination.

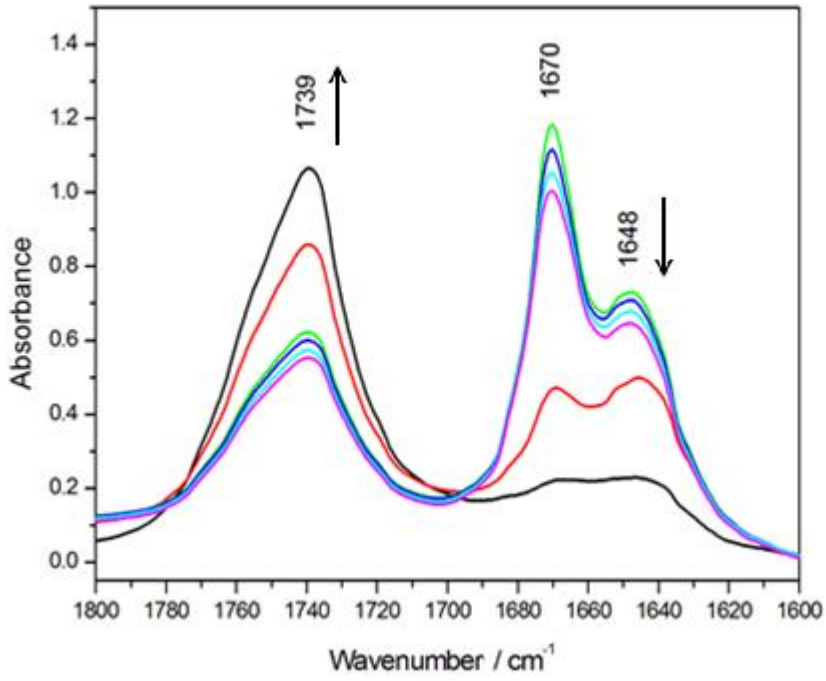

Figure 3.14. Series of FT-IR spectra of $As(NO_3)_3$ in acetonitrile at room temperature over a period of 10 mins. The green line is the initial spectrum.

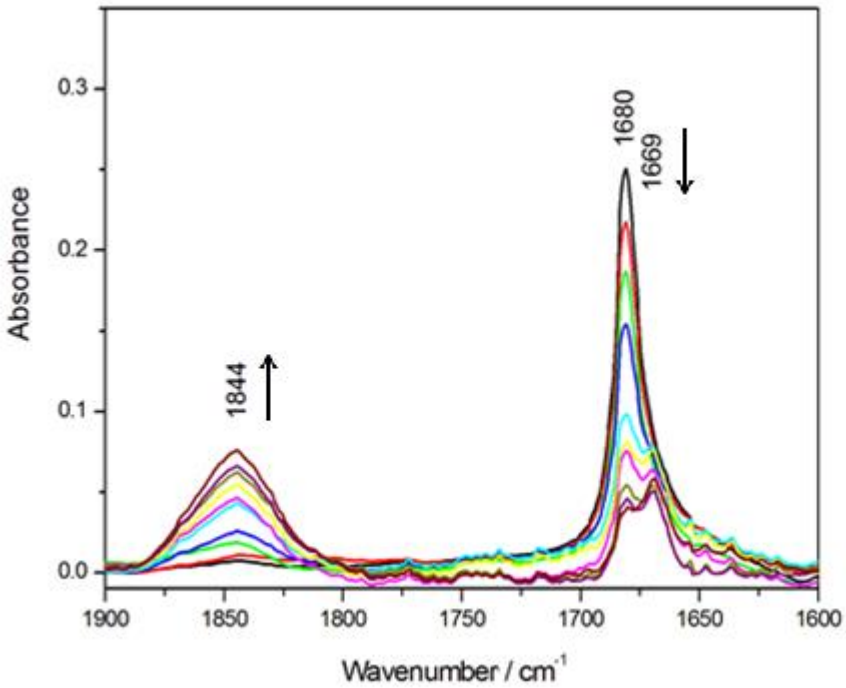

Figure 3.15. Series of FT-IR spectra of the $AsCl_3$ / silver nitrate reaction mixture in dichloromethane recorded over a period of 75 minutes at room temperature. The black line is the initial spectrum.

3.2.2.2 Single crystal X-ray diffraction

Crystals of **5** suitable for single crystal X-ray diffraction studies were obtained from cooling a saturated dichloromethane solution of **5** from 0°C to −28°C slowly over a period of 16 hrs. The compound crystallises in the space group *P*21/c and the nitrato groups are coordinated in a monodentate fashion. The As atom is four coordinate with a stereochemical active lone pair lying in the equatorial plane giving an see-saw geometry for the complex. Both of the nitrato ligands occupy axial coordination sites, leaving the chlorine atoms in the equatorial sites. Positional disorder is observed for one of the nitrato groups. One position is where the nitrato group is in the plane with the nitrato group *trans* to it, whereas the other position is where the nitrato group is twisted by approximately 75° with respect to the nitrato group *trans* to it. Figure 3.18 shows the thermal ellipsoid plots of the two disordered components of $[As(NO_3)_2Cl_2]^-$. Due to repulsion between the lone pair and the ligands the angle between O−As−O, Cl−As−O and Cl−As−Cl deviates from the ideal 180, 90 and 120° to 160(1)°, 78(1)° and 100(1)°.

The N−O bond lengths in this molecule are considerably different to the N−O bond lengths seen in $(PPN)_2Si(NO_3)_6$. Most significantly in the N−OAs bond, **5** has an average bond length of 1.22(1) Å compared to 1.35 Å in $[Si(NO_3)_6]^{2-}$. One of the terminal N−O bond lengths in each nitrato ligand is similar to $[Si(NO_3)_6]^{2-}$ whereas a second is slightly longer, this is N2−O3, N3−O5A and N3−O5B. These bond lengths are 1.26(1), 1.30(1) and 1.42(1) Å respectively, unusually long and closer to N−O single bonds. The reason for this elongation is due to the secondary coordination of the nitrato ligand. This paramter, ΔEO, is the difference between the E−O bond and the E···O secondary interaction distance. It can be used as a measure whether the nitrato ligand is monodentate or bidentate. In a review by Addison, he defined that if the difference is 0 then the coordination is symmetrically bidentate, between 0.2−0.7 unsymmetrically bidentate and > 0.7 is monodentate.[35] In this molecule the three ΔEO values are 0.6, 0.6 and 0.5, therefore the nitrato groups are unsymmetrically bidentate. It is worth noting that this mode appears to be indiscernible from mondentate coordination in the IR spectrum. The value of 0.6 belong to the symmetrically equivalent nitrates whereas the twisted nitrate has the slightly smaller ΔEO. This secondary interaction has a knock on effect on the E−O−N bond angle which are significantly more acute than 120° ranging

between 104 and 112°. In stark contrast with $[E(NO_3)_6]^{2-}$ which have ΔEO values of 1.0 (Sn), 1.2 (Ge) and 1.3 (Si) and E−O−N angles between 122 to 130°.

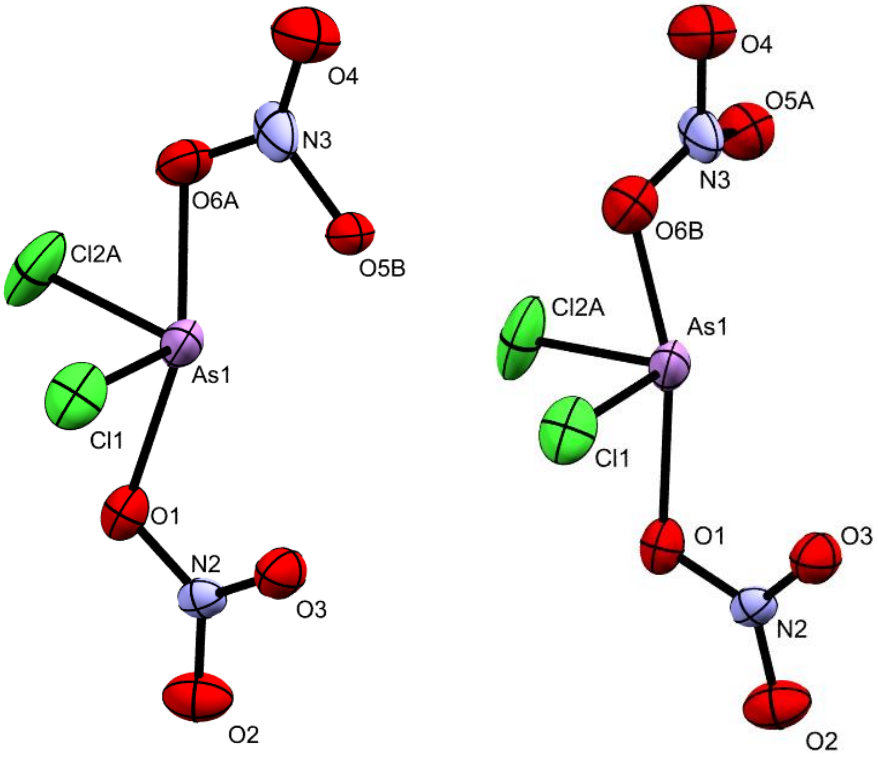

Figure 3.18. Thermal ellipsoid plot of both arrangements of the anion $[As(NO_3)_2Cl_2]^-$ in **5**. Thermal ellipsoids are set at the 50% probability level. Selected bond lengths (Å) and angles (°): As1−O1 2.131(2), As1−O6A 2.010(5), As1−O6B 2.204(6), As1−Cl1 2.1803(10), As1−Cl2 2.1677(11), N2−O1 1.299(3), N2−O2 1.212(3), N2−O3 1.256(4), N3−O4 1.249(4), N3−O5A 1.297(7), N3−O5B 1.424(6), N3−O6A 1.217(7), N3−O6B 1.150(7), O1−As1−Cl1 87.28(7), O1−As1−Cl2 83.04(7), O6A−As1−O1 159.24(18), O6B−As1−O1 160.58(17), O6A−As1−Cl1 95.54(17), O6A−As1−Cl2 76.20(17), Cl2−As1−Cl1 99.55(4), Cl2−As1−O6B 95.31(17), Cl1−As1−O6B 73.87(17), O2−N2−O1 119.5(3), O3−N2−O1 117.6(2), O2−N2−O3 122.9(3), O6A−N3−O4 133.2(4), O6B−N3−O4 119.9(4), O6A−N3−O5A 77.2(4), O6B−N3−O5B 88.9(4), O4−N3−O5A 110.4(4), O4−N3−O5B 112.4(4), N2−O1−As1 109.04(19), N3−O6A−As1 112.8(4), N3−O6B−As1 104.2(4).

3.3 Conclusions

The successful synthesis of a variety of novel Main Group nitrato complexes *via* a two-step process using silver nitrate and $(PPN)NO_3$ has provided a new and safer route for the preparation of a novel homoleptic nitrato complexes. The use of bulky cations and the formation of hypercoordinate complexes has allowed for the preparation of stable polynitrato silicon, germanium and tin anions. This new two-step process *via* the

thermally labile neutral tetranitrato species removes the need for dry-N_2O_5 as used in the preparation of other covalent nitrato compounds. Previously inaccessible nitrato complexes have also been obtained. Formation of complex salts increases thermal stability dramatically, with $Si(NO_3)_4$ decomposing within minutes at room temperature whereas crystalline $(PPN)_2Si(NO_3)_6$ is stable up to 138°C. The loss of varying amounts of NO_2 and O_2 in a two-stage process shows that despite the similarity between the complexes $(PPN)_2E(NO_3)_6$ (E = Si, Ge, Sn), especially for Si and Ge, different final products are obtained after thermal decomposition. A different cation to (PPN) will be necessary to determine any more insight into the thermal decomposition as the decomposition of the cation masks any later stage nitrate-related decomposition. NO^+ or NO_2^+ would be ideal candidates as either would remove any oxidisable material present from carbon or hydrogen impurities. The combination of the N_2O_5 and silver nitrate methods would be necessary to prepare a complex such as $(NO)_2Si(NO_3)_6$ or $(NO_2)_2Si(NO_3)_6$.

Limited success was obtained in the synthesis of arsenic nitrates. It was found that arsenic nitrates are significantly more thermally labile than Group 14 nitrates. Nevertheless, it was possible to prepare two new neutral arsenic nitrates in solution and a third in the solid state at low temperature, $As(NO_3)_3$, $AsCl_2(NO_3)$ and $(PPN)AsCl_2(NO_3)_2$. Despite the similarities of the IR signature of bidentate coordination and bridging coordination modes it has been possible to distinguish between the two coordination modes based on the gas evolved on thermal decomposition. Addition of $(PPN)NO_3$ to the acetonitrile solution of $As(NO_3)_3$ resulted in no reaction as no gain in lattice enthalpy is obtained from converting $(PPN)NO_3$ to $(PPN)As(NO_3)_4$. Therefore, even if it was possible to prepare $(PPN)As(NO_3)_4$ it would most likely dissociate in the presence of a coordinating solvent, such as acetonitrile of THF.

From the synthesis of these hypercoordinate polynitrato complexes it is clear the coordination chemistry of the nitrato ligand is diverse. Despite the nitrato ligand being a sterically demanding ligand the flexibility of the N−O bonds minimises inter-ligand steric repulsion. The classification of monodentate and bidentate coordination limits the true nature of the bonding in such complexes, competing steric and electronic interactions often gives a coordination mode between monodentate and bidentate. A subtle difference in the secondary interaction of the nitrato ligand, even though it would still be classified as monodentate, can result in different geometries of complexes in the solid state. The understanding of the nitrato coordination is therefore, an important

aspect not just for chemical reactivity but also structural studies and thermal decomposition pathways.

4. HALOGEN BONDING IN ENERGETIC COMPLEXES

4.1 Introduction

Energetic supramolecular chemistry is a relatively new field of study though has its origins as early as 1982. Patil *et al* prepared mixed hydrazine metal complexes with NO_3^-, N_3^- or ClO_4^- counterions, $(M(L)_2(N_2H_4)_2$ (L = NO_3, M = Mn, Fe, Co, Ni, Zn, Cd; L = N_3, M = Mg, Co, Ni, Zn; L = ClO_4, M = Mg).[131] Another report in 1996 by Narang *et al* prepared the same metal hydrazine azides with Co, Ni, Zn and Cd.[21] However, it was not until 2011 when a re-emergence in the field prompted a new synthesis of $[Zn(N_3)_2(N_2H_4)_2]_n$. The solid state structure of which is a 1-D polymer as determined by single crystal X-ray diffraction, Figure 4.1.[22]

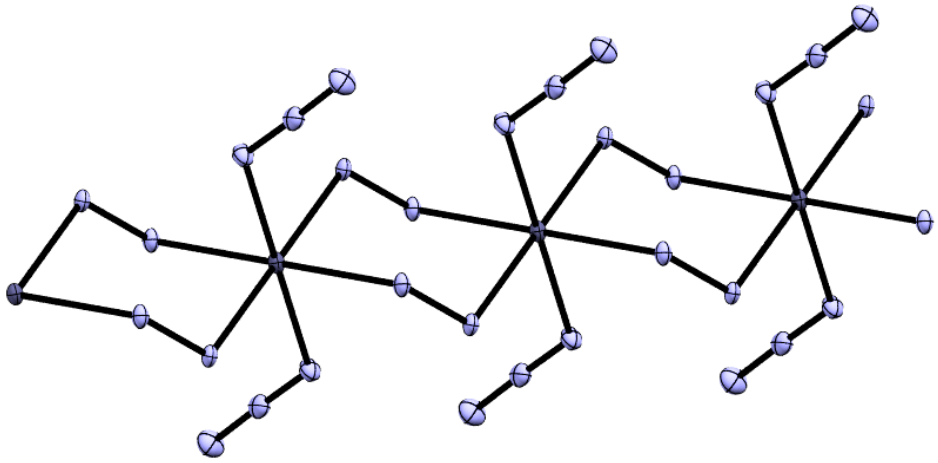

Figure 4.1. Thermal ellipsoid plot of $[Zn(N_3)_2(N_2H_4)_2]_n$. Dark grey: Zn; light blue: nitrogen. Image generated from cif file from reference 22.

An assortment of nitrogen and oxygen containing polydentate ligands, such as tetrazole and furazan derivatives, combined with a variety of metal centres has resulted in several interesting energetic supramolecular compounds coined "energetic metal-organic frameworks".[15,132–135] The complexes mentioned above are extremely shock and friction sensitive and possess very high heats of detonation, comparable to that of powerful organic explosives. Herein lies the next problem with these new energetic materials; their extremely high shock and friction sensitivities. It was postulated that extending the structure into higher dimensions would impart an increase in stability. In 2013 the direct modification of the hydrazine ligand in

$[Co(N_2H_4)_2](ClO_4)_2$ and $[Zn(N_2H_4)_2](ClO_4)_2$ with atmospheric CO_2 prepared new coordination polymers containing the hydrazincarboxylate ligand.[132] These new complexes did possess 2-D structures (Figure 4.2) and, more importantly, had the desired effect and were much safer to handle. Energetic output was reduced, however, still remaining comparable to common organic secondary explosives.

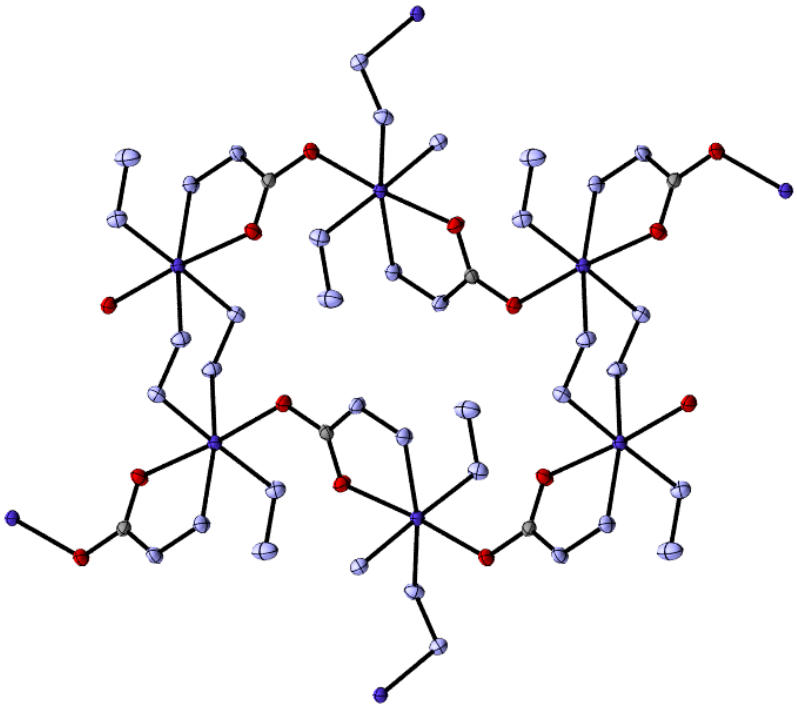

Figure 4.2. Thermal ellipsoid plot of the extended structure of $[Co_2(\mu^2\text{-}N_2H_4)_2(N_2H_2)_2(OC(O)NHNH_2)_2\text{-}\mu^2\text{-}(O,O')\text{-}\kappa^2\text{-}(N,O)](ClO_4)_2$, with perchlorate anions omitted. Purple: Co; grey: carbon; red: oxygen. Image generated from cif file from reference 132.

Extension into the third dimension has been achieved using a variety of triazole, tetrazole, triazine, tetrazine and furazan based ligands. Recent reviews have catalogued the incredible structures that have been successfully synthesised, varying from 2-D sheets to porous 3-D frameworks.[15,135] Instead of combining energetic polydentate ligands and metal ions to obtain energetic scaffolds, a further avenue of research would be to incorporate energetic coordination complexes into coordination networks through intermolecular interactions. Hydrogen bonding has been extensively studied in the field of energetic coordination complexes, especially for transition metals, however, halogen bonding networks have66 seen very little attention.

The halogen bond is a highly directional non-covalent interaction between a covalently bound halogen and a Lewis base.[136–143] Halogen atoms are usually considered as having partial negative charges, therefore it is counter-intuitive that a

halogen bond would be a favourable interaction. Insight into this bonding interaction can be gained by considering the electrostatic potentials, $V_S(r)$, of a halogen atom when as part of a molecule. For a ground-state spherically symmetric atom the electrostatic potential is positive as the nucleus has a stronger effect than the electrons on the overall potential. When an atom bonds to form a molecule the rearrangement of charge produce regions of negative electrostatic potential over the molecule usually as a consequence of differing electronegativies.[140] Figure 4.3 shows the $V_S(r)$ of CF_3X (X= F, Cl, Br, I) determined by Politzer *et al*. The obvious trend is the increase of the positive region, growing at the point along the C−X bond, going down the halogens. This positive region is what is known as the σ-hole and accounts for why a covalent halogen can form a favourable bonding interaction with areas of negative charge. Each halide has a σ bonding orbital and three electron pairs residing in two perpendicular *p*-orbitals and one in a partially hybridised *s*-orbital and *p*-orbital.[140] The component of the σ bond from the halogen is primarily from a *p*-orbital and when considering X= Cl, Br and I the distribution of the shared electrons is approximately 50% between C and X (71% towards F in C–F).

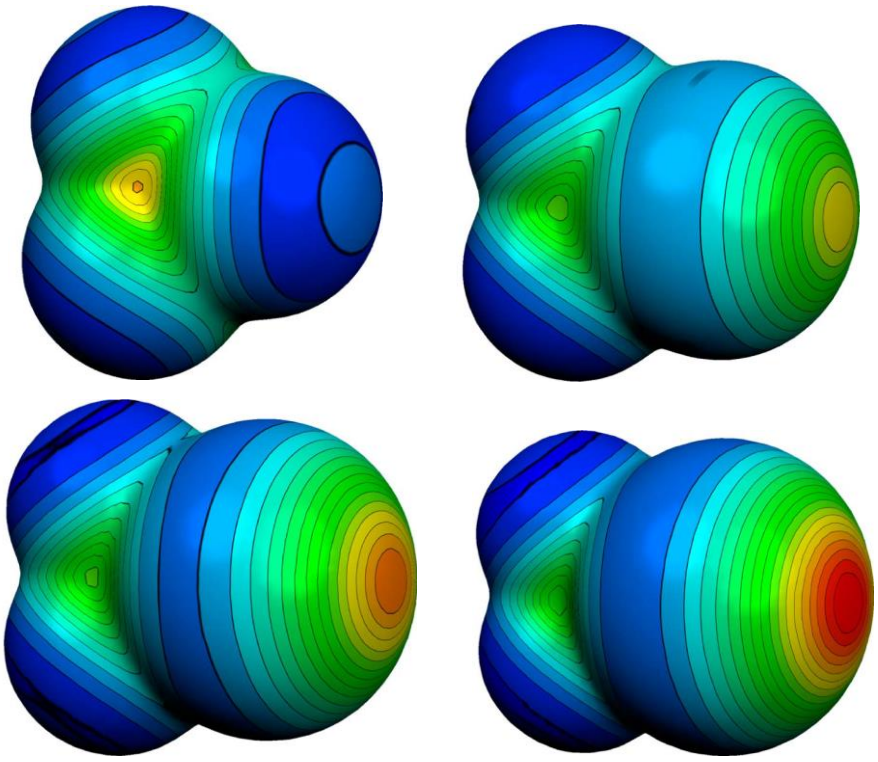

Figure 4.3. The molecular electrostatic potentials of CF_4 (top left), CF_3Cl (top right), CF_3Br (bottom left) and CF_3I (bottom right). Blue indicates regions of negative electrostatic potential while all other colours indicates positive electrostatic potential with red being the highest. Images reproduced from reference 140 with permission, copyright Springer.

Halogen bonds between organohalides (C−X) and many different metal ligand systems have been extensively studied and reviewed.[136,139,141,142] Ligands investigated vary from oxo- and nitride- groups to π-acceptor groups such as CO, NO^+ and CN^- and can exhibit extended structures in the solid state as result of the high directionality and the strength of the halogen bond. The nitrato and the azido ligand both possess electronegative atoms that bear partial negative charges. Complexes bearing these ligands open up the possibility of halogen bonding interactions resulting in supramolecular systems containing energetic molecular fragments. These interactions could lead to an increase in stability and decrease in the sensitivity of the energetic molecule in question. Two routes are possible, either; (i) a Lewis base adduct using a Lewis base containing a halogen atom, or (ii) a counterion containing a halogen atom for a hypercoordinate anionic species.

4.2 Results and Discussion

4.2.1 Halopyridine adducts of $Si(N_3)_4$

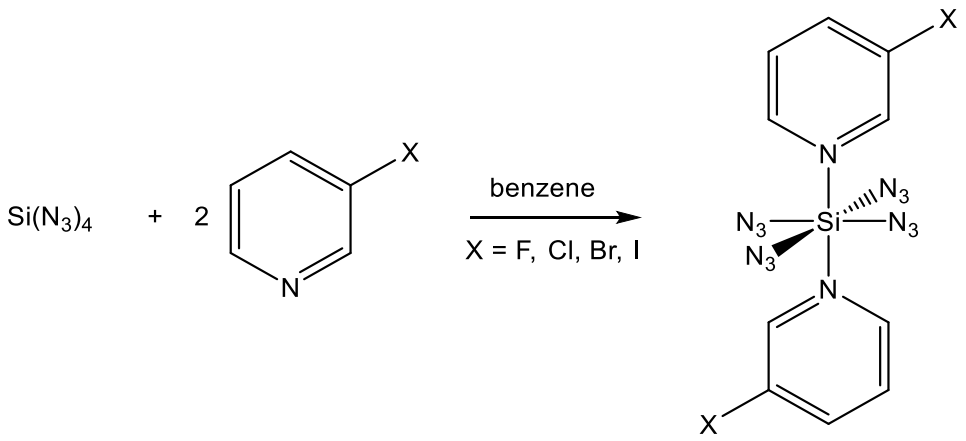

Scheme 4.1. Synthesis of halopyridine adducts of $Si(N_3)_4$.

Scheme 4.1 shows the general synthesis of the halopyridine adducts of $Si(N_3)_4$ in a simple one step process. The main difficulties lie in the synthesis of $Si(N_3)_4$ as it is not only shock and friction sensitive but also highly air sensitive too, making it difficult to prepare and handle.[54] $Si(N_3)_4$ has to be stored as a stock solution in benzene at concentrations as low as 0.1 mmol mL^{-1} under an inert atmosphere, however, is then stable for up to several months. The initial synthesis of $Si(N_3)_4$ was attempted by Wiberg and Horst in 1954 by refluxing $SiCl_4$ and a large excess of sodium azide in benzene for 20-30 hours,[144] resulting in incomplete chlorine / azide exchange. In order to obtain full exchange the mixture requires refluxing for 120 hours followed by filtration onto a second batch of sodium azide and a further 120 hours of reflux, any less time and conversion remains incomplete. Due to the low concentration of the stock solution all reagents involving $Si(N_3)_4$ must be thoroughly dried before use. Addition of $Si(N_3)_4$ in benzene to the appropriate dry halopyridine gave quantitative yields of (3-fluoropyridine)$_2$Si$(N_3)_4$ (**6**), (3-chloropyridine)$_2$Si$(N_3)_4$ (**7**), (3-bromopyridine)$_2$Si$(N_3)_4$ (**8**) and (3-iodopyridine)$_2$Si$(N_3)_4$ (**9**).

All four compounds are moisture sensitive colourless solids. Compounds **6**, **7** and **8** crystallise from the respective halopyridines whereas compound **4** can be recrystallised from benzene. The FT-IR spectra of **6**-**9** as nujol mulls between 2200 and 2000 cm^{-1} are displayed in Figure 4.4. In between these wavenumbers, compounds **6**, **7** and **8** look similar while compound **9** differs in the number of bands present. Compounds **6**, **7** and

8 show multiple peaks between 2167 and 2118 cm^{-1} while **9** only has a single peak maximum at 2118 cm^{-1}. The peak shapes in all the spectra are not very well defined and considerably broad and showing shoulders around the main peaks, a consequence of deviation from idealised symmetry on sample preparation. In principle, it would be expected that **6-9** would have the same molecular point group. There are two possible isomers of these complexes, *trans* or *cis* pyridines. Pyridine adducts of silicon tetrahalides are all the *trans* isomer, therefore, it can be assumed these compounds would be the *trans* isomer as well.[145–147] This would imply that **6-9** have C_i symmetry and would be expected to display two bands in the FT-IR spectrum for the $\nu_{as}(N_3)$. The complicated IR band structure makes an accurate structural determination not possible.

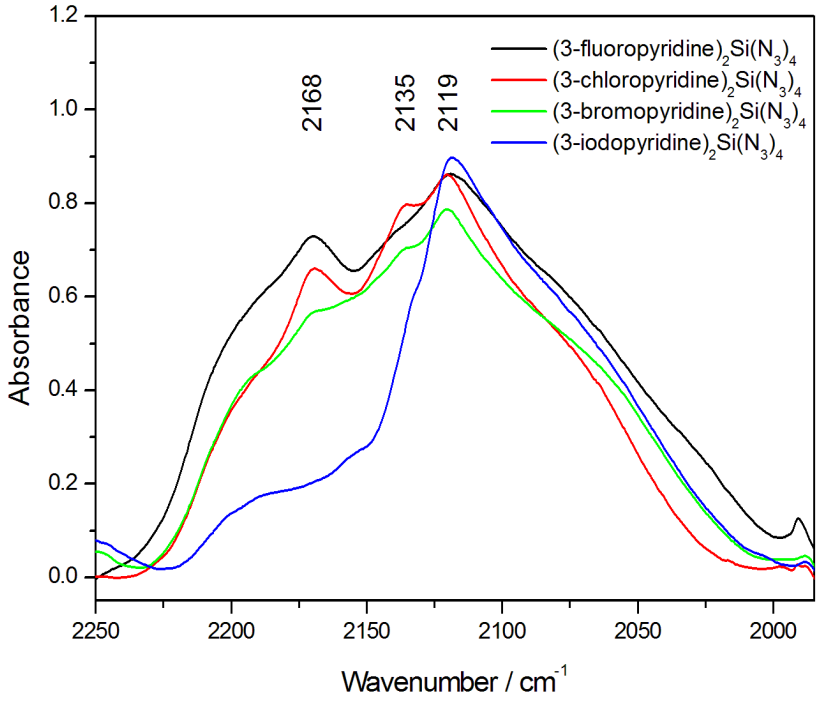

Figure 4.4. FT-IR spectra of **6-9** as nujol mulls between 2250 and 1900 cm^{-1}.

Crystals of **6-9** were investigated by single crystal X-ray diffraction. All four molecules have C_i symmetry and both halopyridines are in a *trans* conformation with the halogens also arranged mutually *trans* to one another. Compounds **6** and **7** crystallise in the space group $P\bar{1}$ with only one formula unit in the unit cell, whereas compounds **8** and **9** crystallise in the space group *C*2/c with four formula units in the unit cell. Table 4.1 shows some structural information for each of the four compounds. From this data, there appears to be very little difference between the structural

parameters of **7** and **8**, whereas compounds **6** and **9** are different, exemplified by the ΔNN parameter.

Compound	Si−N_{Xpy}	Si−N_{azide}	N(α)−N(β)	N(β)−N(γ)	ΔNN
6	2.01(1)	1.83(1)	1.224(4)	1.137(3)	8.7(5)
7	2.01(1)	1.84(1)	1.212(4)	1.137(5)	7.5(6)
8	1.99(1)	1.83(1)	1.213(4)	1.140(3)	7.3(5)
9	1.98(1)	1.84(1)	1.195(10)	1.148(11)	4.7(15)

Table 4.1. Average bond lengths of selected bonds of compounds **1-4** in angstroms. The ΔNN parameter is quoted in pm and calculated as a difference between N(α)−N(β) and N(β)−N(γ).

The silicon atom in each of the four compounds has ideal octahedral geometry with average N−Si−N angles of 90 and 180°. The average Si−N(α) bond length is 1.83Å, this value is shorter than the Si−N(α) bond length of $[Si(N_3)_6]^{2-}$ and longer than tetrahedral azidosilanes but very similar to (2,2'-bipyridine)$Si(N_3)_4$ and (1,10-phenanthroline)$Si(N_3)_4$.[54,55,66] The N−N bond lengths are in the expected region for coordinated azido ligands and the Si−N−N and N−N−N bond angles are consistent with the bent coordination and linear azido group. The pyridine adduct, $(py)_2Si(N_3)_4$, has not been reported and so no comparison can be made, the closest molecule for comparison would be (2,2'-bipyridine)$Si(N_3)_4$. This compound has ΔNN values of 7.0 and 7.9 pm for the axial and equatorial sets of azides respectively. These values are either side of the values for **7** and **8** suggesting the electronic structure of the Si−N_3 bond is similar. When considering **6**, the ΔNN value is 8.7 pm, a significant increase from the other compounds. One explanation is the highly electronegative fluorine atom withdrawing electron density from the pyridine ligand reducing the strength of the Lewis base. Therefore, the electronics of the E−N−N−N moiety closer resembles the situation in the previously reported tetrahedral azidosilanes, Ph_3SiN_3 (ΔNN = 10 pm) and (^{t}BuNCH=HN^{t}Bu)$Si(N_3)N(SiMe_3)_2$ (ΔNN = 9.1 pm).[64,146] Compound **9** has a much lower ΔNN parameter (4.5 pm), which is most likely related to the error in the N−N bond lengths of compound **9**. Figures 4.5, 4.6, 4.7 and 4.8 show the thermal ellipsoid plots of **6-9**.

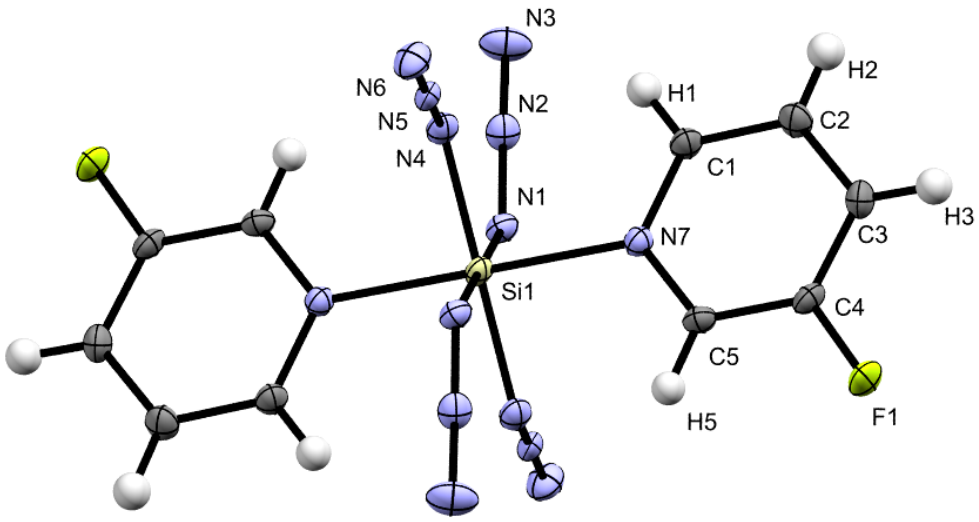

Figure 4.5. Thermal ellipsoid plot of **6**. Thermal ellipsoids set at the 50% probability level. Selected bond lengths (Å) and bond angles (°): Si1–N4 1.8271(19), Si1–N1 1.8353(19), Si1–N7 2.0058(17), N1–N2 1.222(2), N5–N6 1.134(2), N5–N4 1.226(3), N2–N3 1.141(2), N4–Si1–N4 180.0, N4–Si1–N1 90.17(9), N4–Si1–N1 89.83(9), N4–Si1–N7 90.49(7), N4–Si1–N7 89.51(7), N1–Si1–N7 89.10(8), N1–Si1–N7 90.90(8), N7–Si1–N7 180.0

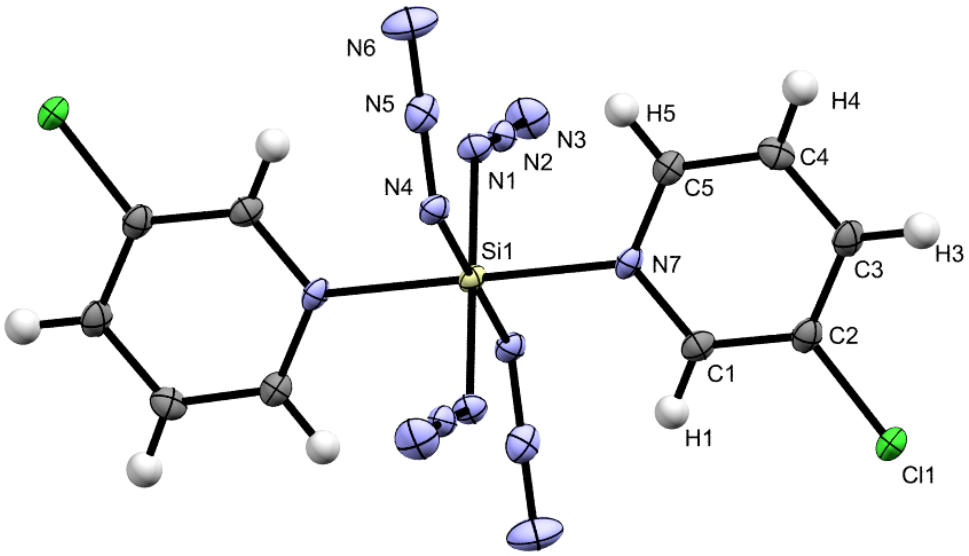

Figure 4.6. Thermal ellipsoid plot of **7**. Thermal ellipsoids set at the 50% probability level. Selected bond lengths (Å) and bond angles (°): Si1–N1 1.823(2), Si1–N4 1.844(2), Si1–N7 2.005(2), N4–N5 1.208(3), N1–N2 1.218(3), N5–N6 1.140(4), N2–N3 1.133(3), N1–Si1–N1 180.0, N1–Si1–N4 90.24(10), N1–Si1–N4 89.76(10), N4–Si1–N4 180.0, N1–Si1–N7 89.61(10), N1–Si1–N7 90.39(10), N4–Si1–N7 89.85(10), N4–Si1–N7 90.15(10), N7–Si1–N7 180.0, N5–N4–Si1 125.3(2), N2–N1–Si1 124.1(2), N6–N5–N4 175.9(3), N3–N2–N1 176.1(3).

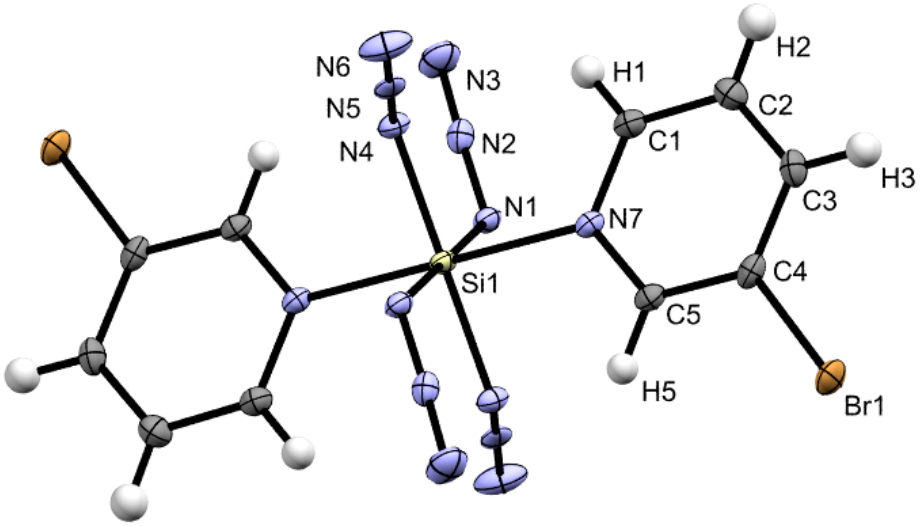

Figure 4.7. Thermal ellipsoid plot of **8**. Thermal ellipsoids set at the 50% probability level. Selected bond lengths (Å) and bond angles (°): Si1–N1 1.8391(17), Si1–N4 1.8287(17), Si1–N7 1.9918(17), N2–N3 1.139(3), N2–N1 1.216(2), N5–N6 1.140(3), N5–N4 1.217(2), N4–Si1–N4 180.0, N4–Si1–N1 90.39(7), N4–Si1–N1 89.62(7), N1–Si1–N1 180.0, N4–Si1–N7 88.94(7), N4–Si1–N7 91.06(7), N1–Si1–N7 90.95(7), N1–Si1–N7 89.05(7), N3–N2–N1 175.7(2), N2–N1–Si1 124.92(14), N6–N5–N4 175.7(2). N5–N4–Si1 122.56(14).

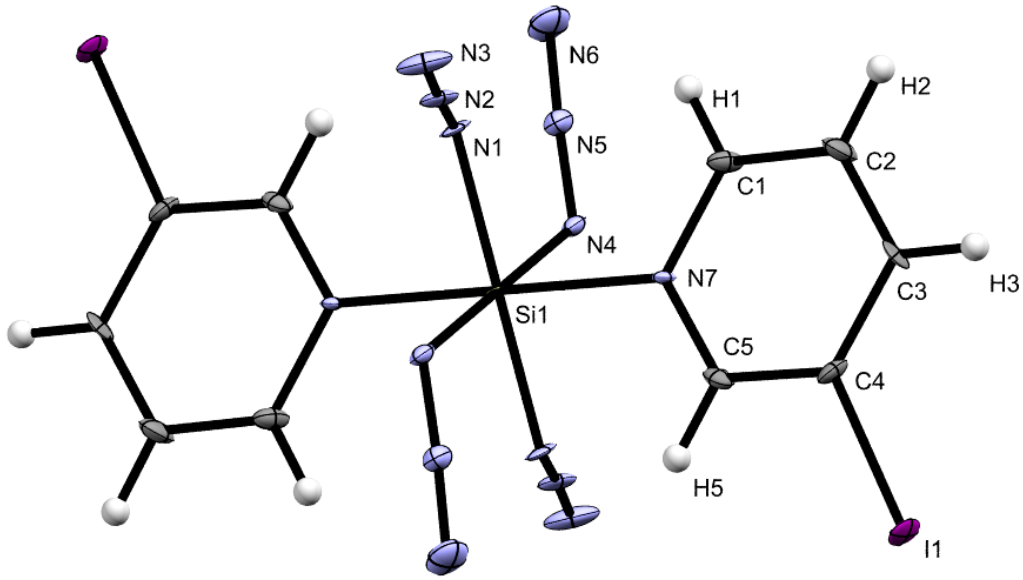

Figure 4.8. Thermal ellipsoid plot of **9**. Thermal ellipsoids set at the 50% probability level. Selected bond lengths (Å) and bond angles (°): Si1–N1 1.833(5), Si1–N4 1.838(5), Si1–N7 1.978(5), N5–N6 1.149(8), N5–N4 1.190(7), N2–N3 1.147(8), N2–N1 1.200(8), Si1–N1 180.0, N1–Si1–N4 90.1(2), N1–Si1–N4 89.9(2), N4–Si1–N4 180.0(3), N1–Si1–N7 89.0(2), N1–Si1–N7 91.0(2), N4–Si1–N7 91.3(2), N4–Si1–N7 88.7(2), N7–Si1–N7 180.0, N6–N5–N4 176.6(6), N5–N4–Si1 126.4(4), N3–N2–N1 176.1(6), N2–N1–Si1 123.5(4). Appropriate SIMU and DELU restraints have been applied and the ellipsoids still remain badly shaped despite an R-factor over all data of 3.31 %.

The interactions between the molecules in the crystal structure differ greatly between **6**-**9**. There is a clear shift in the intermolecular interaction holding the structure together between the four compounds. Compound **6** has two weak "hydrogen bonds" that are better described as van der Waals interactions owing to the large distance between donor and acceptor. One of these interactions is between C−F···H−C with a donor acceptor distance of 3.218(3) Å and the other is between N−N···H−C with a donor acceptor distance of 3.242(4) Å. Both interactions are not linear and are bent to angles of 135 and 124° respectively. There are no π-π stacking interactions, therefore, the two "hydrogen bonds" account for the structure observed. Figure 4.9 shows the unit cell of **6** with the distance between the fluorine and carbon atoms, the nitrogen and carbon atoms, and the distance between the aromatic rings labelled.

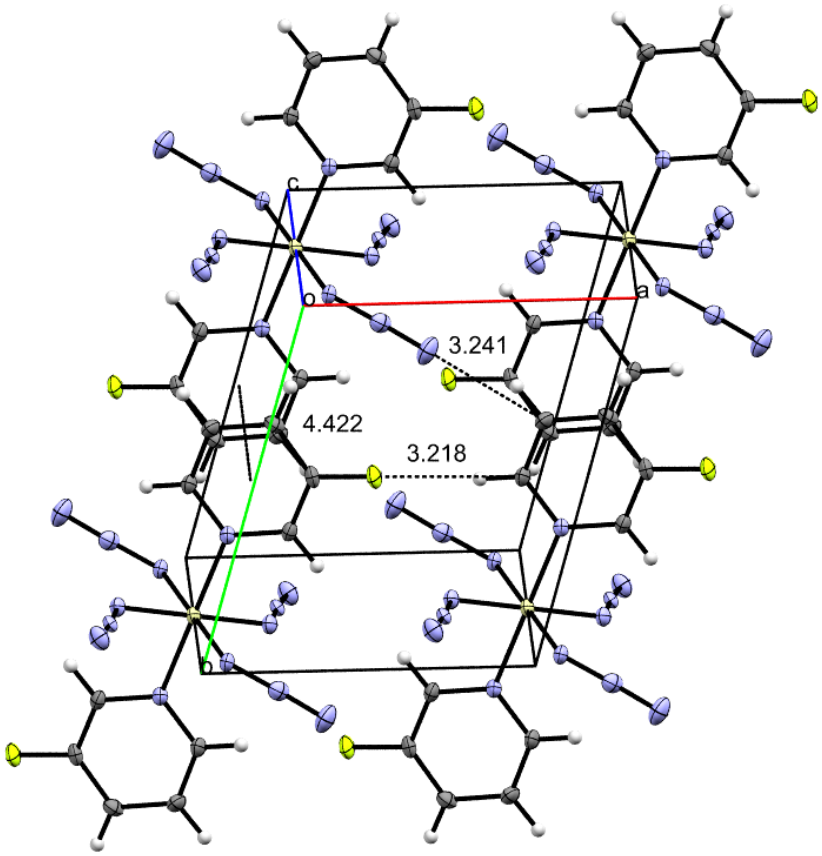

Figure 4.9. Unit cell of **6** with the relevant intermolecular interactions labelled.

In the packing of compound **7**, the chlorine atoms are not involved in any intermolecular interactions shorter than the van der Waals radii at variance to the structure of **6**. The only notable interactions are a weak interaction between C−H···N−N which has a donor acceptor distance of 3.336(4) Å and angle between N···H−C of 150°

slightly more linear but also a larger distance than the same interaction in **6**. The distance between the aromatic rings is 3.95 Å, above the upper limit of the accepted π-π stacking interaction distance (3.8 Å).[149] This distance is shorter than the distance in **7**, however, the weak C−H···N−N interaction remains the driving force for the packing of the crystal structure.

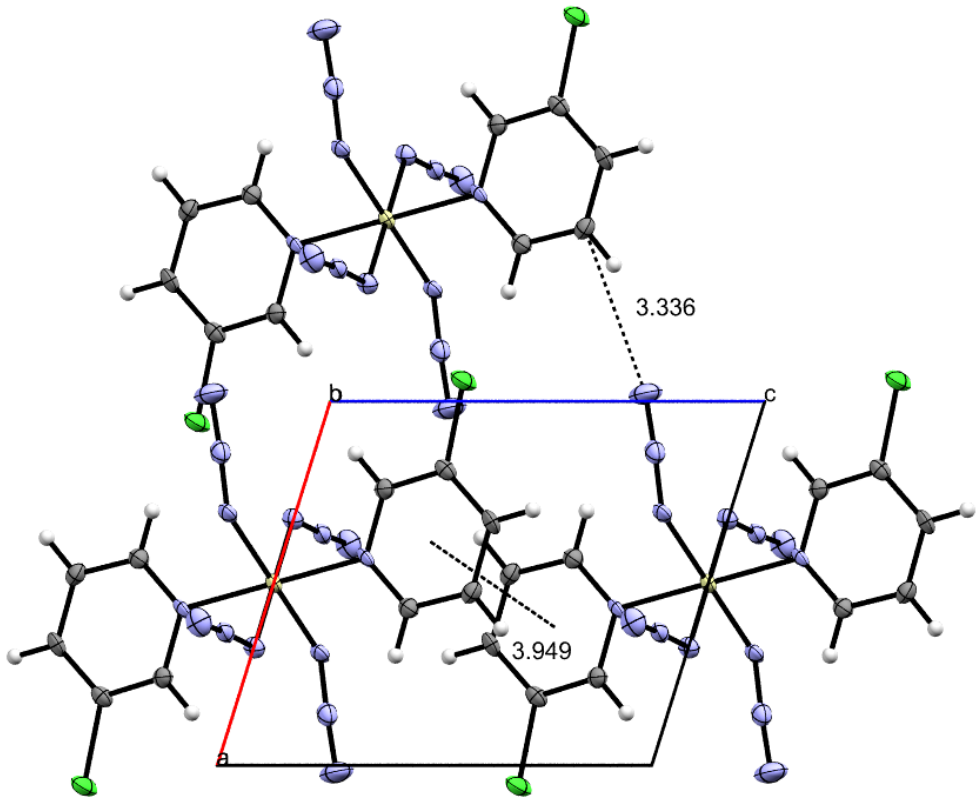

Figure 4.10. Unit cell of **7** viewed down the crystallographic *b*-axis with the relevant intermolecular interactions labelled.

Compounds **8** and **9** have significantly different intermolecular interactions to **6** and **7** in the crystal structure. There are several interactions between the phenyl ring hydrogen atoms and the azido groups, but the structures also contain halogen-azide interactions. In compound **8** the Br···N distance is 3.266(2) Å, 93 % of the sum of van der Waals radii of bromine and nitrogen,[150] and the angles between C−Br···N and N−N···Br are 167(1) and 108(1)° respectively. The distance is very close to the sum of the van der Waals radii so cannot be described as a true halogen bond but a van der Waals interaction between the Br atom and the N atom. The geometry about this interaction is indicative of an electrostatic interaction between the lone pair on the nitrogen atom and the σ-hole of the bromine atom. The effect of the weak Br···N interaction results in a very different crystal packing than to what is seen in **6** and **7**. Lines of the molecule are

arranged parallel to the crystallographic *a*-axis and *b*-axis with the Br···N interaction directed parallel to the crystallographic *c*-axis. The combination results in a "ribbon" like structure perpendicular to the *c*-axis as shown in Figure 4.11. The ribbon pattern is parallel to the *a*-axis and there are no short contacts between ribbons.

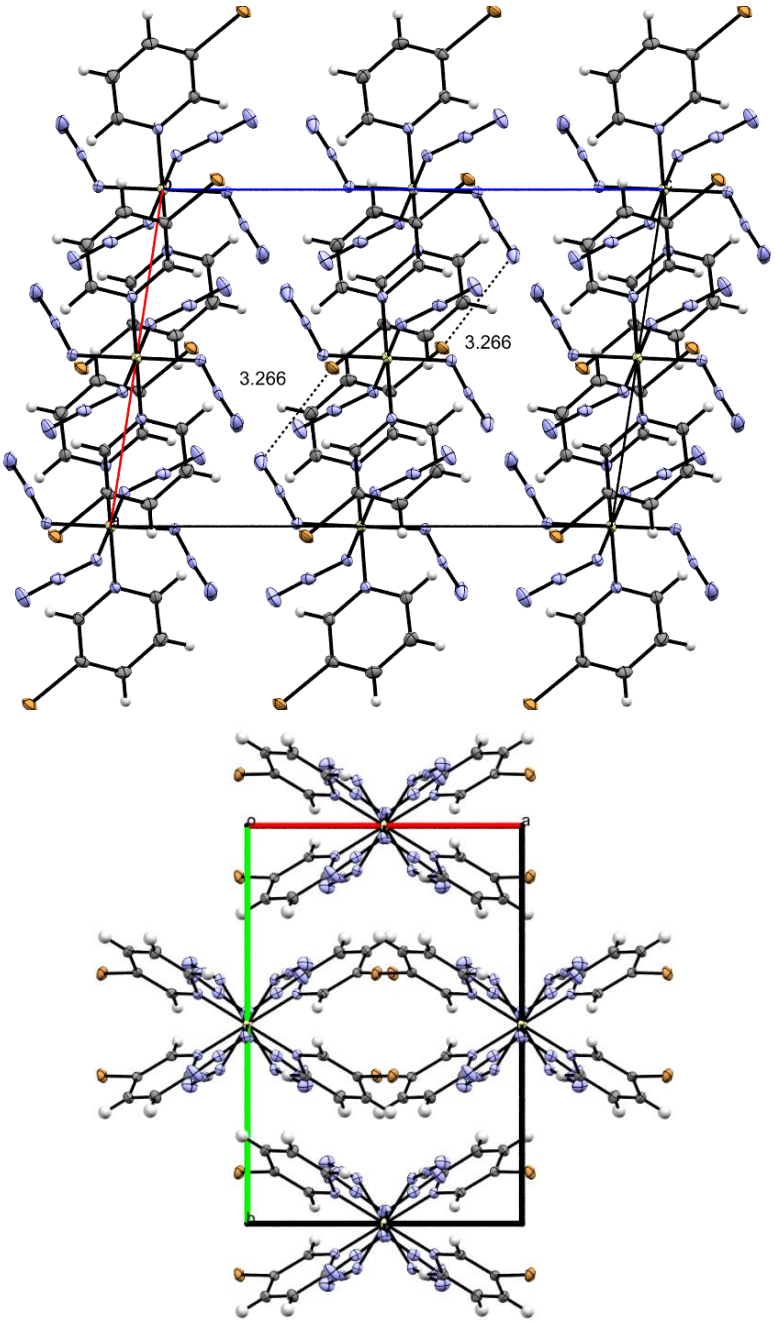

Figure 4.11. Top: unit cell of **8** viewed down the crystallographic *b*-axis showing the interaction between the bromine and the azido group. Bottom: unit cell of **8** viewed down the crystallographic *c*-axis.

The crystal structure of **9** is similar to **8**. A weak I···N interaction is present with a distance of 3.384(6) Å, 93 % of the sum of van der Waals radii of iodine and nitrogen,

and the relevant bond angles of 166(2) and 108(4)°. One noticeable difference, is the presence of an interaction between two iodine atoms, a type I halogen-halogen interaction, C−I···I−C, with a distance of 3.959(4) Å. The interaction is symmetric, unlike the C−I···N−N interaction, with a C−I···I angle of 131(2)° but also lies parallel to the *c*-axis. Both interactions point in the same direction as the halogen azide interaction in **8**, therefore, the crystal structure has the same ribbon pattern.

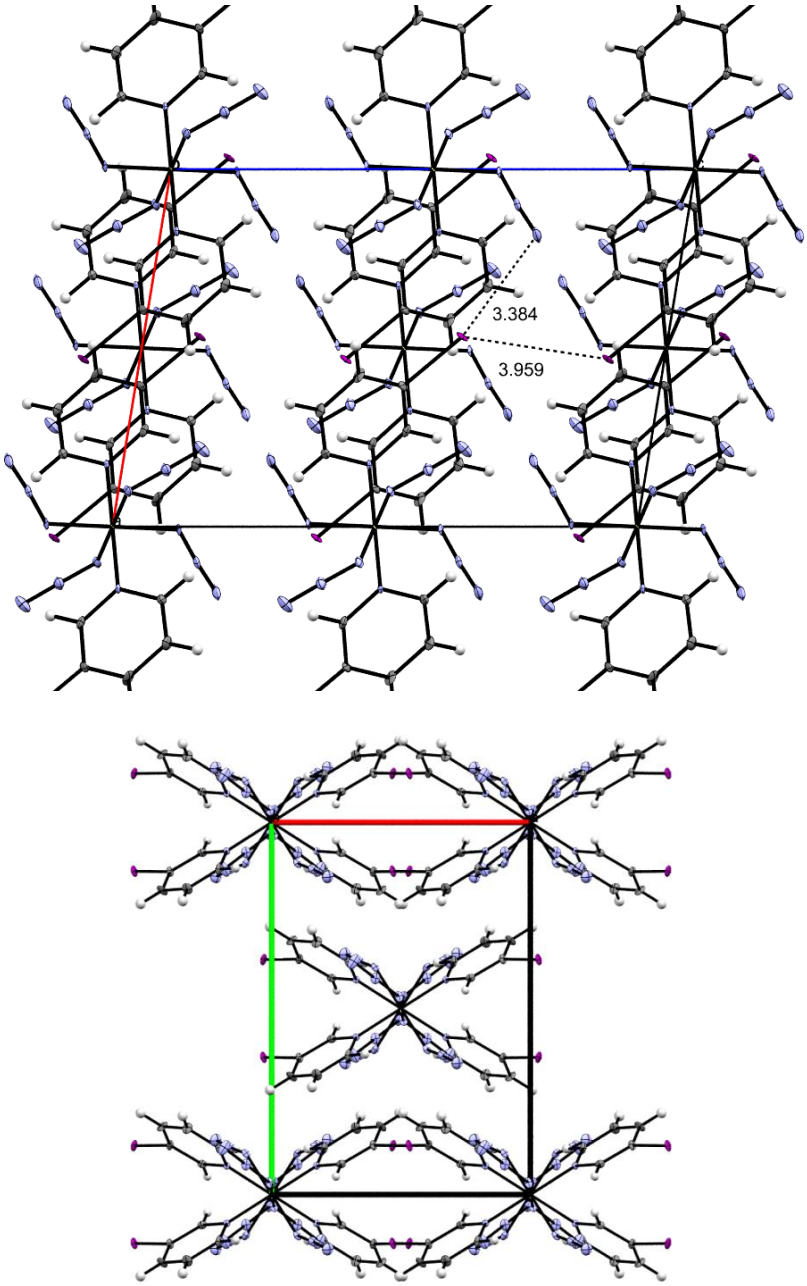

Figure 4.12. Top: unit cell of **9** viewed down the crystallographic *b*-axis showing the interaction between the iodine and the azido group. Bottom: unit cell of **9** viewed down the crystallographic *c*-axis.

Compound	Intermolecular interaction (CX···A)	d(CX···A) / Å	∠(C−X···A) / °	∠(X···N−N) / °
6	CH···N	3.242(4)	124	-
	CH···F	3.214(3)	135	-
7	CH···N	3.336(4)	150	-
8	CBr···N	3.266(2)	167(1)	108(1)
9	CI···N	3.384(6)	166(2)	108(4)

Table 4.2. Summary of the intermolecular interactions in the crystal structures of **6**-**9**. A is the halogen/hydrogen bond acceptor. X is either a halogen or a hydrogen.

Table 4.2 summarises the intermolecular interactions present in the crystal structures of **6**-**9**. It is clear that changing the halogen causes a change in the interaction between molecules in the crystal lattice. It is not unexpected that fluorine and chlorine do not participate in any form of halogen bonding interaction while bromine and iodine do.

A search in the Cambridge Structural Database (CSD) for organic molecules containing both an azide and an iodine atom gives a handful of known structures, none of which show any halogen bonding interactions between the azido group and the iodine atom. Extension of the search to metal azides and an iodine atom resulted in only one example which displays a halogen bonding interaction, an iridium complex shown in Figure 4.13.[151] The molecule has a N−N···I−C distance of 3.192 Å, shorter than the contact distance in **9**, and the angles are 113 and 171° for N−N···X and N···X−C respectively.[152] No metalloid or non-metal, besides carbon, compounds of the same criteria are in the CSD.

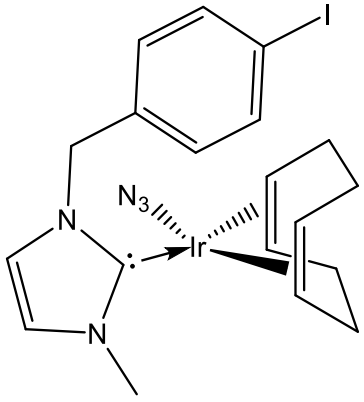

Figure 4.13. The only compound with a metal azide and an iodine atom that possesses a halogen bonding in the solid state in the CSD.

The C−I···N−N interaction present in the solid-state structure of this complex and compound **9** is very different. When considering the azido groups, both Si−N_3 and Ir−N_3 bonds have significant colvalent character, however, Ir(I) has 8 *d*-electrons and as the azide is a π-acceptor these electrons will participate in back-bonding to the π* orbital of the azide. Increasing the electron density of the nitrogen atoms due to the back-bonding results in a stronger halogen bond acceptor. Therefore, metal azides may be more appropriate than *p*-block azides for potential halogen bonding interactions in supramolecular chemistry.

4.2.2 Counterions containing halogens for Group 14 nitrato complexes

Hypercoordinate anionic nitrato complexes of Group 14 elements are thermally robust (discussed in chapter 3). Therefore, $[E(NO_3)_6]^{2-}$ (E = Ge, Sn) was prepared with a cation containing a halogen to investigate any halogen bonding interactions between the two ions. Both 1-methyl-3-iodopyridinium nitrate (**10**) and 1-methyl-3-bromopyridinium nitrate (**11**) can be easily prepared *via* salt metathesis between the appropriate iodide salts and silver nitrate as colourless needle crystals.

The molecular structure of **10** is shown in Figure 4.14 and the unit cell in Figure 4.15. Compound **10** crystallises in the space group $P2_1/c$ and contains four formula units per unit cell. All N−O bond lengths are similar, 1.241(14)-1.256(14) Å, demonstrating the fully delocalised structure of the nitrate anion. The three O−N−O bond angles range between 118(1) and 122(1)°. The iodine atom and oxygen atom are separated by 2.95(1) Å, 81 % of the sum of van der Waals radii of iodine and nitrogen, displaying a halogen bonding interaction with C−I···O and I···O−N bond angles of 171(1) and 150(1)° respectively. Both molecules are co-planar to one another due to the weak interactions between the non-halogen-bonded oxygen atoms on the nitrate anion and the hydrogen atoms on the pyridinium ring. The overall result is parallel sheets with an inter-layer distance of approximately 3.4 Å. Each sheet contains alternating cations and anions as shown in Figure 4.15.

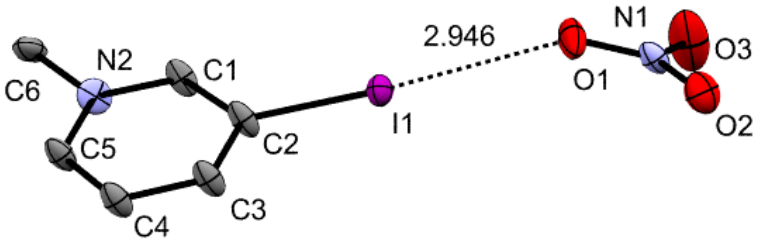

Figure 4.14. Thermal ellipsoid plot of **10** displaying the halogen bond between the iodine atom and the nitrate anion. Hydrogen atoms have been omitted. Thermal ellipsoids set to 50 % probability. Selected bond lengths (Å) and bond angles (°):C1–N2 1.322(16), C1–C2 1.389(17), C2–C3 1.404(15), C2–I1 2.063(12), C3–C4 1.400(16), C4–C5 1.400(16), C5–N2 1.311(16), C6–N2 1.514(15), N1–O2 1.241(14), N1–O3 1.254(14), N1–O1 1.256(14), O2–N1–O3 118.7(11), O2–N1–O1 122.9(11), O3–N1–O1 118.5(11).

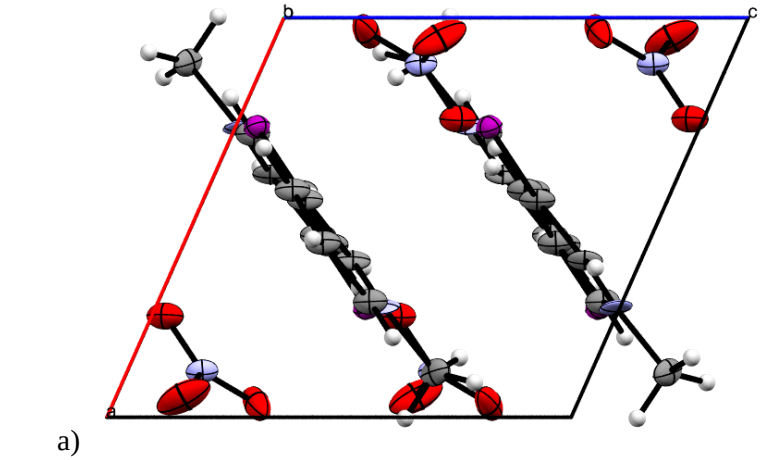

a)

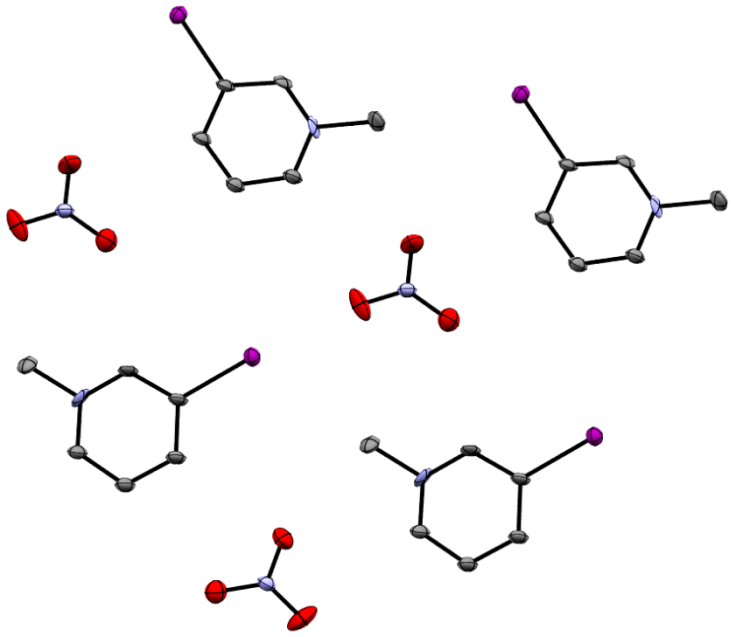

b)

Figure 4.15. a): Unit cell of **10** viewed down the crystallographic *b*-axis. b): One layer of the crystal structure of **10**.

The packing of **11** in the crystal structure, shown in Figure 4.16, is considerably different to the structure of **10**. Compound **11** crystallises in the space group $P2_1/n$ with four formula units per unit cell. The N−O bond lengths are slightly larger in **11**, 1.258(7)-1.271(7) Å, compared to **10** and the O−N−O bond angles are 120°, not distorted from the ideal trigonal planar structure as they are in **10**. There is no interaction between the nitrate anion and the bromine atom accounting for why the anion in **11** is not distorted in the same way as **10**. The only interaction the nitrate anion has is with hydrogen atoms from the pyridinium ring. However, there is a weak type I interaction between the bromine atoms on neighbouring cations with a distance of 3.684(1) Å, shown in Figure 4.17, and the C−Br···Br angles are identical at 133(1)°. The overall structure is alternating layers of cation and anions, at variance to the packing of **11**. The layers of anions are planar whereas the layers of cations are slightly puckered as a consequence of the Br···Br interaction. Bromine is a weaker halogen bond donor compared to iodine and does not interact with the oxygen of the ionic nitrate in this system. The oxygen atom of the nitrate anion appears to be a strong halogen bond acceptor despite this, as recognised by the strong interaction between the oxygen atom and the iodine atom in **10**. There is also minimal distortion of the nitrate anion from the result of halogen bonding with the 1-methyl-3-iodopyridinium cation.

The IR spectra of **10** and **11** are very similar. The $\nu_{as}(NO_2)$ is at 1347 and 1341 cm^{-1} in **10** and **11** respectively despite the different structures in the solid state. IR spectroscopy does not appear to be a sensitive enough technique to detect any structural differences in these types of compounds.

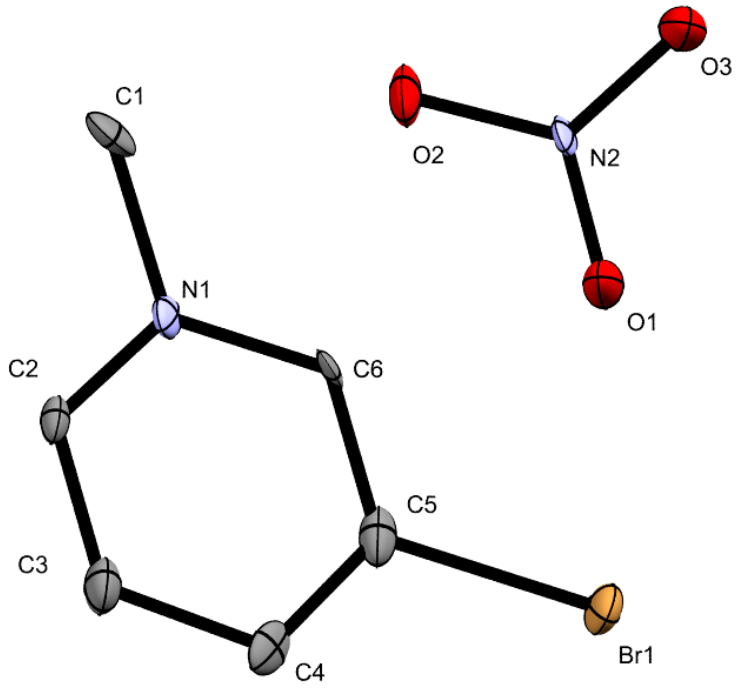

Figure 4.16. Thermal ellipsoid plot of **11**. Hydrogen atoms have been omitted. Thermal ellipsoids set to 50% probability. Selected bond lengths (Å) and bond angles (°): Br1–C5 1.889(6), C1–N1 1.506(9), C2–N1 1.344(9), C2–C3 1.372(10), C3–C4 1.403(9), C4–C5 1.376(10), C5–C6 1.382(10), C6–N1 1.360(8), N2–O3 1.258(7), N2–O1 1.258(8), N2–O2 1.271(7), O3–N2–O1 119.9(5), O3–N2–O2 120.5(6), O1–N2–O2 119.6(5).

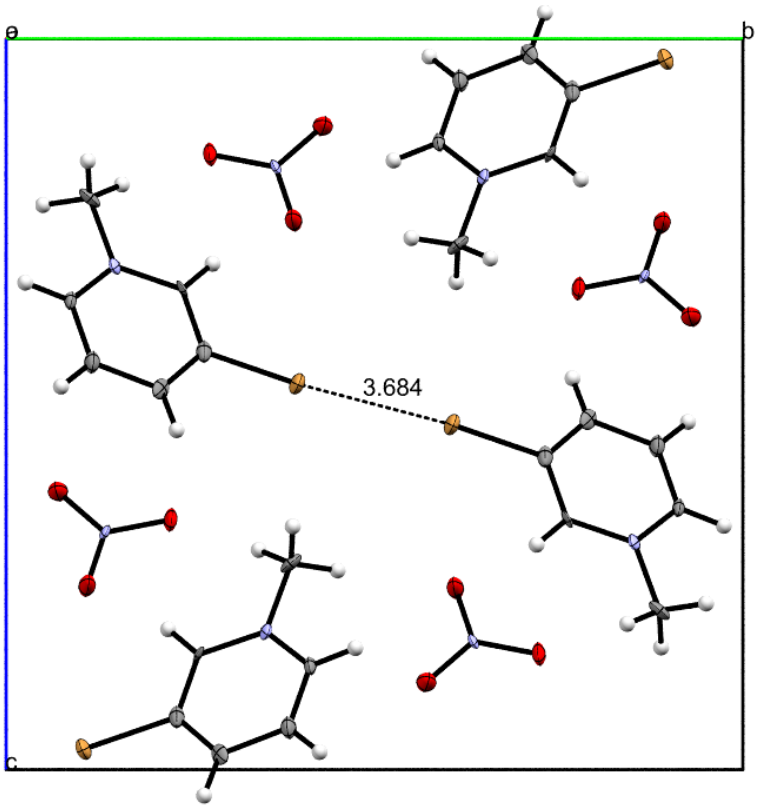

Figure 4.17. Unit cell of **11** viewed along the crystallographic *a*-axis.

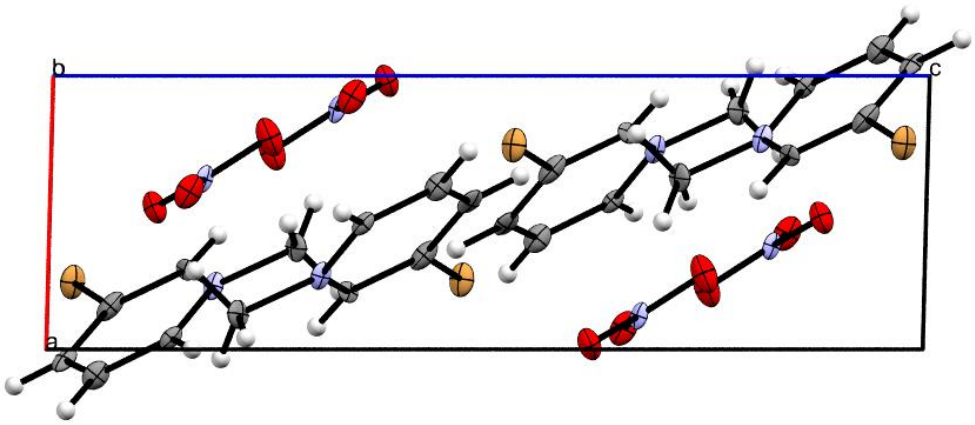

Figure 4.18. Unit cell of **11** viewed along the crystallographic *b*-axis.

These ionic salts are ideal for the preparation of halogen bonding hypercoordinate polynitrato complexes. The hexanitrato anions of the Group 14 elements can be prepared in a two-step process as discussed earlier in chapter 3. Addition of **11** to a solution of $Ge(NO_3)_4$ or $Sn(NO_3)_4$ in acetonitrile selectively prepares the corresponding hexanitrato complexes, (1-methyl-3-bromopyridinium)$_2$Ge$(NO_3)_6$ (**12**) and (1-methyl-3-bromopyridinium)$_2$Sn$(NO_3)_6$ (**13**), which can be recrystallised from acetonitrile as large, colourless block crystals.

The structures of both compounds were determined by single crystal X-ray crystallography. Compound **12** crystallises in the space group *P*bca and has four formula units per unit cell. The overall structure of the compound is a cubic close packed (CCP) anti-fluorite structure with the anion at the lattice points and the cations in the tetrahedral holes. The $[Ge(NO_3)_6]^{2-}$ anion has approximate D_{3d} symmetry, different to the symmetry of the anion in $(PPN)_2Ge(NO_3)_6$, which has C_{2h} symmetry. This is because of a halogen bond between an oxygen atom of the nitrato ligand and the bromine atom from the cation. The oxygen atom in question is the one involved in the secondary interaction of the nitrato ligand with the coordination centre. There are two type II halogen bonding interactions between one anion and two different cations. Figure 4.19 shows the structure of the anion in **12** and Figure 4.24 shows the interactions between the anion and two cations. The C−Br···O−N distance is 3.046(2) Å, 89 % of the sum of van der Waals radii of bromine and nitrogen, and the C−Br···O and Br···O−N angles of 175(1) and 123(1)° respectively. Overall, it shows that the halogen bond in this salt is a favourable enough interaction to overcome the steric repulsion between nitrato groups giving rise to D_{3d} symmetry for the $[Ge(NO_3)_6]^-$ anion. The

enforced symmetry change has little effect on the structural parameters of the bonds of the anion. All the N−O and O−N−O bond lengths and angles are very similar between the anion in **12** and the anion in $(PPN)_2Ge(NO_3)_6$, including the secondary E···O interaction. The main difference is the O−E−O angle, which is to account for the D_{3d} symmetry. These values are between 81.3 and 98.8°, a larger deviation from the ideal 90° that is seen in the C_{2h} structure but similar to the distortion in the anion $(PPN)_2Sn(NO_3)_6$ which has the same symmetry.

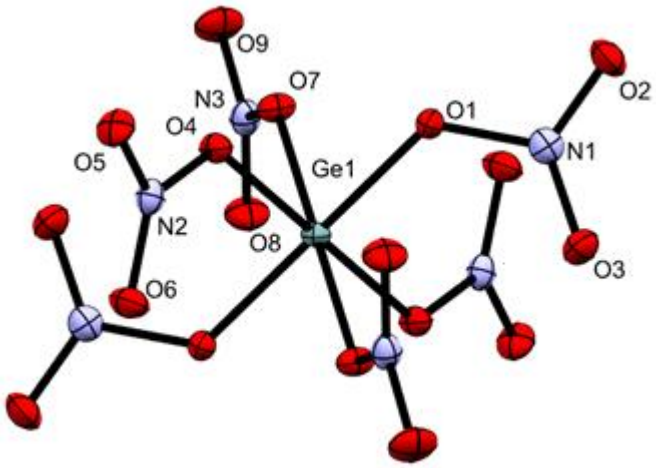

Figure 4.19. Thermal ellipsoid plot of the $[Ge(NO_3)_6]^{2-}$ in **12**. Thermal ellipsoids set to 50% probability. Selected bond lengths (Å) and bond angles (°): Ge1–O7 1.9014(15), Ge1–O7 1.9014(15), Ge1–O1 1.9035(16), Ge1–O1 1.9035(16), Ge1–O4 1.9063(15), Ge1–O4 1.9063(15), N1–O2 1.221(3), N1–O3 1.221(2), N1–O1 1.343(2), N2–O5 1.214(2), N2–O6 1.220(2), N2–O4 1.350(2), N3–O8 1.215(3), N3–O9 1.216(3), N3–O7 1.345(2), O7–Ge1–O7 180.0, O7–Ge1–O1 98.31(7), O7–Ge1–O1 81.70(7), O7–Ge1–O4 81.25(7), O7–Ge1–O4 98.75(7), O1–Ge1–O4 97.72(7), O1–Ge1–O4 82.28(7), O2–N1–O3 126.0(2), O2–N1–O1 114.18(18), O3–N1–O1 119.79(18), O5–N2–O6 126.0(2), O5–N2–O4 114.47(18), O6–N2–O4 119.49(18), O8–N3–O9 126.2(2), O8–N3–O7 119.75(18), O9–N3–O7 114.08(18), N1–O1–Ge1 123.92(13), N2–O4–Ge1 124.36(13), N3–O7–Ge1 125.80(13)

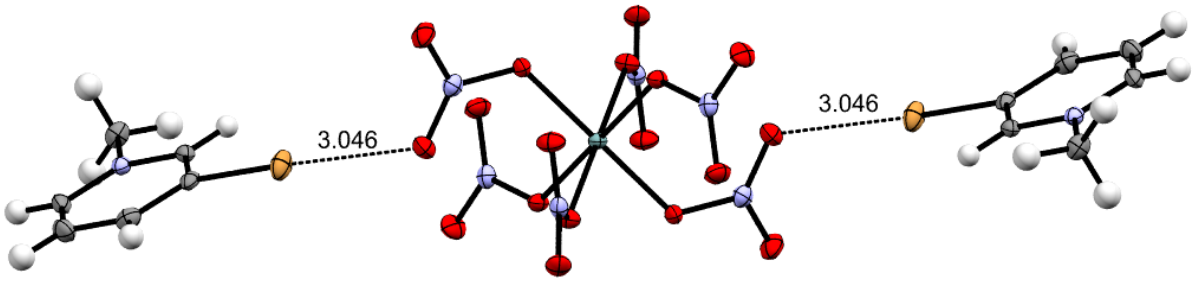

Figure 4.20. Thermal ellipsoid plot of **12** showing the halogen bonding interaction. Thermal ellipsoids set to 50% probability.

Compound **13** is isostructural to compound **12**. It crystallises in the space group *P*bca and has the CCP anti-fluorite structure. The anion also has D_{3d} symmetry and the bond

lengths and angles are also very similar to that of $(PPN)_2Sn(NO_3)_6$. The halogen bond is between the same oxygen atom of the nitrato group as in **12**, and the Br···O distance is 3.071(3) Å, 90 % of the sum of van der Waals radii of bromine and nitrogen and slightly larger than in **12**, and appropriate bond angles are 175(1) and 120(3)°.

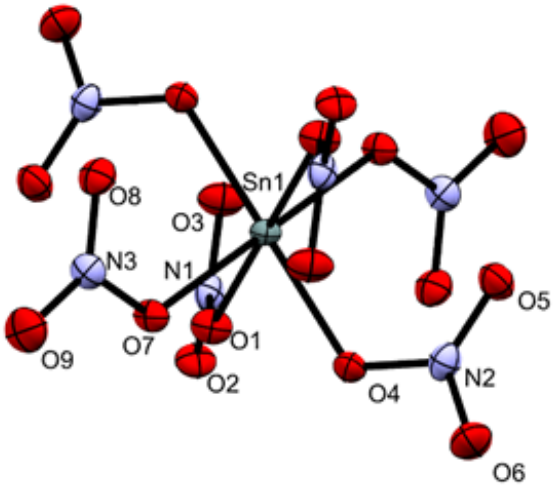

Figure 4.21. Thermal ellipsoid plot of the anion in **13**. Thermal ellipsoids set to 50% probability. Selected bond lengths (Å) and bond angles (°): Sn1–O1 2.074(3), Sn1–O4 2.074(3), Sn1–O7 2.071(3), O2–N1 1.219(4), O1–N1 1.336(4), O3–N1 1.225(4), O4–N2 1.342(4), O5–N2 1.220(4), O7–N3 1.342(4), O8–N3 1.227(4), O9–N3 1.215(4), O1–Sn1–O1 180.00(11), O1–Sn1–O7 99.73(11), O1–Sn1–O7 80.27(11), O7–Sn1–O7 180.0, O1–Sn1–O4 98.62(12), O1–Sn1–O4 81.38(12), O7–Sn1–O4 80.42(11), O7–Sn1–O4 99.58(11), N1–O1–Sn1 121.3(2), N2–O4–Sn1 121.1(3), N3–O7–Sn1 122.5(3), O6–N2–O5 126.7(4), O6–N2–O4 114.3(4), O5–N2–O4 118.9(4), O2–N1–O3 126.2(4), O2–N1–O1 115.3(4), O3–N1–O1 118.5(3), O9–N3–O8 126.5(4), O9–N3–O7 115.0(4), O8–N3–O7 118.5(4)

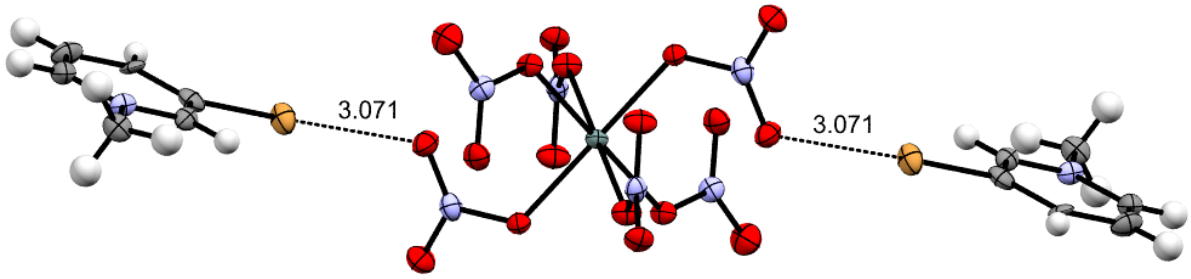

Figure 4.22. Thermal ellipsoid plot of **13** showing the halogen bonding interaction. Thermal ellipsoids set to 50% probability.

Both of these complexes highlight the difference between the ionic nitrate and coordinated nitrato group. The ionic nitrate anion is clearly a weaker halogen bond acceptor than the covalent nitrato ligand. This may be a result of an increased amount of delocalisation over the nitrate anion spreading the negative charge over three oxygen

atoms. Whereas in the coordinated nitrato group, the charge is spread over two oxygen atoms, exemplified by the shorter terminal N−O bond lengths in the coordinated group.

Compound	$\nu_{as}(NO_2)$	$\nu_{sym}(NO_2)$	ν(ON)
$(PPN)_2Ge(NO_3)_6$	1561	1298	959
12	1579, 1541	1277	941
$(PPN)_2Sn(NO_3)_6$	1547	1280	964
13	1561, 1539	1286	956

Table 4.3. IR absorption (cm^{-1}) of the nitrato groups in $(PPN)_2E(NO_3)_6$, **12** and **13**. (E = Ge, Sn)

Table 4.3 shows the IR spectroscopic data of $(PPN)_2Ge(NO_3)_6$, $(PPN)_2Sn(NO_3)_6$, **12** and **13**. The main difference is the splitting of the $\nu_{as}(NO_2)$ band in the halogen containing compounds. In both **12** and **13** the anion has D_{3d} symmetry, and as $(PPN)_2Sn(NO_3)_6$ displays a single band for $\nu_{as}(NO_2)$ and also has D_{3d} symmetry, it can be inferred that the presence of halogen bonding is causing the splitting of the bands. Even with this change, IR spectroscopy remains unsuitable for the identification of halogen bonding in nitrato complexes without prior understanding of the spectroscopic detail of the polynitrato complex.

Halogen bonding has an effect on the thermal properties of the $[Ge(NO_3)_6]^{2-}$ anion. $(PPN)_2Ge(NO_3)_6$ decomposes at 145°C and 260°C (*vide supra*), whereas **12** decomposes initially at 120°C and a second step at 250°C as determined during a melting point measurement. On the first decomposition step the glass capillary filled with a brown gas, while it could be bromine, it was most likely NO_2. Interestingly, at the second step the brown gas turns colourless. Further investigations are necessary to determine the processes occurring. However, the effect of halogen bonding does appear to reduce thermal stability.

A survey of the CSD searching for metal nitrates with halogen bonding interactions was completed. Very few examples are in the database, none containing bromine and there was no discussion of these interactions for those containing iodine. The most interesting structure is a nitrato copper complex containing bis(iodopyrazoyl)methane ligands.[153,154] This compound was crystallised with and without water as a ligand. Without the water both nitrates have the $\kappa^2(O,O')$ coordination mode. The effect of the water ligand causes a change of one of the nitrates to $\kappa^1(O)$ coordination giving an opportunity to compare which coordination mode is the better halogen bond acceptor.

The first point to note is the halogen bonding interaction is between the iodine atom and the coordinated oxygen atom of the bidentate nitrato ligand and not the terminal oxygen atom. For the compound with both $\kappa^2(O,O')$ nitrato ligands the I···O distance is 3.201 Å and the bond angles are 151 and 142°. In the complex bearing a monodentate nitrato coordination the halogen bonding interaction is between the terminal oxygen atom closest to the coordination centre, as seen in **12** and **13**. There is no interaction between the bidentate nitrato group and the halogen atom. The presence of water molecules in the structure results in a hydrogen bonding interaction between the nitrato groups and the water. Therefore, it is hard to determine if the monodentate nitrato group is a stronger halogen bond acceptor than the bidentate nitrato group or the presence of hydrogen bonding is disrupting any halogen bonding interactions.

Attempts to isolate the iodo analogues of **12** and **13** proved to be unsuccessful. The addition of $Sn(NO_3)_4$ and $Ge(NO_3)_4$ solutions to **10** resulted in clear solutions that over time would precipitate a white solid. The solid shows no signals in the FT-IR spectrum suggesting the formation of AgI from the reaction between **10** and unreacted silver nitrate in the solutions of $Sn(NO_3)_4$ and $Ge(NO_3)_4$. This appeared to prevent the crystallisation of (1-methyl-3-iodopyridinum)$_2$E$(NO_3)_6$ from the reaction solution.

4.3 Conclusions

The investigation into halogen bonding in energetic Main Group complexes has yielded two methods to exploit halogen bonding interactions. The interaction between a charge-neutral Lewis acid-base complex of $Si(N_3)_4$ and 3-halopyridines has demonstrated that despite a weak halogen-azide interaction significant changes in the crystal structure of the complexes can occur. This opens up the possibility of using Lewis acid-base complexes of $Si(N_3)_4$ and potentially transition metal azides, which appear to be stronger halogen bond acceptors, as an energetic component of supramolecular frameworks. Other, stronger, halogen bond donor bases would need to be investigated to maximise the interaction between the azido group and the halogen. Halogen bonding may have use in stabilising $Si(N_3)_4$ in the solid state. Co-crystallisation of $Si(N_3)_4$ with a strong halogen bond donor, such as I_2, may make it possible to study the sensitive compound in the solid state without the need for hypercoordination.

The use of halogenated methylpyridinium cations as counterions for Main Group nitrato complexes further highlighted the diversity of the coordination chemistry of the nitrato ligand previously discussed in chapter 3. It appears that the monodentate coordination mode may be a stronger halogen bond acceptor over bidentate coordination, however, it remains unclear and would require further investigation. Covalent nitrato groups are stronger halogen bond acceptors over ionic nitrates. Therefore, not only do these species have a stronger interaction in such systems, but more nitrato groups can be present for every halogen bond donor cation as a polynitrato coordination complex. This would help provide a higher oxygen content that could help with combustion of organic substrates.

It is not possible from these complexes to determine which is the stronger halogen bond acceptor, nitrate or azide, as the nitrato species were ionic salts and the azido species were charge-neutral coordination complexes. However, halogen bonding adds to the tools available to stabilise such shock and friction sensitive species, which has previously relied upon phlegmatising cations or ligands. This opens a number of routes for research in energetic coordination complexes, including anionic polyazido complexes with halogen bonding cations or halogen bonding bases with neutral polynitrato complexes.

5. GE(II) AND SN(II) AZIDO AND NITRATO COMPLEXES

5.1 Introduction

The stability of low valent Main Group complexes increases going down a group in the *p*-block, to an extent where it becomes more stable for an element to be in a lower oxidation state than the principle oxidation state of that specific group. Considering Group 14 as an example, Sn(II) and Pb(II) chloride are air stable compounds and show a higher degree of stability with regards to dissociation in comparison to their +4 counterparts, $PbCl_4$ decomposes above 50°C to $PbCl_2$ and chlorine gas. $SnCl_2$ is a coordination polymer with bridging chloride ligands giving a tin atom with a trigonal pyramidal coordination environment forming infinite chains.[155] The lighter congener, $GeCl_2$, is unstable and can be formed *in situ* through thermolysis of $HGeCl_3$.[156] It is often isolated as a colourless crystalline solid as an adduct with 1,4-dioxane, a 1-D coordination polymer with the dioxane molecule bridging between germanium atoms. The germanium atom has a see-saw geometry with oxygen atoms in the axial sites, and chlorine atoms and a stereochemical active lone pair in equatorial sites.[157]

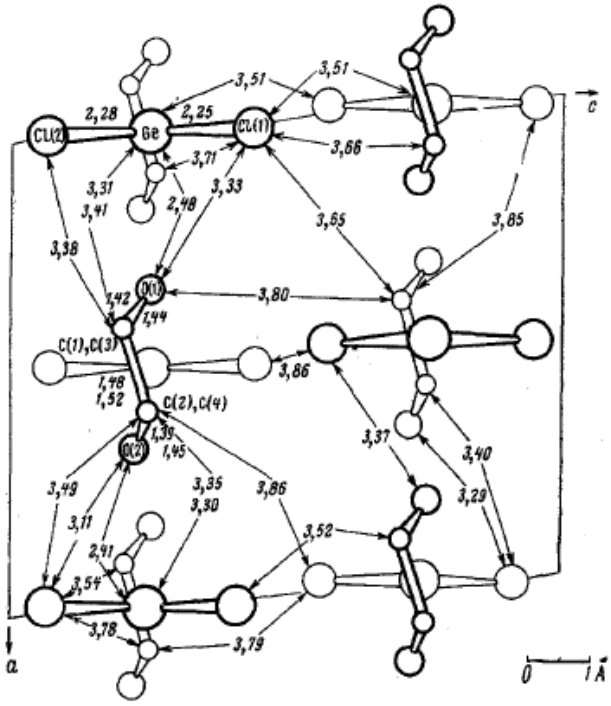

Figure 5.1. Ball and stick diagram of $GeCl_2$(1,4-dioxane). Reproduced from reference 157 with permission, copyright Springer.

Both of these compounds are versatile reagents for preparing a variety of Ge(II) and Sn(II) complexes. Azido complexes of base stabilised Ge(II) and Sn(II) centres have been known for many years, however, all of which are monoazides. It was not until 2013 when a base stabilised Ge(II) diazide was prepared using the N-heterocyclic carbene bis(2,6-diisopropylphenyl)imidazol-2-ylidene (IPr) as the ancillary ligand.[158] The only known compounds are $(HB(3,5\text{-}Me_2Pz)_3)GeN_3$, *trans*-$(\eta^5\text{-}C_5Me_5)W(CO)(PMe_3)_2[Ge(N_3)_3]$, $[CpCo(P(O)(OEt)_2)_3]GeN_3$, $((n\text{-}Pr)_2ATI)EN_3$ $(HB(3,5\text{-}(CF_3)_2Pz)_3)AgE(N_3)((n\text{-}Pr)_2ATI)$, (^{mes}Nacnac)$EN_3$ $\{(^tBuO(Me_2)\text{-}Si)_2NGeN_3\}_2$, $(Me_2NCH_2CH_2O)EN_3$ and $(IPr)Ge(N_3)_2$.[158–165] (E = Ge/Sn; Pz = pyrazoyl, (^{mes}Nacnac = bis(2,4,6-trimethylphenyl)-1,5-*β*-diketiminate), $(n\text{-}Pr)_2$ATI = N-(n-propyl)-2-(n-propylamino)-aminotroponiminate).

From the two structures of $SnCl_2$ and $GeCl_2$(1,4-dioxane) above it is clear that these low valent centres can form extended structures through bridging chlorines. Equally, the azido ligand has the ability to bridge between coordination centres and this phenomenon is observed in the solid-state structures of $((n\text{-}Pr)_2ATI)SnN_3$ and (^{mes}Nacnac)SnN_3.[162,163] Interestingly, this is not seen in the germanium analogues. Both of these tin compounds form discrete dimers in the solid state where the N(α) is bridging to a second tin atom to form a weakly bound Sn_2N_2 ring. It is also possible for the azido ligand to act as a bridging ligand *via* the N(γ) site to a nearby coordination site, as seen in the crystal structure of $(Me_2NCH_2CH_2O)SnN_3$.[164]

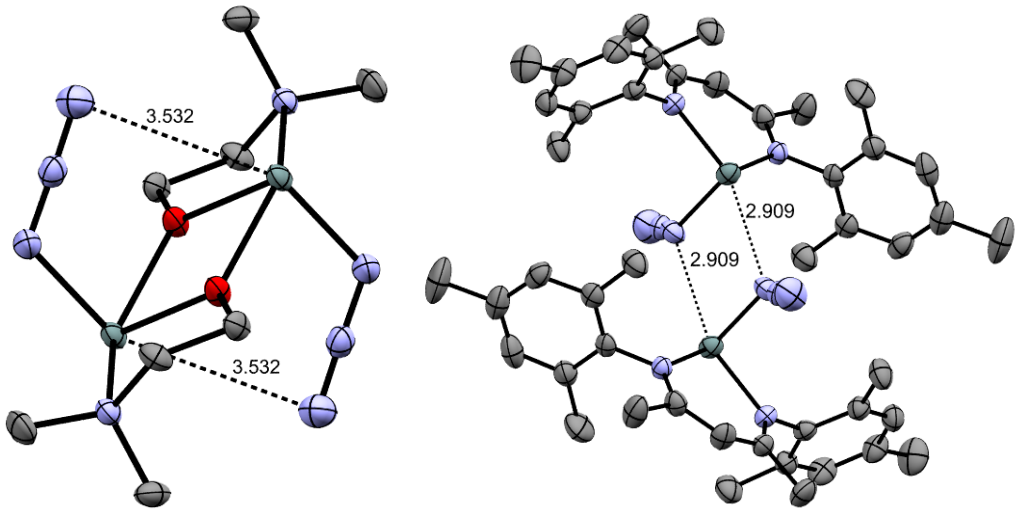

Figure 5.2. Thermal ellipsoid plot of $(Me_2NCH_2CH_2O)SnN_3$ (Left) and (^{mes}Nacnac)SnN_3. Blue = nitrogen; grey = carbon; light grey = tin; red = oxygen. Images generated from cif files from references 163 and 164.

Ge(II) azides have been used as versatile reagents to prepare novel Ge(IV) azido compounds. $[CpCo(P(O)(OEt)_2)_3]Ge(N_3)_3$ and $(HB(3,5\text{-}Me_2Pz)_3)Ge(N_3)_3$ cannot be made directly from the corresponding Ge(IV) halide, however the appropriate Ge(II) azide can be made from the analogous halide. Oxidation of these Ge(II) species using HN_3 selectively produces $[CpCo(P(O)(OEt)_2)_3]Ge(N_3)_3$ and $(HB(3,5\text{-}Me_2Pz)_3)Ge(N_3)_3$ demonstrating a unique reactivity of these compounds.

The use of Lewis bases has clearly been demonstrated for the synthesis of stable Ge(II) and Sn(II) azides. However, no such examples of Ge(II) or Sn(II) nitrates are known. In fact, the only known low valent Main Group nitrate is $Pb(NO_3)_2$. Instead of using Lewis bases to stabilise Ge(II) or Sn(II) coordination centres, WCCs may be used to isolate homoleptic Ge(II) and Sn(II) containing salts. Evident in the isolation of the $[GeCl_3]^-$ and $[SnCl_3]^-$ anions. The first structure of the $[SnCl_3]^-$ anion was reported in 1962 as the $KCl{\cdot}KSnCl_3$ hydrate,[166] however, the Sn−Cl bond lengths are longer than would be expected. It was not until 1982 when the molecular structure of $(PPh_4)SnCl_3$ was determined.[167] The structure of $(PPh_4)GeCl_3$ was determined in 1998 as a reference compound in the preparation of gold complexes with $[GeCl_3]^-$ ligands.[168] These anions are ideal starting materials for the preparation of azido or nitrato Ge(II) and Sn(II) anions.

5.2 Results and discussion

5.2.1 A nitrato group on a low valent Main Group coordination centre?

The nitrato group is oxygen-rich and a known oxidising agent, therefore, coordination to a low valent Main Group centre results in possible difficulty. Methods described previously in chapter 3 will not be suitable for Ge(II) or Sn(II), in particular the use of silver nitrate due to the oxidising potential of Ag(I). A different method was attempted using $(PPN)NO_3$ and sodium nitrate as the ionic nitrate exchange agent.

$$GeCl_2(1,4\text{-dioxane}) + (PPN)NO_3 \xrightarrow{THF} \underset{\mathbf{14}}{(PPN)GeCl_2(NO_3)} + 1,4\text{-dioxane}$$

Scheme 5.1. Proposed reaction scheme for the synthesis of $(PPN)GeCl_2(NO_3)$ (**14**).

One equivalent of $(PPN)NO_3$ was added to $GeCl_2$(1,4-dioxane) and dissolved in THF to give $(PPN)GeCl_2(NO_3)$ (**14**). The colourless solution that formed was analysed by FT-IR spectroscopy and resulted in the spectrum shown in Figure 5.3. The main feature of the spectrum is the intense peak at 1517 cm^{-1} for $\nu_{as}(NO_2)$, $\kappa^1(O)$ coordination. The peak at 1588 cm^{-1} is indicative of the (PPN) cation.

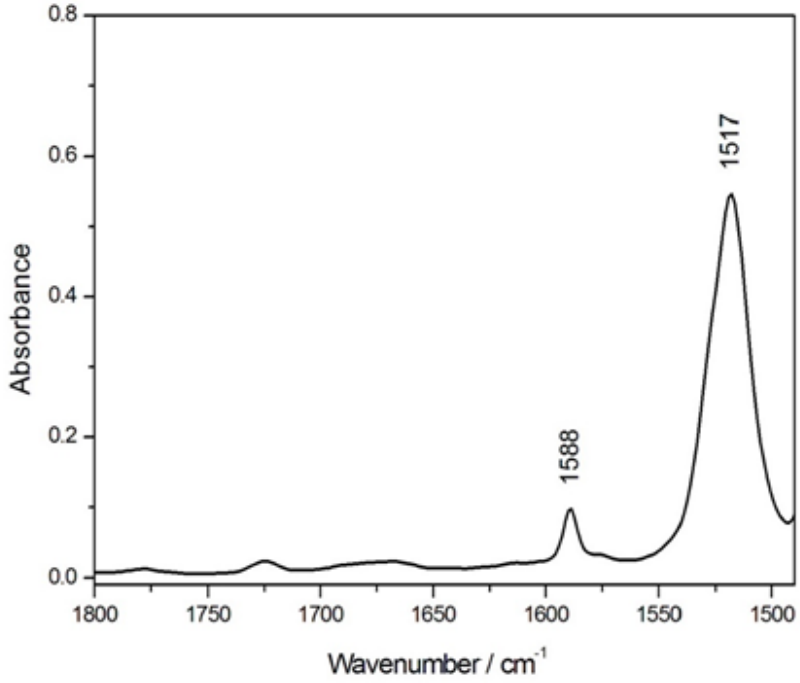

Figure 5.3. FT-IR spectrum of **14** in THF.

After stirring this THF solution over sodium nitrate for several days no change was obvserved in the FT-IR spectrum. It was clear that no reaction had occurred between **14** and sodium nitrate and so a solid was isolated from the solution in an attempt to elucidate the structure of the synthesised complex. Block crystals were obtained and studied using single crystal X-ray diffraction. The identity of the crystals was confirmed to be $(PPN)GeCl_3$ and $(PPN)Ge(NO_3)Cl_2$ as a solid solution. The molecular structures of the anions are shown in Figures 5.4 and 5.5.

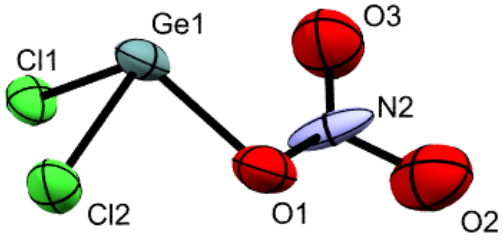

Figure 5.4. Thermal ellipsoid plot of the $[GeCl_2(NO_3)]^-$ anion in $(PPN)GeCl_3/GeCl_2(NO_3)$. Thermal ellipsoids are set at the 50% probability level. Selected bond lengths (Å) and angles (°): Ge1−Cl2 2.2773(11), Ge1−O1 1.921(7), N8−O1 1.119(10), N2−O3 1.189(9), N2−O2 1.332(10), N2−O1−Ge1 102.0(6), O1−N2−O3 135.2(9), O1−N2−O2 113.2(8), O3−N2−O2 111.0(8).

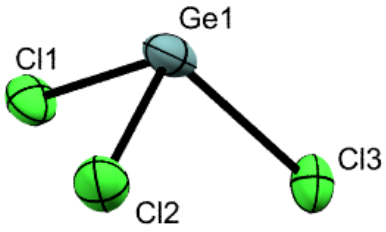

Figure 5.5. Thermal ellipsoid plot of the $[GeCl_3]^-$ anion in $(PPN)GeCl_3/GeCl_2(NO_3)$. Thermal ellipsoids are set at the 50% probability level. Selected bond lengths (Å) and angles (°): Ge1−Cl2 2.2779(12), Ge1−Cl1 2.2917(11), Cl2−Ge1−Cl1 96.03(4). The Ge1−Cl3 bond length is 2.401 Å as measured in the Mercury program.

The space group of the solid solution is $P\bar{1}$ and contains two formula units per unit cell. For each PPN cation there is a germanium centre with chloro ligands in two of the coordination sites and a half occupancy chloro or nitrato ligand in a third site giving an overall pyramidal structure with a stereochemical active lone pair residing in the apical site. The substitutional disorder indicates a solid solution of $(PPN)GeCl_3$ and $(PPN)GeCl_2(NO_3)$. Bond lengths and bond angles of the non-disordered Ge−Cl components are very similar to that of $(PPh_4)GeCl_3$.[168] The position of the third chlorine atom is effected in the model by the position of the nitrato group resulting in a slightly elongated Ge−Cl bond. The Ge−O and N−O bond lengths are longer in this structure than in $(PPN)_2Ge(NO_3)_6$, summarised in Table 5.1. Remarkable differences are in the bond angles between the two molecules. In $[Ge(NO_3)_6]^{2-}$ the Ge−O−N bond angle is close to 120° (Table 5.2), whereas in $[GeCl_2(NO_3)]^-$ the bond angle is 102.0°, which has a knock-on effect on the O−N−O bond angles in the nitrato group. The O(1)−N−O(3) bond angle is significantly larger than 120° at 135.2° and the other two angles are smaller than 120° at 113.2 and 111.0°, summarised in Table 5.2.

	Average bond length (Å)		
Compound	E−O	O−N	N−O
$[Ge(NO_3)_6]^{2-}$	1.90(1)	1.34(1)	1.21(1)
$[GeCl_2(NO_3)]^-$	1.92(1)	1.33(1)	1.19(1)

Table 5.1. Average bond lengths of $[Ge(NO_3)_6]^{2-}$ and $[GeCl_2(NO_3)]^-$.

	Average bond angle (°)			
Compound	Ge−O−N	O(1)−N−O(3)	O(1)−N−O(2)	O(2)−N−O(3)
$[Ge(NO_3)_6]^{2-}$	126.2(1)	114.9(3)	120.0(3)	125.7(3)
$[GeCl_2(NO_3)]^-$	102.0(6)	135.2(9)	113.2(8)	111.0(8)

Table 5.2. Average bond angles in $[Ge(NO_3)_6]^{2-}$ and $[Ge(NO_3)Cl_2]^-$.

The secondary Ge···O distance is 2.580 Å and the difference between this distance and the Ge−O bond length, ΔEO, is 0.66 Å. Compared to $[Ge(NO_3)_6]^{2-}$ this value is significantly lower (1.2 Å for $[Ge(NO_3)_6]^{2-}$) due to the reduced steric congestion around the germanium centre. From the narrow Ge−O−N bond angle and the ΔEO value, it can be inferred that the nitrato group is bound in an unsymmetrically bidentate coordination mode rather than monodentate coordination mode. This coordination mode is very similar to that of $(PPN)As(NO_3)_2Cl_2$ discussed in chapter 3. Both coordination centres have stereochemical active lone pairs which is the primary reason for the prevention of bidentate nitrato coordination. However, enough space is available to allow for the secondary interaction in these molecules. One noticeable difference between the two molecules is that the arsenic compound is temperature sensitive whereas the Ge(II) compound is not, demonstrating that the coordination mode does not account for temperature sensitivity but rather the element the nitrato group to which it is coordinated.

Sodium nitrate is too weak a nucleophile to displace a chlorine atom in these molecules under these conditions. The presence of trichlorogermanate in the crystal structure shows that some exchange must occur to provide the chloride anions to form the $[GeCl_3]^-$ anion, resulting in an equilibrium between $[Ge(NO_3)_3]^-$ and $[GeCl_3]^-$ and the substituted products in between, Scheme 5.2. Preferentially the mixed salt of

(PPN)$GeCl_3$/$GeCl_2(NO_3)$ crystallises from the recrystallisation conditions used. To further push the exchange to completion a different source of nitrate anions would have to be used of which there are two choices.

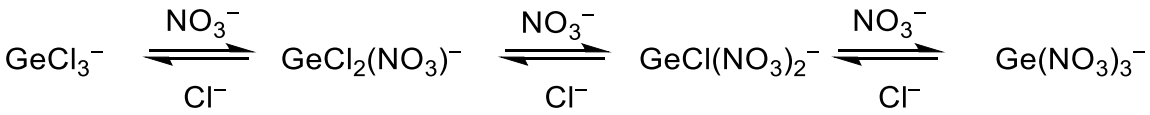

Scheme 5.2. Equilibrium of nitrato(chloro)germanates in THF solution.

Silver nitrate represents the most obvious choice, however, due to its oxidising properties cannot be used. An alternative is the *covalent* nitrate Me_3SiONO_2. Though this reagent has two potential issues, (i) exchange usually requires an E−F bond, i.e. SnF_2, as the formation of Si−F bonds are a large thermodynamic driver; (ii) the compound decomposes in a few hours at room temperature. There is no reagent to generate GeF_2 *in situ* in the way that $GeCl_2$(1,4-dioxane) is a source of $GeCl_2$, though it is worth noting (Nacnac)GeF is a known compound, that leaves SnF_2 as an ideal starting point for investigation.[169]

Trimethylsilyl nitrate can be prepared as a stock solution in acetonitrile by treating Me_3SiCl with silver nitrate at 0°C.[170] The solution has to be kept below 0°C otherwise decomposition of the silyl nitrate occurs. Combination of SnF_2 and (PPN)NO_3 and Me_3SiONO_2 in acetonitrile affords a colourless solution. Removal of the solvent resulted in a viscous oil that did not display coordinated nitrato bands in the FT-IR spectrum and showed the characteristic signals of (PPN)NO_3. Conversion using trimethylsilyl reagents, such as Me_3SiN_3,[171] often require elevated temperatures and so at the low temperatures required to handle Me_3SiONO_2, conversion appears to not be possible.

The synthesis of nitrato complexes of low valent elements is hampered as common nitrato exchange reagents are unsuitable. Azido complexes, however, should have fewer difficulties.

5.2.2 Homoleptic azido Ge(II) and Sn(II) complexes

5.2.1.1 Syntheses and IR spectroscopy

Information on homoleptic Ge(II) and Sn(II) azides is scarce. In fact, the only report is for the isolation of $Sn(N_3)_2$ in 2014 and very little information is provided. The IR absorption for $\nu_{as}(N_3)$ is quoted as 2200 to 1900 cm^{-1} and elemental analysis values are too low.[172] Otherwise the only Ge(II) and Sn(II) azido complexes known are base stabilised Lewis adducts. To demonstrate that azido complexes of Ge(II) do not require bulky stabilising ligands, an attempt to synthesise the triazidogermanate anion, $[Ge(N_3)_3]^-$, was made. As well as the triazidostannate anion, $[Sn(N_3)_3]^-$.

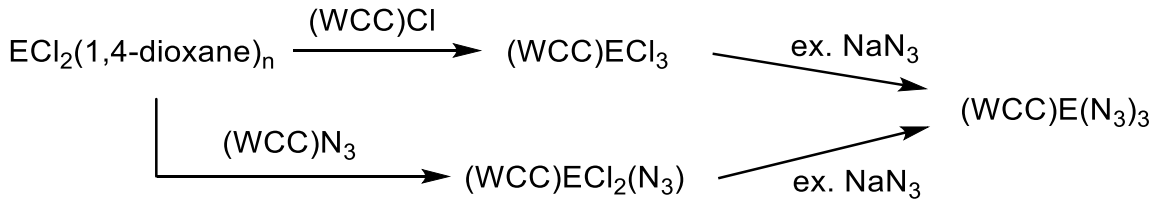

Scheme 5.3. Synthesis of azido(chloro) germanates(1−) and stannates(1−). E = Ge (n = 1), Sn (n = 0). WCC = (PPh_4), (PPN), $(AsPh_4)$.

Two different syntheses were devised: (i) addition of $(WCC)N_3$ to ECl_2 followed by salt metathesis with sodium azide, or (ii) addition of (WCC)Cl to ECl_2 followed by salt metathesis with sodium azide, Scheme 5.3. Figure 5.6 shows the FT-IR spectrum obtained from a solution of $(PPh_4)N_3$ and $GeCl_2$(1,4-dioxane) in acetonitrile between 2000 and 2200 cm^{-1}. The dominant peak at 2075 cm^{-1} is the complex $(PPh_4)GeCl_2(N_3)$ and the other peak at 2062 cm^{-1} indicates $(PPh_4)GeCl(N_3)_2$. The latter complex should have two absorptions in the $\nu_{as}(N_3)$ region, however, only one is observed, most likely that the second peak, which should be at higher energy, is hidden by the larger peak at 2075 cm^{-1}.

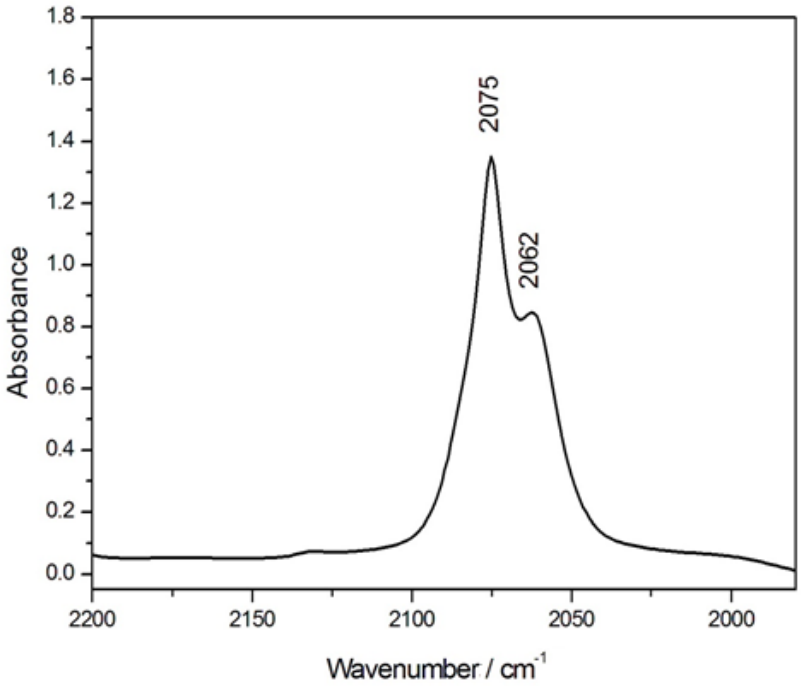

Figure 5.6. FT-IR spectrum of the solution of $(PPh_4)N_3$ and $GeCl_2$(1,4-dioxane) in acetonitrile.

Only a single equivalent of $(PPh_4)N_3$ was added to $GeCl_2$(1,4-dioxane), therefore, for the $[GeCl(N_3)_2]^-$ to form extra azide anions must be present in the reaction solution. An equilibrium between $[GeCl_3]^-$ and $[Ge(N_3)_3]^-$ and all the other degrees of substitution establishes to provide a source of chloride and azide anions. The overall position of the equilibrium appears to be a mixture of $[GeCl_3]^-$, $[GeCl_2(N_3)]^-$ and $[GeCl(N_3)_2]^-$ with the monoazido complex the most prevalent. Scheme 5.4 shows the equilibrium.

$$GeCl_3^- \underset{Cl^-}{\overset{N_3^-}{\rightleftharpoons}} GeCl_2(N_3)^- \underset{Cl^-}{\overset{N_3^-}{\rightleftharpoons}} GeCl(N_3)_2^- \underset{Cl^-}{\overset{N_3^-}{\rightleftharpoons}} Ge(N_3)_3^-$$

Scheme 5.4. Equilibrium of the azido(chloro)germanates(1−) in acetonitrile solution.

Removal of the acetonitrile solvent resulted in an off-white solid which was combined with a large excess of sodium azide in THF to drive the equilibrium towards the $(PPh_4)Ge(N_3)_3$ (**14a**). The FT-IR spectrum of the new solution is shown in Figure 5.7. There are two IR absorptions in the $\nu_{as}(N_3)$ region at 2091 and 2058 cm^{-1} indicative of **14a**. A small absorption at 2130 cm^{-1} for HN_3 and at 1997 cm^{-1} for $(PPh_4)N_3$ is also

observed. Identical spectra are obtained when using (PPN)N_3 instead of (PPh_4)N_3 to give (PPN)$Ge(N_3)_3$ (**14b**) or ($AsPh_4$)N_3 to give ($AsPh_4$)$Ge(N_3)_3$ (**14c**).

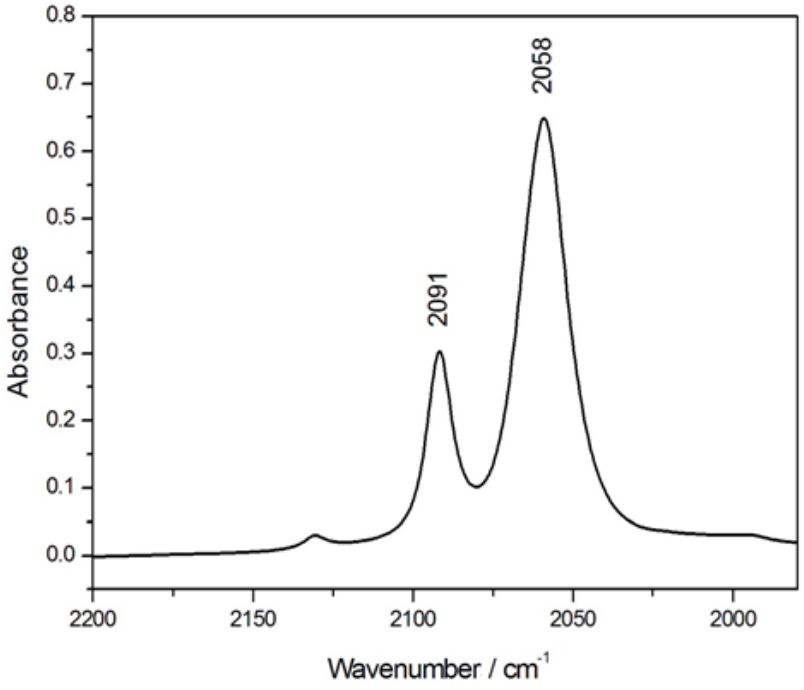

Figure 5.7. FT-IR spectrum of **14a** in THF.

Two bands in the IR spectrum represent a molecule with symmetry as there are three azido groups. The most likely point group of $[Ge(N_3)_3]^-$ is C_3, which would display two bands in the IR spectrum. Other possible point groups, C_{3h}, C_{3v} and C_s, are unlikely because of the expected geometric restrictions enforced by the lone pair on the germanium atom and the bent coordination of the azido ligand. Figure 5.8 is a representation of the stereoprojection of $[Ge(N_3)_3]^-$ in the C_3 point group.

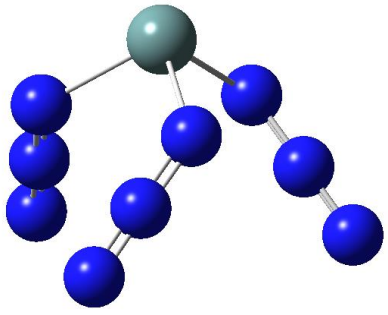

Figure 5.8. Stereoprojection of $[Ge(N_3)_3]^-$ in the C_3 point group.

The analogous higher coordinate Ge(IV) anion, $[Ge(N_3)_6]^{2-}$, shows a single absorption at 2083 cm^{-1} in acetonitrile.[173] In THF solution the most dominant peak of

14a at 2058 cm^{-1} is consistent with other Ge(II) azido complexes (2075−2048 cm^{-1}) and lower than Ge(IV) azido complexes (2083−2120 cm^{-1}), Table 5.3. The lower position of the wavenumbers implies a less covalent nature of the Ge−N bond in the reduced species. As the Ge atom is in a lower oxidation state there is less *s* character in the bonding, elongating the bond and effectively reducing the covalency of the Ge−N bond.

Compound	$\nu_{as}(N_3)$ / cm^{-1}	Medium
14a	2091, 2058	THF
$(IPr)Ge(N_3)_2$ [158]	2075	ATR
$(ATI)Ge(N_3)$ [162]	2048	KBr
$L^3Ge(N_3)$ [161]	2053	THF
$(PPN)_2Ge(N_3)_6$ [173]	2083	MeCN
$(bipy)Ge(N_3)_4$ [173]	2120, 2097, 2091	MeCN

Table 5.3. IR absorptions of selected Ge(II) and Ge(IV) azido complexes. The azide symmetric stretch is obscured by ancillary ligands on some complexes and so has not been included. IPr: 1,3-bis(2,6-diisopropylphenyl)imidazole-2-ylidene; ATI: *N*-(n-propyl)-2-(n-propylamino)-troponiminate; L^3: $(C_5H_5)Co\{P(O)(OEt_2)_3\}$; bipy: 2,2'-bipyridine.

The analogous tin(II) complex, $(PPh_4)Sn(N_3)_3$ (**15**), can be prepared in an identical method as **14a** starting from $SnCl_2$. The FT-IR spectrum of a THF solution containing PPh_4N_3 and $SnCl_2$ is shown in Figure 5.9. As before with **14a**, multiple peaks are observed despite only a single equivalent of azide anions present. Two peaks at 2050 and 2064 cm^{-1} and a shoulder at 2072 cm^{-1} suggest $(PPh_4)SnCl_2(N_3)$ and $(PPh_4)SnCl(N_3)_2$. It is worth noting that the intensity of the $SnCl(N_3)_2$ is much greater than what is observed in the synthesis of $(PPh_4)GeCl_2(N_3)$. Stirring this solution over a large excess of sodium azide results in a solution which displays two bands at 2051 and 2081 cm^{-1} for $[Sn(N_3)_3]^-$ and a much weaker peak at 2130 cm^{-1} in its FT-IR spectrum, Figure 5.10. The band shape of the peak at 2081 cm^{-1} suggests another peak is present under the peak, which is most likely due to the $[Sn(N_3)_6]^{2-}$ anion (2078 cm^{-1} in MeCN).[171] The presence of which can be explained by oxidation of **15** with HN_3.

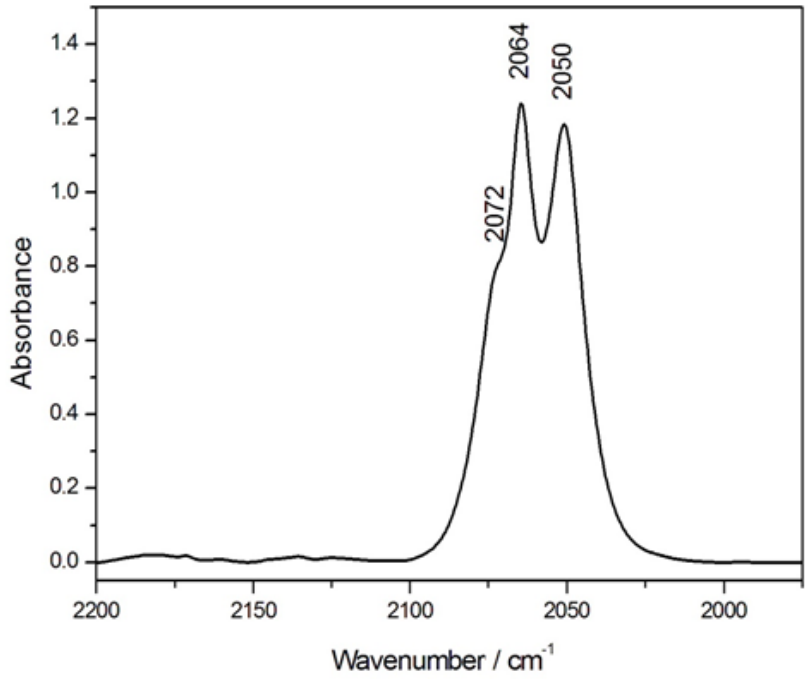

Figure 5.9. FT-IR spectrum of the solution of $(PPh_4)N_3$ and $SnCl_2$ in THF.

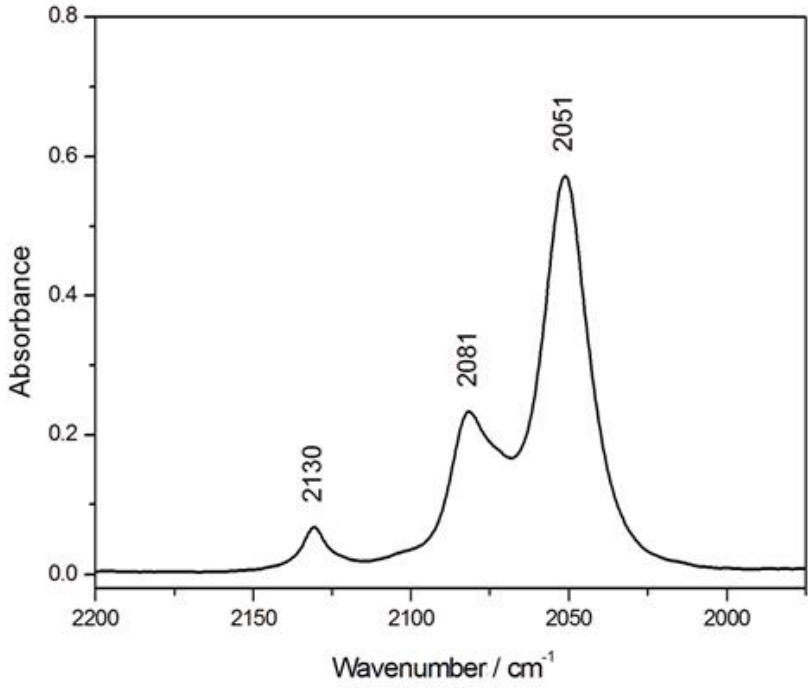

Figure 5.10. FT-IR spectrum of $(PPh_4)Sn(N_3)_3$ in THF.

Table 5.4 shows the IR absorption frequencies of Sn(II) and Sn(IV) azido complexes. Firstly, as is common when changing the coordination centre to a heavier element in the same group the frequency of $\nu_{as}(N_3)$ decreases, the $\nu_{as}(N_3)$ for **15** is at lower wavenumbers than **14a**. Similarly to **14a**, the absorption appears at a lower wavenumber than the $[Sn(N_3)_6]^{2-}$ anion and falls in the region of previously determined Sn(II) azido

complexes. The difference between the two peaks in the FT-IR spectrum of **15** is 30 cm^{-1} and is similar to the difference between the peaks of **14a** (33 cm^{-1}). This suggests both anions have very similar structures in solution.

Compound	$\nu_{as}(N_3)$ / cm^{-1}	Medium
15	2081, 2051	THF
(ATI)Sn(N_3)	2039	KBr
(^{mes}Nacnac)Sn(N_3)	2060	KBr
$(PPN)_2Sn(N_3)_6$	2079	MeCN
(bipy)Sn$(N_3)_4$	2112, 2085	MeCN

Table 5.4. IR absorptions of selected Ge(II) and Ge(IV) azido complexes. The azide symmetric stretch is obscured by ancillary ligands on some complexes and so has not been included. ^{mes}Nacnac: 2,4-dimethyl-*N,N′*-bis(2,4,6-trimethylphenyl)-1,5-diazapentadienyl.

The $[Ge(N_3)_3]^-$ anion was prepared with the PPh_4^+, PPN^+ and $AsPh_4^+$ cations. Attempts to crystallise the $AsPh_4$ salt resulted in only off-white solids, while the PPN salt (**14b**) formed small colourless block crystals by solvent evaporation of THF in a glovebox. The PPh_4 salt could be crystallised by the slow cooling of a THF and diethyl ether (1:10) solution of **14a** to give colourless needle crystals. Only the PPh_4 salt of the $[Sn(N_3)_3]^-$ anion was prepared and crystallised in the same method as **14a**.

Figure 5.11 shows the FT-IR spectrum of **15** as a nujol mull. There are striking differences between the IR spectra obtained in solution and as a nujol mull. Three peaks are present in the nujol mull spectrum at 2068, 2058 and 2034 cm^{-1} at variance to the THF solution FT-IR spectrum which displays two bands at 2081 and 2051 cm^{-1}. The significance of this is that the $[Sn(N_3)_3]^-$ has a different structure in solution than in the solid-state.

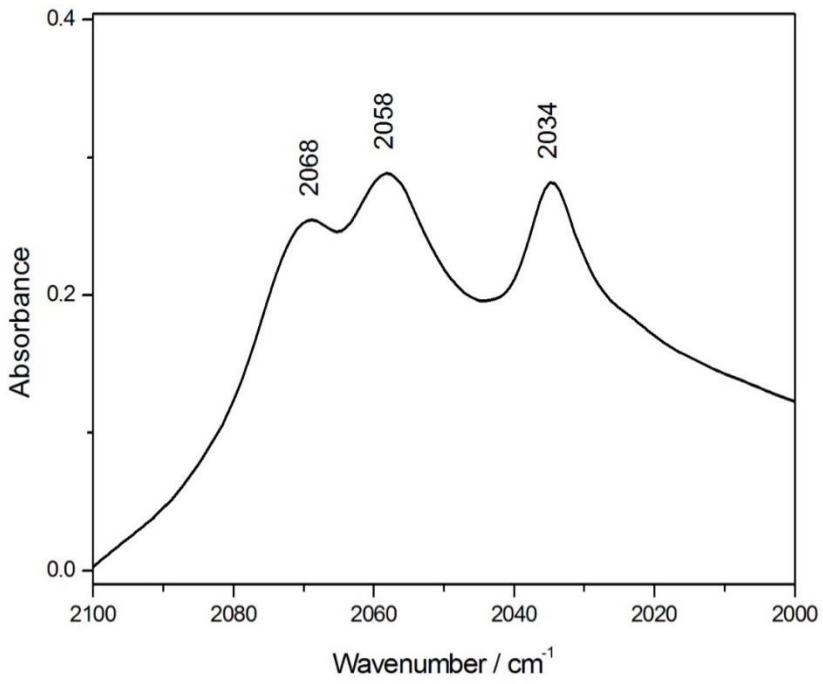

Figure 5.11. FT-IR spectrum of **15** as a nujol mull.

5.2.1.2 Single crystal X-ray diffraction

Single crystal X-ray diffraction studies were performed on **14a**, **14b** and **15**. (PPN)Ge(N_3)$_3$ crystallises in the space group $P2_1$, however, it was not possible to completely solve the structure. The germanium atoms and PPN cation could be located, however, the nitrogen atoms of the azido group could only be partially located. Despite attempting different models the location of the azido groups could not be fully determined. Figure 5.12 shows the packing of the PPN cation, from the attempted structure solution, which dominates the packing of the crystal structure. There are two cavities in the unit cell available for the [Ge(N_3)$_3$]$^-$ to be positioned and one is significantly larger than the other. In the small cavity the anion can fit, however, in the larger cavity there is more freedom for the [Ge(N_3)$_3$]$^-$ making the exact location of the anion difficult to find, up to a point where it could not be located definitively.

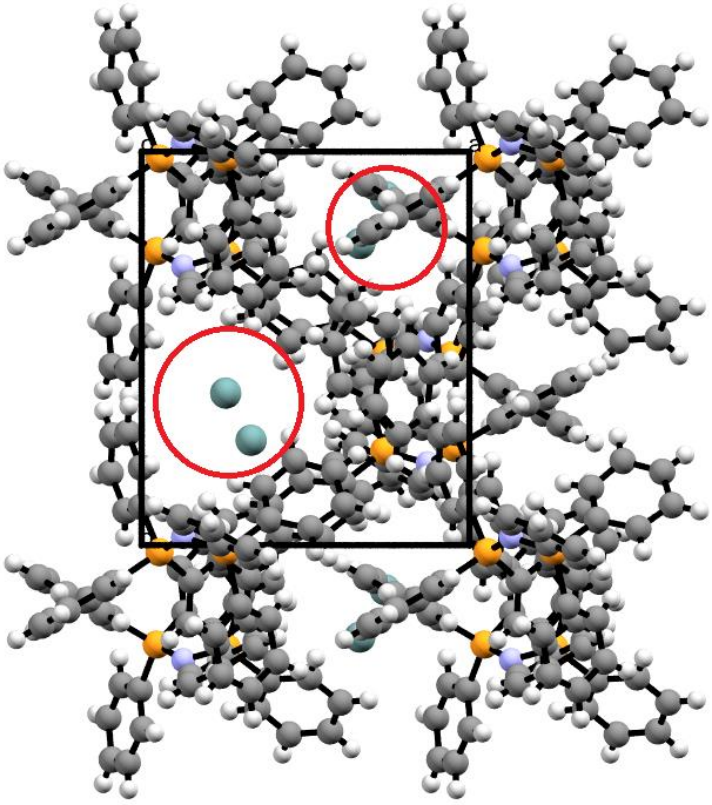

Figure 5.12. Unit cell of **14b** only showing the PPN cation and germanium atoms viewed down the crystallographic *c*-axis. Cavities marked with red rings. Grey: carbon; blue: nitrogen; orange: phosphorus; white: hydrogen; turquoise: germanium.

As the packing of **14b** is dominated by the PPN cation, it was thought the smaller PPh_4 cation would result in structure which could be completely resolved. The moderately air sensitive crystals of **14a** were put under nujol on a microscope slide and after a period of 15 mins bubbles had formed on the surface of the crystals, shown in Figure 5.13. The identity of the gas is unknown but most likely HN_3.

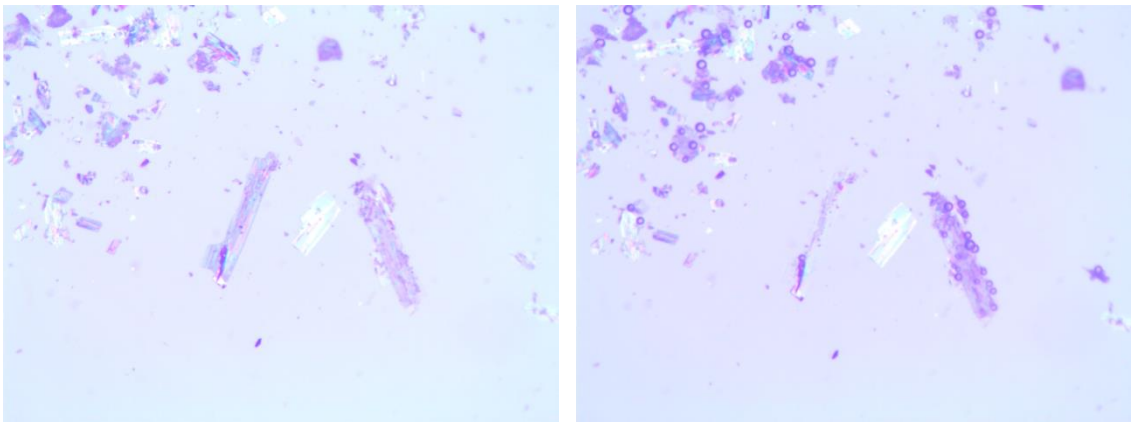

Figure 5.13. Crystals of **14a** under nujol in air at various times. Left: t = 0 min; right: t = 15 min. Scale: 1.25 cm : 1 mm.

Compound **14a** crystallises in the space group $P\bar{1}$ with a unit cell that contains two formula units. Only weak van der Waals interactions are present between anion and cation resulting in channels of unperturbed cations and anions along the crystallographic *a*-axis. There are no bridging interactions between $[Ge(N_3)_3]^-$ anions with the shortest intermolecular Ge···N and N···N distances being 4.13 and 5.07 Å respectively. The germanium atom is three coordinate with three essentially linear azido ligands arranged in a trigonal-pyramidal geometry around the germanium, giving C_1 symmetry, contradictory to the solution cell FT-IR spectrum. The average N(α)−Ge−N(α) bond angle is 92.98(18)°, indicative of a stereochemical active lone pair consistent with other three coordinate Ge(II) azido complexes.[158,162,163]

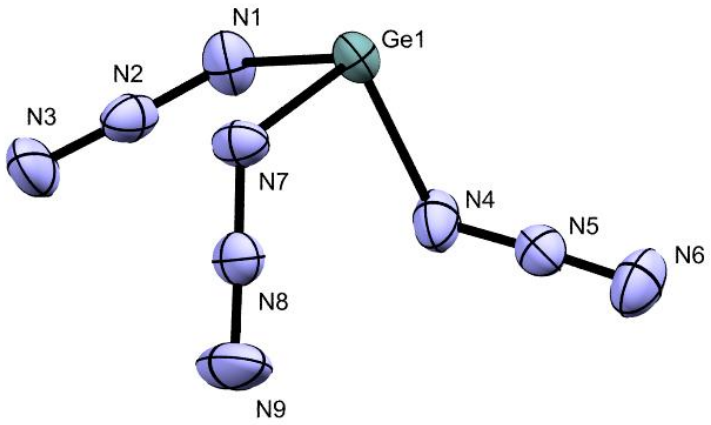

Figure 5.14. Thermal ellipsoid plot of the anion $[Ge(N_3)_3]^-$ in **14a**. Thermal ellipsoids are set at the 50% probability level. Selected bond lengths (Å) and angles (°): Ge1–N1 1.988(3), Ge1–N4 2.011(3), Ge1-N7 1.984(2), N1–N2 1.213(3), N2–N3 1.148(3), N4–N5 1.209(3), N5–N6 1.142(3), N7–N8 1.206(3), N8–N9 1.140(3), N1–Ge1–N4 91.05(11), N7–Ge1–N1 93.59(10), N7–Ge1–N4 94.29(10), N2–N1–Ge1 116.4(2), N3–N2–N1 177.6(3), N5–N4–Ge1 118.7(2), N6–N5–N4 177.4(3), N8–N7–Ge1 121.3(2), N9–N8–N7 175.2(3).

The Ge−N(α) bond lengths (1.984(2)−2.011(3) Å) are shorter than tetracoordinate Ge(II) azido complexes (2.088−2.094 Å)[159,161] and falls in the range of known tricoordinate Ge(II) azido complexes (1.969–2.047 Å).[158,162,163,174] The Ge(IV) azido compound, $(PPN)_2Ge(N_3)_6$, has shorter Ge−N(α) bond lengths (1.969−1.980 Å) than those in **14a**, Table 5.5. An increase in the coordination number around the germanium centre accounts to why the tetracoordinate Ge(II) complexes have a longer bond. The effect of the negative charge appears to have very little effect on the bond length after comparing with other tricoordinate Ge(II) azido complexes. The N(α)−N(β) and N(β)−N(γ) bond lengths of the azido ligands fall in the expected range for a covalent azide with the former being longer than the latter (1.206(3)−1.213(3) Å and

1.140(3)−1.148(3) Å). The difference between these two bond lengths for this anion is 6.6 pm on average. A value similar to $(PPN)_2Ge(N_3)_6$ (6.5 pm). As this parameter is an indicator of the degree of covalency of the Ge−N bond, this implies very little difference between **14a** and $(PPN)_2Ge(N_3)_6$ contrary to the differences in the Ge−N bond lengths between the two compounds. The FT-IR spectrum of **14a** also suggests an increase in the ionicity of the germanium azide bond.

Compound	Average bond lengths			ΔNN / pm
	Ge−N	N(α)−N(β)	N(β)−N(γ)	
14a	1.994(5)	1.209(5)	1.143(5)	6.7(7)
$(IPr)Ge(N_3)_2$ [158]	1.969	1.209	1.152	5.7
$(ATI)Ge(N_3)$ [162]	2.047	1.197	1.144	5.3
$L^3Ge(N_3)$ [161]	2.094	1.180	1.159	2.1

Table 5.5. Average bond lengths of Ge(II) azido complexes. Bond lengths are in units of Å and ΔNN (D(N(α)−N(β))−D(N(β)−N(γ))) in units of pm. L^3: $(C_5H_5)Co\{P(O)(OEt_2)_3\}$.

Table 5.5 shows the bond lengths for a selection of Ge(II) complexes. The ΔNN parameter is much larger in **14a** compared to the Ge(II) azides that contain Lewis bases. It appears that the greater electron withdrawing properties of the azido groups over the strong σ-donor strength of the ancillary ligands results in a larger ΔNN parameter for $[Ge(N_3)_3]^-$.

The solid-state structure of **15** is different to that of **14a.** Single crystal X-ray diffraction studies show compound **15** crystallises in the space group $P\bar{1}$ with two formula units per unit cell. Unlike in **14a**, which has only weak van der Waals interactions between anion and cation, **15** displays two Sn···N(α) contacts and two long Sn···N(γ) contacts resulting in the formation of discrete $\{[Sn(N_3)_3]\}_2^{2-}$ dimers, Figure 5.15. The contacts are asymmetric $\mu_{1,1}$-N_3 bridges giving an Sn_2N_2 ring with short and long Sn−N(α) bonds (2.203 and 2.672 Å). The Sn_2N_2 ring is planar and the bond angles imply sp^2 hybridisation for the nitrogen atoms. Other Sn(II) azido complexes display a similar feature. Table 5.6 summarises the structural features of **15** and other Sn(II) azido complexes.

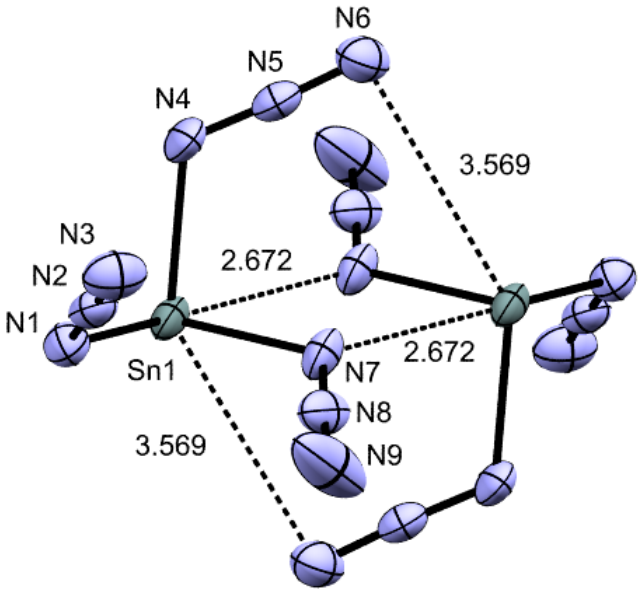

Figure 5.15. Thermal ellipsoid plot of $\{[Sn(N_3)_3]\}_2^{2-}$ in crystals of **3**. Thermal ellipsoids are set at the 50% probability level. Selected bond lengths (Å) and angles (°): Sn1−N1 2.263(4), Sn1−N4 2.203(4), Sn1−N7 2.203(4), N1−N2 1.197(6), N2−N3 1.151(6), N4−N5 1.205(6), N5−N6 1.142(6), N7−N8 1.186(6), N8−N9 1.160(7), N1−Sn1−N4 88.15(15), N7−Sn1−N1 88.71(15), N7−Sn1−N4 89.24(16), N2−N1−Sn1 123.8(3), N3−N2−N1 177.5(5), N5−N4−Sn1 118.8(3), N6−N5−N4 177.0(5), N8−N7−Sn1 123.7(3), N9−N8−N7 176.5(5).

Compound	Average bond length				ΔNN
	Sn−N	Sn···N(α)	N(α)−N(β)	N(β)−N(γ)	
15	2.223(7)	2.672	1.196(10)	1.151(11)	4.0(15)
(ATI)Sn(N_3) [162]	2.253	2.870	1.188	1.156	3.2
(^{mes}Nacnac)Sn(N_3) [163]	2.198	2.910	1.208	1.109	9.9

Table 5.6. Average bond lengths of Sn(II) and Sn(IV) azido complexes. Bond lengths are in units of Å and ΔNN is in units of pm.

The dimerisation feature in this structure has the shortest Sn···N(α) interaction for Sn(II) azides known to date. The primary reason is due to less steric crowding around the tin centre. Ligands such as ATI or (^{mes}Nacnac) are large and crowd the coordination sphere of the tin atom resulting in a longer distance between the nitrogen atom and the tin atom. Other than this interaction, the $[Sn(N_3)_3]^-$ anion is similar to $[Ge(N_3)_3]^-$. The $[Sn(N_3)_3]^-$ anion has a trigonal-pyramidal tin atom with a stereochemical active lone pair. As with **14a**, the E−N bond length is longer than the E(IV) analogue and falls in the range of other Sn(II) azido complexes. Interestingly, the difference in the ΔNN parameter between **15** and $(PPN)_2Sn(N_3)_6$ is much greater than between **14a** and $(PPN)_2Ge(N_3)_6$. In **15** the ΔNN is 4.0(15) pm, whereas for $(PPN)_2Sn(N_3)_6$ it is 6.8 pm.

The large difference is most likely due to the bridging interaction. The azido ligand which is not involved in any intermolecular interactions with another $[Sn(N_3)_3]^-$ has N(α)−N(β) and N(β)−N(γ) bond lengths of 1.197(6) and 1.151(6) Å. Whereas the azido ligand involved with the N(γ) interaction has a larger N(α)−N(β) bond length (1.205(6) Å) and a shorter N(β)−N(γ) bond length (1.142(6) Å). The azido ligand bridging *via* N(α) has a N(α)−N(β) bond length of 1.186(6) Å, shorter than the other two azido ligands, and N(β)−N(γ) bond length of 1.160(7) Å, longer than the other two azido ligands. A simple electrostatic argument explains these differences, as electron density is removed from the bridging nitrogen towards the tin centre effectively pulling the central N(β) towards the bridging nitrogen.

The structures of **14a** and **15** in the solid state are very different, however, are similar when dissolved in THF, suggesting discrete anions of $[Sn(N_3)_3]^-$ to be present in solution.

5.2.2.3 Nuclear Magnetic Resonance spectroscopy

The ^{14}N NMR resonances of **14a** were determined in CD_2Cl_2 to be at −264, −136 and −208 ppm for the N(α), N(β) and N(γ) atoms respectively, with FWHM values of 552 and 24 Hz for N(α) and N(β). Whereas the ^{14}N NMR spectrum of **15**, recorded in CD_3CN, had resonances at −260 and −218 ppm with FWHM of 166 and 32 Hz. The N(β) resonance of **15** is obscured by the resonance of CD_3CN. Compared to $[Ge(N_3)_6]^{2-}$ and $[Sn(N_3)_6]^{2-}$, the ^{14}N signals of the azido ligands of **14a** and **15** are more deshielded. Similarly with IR spectroscopy and ΔNN values, insight into the electronic structure of the azido group can be made from the position of the resonances. If the difference between the N(α) and N(γ) resonances, ΔN(α)N(γ), is equal to zero then the azido group is ionic, and more accurately the azide anion, and a larger value indicates a more covalent azido group. The ΔN(α)N(γ) values of **14a** and **15** are 56 and 42 Hz respectively, lower than the Ge(IV) and Sn(IV) analogues (both 81 Hz). The lower values are indicative of the increase in ionicity of the E−N bond as evidenced by IR spectroscopy and the structure determination. Table 5.7 shows the ^{14}N NMR data of Ge(II) azido complexes and the ^{14}N and ^{119}Sn NMR data of Sn(II) azido complexes.

Compound	$^{14}N(\alpha)$	$^{14}N(\beta)$	$^{14}N(\gamma)$	^{119}Sn	Solvent
14a	−264	−137	−208	−	CD_2Cl_2
15	−260	*	−218	−221	CD_3CN
(^{mes}Nacnac)Ge(N_3) [163]	−291	−136	−215	−	CD_2Cl_2
(ATI)Ge(N_3)[162]	−250	−135	−213	−	CD_2Cl_2
(IPr)Ge(N_3)$_2$ [158]	−295	−137	−213	−	THF-d_8
(^{mes}Nacnac)Sn(N_3) [163]	−292	−136	−223	−276	CD_2Cl_2
(ATI)Sn(N_3) [162]	−256	−136	−202	−122	CD_2Cl_2
$(PPN)_2Ge(N_3)_6$ [173]	−289	*	−208	−	CD_3CN
$(PPN)_2Sn(N_3)_6$ [171]	−299	*	−218	−	CD_3CN

Table 5.7. NMR data of selected Ge(II) and Sn(II) azido complexes and $(PPN)_2Ge(N_3)_6$ and $(PPN)_2Sn(N_3)_6$. Units of resonances in Hz. * overlaps with solvent signal.

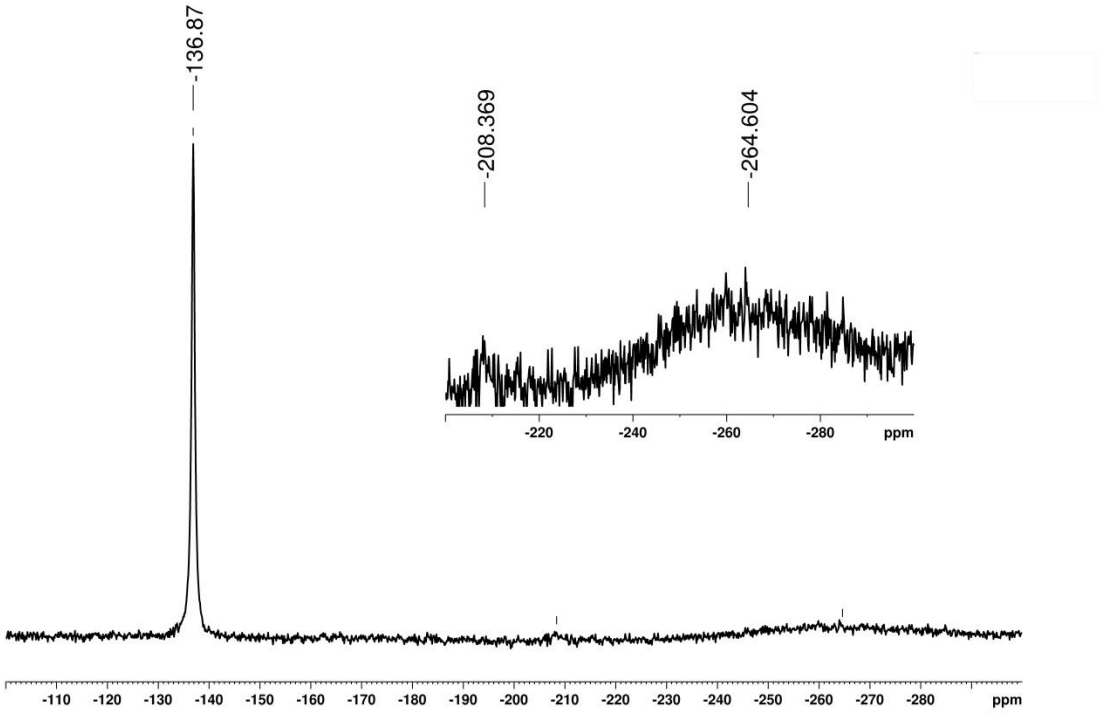

Figure 5.16. ^{14}N NMR spectrum of **14a** in CD_2Cl_2.

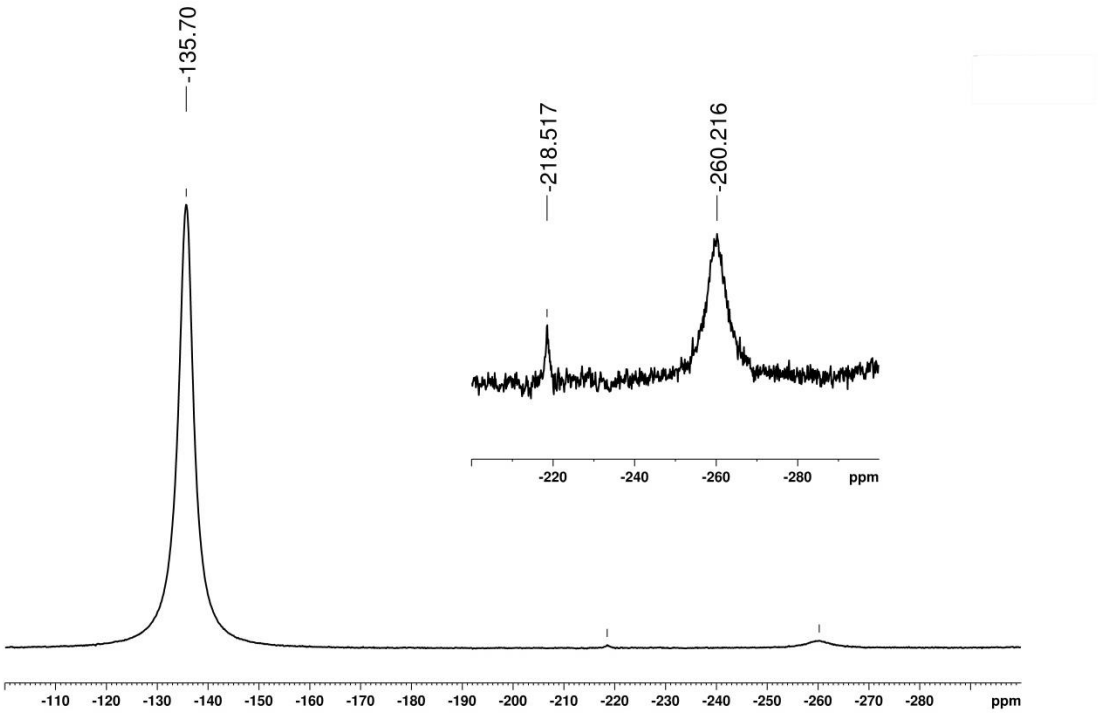

Figure 5.17. ^{14}N NMR spectrum of **15** in CD_3CN.

Other Ge(II) and Sn(II) azido complexes have different shifts for the ^{14}N resonances of the azido group depending on the ancillary ligand. The complexes containing the ligands ^{mes}Nacnac and IPr have lower chemical shifts compared to **14a** and **15** and the complexes containing the ATI ligand. The ^{119}Sn NMR spectrum of **15**, Figure 5.17, displays a signal at −221 ppm, in between those of (^{mes}Nacnac)SnN_3 (−276 ppm) and (ATI)SnN_3 (−122 ppm). The ^{119}Sn resonance for $[Sn(N_3)_6]^{2-}$ is not published, however, $(NMe_4)_2SnCl_6$ has been reported as −732 ppm in CH_2Cl_2.[175] The resonance for $[SnCl_3]^-$ has been previously determined by combining various amounts of $SnCl_2$ with 1-*n*-octane-3-methylimidazolium chloride, which gives an ionic liquid. Various signals for the ^{119}Sn resonance are found between −48 and −248 ppm depending on the quantity of $SnCl_2$ added.[176] Low valent coordination centres appear to be more deshielded than the hypercoordinate species, and **15** is in the correct region.

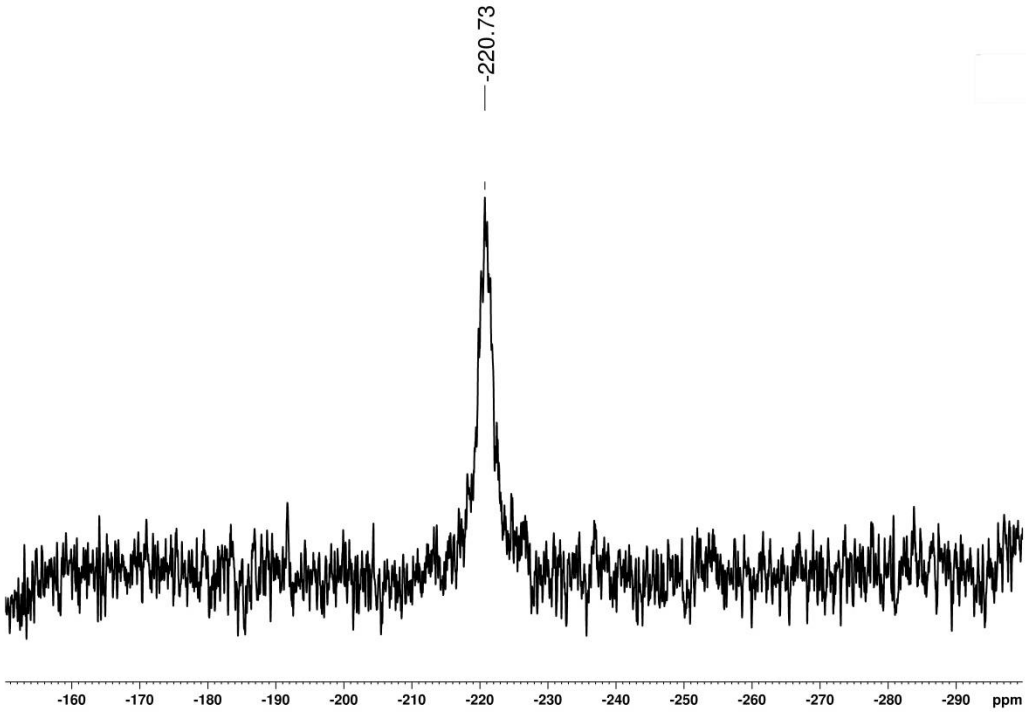

Figure 5.18. ^{119}Sn NMR spectrum of **15** in CD_3CN.

5.2.2.4 Thermal properties and reactivity of $[E(N_3)_3]^-$

The nitrogen content of **14a** and **15** are 23.42 % and 21.58 % respectively. These values are not high enough to be considered a nitrogen-rich compound, however, the anion combined with the appropriate counterion could be. These compounds are appropriate for the safe study of the $[Ge(N_3)_3]^-$ and $[Sn(N_3)_3]^-$ anions. Figures 5.19 and 5.20 show the differential scanning calorimetry (DSC) thermograms of compounds **14a** and **15**. Compound **14a** first melts at 63°C and then decomposes in two steps at 108°C and 317°C. The first step corresponds to an energy release of −145 kJ mol^{-1} and the second step an energy release of −251 kJ mol^{-1}. The significance of the second decomposition is that the temperature is very close to that of the second decomposition step of $(PPN)_2Ge(N_3)_6$ (317°C *vs.* 312°C).[173] Also the energy release for $(PPN)_2Ge(N_3)_6$ is approximately double that of **14a** (−251 kJ mol^{-1} *vs.* −481 kJ mol^{-1}), scaling with the charge of the anion. Combination of these two facts suggests that the second step is due to the decomposition of $(WCC)N_3$ for both compounds. Step one is considerably lower in energy than that of $(PPN)_2Ge(N_3)_6$, even when considering the scaling of the charge, and occurs at a much lower temperature. A sample of **14a** heated

to 150°C resulted in a material which displayed $(PPh_4)N_3$ suggesting decomposition is initiated with the loss of N_3^-.

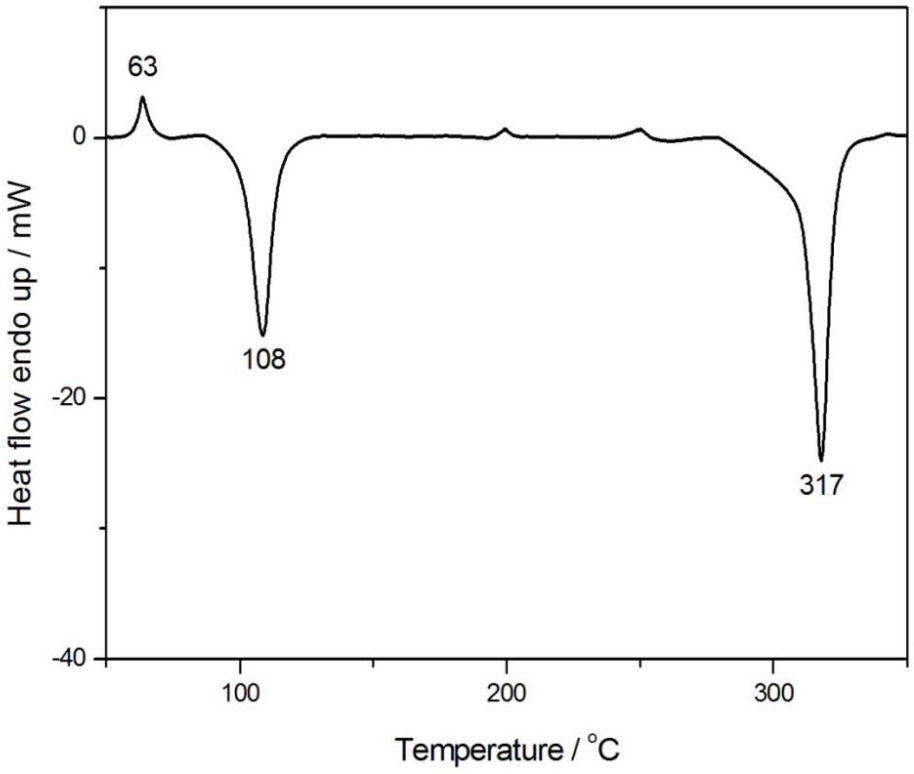

Figure 5.19. DSC thermogram of **14a**. Heating rate at 10°C / min. Compound **15** melts at 63°C and decomposes at 108°C and 317°C. Two other phase changes are observed at 199°C and 250°C.

The $[Sn(N_3)_3]^-$ anion decomposes in a different pattern to that of $[Ge(N_3)_3]^-$ occurring at higher temperatures. Compound **15** melts at 124°C and decomposes in a three step process at 226, 252 and 331°C, slightly lower temperatures than $(PPN)_2Sn(N_3)_6$ (300 and 365°C)[171]. The first and second steps overlap and are considerably lower in energy than the step at 331°C. The difference is potentially related to the dimeric structure of the compound in the solid state.

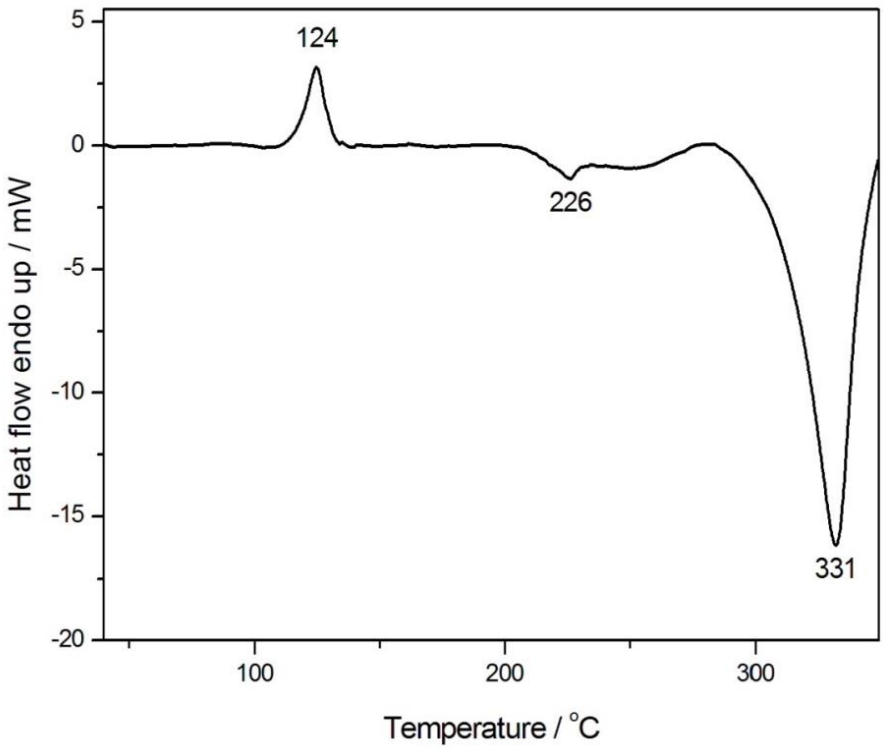

Figure 5.20. DSC thermogram of **3**. Heating rate at 10°C / min. Compound **3** melts at 124°C and decomposes at 226°C, 252°C and 331°C

Both **14a** and **15**, as low-valent species, are prone to oxidation. The FT-IR spectrum of **15** in THF, Figure 5.10 (*vide supra*), shows a small peak for $[Sn(N_3)_6]^{2-}$ assumed to be due to the oxidation from HN_3 produced on hydrolysis of **15**. The reaction of **14a** and **15** with HN_3 was investigated by IR spectroscopy. Figure 5.21 shows the IR spectral series of the reaction between HN_3 and **14a** in THF over a period of approximately 19 hrs. The initial spectrum before HN_3 was added shows the two peaks at 2058 and 2091 cm^{-1}. Addition of HN_3 (appears at 2130 cm^{-1} in THF) results in the decrease of these two peaks and the growth of a new peak at 2086 cm^{-1}, which corresponds to $[Ge(N_3)_6]^{2-}$. The low intensity of this peak is due to the low solubility of $(PPh_4)_2Ge(N_3)_6$ in THF. Compound **15** shows the same reactivity converting $(PPh_4)Sn(N_3)_3$ to $(PPh_4)Sn(N_3)_6$. However, is completed in fewer than 70 mins, faster than the germanium analogue. The mechanism for such a reaction is currently unknown and possibly occurs via $(PPh_4)E(H)(N_3)_4$.

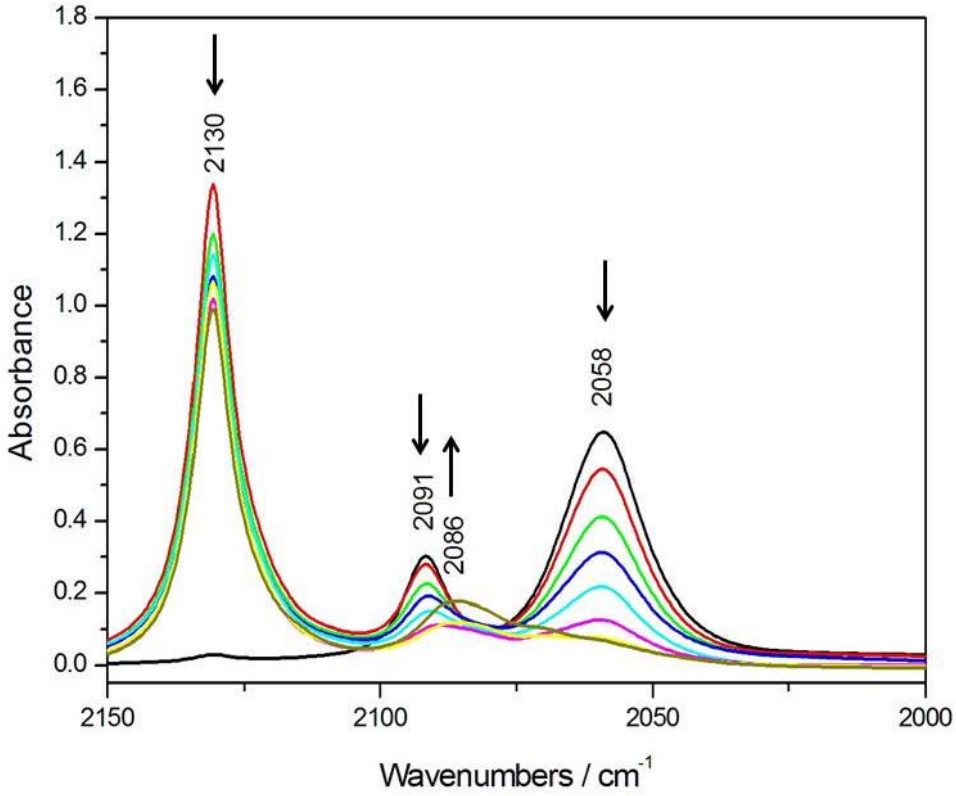

Figure 5.21. FT-IR spectral series of a solution of HN_3 and compound **14a** in THF recorded over a period of 16 h. Black line: t = 0 mins; red line: t = 17 mins; green line: t = 37 mins; dark blue line: t = 49 mins; light blue line: t = 67 mins; pink line: t = 97 mins; yellow line: t = 162 mins; gold line: t = 1125 mins.

5.3 Conclusion

Main Group coordination complexes where the coordination centre is in a lower oxidation state than the principal oxidation state often have different chemical properties. This is also true for azido complexes of low valent Main Group elements. Like their higher coordinate homologues, $[E(N_3)_6]^{2-}$, the $[E(N_3)_3]^-$ anions can be isolated bearing bulky, non-coordinating counterions. Thus removing the need for bulky, strong σ-donor ligands, such as IPr or ^{mes}Nacnac, in the preparation of Ge(II) and Sn(II) azido complexes. The presence of a low-valent coordination centre results in different structural and chemical properties of anionic homoleptic azido complexes. Spectroscopic measurements, ^{14}N NMR and IR spectroscopies, show an increased degree of ionicity in the E−N bond for the Ge(II) and Sn(II) over Ge(IV) and Sn(IV), as a result of less *s*-character in the bonding. Structurally, $[Sn(N_3)_3]^-$ shows an interesting dimerisation feature *via* μ(1,1')-N_3 and μ(1,3)-N_3 bridges. In the germanium complex no such feature is observed. Despite being a low coordinate centre, the germanium atom is

too small to accommodate bridging interactions giving discrete anions of $[Ge(N_3)_3]^-$ in the solid-state structure of **14a**. The lone pair in both $[Ge(N_3)_3]^-$ and $[Sn(N_3)_3]^-$ is stereochemically inactive.

Differences in the thermal properties of $[E(N_3)_3]^-$ and $[E(N_3)_6]^{2-}$ can also be explained by the low-valent coordination centre. Decomposition temperatures of the low-valent anions are considerably lower than that of the hypercoordinate anions. The molar enthalpies of the second step of **14a** and $(PPN)_2Ge(N_3)_6$ scale approximately with unit charge implying this step is the decomposition of $(WCC)N_3$. The other decomposition step has too low an energy release to be considered the decomposition of $Ge(N_3)_2$ (addition of an azido group results in an approximate increase of 200 kJ mol^{-1} of energy).

To extend low valent Main Group azide chemistry further the reactivity of such species requires investigation. Inorganic azido complexes are known to undergo [3+2] cycloaddition with nitriles to prepare tetrazoles and tetrazolato coordination complexes.[177–179] The presence of a low-valent Main Group coordination centre offers the potential for different reaction routes and reactivity, while also remaining as a possible precursor for other Ge(II) and Sn(II) tetrazolato complexes. Other coordination centres also remain open for investigation such as, Ga(I) and In(I), as well as the lighter elements of the *p*-block: Al(I), Si(II), P(I). The latter of which will require new methodologies and requirements to ensure stability of such a reactive coordination centre.

In attempts to prepare $[Ge(NO_3)_3]^-$ sodium nitrate is too weak a nucleophile to displace the chloro ligands from $(PPN)GeCl_2(NO_3)$ completely. Current synthetic methods of nitrato / chloro exchange would be unsuitable in the preparation of the desired anion. The common reagent N_2O_5 would be strongly oxidising, it is also prepared in ozone, and therefore be reactive towards Ge(II) centres. Trimethylsilyl nitrate appears to be unreactive towards Main Group halides below its decomposition temperature. Like N_2O_5, silver nitrate would equally be oxidising due to the presence of Ag(I) ions. New methods of nitrato / halo exchange would be required to prepare the $[Ge(NO_3)_3]^-$, such as using other covalent metal nitrates as a potential source of the nitrato ligand. The anion that was obtained, $(PPN)GeCl_2(NO_3)$, could only be isolated as a solid solution with $(PPN)GeCl_3$. Structurally the anion is similar to $[AsCl_2(NO_3)_2]^-$ in that the nitrato coordination is unsymmetrically bidentate. However, is thermally more robust than the arsenic complex. Further coordination of nitrato groups to form

$[Ge(NO_3)_3]^-$ would result in an interesting species and the method for its preparation remains elusive.

6. A THIRD ROW LOW-VALENT AZIDO COMPLEX?

6.1 Introduction

After the success in the preparation of a homoleptic Ge(II) and Sn(II) azido complex the next progression was a third row low valent azido complex. Such a species would have potential to be a highly reactive compound and, therefore, have a diverse and interesting chemistry. A variety of Si(II) compounds have been treated with a range of organoazides: NHC stabilised silicon dichloride, saturated N-heterocyclic silylene and an unsaturated N-heterocyclic silylene, Figure 6.1.[66,69,80,180–183] Dependant on the organic group bonded to the azide a different Si−N containing product is obtained. The first report by West *et al* in 1994 concerned the reactivity of silylene **A** (Figure 6.1) towards Me_3SiN_3 and $PhCN_3$. Addition of two equivalents of Me_3SiN_3 with silylene **A** resulted in the evolution of nitrogen gas even at temperatures as low as −78°C in THF. The product obtained was a Si(IV) species, $LSi(N_3)(N(SiMe_3)_2)$, identified by X-ray crystallography, the only isolable compound from the reaction. The proposed intermediate, $LSi{=}NSiMe_3$, could not be detected by NMR spectroscopy and has only neen assumed. Interestingly, the reaction between the same silylene and Ph_3CN_3 resulted in the iminosilane, $LSi{=}NCPh_3$.

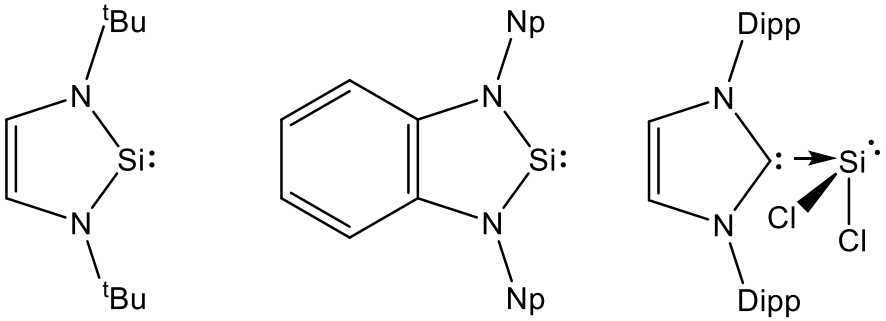

A **B** **C**

Figure 6.1. A selection of Si(II) compounds that have been treated with covalent azides. Np: $CH_2{}^tBu$. Dipp: 2,6-diisopropylphenyl.

In 1996 the treatment of silylene **A** with adamantyl-N_3 (Ad-N_3) was investigated by West and Denk. The product was determined to be a silatetrazoline by NMR spectroscopy, however structural evidence was lacking. Later work by Lappert in 2004

using silylene **B** and either Me_3SiN_3 and Ad-N_3 also suggested the formation of a silatetrazoline. However, a different intermediate to the iminosilane was proposed. Two equivalents of the silylene to one equivalent of Ad-N_3 or Me_3SiN_3 resulted in a material the authors suggested to be a 1,3-disila-2-azacyclopropane derivative evidenced by NMR spectroscopy and elemental analysis.

It was not until 2005 structural evidence was obtained for the silatetrazoline product from these reactions. Phenylazide and silylene **A** resulted in the corresponding silatetrazoline which could be crystallised from hexane. The structure displays a spirocyclic silicon centre with two orthogonal rings. The differing products obtained, either a silatetrazoline or azidoamidosilane, can be attributed to the sterics of the organic azides used. The bulkier Ad-N_3 and PhN_3 prepare the silatetrazoline to relieve the steric clash that would be present in the formation of the azidoamidosilane that forms on reaction with Me_3SiN_3. Two different intermediates are possible for the formation of these compounds: the iminosilane LSi=NR or the 1,3-disila-2-azacyclopropane, LSi(μ_2-NR)SiL. Scheme 6.1 summarises the products identified from these reactions.

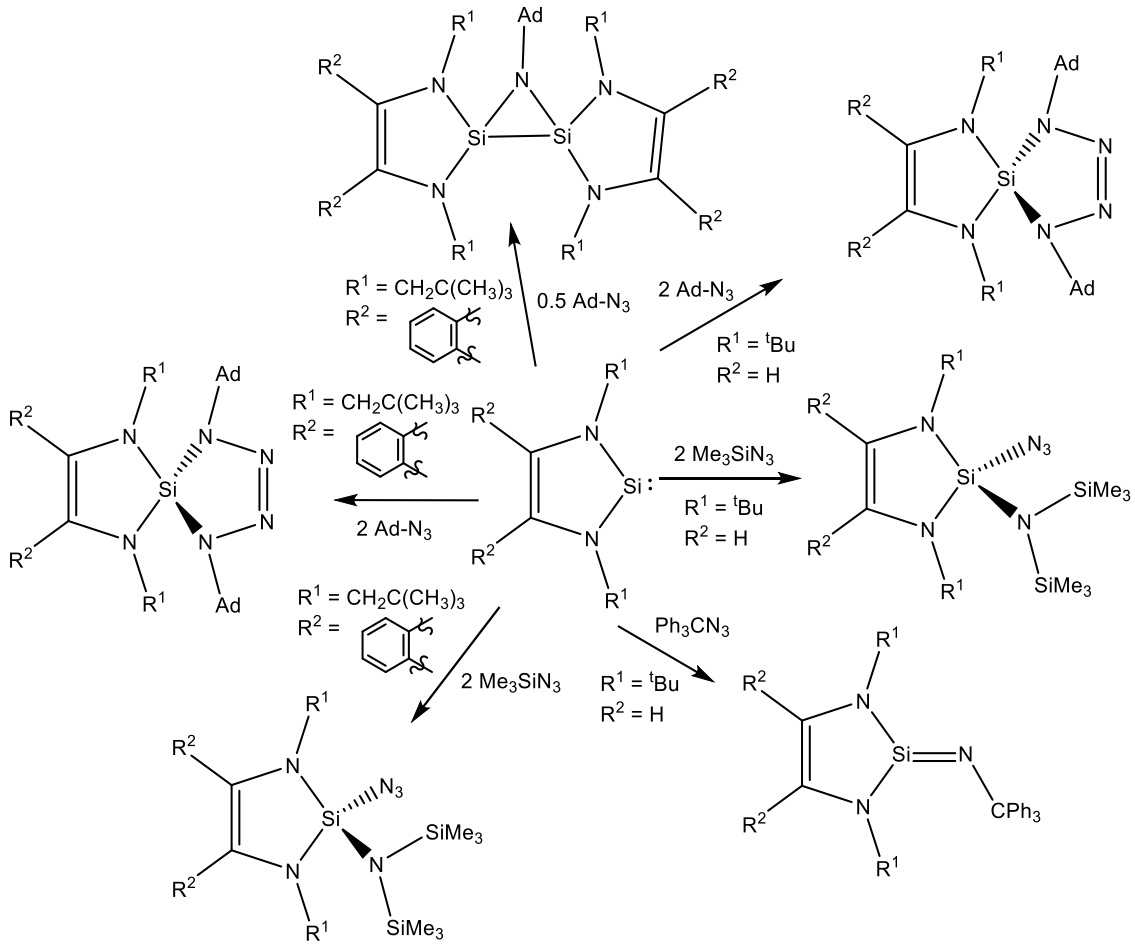

Scheme 6.1. Reactions of N-heterocyclic silylenes with covalent azides.

Silylene **C**, in Figure 6.1, is noticeably different to the other silylenes discussed and that is the compound is a precursor for $SiCl_2$. The only reports concern the reactivity of silylene **C** with the organoazides Ad-N_3, Ph_3CN_3, Dipp-N_3 and 2,4,6-triisopropylphenylazide (Triip-N_3). The latter three give silaimines with loss of N_2 whereas Ad-N_3 results in the functionalisation of the NHC.[80] The reaction between silylene **C** and Ad-N_3 is assumed to pass through an iminosilane intermediate which abstracts a proton from the imidazole backbone before rearranging to give the molecule shown in Figure 6.2. The NHC is coordinated to the silicon in what is known as the abnormal coordination mode of an NHC, the C4 or C5 site of the NHC. Abnormal NHC coordination is rare among the *p*-block elements, especially when the C2 site is not blocked or coordinated to a metal centre.

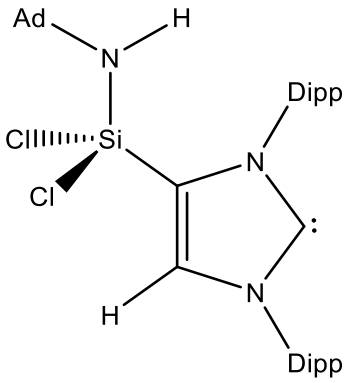

Figure 6.2. Diagram of the product obtained from the reaction of $IPrSiCl_2$ and Ad-N_3.

All of the above reactions involve the reduction of organoazides using Si(II), which is in turn oxidised to Si(IV). Other reducing agents have been used with organoazides and instead of eliminating N_2 the azido groups are reductively coupled together to produce N_6 chains, hexazenes.[49–52] The first of which was an iron hexazene prepared in 2009 by Holland *et al*. using a dimeric diketiminate iron(I) dinitrogen complex. Further examples of reducing agents include diketiminate magnesium(I) dimers and diketiminate zinc(I) dimers. Figure 6.3 summarises the known hexazene complexes prepared by reductive coupling of azido ligands.

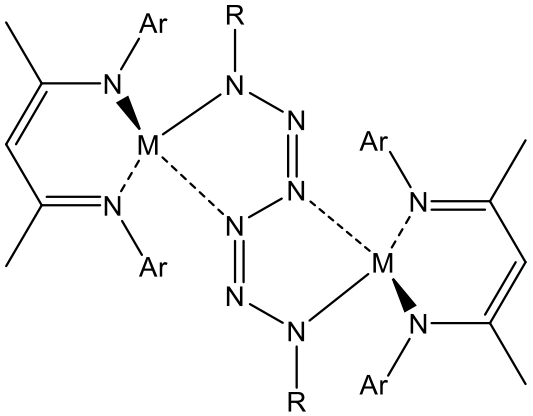

M = Mg; R = Ad; Ar = Mes, Dipp
M = Zn; R = Ph, Dipp; Ar = Mes
M = Fe; R = Ad; Ar = Dipp

Figure 6.3. Known metal hexazene complexes.

In all the complexes shown in Figure 6.3, the metal centre has a distorted tetrahedral geometry from two different bidentate ligands. The hexazene ligand is planar and acts as a four electron donor with two negative charges towards two metal centres forming a bicyclic M_2N_6 unit. The (^{R}Nacnac)Zn(I) dimer has also been used to reduce trimethylsilyl azide and trimethylstannyl azide. In both cases the azido group was not

reduced, but, rather the silicon or tin atom giving hexamethyldisilane or hexamethyldistannane and (^{R}Nacnac)ZnN_3.

It is clear that the azido group can be reduced with loss of dinitrogen gas to give a variety of different products. Attempts to reduce a polyazido silicon(IV) species offers a number of potential reaction sites for the reduction to take place. Third row low valent coordination centres, such as phosphorus and silicon, are highly reactive species and prompted an investigation into the attempted preparation of Si(II) and P(I) azido complexes.

6.2 Results and discussion

6.2.1 Salt metathesis of the Si(II) halides IPrSiX_2

Two methods have been devised to prepare a Si(II) azido complex: (i) salt metathesis reaction between a Si(II) halide and sodium azide; (ii) reduction of an appropriate Si(IV) azido complex. Traditionally, salt metathesis reactions involving an ionic azide transfer agent require a polar solvent such as THF or acetonitrile. Solvents that are potentially unsuitable as Si(II) is known to undergo bond insertion reactions with polar bonds. Despite this, the reaction of IPrSiI_2 and IPrSiCl_2 with sodium azide was attempted using either THF or benzene as solvents, Scheme 6.2.

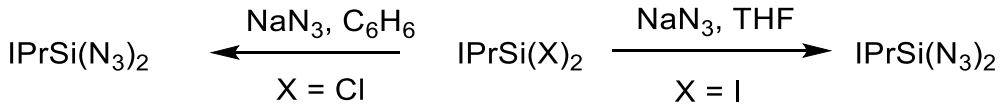

Scheme 6.2. Proposed reaction scheme for salt metathesis reaction to prepare IPrSi$(N_3)_2$.

A suspension of sodium azide and IPrSiI_2 in THF in a 20:1 ratio results in an orange suspension over a period of 24 hrs. The FT-IR spectrum of this solution displays one band between 2000 and 2200 cm^{-1} at 2152 cm^{-1}. The presence of a single band in the $\nu_{as}(N_3)$ region reduces the likelihood that IPrSi$(N_3)_2$ is present, as such species would be expected to have two bands present similarly to IPrGe$(N_3)_2$.[158] More evidence for the unlikeliness of synthesising the desired compound is that the absorption is at a relatively high wavenumber. Reduction from a E(IV) azide to a E(II) azide results in a decrease of the stretching frequency as seen between $[Ge(N_3)_6]^{2-}$ and $[Ge(N_3)_3]^{-}$ (2083 cm^{-1} to 2058 cm^{-1} and a weaker band at 2092 cm^{-1}). The presence of a band at 2152 cm^{-1} suggest a

Si(IV) centre, which implies the Si centre is oxidised over the course of the reaction. It is possible the Si(II) centre reacts with THF, however, there is a distinct possibility that $IPrSi(N_3)_2$ would decompose with elimination of dinitrogen to form $IPrSi(N_3)(\mu^2\text{-}N)_2Si(N_3)IPr$ as a possible product akin to the reactions shown in Scheme 6.1. The reaction solvent was changed to benzene to eliminate any potential reaction with solvent. The Si(II) halide was also changed to $IPrSiCl_2$ as it is easier to prepare this compound in larger quantities.

$IPrSiCl_2$ and 10 equivalents of sodium azide were suspended in benzene and stirred for several days. The FT-IR spectrum of this solution showed weak signals in the $\nu_{as}(N_3)$ region indicating that the product of the reaction is only sparingly soluble in benzene. The strongest peak appeared at 2014 cm^{-1}, indicative of the ionic azide $(IPrH)N_3$ a by-product of hydrolysis, and two weaker peaks 2086 and 2102 cm^{-1}, possibly the desired $IPrSi(N_3)_2$, and another peak at 2154 cm^{-1}. The peak at 2154 cm^{-1} appears at a similar position to the band observed in the THF experiment suggesting the same product is formed in both the THF and benzene experiments. Both of these reactions point to the transfer of the azido ligand to the Si centre, though no silicon containing product has been obtainable so far.

6.2.2 Main Group azido complexes: Precursors for reduction reactions

6.2.2.1 Syntheses and spectroscopy

To reduce a Main Group azido complex an appropriate azido complex with the correct ancillary ligand has to be prepared. The most common Lewis base stabilised azido complexes contain pyridyl type ligands, such as 2,2'-bipyridyl, 1,10-phenanthroline and *para*-dimethylaminopyridine as examples.[54,56,173,184] These ligand choices are not ideal for the preparation of low valent complexes as they lack the appropriate steric bulk and electronic factors usually required. Three types of ligands that are suitable are N-heterocyclic carbenes, amidinato and β-diketiminato ligands, Figure 6.4. N-heterocyclic carbenes are ideal candidates, however, it is known that NHCs react with covalent azides. Organic azides react with NHCs to give asymmetric triazenes, while Me_3SiN_3 reacts with NHCs *via* a Staudinger type reaction to give

imidazolin-2-imidosilanes.[185–189] An investigation was made regarding the reactivity between IPr and 1,3-di-*tert*-butyl-imidazol-2-ylidene (I^{t}Bu) with $Si(N_3)_4$ and $NaP(N_3)_6$.

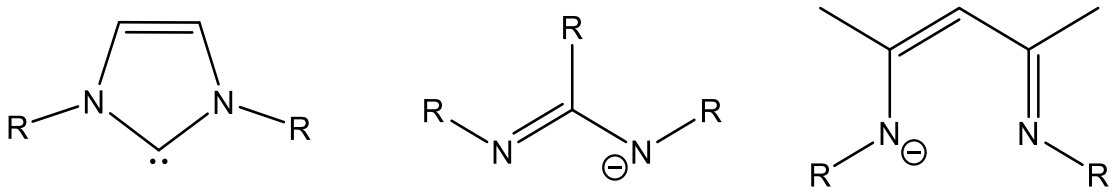

Figure 6.4. Basic structure of NHC, amidinato and β-diketiminato ligands (Nacnac). R is often bulky alkyl or aromatic groups.

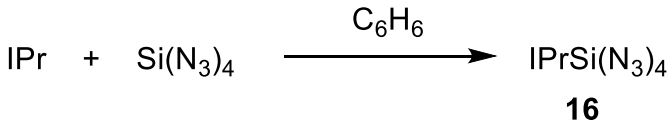

Scheme 6.3. Reaction scheme for the synthesis of $IPrSi(N_3)_4$.

Addition of $Si(N_3)_4$ to one equivalent of IPr results in the precipitation of an off-white solid within minutes. The FT-IR spectrum of the solid as a nujol mull shows four distinct bands in the $\nu_{as}(N_3)$ region at 2150, 2134, 2118 and 2102 cm^{-1}. In between the IR spectral position of $Si(N_3)_4$ (2174 cm^{-1}) and $[Si(N_3)_6]^{2-}$ (2108 cm^{-1}). The presence of four bands indicates four azido groups, either symmetrically independent or two groups of two azides related by symmetry. Regardless of which, the product can be identified as $IPrSi(N_3)_4$ (**16**). As the silicon atom has a coordination number of five, the most likely geometry is trigonal bipyramidal and the IPr ligand can sit in either the equatorial or the axial plane. Due to the large steric demand of the IPr ligand it would be assumed the ligand would reside in the equatorial plane. In the $IPrSiX_4$ series (X = Cl, Br, I) the IPr ligand is located in the equatorial site.[190] As the $Si{-}N_{ax}$ bonds should be longer than the $Si{-}N_{eq}$ the effective result would be this bond is slightly more ionic in nature. If this is correct, a tentative assignment can be made that the bands at 2118 and 2102 cm^{-1} in the FT-IR spectrum are due to the vibrations of the axial azido ligands and the bands at 2150 and 2134 cm^{-1} are due to the vibrations of the equatorial azido ligands. The FT-IR spectrum of a benzene solution of **16** displays four bands at 2153, 2139, 2120 and 2111 cm^{-1}. However, as a trigonal bipyramidal molecule there is possibility for Berry pseudo rotation (BPR) rendering all azido groups equivalent in solution. To determine if BPR is a possibility the ^{1}H-NMR spectrum in CD_2Cl_2 was recorded, as shown in Figure 6.5.

One possible point group of **16** is C_2, the other most likely point group being C_1. The expected number of resonances, if **16** is C_2 symmetric, would be ten as is observed in the spectrum in CD_2Cl_2. The ^{1}H NMR spectrum of **16** shows four doublets between 1.0 and 1.5 ppm, two septets at 2.67 and 2.76 ppm, a doublet at 7.20 ppm, and multiplets between 7.36 and 7.60 ppm. The other peaks present are residual solvent, silicone grease and the imidazolium cation from hydrolysis. The fact only one set of signals are present either implies there is no BPR or the phenomenon is faster than the NMR timescale. In the ^{19}F NMR of $IPrSiF_4$ a singlet is observed even at temperatures as low as −78°C implying a very fast exchange process.[190] The azido ligand is significantly larger than fluorine, however, the NHC acts as an anchor and can allow the process to happen rapidly.

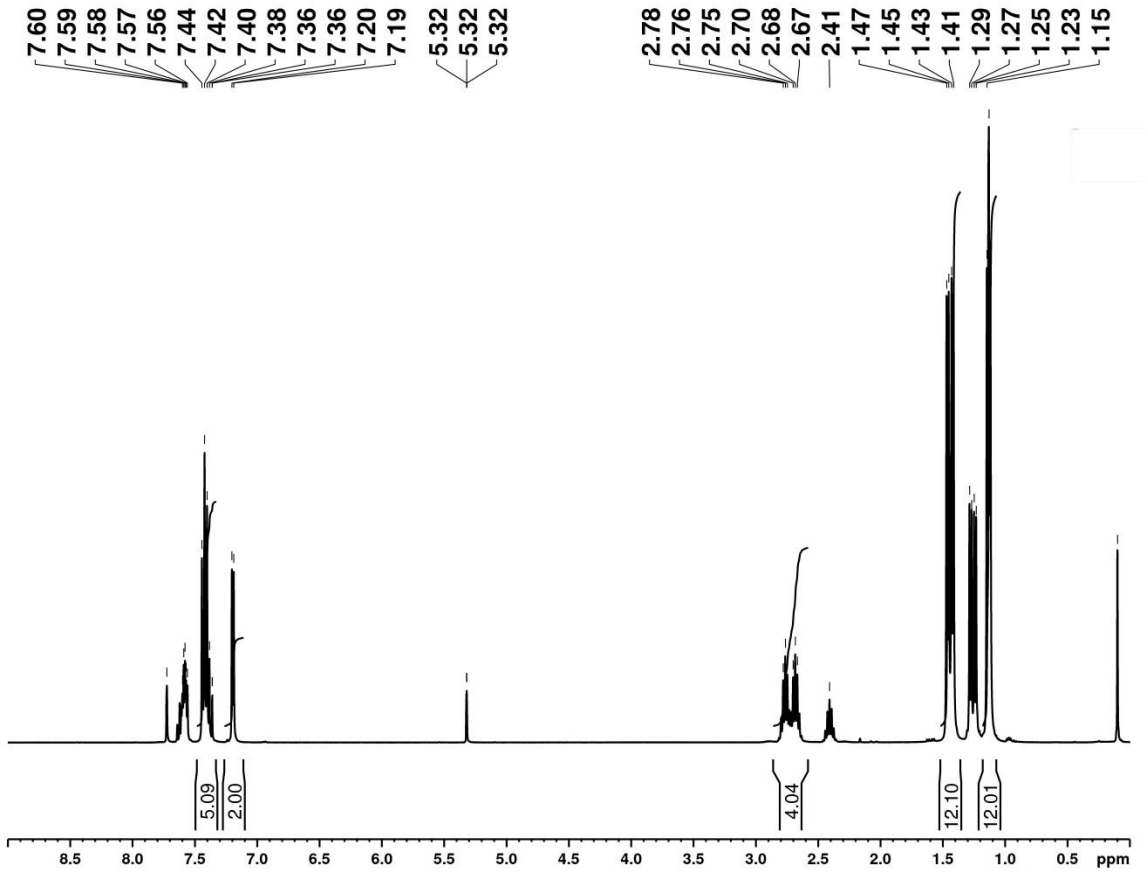

Figure 6.5. ^{1}H-NMR spectrum of **16** in CD_2Cl_2. The signal at 5.32 ppm is the solvent residual peak of CH_2Cl_2. The peak at 0.1 ppm is silicone grease. The other non-integrated peaks are the imidazolium cation produced by hydrolysis of **16** on sample measurement.

The ^{14}N NMR spectrum of **16** would be more indicative of any fluxionality. In the ^{14}N NMR spectrum only two resonances are observed at −146 (FWHM = 173 Hz) and

−201 ppm (FWHM = 368 Hz) for N(β) and N(γ) respectively. No signal is observed for the N(α) resonance in the spectrum. Fluxionality of the molecule would result in the broadening of a typically broad signal and could explain as to the reason for not observing the N(α) resonance. The resonance for the NHC nitrogen atom is typically a broad signal and masked by the N(γ) resonance. There is no ^{14}N NMR data on other charge-neutral Lewis base stabilised $Si(N_3)_4$ complexes, most likely due to their poor solubility, and so a comparison can only be made with $Si(N_3)_4$ and the $[Si(N_3)_6]^{2-}$ anion. The tetrahedral molecule has N(β) and N(γ) resonances of −150 and −189 ppm and the octahedral molecule has a N(γ) resonance of −215 ppm. The value of N(β) of $[Si(N_3)_6]^{2-}$ is obscured by the resonance for acetonitrile, the solvent used for the measurement, therefore the resonance appears around −135 ppm. Similarly with the IR spectroscopic data, the NMR resonances for **16** fall in between those of $Si(N_3)_4$ and $[Si(N_3)_6]^{2-}$. This trend can be explained by the degree of covalency of the Si−N bond. The Si−N bond in $Si(N_3)_4$ has the highest degree of covalency and on increasing the coordination number from four coordinate to five coordinate to six coordinate decreases the covalency of that bond.

This method prepares $IPrSi(N_3)_4$ in very high yields, however, a low quantity of product is obtained due to the limiting amount of $Si(N_3)_4$ that can be used. $Si(N_3)_4$ can only be prepared as a dilute solution in benzene, due to its high shock sensitivity, in a time-consuming synthesis with strict exclusion of air and moisture. Therefore, an alternative procedure to prepare $IPrSi(N_3)_4$ *via* $IPrSiCl_4$ was attempted. $IPrSiCl_4$ was prepared according to a published procedure and suspended with sodium azide in dichloromethane.[73]

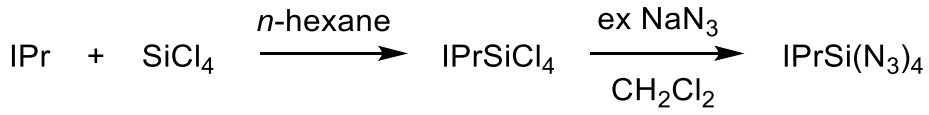

Scheme 6.4. Proposed alternative synthesis of **16**.

After 5 days of stirring a pale green solid was isolated which displays only three bands in the $\nu_{as}(N_3)$ region indicating incomplete azide/chlorine exchange, which is common when the solvent used is dichloromethane. Acetonitrile and THF are more commonly used for azide exchange, however, acetonitrile causes dissociation of **16** to $Si(N_3)_4$ and IPr. Therefore, the $Si(N_3)_4$ reacts with sodium azide to form $Na_2Si(N_3)_6$. In

THF there is evidence of azide exchange by IR spectroscopy of the reaction solution, however, exchange is incomplete. After longer reaction times, several days, or raising the temperature of the suspension the IR spectrum only displays $[Si(N_3)_6]^{2-}$ suggesting over time some degree of dissociation must occur and the formation of $Na_2Si(N_3)_6$ acts as a thermodynamic sink.

Compound **16** is an ideal candidate for investigating the reduction chemistry of Si(IV) azides, as the NHC would potentially stabilise the Si(II) centre. The properties of NHCs differ depending on the R-group attached to the nitrogen atoms of the NHC. The *tert*-butyl group is a stronger σ-donor compared to the 2,6-diisopropylphenyl group increasing the nucleophilicity of the NHC. Consequently, a reaction may occur with the azido groups instead of coordination to the silicon centre. Bubbles form on the addition of $Si(N_3)_4$ to I^{t}Bu. The FT-IR spectrum of the solution shows two bands in the $\nu_{as}(N_3)$ region at 2144 and 2117 cm^{-1} and two strong bands at 1713 and 1645 cm^{-1}, in the ν(C=N) region, as well as a signal for unreacted $Si(N_3)_4$. A further equivalent of I^{t}Bu was added and further effervescence was observed. The FT-IR spectrum of this solution showed the same bands as the previous spectrum and no $Si(N_3)_4$. Bubble formation is from the elimination of N_2 gas from the reaction of I^{t}Bu with the azido group of $Si(N_3)_4$, analogous to the Staudinger reaction with phosphines and organoazides.[191] Large, colourless needle crystals can be obtained by recrystallization of the crude product from toluene. Combining the data from the FT-IR spectrum and stoichiometry with the production of dinitrogen gas gives the identity of $(I^tBu{=}N)_2Si(N_3)_2$ (**17**).

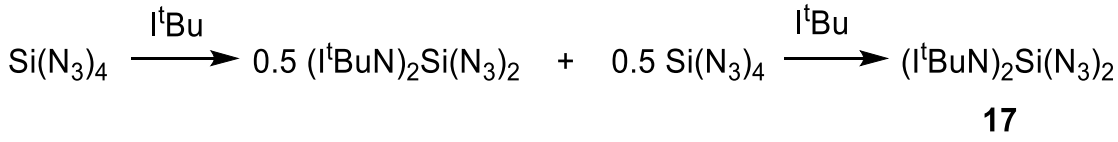

Scheme 6.5. Reaction scheme for the synthesis of **17**.

The ^{1}H NMR spectrum in $CDCl_3$ of **17** displays two singlets at 1.57 and 6.34 ppm for the t-butyl group and imidazolium backbone respectively, therefore **17** has C_2 symmetry. The peak of the backbone protons is more shielded than those in free I^{t}Bu (7.16 ppm). The ^{15}N NMR spectrum of **17** was recorded as a solid state sample. Six resonances are observed at 236, 168, 160, 159, 113 and 71 ppm, Figure 6.6. Assignment of the signals has currently not been possible.

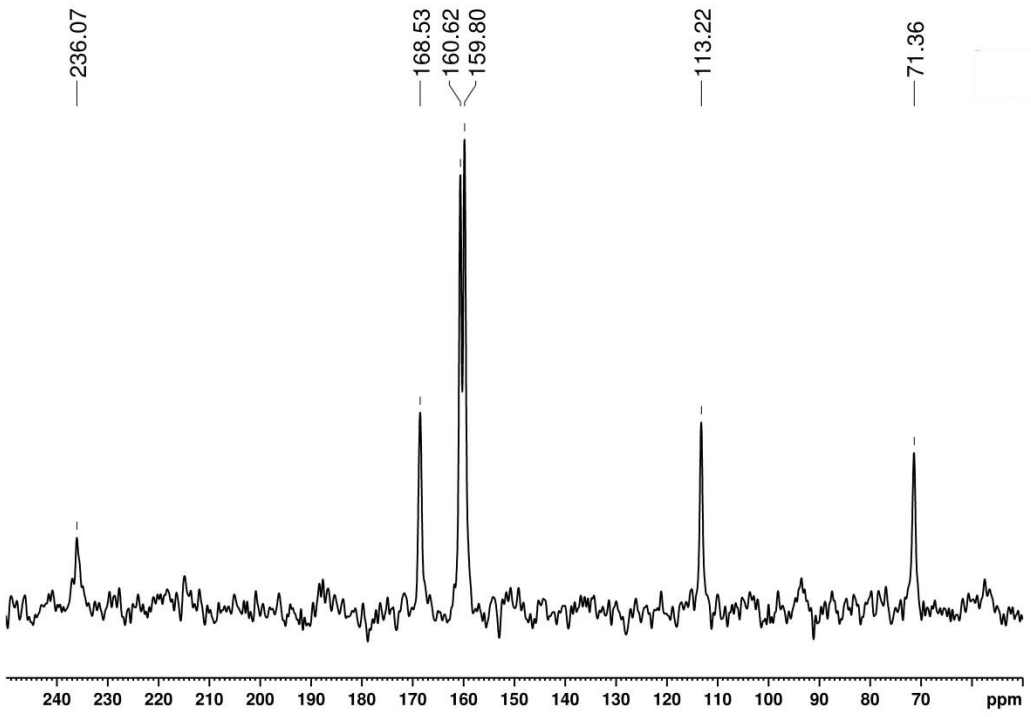

Figure 6.6. Solid state ^{15}N NMR spectrum of **17**.

Clearly, the reactivity varies depending on the NHC, however, it also offers some insight into the reactivity of silicon tetraazide in comparison with Me_3SiN_3. IPr reacts with Me_3SiN_3 in this N_2 elimination reaction but not with $Si(N_3)_4$. The formation of a Lewis acid-base adduct implies $Si(N_3)_4$ is a stronger Lewis acid than Me_3SiN_3, as expected. The addition of methyl groups to the silicon centre results in a decrease in Lewis acidity and, therefore, the NHC is more likely to react at the azido group. It is unclear if the mechanism is *via* coordination of the NHC to the silicon centre followed by subsequent attack on the azido group or directly attacks the azido group as is proposed for the Staudinger reaction.[192] Regardless, in terms of potential reduction chemistry only **16** is a viable candidate as it possesses a coordinated NHC.

Low valent complexes of phosphorus are equally interesting species as low valent silicon, however, less work on the reactivity of such compounds is in the literature.[72] Phosphazenes are a versatile class of compounds and have found a variety of applications from non-stick coatings to fire retardant materials.[193–196] Phosphorus azides offer a potential new route for phosphorus nitrogen bond forming reactions and adding to that a reduced phosphorus species could result in unique and new chemistry. The main difference between silicon and phosphorus are the two easily accessible oxidation

states for phosphorus, P(III) and P(V). The previous synthesis applied for **16** is not applicable for the synthesis of IPrP$(N_3)_5$ as $P(N_3)_5$ is an unknown compound. The binary P(III) azide, $P(N_3)_3$, is known and offers a viable starting point.[197]

PCl_3 and sodium azide suspended and stirred in acetonitrile for two days gives a solution that displays a very broad signal in the FT-IR spectrum at 2164 cm^{-1} and a peak at 2138 cm^{-1} which corresponds to HN_3 from hydrolysis in sample measurement. When this solution is added to IPr a turbid, oily, red solution is formed. The FT-IR spectrum of this solution displays two bands at 2152 cm^{-1} and 2005 cm^{-1}, indicating the presence of both covalent and ionic azido groups. Figure 6.7 shows an overlay of the two solution spectra from this reaction. After several attempts of crystallisation in a variety of solvents only a deep red oil could be obtained. The presence of the ionic azide could be due to imidazolium azide formed from the reaction of IPr and HN_3. Though HN_3 was present in the FT-IR spectrum of the $P(N_3)_3$ solution, there is not enough present to account for the size of the ionic peak in the second spectrum. Another possibility is that the NHC displaces an azido group from $P(N_3)_3$ giving the positively charged species, $[IPrP(N_3)_2]^+$, with an azide anion acting as the counterion. A similar cation has been previously prepared and fully characterised by Weigand and co-workers in 2015 where the NHC used was 1,3-bis(dipp)-4,5-dichloroimidazol-2-ylidene and the counterion was a triflate anion, $[(NHC)P(N_3)_2](F_3CSO_3)$.[198] No other evidence was obtained for the identity of the red oil.

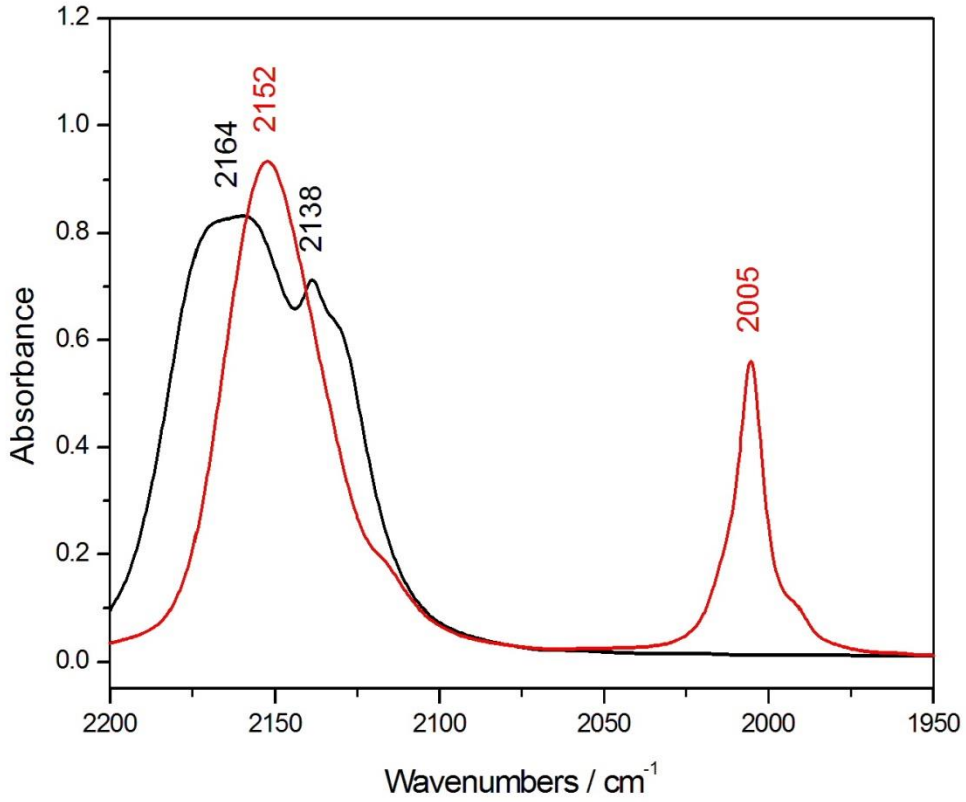

Figure 6.7. FT-IR spectra of an acetonitrile solution of $P(N_3)_3$ and after IPr was added to the solution. Black line is $P(N_3)_3$ in MeCN. Red line is $P(N_3)_3$ and IPr in a 1:1 ratio in MeCN.

With no success in preparing $IPrP(N_3)_3$, the synthesis of the P(V) analogue, $IPrP(N_3)_5$, was attempted but as $P(N_3)_5$ is unknown a different method had to be used. $NaP(N_3)_6$ can be easily prepared as an acetonitrile stock solution from the reaction between PCl_5 and sodium azide in acetonitrile, though care must be taken as it is a highly moisture sensitive compound.[199] Addition of this solution to IPr results in the precipitation of sodium azide and $IPrP(N_3)_5$ (**18**), the first example of a charge-neutral Lewis adduct of $P(N_3)_5$. The desired compound can be extracted and crystallised using THF. After filtration of the solvent the crystals begin to degrade within 1 hr to white blocks, though there is no decomposition of the compound.

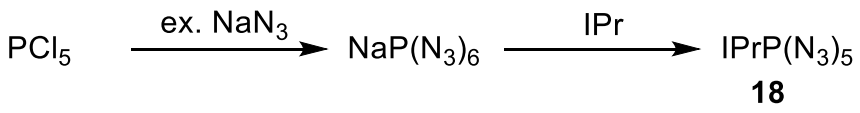

Scheme 6.6. Reaction scheme for the synthesis of **18** by-products omitted.

The FT-IR spectrum of the material displays four bands corresponding to the $\nu_{(as)}N_3$ vibration at 2138, 2126, 2114 and 2080 cm^{-1}, lower than that observed for **16**.

Phosphorus azides often have slightly higher wavenumber values for the $\nu_{as}(N_3)$ than their analogous silicon counterparts, e.g. $[Si(N_3)_6]^{2-}$ and $[P(N_3)_6]^-$ appear at 2104 and 2112 cm^{-1} respectively. The asymmetric and symmetric vibrations of the azido group is affected by the bond between the element acting as a coordination centre and the nitrogen atom and thus the geometry of the overall complex, as described earlier. Therefore, the $\nu_{(as)}N_3$ vibration of the trigonal bipyramidal $IPrSi(N_3)_4$ will appear at a slightly higher wavenumber compared to the octahedral $IPrP(N_3)_5$.

The ^1H and ^{13}C NMR spectra show the expected resonances for the IPr ligand. A singlet at −199 ppm is observed in the ^{31}P NMR spectrum. This value is upfield compared to the ^{31}P resonance of the $[P(N_3)_6]^-$ anion (−178 ppm, CD_3CN), and the cyclic P(V) azides (*cyclo*-$[NP(N_3)_2]_3$) (13.6 ppm, C_6D_6) and {*cyclo*-$P(N_3)_3(NPh_2)\}_2$ (−87 ppm, CD_2Cl_2).[19,200] An NMR study of the reaction between $(py)PCl_5$ and lithium azide was carried out in 1981.[201] Stoichiometric quantities of lithium azide were added to demonstrate the stepwise exchange of chloro ligands with azido ligands. No signal for $(py)P(N_3)_5$ was observed in the study, however, a value was calculated by extension of the series $(py)PCl_{5-x}(N_3)_x$ (x = 0-4) of −189 ppm. Not too dissimilar to the signal observed for **18**. The ^{14}N NMR spectrum of **18** is shown in Figure 6.8. Some of the peaks are not uniform. To gain insight into the position and FWHM of the peaks a Lorentzian curve was fitted to the raw data, Figure 6.9.

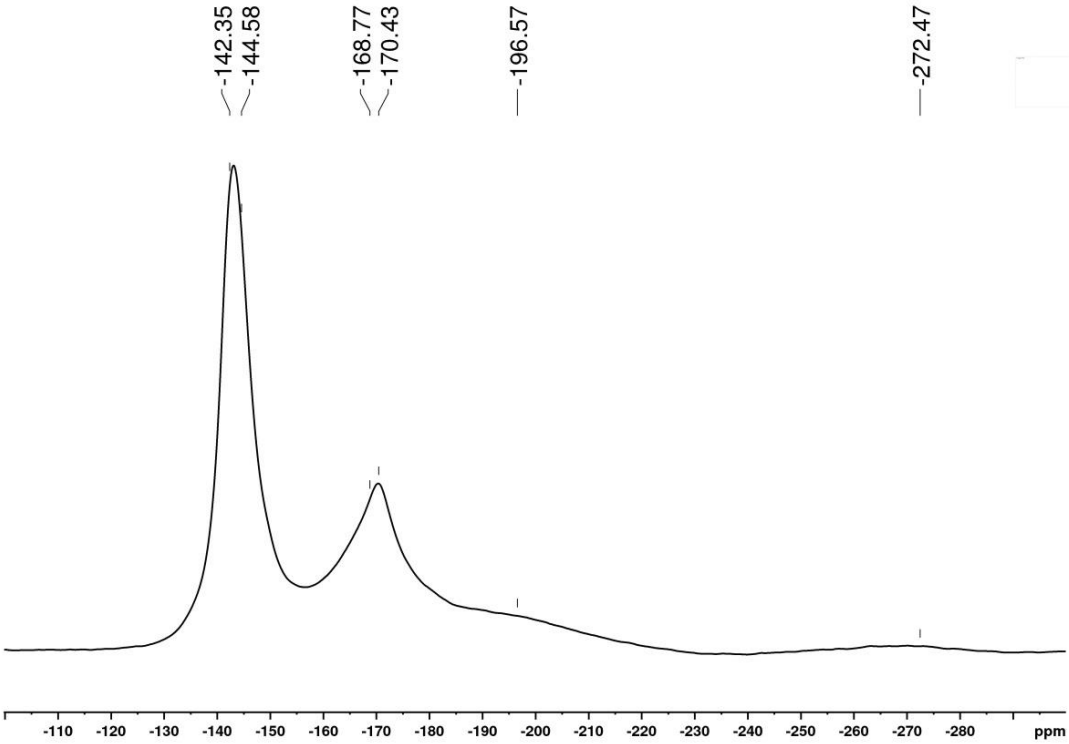

Figure 6.8. ^{14}N NMR spectrum of **18** in CD_2Cl_2. Peak labels determined from peak fitting shown in Figure 6.9.

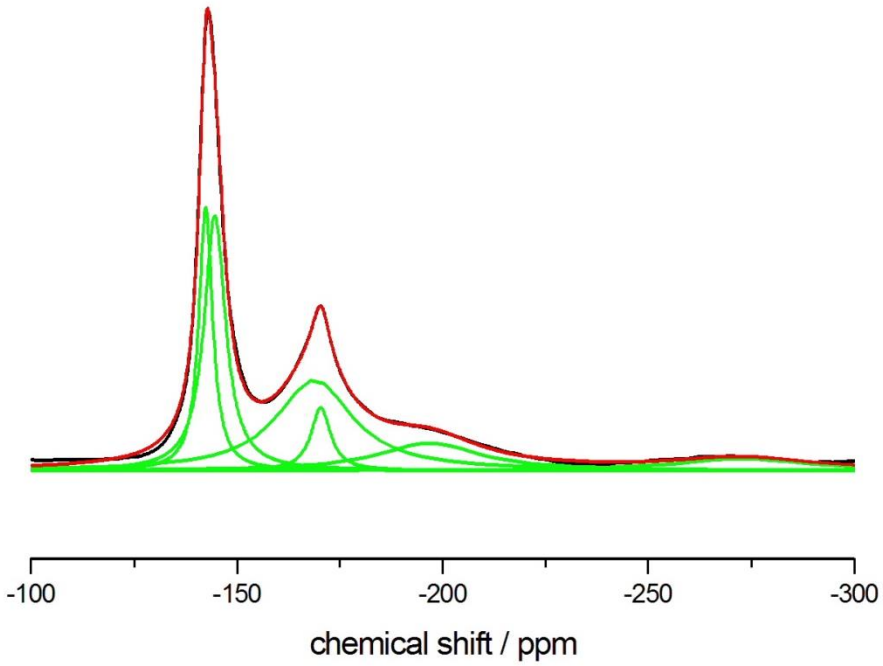

Figure 6.9. Lorentzian curve fitting plot of the ^{14}N NMR data of **18**. Black line is the NMR spectrum. Green lines represent the model of each peak. Red line is the sum of all green lines.

Peak position / ppm	FWHM / Hz
−142	115
−144	181
−168	651
−170	166
−196	865
−272	1159

Table 6.1. ^{14}N NMR data for compound **18** as determined by fitting a Lorentzian curve to the original spectrum.

From the curve fitting analysis, there are six resonances observed for compound **18** in the ^{14}N NMR spectrum. Two N(β) and two N(γ) signals at −142 and −144, and −168 and −170 ppm respectively. The size of the signal at −170 ppm is much smaller than the peak at −168 ppm suggesting this resonance belongs to the azido group *trans* to the NHC. Whereas the −168 ppm signal is due to the four equivalent azido groups *cis* to the IPr ligand. The resonance at −196 ppm is due to the nitrogen atom of the NHC,[202] and the final resonance at −272 ppm is due to the N(α) of the azido groups. Only one signal is present for N(α). Most likely the N(α) of the azido group *trans* to the NHC is missing and hidden due to the broadness of the other N(α) signal present.

As well as a potential reduction candidate, **18** may be a source for $P(N_3)_5$, an unknown compound. It was originally described as the product from the reaction between PCl_5 with sodium azide in acetonitrile, however, that was later disproven and the product of that reaction is $NaP(N_3)_6$. The reaction of PCl_5 towards lithium azide in $PhNO_2$ resulted in the formation of cyclophosphazenes and the conclusion was that a Lewis base is required to stabilise $P(N_3)_5$. A sample of **18** was evacuated in a Schlenk tube and heated to 150°C in an oil bath at which a sudden decomposition occurred accompanied with a high-pitched popping sound and the formation of a sticky brown residue. The residue displayed no azide bands in the FT-IR spectrum as a nujol mull. The chemical reactivity of **18** towards HN_3, $(PPN)N_3$, H_2NCN, pyridine and ethereal HBF_4 was investigated.

Addition of ethereal HN_3 to a sample of **18** dissolved in THF displayed a single band in the $\nu_{(as)}N_3$ region at 2112 cm^{-1} indicative of the $[P(N_3)_6]^-$ anion. Imidazolium acts as the counterion, formed on protonation of IPr. $(PPN)N_3$ and **18** were combined in acetonitrile, due to the insolubility of $(PPN)N_3$ in THF, and similarly the IR spectrum of

the solution displayed a single band for the $[P(N_3)_6]^-$ anion. Cyanamide, H_2NCN, is a diprotic molecule that has been used as a bridging ligand between two coordination centres.[203–206] In theory, cyanamide could bridge between two $P(N_3)_5$ molecules forming a dianion with two imidazolium counterions, $(IPrH)_2[(N_3)_5P{-}N{=}C{=}N{-}P(N_3)_5]$. However, on combining **18** with cyanamide in THF results in the loss of the cyanamide signal at 2250 cm^{-1} and the most dominant peaks were that of HN_3 and $[P(N_3)_6]^-$. Demonstrating that the cyanamide is a strong enough acid to protonate both IPr and the azido groups.

The reaction between ethereal HBF_4 and **18** in dichloromethane was also investigated. If the HBF_4 protonated IPr to give $(IPrH)BF_4$ this relatively inert species would unlikely act as a Lewis base and release $P(N_3)_5$. The FT-IR spectrum of the reaction solution displayed four bands in the $\nu_{as}(N_3)$ region at 2188, 2174, 2156 and 2137 cm^{-1} the latter peak being the result of the presence of HN_3. Again, it appears that the azido group is protonated, however, it would not be possible to determine if the IPr had been removed by solution cell IR spectroscopy. However, the high wavenumbers imply an azido complex with a low coordination number. After cooling at −28°C overnight colourless block crystals were obtained. The crystals immediately degraded on removal of the solvent to a white solid making it very difficult to obtain good single crystal X-ray diffraction data. As a result crystallographic data could not be obtained to determine the structure of this compound. The compound was identified as $IPrPF_5$ by ^{31}P and ^{19}F NMR spectroscopy, the spectra shown in Figures 6.10 and 6.11. The ^{31}P NMR spectrum of this material in $CDCl_3$ displays an overlapping doublet of quintets at −149 ppm with $^1J_{PF}$ of 757 and 790 Hz. Whereas the ^{19}F NMR spectrum shows two peaks: a doublet of doublets at −52 ppm with $^2J_{FF}$ of 56 and $^1J_{PF}$ of 790 Hz for the four F atoms *cis* to IPr and a doublet of quintets at −76.5 ppm with $^2J_{FF}$ of 56 and $^1J_{PF}$ of 757 Hz for the F atom *trans* to IPr. Therefore, the reaction of $(IPr)P(N_3)_5$ and HBF_4 results in an azide/fluoride exchange giving $IPrPF_5$, $HB(N_3)_4$ and HN_3 as products of the reaction.

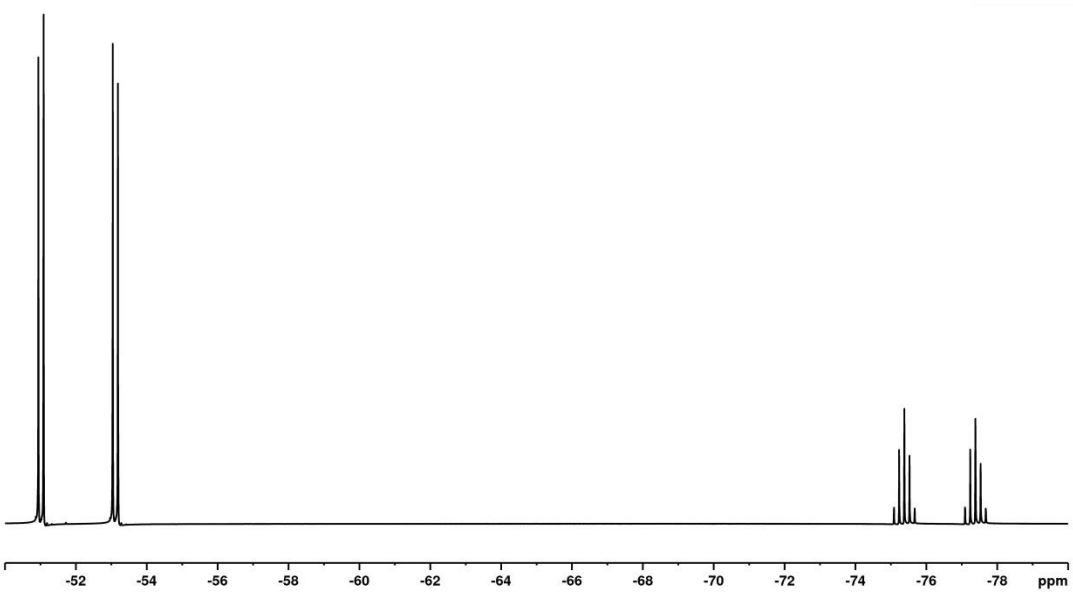

Figure 6.10. ^{19}F NMR spectrum of $IPrPF_5$.

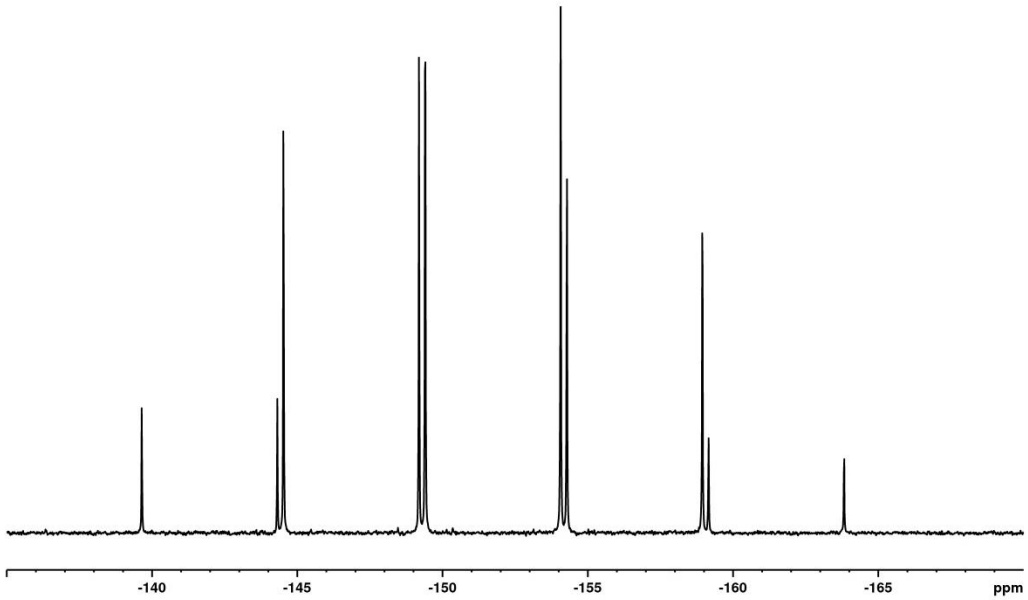

Figure 6.11. ^{31}P NMR spectrum of $IPrPF_5$.

An attempt to replace the NHC from **18** with pyridine was investigated by dissolving a small amount of **18** in pyridine. The solution over a period of 24 hrs had turned orange. The FT-IR spectrum of the solution displayed three signals. A very weak signal at 2124 cm^{-1}, which belongs to HN_3, a signal at 2113 cm^{-1}, most likely the $[P(N_3)_6]^-$ anion, and a signal at 2136 cm^{-1}. If pyridine displaces IPr and forms $(py)P(N_3)_5$, the presence of $[P(N_3)_6]^-$ in the IR spectrum indicates that $(py)P(N_3)_5$ is not the complex observed in solution. The complex could potentially be $[(py)_2P(N_3)_4]P(N_3)_6$ in solution

to account for the FT-IR spectrum. The $[(py)_2P(N_3)_4]^+$ component giving rise to the band at 2136 cm^{-1}. The ^{31}P NMR of **18** in d_5-pyridine displays two signals at −197 and 22 ppm. The signal at −197 ppm is only two ppm upfield of **18** in CD_2Cl_2, however, the resonance at 22 ppm is a possible indication of a phosphonium cation. From the Bruker Almanac $[PCl_4]^+$ has a resonance of 86 ppm in an unspecified solvent. All attempts to crystallise from the solution were unsuccessful, only giving oils. Therefore, the result still remains inconclusive.

IPr eliminates sodium azide from $NaP(N_3)_6$ in acetonitrile. To investigate whether pyridine does the same elimination reaction, an acetonitrile solution of $NaP(N_3)_6$ was added to an equivalent volume of pyridine. No precipitation was observed after several hrs of stirring and after cooling to −28°C overnight colourless needle crystals were present in the solution. The FT-IR spectrum of the crystals as a nujol mull displayed two signals between 2200 and 2000 cm^{-1} at 2146 and 2125 cm^{-1}. Considerably different to that of **18**, which has four bands in the FT-IR spectrum, and $(PPN)P(N_3)_6$, which has a single band in the FT-IR spectrum at 2113 cm^{-1}. As there was no sodium azide observed when the $NaP(N_3)_6$ was added to pyridine the identity of the crystals was most likely $NaP(N_3)_6$. Therefore, a crystal was very carefully removed from the solution and analysed by single crystal X-ray diffraction. The identity of the crystal was determined to be $NaP(N_3)_6{\cdot}6py$ (**19**). The structure of which is fully discussed later in **6.2.2.2**, however, one interesting feature is the point group of the $[P(N_3)_6]^-$ anion is S_6. This accounts for the multiple bands observed in the FT-IR spectrum, as the $[P(N_3)_6]^-$ anion in $(PPN)P(N_3)_6$ displays a single band at 2113 cm^{-1} and has C_i symmetry.

Rather than NHCs, another suitable ligand for the stabilisation of low valent coordination centres is the amidinato type ligand, ^{dipp}NCN, a bulky, monoanionic bidentate ligand with a small bite angle (approximately 68°). Bonded to each of the nitrogen atoms are 2,6-diisopropylphenyl groups and on the carbon atom a 4-^{t}butylphenyl group, which aids solubility in non-coordinating solvents like *n*-hexane and toluene. Addition of Li(^{dipp}NCN) to the appropriate Main Group halide gives (^{dipp}NCN)ECl_x (where E = Si, x = 3; E = P, x = 2 or 4) in a high yield. Azide exchange is completed using sodium azide suspended in THF. Recrystallisation of the crude material obtained from THF can be achieved by cooling warm *n*-hexane solutions to −28°C overnight giving colourless block crystals of (^{dipp}NCN)$Si(N_3)_3$ (**20**), (^{dipp}NCN)$P(N_3)_2$ (**21**) and (^{dipp}NCN)$P(N_3)_4$ (**22**). Table 6.2 summarises the IR spectroscopic data between 2200 and 2000 cm^{-1} of these three compounds.

Compound	Wavenumbers / cm^{-1}
20	2160, 2141, 2121
21	2130, 2117
22	2138, 2127, 2115, 2095

Table 6.2. Band position of the $\nu_{as}N_3$ vibrations in compounds **20**-**22** in toluene solution.

The number of bands present in **20**, **21** and **22** is equal to the number azido groups in the molecule. Due to the size of the ancillary ligand the point group of each of the molecules is most likely C_1. Similarly to **16** and **18**, the position of the bands are lower for the phosphorus complexes than the silicon complex due to geometry of the individual complex (octahedral *vs* trigonal bipyramidal). There is little difference between the position between the P(III) and P(V) complexes unlike Group 14 complexes which show a noticeable decrease between E(IV) and E(II) azido complexes. All three complexes are potential candidates for the synthesis of low-valent Main Group azido complexes.

6.2.2.2 Single crystal X-ray diffraction

Single crystal X-ray diffraction measurements were completed on **16**-**22**. Figure 6.12 shows the molecular structure of **16**. The compound crystallises in the space group $P2_1$. The silicon atom has trigonal bipyramidal geometry with two azido groups in the axial positions and two azido groups in the equatorial positions. Leaving the NHC occupying the final equatorial site, as seen in $IPrSiCl_4$, $IPrSiBr_4$ and $IPrSiI_4$.[73,76,84,190] The azido ligands in the axial plane are not related by symmetry, rendering the molecule C_1 symmetric. The axial Si−N bond lengths are noticeably longer than the equatorial Si−N bonds at 1.848(4) and 1.759(4) Å respectively as expected for trigonal bipyramidal molecules. The equatorial Si−N bond lengths are closer in size to tetracoordinate azidosilanes (1.760-1.814 Å) while the axial Si−N bond lengths are comparable to octahedral silicon azido complexes, $[Si(N_3)_6]^{2-}$ and (2,2'-bipyridyl)$Si(N_3)_4$ (1.871 and 1.841 Å). The difference between N(α)−N(β) and N(β)−N(γ), ΔNN, is different for the axial and the equatorial azides, 6.8 pm and 10.7 pm respectively. The Si−C bond length is 1.926(3) Å, similar to that of $IPrSiCl_4$ (1.928 Å) and $IPrSiBr_4$ (1.935 Å). The angle between equatorial azido groups, $N_{eq}(\alpha)-Si-N_{eq}(\alpha)$, is 124.1(2)° while the

C−Si−N_{eq}(α) on average is 117.9(3)°. Opposite to what is observed for IPrSiCl_4 (Cl_{eq}−Si−Cl_{eq} = 117.1°; average C−Si−Cl_{eq} = 121.4°). The average bond angle between N_{ax}(α)−Si−C is 88.2(3)° implying that the azido group position is influenced more by the steric repulsion of the other azido groups than IPr. This structure is the first pentacoordinate Lewis adduct of Si$(N_3)_4$.

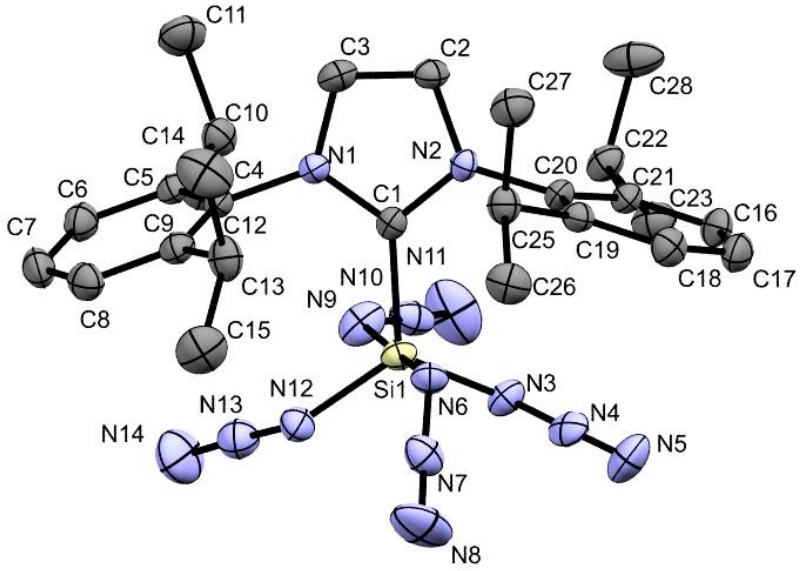

Figure 6.12. Thermal ellipsoid plot of **16**. Hydrogen atoms omitted for clarity. Thermal ellipsoids are set at the 50% probability level. Selected bond lengths (Å) and angles (°):Si1–N12 1.759(3), Si1–N3 1.759(3), Si1–N9 1.848(3), Si1–N6 1.848(3), Si1–C1 1.926(3), C1–N1 1.345(4), C1–N2 1.354(4), N4–N5 1.129(4), N4–N3 1.247(4), N6–N7 1.211(4), N7–N8 1.141(4), N10–N11 1.143(5), N10–N9 1.210(4), N12–N13 1.234(4), N13–N14 1.135(4), N12–Si1–N3 124.18(14), N12–Si1–N9 91.16(15), N3–Si1–N9 89.54(15), N12–Si1–N6 88.33(13), N3–Si1–N6 94.42(14), N9–Si1–N6 175.53(15), N12–Si1–C1 117.92(14), N3–Si1–C1 117.91(14), N9–Si1–C1 88.77(13), N6–Si1–C1 87.54(13), N1–C1–N2 105.7(2), N1–C1–Si1 126.8(2), N2–C1–Si1 127.4(2), N5–N4–N3 175.6(4), N4–N3–Si1 121.3(2), N7–N6–Si1 124.1(2), N8–N7–N6 175.9(4), N11–N10–N9 175.6(4), N10–N9–Si1 127.2(3), N13–N12–Si1 124.0(2), N14–N13–N12 173.8(4).

Compound **18** crystallises in the space group $P2_1/m$ and has a distorted octahedral structure with four azides in a pseudo C_4 plane where three azides point up away from the NHC and one flat in the plane. There is disorder in the position of the azides *cis* to IPr where they are arranged like a propeller and all point in a clockwise direction or anticlockwise direction. The azido group *trans* to the IPr ligand is always in the same position and causes an azide in the "C_4" plane to lie in the plane. The P−N_{trans}(α) bond length is significantly longer than the average P−N_{cis}(α) at 1.837(2) Å and 1.784(4) Å respectively. These values lie either side of the P−N bond lengths observed in the $[P(N_3)_6]^-$ anion in (PPN)P$(N_3)_6$, demonstrating the increased *trans effect* of IPr over the

azido group. In comparison to the previously reported (*p*-dmap)As$(N_3)_5$ and (*p*-dmap)Sb$(N_3)_5$ (*p*-dmap = *para*-dimethylaminopyridine) the *trans* azide E−N bond length is shorter than the *cis* azide E−N showing that IPr is a stronger σ donor than the *p*-dmap ligand. However, like the reported As and Sb structures and also **16**, the $N_{cis}(\alpha)$−P−C bond angle of the *cis* azido groups is less than 90° at 89.0(2)°. Providing further evidence that the azido group position is influenced as much by the other azido ligands as the NHC. This is the first example of a charge-neutral complex bearing a $P(N_3)_5$ fragment, however, other neutral P(V) azides are known such as the cyclic phosphazanes *cyclo*-$[NP(N_3)_2]_3$ and {*cyclo*-$P(N_3)_3(NPh_2)\}_2$.[19,200,207] The former compound has a P−N(α) bond length shorter than **18** at 1.67 Å, while the latter compound has a range of P−N(α) bond lengths between 1.703 and 1.804 Å, shorter than the $P-N_{trans}(\alpha)$ but either side of the $P-N_{cis}(\alpha)$ bond lengths in **18**.

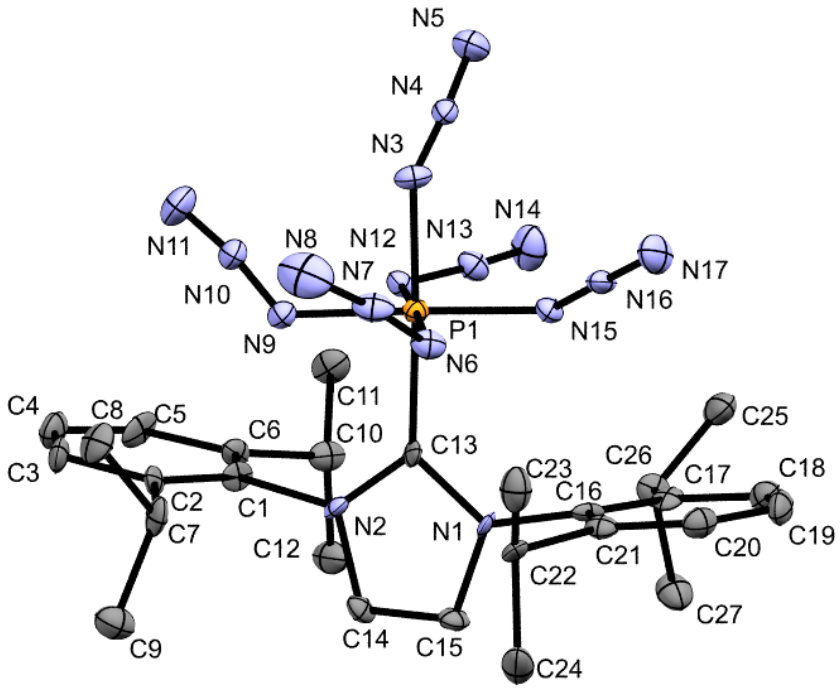

Figure 6.13. Thermal ellipsoid plot of one component of the disordered structure of **18**. Hydrogen atoms omitted for clarity. Thermal ellipsoids set at 50% probability. Selected bond lengths (Å) and angles (°): P1−N3 1.8369(16), P1−N12 1.792(2), P1−N6 1.792(2), P1−N9 1.783(2), P1−N15 1.769(2), N3−N4 1.223(2), N4−N5 1.141(2), N6−N7 1.226(3), N7−N8 1.185(3), N12−N13 1.232(3), N13−N14 1.112(3), N9−N10 1.239(3), N10−N11 1.138(3) N15−N16 1.229(4), N16−N17 1.136(3), P1−C13 1.9273(18), C13−P1−N6 86.74(9), C13−P1−N12 90.37(9), C13−P1−N3 175.10(8), N3−P1−N6 88.99(9), N3−P1−N12 93.86(8), N3−P1−N9 92.45(7), N3−P1−N15 88.5(8), N12−P1−N15 89.41(12), N6−P1−N9 91.05(11), P1−N3−N4 119.97(13), N3−N4−N5 175.0(2), P1−N6−N7 119.02(19), N6−N7−N8 175.3(3), P1−N12−N13 122.22(19), N12−N13−N14 170.0(2), P1−N9−N10 118.0(2), N9−N10−N11 176.2(3), P1−N15−N16 118.5(2), N15−N16−N17 174.5(3), N9−P1−N15 178.7(2), C13−P1−N9 90.25(1), N6−P1−N12 176.91(1), C13−P1−N15 90.25(2).

In an attempt to prepare (py)P(N_3)$_5$ from NaP(N_3)$_6$, only NaP(N_3)$_6$ solvated by six pyridine molecules was isolated. The compound crystallises in the space group *R*-3 with three formula units per unit cell. The structure contains discrete [P(N_3)$_6$]$^-$ anions of S_6 symmetry and Na cations coordinated by six pyridine ligands. At variance to the [P(N_3)$_6$]$^-$ anion in (PPN)P(N_3)$_6$ which has C_i symmetry. The pyridine molecules are not coplanar and slightly offset with a Na−N−C3 bond angle of 165°. The P−N, N(α)−N(β) and N(β)−N(γ) bond lengths and associated bond angles are almost identical to those of the previously determined [P(N_3)$_6$]$^-$ anion in the salt (PPN)P(N_3)$_6$.[199] The only other known structure of a pyridine adduct of a Main Group polyazido complex bearing sodium counterions is that of [Na(py)$_2$]In(N_3)$_4$(py)$_2$ which is made up of a network of bridging azides between In and Na.[208] The distance between the nitrogen donor atom of

the pyridine and the sodium is slightly larger in **19** than the indium structure at 2.53(1) and 2.48 Å, respectively. Other sodium salts of polyazido *p*-block elements including $[Ge(N_3)_6]^{2-}$, $[Al(N_3)_4]^-$ and $[Ga(N_3)_4]^-$ have been isolated with varying degrees of solvation by THF and Et_2O.[173,208] All of these structures, including the indium structure, show some interaction between the sodium and either N(α) or N(γ) of an azido group, making this structure the first sodium salt of a Main Group polyazido complex with no covalent interaction between the two ions.

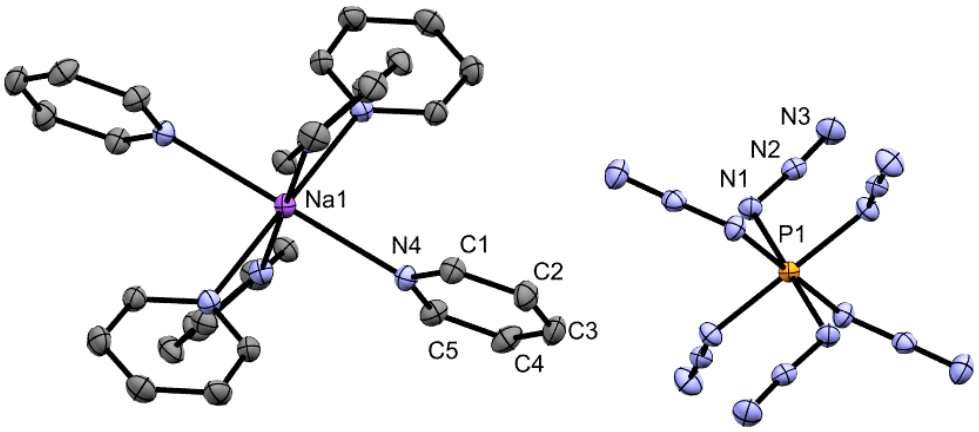

Figure 6.14. Thermal ellipsoid plot of **19**. Hydrogen atoms omitted for clarity. Thermal ellipsoids set at 50% probability. Selected bond lengths (Å) and angles (°): P1−N1 1.8083(9), N1−N2 1.2259(13), N2−N3 1.1344(14), Na1−N4 2.5317(9), N4−C1 1.3396(14), C1−C2 1.3824(16), C2−C3 1.3829(17), C3−C4 1.3831(18), C4−C5 1.3842(17), C5−N4 1.3398(15), P1−N1−N2 177.87(7), N1−N2−N3 175.54(11), Na1−N4−C5 115.22(7), Na1−N4−C1 126.13(7), N4−C5−C4 123.60(10), C5−C4−C3 118.93, C4−C3−C2 118.18(11) C3−C2−C1 119.05(11)

Compound **17** is very different to both compounds **16** and **18** in that it contains an imidazolin-2-imido ligand, as the NHC, I^{t}Bu, reacts with the azido groups. The compound crystallises in the space group *C*2/c. The silicon atom is four coordinate and has a distorted tetrahedral geometry with N−Si−N angles between 100.8(1) and 122.0(1)°. The N_{azide}−Si−N_{Im} bond angles range between 110.4(1) and 105.9(1)°. The bond angle N_{azide}−Si−N_{azide} is 100.8(1)° to accommodate the bulk of the two N=I^{t}Bu groups which have a large N−Si−N angle of 122.0(1)°. A remarkable feature of the molecule is the Si−N−C bond angle at 166.3(1)°, much more obtuse than the expected 120°, and an almost linear arrangement. The Si−N bond length of this unit is 1.619(1) Å, much shorter than the Si−N bond lengths of the azido ligands (1.783(1) Å) in this molecule. It is of comparable length to the Si=N bond length in the silaimine, (^{t}BuNCH=CHN^{t}Bu)Si=NCPh$_3$·THF, prepared by West and co-workers in 1994 (1.599 Å).[66] Overall, suggesting double bond character between the silicon and nitrogen atom

of the imidazolin-2-imido ligand. If there are two double bonds from the two imidazolin-2-imido ligands and a single bond from each azido ligand then the silicon atom formally has six bonds while remaining tetrahedral. Similar systems have been prepared with $Me_3Si(N_3)$ and a variety of NHCs to give (NHC)N=$SiMe_3$, though only a few have structural data.[189] All the Si−N bonds lengths in those compounds fall between 1.65(1) and 1.68(1) Å and the N−C bond lengths are approximately 1.26(1) Å. Whereas in **17** the N–C bond is slightly longer at 1.286 Å with the overall observation that the Si–N bond has more double bond character than the N−C bond in this system.

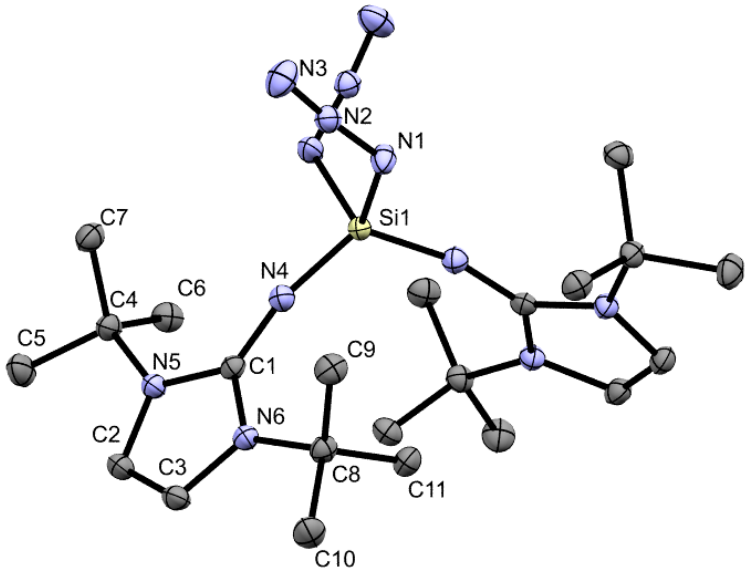

Figure 6.15. Thermal ellipsoid plot of **17**. Hydrogen atoms omitted for clarity. Ellipsoids set at 50% probability level. Selected bond lengths (Å) and angles (°): Si1–N4 1.6194(11), Si1–N1 1.7830(11), N2–N3 1.1388(16), N2–N1 1.2151(15), N5–C1 1.3866(16), N6–C1 1.3908(16), N4–C1 1.2856(16), N4–Si1–N4 121.99(8), N4–Si1 N1–110.13(5), N4–Si1–N1 105.89(5), N1–Si1–N1 100.81(8), N3–N2–N1 174.36(13), N2–N1–Si1 124.83(9), C1–N4–Si1 166.26(10), N4–C1–N5 127.04(11), N4–C1–N6 127.80(11), N5–C1–N6 105.14(10).

The compounds containing the amidinato ligand are easily crystallised from *n*-hexane. Compound **20** crystallises with $P2_1/c$ symmetry with two molecules in the asymmetric unit. The molecule has a distorted trigonal bipyramidal structure with two azido groups in the equatorial plane, a third in the axial plane and the ^{dipp}NCN ligand occupying an axial and an equatorial site. The ^{dipp}NCN ligand has a narrow bite angle of 69.7(2)° consequently widening the bond angle between all the other N_{ax}−Si−N_{eq} bonds above 90°. The Si−N bond lengths between the silicon and nitrogen atoms of the ^{dipp}NCN ligand are 1.791(4) and 1.924(4) Å for the axial and equatorial nitrogen atoms respectively. Both of the bond lengths are shorter than that of (^{dipp}NCN)$SiCl_3$ (axial:

1.798; equatorial: 1.963 Å) most likely due to the smaller nitrogen atoms of the azido groups being less sterically hindering than the chloro ligands around the coordination sphere.[85] The Si−N bond lengths between the silicon atom and the nitrogen of the azido groups are 1.797(5) and 1.740(7) Å for the equatorial and axial groups respectively. Similar to those seen for tetracoordinate azidosilanes. Like the IPrSi$(N_3)_4$ structure there is a difference in the ΔNN parameter for the axial and equatorial azido groups. The axial azido group has a ΔNN value of 6.9(9) pm and the equatorial azido groups have an average value of 11.1(12) pm.

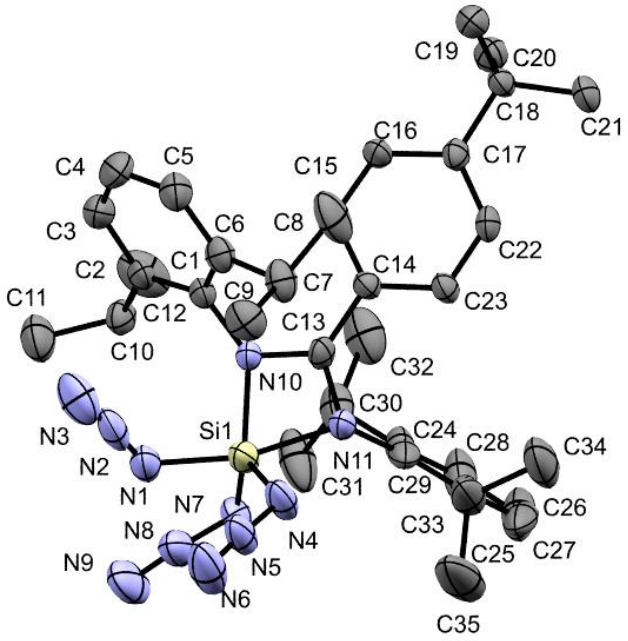

Figure 6.16. Thermal ellipsoid plot of **20**. Hydrogen atoms omitted for clarity. Thermal ellipsoids set at 50% probability. Selected bond lengths (Å) and angles (°): N1−N2 1.228(7), N1−Si1 1.797(5), N2−N3 1.159(7), N4−N5 1.230(6), N4−Si1 1.748(4), N5−N6 1.130(6), N7−N8 1.240(6), N7−Si1 1.732(5), N8−N9 1.117(6), N10−Si1 1.794(4), N11−Si1 1.924(4), N2−N1−Si1 126.2(4), N3−N2−N1 175.4(6), N5−N4−Si1 121.0(3), N6−N5−N4 176.1(5), N8−N7−Si1 123.8(4), N7−Si1−N4 115.9(2), N7−Si1−N10 123.1(2), N4−Si1−N10 117.0(2), N7−Si1−N1 94.2(2), N4−Si1−N1 98.6(2), N10−Si1−N1 97.15(19), N7−Si1−N11 90.3(2), N4−Si1−N11 91.46(19), N10−Si1−N11 69.25(17), N1−Si1−N11 165.83(19)

Compound **21** crystallises in the space group $P2_1/n$. The phosphorus is three coordinate and has a distorted pyramidal geometry. The commonly bidentate amidinato ligand is monodentate and only bound through a single nitrogen atom. As a result the phosphorus atom does not sit in the plane with the (^{dipp}NCN) ligand, but rather above or below the plane. Disorder is present in the structure where the phosphorus atom is either bonded to N1 or N2 of the amidinato ligand. This leads to the N(γ) of the azido group in one component being shared with the N(β) of the azido group in the other. Appropriate

SADI, SIMU and DELU commands have been applied to the nitrogen atoms of the azido groups to ensure linearity of the azide and produce sensible ellipsoids. As a result the N−N bond lengths are unreliable (N(α)−N(β) is too long and N(β)−N(γ) is short). The ΔNN parameter is 15.7 pm, larger than any other azide containing crystal structure determined, except $[C(N_3)_3]^+$ (ΔNN = 24 pm).[59] Which makes the N−N bond lengths in this structure unlikely as the wavenumber of $\nu_{as}(N_3)$ are 2130 and 2117 cm^{-1}. The P−N bond length of the amidinato ligand is 1.829(3) Å shorter than the two bond lengths in **22** (1.854 Å average). The second nitrogen atom of the ligand is 2.411 Å away from the phosphorus atom implying there is an interaction between the two atoms but the steric influence of the ligand prevents bond formation. The ligand has a bite angle of approximately 70° and therefore ideal to occupy an axial and equatorial site of the see-saw geometry. However, due to the influence of the electron lone pair the molecule has distorted pyramidal geometry.

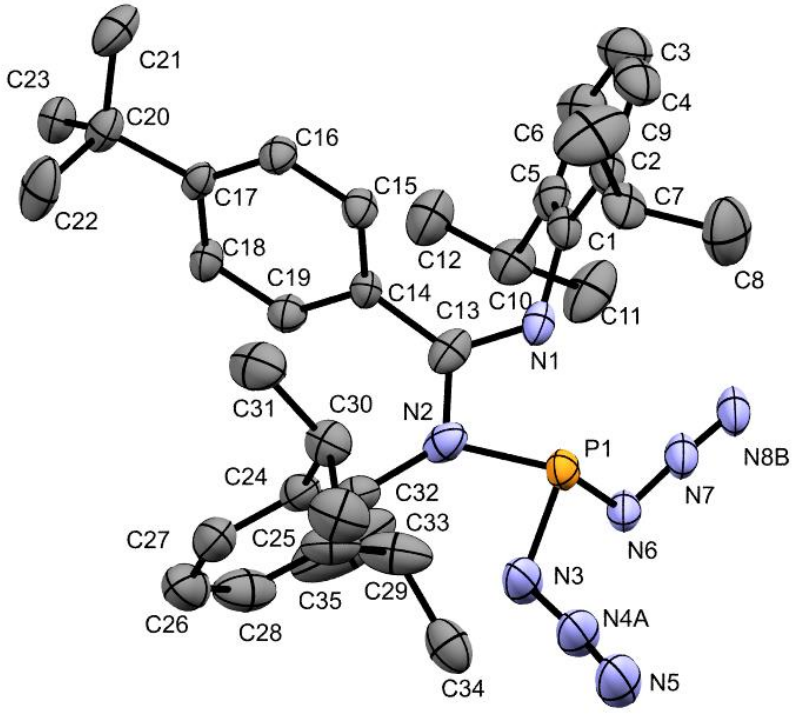

Figure 6.17. Thermal ellipsoid plot of one of the disordered components of **21**. Hydrogen atoms omitted for clarity. Thermal ellipsoids set at the 50 % probability level. Selected bond lengths (Å) and bond angles (°): N2−P1 1.829(3), N4A−N5 1.083(6), N4A−N3 1.267(7), N8B−N7 1.105(7), P1−N3 1.734(5), P1−N6 1.750(5), N6−N7 1.234(6), N3−P1−N2 88.99(19), N6−P1−N2 103.88(18), N7−N6−P1 116.0(4), N8B−N7−N6 174.6(7), N4A−N3−P1 117.7(5), N5−N4A−N3 173.5(9).

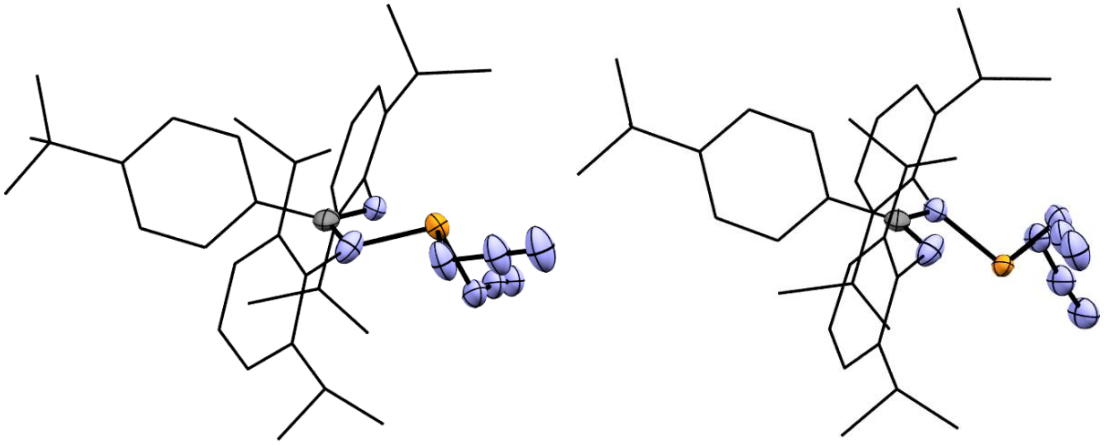

Figure 6.18. Diagrams of the two disordered components of **21**.

Compound **22**, the P(V) analogue of **21**, crystallises in the space group $P2_1/c$ with one equivalent of hexane per formula unit. The molecule itself possesses a C_2 axis in between the P−N bonds of the amidinato ligand. The phosphorus atom has a significantly distorted octahedral geometry as a consequence of the narrow bite angle of the amidinato ligand at 69.6(1)°. This results in a noticeable increase of the N−P−N angle between the azides *trans* to the amidinato ligand with a bond angle of 97.6(1)°. The other N−P−N angles between the azides are also slightly larger than the ideal 90° but distorted to a lesser extent. Both P−N bond lengths between the phosphorus and the amidinato ligand (1.85(1) Å) are longer than previously reported amidinato phosphorus compounds (1.80-1.81Å) as well as longer than the P−N bond length of the azido ligands in this molecule.[209,210] The P−N bond lengths for the azides differ depending on the group *trans* to the azido group. Where the amidinate is *trans* to the azide the P−N bond length is shorter (1.77(1) Å) than when another azido group is *trans* to it (1.79(1) Å). These lengths are slightly shorter than $[P(N_3)_6]^-$ and fall in the region of other neutral P(V) azido compounds.[19,199,200,211] The ΔNN parameter is slightly different for the two sets of the azido groups. The two azido groups trans to the amidinato ligand have an average ΔNN of 9.5(2) pm, while the other two azido groups have an average of 9.0(2) pm. Highlighting the slight difference in the *trans* influence between the azido and amidinato ligands. One intriguing feature of the molecular structure of **22**·C_6H_{14} is the conformation of the hexane molecule. Rather than be in its more favoured *trans* conformation one of the terminal carbon atoms is in a *cis* conformation with respect to the rest of the chain and points towards the (^{dipp}NCN)P$(N_3)_4$. There are no contacts

between the C−H and the azides shorter than the van der Waals radii; however, the carbon atom is directed towards a cavity formed by the arrangement of the azido groups. The incredibly large size of the ^{dipp}NCN ligand dictates the packing in the crystal structure, therefore, the hexane molecule must only be able to fit in this higher energy conformation.

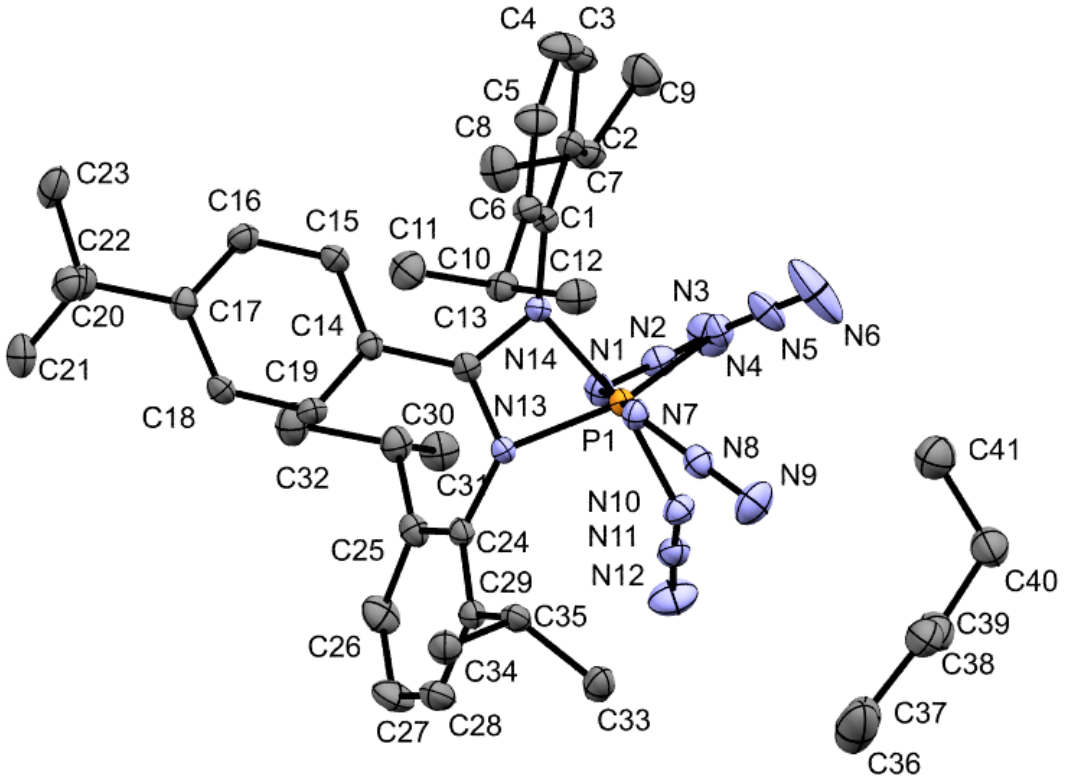

Figure 6.19. Thermal ellipsoid plot of **22**·C_6H_{14}. Hydrogen atoms omitted for clarity. Thermal ellipsoids set at 50% probability. Selected bond lengths (Å) and angles (°): P1−N1 1.7923(15), P1−N4 1.7731(14), P1−N7 1.7975(15), P1−N10 1.7739(14), P1−N13 1.8524(13), P1−N14 1.8566(13), N1−N2 1.2280(18), N2−N3 1.1396(19), N4−N5 1.222(2), N5−N6 1.130(2), N7−N8 1.2285(19), N8−N9 1.1366(19), N10−N11 1.2311(19), N11−N12 1.133(2), N1−P1−N4 93.73(7), N4−P1−N10 97.58(6), N1−P1−N4 89.33(7), N7−P1−N10 88.54(7), N4−P1−N7 88.54(7), N1−P1−N7 176.01, N10−P1−N13 96.79(6), N4−P1−N13 165.31N(6), N1−P1−N13 86.66(6), N7−P1−N13 89.81(6), N10−P1−N14 165.49(7), N4−P1−N14 96.37(6), N1−P1−N14 90.41(7), N7−P1−N14 86.61(6), N13−P1−N14 69.55(6), N2−N1−P1 121.22(12), N3−N2−N1 173.68(19), N5−N4−P1 120.19(12), N6−N5−N4 174.6(2), N8−N7−P1 120.47(12), N9−N8−N7 173.93(18), N11−N10−P1 120.34(12), N12−N11−N10 173.96(18).

			Average bond lengths of azido group		
Compound	Orientation	E−N / Å	N(α)−N(β) / Å	N(β)−N(γ) / Å	ΔNN / pm
16	axial	1.848(4)	1.211(6)	1.142(6)	6.9(8)
	equatorial	1.759(4)	1.240(6)	1.132(6)	10.8(8)
17		1.783(1)	1.215(1)	1.139(2)	7.6(3)
18	*trans*	1.837(2)	1.223(2)	1.141(2)	8.2(3)
	cis	1.784(4)	1.232(6)	1.137(6)	9.5(8)
19		1.808(1)	1.226(1)	1.134(1)	9.2(1)
20	axial	1.797(5)	1.228(7)	1.159(7)	6.9(10)
	equatorial	1.740(8)	1.235(8)	1.123(8)	11.2(12)
21		1.742(7)	1.251(9)	1.094(9)	15.7(13)*
22	*trans*	1.774(3)	1.227(3)	1.132(3)	9.5(4)
	cis	1.795(3)	1.228(3)	1.138(3)	9.0(4)

Table 6.3. Selected structural data of azido complexes **16**-**22**. E = P or Si. Trans and cis orientation are the position of the azido groups with respect to the ancillary ligand. * restraints applied to the model due to disorder in the structure renders the bond lengths in the azido group unreliable.

Table 6.3 shows the average E−N and N−N bond lengths for **16**-**22**. A direct observation from the data is the azido groups *trans* to IPr, i.e. the axial azido group and the trans azido group in **16** and **18** respectively, have the longest E−N bonds. The strong σ-donor strength of the IPr ligand causes a large *trans effect* effectively pushing the azido ligand away. The differences between phosphorus and silicon as a coordination centre are harder to determine as there are fundamental differences on the complexes formed. The effect of the overall geometry on the complex appears to be a greater influence on the nature of the coordination bond, and in turn the electronic structure of the azido group, than the coordination centre.

6.2.3 Reduction reactions of Main Group polyazido complexes

6.2.3.1 Potassium graphite as the reducing agent

The original syntheses for Si(II) halides involved reduction of the parent base stabilised Si(IV) halide with potassium in the form of potassium graphite, KC_8. The reducing agent is prepared by stirring small pieces of potassium with graphite at 200°C until the mixture turns bronze.[212] Compound **16** is only sparingly soluble in toluene,

therefore, **16** was added as a solid to KC_8 and suspended in toluene. Immediately a black suspension, black solid in a yellow solution, had formed and after two hours the FT-IR spectrum of the yellow solution between 2200 and 2000 cm^{-1} displayed a sharp band at 2103 cm^{-1} and two broad signals at 2150 and 2014 cm^{-1}. The signal at 2014 cm^{-1} is indicative of (^{dipp}ImH)N_3 and the peak at 2103 cm^{-1} is a signature of **16**. The signal at 2150 cm^{-1} is similar to the peak observed in the metathesis experiments described in **6.2.1** suggesting both experiments give the same product. From the salt metathesis experiments the conclusion was the azido group was exchanged onto the Si(II) centre and then simultanesously reduced by the Si(II) centre. As the azido groups are already present on the silicon centre in the reduction experiment it is possible that IPrSi$(N_3)_2$ is formed in both experiments and is too reactive to be isolated. IPrSi$(N_3)_2$ potentially reacts with a second molecule of IPrSi$(N_3)_2$ to give an iminosilane, shown in Scheme 6.7. No solid material could be obtained, only yellow oils, from the experiment to obtain conclusive proof.

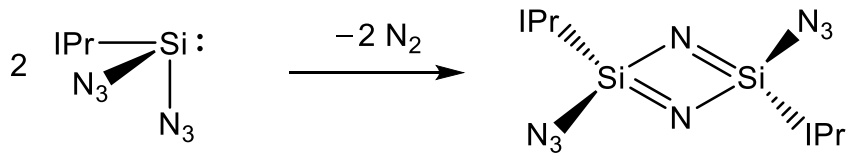

Scheme 6.7. Possible decomposition product of IPrSi$(N_3)_2$.

The only drawback to this hypothesis is the lack of effervescence of the reaction mixture. However, the quantities used, less than 0.5 mmol, and the presence of starting material in the FT-IR spectrum implies very little dinitrogen gas would be released. One common problem with reducing IPrSiX_4 (where X is a halide) or (^{R}NCN)$SiCl_3$ with KC_8 is the yield of the Si(II) product is often as low as 10 %.[73,213] It appears that the desired IPrSi$(N_3)_2$ product is unstable and decomposes readily. The germanium analogue, IPrGe$(N_3)_2$, is a known and fully characterised compound, clearly showing no reactivity between the Ge(II) centre and azides. Only carbenes or silylenes show this kind of reactivity. A testament to the increased reactivity of the Si(II) oxidation state (and carbenes) compared to the heavier congeners. There are two possible methods of attack: the Si(II) centre acts as a Lewis acid or the Si(II) centre acts as a nucleophile. The former is unlikely as the empty orbital present in the low valent species (see chapter **1.2**) is occupied by the NHC. Therefore, it is much more likely that the lone pair on the

silicon atom attacks the azido group. Whether it attacks N(α) or N(γ) is uncertain. Only a qualitative explanation based on first principles can be made to why Ge(II) does not react with azido groups but Si(II) does, rather than a quantitative explanation. The energy difference between the electronic structure of E(IV) (four sp^3 orbitals) and the electronic structure of E(II) (three sp^2 and one p orbitals) is greater for germanium than silicon. Effectively increasing the stability of the lone pair on germanium. Extensive calculations would need to be completed to determine the reaction dynamics, where it may be possible to then design an NHC able to stabilise $Si(N_3)_2$.

Reduction of compound **20** would give (^{dipp}NCN)SiN_3 and potassium azide as the products. The (^{dipp}NCN) ligand is larger than IPr, especially around the coordination centre potentially imparting extra kinetic stability. Another advantage is the synthesis of **20** can be easily upscaled unlike the synthesis of **16**. Therefore, the reduction experiment can be attempted on a much larger scale. On reduction of **20** with KC_8 a yellow oil was obtained. The FT-IR spectrum between 2200 and 2000 cm^{-1} of this oil shows four bands at 2147, 2129, 2119 and 2044 cm^{-1}. The three at higher energy indicate compound **20**. The new band at 2044 cm^{-1} satisfies the criteria that the band should appear at lower wavenumbers than the Si(IV) analogue. However, if making a prediction by calculating the difference between the IR frequencies of the azido group of Ge(II) and Ge(IV), and Sn(II) and Sn(IV) complexes, Table 6.4, the frequency of the observed band is too low.

E(IV) compound	$\nu_{(as)}N_3$ / cm^{-1}	E(II) compound	$\nu_{(as)}N_3$ / cm^{-1}	Δ / cm^{-1}
$(PPh_4)_2Ge(N_3)_6$	2086	$(PPh_4)Ge(N_3)_3$	2058, 2091	12
$(PPh_4)_2Sn(N_3)_6$	2082	$(PPh_4)Sn(N_3)_3$	2051, 2081	16
$IPrGe(N_3)_4$	2128, 2108, 2088, 2077	$IPrGe(N_3)_2$	2075	25
$(^{dipp}NCN)Ge(N_3)_3$	2127, 2109, 2099, 2089	$(^{dipp}NCN)GeN_3$	2070	36
$IPrSi(N_3)_4$	2150, 2136, 2117, 2102	$IPrSi(N_3)_2$	*2101*	*25**
$(^{dipp}NCN)Si(N_3)_3$	2159, 2138, 2128, 2116	$(^{dipp}NCN)SiN_3$	*2099*	*36**

Table 6.4. IR data of selected Si(IV), Ge(II), Ge(IV), Sn(II) and Sn(IV) azido compounds as nujol mulls and the absorptions calculated for Si(II) azido species. Δ column is the subtraction of the azido frequency of the E(II) compound from the analogous E(IV) compound. Where multiple signals are observed in the $\nu_{(as)}N_3$ region an average of the peak positions has been taken. Italicised numbers are theoretical. * Value taken from the Ge analogue. $IPrGe(N_3)_4$, $(^{dipp}NCN)Ge(N_3)_3$ and $(^{dipp}NCN)GeN_3$ were synthesised as comparison compounds, details in the experimental section.

The yellow oil obtained could be turned into a foam by placing under high vacuum and forcing the remainder of the solvent out of the oil. The foam is readily soluble in *n*-hexane and pentane to give yellow solutions, however no solid material has been obtained from this reaction. As there are no purification steps ^{1}H-NMR spectra obtained of these oils are very complicated, containing starting material, signs of hydrolysis and new peaks, and not a lot of information can be determined from them. Chemical shifts of the starting material and any products containing the ^{dipp}NCN would be very similar. Therefore, it is difficult to ascertain or even to speculate the identity of the new band at 2044 cm^{-1}. If the band at 2044 cm^{-1} in the IR spectrum is due to $(^{dipp}NCN)SiN_3$, it is likely that the structure of the molecule is more complex than a simple monomer. A higher wavenumber for the $\nu_{as}(N_3)$ would be expected if $(^{dipp}NCN)SiN_3$ was monomeric. A possible structure is a dimeric species with bridging azido ligands between two silicon centres. There are two possible bridging modes *via* the N(α) in a $\mu_{1,1}$-N_3 end-on bridge or *via* the N(γ) in a $\mu_{1,3}$-N_3 end-to-end bridge. Both of these structural features are rare in Main Group azide chemistry but common for transition metal azido complexes, as has been recently reviewed in 2013 by Fehlhammer and Beck.[33] As there are very few examples of bridging azido groups in complexes of Main

Group elements it is difficult to definitively conclude how the bridging interactions affect the stretching vibrations of the azido ligand.

6.2.3.2 ($^{dipp/mes}$Nacnac)Mg dimers as reducing agents

With no silicon containing products isolated from reactions with potassium graphite the reducing agent was changed to Jones's β-diketiminate magnesium(I) dimer, [(^{R}Nacnac)Mg]$_2$.[50,214] Two different magnesium(I) dimers were prepared based on published procedures: [(^{dipp}Nacnac)Mg]$_2$ and [(^{mes}Nacnac)Mg]$_2$. The advantage using these compounds as reducing agents is that they are soluble in toluene. Therefore, it is significantly easier to add these reagents stoichiometrically. However, there is one drawback with respect to their reactivity. As described earlier in this chapter, [(^{R}Nacnac)Mg]$_2$ reductively couples organic azides to form hexazenes. Therefore, a silyl azide will have two potential reduction sites, the azido ligand or the silicon atom. This offers a possible competing reaction, though the more likely site of reaction is the silicon atom, as was found from the reaction of Me_3SiN_3 with [(^{mes}Nacnac)Zn]$_2$ by Schulz *et al*.[51] The two different magnesium(I) dimers were reacted with $Si(N_3)_4$, **16**, **20** and **21**.

The magnesium dimers are unstable in coordinating solvents so the reaction solvent used was either benzene or toluene. $Si(N_3)_4$ in benzene was added to [(^{mes}Nacnac)Mg]$_2$, a yellow solid, giving a white suspension. The FT-IR spectral series of the experiment is shown in Figure 6.20. The initial spectrum, black line, is that of $Si(N_3)_4$ before addition of [(^{mes}Nacnac)Mg]$_2$. It shows a signal for $Si(N_3)_4$ at 2170 cm^{-1} and HN_3 at 2133 cm^{-1}. On addition of the magnesium dimer the peak at 2170 cm^{-1} has decreased and new peaks have appeared at 2156 cm^{-1} and 2108 cm^{-1}. The peak at lower wavenumbers is indicative of the $[Si(N_3)_6]^{2-}$ anion. The presence of only one other band in the $\nu_{as}(N_3)$ region indicates it is unlikely that the azido group has been reductively coupled to a hexazene, unless all but one azido group has been reductively coupled. Therefore, the identity of the molecule giving rise to the band at 2156 cm^{-1} is most likely (^{mes}Nacnac)MgN_3 (**23**). As no other bands in this region are present suggest that no other benzene soluble azido containing compound is present. It appears that nearly all the $Si(N_3)_4$ has reacted with the magnesium(I) dimer despite the stoichiometry of 1:1. At that stoichiometry only half of the $Si(N_3)_4$ can react. One possible explanation is

hydrolysis, $Si(N_3)_4$ is extremely moisture sensitive and HN_3 is present in the FT-IR spectrum. At low concentrations of $Si(N_3)_4$ it becomes increasingly more difficult to observe in the IR spectrum due to hydrolysis.

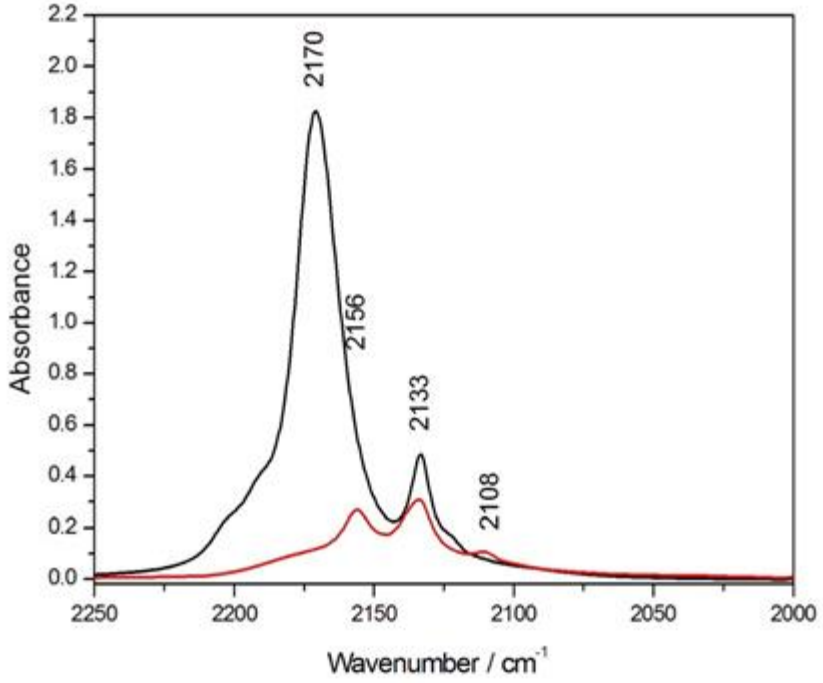

Figure 6.20. FT-IR spectral series of the reaction of $[(^{mes}Nacnac)Mg]_2$ and $Si(N_3)_4$ in benzene. Black line is the spectrum of $Si(N_3)_4$. Red line is after addition of $[(^{mes}Nacnac)Mg]_2$.

The white precipitate that formed in the reaction was dried and analysed by IR spectroscopy as a nujol mull. Two bands are present in the $\nu_{as}(N_3)$ region at 2160 and 2116 cm^{-1}. These two bands most likely belong to the bands observed from the solution IR spectrum, $(^{mes}Nacnac)MgN_3$ and $[Si(N_3)_6]^{2-}$. With no other band in the $\nu_{as}(N_3)$ region, in solution or the precipitate, it appears that the magnesium(I) dimer selectively reduces the silicon centre by the number of azido groups present.

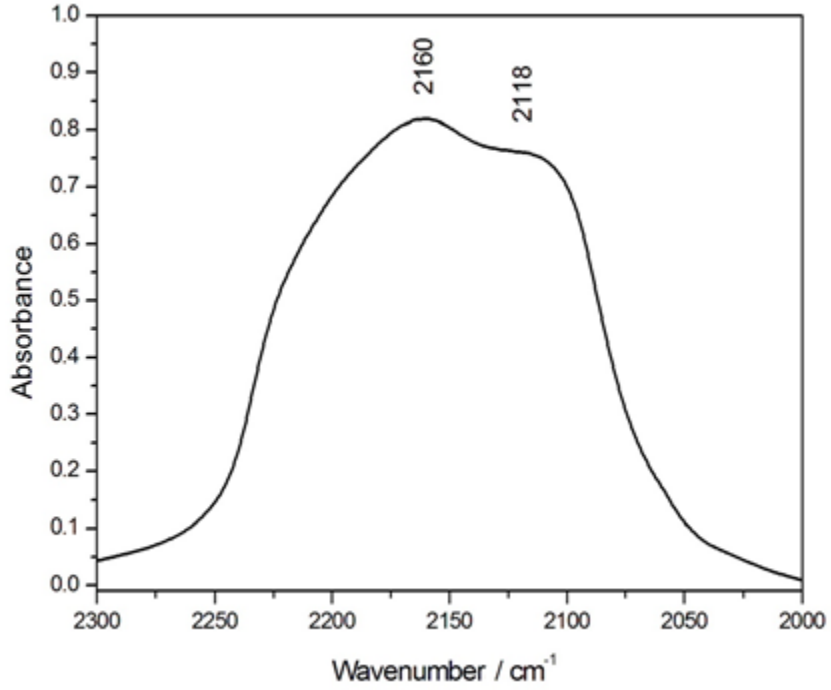

Figure 6.21. FT-IR spectrum of white precipitate obtained from the reaction of $Si(N_3)_4$ with $[(^{mes}Nacnac)Mg]_2$ as a nujol mull.

The magnesium(I) dimer, $[(^{mes}Nacnac)Mg]_2$, was also combined with **21** in toluene in a 0.5:1 ratio and affords an orange solution. The IR spectral series of this experiment is shown in Figure 6.22. Compound **21** has two bands in the $\nu_{as}(N_3)$ region in a solution cell FT-IR spectrum in toluene, the black line, at 2129 and 2116 cm^{-1}. After addition of $[(^{mes}Nacnac)Mg]_2$, the red line, these two peaks decrease and a new broad peak appears at 2176 cm^{-1}. It appears a similar reaction as described previously occurs and the magnesium(I) dimer selectively reduces **21** from P(III) to P(I) by removing all the azido ligands. The orange colour comes from the $(^{dipp}NCN)P$, which most likely dimerises as $(^{dipp}NCN)Si$, IPrSi, IPrP and IPrPCl do.[72]

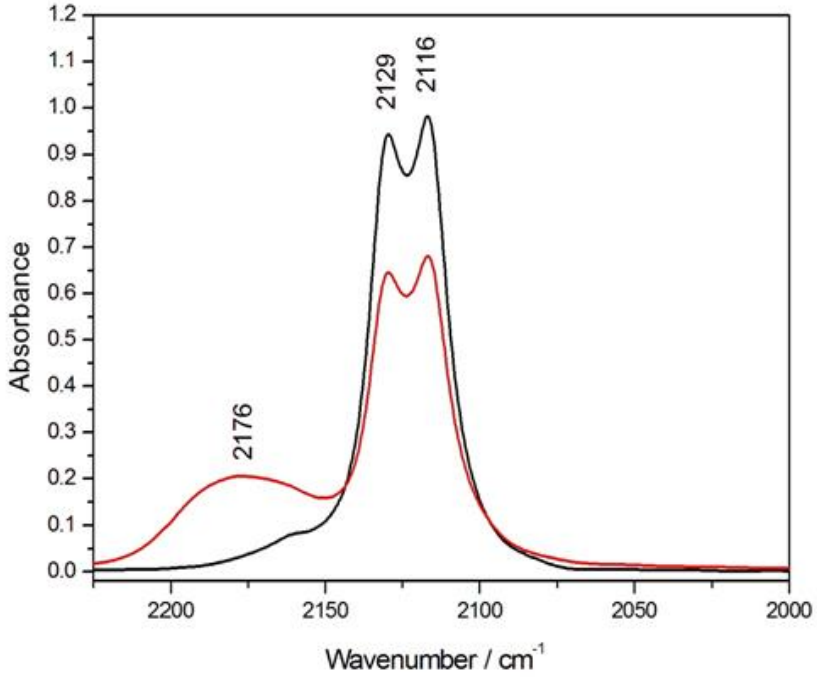

Figure 6.22. FT-IR spectra series of the reaction of [(^{mes}Nacnac)Mg]$_2$ and **21** between 2250 and 2000 cm^{-1}. Black line is FT-IR spectrum of **21** dissolved in toluene. Red line is FT-IR spectrum after addition of half an equivalent of [(^{mes}Nacnac)Mg]$_2$.

The position of the $\nu_{as}(N_3)$ vibration is much higher than would be expected. Magnesium is an electropositive element and, therefore, the IR absorption should be around the ionic region of the range of the asymmetric azide vibration. The absorption is only slightly lower than $Si(N_3)_4$ and higher than those of **16**-**22**.

The [(^{mes}Nacnac)Mg]$_2$ selectively reacts with all the azido groups on a Main Group polyazido complex. It has been reported that [(^{dipp}Nacnac)Mg]$_2$ is less reactive than the mesityl analogue, therefore it was used in attempts to reduce **16** and **20**. Compound **16** is sparingly soluble in toluene and so both solids were combined in a Schlenk tube and suspended in toluene. The mixture turned orange and the solvent was evaporated to give an orange solid. The FT-IR spectrum of the solid as a nujol mull is shown in Figure 6.23 and displays five bands between 2200 and 2000 cm^{-1} at 2195, 2150, 2135, 2119 and 2103 cm^{-1}. The four bands at lower wavenumbers belong to **16**, therefore, the band at 2195 cm^{-1} belongs to (^{dipp}Nacnac)MgN$_3$ (**24**). Again, as with the [(^{mes}Nacnac)Mg]$_2$ experiments, all the azido groups of the complex appear to be removed selectively. The orange colour in the experiment comes from the production of the orange IPrSi dimer.

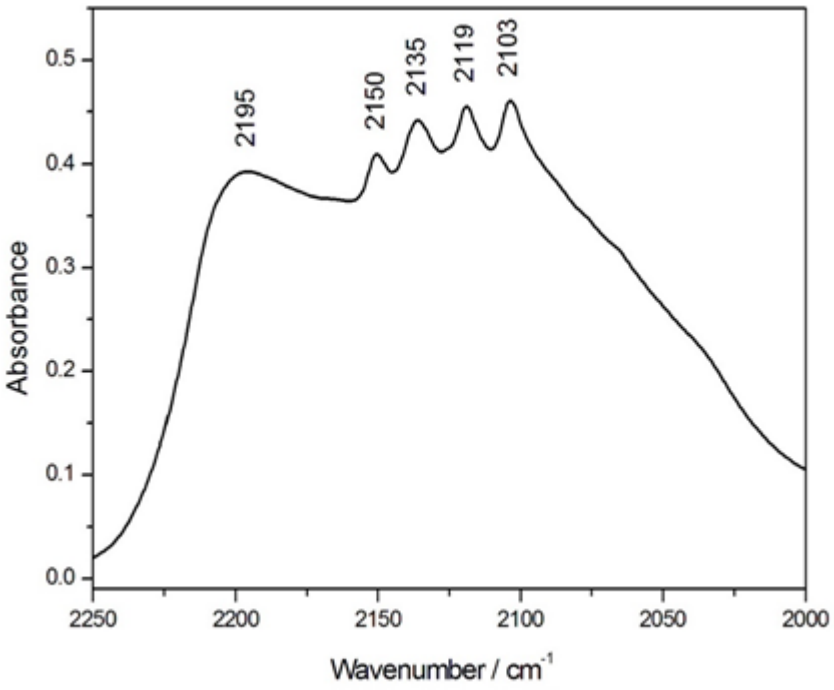

Figure 6.23. FT-IR spectrum of solid obtained from a solution of $IPrSi(N_3)_4$ and $[(^{dipp}Nacnac)Mg]_2$ as a nujol mull.

For completeness **20** was also reduced with one equivalent of $[(^{dipp}Nacnac)Mg]_2$. The initial yellow solution turns green and displays bands for **20** and **24** in the FT-IR spectrum. After adding another half equivalent of $[(^{dipp}Nacnac)Mg]_2$ the reaction solution turns blue, the colour of $[(^{dipp}NCN)Si]_2$, shown in Figure 6.24. Only an IR band for **24** is observed in the FT-IR spectrum of the blue solution demonstrating again that magnesium(I) dimers selectively removes all azido groups from the silicon and phosphorus complexes.

(a) (b)

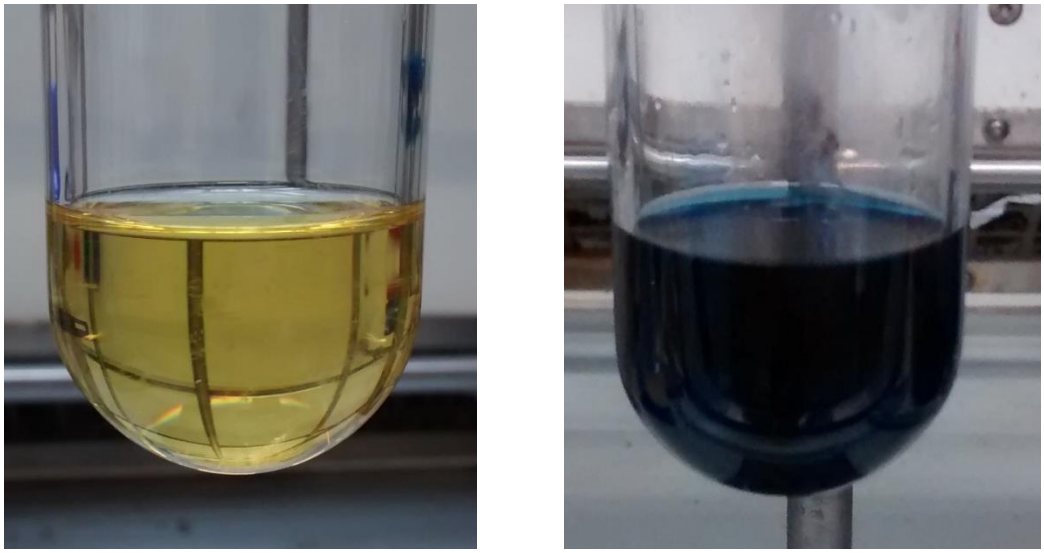

Figure 6.24. (a): [(^{dipp}Nacnac)Mg]$_2$ dissolved in toluene. (b): 1.5 equivalents of [(^{dipp}Nacnac)Mg]$_2$ and **20** dissolved in toluene.

Interestingly, there are significant differences of the position of $\nu_{as}(N_3)$ between **23** and **24**. In a toluene solution, **23** displays a band at 2176 cm^{-1} and **24** at 2195 cm^{-1}. Both of these compounds can be crystallised from *n*-hexane and both were investigated by single crystal X-ray diffraction. Compounds **23** and **24** form unusual cyclic oligomeric species when crystallised from *n*-hexane. The $\nu_{as}(N_3)$ band position of **24** as a nujol mull is at the same position as the toluene solution cell FT-IR spectrum, implying the same structure in the solid state and when dissolved in toluene.

The molecular structure of **23** is shown in Figures 6.25 and 6.26. Compound **23** crystallises from *n*-hexane as the solvate (^{mes}Nacnac)MgN$_3$·0.33C$_6$H$_{14}$ in the space group $P\bar{1}$. The magnesium atom has a distorted tetrahedral geometry with two coordination sites occupied by the Nacnac ligand and a third site occupied by the azido ligand. The fourth coordination is from a $\mu_{1,3}$-N$_3$ end-to-end bridge with a neighbouring azido ligand from another (^{mes}Nacnac)MgN$_3$. This results in an extended structure where six (^{mes}Nacnac)MgN$_3$ molecules come together to give a 24-atom ring.

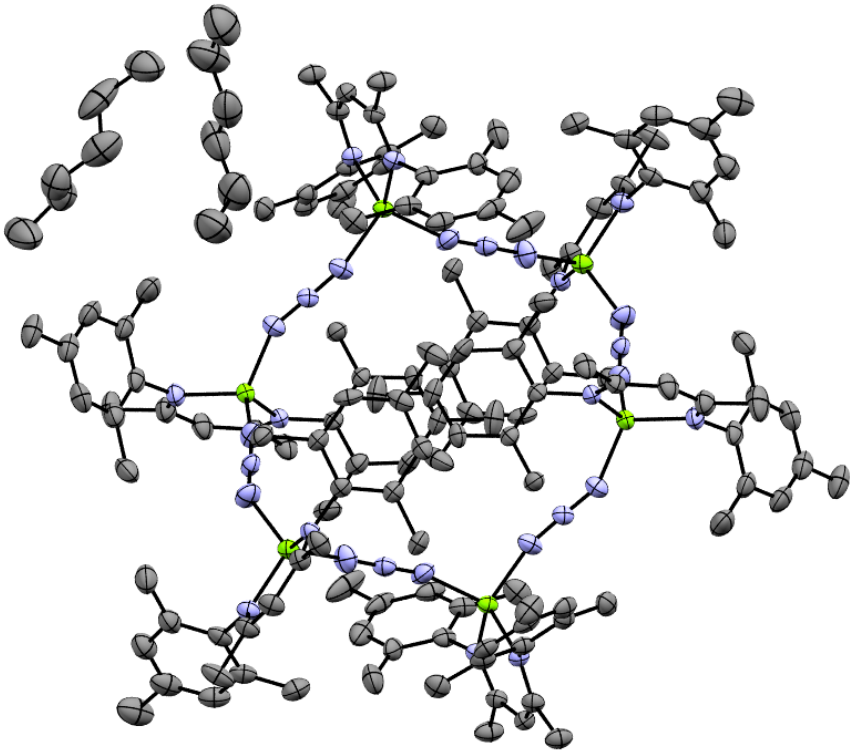

Figure 6.25. Thermal ellipsoid plot of {(^{mes}Nacnac)MgN_3}$_6$·2C_6H_{14}. Hydrogen atoms omitted.

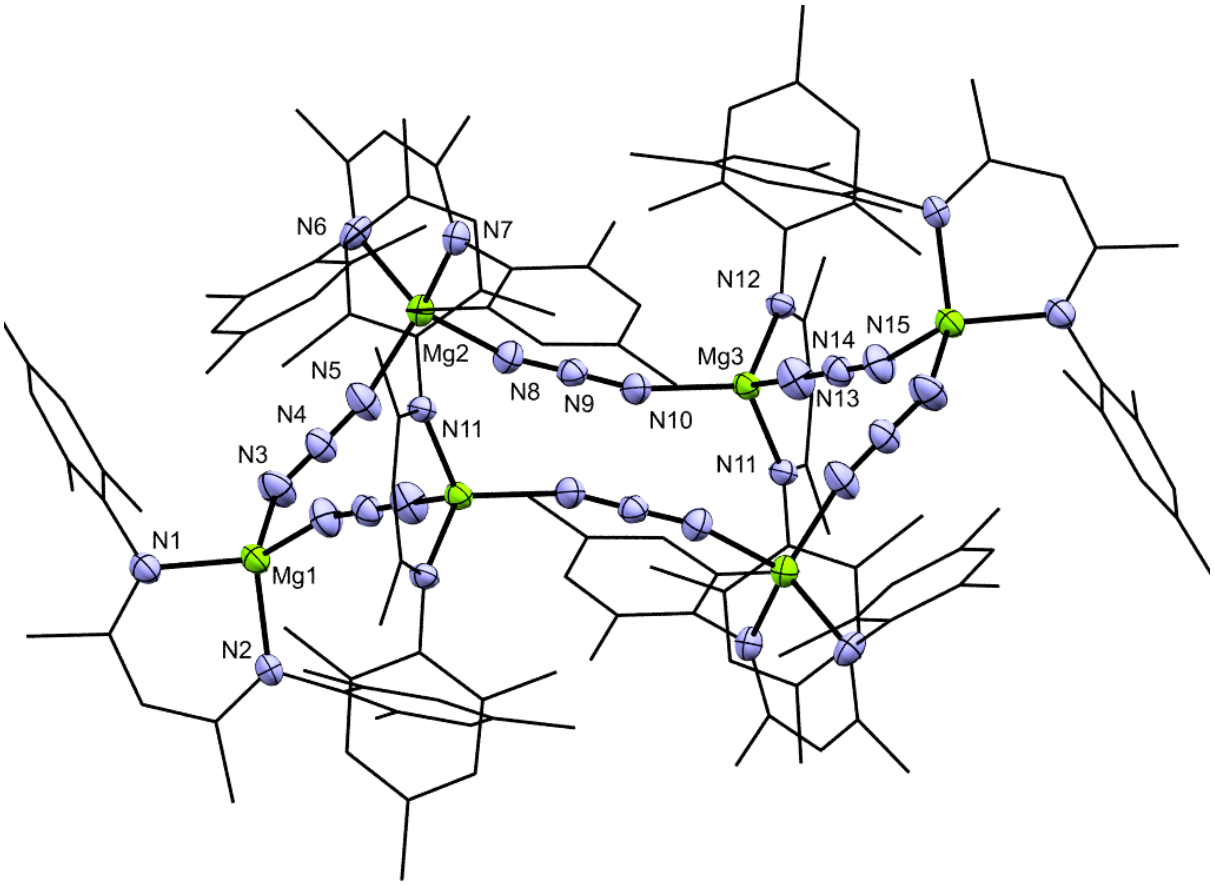

Figure 6.26. Thermal ellipsoid plot of $\{(^{mes}Nacnac)MgN_3\}_6$ hexamer from the crystal structure of $\{(^{mes}Nacnac)MgN_3\}_6 \cdot 2C_6H_{14}$. Ellipsoids set at the 50 % probability level. Hydrogen atoms have been omitted and all carbon atoms are represented in the wire frame. Selected bond lengths (Å) and bond angles (°): Mg1−N1 2.009(3), Mg1−N3 2.015(3), Mg1−N15 2.015(4), Mg1−N2 2.015(3), Mg2−N5 1.994(3), Mg2−N7 2.012(3), Mg2−N6 2.013(3), Mg2−N8 2.031(3), Mg3−N10 2.008(3), Mg3−N11 2.014(3), Mg3−N12 2.026(3), Mg3−N13 2.025(4), N3−N4 1.164(4), N4−N5 1.156(4), N8−N9 1.163(4), N9−N10 1.165(4), N13−N14 1.151(4), N14−N15 1.158(5), N1−Mg1−N3 114.40(15), N1−Mg1−N15 117.90(14), N3−Mg1−N15 101.02(16), N1−Mg1−N2 94.93(12), N3−Mg1−N2 114.88(14), N15−Mg1−N2 114.65(14), N5−Mg2−N7 117.69(14), N5−Mg2−N6 113.40(14), N7−Mg2−N6 93.83(13), N5−Mg2−N8 102.05(15), N7−Mg2−N8 112.03(13), N6−Mg2−N8 118.78(14), N10−Mg3−N11 114.42(13), N10−Mg3−N12 116.71(13), N11−Mg3−N12 94.28(12), N10−Mg3−N13 103.32(14), N11−Mg3−N13 114.47(15), N12−Mg3−N13 114.21(14), N4−N3−Mg1 142.5(3), N5−N4−N3 178.5(4), N4−N5−Mg2 168.2(3), N9−N8−Mg2 147.4(3), N8−N9−N10 178.2(4), N9−N10−Mg3 161.3(3), N14−N13−Mg3 164.9(3), N13−N14−N15 178.8(4), N14−N15−Mg1 164.6(3).

Four mesityl groups lie above and below a cavity formed by the ring of magnesium and nitrogen atoms, whereas the other mesityl groups are directed away from the ring. Each magnesium centre occupies a vertex in a chair confirmation akin to cyclohexane. The distortion of the tetrahedron skeleton of the $[MgN_4]$ unit is caused by the small bite angle of the ^{mes}Nacnac ligand (94.93-93.83°). The azido ligands are coordinated to two different magnesium centres with two different Mg−N−N bond angles but almost identical Mg−N bonds. The average bond angle between Mg−N(α)−N(β) is 151(2)°,

more obtuse than the usual 120° for E−N(α)−N(β), and the average angle between N(β)−N(γ)−Mg is 165(2)°. A simple Lewis structure of a coordinated azide has a single bond between N(α)−N(β) and a triple bond between N(β)−N(γ), therefore, N(γ) would be considered *sp* hybridised and so should form a linear bond to a coordination centre. In this system, the bond angle between N(β)−N(γ)−Mg is significantly more acute than 180°. The average bond lengths between N(α)−N(β) and N(β)−N(γ) are 1.159(7) and 1.160(7) Å respectively. Combination of these two facts point to an ionic azide group, and N(α) and N(γ) are inherently the same and there is no true terminal nitrogen.

Unlike **23**, compound **24** exhibits a trimeric structure. It is worth noting that the single crystal x-ray diffraction data collected for compound **24** was of a low quality due to the crystal decaying almost immediately after removing from the supernatant solution. Consequently, a weak diffraction pattern was obtained. Figure 6.27 shows the molecular structure determined. The ellipsoids, especially the terminal carbon atoms, are incredibly large as well as some of the nitrogen atoms belonging to the azido group.

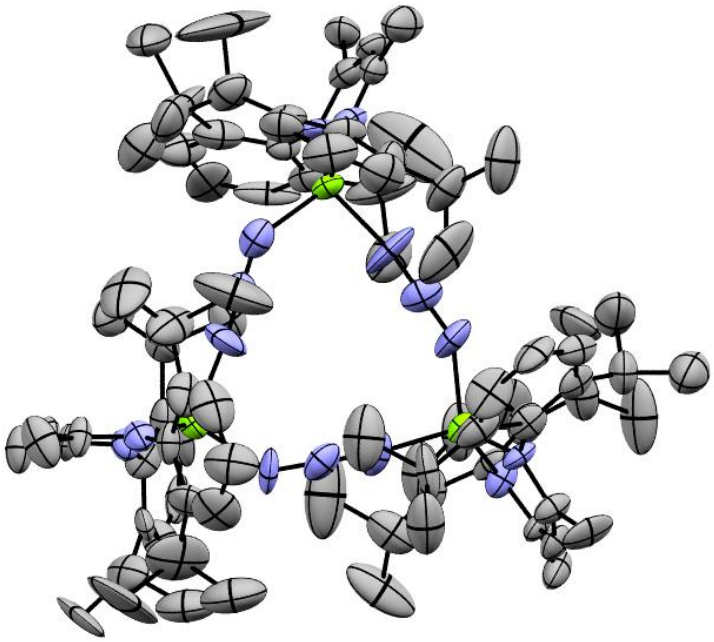

Figure 6.27. Thermal ellipsoid plot of $\{(^{dipp}Nacnac)MgN_3\}_3$. Hydrogen atoms omitted.

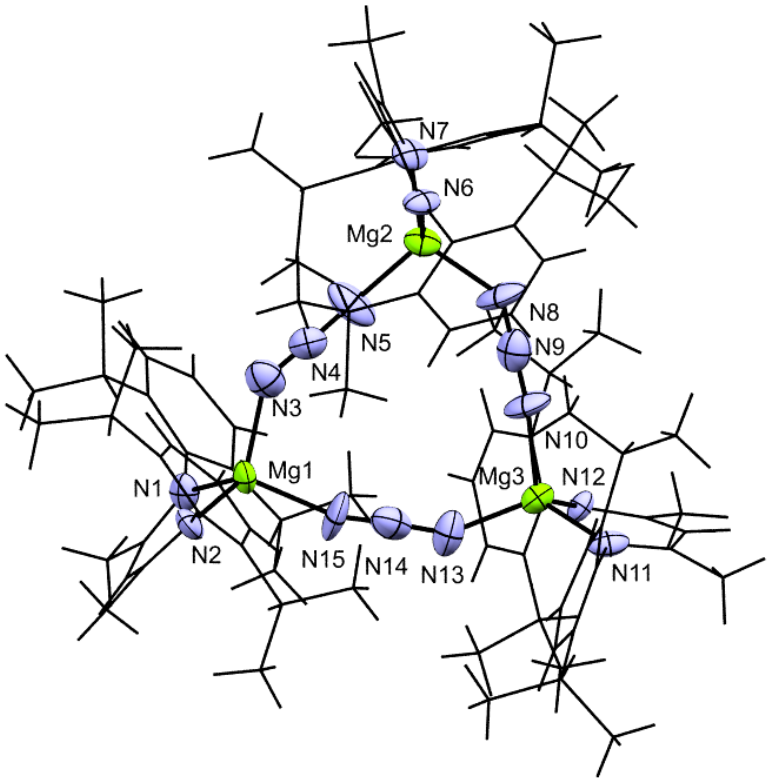

Figure 6.28. Thermal ellipsoid plot of {(^{dipp}Nacnac)MgN_3}$_3$. Ellipsoids set at the 50 % probability level. Hydrogen atoms have been omitted and all carbon atoms are represented in the wire frame. Selected bond lengths (Å) and bond angles (°): Mg1−N1 1.982(11), Mg1−N2 2.004(11), Mg1−N15 2.023(14), Mg1−N3 2.030(13), Mg2−N8 1.945(14), Mg2−N5 1.956(13), Mg2−N7 2.028(11), Mg2−N6 2.042(10), Mg3−N13 1.960(14), Mg3−N10 1.965(12), Mg3−N12 1.978(10), Mg3−N11 1.982(11), N3−N4 1.142(14), N4−N5 1.185(15), N8−N9 1.229(17), N9−N10 1.197(16), N13−N14 1.216(18), N14−N15 1.155(17), N1−Mg1−N2 95.8(4), N1−Mg1−N15 116.8(5), N2−Mg1−N15 112.3(5), N1−Mg1−N3 109.3(5), N2−Mg1−N3 122.6(5), N15−Mg1−N3 101.0(6), N8−Mg2−N5 100.7(6), N8−Mg2−N7 120.3(5), N5−Mg2−N7 113.0(5), N8−Mg2−N6 114.8(5), N5−Mg2−N6 115.6(5), N7−Mg2−N6 93.4(4), N13−Mg3−N10 102.3(6), N13−Mg3−N12 120.9(5), N10−Mg3−N12 111.7(5), N13−Mg3−N11 114.4(5), N10−Mg3−N11 112.8(5), N12−Mg3−N11 95.2(5), N4−N3−Mg1 142.2(11), N3−N4−N5 177.6(13), N4−N5−Mg2 172.9(10), N9−N8−Mg2 140.3(12), N10−N9−N8 177.9(15), N9−N10−Mg3 173.5(12), N14−N13−Mg3 147.8(11), N15−N14−N13 174.3(14), N14−N15−Mg1 162.3(12).

Similarly to the structure of **23**, **24** also crystallises in the space group $P\bar{1}$. Three molecules of **24** come together and are bonded together through $\mu_{1,3}$-N_3 end-to-end bridges to give a planar 12-atom ring. The magnesium atoms have a distorted tetrahedral geometry again as a result of the narrow bite angle from Nacnac ligand. The average Mg−N(α) and Mg−N(γ) bonds are identical (1.984(15) Å and 1.981(13) Å) within the e.s.d and slightly smaller than those in **23**. Both of the N−N bonds in the azido group are similar in length, though the N(α)−N(β) bond is slightly longer than N(β)−N(γ) like a traditional coordinated azido group. The ΔNN parameter is 1.7 pm, a

low value due to the bridging interaction. The similarity of the Mg−N and N−N bond lengths, and the fact the ring is planar, results in the three magnesium atoms occupying the vertex of an equilateral triangle. The bond angle between Mg−N(α)−N(β) is 143(1)°, again larger than the expected 120°, and the N(β)−N(γ)−Mg bond angle is 170(1)°. The shape of the ellipsoids for the azido group nitrogen atoms are larger for N(α) and N(γ). This could be a consequence of low quality diffraction data, however, there is a possibility the coordinated nitrogen atoms are split over two positions or the nitrogen atoms have enough thermal energy to vibrate, even at 100 K.

Compound	Mg−N(α)	Mg−N(γ)	N(α)−N(β)	N(β)−N(γ)	ΔNN
23	2.024(4)	2.006(4)	1.159(7)	1.160(7)	−0.1(10)
24	1.984(23)	1.981(23)	1.196(26)	1.179(28)	1.7(38)

Table 6.5. Bond length data (Å) of hexameric (^{mes}Nacnac)MgN_3 and trimeric (^{dipp}Nacnac)MgN_3.

Compound	Mg−N(α)−N(β)	N(α)−N(β)−N(γ)	N(β)−N(γ)−Mg
23	151(1)	178(1)	165(1)
24	143(1)	175(1)	170(1)

Table 6.6. Bond angle data (°) of hexameric (^{mes}Nacnac)MgN_3 and trimeric (^{dipp}Nacnac)MgN_3.

Tables 6.5 and 6.6 show some of the structural data of the oligomeric structures. An interesting feature is the relationship between the Mg−N(α)−N(β) and N(β)−N(γ)−Mg bond angles and the N−N bond lengths. In the structure of **23** the bond lengths are equal whereas in **24** they are slightly different which results in a larger difference between the angles of the magnesium azide bonds. From this it can be said that the N(γ) in **24** is closer to *sp* hybridisation and in **23** it is relatively closer to sp^2 hybridisation. In the literature, there are three examples of transition metal azides that contain diketiminate ligands that possess a $\mu_{1,3}$-N_3 end-to-end bridge. The examples, (^{dipp}Nacnac)FeN_3, (^{dipp}Nacnac)Cr(THF)N_3 and (^{Ph}Nacnac)V(O^{dipp})N_3, are dimeric and the N(β)−N(γ)−M bond angle is much more acute than in **23** and **24**.[215–217]

In terms of the compounds IR spectra, the differences in the azido groups from the crystal structure explain the difference in the position of the $\nu_{as}(N_3)$. Compound **23** has an absorption at 2160 cm^{-1} and **24** has an absorption at 2195 cm^{-1}. The azido group in the hexameric structure is effectively more ionic than in the trimeric structure exemplified by the ΔNN values from the two structures. This, however, does not

explain why the peak position is at such high wavenumbers to begin with. To prove it is because of the oligomerisation, compound **23** was dissolved in THF. The FT-IR spectrum of this solution displays an IR absorption at 2123 cm^{-1}. Unfortunately, crystals could not be obtained from a THF solution so it was not possible to prove a monomeric species but the absorption is in a plausible position. Oligmerisation is the reason for the high wavenumbers for the IR absorption. Electron density is donated from the terminal nitrogen atom to the second magnesium centre, therefore, for the wavenumbers to increase the electrons must be situated in an antibonding orbital. Loss of electron density from this orbital strengthens the N−N bonds and despite the azide appearing ionic in the solid-state the position of the absorption is close to that of ν(N≡N). At this point this is only speculation. DFT calculations would be required to provide any more insight into the spectroscopic effect of oligomerisation in Main Group azides.

Reduction of Si(IV) polyazides appears to not be a viable method partly due to instability of the potential products or over reduction to Si(I) or Si(0). The other common method for the preparation of low valent silicon centres is *via* hydrido(chloro)silanes. Therefore, the next course of investigation was attempts to prepare hydrido(azido)silanes.

6.2.4 Hydrido(azido)silicon compounds

6.2.4.1 Syntheses and spectroscopy

The simplest hydrido(azido)silane is $HSi(N_3)_3$, an unknown compound. Starting from trichlorosilane a similar method for the preparation of $Si(N_3)_4$ was attempted. After refluxing $HSiCl_3$ dissolved in benzene over sodium azide for 10 days the FT-IR spectrum of the solution displayed two bands between 2200 and 2000 cm^{-1} at 2170 and 2133 cm^{-1}, indicative of $Si(N_3)_4$ and HN_3 respectively. For $Si(N_3)_4$ to form either HN_3 or H_2 must be released. The presence of HN_3 in the FT-IR spectrum clearly points to the release of HN_3. The signal is too large to be accounted for by hydrolysis of $Si(N_3)_4$. The mechanism to form $Si(N_3)_4$ would be complicated with possibilities of the loss of HN_3 from $HSi(N_3)_3$ to give $Si(N_3)_2$, which would be unstable, or an equilibrium between $HSi(N_3)_3$ and $H_2Si(N_3)_2$ and $Si(N_3)_4$.

Unfortunately, $HSi(N_3)_3$ cannot be made this way and may not be a stable molecule. From this, the next reactions attempted involved adding the bulky ligands to $HSiCl_3$ followed by choro / azido exchange using sodium azide. N-heterocylic carbene

complexes of $HSiCl_3$, $(NHC)SiHCl_3$, are often unstable in solution; liable to release of HCl or *via* a dismutation process to form $(NHC)SiCl_4$ and $(NHC)SiH_2Cl_2$.[218] Amidinato complexes of the type $(^{R}NCN)SiHCl_2$ are known. [79] Therefore, $(^{dipp}NCN)SiHCl_2$ was prepared by the reaction of Li(^{dipp}NCN) and $HSiCl_3$. Azido / chloro exchange was completed using sodium azide as an ionic azide transfer reagent to form $(^{dipp}NCN)SiH(N_3)_2$ (**25**).

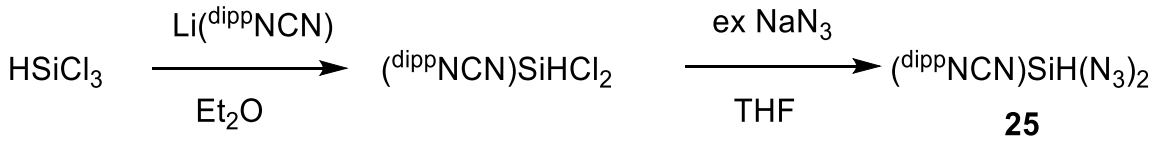

Scheme 6.8. Reaction scheme for the synthesis of $(^{dipp}NCN)SiH(N_3)_2$.

Diketiminato ligands have been used to prepare Si(II) compounds, however, not in the same way as the amidinato ligand. Unlike the amidinato ligand, diketiminato ligands have an unexpected reactivity towards silicon halides. The reaction of Li(^{dipp}Nacnac) and $SiBr_4$ in the presence of tetramethylethylenediamine (tmeda) gives the molecule shown in Figure 6.29. The (^{dipp}Nacnac) loses a hydrogen atom and is reduced from a monoanionic ligand to a dianionic ligand.[219]

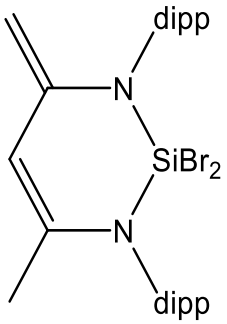

Figure 6.29. Compound obtained from the reaction of $SiBr_4$·(tmeda) and Li(^{dipp}Nacnac).

When Li(^{dipp}Nacnac) was treated with $HSiCl_3$ a voluminous colourless precipitate of LiCl formed and after the reaction work-up colourless crystals of $(^{dipp}Nacnac)SiHCl_2$ (**26**) were obtained. As the product of this reaction was the desired hydrido(chloro)silane it appears there the silicon coordination sphere is too crowded for $(^{dipp}Nacnac)SiBr_3$ to form. The hydrido and chloro ligands are obviously smaller than a

bromo ligand allowing more space around the silicon centre to accommodate the bulky (^{dipp}Nacnac) ligand.

When **26** and sodium azide were suspended in THF the suspension turned purple. The colour change was unexpected and after work-up of the reaction solution colourless crystals were obtained from a purple solution. The crystals were identified as (^{dipp}Nacnac)SiH(N_3)$_2$ (**27**) by single crystal X-ray diffraction measurements. The structure of **26** was also determined by single crystal X-ray diffraction measurements, both of which are discussed in detail in **6.2.4.2**. Interestingly, the molecules have different geometries. In **26** the silicon atom has tetrahedral geometry and the (^{dipp}Nacnac) is bound in a κ^1(*N*) fashion. Whereas in **27** the silicon atom has trigonal bipyramidal geometry and the (^{dipp}Nacnac) is bound in the traditional κ^2(*N*,*N'*) fashion. The chloro ligand is more sterically demanding than the azido ligand and this is exemplified in the differing geometries of the two complexes and the different coordination modes of the Nacnac ligand. The identity of the purple colour could not be determined. However, the ^{1}H-NMR spectrum of the purple oil displays the presence of ^{dipp}NacnacH. It is possible that the molecule slowly decomposes in THF solution and the ^{dipp}Nacnac ligand removes the hydride from the silicon centre and eliminates ^{dipp}NacnacH forming Si(N_3)$_2$, which would be unstable. This is only speculation at this point.

The ^{1}H NMR spectra of compounds **25-27** display resonances for the hydride between 6.13 and 5.54 ppm, summarised in Table 6.7. The hydride resonance for compound **25** is 6.13 ppm with a $^1J_{SiH}$ of 311 Hz. The resonance of the hydride in **25** is at a lower chemical shift compared to (^{dipp}NCN)SiHCl$_2$ (6.47 ppm, $^1J_{SiH}$ 298 Hz). Both of these compounds are trigonal bipyramidal, therefore, the chemical shift is lower because of the electron withdrawing property of the azido group. For compounds **26** and **27** the opposite is true. The azido compound has a hydride chemical shift of 5.91 ppm ($^1J_{SiH}$ 322 Hz) while the chloro compound has a lower hydride chemical shift (5.54 ppm, $^1J_{SiH}$ 338 Hz). As the compounds have differing geometries, that is the reason for the different chemical shifts. Compound **26** is tetrahedral and, therefore, the bonding has more *s*-character compared to the trigonal bipyramidal compound **27** and the hydride has a lower chemical shift.

Compound	δ / ppm	J / Hz
(^{dipp}NCN)SiHCl$_2$	6.47	298
25	6.13	311
26	5.54	338
27	5.91	322

Table 6.7. ^{1}H NMR chemical shift of the hydride in hydrido(chloro)silanes and hydrido(azido)silanes.

The ^{14}N NMR spectrum of **25** only displays two resonances between −100 and −300 ppm at −143 and −204 ppm for N(β) and N(γ) respectively. The resonance for N(α) is missing from the spectrum. As compound **25** has a very large molecular mass the concentration of azido groups is low and consequently the very broad N(α) signal is not observed.

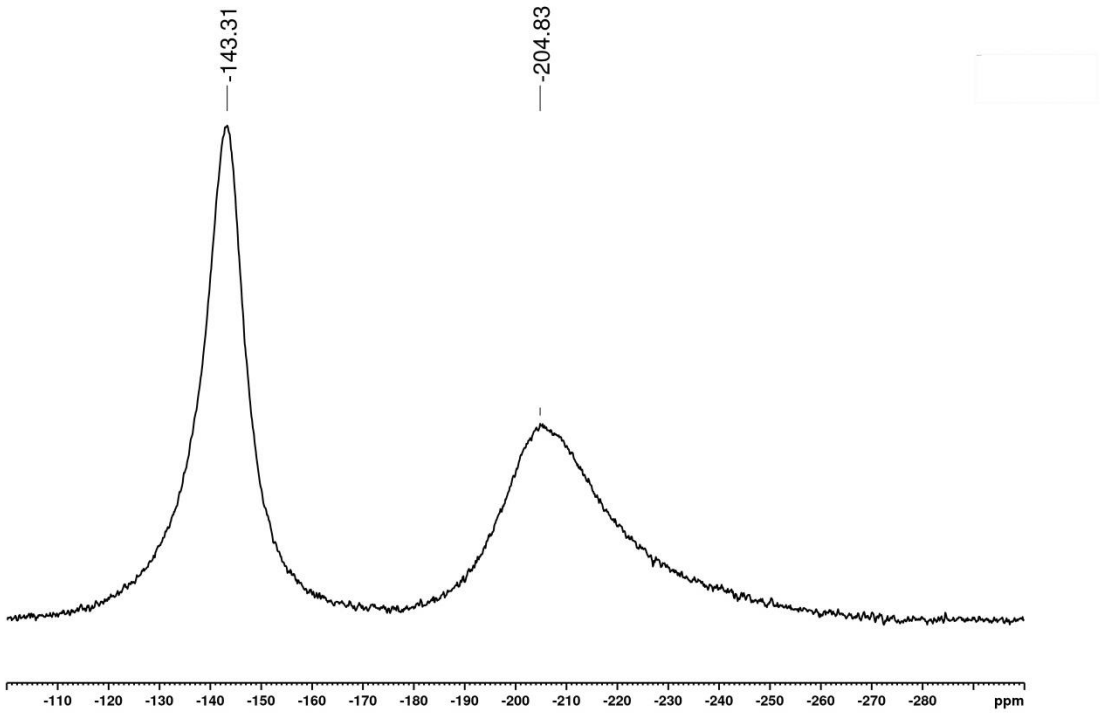

Figure 6.30. ^{14}N NMR spectrum of **25**.

The assignment of the bands in the IR spectra of compounds **25** and **27** is complicated by the fact that the ν(Si−H) and $\nu_{as}(N_3)$ vibrations are observed in the same region. Three absorptions are observed at 2117, 2142 and 2157 cm^{-1} for compound **25** and four absorptions at 2104, 2123, 2144 and 2157 cm^{-1} for compound **27**. Compound

27 was not isolated as a pure compound, the crystals were coated with a sticky purple oil, which may have an influence on why a fourth band is observed. Regardless, the bands of **25** and **27** appear at very similar positions. The two other pentacoordinate azido complexes prepared in this work, **16** and **20**, also have similar positions for the $\nu_{as}(N_3)$ vibration.

Compound	ν / cm^{-1}
25	2117, 2142, 2157
27	2104, 2123, 2144, 2157

Table 6.8. IR absorptions between 2200 and 2000 cm^{-1} of compounds **25** and **27**.

Compound **27** was not isolated as a pure compound, however, compound **25** was and is an ideal candidate for a "deazoimidation" reaction, akin to the dehydrochlorination reactions of $HSiCl_3$ and $(({}^tBuN)_2CPh)SiHCl_2$.

6.2.4.2 Single crystal X-ray diffraction

The molecular structures of compounds **25**-**27** were investigated by single crystal X-ray crystallography. Compound **25** crystallises in the space group *P*bca with four formula units per unit cell. The silicon atom has a distorted trigonal bipyramidal geometry with the amidinato ligand occupying an axial and an equatorial site, as observed in compound **20**. Two azido ligands occupy an equatorial site and an axial site. Counter-intuitively, the final equatorial site is occupied the hydride ligand. As the smallest ligand it would be expected that the hydride would be positioned in the axial position. The amidinato ligand is restricted in its orientation as a result of the narrow bite angle (68.8(1)°). Electronically, the electronegative nitrogen atom is more electron withdrawing than the hydride ligand. In the axial sites there is less competition for the electron density as there are only two groups along that axis. Therefore, despite the steric preference for the equatorial position the azido group is in the axial position due to electronic effects. The trigonal bipyramidal skeleton is distorted to a lesser extent in compound **25** in comparison to compound **20**. The small hydride ligand allows for bond angles in the equatorial plane closer to 120° with a range of 118.1(1)-120.4(1)° (113.7-126.7° for compound **20**).

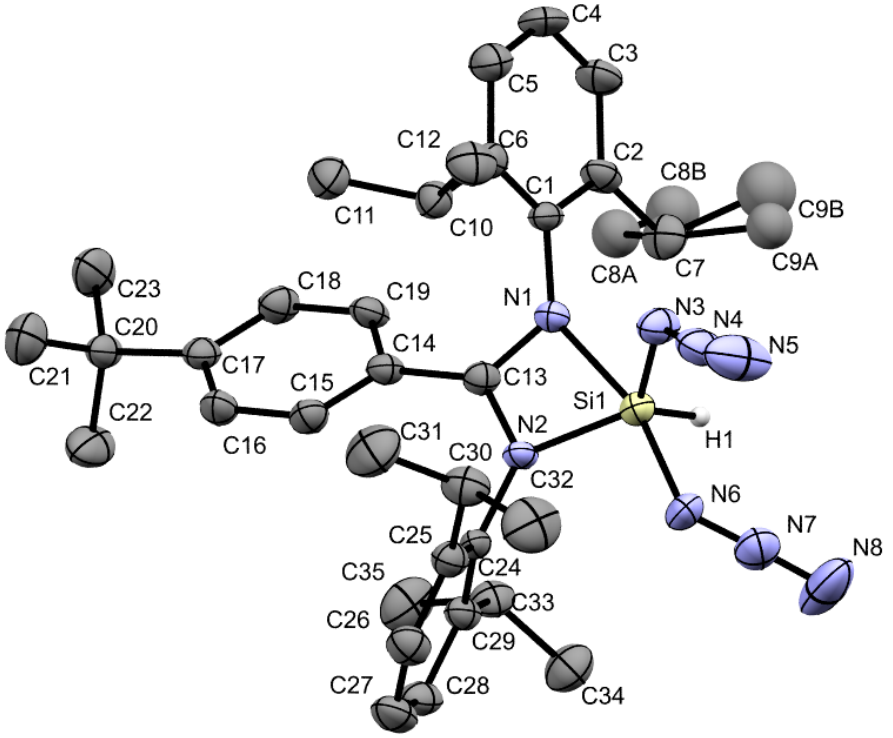

Figure 6.31. Thermal ellipsoid plot of compound **25**. Hydrogen atoms, except the hydride, omitted for clarity. Thermal ellipsoids set at 50 % probability level. C8 and C9 are split over two sites with 50% occupancy in each site. Selected bond lengths (Å) and bond angles (°): Si1−H1 1.319, Si1−N3 1.748(3), Si1−N2 1.785(3), Si1−N6 1.803(3), Si1−N1 1.967(3), N3−N4 1.235(4), N4−N5 1.137(4), N6−N7 1.208(4), N7−N8 1.145(4), N3−Si1−N2 117.83(14), N3−Si1−N6 97.89(15), N2−Si1−N6 94.89(14), N3−Si1−N1 88.75(14), N2−Si1−N1 68.77(12), N6−Si1−N1 163.56(14), N4−N3 Si1 122.4(3), N5−N4−N3 173.9(4), N7−N6−Si1 121.7(3), N8−N7−N6 176.4(4)

The Si−N bonds of **25** are slightly different to those in **20**. The Si−N_{ax} is 1.967(3) Å and the Si−N_{eq} is 1.785(3) Å (1.924 and 1.794 Å in **20**). As with the amidinato ligand, both of the azido ligands have differing Si−N bond lengths due to their orientation, 1.803(3) and 1.748(3) Å for axial and equatorial azido groups respectively. The N−N bonds lengths are typical of coordinated azido groups. The ΔNN parameter for the axial and equatorial azido groups in compound **25** is similar to that of compound **20** (6.3(4) and 9.8(4) pm *vs.* 6.9 pm and 11.2 pm, respectively). As the ΔNN parameter is closely related to the E−N bond length, the ΔNN is larger in **20** than in **25** as E−N is shorter in **20** than in **25** as expeceted. The hydride ligand is less sterically demanding than the azido group and consequently the Si−N bond lengths of the azido groups are shorter in **25**.

Figure 6.31 shows the molecular structure of **26**. The compound crystallises in the space group $P\bar{1}$ with one equivalent of hexane. The silicon atom has a distorted tetrahedral geometry with two chloro ligands, one hydrido ligand and one nitrogen

ligator from the Nacnac ligand occupying the four coordination sites. The Cl−Si−Cl bond angle is narrower than the ideal 109.5° at 105.9(1)°, while both N−Si−Cl bond angles are identical at 113.3°. Both dipp groups are twisted, almost orthogonal, with respect to one another. Also, due to the bulk of the dipp groups, the Nacnac ligand is orientated in a *trans* conformation. The Si−N bond length is 1.711(3) Å, shorter than the two silicon amidinato complexes **20** and **25**. In the NCCCN chain there are two different N−C bonds, a single and a double bond. The nitrogen atom bonded to the silicon atom has the longer N−C bond, 1.423(5) Å, while the other nitrogen atom has the shorter N−C bond, 1.281. The Si−H bond length is 1.341 Å, slightly larger than in compound **25**.

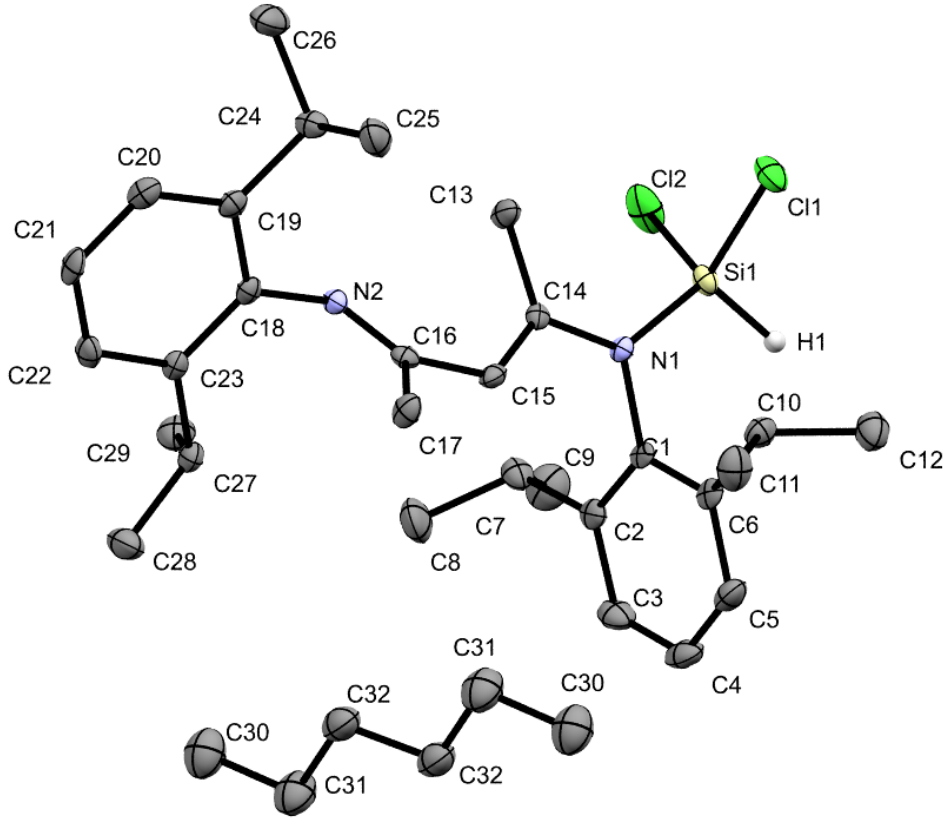

Figure 6.32. Thermal ellipsoid plot of **26**·C_6H_{14}. Hydrogen atoms, except the hydride, have been omitted. Thermal ellipsoids set at the 50% probability level. Selected bond lengths (Å) and bond angles (°): Si1−H1 1.341, Si1−N1 1.711(3), Si1−Cl1 2.0384(15), Si1−Cl2 2.0393(16), C14−C15 1.338(5), C14−N1 1.423(5), C15−C16 1.480(5), C16−N2 1.281(5), N1−Si1−Cl1 113.26(12), N1−Si1−Cl2 113.31(12), Cl1−Si1−Cl2 105.87(7)

Compound **27** crystallises in the space group $P2_1/c$ and the silicon atom has trigonal bipyramidal geometry. In this structure the Nacnac ligand is bidentate and, as with the amidinato ligand, occupies an equatorial site and an axial site. The bite angle of the

Nacnac ligand is larger than the amidinato ligand at 93.8(1)° and consequently results in a less distorted trigonal bipyramidal structure in comparison to compounds **20** and **25**. As with compound **20**, the hydride ligand occupies an equatorial site and the azido groups occupy the final equatorial and axial sites. The bond angles in the equatorial plane, which should be 120°, range between 110.6(1) and 125.0(1)°. The range is much narrower in compound **25** (118.1 and 120.4°) as the amidinato ligand is less sterically demanding than the Nacnac ligand.

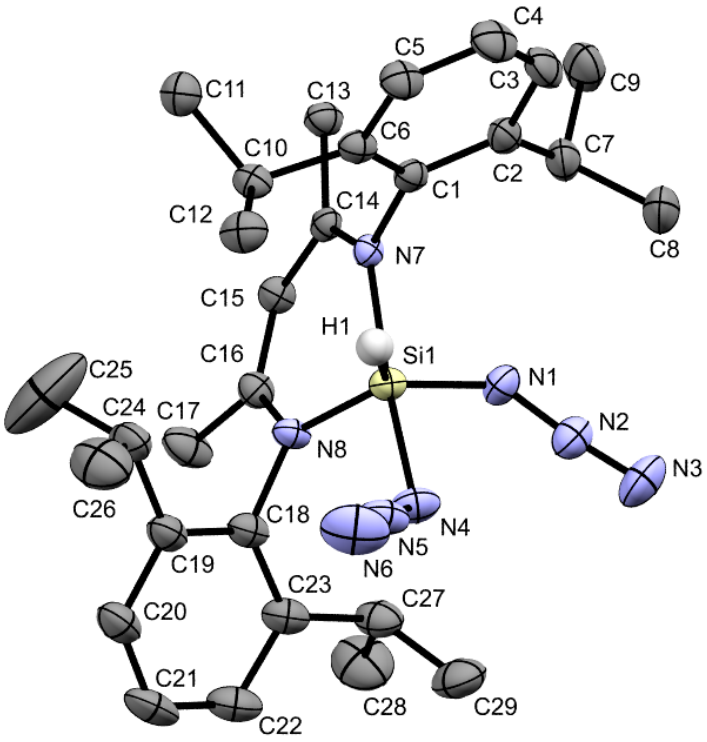

Figure 6.33. Thermal ellipsoid plot of **26**. Hydrogen atoms, except the hydride, have been omitted. Thermal ellipsoids set at the 50% probability level. Selected bond lengths (Å) and bond angles (°): Si1−H1 1.349, Si1−N1 1.769(2), Si1−N8 1.796(2), Si1−N4 1.870(2), Si1−N7 1.926(2), N1−N2 1.228(3), N2−N3 1.134(3), N4−N5 1.216(3), N5−N6 1.143(3), N1−Si1−N8 110.55(10), N1−Si1−N4 91.71(11), N8−Si1−N4 93.56(10), N1−Si1−N7 88.19(9), N8−Si1−N7 93.75(9), N4−Si1−N7 172.23(10), N2−N1−Si1 124.77(19), N3−N2−N1 173.2(3), N5−N4−Si1 116.53(19), N6−N5−N4 179.0(3)

The Si−N bond lengths of the Nacnac ligand are 1.926(2) and 1.796(2) Å for the axial nitrogen and equatorial nitrogen atom respectively. Both of these bond lengths are shorter than the values of the Si−N bond lengths of the amidinato ligand in compound **25**, most likely as the six-membered ring is less strained than the four-membered ring in compound **25**. The Si−N bond lengths of the azido group are 1.870(2) and 1.769(2) Å for the axial and equatorial azido groups respectively. Table 6.9 summarises the structural parameters of the azido ligands in **25** and **27**. It is often observed that the longer the E−N bond the lower the ΔNN parameter. However, when considering

complex **27** the trend is not followed for the axial azido group. The Si−N bond length for this azido group is 1.870 Å, the largest Si−N bond length determined in this work, and yet the ΔNN parameter is high at 7.3 pm. For comparison, the $[Si(N_3)_6]^{2-}$ anion has an average Si−N bond length of 1.871 Å and the ΔNN parameter is 5.7 pm. The ellipsoids in the solved structure of **27** are sensible, the r-factor is 5.73% and there is no disorder in the structure, therefore, the bond lengths are reliable. The unusually long Si−N bond length for this azido group must be a result of a steric influence from the Nacnac ligand. The Si−H bond length is 1.349 Å, longer than both **25** and **26**.

Compound	Orientation	E−N	N(α)−N(β)	N(β)−N(γ)	ΔNN
25	axial	1.803(3)	1.208(4)	1.145(4)	6.3(6)
	equatorial	1.748(3)	1.235(4)	1.137(4)	9.8(6)
27	axial	1.870(2)	1.216(3)	1.143(3)	7.3(4)
	equatorial	1.769(2)	1.228(3)	1.134(3)	9.4(4)

Table 6.9. Bond lengths (Å) and ΔNN parameter (pm) associated with the azido group in **25** and **27**.

6.2.5 Attempted 'deazoimidation' of hydrido(azido) silicon compounds

Compound **25** was treated with a variety of bases in the aims of eliminating HN_3 from the molecule in a reductive elimination reaction, akin to the dehydrochlorination reaction of $(^{R}NCN)SiHCl_2$. The base chosen needs to ideally be bulky and non-nucleophilic to prevent coordination to the silicon centre and a strong enough base to remove the hydride. Bases previously used for dehydrochlorination of $((^{t}BuN)_2CPh)SiHCl_2$ were I^{t}Bu and $LiN(SiMe_3)_2$. In this work four bases have been used: Li(^{dipp}Nacnac), $LiN(SiMe_3)_2$, IPr, and I^{t}Bu.

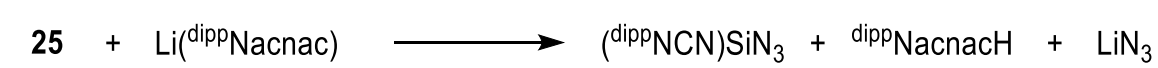

Scheme 6.9. Proposed reaction scheme for the preparation of $(^{dipp}NCN)SiN_3$ from **25** and Li(d^{ipp}Nacnac).

Considering Li(^{dipp}Nacnac) first, the compound was combined with **25** in toluene in a Schlenk tube and stirred. The solution had turned slightly yellow over a 24 hr period, however, no other change was observed. If the intended reaction had occurred a

precipitation of lithium azide should have been apparent, Scheme 6.9. Colourless crystals were obtained after evaporating the toluene and recrystallizing the residue from *n*-hexane. The FT-IR spectrum of those crystals as a nujol mull displayed two signals at 2173 and 2147 cm^{-1}. The increase in wavenumbers of the absorption between these crystals and **25** (2157, 2142 and 2117 cm^{-1}) combined with the fact no lithium azide had formed indicates that compound **25** and Li(^{dipp}Nacnac) co-crystallise. The ^{1}H NMR spectrum of the crystals in C_6D_6 showed that the resonance for the hydride is at the same chemical shift as in **25** in C_6D_6 and there is no interaction between the two compounds in solution.

Earlier it was determined that a $\mu_{1,3}$-N_3 end-to-end bridge results in an increase in the wavenumbers of $\nu_{as}(N_3)$. A similar interaction between Li(^{dipp}Nacnac) and compound **25** is present in the solid-state structure giving a plausible reason to the high wavenumber observed in the FT-IR spectrum obtained. The identity of the crystals was confirmed to be (^{dipp}NCN)SiH$(N_3)_2$·Li(^{dipp}Nacnac) (**28**) by single crystal X-ray diffraction measurements. Figure 6.34 shows the molecular structure of **28**. Compound **28** crystallises in the space group $P2_1$ with two formula units per unit cell. The silicon atom has trigonal bipyramidal geometry and has the same arrangement of ligands as compound **25**. The lithium atom is trigonal planar with the (^{dipp}Nacnac) ligand symmetrically bidentate and occupying two coordination sites. A long Li−N bond with the N(γ) atom of the axial azido ligand of the trigonal bipyramidal component, forming an asymmetric bridge, completes the arrangement.

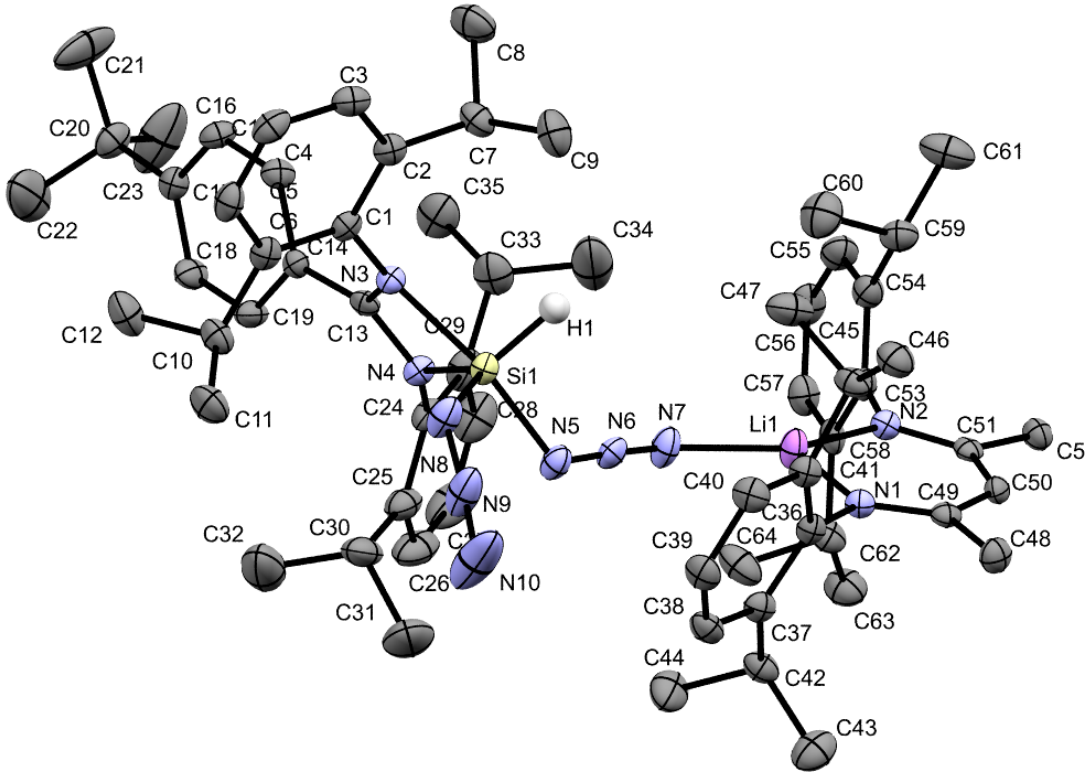

Figure 6.34. Thermal ellipsoid plot of **28**. Thermal ellipsoids set at the 50% probability level. Hydrogen atoms, except the hydride, have been omitted for clarity. Selected bond lengths (Å) and bond angles (°): Si1−H1 1.526, Si1−N8 1.743(2), Si1−N4 1.791(2), Si1−N5 1.846(2), Si1−N3 1.950(2), Li1−N1 1.891(5), Li1−N2 1.893(5), Li1−N7 2.005(5), N5−N6 1.205(3), N6−N7 1.144(3), N8−N9 1.225(4), N9−N10 1.126(4), N8−Si1−N4 119.97(11), N8−Si1−N5 95.55(11), N4−Si1−N5 95.18(10), N8−Si1−N3 90.53(10), N4−Si1−N3 68.91(9), N5−Si1−N3 163.87(10), N1−Li1−N2 99.3(2), N1−Li1−N7 109.3(2), N2−Li1−N7 151.4(3), N6−N5−Si1 120.10(18), N7−N6−N5 177.3(3), N6−N7−Li1 149.7(2), N9−N8−Si1 124.1(2), N10−N9−N8 174.1(3)

The bond lengths of the ligands to the silicon centre are similar to compound **25**, except the Si−H bond and Si−N bond of the axial azido ligand. The Si−H bond is 1.526 Å, much longer than the same bond in compounds **25**, **26** and **27**. There is also a significant degree of distortion in the equatorial plane of the trigonal bipyramid resulting in a range of bond angles in this plane between 105(1) and 132(1)°. The extra bulk from the ^{dipp}Nacnac ligand causes the amidinato ligand to crowd the coordination sphere around the silicon more than in **25** and pushes the hydride closer towards the azido ligand. The change in the axial ligand is caused by the effect of the lithium coordination. Unlike the magnesium azides, **23** and **24**, there is still a difference between the N−N distances of the bridging azido ligand, ΔNN is 6.1(4) pm. The bridging interaction is similar to the bridging interaction present in metal diketiminato azides mentioned earlier. Corroborated by the bond angle between N(β)−N(γ)−Li,

which is 149.7(2)°. Table 6.10 summarises the spectral position of $\nu_{as}(N_3)$ and the angle between the azide and bridging metal of diketiminato metal azido complexes.

Compound	$\nu_{as}(N_3)$ / cm^{-1}	N(β)−N(γ)−M / °
24	2195	170
23	2176	165
28	2173 or 2147*	150
(^{dipp}Nacnac)Cr(THF)N_3 [216]	-	136
(^{dipp}Nacnac)V(Odipp)N_3 [215]	2087	134
(^{dipp}Nacnac)FeN_3 [217]	2129	128

Table 6.10. Wavenumbers of $\nu_{as}(N_3)$ and the bond angle between N(β)−N(γ)−M for diketiminato containing bridging azido complexes. *As a polyazide, compound **28** has two absorptions either of which could be the bridging azide, the terminal azide, or the Si−H bond. No IR data was provided for the chromium complex.

Caution needs to be taken when comparing transition metal azido complexes with Main Group azido complexes because of electron donation from metal *d*-orbitals to the π* orbitals of the azido ligand. However, there appears to be a general trend that a less obtuse angle for N(β)−N(γ)−M is accompanied with a lower wavenumber for the $\nu_{as}(N_3)$.

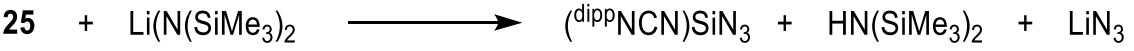

Scheme 6.10. Proposed reaction scheme for the preparation of (^{dipp}NCN)SiN_3 from **25** and Li(N($SiMe_3$)$_2$).

Addition of LiN($SiMe_3$)$_2$ to a toluene solution of **25** results in an immediate white precipitate and a pale yellow solution. The FT-IR spectrum of the white solid is shown in Figure 6.35. There is a broad signal between 2200 and 2000 cm^{-1} at 2136 cm^{-1}, and two signals at 3523 and 3405 cm^{-1} suggesting lithium azide. Sodium azide also has two signals in the same region at 3390 and 3299 cm^{-1}.

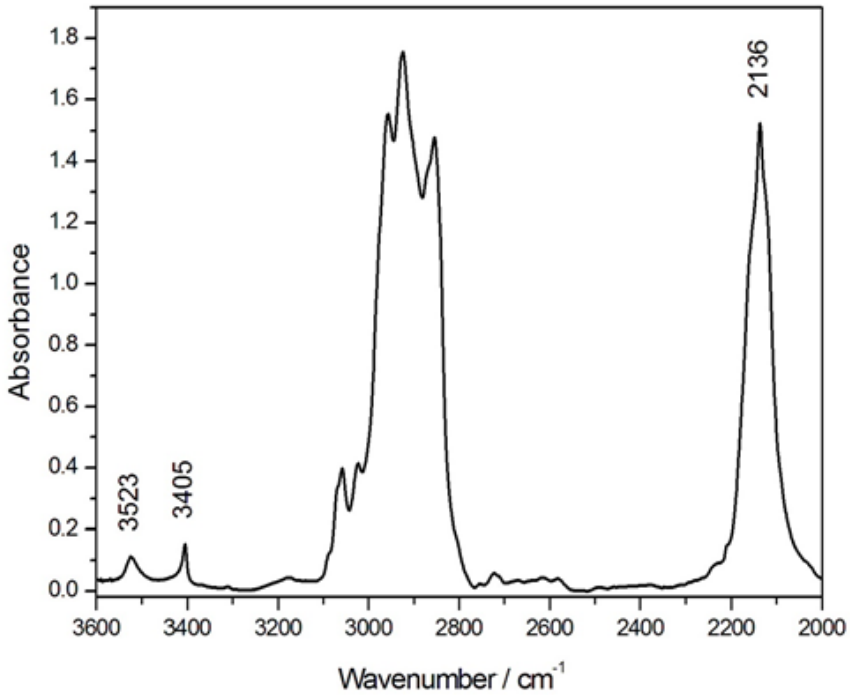

Figure 6.35. FT-IR spectrum of LiN_3 between 3600 and 2000 cm^{-1}.

Scheme 6.10 suggests that the other by-product of the reaction is the silyl amine, $HN(SiMe_3)_2$. This is a volatile liquid and is removed by evaporation along with the reaction solvent. The residue can be recrystallized from *n*-hexane to give colourless block crystals. The FT-IR spectrum of these crystals as a nujol mull displays signals at 2225 (νSiH) and 2153 cm^{-1} ($\nu_{as}(N_3)$). The presence of Si−H bonds in the FT-IR spectrum and the precipitation of lithium azide points to an exchange between the azido group and $N(SiMe_3)_2$. Therefore, the product from the reaction of **25** and $Li(N(SiMe_3)_2)$ is (^{dipp}NCN)SiH(N_3)($N(SiMe_3)_2$) (**29**).

Compound **29** crystallises in the space group $P\bar{1}$ with four formula units per unit cell with two unique molecules in the asymmetric unit. As with compound **21**, the amidinato ligand is bound in a κ^1N fashion and not the more common bidentate coordination mode. In turn the silicon atom has a tetrahedral geometry and not trigonal bipyramidal. This silicon atom has four different substituents, thus rendering the molecule chiral. Both enantiomers are present in the crystal structure. The bis(trimethylsilyl)amide group is bulky enough to prevent bidentate coordination of the amidinato ligand exemplified by the large N−Si−N bond angle between these two ligands, 124(1)°. Si1, as labelled in Figure 6.36, is coordinated to three nitrogen atoms from three different ligands. The Si−N bond lengths range between 1.705(2) to 1.780(2) Å with the bis(trimethylsilyl) amide ligand being the shortest and the amidinato ligand having the longest Si−N bond.

The two Si−N bond lengths, between the trimethylsilyl groups and the nitrogen atom of the amide, are very similar at 1.765(2) and 1.772(2) Å. As the bond to Si1 from the nitrogen is 1.705(2) Å, significantly shorter than Si2−N6 and Si3−N6, suggests there is a degree of double bond character between Si1 and N6. The structural parameters associated with the azido group are consistent with that of other tetrahedral azidosilanes; the Si−N bond length is 1.761(3) Å and the ΔNN parameter is 9.3(4) pm. The Si−H bond length is 1.391 Å, larger than that of **25**-**27** but shorter than **28**. Unlike the Si−N bond length of azido groups, the Si−H bond length does not seem to depend on the geometry of the complex but rather the steric hindrance around the coordination sphere.

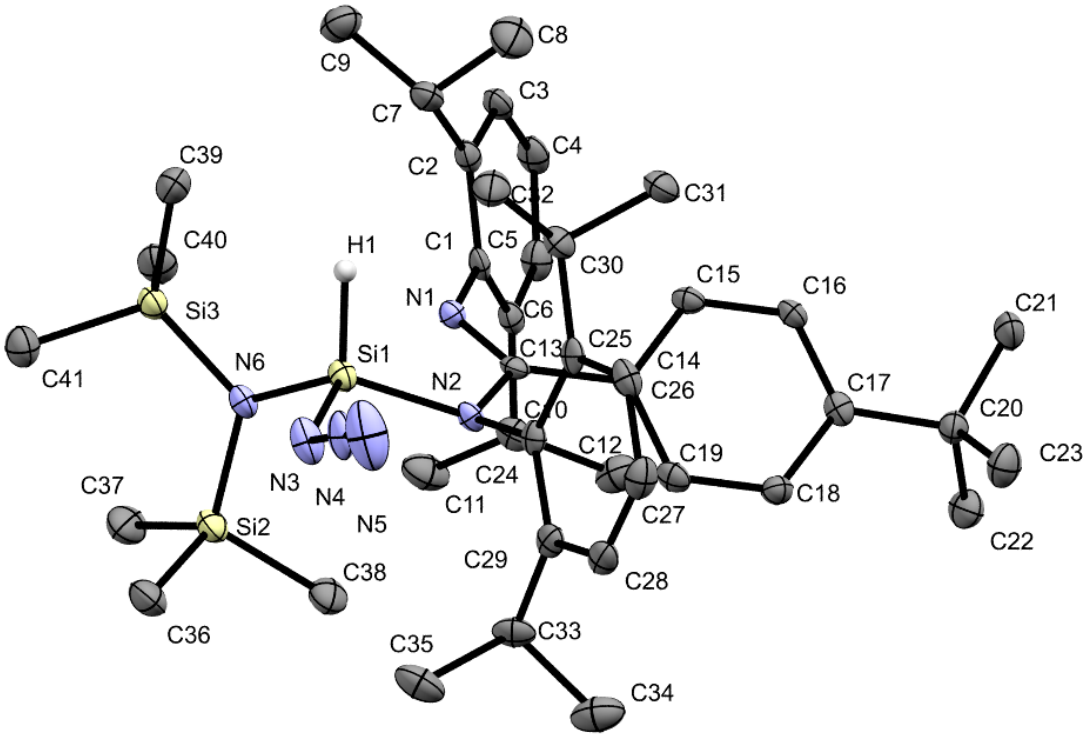

Figure 6.36. Thermal ellipsoid plot of the s-isomer of **29**. Thermal ellipsoids set to the 50% probability level. Hydrogen atoms, except the hydride, have been omitted. Selected bond lengths (Å) and bond angles (°): Si1−H1 1.391, Si1−N6 1.705(2), Si1−N3 1.761(3), Si1−N2 1.780(2), Si2−N6 1.765(2), Si3−N6 1.772(2), N3−N4 1.225(3), N4−N5 1.132(3), N6−Si1−N3 102.85(11), N6−Si1−N2 124.18(11), N3−Si1−N2 103.11(11), N6−Si3−C40 109.67(13), N6−Si3−C39 113.96(12), C40−Si3−C39 107.15(14), N6−Si3−C41 109.88(12), C40−Si3−C41 113.40(14), C39−Si3−C41 102.68(14), N6−Si2−C36 109.61(13), N6−Si2−C38 111.29(12), C36−Si2−C38 110.42(14), N6−Si2−C37 112.63(12), C36−Si2−C37 108.79(15), C38−Si2−C37 103.96(14), N12−Si4−N9 100.52(11), N4−N3−Si1 130.6(2).

The overall driving force for the reaction is the insolubility of the lithium azide and the enthalpic gain accompanied with its precipitation. The bis(trimethylsilyl)amide is

too nucleophilic and is small enough to coordinate to the silicon centre. It may be that the planned reaction is occurring, however, there is then a reaction between the desired product and the by-product bis(trimethylsilyl)amine, Scheme 6.11.

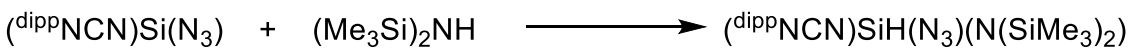

Scheme 6.11. Proposed reaction equation between desired product and bis(trimethylsilyl)amine.

In both lithium based bases experiments a Si(II) species was not isolated. The next two bases used were the NHCs IPr and I^{t}Bu. The expected reaction between **25** and an NHC would form the Si(II) azide and the corresponding imidazolium azide, Scheme 6.12.

Scheme 6.12. Proposed reaction scheme for the reaction between **25** and NHCs.

The combination of IPr and **25** in toluene affords a slightly turbid solution, which after work-up resulted in colourless needle crystals. The FT-IR spectrum of these crystals as a nujol mull between 3500 and 2000 cm^{-1} is shown in Figure 6.37. There are four bands present in the $\nu_{as}(N_3)$ region at 2157, 2141, 2113 and 2091 cm^{-1}.

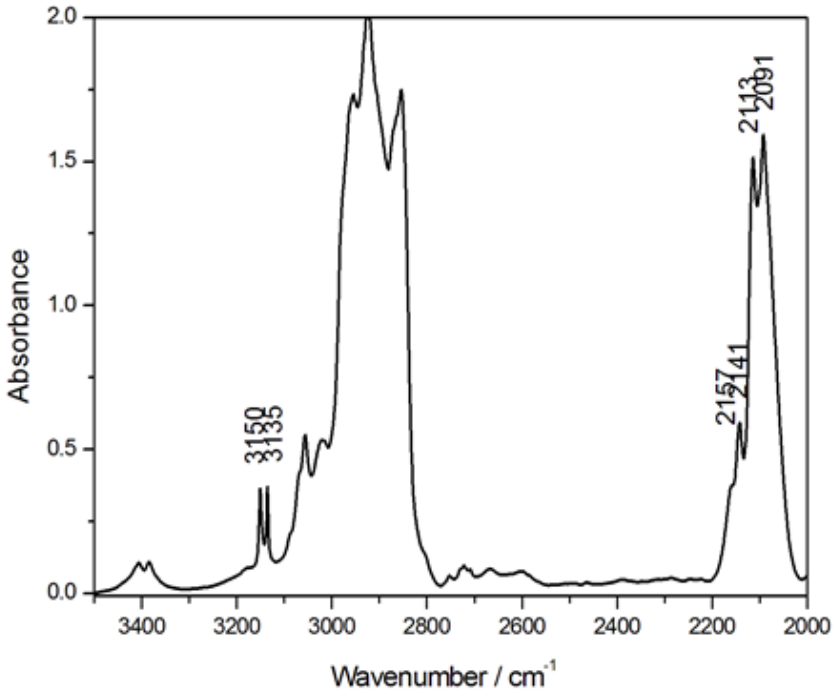

Figure 6.37. FT-IR spectrum of **30** as a nujol mull between 3500 and 2000 cm^{-1}. Relevant peaks labelled.

There is no absorption present around 2000 cm^{-1} for the imidazolium azide immediately indicating the proposed reaction has not occurred. The identity of the product could be determined from the FT-IR spectrum. Two peaks at 3150 and 3135 cm^{-1} are indicative of coordinated IPr and the postion of the $\nu_{as}(N_3)$ vibration suggests octahedral geometry, therefore, the compound is (^{dipp}NCN)SiH$(N_3)_2$(IPr). The ^{1}H-NMR spectrum shows the resonances for both ^{dipp}NCN and IPr. Interestingly the peaks for the imidazole protons are significantly down field of both free IPr and **16** at 7.66 and 7.68 ppm (IPr = 6.62 ppm; **16** = 7.18 and 7.20 ppm). This indicates that IPr is not coordinated in the traditional fashion *via* C2, but rather in what is known as the abnormal coordination mode *via* C4.[220] Over the course of the reaction the IPr ligand has tautomerized and coordinated to **25**, as confirmed by single crystal X-ray diffraction studies, to form (^{dipp}NCN)SiH$(N_3)_2$(*ab*-IPr) (**30**).

Compound **30** crystallises in the space group $P\bar{1}$ as a hemi solvate with toluene and has two formula units per unit cell. The silicon atom has a significantly distorted octahedral geometry with one azido group *trans* to a hydride and another azido group *trans* to one of the nitrogen atoms of the amidinato ligand. IPr is *trans* to a nitrogen atom of the bidentate amidinato ligand bound in the abnormal coordination mode. The bite angle of the amidinato ligand is 67.36(8)°, comparable to that of the other compounds synthesised thus far. The bond angle between the NHC and the *cis* nitrogen

atom of the amidinato group is larger than the ideal 90° at 99.18(8)°. This relieves some of the steric hindrance between the dipp groups of the NHC and amidinato ligand. The angle between IPr and the nitrogen atom *trans* to it is 165.77(9)° and the Si−C bond length is 1.969(2) Å, slightly longer than the Si−C bond in **16** which is 1.926 Å. It is not possible to determine if bond is longer due to the abnormal coordination mode or because the molecule is octahedral. For comparison, the Si−C bond between $IPrSiF_4$ and IPr_2SiF_4 is slightly larger in the octahedral molecule.[190] Most likely the longer bond length in **30** is due to the increased coordination number. The traditional coordination mode should have a longer Si−C bond as the bulky groups bonded to the nitrogen atoms will be closer to the coordination centre. The Si−H bond length is 1.568 Å, longer than the other hydrido(azido) silanes prepared so far. The Si−N bond lengths for the amidinato ligand are different lengths at 1.951(2) and 1.917(2) Å. The nitrogen atom *cis* to IPr has the longer Si−N bond length due to its closer proximity to the NHC than the other nitrogen atom of the amidinato ligand. The azido ligand *cis* to IPr and both amindinato nitrogen atoms has the longer Si−N bond of the two groups at 1.915(2) Å. The other azido group has a Si−N bond length of 1.854(2) Å. Though in different environments both the azido groups have almost identical N−N bond lengths and the ΔNN parameters are 5.9(3) and 6.0(3) ppm. This is despite the two different $Si-N_{azide}$ bond lengths.

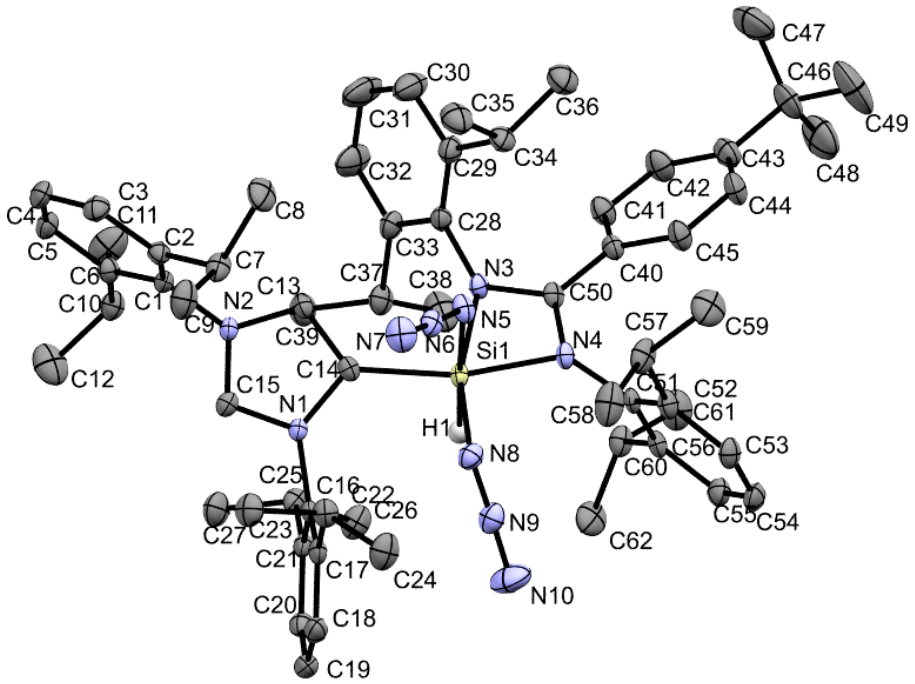

Figure 6.38. Thermal ellipsoid plot of **30**. Thermal ellipsoids set at 50 % probability. Hydrogen atoms, except the hydride, have been omitted for clarity. Selected bond lengths (Å) and bond angles (°): Si1−H1 1.568, C14−Si1 1.969(2), C15−N2 1.329(3), C15−N1 1.343(3), C13−C14 1.366(3), C13−N2 1.387(3), N3−Si1 1.9509(18), N4−Si1 1.9165(18), N5−N6 1.209(3), N5−Si1 1.9147(19), N6−N7 1.150(3), N8−N9 1.211(3), N8−Si1 1.854(2), N9−N10 1.151(3), N6−N5−Si1 121.80(16), N7−N6−N5 177.4(2), N9−N8−Si1 123.26(16), N10−N9−N8 175.2(2), N8−Si1−N5 89.11(9), N8−Si1−N4 96.27(8), N5−Si1−N4 87.12(8), N8−Si1−N3 163.23(9), N5−Si1−N3 86.50(8), N4−Si1−N3 67.36(8), N8−Si1−C14 96.79(9), N5−Si1−C14 87.46(9), N4−Si1−C14 165.77(9), N3−Si1−C14 99.18(8)

Table 6.11 shows the spectroscopic and structural properties of the silicon hydride bond in compounds **25**, **28**, **29** and **30**. IR spectroscopic data is not included as in some instances it is not possible to determine the absorption from the FT-IR spectrum as the ν(Si−H) region overlaps with the $\nu_{as}(N_3)$ region. It would be expected that the chemical shift of the hydride signal should decrease with an increased coordination number and this can be seen between the trigonal bipyramidal and octahedral complexes **25** and **30**. The tetrahedral compound **29** does not fit this trend; however, the ligands are different. The azido ligand is different to the bis(trimethylsilyl)amido ligand both sterically and electronically and so it is not possible to draw a direct comparison. There is a clear correlation between the chemical shift and the Si−H bond length. The longer the Si−H bond, the lower the chemical shift. Compound **28** has a longer Si−H bond than compound **25** despite both being trigonal bipyramidal molecules. However, the presence of the Nacnac ligand in compound **28** results in more steric crowding around the coordination sphere and so affects the length of the Si−H bond.

Compound	Si−H bond length / Å	δ / ppm	J / Hz
25	1.319	6.13	311
28	1.526	6.13	313
29	1.391	5.98	286
30	1.568	5.93	-*

Table 6.11. Spectroscopic and structural data of the silicon hydride. * sample too dilute to observe ^{29}Si satellites.

IPr could not break the Si−H bond to form (IPrH)N_3, therefore, I^{t}Bu was also investigated. The t-butyl groups are more electron donating than the Dipp groups resulting in an increased amount of electron density on the imidazolylidene ring and increasing the nucleophilicity of the NHC. Compound **25** and I^{t}Bu were suspended in hexane and stirred for 24 hrs. Figure 6.39 shows the FT-IR spectrum of the reaction solution. The original three signals of compound **25** at 2159, 2143 and 2123 cm^{-1} have disappeared and new signals at 2152, 2133, 2109, 2099 and 2008 cm^{-1} are present. The peak at 2133 cm^{-1} indicates HN_3 from hydrolysis of the silicon azide in sample measurement. The size of which indicating how sensitive the compound formed is. The peak at 2008 cm^{-1} is due to (I^{t}BuH)N_3. This leaves the other three peaks to be due to the new product. Multiple peaks implies that either (I^{t}BuH)N_3 reacts with (^{dipp}NCN)SiN_3 or unreacted starting material to give a new silicon polyazide.

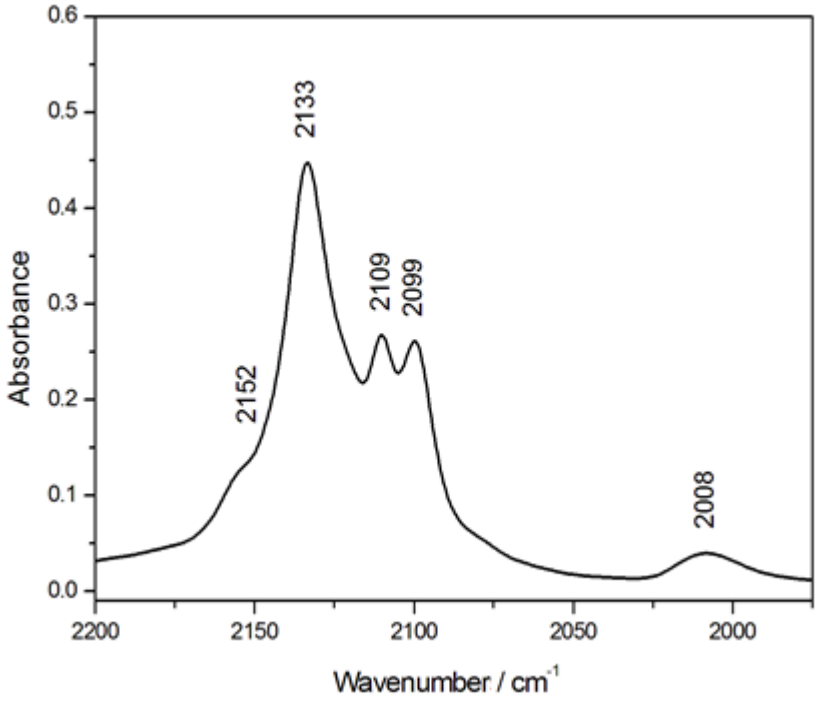

Figure 6.39. FT-IR spectrum of a hexane solution of **25** and I^{t}Bu after stirring for 24 hrs.

Regardless, it appears that the reaction between **25** and I^{t}Bu proceeds by the proposed reaction scheme, Scheme 6.12. Concentration of the reaction solution and cooling to −28°C affords small, colourless block crystals. The FT-IR spectrum of the crystals as a nujol mull is shown in Figure 6.40. Between 2050 and 2160 cm^{-1} there are several overlapping and broad peaks, as a result it is difficult to ascertain how many peaks are actually present, except for a clear signal at 2123 cm^{-1}. There is a small peak for (I^{t}BuH)N_3 at 2015 cm^{-1}. After air exposure of the sample on the sodium chloride windows for as little as four mins and rerecording the FT-IR spectrum of the sample shows a significant increase in the peak at 2015 cm^{-1}, and only a small signal at 2122 cm^{-1} remains between 2050 and 2160 cm^{-1}. From this it is clear the compound prepared is extremely air sensitive and more sensitive than all the other hydrido(azido)silanes prepared in this work.

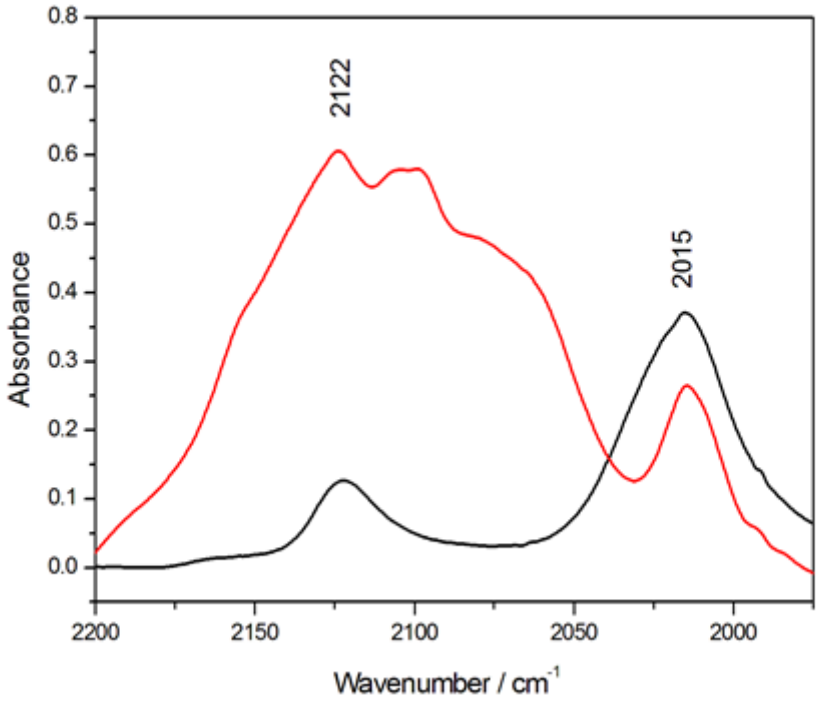

Figure 6.40. Black: FT-IR spectrum of crystals obtained from the reaction between I^{t}Bu and **25** as a nujol mull. Red: FT-IR spectrum of the sample that produced the black line after air exposure of 4 mins.

The crystals obtained from this reaction were investigated by single crystal X-ray diffraction studies. The best model obtained from the study was that of (I^{t}BuH)[(^{dipp}NCN)SiH(N_3)$_3$] (**31**), as a hexane solvate. Disorder in the position of the azido groups causes ambiguity in the overall model. In the hope of rectifying this, the material was also recrystallized from toluene. However, the model determined from the crystal obtained from toluene has similar issues as the crystal grown from hexane. In both structures, **31**·C_6H_{14} and **31**·C_7H_8, the compounds crystallises in the space group $P\bar{1}$. The silicon atom has octahedral geometry with the amidinato ligand occupying two sites and an azido group in the same plane. This azido group is the only azido group in the structures with an occupancy of one. Four other azido groups are shared over three sites with an overall occupancy of two giving an overall three azido groups in the molecule. Due to this disorder the position of the hydride cannot be determined. However, as two azido groups are shared in one coordination site, in the plane with the amidinato ligand, the hydride must therefore be split between the two sites *cis* to the amidinato ligand. Figures 6.41 and 6.42 show the molecular structures of **31**·C_6H_{14} and **31**·C_7H_8 and Figure 6.43 shows the two disordered components of **31** as determined from the diffraction studies.

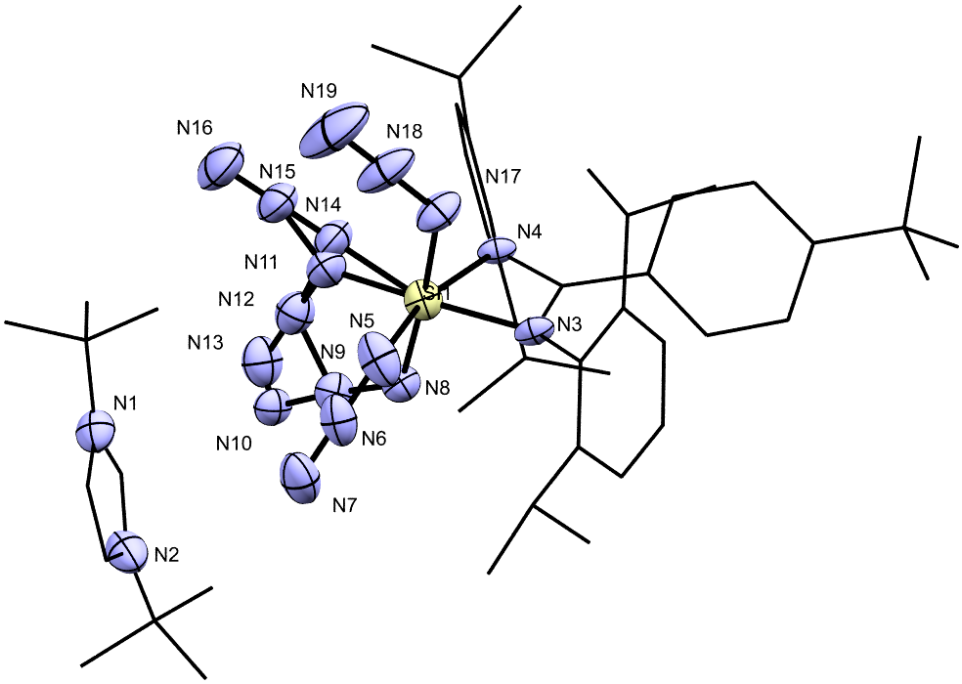

Figure 6.41. Thermal ellipsoid plot of **31**·C_7H_8. Thermal ellipsoids set at the 50 % probability level. Toluene and hydrogen atoms omitted for clarity. Carbon atoms represented as wireframe. Selected bond lengths (Å) and bond angles (°): Si1−N5 1.797(6), Si1−N17 1.823(4), Si1−N8 1.832(7), Si1−N11 1.874(3), Si1−N3 1.896(3), Si1−N14 1.89(2), Si1−N4 1.925(3), N5−N6 1.230(8), N6−N7 1.163(9), N8−N9 1.224(9), N9−N10 1.160(9), N11−N12 1.204(4), N12−N13 1.155(4), N14−N15 1.16(2), N15−N16 1.11(2), N17−N18 1.211(5), N18−N19 1.142(5), N5−Si1−N3 96.2(2), N17−Si1−N3 90.63(16), N8−Si1−N3 163.3(2), N11−Si1−N3 96.09(13), N3−Si1−N14 162.2(7), N5−Si1−N4 91.4(2), N17−Si1−N4 90.18(14), N8−Si1−N4 96.5(2), N11−Si1−N4 163.75(13), N3−Si1−N4 67.71(12), N14−Si1−N4 99.5(6), N6−N5−Si1 121.6(5), N7−N6−N5 175.8(8), N9−N8−Si1 118.7(5), N10−N9−N8 178.6(8), N12−N11−Si1 120.8(2), N13−N12−N11 176.2(3), N15−N14−Si1 117.9(17), N16−N15−N14 176(2), N18−N17 Si1 122.7(4), N19−N18−N17 177.3(6).

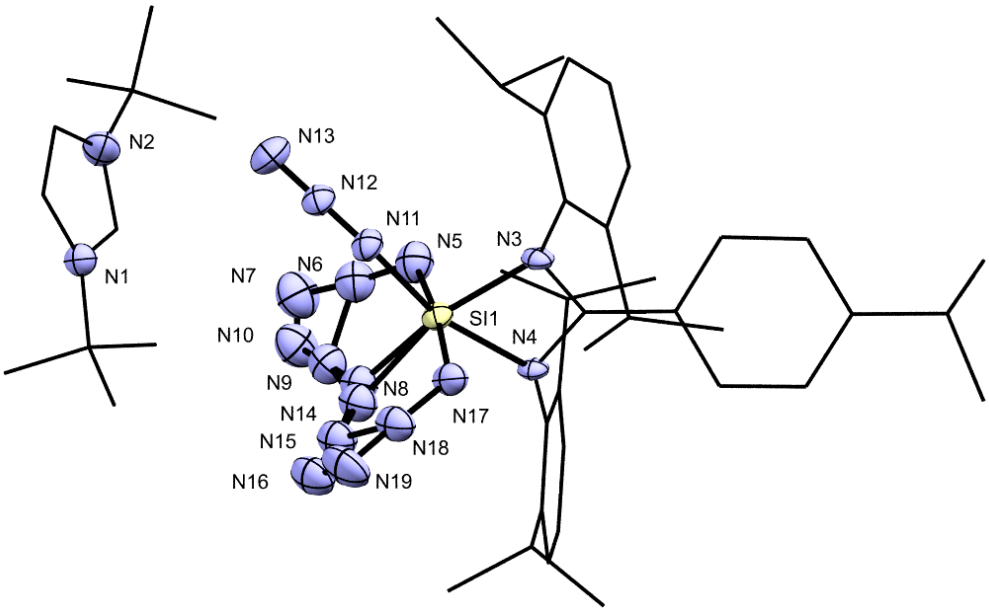

Figure 6.42. Thermal ellipsoid plot of **31**·C_6H_{14}. Ellipsoids set at 50 % probability. Hexane and hydrogen atoms omitted for clarity. Carbon atoms represented as wireframe Selected bond lengths (Å) and bond angles (°): Si1−N5 1.798(6), Si1−N17 1.823(4), Si1−N8 1.833(7), Si1−N11 1.874(3), Si1−N3 1.897(3), Si1−N14 1.90(2), Si1−N4 1.925(3), N5−N6 1.227(8), N6−N7 1.165(9), N8−N9 1.223(9), N9−N10 1.161(9), N11−N12 1.204(4), N12−N13 1.155(4), N14−N15 1.15(2), N15−N16 1.10(2), N17−N18 1.211(5), N18−N19 1.141(6), N5−Si1−N3 96.2(2), N17−Si1−N3 90.62(16), N8−Si1−N3 163.3(2), N11−Si1−N3 96.08(13), N3−Si1−N14 162.2(7), N5−Si1−N4 91.4(2), N17−Si1−N4 90.19(15), N8−Si1−N4 96.5(2), N11−Si1−N4 163.73(13), N3−Si1−N4 67.69(12), N14−Si1−N4 99.5(6), N6−N5−Si1 121.7(5), N7−N6−N5 175.9(8), N9−N8−Si1 118.7(5), N10−N9−N8 178.6(8), N12−N11−Si1 120.8(2), N13−N12−N11 176.2(3), N15−N14−Si1 117.9(17), N16−N15−N14 177(3), N18−N17−Si1 122.7(4), N19−N18−N17 177.2(6).

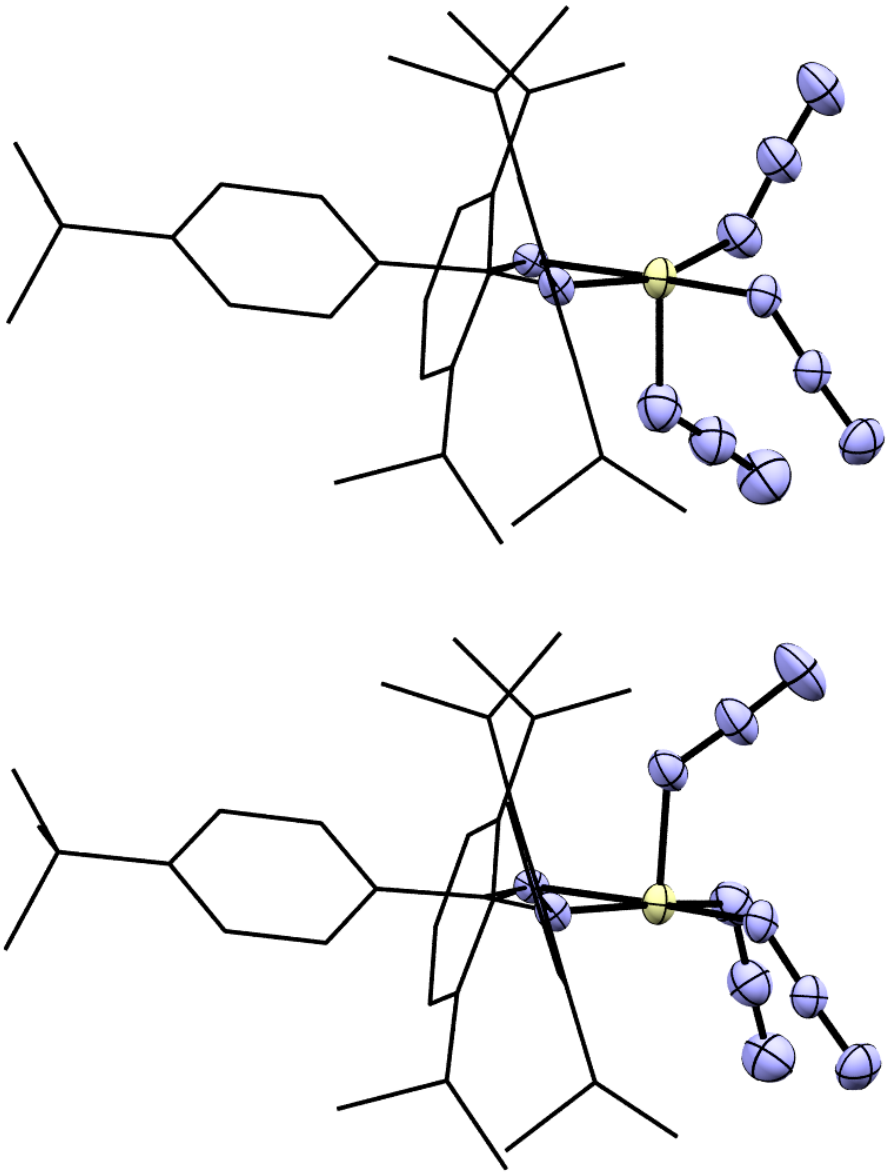

Figure 6.43. Representation of the two disordered components of the anion of **31**. Hydride is missing as it could not be determined from the crystal structure determination.

The structure determined from the crystal obtained from hexane has a better data set than the crystal obtained from toluene and, therefore, a more reliable structure. The octahedral skeleton about the silicon atom is significantly distorted by the narrow bite angle of the amidinato ligand, 67.69(12)°, as with the other amidinato structures determined thus far. Each of the N−Si−N(α) bond angles are greater than 90° with a range between 90.2(2) and 99.5(6)°. The angle between N_{NCN}−Si−$N(\alpha)_{trans}$ is narrower than 180° at 162.2(2) and 163.3(7)° demonstrating the steric influence of the amidinato ligand. The Si−N bond lengths are longer for the bonds between the silicon and the amidinato ligand compared to the Si−N bond lengths between the silicon and the azido groups. All five $Si-N_{azide}$ bonds are different in length varying between 1.799 and 1.894

Å. The Si−N_{azide} bonds in the plane with the amidinato ligand are slightly longer than the Si−N_{azide} bonds *cis* to the amidinato ligand.

Table 6.13 shows the structural data of the silicon azide bonds from compounds **25**, **28**, **29**, **30** and **31**·C_6H_{14}. The size of the bond lengths and ΔNN parameter follow the trend that increasing the coordination number results in an increase in the E−N bond length and decrease in ΔNN. Compound **30** has smaller ΔNN parameters than compound **31** despite the latter compound having an anionic charge. This is different compared to $(PPN)_2Si(N_3)_6$ and (bipy)$Si(N_3)_4$, where the ΔNN parameter is smaller for the anionic complex. It appears that the increased steric hindrance, due to IPr, about the coordination sphere results in the lower value for ΔNN for compound **30** over compound **31**.

Compound	Orientation	E−N	N(α)−N(β)	N(β)−N(γ)	ΔNN
25	axial	1.803(3)	1.208(4)	1.145(4)	6.3(6)
	equatorial	1.748(3)	1.235(4)	1.137(4)	9.8(6)
28	axial	1.846(2)	1.205(4)	1.144(4)	6.1(6)
	equatorial	1.743(2)	1.225(3)	1.126(3)	9.9(4)
29		1.761(3)	1.225(3)	1.132(3)	9.3(4)
30	In plane with (^{dipp}NCN)	1.854(2)	1.211(3)	1.151(3)	6.0(4)
	trans to H	1.915(2)	1.209(3)	1.150(3)	5.9(4)
31·C_6H_{14}	In plane with (^{dipp}NCN)	1.877(7)	1.203(8)	1.138(7)	6.5(10)
	Orthogonal to (^{dipp}NCN)	1.838(8)*	1.201(9)	1.139(9)	6.2(12)

Table 6.13. Selected structural properties of compounds **25**, **28**, **29**, **30** and **31**·C_6H_{14}. Bond lengths are in Å and ΔNN in pm. *bond length potentially shorter than expected due to disorder model currently applied, which does not account for the position of the hydride along the same bond.

Instead of forming (^{dipp}NCN)SiN_3 the reaction of (^{dipp}NCN)$SiH(N_3)_2$ with various bases has resulted in the formation of numerous hydrido(azido)silicon complexes. Only I^{t}Bu appears to be capable of eliminating HN_3 from **25**, however, the resulting imidazolium azide reacts with unreacted **25** to give **31**. This suggests that the desired (^{dipp}NCN)SiN_3 has formed, however, it could not be isolated.

6.3 Conclusion

Formation of the two Si(II) azides IPrSi$(N_3)_2$ and (^{dipp}NCN)SiN_3 have been inferred but not conclusively proven or isolated as a pure compound. The synthesis of a Si(II) azide was attempted by two methods: (i) ligand exchange of a Si(II) halide and (ii) reduction of a Si(IV) azide. Salt metathesis between sodium azide and IPrSiX_2 (X = I or Cl) forms a product with the same physical appearance and FT-IR spectrum as the product obtained from the reduction of **16** with KC_8. This provides evidence for the formation of IPrSi$(N_3)_2$, however, the spectroscopic data obtained suggests the product of the reactions is a Si(IV) azide. Most likely the formation of which is from the reaction of IPrSi$(N_3)_2$ with another molecule of IPrSi$(N_3)_2$. Despite the steric protection and the electronic influences of the IPr ligand, IPrSi$(N_3)_2$ is unstable at room temperature. Si(II) centres are well known to react with organoazides, and it appears that IPrSi$(N_3)_2$ reacts in a similar way. It may only be possible to prepare a NHC stabilised Si(II) azide by blocking the lone pair of the Si(II) centre with an appropriate Lewis acid. Transition metal complexes are well known Z-type ligands for Si(II) complexes, however, three coordinate boron complexes are also viable candidates. The reagent (PPN)B$(N_3)_4$ may be a viable candidate as a halo / azido exchange reagent with IPrSiX_2 to give (PPN)X and IPrSi$(N_3)_2$B$(N_3)_3$ as reaction products.

The balance between nucleophilicity and the basicity of a reducing agent is an important factor in the reactivity of the agent with Si(IV) azides and hydrido(azido) silicon compounds. NHCs are reactive towards organosilylazides to give imidazolin-2-imido silyl complexes. Si$(N_3)_4$ has a different reactivity towards NHCs depending on the nucleophilicity of the NHC. The product obtained between IPr and Si$(N_3)_4$ is the Lewis acid base adduct **16**. For the preparation of imidazolin-2-imido ligands, the mechanism is thought to occur *via* a triazene intermediate. When IPr coordinates to Si$(N_3)_4$ it cannot attack the nitrogen atom of the azide and eliminate dinitrogen from the azido group. I^{t}Bu is a stronger nucleophile than IPr and undergoes the dinitrogen elimination reaction and does not coordinate to the silicon atom. The reactivity of IPr and I^{t}Bu with compound **25** is also different due to strength of the nucleophilicity of the NHCs. IPr is too weak a base to eliminate HN_3 and tautomerizes to be able to coordinate to the silicon centre. I^{t}Bu, on the other hand, can eliminate HN_3 from compound **25**, however, the resulting (I^{t}BuH)N_3 reacts with compound **25**.

Lithium bases, Li(N(SiMe$_3$)$_2$) and Li(^{dipp}Nacnac), are unsuitable to eliminate HN_3 from compound **25**, even though Li(N(SiMe$_3$)$_2$) can eliminate HCl from (PhC(^{t}BuN)$_2$)SiHCl$_2$. The removal of the hydride is prevented due to the nucleophilicity of the trimethylsilyl amide in Li(N(SiMe$_3$)$_2$). The ideal base for "deazoimidation" of compound **25** would be a lithium base with a large bulky counterion to prevent coordination to the silicon atom, such as a hypersilyl lithium base Li(N(Si(SiMe$_3$)$_3$)$_2$). A strong neutral organic base is not suitable because the azide anion is too strong a nucleophile and reacts with compound **25**. The organic counterion that forms concurrently helps solubilise the anion making competing reactions more likely to occur.

A number of reducing agents are available. Group 1 metals are strong reducing agents, however, have issues associated with stoichiometry. Yields of reactions between IPrSiX$_4$ (X = Cl, Br, I) and KC_8 are also often very low. The ($^{mes/dipp}$Nacnac)Mg dimer offers answers to these problems, however, the reaction with **16** and **20** results in over reduction, despite stoichiometry, from Si(IV) to Si(0) and Si(I) respectively. A possible alternative reaction to a redox reaction between a Group 1 or Group 2 metal and Si(IV) is a comproportionation reaction. The Si(I) dimer, [(^{dipp}NCN)Si] may react with **16** to give two different Si(II) compounds: IPrSi(N$_3$)$_2$ and (^{dipp}NCN)SiN$_3$.

Despite the lack of success in preparing and isolating a Si(II) azide a number of novel silicon and phosphorus azides have been prepared. Figure 6.44 shows the relationship between coordination number and the Si−N$_3$ bond length and the $\nu_{as}(N_3)$ of the polyazido silicon complexes prepared in this work. Other than the equatorial Si−N$_3$ bond lengths of trigonal bipyramidal complexes, which are shorter than the other Si−N$_3$ bond lengths, there is a general trend that as the coordination number increases the Si−N$_3$ bond length also increases and, therefore, the ionicity of the Si−N$_3$ bond. This is also seen in the plot showing the relationship between $\nu_{as}(N_3)$ and coordination number, where the $\nu_{as}(N_3)$ decreases in wavenumbers as coordination number increases. These plots give a tool for the prediction of the spectroscopic and structural properties of new polyazido silicon compounds helping investigations in determining the identity of intermediates and products in Main Group azido chemistry. The electronic structure of the azido groups can, therefore, be inferred from this data. Shorter Si−N bonds results in a higher wavenumber for the $\nu_{as}(N_3)$ vibration and a higher degree of covalency for the

Si−N bond. Geometry of the complex has more of an effect on the electronic structure of the azido groups than the ancillary ligands of the complex.

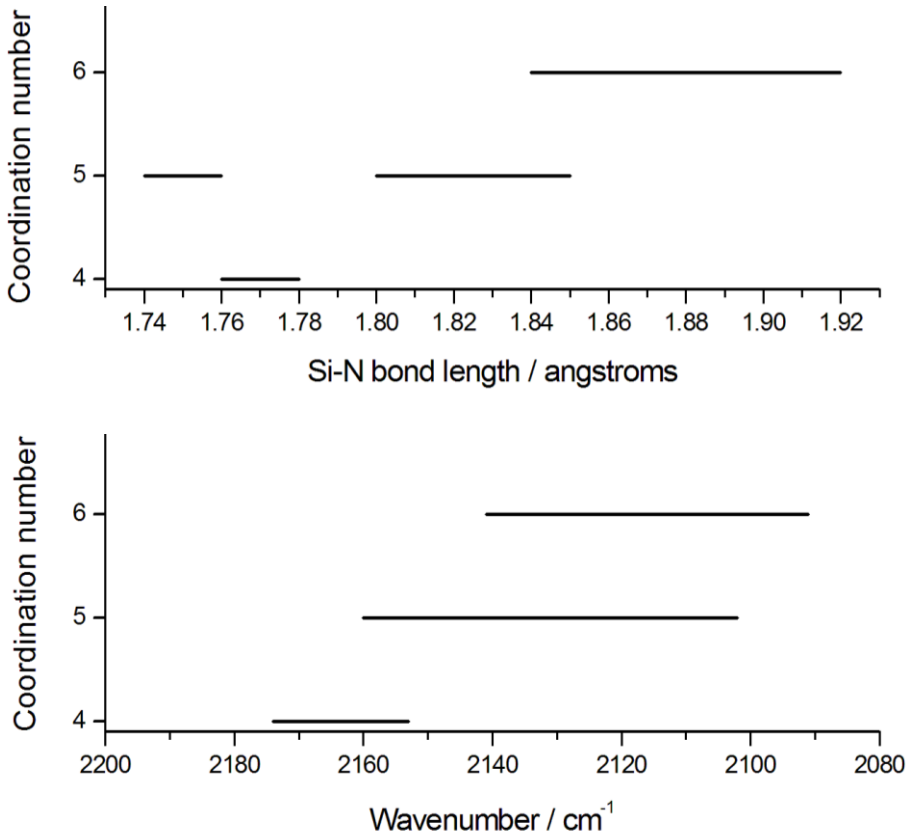

Figure 6.44. Top: Plot showing the relationship between coordination number and the Si−N bond length of a variety of tetra-, penta- and hexa- coordinate polyazido silanes. Bottom: Plot showing the relationship between coordination number and the $\nu_{as}(N_3)$ of a variety of tetra-, penta- and hexa- coordinate polyazido silanes.

A Si(II) azide still remains elusive and a sought-after molecule. While a number of methods have been attempted there are still other avenues available for further investigation.

7. TRIAZENIDO LIGANDS FOR MAIN GROUP CENTRES

7.1 Introduction

Charge-neutral ligands, L-type ligands using the MLX classification, in the field of energetic coordination chemistry are primarily based on tetrazole and triazole rings. Tetrazole itself is capable of acting as an L type ligand towards transition metals. The one advantage of tetrazole is the ease at which it can be modified and additional groups can be added at the 1N, 2N and 5C positions. Tetrazole rings can also be coupled together to synthesise bis(tetrazole), which has potential as a bidentate ligand.[18,53,221–224] The main problem associated with such compounds is the fact that tetrazole rings are strongly electron withdrawing, effectively reducing the ability of the compound acting as a ligand. This makes anionic nitrogen-rich ligands a more viable option, as they are often stronger ligands due to the negative charge. When considering Main Group coordination centres anionic ligands are almost always required to prepare a complex.

There is a short list of anionic ligands suitable as candidates for energetic coordination complexes. Common ligands are the azide anion, tetrazolate anion and the nitrate anion, but after these there are no more readily available. Pentazolate (N_5^-) is an ideal candidate. Attempts have been made to use substituted pentazoles as a source of the pentazolate anion, but it still remains elusive to date.[36,225–228] Another ligand that has potential is the triazenido ligand, a negatively charged chain of three nitrogen atoms bridging between two organic groups, most commonly aryl groups.

A number of coordination modes are available for the triazenido ligand, as shown in Figure 7.1. These are monodentate through either the 1 or 2 positions, as a bidentate ligand to a single metal centre through positions 1 and 3 and bridging between two metal centres through a covalent bond and a coordinate dative bond. If an appropriate R group is attached, further coordination is possible giving a polydentate ligand. The identity of the R group is most commonly aromatic rings, and recently 1-methyltetrazole and 2-methyltetrazole.[53] The latter of which, (1,3-bis(2-methyltetrazol-5-yl)triazenide), has been used as a ligand in complexes with Zn(II), Fe(II) and Co(II) as coordination centres.[229,230] This ligand is a terdentate ligand

through the central nitrogen of the triazenido chain and from each tetrazole ring, Figure 7.2.

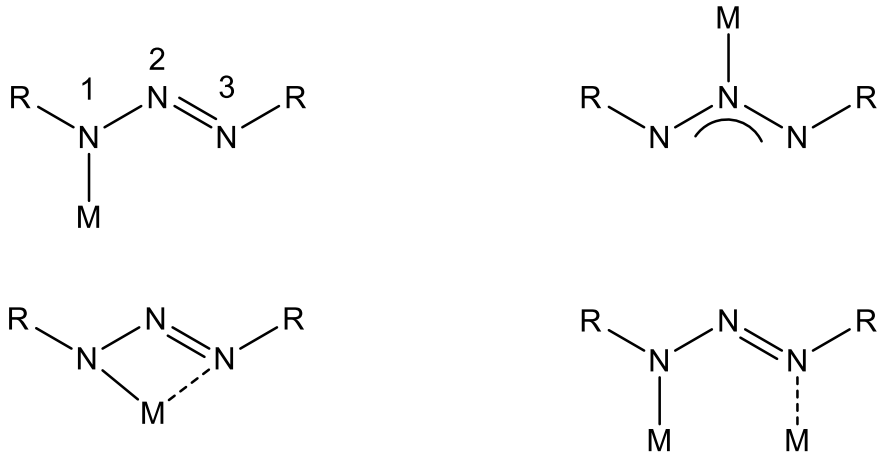

Figure 7.1. Coordination modes of the triazenido ligand.

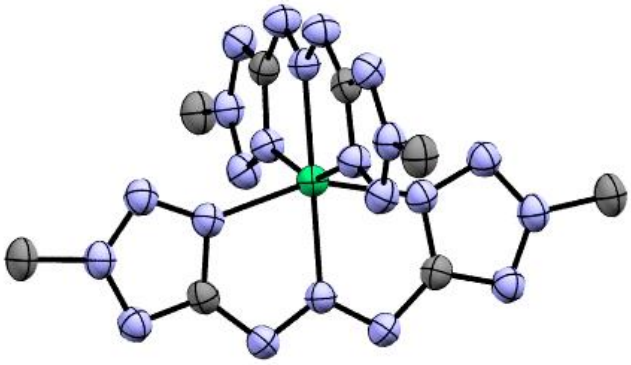

Figure 7.2. Thermal ellipsoid plot of bis[1,3-bis(2-methyltetrazol-5-yl-κ^3*N*, *N*, *N*)triazenido]nickel(II). Turquoise: Nickel. Hydrogens omitted for clarity.

To synthesise the triazenide anion the corresponding triazene is deprotonated. Triazenes are formed by the reaction of a diazonium salt and an amine, first achieved in the mid-19th century.[231] The coordination chemistry of triazenides was first investigated as early as the 1920s with transition metals.[232] Extension to the *p*-block elements has seen several structures of triazenido aluminium complexes, with the first appearing in 1989 of tris(1,3-diphenyltriazenido)aluminium.[47] The analogous gallium and indium complexes were published in the same report. An interesting structure of a reduced aluminium triazenido complex was published in 1995.[48] The complex, (PPN)Al(PhNNNPh)$_3$, was prepared by reduction of the parent Al(PhNNNPh)$_3$ with sodium metal followed by salt metathesis with (PPN)Cl. The only known silicon

complex bearing a triazenido ligand is $Me_3Si(PhNNNPh)$, prepared in 1978 for use as a "triazenido transfer reagent".[42] Triazenides can clearly be used as ligands and using a nitrogen-rich aryl group could result in a new energetic ligand for Main Group coordination complexes.

Recently the sodium salt of 1,3-bis(1-methyltetrazol-5-yl)triazenide (b1mtt) was isolated as a pentahydrate, a potential starting material for the preparation of coordination complexes.[53] However, the presence of water is an issue for the moisture sensitive *p*-block halides. Removal of the water requires heating a sample under vacuum, which may result in decomposition of the compound. A salt metathesis reaction of Na(b1mtt) with (PPN)Cl would give (PPN)(b1mtt), which would be a hydrophobic salt and easier to dry.

Aminotetrazole has three different isomers, as discussed in chapter 1. However, it is worth noting that the diazonium salt of 5-aminotetrazole is unstable at 0°C and as a result substituted tetrazoles are used instead, most commonly 1-methyl-5-aminotetraole. The only known triazenides bearing tetrazole rings are prepared from 5-aminotetrazole derivatives, as 5-aminotetrazole is readily available and can be purchased at a relatively low price (100 g is £43), whereas 1-aminotetrazole is not commercially available. The first method for the synthesis of 1-aminotetrazole, reported in 1965, is *via* hydrolysis of 1-benzylideneaminotetrazole, however, the procedure is not very well detailed.[233,234] An alternative synthesis was reported in 1969 using hydroxylamine-O-sulfonic acid as a reagent, which is not only expensive, but more hazardous, as well as giving a mixture of isomers.[235]

Despite the difficulties in preparing 1-aminotetrazole, it has been used to prepare azobis(tetrazoles) which possess ten consecutive nitrogen atoms.[236] No attempts to prepare triazenes or triazenides from 1-aminotetrazoles have been reported. Though there was a report from 2013 on the synthesis of 1,3-bis(5-aminotetrazol-1-yl)triazenium chloride obtained from the attempted diazotisation of 1,5-diaminotetrazole.[237] This compound has eleven consecutive nitrogen atoms, which is the record for the most sequential nitrogen atoms in a single molecule. Attempts to remove HCl to generate the neutral compound resulted in decomposition into 1,5-diaminotetrazole and 5-aminotetrazole with the evolution of dinitrogen gas. Unfortunately, as a positively charged species the molecule would be a very weak ligand.

Nitrogen-rich triazenides are known, however, investigations into their coordination chemistry with *p*-block elements are limited to very few structures. Therefore, the investigation of (b1mtt) as a ligand for Main Group complexes has been made. As well as the attempted synthesis of another isomer of the ligand to prepare 1,3-bis(5-methyltetrazol-1-yl)triazenide (b5mtt), and test its potential as a ligand towards Main Group coordination centres.

7.2 Results and discussion

7.2.1 Group 14 triazenido complexes

7.2.1.1 Syntheses and spectroscopy

A triazenido containing silicon compound is known, $Me_3Si(PhNNNPh)$, however, this contains three methyl groups bonded to the silicon atom. These methyl groups would be very difficult to remove, making the coordination of a second triazenide unlikely. Chloro ligands are much more labile, therefore, using $SiCl_4$ as a starting reagent has the potential of adding more than one triazenido ligand. Due to the potential dangers and shock sensitivity of a bis(tetrazoyl)triazenido complex, it is important to understand the chemistry and reactivity of these types of ligands towards $SiCl_4$. Consequently, the first reactions attempted involved using the sodium salts of 1,3-bis(*p*-tolyl)triazenide (bptt) and 1,3-bis(*p*-anisyl)triazenide (bpat) with $SiCl_4$, Scheme 7.1. In the reaction of $AlCl_3$ and Na(PhNNNPh), regardless of stoichiometry, the fully substituted $Al(PhNNNPh)_3$ was always obtained. Therefore, the most likely product between a triazenide and $SiCl_4$ would be $Si(RNNNR)_2Cl_2$. Any further substitution is unlikely due to steric hinderance around the coordination sphere.

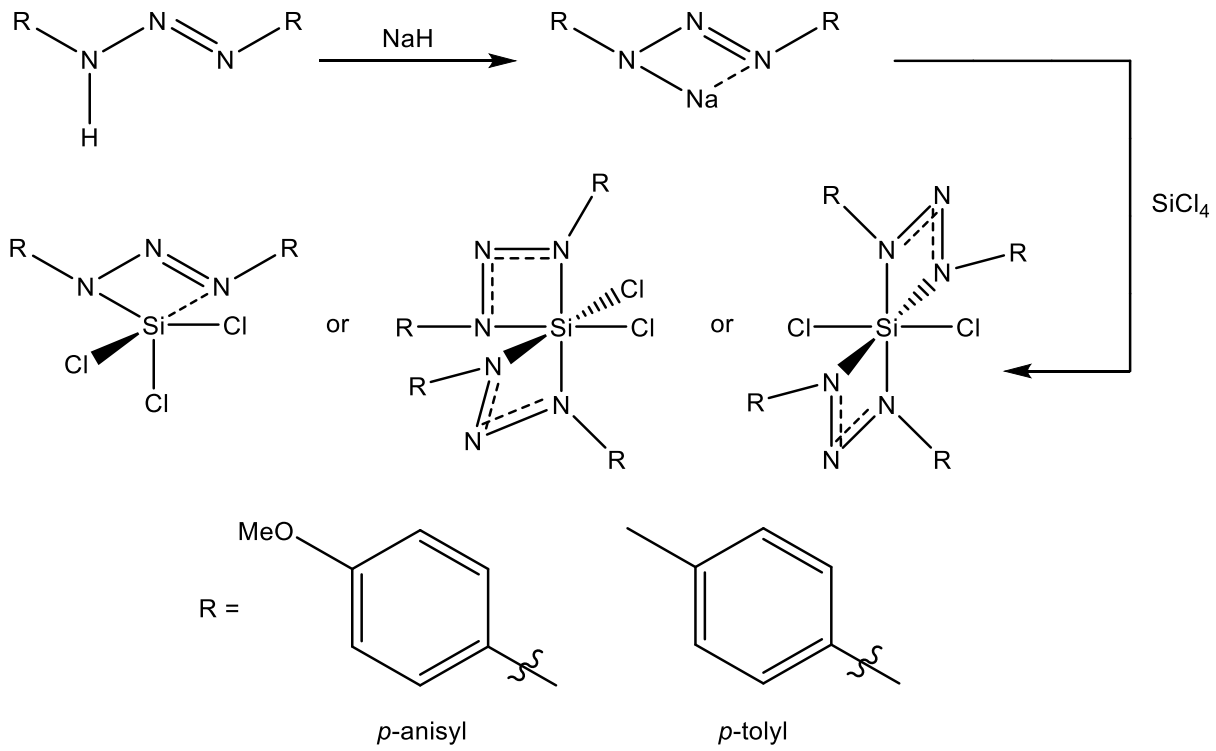

Scheme 7.1. Reaction scheme for the preparation of Na(RNNNR) and possible products on addition of $SiCl_4$.

The triazenes were prepared by the addition of half an equivalent of sodium nitrite and HCl at 0°C in water to the appropriate amine. The deprotonation of both compounds is easily achieved by using NaH in THF giving deep red, almost black, solutions. The solid can be isolated by evaporating the THF or the solution can be used directly. $SiCl_4$ is known to react with THF, however, the reaction between sodium triazenides and $SiCl_4$ can be completed in THF. Addition of one equivalent of $SiCl_4$ to the THF solution of sodium triazenides results in a lightening of the solution to red and the precipitation of a solid. Evaporation of solvent results in a brown, red powder, which can be recrystallised using a 1:1 mixture of THF and diethyl ether to give red needles. The identity of the compounds were confirmed through ^{1}H-NMR spectroscopy and single crystal X-ray diffraction to be *cis*-$(bpat)_2SiCl_2$ (**32**) and *cis*-$(bptt)_2SiCl_2$ (**33**), despite adding only one equivalent of sodium triazenide with respect to $SiCl_4$.

The ^{1}H-NMR spectrum of **32** shows six resonances for the complex, two resonances at 3.26 and 3.08 ppm for the methyl groups and four sets of doublets between 8.02 and 5.49 with a coupling constant of 9 Hz for the phenyl hydrogen atoms. If there are two triazenido ligands present the complex cannot be the *trans* isomer as this would have

three ^{1}H resonances because of a mirror plane parallel to the Cl−Si−Cl axis, therefore, the *cis* isomer is the product. In the *cis* isomer, a C_2 axis is present between the two chloro ligands rendering the phenyl rings on the same triazenido ligand inequivalent, but rather the phenyl rings in different triazenido ligands become equivalent.

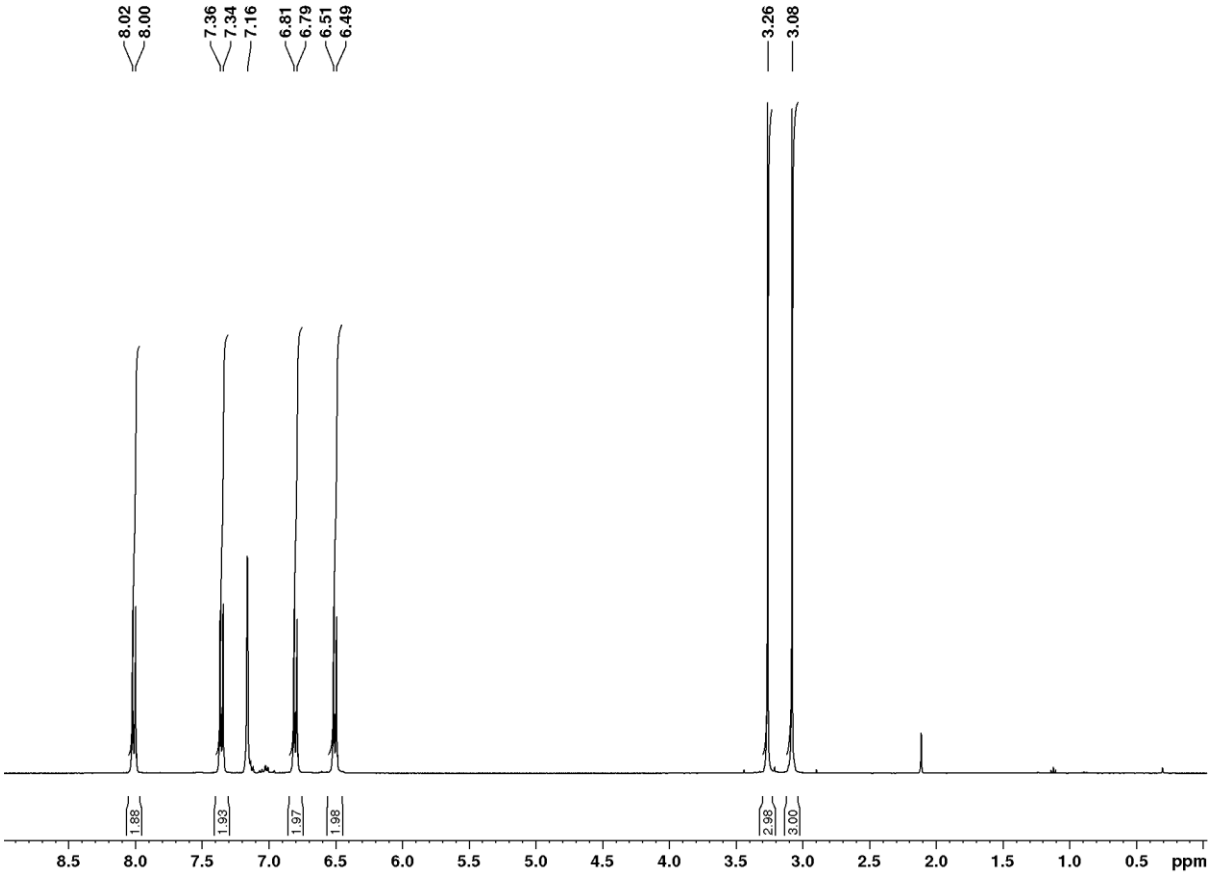

Figure 7.3. ^{1}H NMR spectrum of **32** in C_6D_6.

The FT-IR spectrum of **32** as a nujol mull shows, as expected, only peaks in the fingerprint region. After comparing a spectrum of (bpat)H and (bpat)Na with the spectrum of **32** a tentative assignment for the bidentate ν_{as}(NNN) can be made to the peak at 1333 cm^{-1}. The same absorption in Al(PhNNNPh)$_3$ is assigned to two peaks at 1320 and 1295 cm^{-1}. Similar to compound **32**, the ^{1}H-NMR spectrum of compound **33** displays six resonances, two singlets for the methyl groups at 2.19 and 1.98 ppm and four sets of doublets between 8.12 and 6.78 ppm for the aromatic hydrogen atoms. A peak at 1314 cm^{-1} in the FT-IR spectrum of **33** as a nujol mull is present for the ν_{as}(NNN) absorption.

These complexes give an insight into the reactivity of triazenido ligands towards $SiCl_4$. Similar to $AlCl_3$, the degree of substitution does not depend on the amount of sodium triazenide added. Further substitution, though theoretically possible, is unlikely. The product would most likely be $[Si(RNNNR)_3]Cl$ to maintain the Si(IV) oxidation state. It may be possible to exchange the remaining chloro ligands with other small, anionic, monodentate ligands, such as azides. An attempt to exchange the chloro ligands of **32** using an excess of sodium azide in THF was made. Three bands are present in the $\nu_{as}(N_3)$ region of the FT-IR spectrum of the reaction solution at 2175, 2130 and 2110 cm^{-1} at a much lower absorbance than the other peaks present in the FT-IR spectrum. As an octahedral molecule, $(RNNNR)_2Si(N_3)_2$, the peak at 2175 cm^{-1} would be too high, therefore, must indicate $Si(N_3)_4$ is present in the solution. The identity of the peak at 2130 cm^{-1} is HN_3, from hydrolysis, and the final peak at 2110 cm^{-1} is $[Si(N_3)_6]^{2-}$, from a reaction between $Si(N_3)_4$ and sodium azide. This all suggests that the triazenido ligand is labile in THF and can be replaced in the presence of azide anions.

7.2.2.2 Single crystal X-ray diffraction studies

Compound **32** crystallises in the space group $P2_1/n$ with four formula units per unit cell. The silicon atom is surrounded by four N ligators and two chlorine atoms giving an overall distorted octahedral centre. The molecule has C_1 symmetry as the phenyl rings in one triazenido ligand are co-planar, however, in the other triazenido ligand one of the rings is twisted out of the plane with respect to the other. This is different to what is observed in the solution ^1H NMR spectrum, where the molecule has a C_2 axis due to freedom of rotation of the phenyl ring in solution.

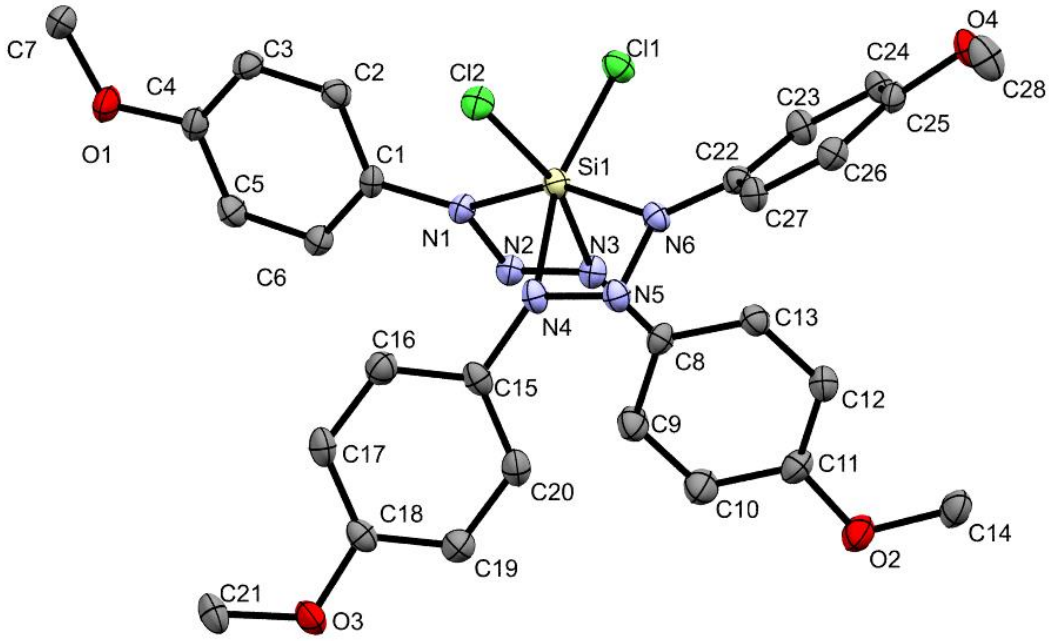

Figure 7.4. Thermal ellipsoid plot of **32**. Ellipsoids set at the 50% probability level. Hydrogen atoms omitted for clarity. Selected bond lengths (Å) and angles (°): Cl1–Si1 2.1136(13), Cl2–Si1 2.1144(13), Si1–N6 1.876(3), Si1–N1 1.884(3), Si1–N4 1.935(3), Si1–N3 1.946(3), N1–N2 1.316(4), N1–C1 1.420(5), N5–N4 1.302(4), N5–N6 1.331(4), N6–C22 1.415(5), N4–C15 1.409(4), N3–N2 1.307(4), N3–C8 1.410(5), N6–Si1–N1 151.52(15), N6–Si1–N4 65.28(13), N1–Si1–N4 93.05(13), N6–Si1–N3 92.77(13), N1–Si1–N3 65.04(13), N4–Si1–N3 82.73(13), N6–Si1–Cl1 98.18(10), N1–Si1–Cl1 100.83(10), N4–Si1–Cl1 91.66(10), N3–Si1–Cl1 164.31(10), N6–Si1–Cl2 99.88(10), N1–Si1–Cl2 98.77(10), N4–Si1–Cl2 164.00(11), N3–Si1–Cl2 92.47(10), Cl1–Si1–Cl2 96.64(6), N2–N1–C1 118.6(3), N2–N1–Si1 97.0(2), C1–N1–Si1 144.0(2), N4–N5–N6 102.8(3), N5–N6–C22 118.5(3), N5–N6–Si1 96.8(2).

The Si−N bonds vary depending on the group *trans* to the nitrogen atom. The average Si−N bond *trans* to a nitrogen atom is 1.88(1) Å, whereas the nitrogen atom *trans* to the chlorine has a longer Si−N bond of 1.94(1) Å giving an overall unsymmetrical bidentate coordination. This difference is partly caused by the difference in electronics between chlorine and nitrogen resulting in a greater *trans* influence from the chlorine atoms. Additionally, a steric effect contributes to the elongation of the Si−N bond. The phenyl rings bonded to the nitrogen atom *trans* to chlorine are brought closer together from the *cis* coordination resulting in a gauche interaction between the two phenyl rings. Both of these Si−N bond lengths are long compared to tetrahedral molecules containing other Si−N functionalities, e.g. azide and bis(trimethylsilyl)amide (between 1.70 and 1.81 Å), but comparable to other octahedral Si−N containing compounds (between 1.84 and 1.98 Å). Interestingly, the N−N bond lengths of the triazenido ligand are different. It would be expected the bonds between N1−N2 and N2−N3 would be the same due to

delocalisation of the electrons of the N−N double bond over all three nitrogen sites as is seen in the molecular structure of $Al(PhNNNPh)_3$, however, the presence of chlorine atoms *trans* to the nitrogen causes the N2−N3 bond (1.307(4) Å) to shorten with respect to the N1−N2 bond (1.316(4) Å). The difference between N4−N5 (1.302(4) Å) and N5−N6 (1.331(4) Å) is even greater, most likely as a consequence of the twisted phenyl ring in this triazenido ligand. All of the N−C bond lengths are very similar and equal to the N−C bond length in *p*-anisidine. Both of the triazenido ligands have bite angles of 65(1)° causing the large distortion of the $[SiN_4Cl_2]$ skeleton. The N−N−N bond angle is 103(1)°, typical of coordinated triazenides from the puckering of the bidentate coordination mode.

Compound **33** crystallises in the space group $P2_1\backslash c$ with four formula units per unit cell as a 1:1 solvate with diethyl ether. Comparable to compound **32**, the silicon atom has a distorted octahedral geometry with the two chloro ligands arranged *cis* to one another. The molecule has C_2 symmetry, at variance to **32**, as the phenyl rings in the triazenido ligand are co-planar in both ligands, retaining the symmetry that is lost in compound **32**. All bond lengths and bond angles are very similar between **32** and **33**.

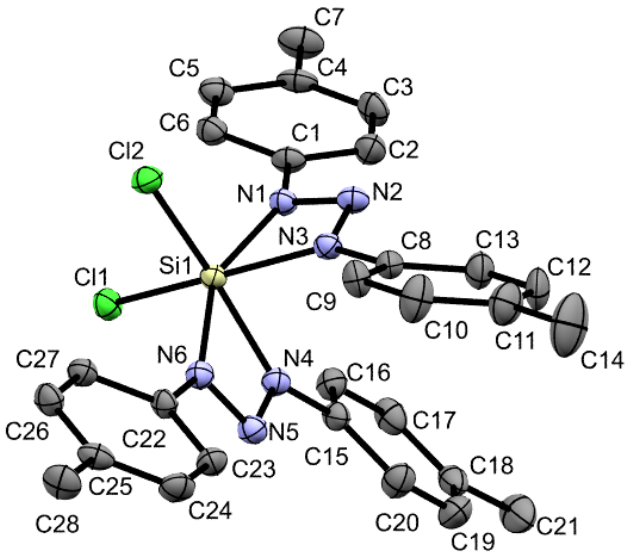

Figure 7.5. Thermal ellipsoid plot of **33**. Ellipsoids set at the 50% probability level. Hydrogen atoms and diethyl ether omitted for clarity. Selected bond lengths (Å) and angles (°): Cl1–Si1 2.1136(13), Cl2–Si1 2.1144(13), Si1–N6 1.876(3), Si1–N1 1.884(3), Si1–N4 1.935(3), Si1–N3 1.946(3), N1–N2 1.316(4), N1–C1 1.420(5), N5–N4 1.302(4), N5–N6 1.331(4), N6–C22 1.415(5), N4–C15 1.409(4), N3–N2 1.307(4), N3–C8 1.410(5), N6–Si1–N1 151.52(15), N6–Si1–N4 65.28(13), N1–Si1–N4 93.05(13), N6–Si1–N3 92.77(13), N1–Si1–N3 65.04(13), N4–Si1–N3 82.73(13), N6–Si1–Cl1 98.18(10), N1–Si1–Cl1 100.83(10), N4–Si1–Cl1 91.66(10), N3–Si1–Cl1 164.31(10), N6–Si1–Cl2 99.88(10), N1–Si1–Cl2 98.77(10), N4–Si1–Cl2 164.00(11), N3–Si1–Cl2 92.47(10), Cl1–Si1–Cl2 96.64(6), N2–N1–C1 118.6(3), N2–N1–Si1 97.0(2), C1–N1–Si1 144.0(2), N4–N5–N6 102.8(3), N5–N6–C22 118.5(3), N5–N6–Si1 96.8(2), C22–N6–Si1 144.3(2), N5–N4–C15 120.3(3), N5–N4–Si1 95.1(2), C15–N4–Si1 144.4(2), N2–N3–C8 119.2(3), N2–N3–Si1 94.4(2), C8–N3–Si1 145.4(2), N3–N2–N1 103.5(3)

7.2.2 Nitrogen-rich triazenides

7.2.2.1 Spectral and structural properties of (PPN)(b1mtt)

As described earlier the nitrogen-rich triazenide, (b1mtt), has been prepared as a sodium salt by Klapötke *et al*. This compound crystallises as a pentahydrate, which would require extensive drying before being used as a reagent for Main Group halides. One method would be to heat the solid under vacuum, however, this may lead to decomposition of the compound and also increase the shock or friction sensitivity of the compound as it is dry. Another method is to convert the sodium salt to a salt with a large bulky organic cation, such as PPN, PPh_4 or $AsPh_4$. This will not only reduce the probability of crystallising as a hydrate but also result in a decrease in any shock and

friction sensitivity of the compound and make it safer to handle. Due to availability PPN was used.

From the commercially available 5-aminotetrazole, the (PPN)(b1mtt) (**34**) salt can be prepared in a multi-step process summarised in Scheme 7.2. Firstly, the methylation of 5-aminotetrazole is achieved using dimethyl sulfate and NaOH in water. This method produces both 1-methyl-5-aminotetrazole and 2-methyl-5-aminotetrazole, however the former is insoluble in cold water and the latter is soluble in water and are easily separated. The diazotisation of the 1-methyl-5-aminotetrazole is completed using the same procedure for other triazenides. After deprotonation with NaOH and salt metathesis with (PPN)Cl **34** is obtained, which is easily recrystallized from acetonitrile to give large, yellow block crystals.

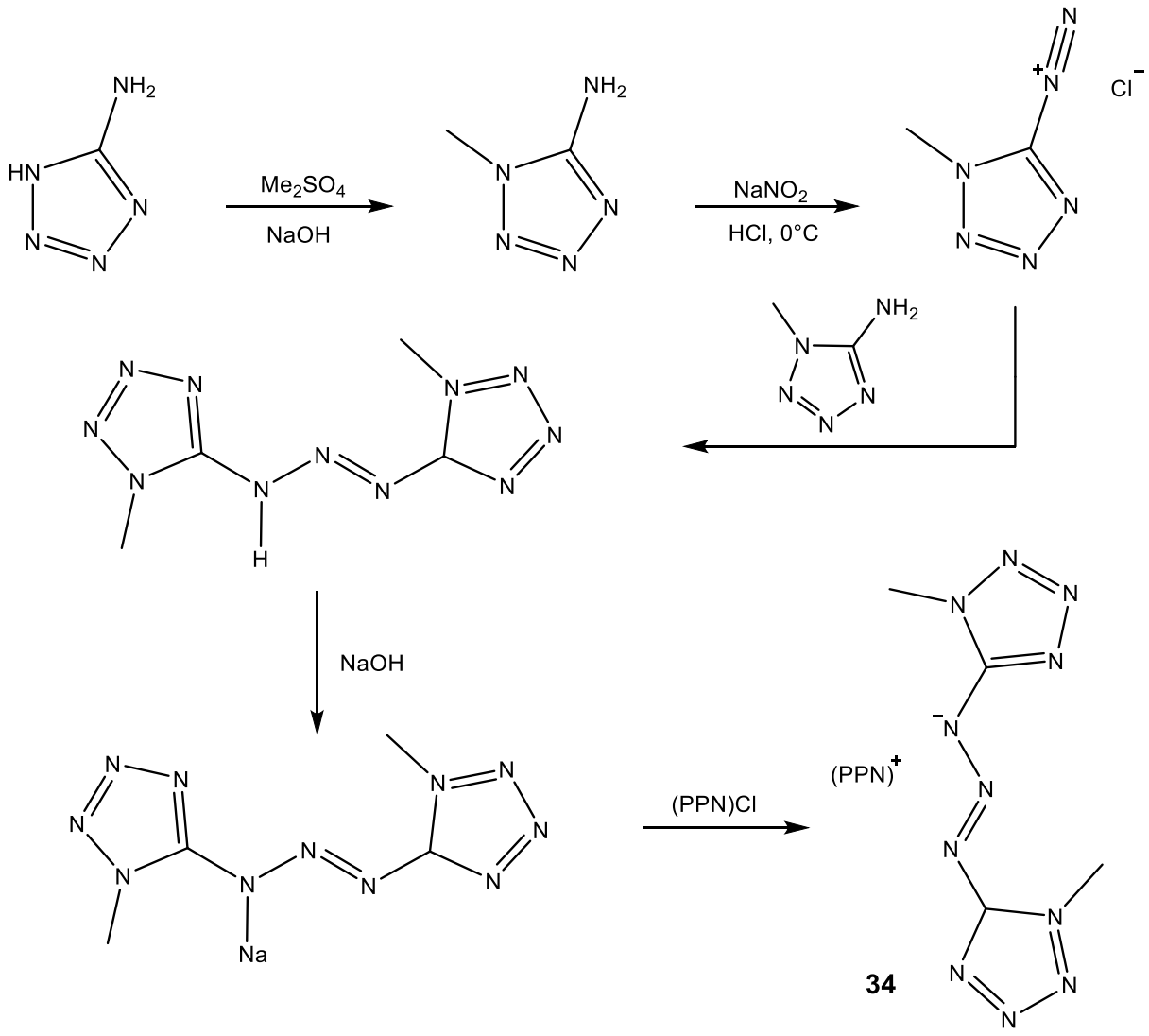

Scheme 7.2. Reaction scheme for the preparation of **34**.

The ^{1}H NMR spectrum of **34** in $CDCl_3$ shows the expected resonance for the (PPN) cation between 7.66 and 7.46 ppm. A singlet peak at 4.05 ppm accounts for the methyl groups on the tetrazole rings, shifted to higher ppm as a consequence of the electron withdrawing nature of the tetrazole rings. The integration ratio of these two peaks is 30:6 implying no (PPN)Cl is present in the crystals as confirmed by elemental analysis. Assignment of the ν_{as}(NNN) absorption in the FT-IR spectrum of **34** as a nujol mull is difficult because of the peaks responsible for the (PPN) cation overlap with the expected region for the triazenide vibration.

The molecular structure of **34**·MeCN was determined by single crystal X-ray diffraction and represents the first bis(tetrazoyl)triazenide with a non-coordinating cation. Compound **34** crystallises in the space group $P\bar{1}$ with two formula units per unit cell. One of the tetrazole rings, C2, N1, N2, N3 and N4 lies in the plane of the triazenide. The other ring, defined by C3, N8, N9, N10 and N11, is twisted out of the plane by approximately 20°. This tetrazole ring has weak contacts between the nitrogen atoms and the C−H on the phenyl rings of the PPN cation as well as contacts with the C−H of the acetonitrile, possibly giving a reason for the slight twist in the molecule. The triazenide is arranged in a *trans* conformation, however, the position of the methyl groups are *cis* relative to one another. The acetonitrile solvate lies between two (b1mtt) anions with one of the C–H moieties directed towards the two outer nitrogen atoms of the triazenide chain and another directed towards a nitrogen atom of the twisted out tetrazole ring.

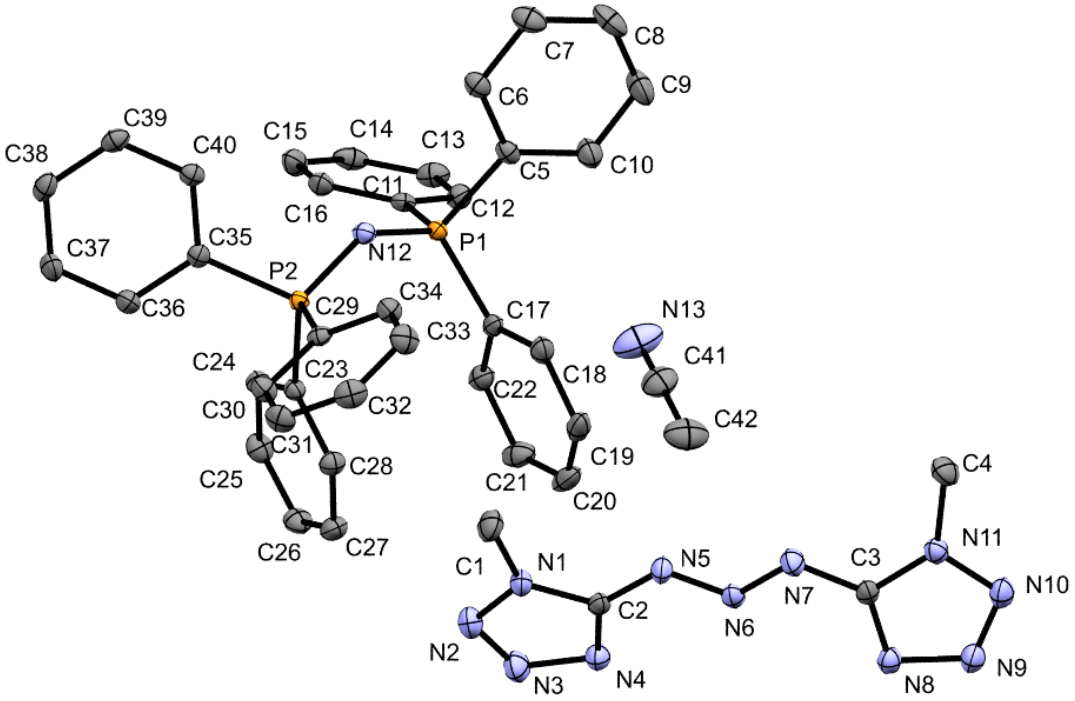

Figure 7.6. Thermal ellipsoid plot of **34**·MeCN. Hydrogen atoms omitted for clarity. Thermal ellipsoids set at the 50% probability level. Selected bond lengths (Å) and bond angles (°): C1–N1 1.451(2), C1–N1 1.451(2), C2–N4 1.333(2), C2–N1 1.350(2), C2–N5 1.375(2), C3–N8 1.333(2), C3–N11 1.348(2), C3–N7 1.377(2), C4–N11 1.455(2), N1–N2 1.3497(19), N2–N3 1.297(2), N3–N4 1.3623(19), N5–N6 1.3120(18), N6–N7 1.3079(19), N8–N9 1.3609(19), N9–N10 1.296(2), N10–N11 1.3512(19), N4 C2 N1 108.21(13), N4–C2–N5 132.85(14), N1–C2–N5 118.93(14), N8–C3–N11 108.26(13), N8–C3–N7 132.60(14), N2–N1–C2 108.63(13), N2–N1–C1 121.87(13), C2–N1–C1 129.46(14), N3–N2–N1 106.27(12), N2–N3–N4 111.43(13), C2–N4–N3 105.46(13), N6–N5–C2 110.71(13), N7–N6–N5 110.52(13), N6–N7–C3 110.88(13), C3–N8–N9 105.31(13), N10–N9–N8 111.71(13), N9–N10–N11 106.00(12), C3–N11–N10 108.72(13), C3–N11–C4 129.68(14), N10–N11–C4 121.44(13).

In comparison with the sodium salt of (b1mtt) determined in 2009, all the bond lengths are slightly shorter in **34**. Unlike in **34**, there are contacts between the cation and the (b1mtt) chain in the sodium salt. The clearest difference between the two structures is the N−N bonds of the triazenide chain. The sodium salt has N−N bond lengths of 1.352 and 1.313 Å, a larger difference than observed in **34**, which has N−N bond lengths of 1.312(2) and 1.308(2) Å.

Compound **34** is an extension to what has already been previously published to increase stability and making the compound easier to work with. However, the isomer of **34** where the triazenide is bonded to the N atom of the tetrazole ring is not known. To prepare the (b5mtt) anion 1-amino-5-methyltetrazole had to be synthesised. It cannot be assumed that 5-aminotetrazole and 1-aminotetrazole will act in the same way, therefore, the methyl group may not be required and so 1-aminotetrazole was also prepared.

7.2.2.2 Synthesis and properties of 1-aminotetrazole derivatives

Of the two methods to prepare 1-aminotetrazole derivatives, the route *via* 1-benzylideneaminotetrazole (**35**) and 1-benzylideneamino-5-methyltetrazole (**36**) was attempted. Firstly, to prepare **35** and **36**, benzylhydrazone, sodium azide and either triethylorthoformate or triethylorthoacetate for **35** and **36**, respectively, are combined in acetic acid, Scheme 7.3. The product in both reactions can be precipitated by adding water to the acetic acid to give a sticky yellow solid which can be recrystallised using ethyl acetate to give a yellow powder of **35** or a white powder of **36** on scales up to 50 g.

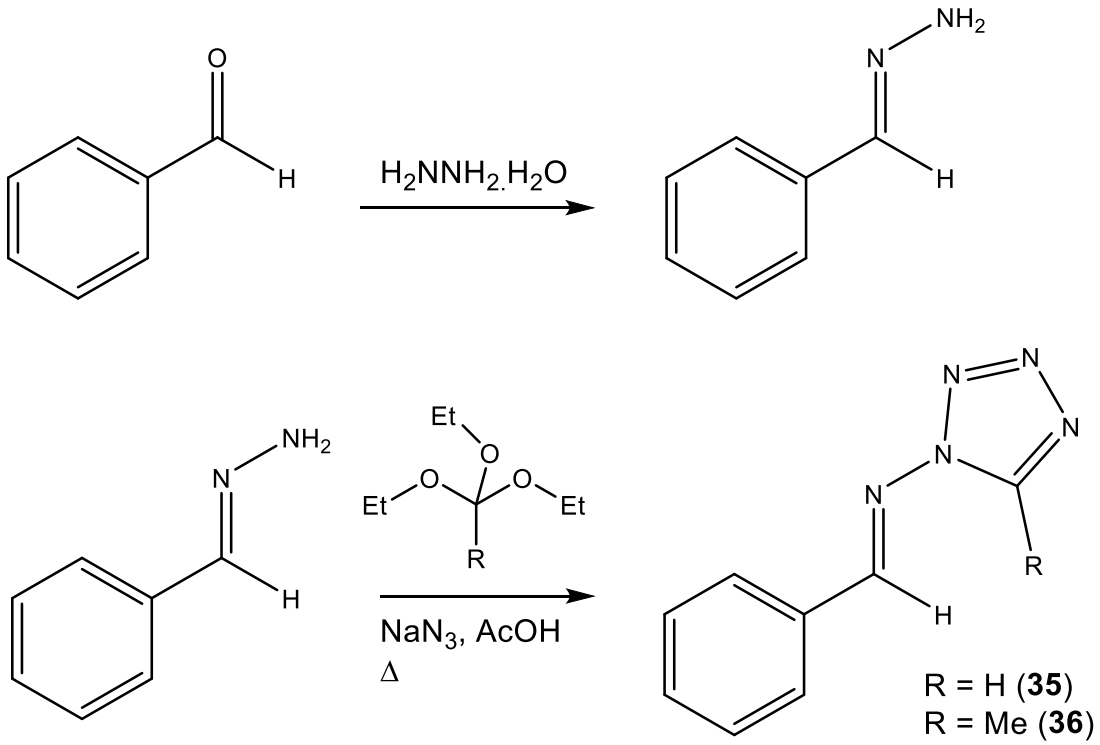

Scheme 7.3. Reaction scheme for the preparation of **35** and **36**.

The ^{1}H NMR spectra of **35** and **36**, Figures 7.7 and 7.8, are noticeably different by the fact that **35** displays two resonances for the imine hydrogen at 9.36 and 8.88 pm. This is indicative of two isomers being present in solution. As there is no rotation about the C=N double bond and only about the N−N bond between the imine and the tetrazole ring, the two rotamers are where the R group is *cis* to the imine hydrogen or where the

R group is *trans* to the imine hydrogen, Figure 7.9. Only a single signal is observed in the spectrum of **36** implying there is no rotation about this bond and the molecule is locked in the *trans* conformation due to a clash that would be present in the other rotamer. The benzylhydrazone imine hydrogen, at 7.70 ppm, is shifted to low field in the spectra of **35** and **36** compared to benzylhydrazone, owing to the electron withdrawing tetrazole group. The methyl group of **36** is shifted to high field compared to 1-methyl-5-aminotetrazole as the carbon is now bound to another carbon atom rather than a nitrogen atom.

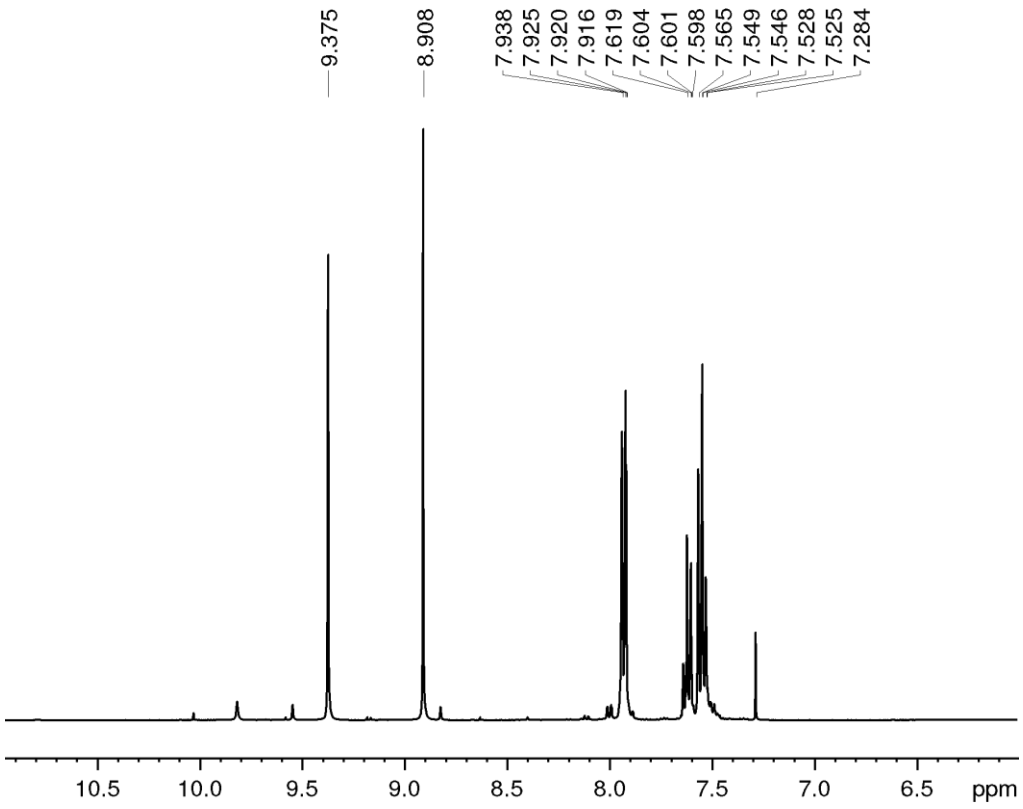

Figure 7.7. ^{1}H-NMR spectrum of **35**.

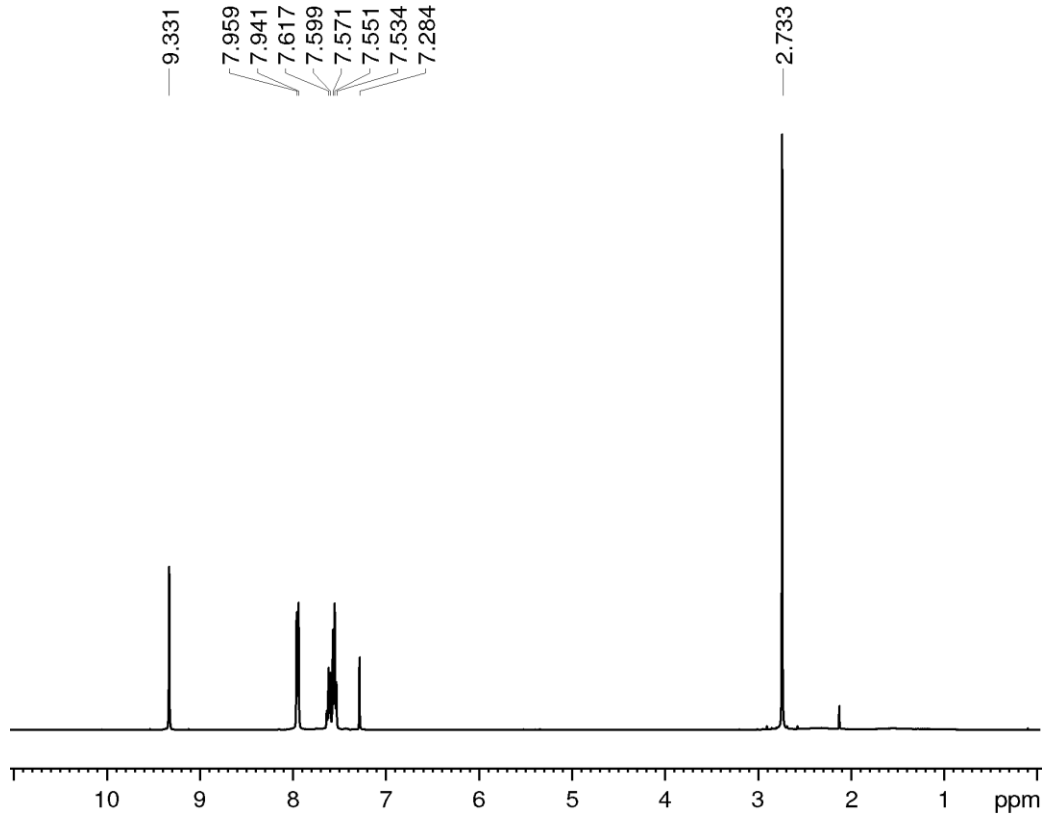

Figure 7.8. ^{1}H-NMR spectrum of **36**.

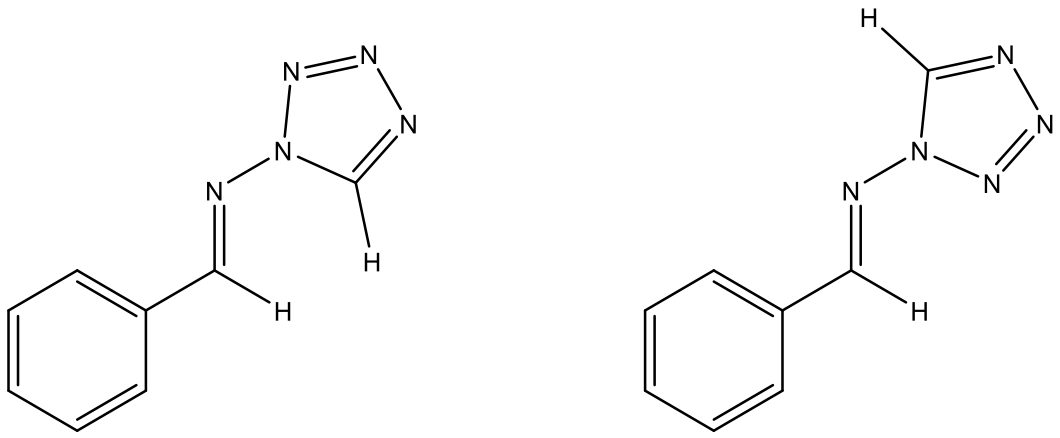

Figure 7.9. Rotamers of compound **35**.

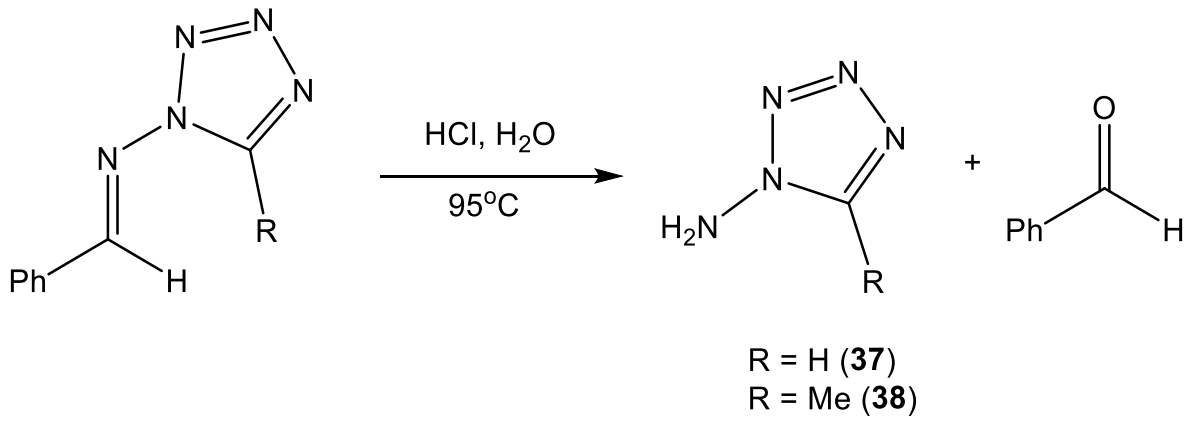

Scheme 7.4. Reaction scheme for the synthesis of 1-aminotetrazoles.

These precursors are hydrolysed under strongly acidic conditions at high temperatures to give benzaldehyde and the corresponding 1-aminotetrazole, Scheme 7.4. However, the experimental details in the literature for this step are sparse. The only information provided is the volumes of water and acid used, and that benzaldehyde was removed by steam distillation. Several attempts to replicate this resulted in very poor yields of impure products. It was possible to obtain pure products by optimising the reaction conditions, however, in low quantities of a few 100 mg of both 1-aminotetrazole (**37**) and 1-amino-5-methyltetrazole (**38**) starting from 10 g of **35** or **36**. Both compounds **37** and **38** are described as yellow oils in the literature,[221] however, **38** was isolated as colourless crystals.

The main issue is the reversibility of the reaction. Any trace amount of benzaldehyde in the presence of the 1-aminotetrazoles results in the preferential formation of **35** or **36**. It is, therefore, essential all benzaldehyde is removed from the reaction mixture. Either **35** or **36** were suspended in equal volumes of water and 35 % HCl and heated at 95°C for 90 mins. The yellow suspension was then distilled under vacuum at 95°C, with a head temperature of 46°C and pressure of 0.1 bar when distillation commenced. It was necessary to add further quantities of HCl and water and repeating the distillation. After two further cycles the reaction mixture became clear and orange, implying all of **35** and **36** had reacted as they are both insoluble in water even at high temperatures. At this point the mixture was distilled to dryness and the sump was suspended in water. After work-up, **37** was obtained as a yellow oil and **38** was isolated as colourless block crystals. The low yield obtained of both compounds could be due to decomposition in the harsh conditions required to prepare them.

The ^{1}H NMR spectrum of **37** displays two resonances, a singlet at 9.27 ppm for the CH and a broad signal at 7.13 ppm for the NH_2. Compared to 1H-tetrazole, the CH signal is at higher field for compound **38** (9.40 ppm for 1H-tetrazole). A broad signal is present for water at 3.72 ppm, which should be at 3.33 ppm in d^6-dmso,[238] implying some degree of interaction between the water and **37**. The ^{1}H NMR spectrum of **38** also displays two singlet resonances, 6.85 ppm for the NH_2 and 2.42 ppm for the CH_3 group. The CH_3 resonance is at a much lower chemical shift compared to 5-amino-1-methyltetrazole (4.15 ppm).[239] This is because the methyl group is bonded to the less electronegative carbon atom instead of nitrogen as in **38**.

The published procedure for **38** describes the product as a yellow oil, however, the compound is a colourless solid, contradictory to the published report. It was possible to crystallise the material in dichloromethane. Compound **38** crystallises in the space group $I4_1$\a with 16 formula units per unit cell. The amino group acts as both a hydrogen bond donor and acceptor. Figure 7.10 shows the molecular structure of **38** and Figure 7.11 displays the hydrogen bonding in the crystal structure of **38**.

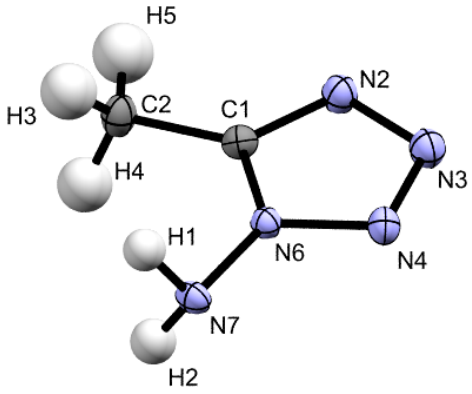

Figure 7.10. Thermal ellipsoid plot of **38**. Ellipsoids set at the 50% probability level. Selected bond lengths (Å) and bond angles (°): C1−C2 1.4823(17), C1−N6 1.3449(15), N2−C1 1.3203(15), N2−N3 1.3734(15), N4−N3 1.2923(15), N4−N6 1.3473(14), N6−N7 1.3991(14), N3−N4−N6 106.02(10), C1−N2−N3 105.97(10), N4−N3−N2 110.84(10), N2−C1−N6 107.75(10), N2−C1−C2 127.58(11), N6−C1−C2 124.66(11), C1−N6−N4 109.42(9), C1−N6−N7 130.68(10), N4−N6−N7 119.90(9).

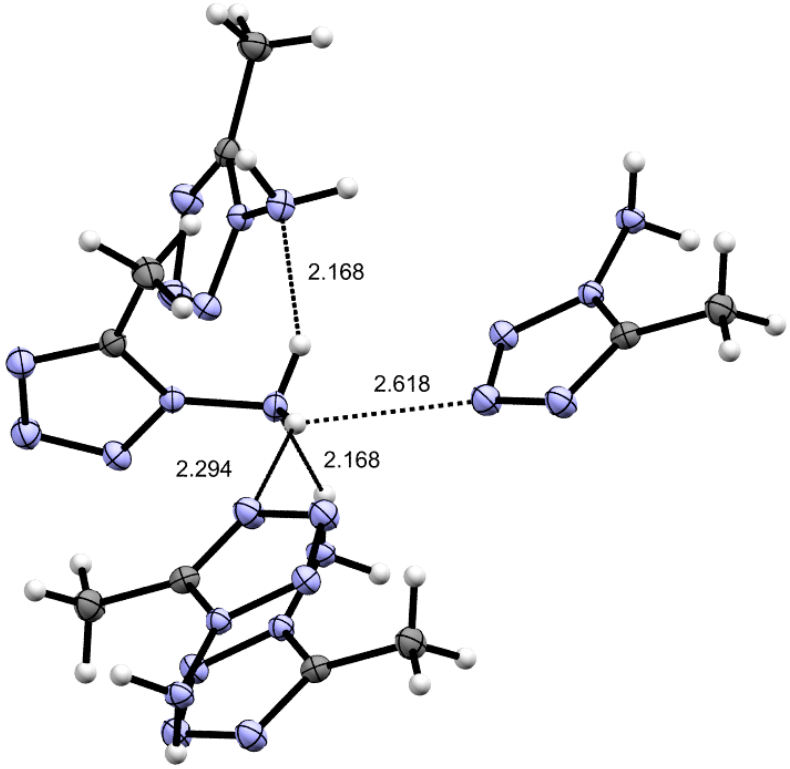

Figure 7.11. Schematic of the hydrogen bonds in the solid-state structure of **38** as determined by single crystal X-ray crystallography.

There are three different hydrogen bonds present in the structure but each amino group is involved in four hydrogen bonding interactions. The amino group acts as a hydrogen bond donor to N2 and N3 of a tetrazole ring and a hydrogen bond acceptor from two neighbouring amino groups. The acceptor donor distances range between 3.021 and 3.045 Å. The longer distances are between amino group and tetrazole ring and the shorter distance is between amino and amino group. There are no interactions involving the methyl group.

Unlike **38**, compound **37** is an oil at room temperature. On leaving at −28°C the oil freezes, it may be possible to place a drop of the oil onto a mylar and cool using the cryostat on the X-ray diffractometer to obtain a suitable crystal for structure determination. Despite the low quantities, enough material of **38** was obtained to attempt to prepare the corresponding triazenide.

7.2.2.3 Attempted syntheses of 1,3-bis(tetrazol-1-yl)triazenides

Two methods were attempted to prepare (PPN)b5mtt from **38**: (i) an aqueous method and, (ii) a non-aqueous method. The aqueous method was the same as what was used

for the preparation of **34**. On addition of half equivalent of $NaNO_2$ to acidified **38** in water, cooled in an ice bath, small bubbles begin to form, indicative of decomposition of the diazonium salt. As the diazonium salt is formed in the presence of the reactant the success of the synthesis depends on which is higher: the rate of the decomposition of the diazonium salt *vs* the rate of reaction between the diazonium salt and **38**. An aqueous solution of sodium hydroxide was added to the reaction solution on which the solution turns a pale yellow. (PPN)Cl was added to this new solution and the water evaporated to give a pale orange residue. Attempts to recrystallize from acetonitrile resulted in an off-white powder and orange crystalline material.

A ^1H NMR spectrum, shown in Figure 7.12, of the material in $CDCl_3$ displays signals for the PPN cation between 7.4 and 7.7 ppm, two singlets at 2.63 and 2.03 ppm and a broad signal at 3.40 ppm. The signal at 2.03 ppm is due to acetonitrile from the crystallisation attempt and the 2.63 ppm signal is due to a methyl group. The integral ratio between the PPN cation signal and the methyl peak should be 30:6, in this spectrum the ratio is 30:2.5. This immediately suggests the presence of more PPN cations, therefore, (PPN)Cl is present. The signal for water in $CDCl_3$ should be at 1.56 ppm, the fact it is shifted to 3.40 ppm implies the water is interacting with the solute in some way. There is no signal for NH_2, therefore, the signal at 2.63 ppm cannot be due to **38**, but rather, a new compound. It could be the b5mtt anion, but further analytical data would be required. The small quantity of material obtained made it difficult to separate the new compound from (PPN)Cl. The metathesis reaction between (PPN)Cl and sodium salts are successful due to the solubility of (PPN)Cl in warm water and the insolubility of the new (PPN) salt. In this reaction, it appears that (PPN)b5mtt is also soluble in warm water.

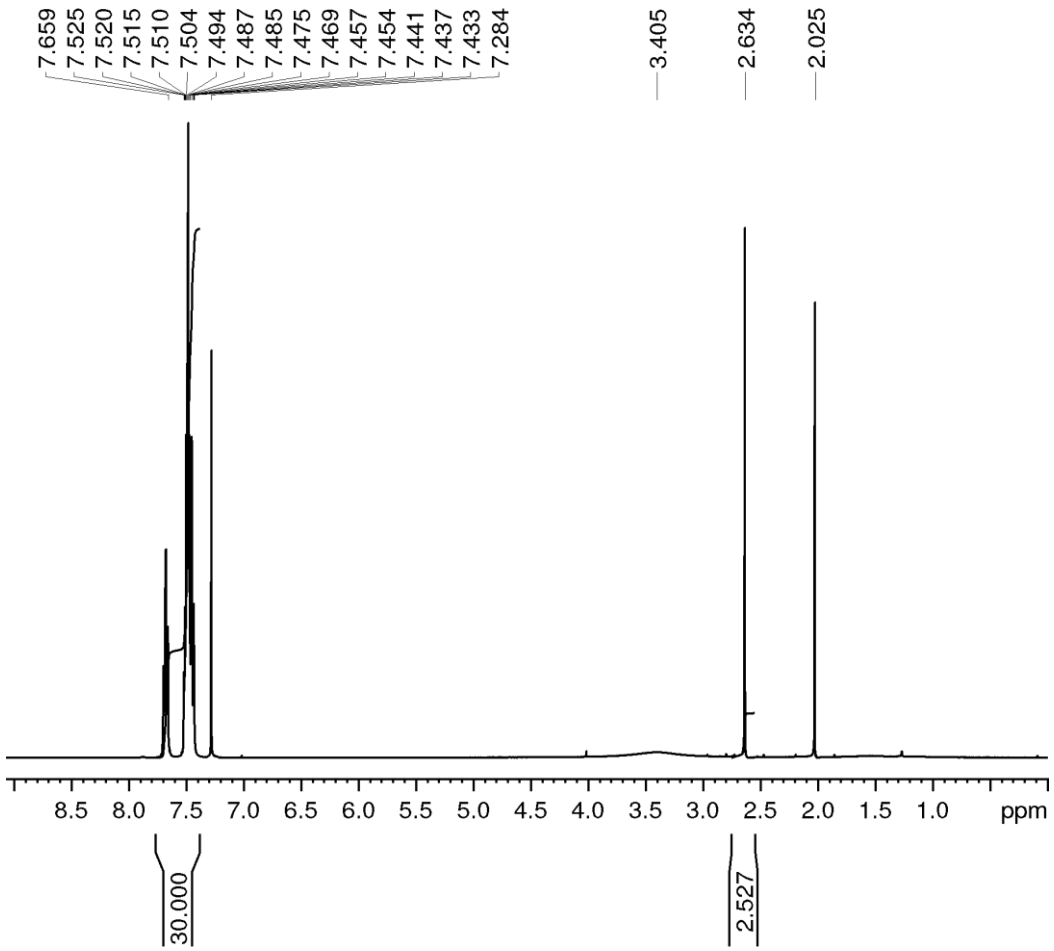

Figure 7.12. ^{1}H-NMR spectrum of the material obtained in the attempt to prepare (PPN)b5mtt *via* the aqueous method.

To achieve a greater level of control in the synthesis of the triazenide, the non-aqueous method was attempted. Instead of using $NaNO_2$, amyl nitrite is used with THF as a solvent at −30°C. The advantage of using THF as the solvent is IR spectroscopy can be used to monitor the reaction. After amyl nitrite and **38** were combined in THF at −30°C and treated with HCl, the FT-IR spectrum of the solution displayed a peak at 2223 cm^{-1} for the ν(N≡N). A further equivalent of **38** was added to the reaction solution to prepare the triazene and then deprotonation with NaH to give Na(b5mtt). (PPN)Cl is insoluble in THF, but on addition of the solution containing the proposed Na(b5mtt), to a suspension of (PPN)Cl in THF the material dissolved. After drying under high vacuum at 65°C for over 24 hrs a viscous yellow oil was all that remained.

The ^{1}H NMR spectrum of the oil, Figure 7.13, showed the presence of amyl nitrite, which was most likely hindering any crystallisation attempts. There are two signals in the expected "methyl region" at 2.84 and 2.59 ppm and a broad signal at 6.44 ppm,

indicative of an NH_2 group. The presence of an NH_2 group and an extra methyl signal suggests the presence of **38**. The integration ratio between the signals 6.44 ppm, 2.84 ppm and 2.59 ppm is 6:3:4. The integration ratio for **38** should be 2:3 (NH_2:CH_3), which is clearly not present. Partnered with the fact there is no signal for water at 1.6 ppm, water is causing the erroneous ratio *via* an interaction with the amino group. Comparing the chemical shift of the methyl group in **34** and 5-amino-1-methyltetrazole (4.05 and 4.15 ppm) the signal has a lower chemical shift in the triazenide. From this, a tentative assignment can be made that the signal at 2.59 ppm may belong to the desired (PPN)bis(5-methyltetrazol-1-yl)triazenide. The ratio between this signal and the PPN resonances is 4:30. Not 6:30, and so a small amount of (PPN)Cl is present. Similarly with the aqueous method pure (PPN)b5mtt could not be obtained, leaving only **34** to be investigated as a ligand towards Main Group coordination centres.

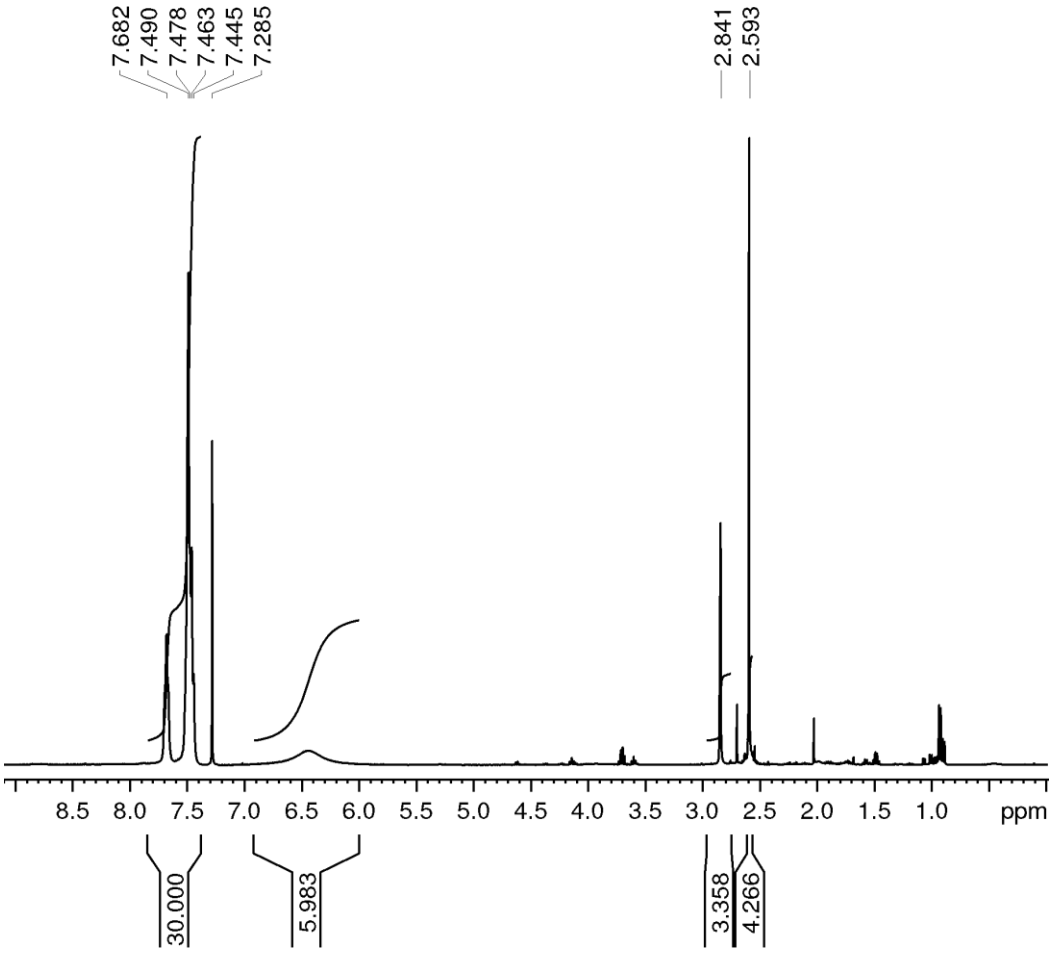

Figure 7.13. ^{1}H-NMR spectrum of the material obtained in the attempt to prepare (PPN)bis(5-methyltetrazol-1-yl)triazenide *via* the non-aqueous method. Unlabelled peaks belong to amyl nitrite.

7.2.3 Nitrogen-rich triazenides as ligands

Several products are possible between the reaction of **34** and a Group 14 tetrahalide summarised in Scheme 7.5. The reaction between $SiCl_4$ and Na(bpat) or Na(bptt) (*vide supra*) formed *cis*-$(RNNNR)_2SiCl_2$ and this remains a possible product between **34** and ECl_4. Due to the potential of the (b1mtt) anion to act as a terdentate ligand through the central nitrogen atom and the tetrazole rings, there is an opportunity only a single (b1mtt) ligand to coordinate and eliminating a single chlorine atom. This would give the octahedral complex, (b1mtt)$SiCl_3$. On the other hand, the PPN salts of small anions are often more soluble in organic solvents, compared with the sodium salts, and so instead of a salt metathesis reaction an addition reaction occurs to give the salt (PPN)[(b1mtt)$SiCl_4$]. It is clear some of these complexes have a high nitrogen content and so to reduce any sensitivity $SnCl_4$ was used to reduce the nitrogen content.

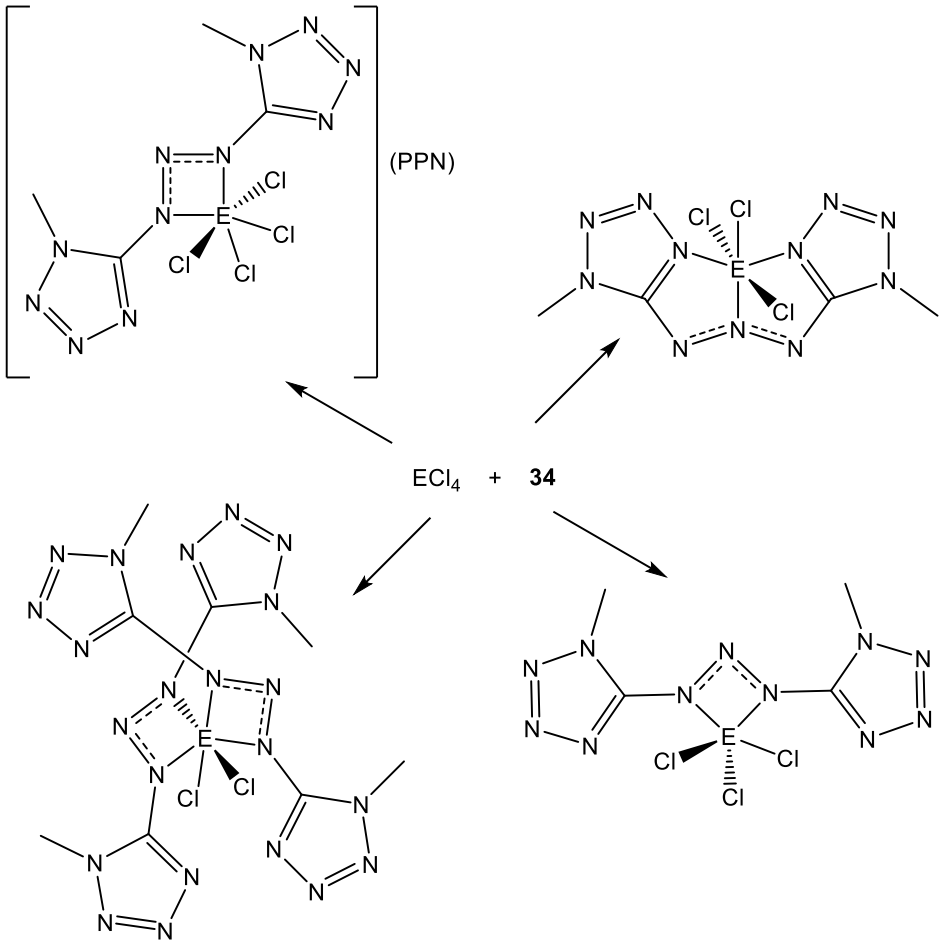

Scheme 7.5. Possible products from the reaction between **34** and ECl_4.

$SnCl_4$ and **34** were combined in acetonitrile in a 1 : 1 ratio. Compound **34** is sparingly soluble in acetonitrile at ambient temperature. On addition of the $SnCl_4$, the material dissolved giving an overall clear, yellow solution. The solvent was evaporated to dryness to give a sticky yellow residue. A ^1H NMR spectrum of the residue was recorded in CD_3CN, Figure 7.14. It shows two peaks at 4.21 and 4.04 ppm, in the ratio 5:1, and resonances for the PPN cation. The signal at 4.04 ppm is unreacted **34** leaving the peak at 4.21 ppm to be the resonances for the new product. Of the four compounds shown in Scheme 7.5, only the complex containing two (b1mtt) ligands would show more than one resonance for the methyl group discounting this compound as the product. All the other three compounds remain as possibilities.

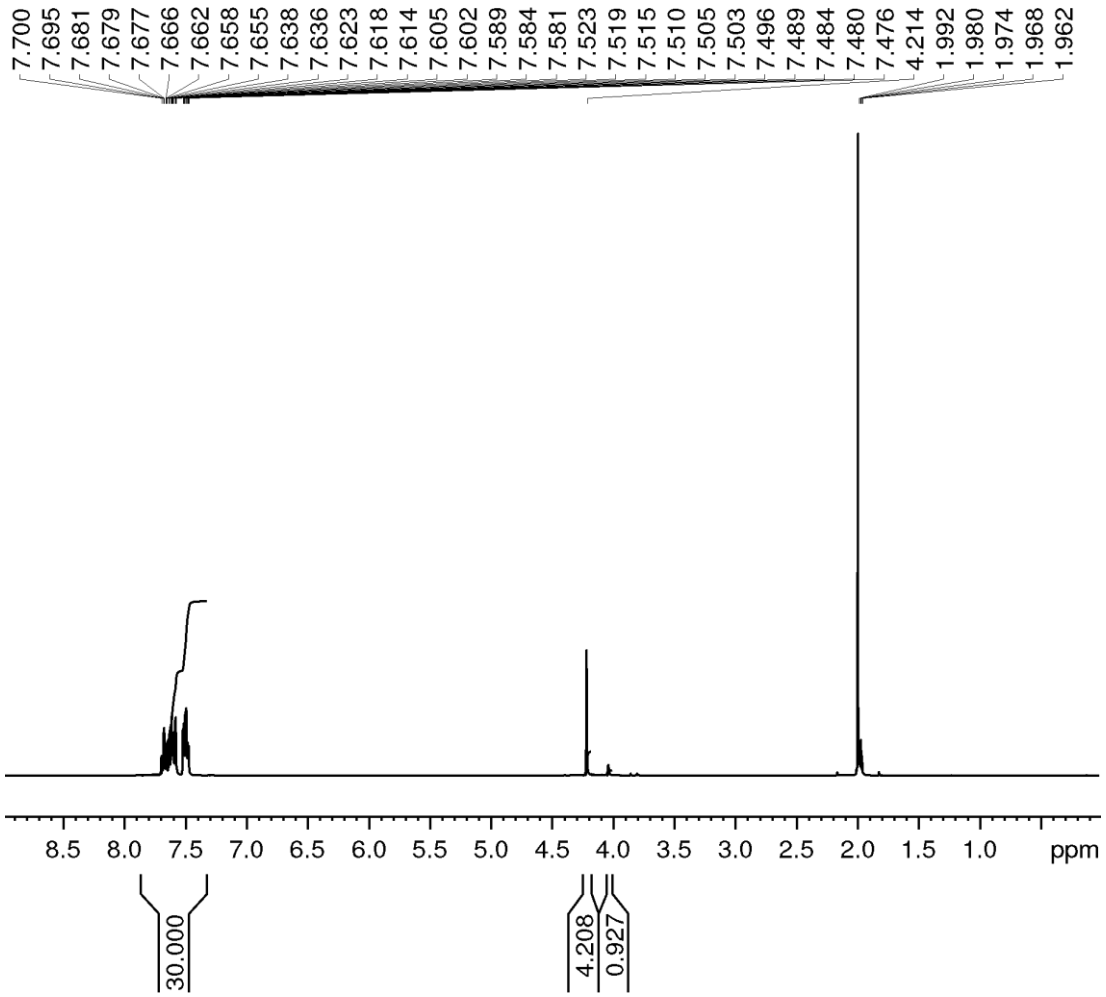

Figure 7.14. ^1H-NMR spectrum of the crude material obtained from the reaction between **34** and $SnCl_4$.

The residue was dissolved in THF and treated with diethyl ether to induce the precipitation of any PPN salts. A white material had precipitated and the supernatant solution remained yellow. Identification of the white material was made by IR spectroscopy to be (PPN)Cl. The presence of (PPN)Cl discounts (PPN)[(b1mtt)$SiCl_4$] as the product of the reaction. The remaining two compounds are constitutional isomers of one another and it would not be possible to determine which of the two is obtained from the current data available. Attempts to crystallise the material proved to be unsuccessful.

If the product from the reaction is the complex bearing the bidentate ligand, addition of a second equivalent of **34** would result in the formation of the bis complex, $(b1mtt)_2SnCl_2$. Consequently, if the product is the complex that contains the terdentate ligand no reaction is likely to occur on the addition of a second equivalent of **34**. When 1.76 mmol of **34** was treated with 0.88 mmol of $SnCl_4$ and stirred for 72 hrs, 0.8 mmol of **34** was recovered from the reaction solution. This equates to a 1:0.9 ratio between $SnCl_4$ and unreacted **34**, approximately 1:1. From this it can be inferred that the product obtained from the the reaction between $SnCl_4$ and **34** is κ^3-*N*,*N'*,*N''*-1,3-bis(1-methyltetrazol-5-yl)$SnCl_3$. It would not be possible to add a further monoanionic terdentate ligand to such a species without the elimination of three chloride anions giving an overall complex with +3 charge. No conclusive structural data was obtainable of the product formed between the reaction of **34** and $SnCl_4$.

Unfortunately it was not possible to obtain a pure Main Group coordination compound containing a bis(tetrazoyl)triazenide, however, evidence for coordination has been obtained.

7.3 Conclusion

Triazenides are viable candidates for a new energetic ligand for Main Group coordination centres. It was clear from the reaction between aryl triazenides and $SiCl_4$ that there was a preference for the formation of the complex *cis*-bis$(RNNNR)_2SiCl_2$ even if a single equivalent of the triazenide was added. Even though the solvent for the reaction was THF, which $SiCl_4$ is known to react with, the complexes were easily obtainable in a reasonable yield. Yet, despite the apparent strength of the triazenide coordination there is evidence for the displacement of the ligand with azide anions. The

structure of these two complexes is the *cis* conformation due to relieving steric interactions that would be present between R-groups in the *trans* isomer.

The successful synthesis of tetrazole triazenides was limited. The PPN salt of bis(5-methyltetrazol-1-yl)triazenide was easily prepared after methylation of 5-aminotetrazole. This compound represents the first bis(tetrazoyl)triazenide with a non-coordinating cation. The phlegmatising property of the PPN cation prevents any interaction between itself and the anion. The ease at which this compound could be prepared is related to the availability of the starting material 5-aminotetrazole. Its regioisomer, 1-aminotetrazole, is much more difficult to obtain. Hydrolysis of (PhCH=NN_4CH) and (PhCH=NN4CMe) proved to be a difficult task. While it was possible to obtain pure products, it was only in very small quantities in yields of 6-11 %. In the presence of benzaldehyde, the 1-aminotetrazole derivatives readily condensed to the appropriate imine, making separation extremely difficult. Therefore, it is imperative for all benzaldehyde to be removed from the reaction solution. Imine hydrolysis is usually a favourable process due to the massive excess of water used. However, in this case hydrolysis only begins to occur at temperatures close to the boiling point of water. The harsh conditions required for the synthesis is the most likely cause for such a low yield of product.

Of the two methods attempted to prepare (PPN)(b5mtt), the non-aqueous method has the advantage that the reaction can be monitored *via* IR spectroscopy, however, it is difficult to remove the associated impurities. The aqueous method is the better method for triazene synthesis, unless the diazonium salt is unstable at ice-bath temperature, as evidenced in the attempts to prepare (PPN)(b5mtt). Using this method, the only impurity was (PPN)Cl, something which can be overcome by adding more Na(b5mtt) if available. In contrast, the non-aqueous method had (PPN)Cl, amyl nitrite and unreacted 1-amino-5-methyltetrazole as impurities. If the synthesis for 1-aminotetrazoles was more reliable, then pure (PPN)(b5mtt) could be made. The method using hydroxylamine-O-sulfonic acid would have to be investigated.

The coordination chemistry of the triazenide ligand depends on the R-group attached either side of the triazenide chain. If the R-group can act as a Lewis base that changes the coordination mode of the triazenide unit from bidentate *via* the two terminal nitrogen atoms to monodentate *via* the central nitrogen atom, as is the case when (b1mtt) was used as a ligand. In turn, this makes the triazenido ligand a highly versatile

ligand towards Main Group coordination centres. Simple functionalisation of the R-group can result in predictable changes in the coordination chemistry of such ligands.

8. SUMMARY

The coordination chemistry of the nitrato as a ligand in “light” Group 14 elements and arsenic has been investigated. With respect to Group 14 it was found it was possible to synthesise the thermally labile $Si(NO_3)_4$ as a 1 : 1 diethyl ether / acetonitrile stock solution at −40°C. The diethyl ether can be evaporated at −60°C which affords an acetonitrile solution of $Si(NO_3)_4$ that can be treated with $(PPN)NO_3$ to prepare $(PPN)_2Si(NO)_6$, as the first isolated compound containg a homoleptic silicon nitrate. It had been previously suggested in the literature that homoleptic anions such as $[Ge(NO_3)_6]^{2-}$ and $[Si(NO_3)_6]^{2-}$ are too unstable to synthesise. However, through the use of weakly coordinating cations it has been possible to prepare such anions. The silicon nitrate shows remarkable thermal stability compared to other silicon nitrates ($Si(NO_3)_4$ decomposes within 0.5 h at room temperature, whereas $(PPN)_2Si(NO_3)_6$ is stable up to 138°C). The heavier congeners, $(PPN)_2Ge(NO_3)_6$ and $(PPN)_2Sn(NO_3)_6$, can be prepared using the same methodology. However, diethyl ether is not required as a reaction solvent and the synthesis can be completed at ambient temperatures to afford acetonitrile solutions of $E(NO_3)_4$ (E = Ge, Sn). Thermal studies of $(PPN)_2E(NO_3)_6$ (E = Si, Ge and Sn) show that the complex anions decompose in two steps by 300°C. A different EO_n product is obtained at these temperatures for each complex salt; Si, n = 2; Ge, n = 0; Sn, n = 1. Further nitrate-related decomposition processes are masked by the decomposition of the (PPN) cation. The crystals of silicon and germanium salts are isostructural and the anion in $(PPN)_2Ge(NO_3)_6$ and $(PPN)_2Si(NO_3)_6$ both possess a crystallographically imposed C_{2h} point group symmetry. In contrast, the anion in $(PPN)Sn(NO_3)_6$ adopts D_{3d} point group symmetry. Throughout, all nitrato groups bond in a monodentate fashion, however, a secondary interaction from another oxygen atom in the ligand is present. The effects of halogen bonding on polynitrato coordination complexes were investigated. Upon changing the cation from PPN to 1-methyl-3-bromopyridinium, halogen bonds appear in the solid state. These are formed between the bromine atom and one oxygen atom of the nitrato ligand in the salts $(1\text{-methyl-3-bromopyrdinium})_2E(NO_3)_6$ (when E = Ge, Sn). This interaction is sufficiently strong so as to force a change in the symmetry of the $[Ge(NO_3)_6]^{2-}$ from C_{2h} (no directed interaction) to D_{3d} (halogen-bond interaction). The covalent nitrato group is a stronger halogen bond acceptor than an ionic nitrate anion.

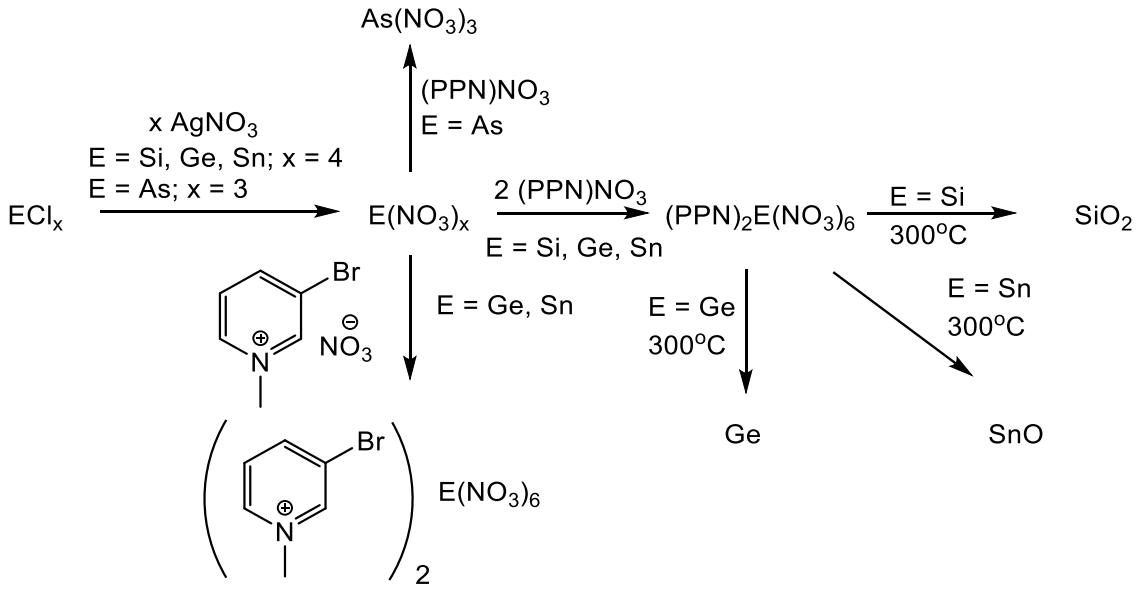

Scheme 8.1. Summary of the synthetic principles for Group 14 and arsenic nitrato complexes.

The synthesis of arsenic(III) nitrates proved to be more challenging owing to two main issues. Firstly, arsenic nitrates are more thermally labile than those of the Group 14 elements. $As(NO_3)_3$ and $AsCl_2(NO_3)$ decompose rapidly at room temperature whilst $(PPN)AsCl_2(NO_3)_2$ decomposes at room temperature within several hours. The second issue is releated to acetonitrile causing the dissociation of the $[AsX_4]^-$ complex into AsX_3 and X^-. Addition of either silver nitrate to $(PPN)AsCl_4$ in acetonitrile, or addition of $(PPN)NO_3$ to $As(NO_3)_3$ in acetonitrile, gives a solution of $As(NO_3)_3$ and $(PPN)NO_3$. IR spectroscopy gave insight into the coordination mode of the nitrato ligand. If bound in a κ^1-*O* or $\mu_{1,3}$-NO_3 fashion, the group decomposes with the release of NO_2 (1740 cm^{-1} in acetonitrile), whereas if bound in a κ^2-*O,O'* fashion the group the decomposition is accompanied by the release of NO (1840 cm^{-1} in acetonitrile). The molecular structure of the $[AsCl_2(NO_3)_2]^-$ anion was determined by single crystal X-ray crystallography and reveals the nitrato group coordination made as unsymmetrically bidentate. It may be possible to prepare $(PPN)As(NO_3)_4$ in dichloromethane. However, due to the low solubility of silver nitrate and the temperature sensitivity of arsenic nitrates, reaction times will be very long.

The classification of monodentate and bidentate coordination modes do not account for the complexity of nitrato coordination in Main Group coordination complexes. IR spectroscopy, while still remaining a vital tool for characterisation, cannot account for

the subtleties in the coordination chemistry of the nitrato ligand. In particular, the strength of the secondary interaction between a second oxygen ligator, of a single nitrato ligand, and the coordination centre. Structural information from X-ray crystallographic measurements is the only reliable characterisation method available to determine the nature of the bonding between coordination centre and the nitrato ligand.

Two other methods for the preparation of nitrato complexes were investigated since the methods applied earlier would not be a suitable method for low-valent Main Group coordination centres. Both of these were found to be ineffective. Sodium nitrate was used as an ionic nitrate transfer agent. It was observed that the nucleophilicity of the nitrate anion is too weak and does not allow the displacement of the chloride ligands in $[GeCl_3]^-$, for instance, efficiently. Consequently, only $(PPN)GeCl_3$ / $(PPN)GeCl_2(NO_3)$ could be crystallised in the form of a solid solution. The presence of the $[GeCl_3]^-$ indicates that there is an equilibrium present between $[Ge(NO_3)_3]^-$ and $[GeCl_3]^-$ and all the degrees of substitution in between. The addition of a large excess of sodium nitrate did not result in forcing the equilibrium towards $(PPN)Ge(NO_3)_3$. An attempt to use trimethylsilylnitrate as a *covalent* nitrato transfer agent was also unsuitable. In this case, the exchange process requires such elevated temperatures at which trimethylsilylnitrate itself readily decomposes at.

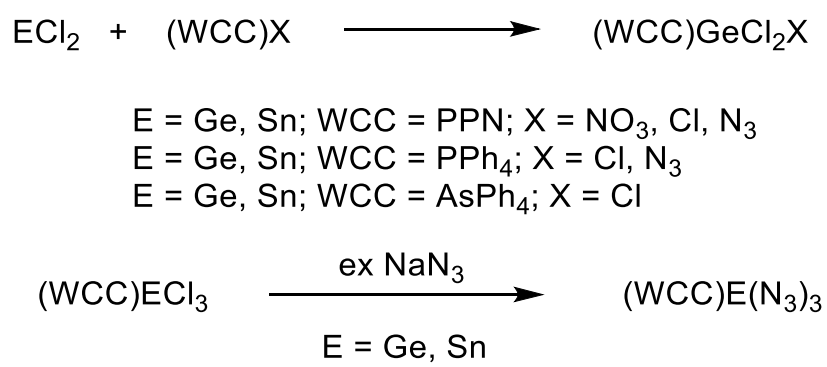

Scheme 8.2. Investigated syntheses of homoleptic germanium(II) and tin(II) complexes.

Using sodium azide as a conventional, good ionic azide transfer agent, it was possible to synthesis and isolate stable anionic homoleptic germanium(II) and tin(II) azido complexes starting from the trichloride complexes $(WCC)ECl_3$. The crystal structures of $(PPh_4)Ge(N_3)_3$ and $(PPh_4)Sn(N_3)_3$ were determined by X-ray crystallography. The $[Ge(N_3)_3]^-$ anion showed only weak interactions between cation and anion with distances in range of the sums of van der Waals' radii. The $[Sn(N_3)_3]^-$ anion forms

discrete dimers, $\{[Sn(N_3)_3]_2\}^{2-}$ in which two long $\mu_{1,1}$-N_3 bridges and two long $\mu_{1,3}$-N_3 bridges hold monomers together. Oxidation of both azido complexes by an excess of HN_3 affords the related homoleptic complexes in the standard oxidation states $(PPh_4)E(N_3)_6$ (E = Ge, Sn).

A variety of interesting compounds were prepared in attempts to access low-valent azido complex of third row elements. For this purpose, Si(IV) azides containing bulky, σ-donor ligands were prepared first as starting complexes, which include $IPrSi(N_3)_4$, $(^{dipp}NCN)Si(N_3)_3$, $IPrP(N_3)_5$, $(^{dipp}NCN)P(N_3)_4$, $(^{dipp}NCN)P(N_3)_2$ and $(^{dipp}NCN)SiH(N_3)_2$. These are the first examples of a *pentacoordinate* Lewis adduct of $Si(N_3)_4$, and charge-neutral Lewis adduct of $P(N_3)_5$. When the N-heterocyclic carbene (NHC) I^tBu was added to $Si(N_3)_4$, a complex containing two imidazolidine-2-imido ligands were formed instead of the anticipated Lewis adduct, $(I^tBuN)_2Si(N_3)_2$. Reduction of these compounds was attempted by either using KC_8 and magnesium(I) dimers or by 'deazoimidation' *via* $Li(NSiMe_3)_2$, IPr and I^tBu. A salt metathesis reaction was also attempted using both $(PPN)N_3$ and sodium azide with $IPrSiCl_2$ as the starting complex already in low oxidation state. The now available evidence suggests that the product from the salt metathesis reaction and reduction of $IPrSi(N_3)_4$ with KC_8 are identical. It is postulated that the desired Si(II) azide, $IPrSi(N_3)_2$, does form but reacts quickly with another molecule of $IPrSi(N_3)_2$ upon elimination of N_2. The exact composition of the product is unknown but is most likely a bridged iminosilane. Reactions with a magnesium(I) dimer reduces $IPrSi(N_3)_4$, $(^{dipp}NCN)Si(N_3)_3$, $IPrP(N_3)_5$ and $(^{dipp}NCN)P(N_3)_3$ to form IPrSiSiIPr, $(^{dipp}NCN)Si$, IPrPPIPr and $(^{dipp}NCN)P$, respectively, regardless of the stoichiometry. The by-product of these reactions was the formaerly unknown $^{R}NacnacMgN_3$. When the R-group is a mesityl group, the compound forms a *hexamer* in non-coordinating solvents and in the solid state, but when dipp groups are present, the compound forms a *trimer* in non-coordinating solvents and in the solid state. Incidentally, these two compounds provide insight into the effect of bridging interactions on the IR stretching frequency of the $\nu_{as}(N_3)$. A $\mu_{1,3}$-N_3 bridge, which both compounds exhibit, results in an increase in the energy of the absorption. The closer the angle between N(β)−N(γ)−M is to 180°, the higher wavenumber of the $\nu_{as}(N_3)$ vibration. One possible explanation for this phenomenon is that electron density is removed from an antibonding orbital, increasing the N−N bond

order and the energy of the harmonic fundamental asymmetric N_3 stretching vibration. This interaction has a remarkable effect on the position of the band in the IR spectrum.

Deazoimidation reactions appeared to be a viable option for preparing a Si(II) azide. However, reactions of (^{dipp}NCN)SiH$(N_3)_2$ with the bases IPr, Li$(NSiMe_3)_2$ and Li^{dipp}Nacnac resulted in Si(IV) compounds (8.3 displays a summary of this part of the investigation). Intriguingly, all these reactions left the Si−H bonds intact. Only when I^{t}Bu was added to (^{dipp}NCN)SiH$(N_3)_2$ was evidence obtained for the breaking of the Si−H bond to give I^{t}BuHN_3. The latter reacts with unreacted hydrido silicon complex to form (I^{t}BuH)[(^{dipp}NCN)SiH$(N_3)_3$], which could be isolated. This observation implies that (^{dipp}NCN)SiN_3 has formed. However, it could not be isolated.

Synthetic methods used for the preparation of Si(II) halides are not applicable for the synthesis of Si(II) azides. Two features of the azido ligand account for why this is the case. Firstly, the azido group is a polar bond and is prone to reduction with elimination of dinitrogen. Secondly, the nucleophilicity of the azide anion can give rise to potential competing reactions that inhibit the isolation of a Si(II) compound. Despite the unsuccessful attempts to prepare a Si(II) azide, a large number of new and interesting Main Group azido complexes have been synthesised. IPrSi$(N_3)_4$ and (^{dipp}NCN)Si$(N_3)_3$ represent the first *pentacoordinate* silicon azido complexes. The structural and spectroscopic data of these complexes, in particular, show that there is a relationship between the covalent nature of the Si−N_3 bond and the coordination number of the silicon atom. Interestingly, the P−N_3 bond of the phosphorus analogues are more ionic in nature than the silicon complexes, due to the fact that the phosphorus complexes have a coordination number of six. In contrast, the complex anions, $[Si(N_3)_6]^{2-}$ and $[P(N_3)_6]^-$, both have coordination numbers of six, however, the Si−N_3 bond appears to be more ionic. A fact which suggests that the coordination number has an equal effect on the nature of the bond between the coordination centre and the azido ligand as the identity of the coordination centre has.

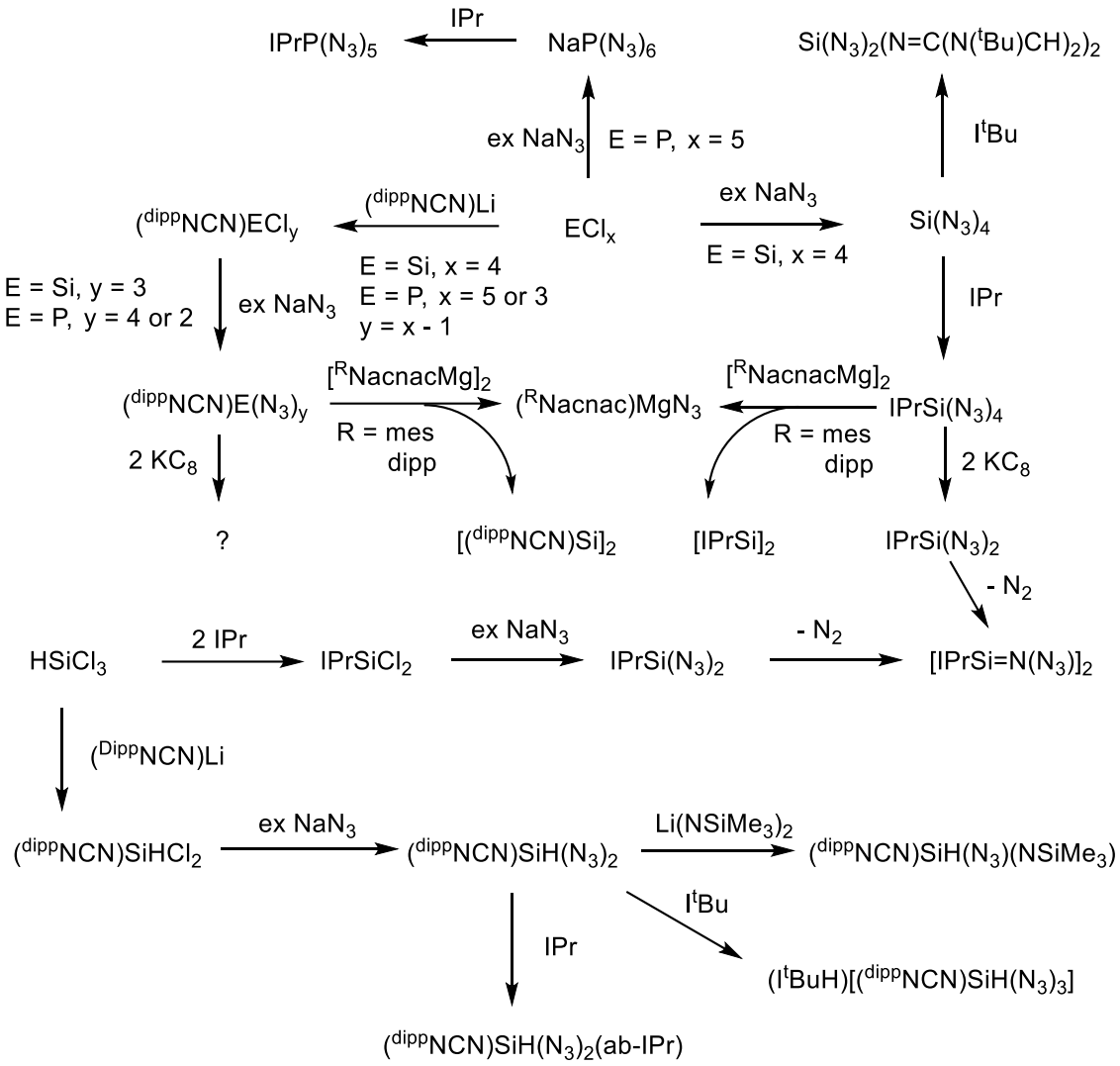

Scheme 8.3. Summary of the reactions investigated in the attempts to prepare a Si(II) azide. Appropriate solvents and by-products omitted for clarity. I^{t}Bu = 1,3-di-*tert*-butylimidazol-2-ylidene, IPr = 1,3-bis(2,6-diispropylphenyl)imidazol-2-ylidene, (^{dipp}NCN) = 1,3-bis(2,6-diisopropylphenyl)-2-(*para*-t-butylphenyl)-amidinate, ^{R}Nacnac = 1,5-β-diketiminate, mes = 2,4,6-trimethylphenyl, dipp = bis(2,6-diisopropyl)phenyl, ab-IPr = abnormal coordination mode of IPr.

The lack of energetic ligands (sufficiently stable nitrogen- and oxygen-rich species) available prompted an investigation into the study of nitrogen-rich triazenides. First, the coordination chemistry of triazenides towards Group 14 elements was investigated using aryltriazenides. It was found that two triazenido ligands add to $SiCl_4$ and coordinate in a κ^2*N,N'* fashion even when only one equivalent of sodium triazenide was added. It was relatively straight-forward to prepare bis(1-methyltetrazol-5-yl)triazenide from 5-amino-1-methyltetrazole, however, the preparation of bis(5-methyltetrazol-1-yl)triazenide suffered from low yields and the difficult and time-consuming synthesis of 1-amino-5-methyltetrazole. Evidence of the formation

(PPN)bis(5-methyltetrazol-1-yl)triazenide was obtained from ^{1}H-NMR spectra of the crude product; however, the complex could not be isolated. The reaction between (PPN)bis(1-methyltetrazol-5-yl)triazenide and $SnCl_4$ suggested that only one triazenido anion coordinates to $SnCl_4$ which is accompanied by the displacement of one chloro ligand. This triazenido ligand acts as a terdenate ligand *via* the central nitrogen atom of the triazene chain and a nitrogen atom on each tetrazole ring.

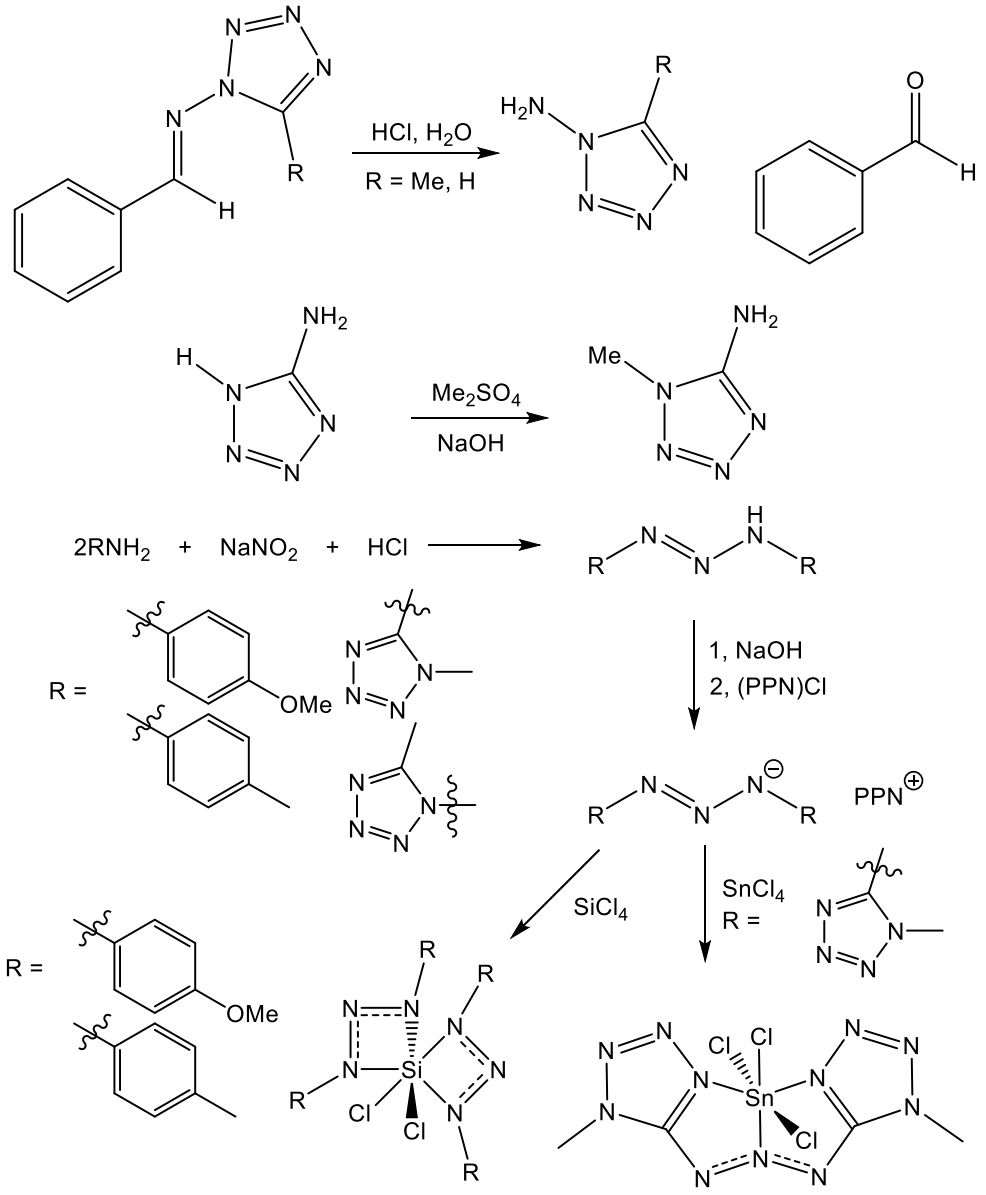

Scheme 8.4. Summary of the synthesis of triazenido coordination complexes. PPN = $(Ph_3P)_2N^+$

New oxygen- and nitrogen- rich coordination complexes of the Main Group elements have been prepared and isolated. Both the azide and nitrate anions appear to be simple

molecules, yet, both are versatile and interesting ligands. The coordination chemistry of these ligands gives rise to a variety of different structural features that have a marked effect on the reactivity of these compounds. Being able to predict the structural and spectroscopic properties results in less risk when working with potentially thermally, shock or friction sensitive compounds. In the field of energetic coordination chemistry, understanding these effects help with the design and synthesis of new energetic coordination complexes.

9. EXPERIMENTAL

9.1 General procedure

Infrared absorption spectra were recorded in the range 500–4000 cm^{-1} on a Bruker Tensor 27 Fourier Transform Infrared spectrometer running the Bruker *OPUS* software package, or Bruker Alpha FT-IR spectrometer running Bruker *OPUS 7.0*, at a spectral resolution of 2 cm^{-1}, either as a nujol mull between NaCl windows or in solution using a Specac CaF_2 solution cell. When Fourier transform infrared spectra are discussed, the following abbreviations will be used to indicate the relative absorbance of bands: vs = very strong, s = strong, m = medium, w = weak, vw = very weak, sh = shoulder, br = broad. Elemental analyses were carried out by the University of Sheffield elemental analysis service on a PerkinElmer 2400 CHNS/O series II elemental analyser in an atmosphere of pure oxygen. ^{1}H, ^{13}C, ^{14}N, ^{31}P Nuclear magnetic resonance (NMR) spectra were recorded using a 400 MHz Bruker Avance 400 spectrometer; ^{119}Sn spectra were kindly recorded by Sue Bradshaw on a 500 MHz Bruker Avance 500 spectrometer. ^{1}H and ^{13}C NMR spectra were calibrated against the residual solvent peak. ^{14}N, ^{31}P and ^{119}Sn were calibrated against $MeNO_2$, 85% H_3PO_4 and $SnMe_4$ respectively. NMR spectra were processed using Bruker *TOPSPIN v3.2*. ^{15}N solid state NMR spectra were kindly recorded by Dr Sandra van Meurs on a 500 MHz Bruker Avance 500 spectrometer and calibrated by adjusting the NMR field such that the higher chemical shift peak of adamantane (C13 spectrum) is at 38.48 ppm. DSC measurements were performed on a PerkinElmer Pyris 1 Differential Scanning Calorimeter operated under nitrogen flow (20 ml min^{-1}) with a heating rate of 10 °C min^{-1}. The instrument was calibrated against a pure indium reference (99.999 %) with a sharp transition at 156.60 °C, with a well-known enthalpy change of 28.45 J g^{-1}. The samples were sealed in PerkinElmer stainless steel high-pressure capsules (30 μL internal volume) with Au-plated Cu seals, which can operate up to 400 °C and 150 bar. Onset temperatures for melting and decomposition were calculated by the intersection of the tangent of maximum gradient with the projected position of the baseline, and quoted values are based on an average of a minimum of 3 measurements unless otherwise stated. Thermogravimetric analysis (TGA) was carried out using a Pyris 1 Thermogravimetric Analyser with a ceramic crucible using a heating rate of 10 °C min^{-1} under nitrogen flow (20 ml min^{-1}). Onset temperatures (T_{on}), mass losses, and decomposition (ΔH_{dec}) were calculated using the data analysis tools within the *Pyris 1*

software. Single crystal X-ray diffraction (XRD) data collections were performed either using graphite-monochromated Mo K_α radiation (λ = 0.71073 Å) at 100 K (unless otherwise specified) on a Bruker Small Molecule Analytical Research Tool (SMART) 4000 diffractometer equipped with a CCD area detector and an Oxford Cryosystems Cobra cryocooler, or on a Bruker Kappa diffractometer equipped with a CCD area detector and an Oxford Cryosystems crysotream cryocooler, or on a Bruker D8 Venture diffractometer using Cu-$K_{\alpha1}$ radiation (λ = 1.54178 Å) equipped with a Bruker PHOTON CMOS detector. Data were collected using Bruker *APEX2* software and integrated using Bruker *SAINT*, absorption correction was applied using Siemens' Area Detector Absorption correction (*SADABS*) within *APEX2*. All structures were solved using direct methods for the location of heavy atoms using *SHELXS-97* within *SHELXTL-2013*.[240,241] Hydrogen atoms bound to heteroatoms were located *via* a Fourier difference map, and their position and isotropic thermal displacement parameters freely refined. Hydrogen atoms bound to carbon were calculated in idealised positions based on the hybridisation of the parent atom and data collection temperature, with isotropic displacement parameters of 1.2U_{eq} of the parent atom, using appropriate HFIX commands within *SHELXL-2014*.[241] Disorder in the N−O groups of **2** is accounted for by a 1:1 disorder model for two independent NO_3 ligands in which the positions of the terminal O atoms are split and geometry and thermal motion related to each other by suitable SADI, SIMU, and DELU restraints. Disorder in $P(N_3)_2$ of **21** is accounted for by an independently refined disorder model for two independent $P(N_3)_2$ units resulting in a 0.6:0.4 ratio of each component. The geometry and thermal motion are related to each other by suitable SADI, SIMU, and DELU restraints.

All solvents were stirred over CaH_2 for a minimum of 24 hrs and purified by trap-to-trap condensation and stored in glass ampoules fitted with Young's taps. Main Group halides were purified by vacuum sublimation or stirring over Na_2CO_3 and transferred by trap-to-trap condensation where appropriate. Acetonitrile (99.9 %, HiPerSolv, ChromaNorm), benzaldehyde (>98 %) and sodium hydroxide (97 %, pellet) were purchased from Fischer. Sodium nitrate (99 %), silver nitrate (99.9 %), germanium tetrachloride (99.9999 %), trimethylsilyl chloride (98 %), tetrafluoroboric acid (50 % w/w in water), magnesium (99+ %) and p-anisidine (99 %) were purchased from Alfa Aesar. Silicon tetrachloride (99 %), diethyl ether, dichloromethane, phosphorus pentachloride (≥ 98 %), toluene, 1,4-dioxane, triethylsilane (99 %), germanium(II) chloride dioxane adduct, tetraphenylarsonium chloride, tetraphenylphosphonium

chloride, glyoxal (40 % weight in water), paraformaldehyde (reagent grade), ethyl acetate, t-butylamine (98 %), sodium hydride (95 %), trichlorosilane (99 %), tetrafluoroboric acid in diethyl ether, p-toluidine (97 %), arsenic trichloride (99.99 %), phosphorus trichloride (98 %), potassium (98 %), acetylacetone (≥ 99 %), lithium(bis(trimethylsilane)amide), hexane, pentane, lithium (99 %), 1-bromo-4-tbutyl-benzene (97 %), nBuLi in hexane (1.5 M), 5-aminotetrazole hydrate (≥ 99 %), hydrazine monohydrate (98 %), triethylorthoformate (98 %), lithium aluminium hydride (powder, reagent grade), methyliodide, 3-iodopyridine, 3-bromopyridine, 3-chloropyridine and 3-fluoropyridine were purchased from Sigma Aldrich. Sodium azide, benzene and triethylorthoacetate were purchased from Merck. 2,6-diisopropylphenylcarbodiimide was purchased from Fluorochem. Sodium nitrite and 2,6-diisopropyphenylamine (90 %) were purchased from Fluka. Acetic acid (glacial), hydrochloric acid (35 %) and sodium carbonate were purchased from VWR. Dimethyl sulfate (99+ %) and graphite were purchased from Acros. (PPN)Cl and $As(NO_3)_3$ were prepared by Andrew Sadler, hydrazoic acid was prepared by Rory Campbell, $IPrSiI_2$ was kindly provided by the Filippou group at the University of Bonn, 3-bromo-methylpyridinium iodide was kindly provided by the Brammer group at the University of Sheffield.

9.2 Preparative procedures

9.2.1 Preparation of (PPN)NO_3. Modified from ref [242]. (PPN)Cl (10.620 g, 19.6 mmol) was dissolved in ~50 mL of water warmed to 60°C and added slowly over a period of ten minutes to a solution of $NaNO_3$ (55.746 g, 0.656 mol) dissolved in ~100 mL of water warmed to 60°C. On addition, a white precipitate was observed and the solution was allowed to stir for a further ten minutes. The solution was cooled in ice for an hour to ensure complete precipitation of the initial white precipitate, after which the precipitate was filtered and dissolved in acetonitrile (50 mL). Organic volatiles were evaporated in vacuum and the solid was recrystallised by dissolving in boiling dichloromethane and left to cool at –28˚C. Colourless, block crystals were isolated by filtration and dried under high vacuum at 100°C. (Mass: 10.123 g, 16.8 mmol in an 86% yield with respect to (PPN)Cl. Elem. anal. calcd. for $C_{36}H_{30}N_2O_3P_2$, 600.57 g mol^{-1}, C, 72.00; H, 5.04; N, 4.66%, found C, 71.92; H, 4.87; N, 4.51%). Melting point 222-224°C. IR (Nujol, cm^{-1}) ν = 3052w, 2955s, 2919vs, 2854.89s, 1588vw, 1463m,

1439m, 1345s, 1297s, 1266s, 1185w, 1155vw, 1115s,1028w, 996w, 801w, 743m, 723s, 691s).

9.2.2 I*n situ* generation of $Si(NO_3)_4$ (1). Modified from ref [128]. A Schlenk tube containing a mixture of $SiCl_4$ (0.250 g, 1.47 mmol) in diethyl ether (5 mL) was immersed in a cold bath at −40°C. After the ethereal solution had attained the bath temperature, a cold solution (−40°C) of silver nitrate (1.03 g, 6.06 mmol) in acetonitrile was added rapidly, upon which AgCl is produced as a white, suspended solid. Immediately after the addition was completed, the Schlenk tube was immersed in liquid nitrogen and then allowed to warm again up to −40°C. The resultant suspension was then rapidly filtered and the filtrate collected into a second Schlenk tube containing diethyl ether (5 mL) precooled to −40°C which resulted in further precipitation of white solid. This step was repeated until no further precipitation occurred. The final resulting colourless solution was cooled further down to −60°C and the diethyl ether removed at this temperature under a dynamic vacuum which affords an acetonitrile solution of $Si(NO_3)_4$ (**1**). Solutions of **1** were used immediately for the synthesis of **2**. (IR (MeCN, Et_2O (1 : 1), cm^{-1}) ν= 1667sh (HNO_3), 1662m, 1617m, 1493w, 1353s, 1297s, 1153s, 1133s, 1115s).

9.2.3 Preparation of $(PPN)_2[Si(NO_3)_6]$ (2). The solution of **1** (approximately 1.5 mmol) was warmed to −40°C and treated with an acetonitrile solution of $(PPN)NO_3$ (1.651 g, 2.75 mmol) also cooled to −40°C resulting in a clear pale green solution. This solution was placed under a dynamic vacuum until all acetonitrile had been evaporated leaving an off-white solid. The solid was washed with cold acetonitrile at −40°C and then dissolved by adding approximately 15 ml acetonitrile and raising the temperature of the resultant suspension to ambient temperature. After concentrating the solution to 5 mL colourless, block-shaped crystals of **2** were obtained upon storage at −28°C within 24 h. The crystals were isolated by filtration, washing (cold acetonitrile) and dried under high vacuum. (Mass: 0.568 g, 0.384 mmol, 24% with respect to $SiCl_4$. Solid **2** is moderately air sensitive and decomposes in air at r.t. within *ca*. 0.5 h. Elem. anal. calcd. for $C_{72}H_{60}N_8O_{18}P_4Si$ (1477.29 g mol^{-1}): C, 58.54; H, 4.09; N, 7.59%; found: C, 58.37; H, 3.84; N, 7.70%. DSC, T_{on}^{ex1} = 146°C, T_p^{ex1} = 154°C, ΔH^1= −93 J g^{-1}, T_{on}^{ex2} = 276°C, T_p^{ex2} = 301°C, ΔH^2= −791 J g^{-1}. IR (Nujol cm^{-1}) ν = 3164w, 1623m, 1589vs, 1569vs, 1563vs, 1557vs, 1548vs 1484s, 1344s, 1322vs, 1293vs, 1287vs, 1274vs, 1267vs 1185w,

1154w, 1117vs, 1072w, 1036w, 998m, 977vs, 950s, 930vs, 824m, 798w, 752s, 724vs, 695vs, 547vs. ^{1}H-NMR (CD_2Cl_2, 250 MHz) δ [ppm] = 7.65 (m), 7.45 (m, 4H, 26H). ^{14}N-NMR (CD_2Cl_2, 29 MHz) δ [ppm] = −5.2 (rel. int. 1.5), −36.7 (rel. int. 0.9), −43.8 (rel. int. 1.0)).

9.2.4 Attempted synthesis of (PPN)As(NO$_3$)$_4$. A Schlenk tube charged with $AsCl_3$ (0.1 mL, 0.210 g, 1.16 mmol) dissolved in dichloromethane (5 mL) cooled to −40°C was added to a suspension of silver nitrate (0.673 g, 3.96 mmol) in dichloromethane (20 mL) also cooled to −40°C *via* a volumetric glass pipette. On addition, no reaction was observed so the solution was allowed to warm up to −20°C over a period of 3 hours. Still no reaction was observed so the solution was then allowed to stir for 1 minute at room temperature before being immersed in a cold bath at −70°C which resulted in the formation of a white precipitate, AgCl. The reaction solution was then filtered into a solution of (PPN)NO_3 (0.688 g, 1.15 mmol) in dichloromethane cooled to −20°C and allowed to stir for 1 hour. The solution was warmed to 0°C and the solvent removed *in vacuo* to a saturated solution which on reducing the temperature to −28°C over a period of 24 hours resulted in the formation of colourless block crystals. The crystals were isolated by filtration, washed with dichloromethane cooled to −50°C and dried under high vacuum. Single crystal X-ray diffraction studies gave the structure (PPN)$AsCl_2(NO_3)_2$ (**5**). (Mass: 173 mg, 0.22 mmol, 19% yield with respect to (PPN)NO_3. Solid **5** is thermally sensitive and over a period of two hours at room temperature the crystals began to turn yellow. IR (CH_2Cl_2 cm^{-1}) ν = 1510m, 1484m, 1439s, 1302s, 1186w, 1116s).

9.2.5 Attempted preparation of (PPN)As(NO$_3$)$_4$ via (PPN)AsCl$_4$. (PPN)Cl (688 mg, 1.20 mmol) was dissolved in dichloromethane in a Schlenk tube and treated with $AsCl_3$ (0.1 mL, 215 mg, 1.19 mmol) *via* a volumetric pipette giving a pale yellow reaction solution. This solution was stirred overnight after which the solvent was removed *in vacuo* producing a viscous oil which on cooling at −18°C crystallised. The remaining supernatant solution was filtered off at −18°C and the crystals were dried, also at −18°C, under dynamic vacuum. These crystals were dissolved in acetonitrile at −40°C and treated with an acetonitrile solution of silver nitrate (816 mg, 4.8 mmol) at the same temperature via a stainless steel cannula, resulting in an immediate white precipitate of AgCl. The resulting suspension was stirred for a further two hours at −40°C after which

the colourless solution was filtered off giving a solution containing $As(NO_3)_3$ and $(PPN)NO_3$. (IR (MeCN cm^{-1}) ν = 1670m, 1603m, 1590m, 1485m, 1304s, 1274vs).

9.2.6 Preparation of $(PPN)PCl_6$. PCl_5 (230 mg, 1.1 mmol) and (PPN)Cl (634 mg, 1.11 mmol) were combined in a Schlenk tube and dissolved in acetonitrile (20 mL). The turbid pale green reaction solution was warmed to 60°C after which became clear. After stirring for 1 hour the solution was allowed to cool to 30°C at which crystallisation started to occur. The solution was reduced in volume by half at 30°C and then cooled to −18°C over a period of 24 hours. After which colourless block crystals had formed and were isolated by filtration. (Mass: 564mg, 0.74 mmol, 67% yield with respect to PCl_5. ^{31}P NMR (CD_2Cl_2, 500 MHz) δ [ppm] = 21.4, –296.8).

9.2.7 Attempted synthesis of $(PPN)P(NO_3)_6$. ($(PPN)PCl_6$ (578 mg, 0.73 mmol) was suspended in acetonitrile (30 mL) at −40°C and treated with an acetonitrile solution of silver nitrate (761 mg, 4.50 mmol) also cooled to −40°C resulting in an immediate white precipitate and black solution. The solution was filtered off and removed under dynamic vacuum to produce a brown oil. No other product was obtained.

9.2.8 Preparation of bis(3-fluoropyridine)tetraazidosilicon (6). $Si(N_3)_4$ (0.1 mmol, 0.5 mL, 0.2 mmol mL^{-1}) in benzene was added to a sample vial in a glovebox and treated with 3-fluoropyridine (25 mg, 0.26 mmol), to give a colourless solution, and stirred for 1 hr. The solvent was allowed to slowly evaporate to afford colourless, block crystals of bis(3-fluoropyridine)tetraazidosilicon. (Mass: 35 mg, 0.089 mmol, 89 % yield with respect to $Si(N_3)_4$. IR (nujol) cm^{-1} = 3431w, 3420w, 3135w, 3132w, 3096w, 3071m, 2169s, 2118vs, 1990vw, 1939vw, 1888vw, 1804vw, 1761vw, 1622m, 1583m, 1538w, 1533w, 1482m, 1442s, 1428s, 1316s, 1263s, 1253m, 1244s, 1190m, 1137w, 1102m, 1070w, 1056m, 1036w, 1018vw, 996m, 946w, 905m, 884w, 854s, 822s, 804w, 770vw, 704m, 695m, 652s, 593s, 576s, 560vs, 545s, 541s, 530s, 516s, 512m).

9.2.9 Preparation of bis(3-chloropyridine)tetraazidosilicon (7). $Si(N_3)_4$ (0.1 mmol, 0.5 mL, 0.2 mmol mL^{-1}) in benzene was added to a sample vial in a glovebox and treated with 3-chloropyridine (24 mg, 0.21 mmol), to give a colourless solution, and stirred for 1 hr. The solvent was allowed to slowly evaporate to afford colourless, block crystals of bis(3-chloropyridine)tetraazidosilicon. (Mass: 41 mg, 0.94 mmol, 94 % yield

with respect to $Si(N_3)_4$. IR (nujol) cm^{-1} = 3436m, 3117m, 3106m, 3064m, 3051m, 2168s, 2135s, 2120vs, 1990vw, 1946vw, 1829vw, 1769vw, 1761vw, 1604m, 1563m, 1425m, 1414m, 1330s, 1320vs, 1263m, 1243w, 1203w, 1189m, 1132w, 1126w, 1104m, 1063m, 1039w 995vw, 954w, 928vw, 915m, 816s, 808s, 792vw, 758m, 718m, 700s, 655s, 594s, 570s, 555s, 528w, 504m).

9.2.10 Preparation of bis(3-bromopyridine)tetraazidosilicon (8). $Si(N_3)_4$ (0.1 mmol, 0.5 mL, 0.2 mmol mL^{-1}) in benzene was added to a sample vial in a glovebox and treated with 3-bromopyridine (42 mg, 0.27 mmol), to give a colourless solution, and stirred for 1 hr. The solvent was allowed to slowly evaporate to afford colourless, block crystals of bis(3-bromopyridine)tetraazidosilicon. (Mass: 48.1 mg, 0.94 mmol, 94 % yield with respect to $Si(N_3)_4$. IR (nujol) cm^{-1} = 3434s, 3116s, 3103m, 3095m, 3060m, 3052m, 2166w, 2134w, 2119vs, 1987vw, 1946vw, 1912vw, 1906vw, 1830vw, 1819vw, 1797vw, 1765vw, 1759vw, 1727vw, 1689vw, 1614vw, 1602s, 1559s, 1421s, 1408m, 1330s, 1322s, 1263w, 1241m, 1200m, 1186m, 1153vw, 1127m, 1112m, 1100s, 1060s, 1036m, 995w, 956w, 918m, 912w, 812m, 805m, 728m, 699s, 692s, 656s, 593m, 569m, 554s, 526s).

9.2.11 Preparation of bis(3-iodopyridine)tetraazidosilicon (9). 3-iodopyridine (41 mg, 0.2 mmol) was dissolved in a sample vial in a glovebox in benzene (1 mL). $Si(N_3)_4$ (0.1 mmol, 0.5 mL, 0.2 mmol mL^{-1}) in benzene was added giving an immediate white precipitate. The suspension was stirred for 1 hr and the solvent decanted off into a second sample vial. Slow evaporation of this solvent affords small, colourless, plate crystals of bis(3-iodopyridine)tetraazidosilicon. The initial precipitate was identified as bis(3-iodopyridine)tetraazidosilicon. (Mass: 51 mg, 0.84 mmol, 84 % yield with respect to $Si(N_3)_4$. IR (nujol) cm^{-1} = 3431w, 3112w, 3099vw, 3089vw, 3065vw, 3052w, 3045w, 2118vs, 1611vw, 1597s, 1562m, 1551s, 1521w, 1481w, 1466s, 1459m, 1413m, 1402s, 1333s, 1322vs, 1259m, 1236m, 1218vw, 1198m, 1186w, 1180vw, 1124m, 1118vw, 1104m, 1095w, 1078w, 1052s, 1032s, 1010m, 979vw, 956w, 946w, 921m, 892w, 809s, 801s, 787s, 710m, 693vs, 675vw, 656s, 618m, 595m, 591m, 556vs, 529s.

9.2.12 Preparation of 3-iodo-methylpyridinium nitrate (10). 3-iodopyridine (4.012 g, 19.5 mmol) was dissolved in ethanol and treated with methyliodide (6 mL, 96.3 mmol). The mixture was heated to reflux and stirred for 16 hrs. After which, a precipitate had

formed and the mixture was cooled to room temperature. The solid was filtered off and washed with ethyl acetate (2 x 50 mL). The 3-iodo-methylpyridinium iodide obtained (2.024 g, 5.83 mmol) was then suspended in acetonitrile and treated with the dropwise addition of silver nitrate (1.032 g, 6.07 mmol) dissolved in acetonitrile giving an immediate white precipitate. After addition, the suspension was stirred for 2 hrs and then filtered off. The solvent was evaporated *in vacuo* resulting in an off-white crystalline solid which was dried under vacuum at 110°C. (Mass: 1.218 g, 4 mmol, 69 % with respect to 3-iodo-methylpyridinium iodide. IR (nujol) cm^{-1} = 3181w, 3120m, 3045m, 3026m, 3014, 2029vw, 1997vw, 1962vw, 1858vw, 1809vw, 1759w, 1744w, 1620m, 1562w, 1492m, 1419m, 1349s, 1325vs, 1274m, 1219vw, 1205w, 1181m, 1167vw, 1145vw, 1111w, 1091w, 1045w, 1026w, 984vw, 932vw, 829m, 722vw, 712vw, 702vw, 679m, 533w).

9.2.13 Preparation of 3-bromo-methylpyridinium nitrate (11). 3-bromo-methylpyridinium iodide (5.673 g, 18.9 mmol) was suspended in acetonitrile and treated with the dropwise addition of silver nitrate (3.219 g, 18.9 mmol) dissolved in acetonitrile giving an immediate white precipitate. After addition, the suspension was stirred for 2 hrs and then filtered off. The solvent was evaporated *in vacuo* resulting in an off-white crystalline solid which was dried under vacuum at 110°C. (Mass: 3.042 g, 12.9 mmol, 68 % yield with respect to 3-bromo-methylpyridinium iodide. IR (nujol) cm^{-1} = 3193w, 3128m, 3092m, 3059w, 3034m, 3018m, 2029vw, 1979vw, 1964vw, 1911vw, 1891vw, 1790vw, 1755w, 1748w, 1626s, 1567m, 1498s, 1462s, 1439w, 1418w, 1411vw, 1347s, 1322s, 1281s, 1181s, 1168s, 1142m, 1112m, 1097m, 1044w, 1029m, 1017w, 967w, 949w, 848m, 827s, 723w, 713w, 693m, 675s, 533w).

9.2.14 Preparation of bis(3-bromo-methylpyridinium)hexanitratostannate (13). A Schlenk tube was charged with silver nitrate (0.678 g, 3.99 mmol) and dissolved in acetonitrile and treated with the dropwise addition of $SnCl_4$ (0.11 mL, 0.94 mmol). An immediate precipitation of a white solid was accompanied with the addition of the $SnCl_4$ and the suspension was stirred for 4 hrs. The suspension was filtered into a second Schlenk tube containing 3-bromo-methylpyridinium nitrate (0.468 mg, 1.99 mmol) suspended in acetonitrile and the new suspension was stirred for 2 hrs. After which, the solid material had dissolved and the solution was clear and pale green. Concentration of the solution to approximately 5 mL and storage at −28°C for 24 hrs

results in large, colourless, needle crystals. (Mass: 0.317 g, 0.3 mmol, 32 % yield with respect to $SnCl_4$. IR (nujol) cm^{-1} = 3203vw, 3137w, 3112w, 3104w, 3080m, 1950vw, 1902vw, 1810vw, 1761vw, 1632m, 1569s, 1549s, 1417m, 1360s, 1328m, 1277s, 1211m, 1188m, 1141w, 1113m, 1095w, 1034vw, 1001vw, 941vs, 906s, 856s, 838vw, 811s, 790s, 778m, 772m, 760m, 706w, 688m, 670m, 633w, 536w)

9.2.15 Preparation of bis(3-bromo-methylpyridinium)hexanitratogermanate (12). The same procedure for bis(3-bromo-methylpyridinium)hexanitratostannate was applied to $GeCl_4$ to prepare bis(3-bromo-methylpyridinium)hexanitratogermanate. (Mass = 0.277 g, 0.34 mmol, 40 % yield with respect to $GeCl_4$. IR (nujol) cm^{-1} = 3203vw, 3137m, 3112m, 3104m, 3081s, 2000vw, 1951vw, 1900vw, 1881vw, 1809vw, 1760vw, 1630m, 1572s, 1548vs, 1495vs, 1462s, 1417m, 1359vs, 1328m, 1276vs, 1236m, 1208s, 1187s, 1141m, 1112s, 1095w, 941vs, 905vs, 855m, 811m, 790m, 778w, 772m, 758m, 706w, 688s, 670s, 537w).

9.2.16 Preparation of $GeCl_2$(dioxane). Modified from ref [243]. $LiAlH_4$ (2.5 mg) was suspended in toluene (100 mL) and treated with 1,4-dioxane (3.0 mL, 35 mmol), $GeCl_4$ (4.0 mL, 35 mmol) and triethylsilane (11.2 mL, 70 mmol) in a Schlenk tube attached to a condenser equipped with a mercury bubbler. The colourless solution was heated to reflux resulting in the production of gas indicated by the bubbler. The reaction time varies and the reaction can take between 2 and 4 hrs. As soon as the solution began to turn yellow the Schlenk tube was immediately cooled in ice resulting in immediate crystallisation of yellow, needle crystals. The Schlenk tube was cooled to −18°C overnight resulting in further crystallisation of $GeCl_2$(dioxane). The crystals were isolated by filtration and dried under high vacuum. (Mass: 0.810 g, 3.5 mmol, 10% yield with respect to $GeCl_4$. ^{1}H-NMR (CD_2Cl_2, 400 MHz) δ [ppm] = 4.09(s)). Note: The filtrate after crystallisation can be heated again to reflux to give a yellow solution which produces further product. If the solution turns orange during the reflux an orange decomposition product forms, which then requires extraction using dichloromethane to give $GeCl_2$(dioxane).

9.2.17 Preparation of (PPN)Ge(NO_3)Cl_2. $GeCl_2$(dioxane) (218 mg, 0.94 mmol) and (PPN)NO_3 (551 mg, 0.92 mmol) were combined in a Schlenk tube and cooled to –90°C. Dichloromethane (20 mL) at room temperature was added via a cannula. The solution

was allowed to warm to room temperature and stirred for one hour resulting in a clear, colourless stock solution of (PPN)Ge(NO_3)Cl_2. The solvent was removed *in vacuo* to produce a colourless oil. (IR (CH_2Cl_2, cm^{-1}) ν = 1589m, 1518s, 1484w, 1439w, 1354m, 1318m, 1284vs).

9.2.18 Attempted preparation of (PPN)Ge(NO_3)$_3$. The oil obtained from **9.2.9** was combined with $NaNO_3$ (0.921 g, 10.8 mmol) in a Schlenk tube and suspended in THF (25 mL). The white suspension was left to stir for 16 hours before being filtered onto a second batch of $NaNO_3$ (0.861 g, 10.1 mmol) and stirred for a further 24 hours. The suspension was filtered resulting in a clear, colourless filtrate. Diethyl ether (15 mL) was added to the filtrate producing an immediate white precipitate. This precipitate was filtered off and discarded, while the new filtrate was cooled to −18°C for 60 hours. Colourless, block crystals were found with the composition (PPN)$GeCl_3$ / (PPN)Ge(NO_3)Cl_2 as a solid solution as determined by single crystal X-ray crystallography. (IR (Nujol, cm^{-1}) ν = 3057w, 1589w, 1576w, 1496m, 1438s, 1298s, 1284s, 1263s, 1184m, 1160m, 1112s, 1072w, 1025w, 998m, 800m, 762w, 744s, 723, 691s, 550m, 529m.)

9.2.19 Preparation of (PPN)$GeCl_3$. $GeCl_2$(dioxane) (0.351 g, 1.51 mmol) and (PPN)Cl (0.851 g, 1.57 mmol) were combined in a Schlenk tube and cooled to −30°C. The solids were dissolved in acetonitrile (20 mL) and left to stir at room temperature for half an hour. The acetonitrile was removed under high vacuum resulting in an off-white precipitate which was dissolved in THF (20 mL). Upon addition of diethyl ether (5 mL) to the THF solution resulted in an immediate white precipitate which was filtered off and discarded. The filtrate solvent was reduced in volume to approximately 2 mL under high vacuum resulting in a cloudy oil. Diethyl ether (30 mL) was added resulting in immediate precipitation of a white solid. The material was isolated by filtration and dried under high vacuum. (Mass: 0.953 g, 1.33 mmol, 88 % yield with respect to $GeCl_2$(dioxane). (Melting point: 170-172°C).

9.2.20 Preparation of ($AsPh_4$)$GeCl_3$. The same procedure for (PPN)$GeCl_3$ was applied to ($AsPh_4$)Cl to prepare ($AsPh)_4GeCl_3$ in a 85 % yield with respect to $GeCl_2$(dioxane).

9.2.21 Preparation of (PPN)Ge(N_3)$_3$ (14b). (PPN)$GeCl_3$ (0.752 g, 1.05 mmol) and sodium azide (1.660 g, 25.5 mmol) were combined in a Schlenk tube and suspended in THF (20 mL). The suspension was stirred for 16 hours at room temperature after which it was filtered into a Schlenk tube containing more sodium azide (1.440 g, 22.2 mmol) and stirred for a further 16 hours. The suspension was filtered giving a colourless solution and treated with diethyl ether (10 mL) giving an immediate white precipitate and turbid solution. On filtering the turbidity of the solution remained while the white precipitate was discarded. The filter solution was reduced in volume to approximately 2 mL and treated with diethyl ether (20 mL) resulting in an immediate white precipitate which was filtered and dried under dynamic vacuum. The solid was dissolved in THF (5 mL) resulting in a solution with slight turbidity which on filtering became colourless. This solution was allowed to evaporate slowly inside a glove box giving colourless, block crystals. (Mass: 0.456 g, 0.62 mmol, 59 % yield with respect to (PPN)$GeCl_3$. (IR (THF cm^{-1}) ν = 2092vs, 2058s).

9.2.22 Preparation of (AsPh_4)Ge(N_3)$_3$ (14c). The same procedure for **14b** can be applied to (AsPh_4)$GeCl_3$ to prepare (AsPh_4)Ge(N_3)$_3$. However, no crystals are formed on solvent evaporation only an off-white powder. (IR (THF cm^{-1}) ν = 2092vs, 2058s).

9.2.23 Preparation of (PPh_4)N_3. PPh_4Cl (4.954 g, 13.2 mmol) was dissolved in H_2O (20 mL) heated to 40°C and added slowly to sodium azide (8.873 g, 136 mmol) also dissolved in H_2O (20 mL) heated to 40°C resulting in an immediate white precipitate. The mixture was stirred for half an hour after which the precipitate was filtered off and washed with diethyl ether (2 x 20mL). Acetonitrile (30 mL) was added to dissolve the crude material and any remaining undissolved material was filtered off and discarded. The acetonitrile solvent was boiled off to approximately 10 mL and cooled back to room temperature. Diethyl ether (100 mL) was added resulting in immediate crystallisation. The solution was cooled to −18°C for 2 hours and the colourless crystals were isolated by filtration. (Mass: 2.869 g, 7.52 mmol, 57 % yield with respect to (PPh_4)Cl. (IR (Nujol, cm^{-1}) ν = 3281w, 3206w, 3079w, 1997vs, 1584m, 1463s, 1341w, 1312w, 1185w, 1158w, 1106s, 996m, 763s, 749m, 722s, 689s, 527vs).

9.2.24 Preparation of $(PPh_4)GeCl_2N_3$. $GeCl_2$(diox) (0.349 g, 1.50 mmol) and $(PPh_4)N_3$ (0.577 g 1.51 mmol) were combined in a Schlenk tube, cooled to −40°C and dissolved in acetonitrile (20 mL). This colourless solution was allowed to warm up to room temperature with stirring and then stirred for a further 0.5 hrs, after which the solvent was removed under a dynamic vacuum precipitating a colourless solid. The solid was dissolved in THF (10 mL) followed with the addition of diethyl ether (1 mL) resulting in a white suspension which was filtered and the residue discarded. The filtrate was concentrated to approximately 2 mL and diethyl ether (20 mL) was added resulting in an immediate white powder which was filtered and washed (cold diethyl ether). (Mass: 0.645 g, 1.23 mmol, 82 % yield with respect to $GeCl_2$(1,4-dioxane). (IR (MeCN) ν = 2075vs, 2062s).

9.2.25 Preparation of $(PPh_4)Ge(N_3)_3$ (14a). Sodium azide (1.840 g, 28.3 mmol) and $(PPh_4)GeCl_2N_3$ (0.643 g, 1.05 mmol) were combined in a Schlenk tube and suspended in THF (20 mL). The suspension was stirred for 16 hours after which the suspension was filtered onto a further 20 equivalents of sodium azide (1.945 g, 29.9 mmol) and stirred for a further 24 hours. The second suspension was filtered giving a clear, colourless supernatant solution and the filter residue was discarded. Diethyl ether (5 mL) was added to the supernatant solution resulting in a white precipitate which was filtered and discarded. The supernatant solution was concentrated to approximately 2 mL and diethyl ether (30 mL) was added resulting in a milky solution. On cooling at −18°C for 48 hours colourless, needle crystals of **14a** were obtained. The crystals were isolated by filtration, washed with diethyl ether and dried under vacuum. (Mass: 0.401 g, 0.75 mmol, 71 % yield with respect to $(PPh_4)GeCl_2N_3$ (Elem. anal. calcd. for $C_{24}H_{20}N_9PGe$ (538.06 g mol^{-1}): C, 53.55; H, 3.75; N, 23.43%; found: C, 53.66; H, 3.83; N, 22.68%. DSC, T_{on}^{endo1} = 60°C, T_p^{endo1} = 63°C, ΔH^1= 94 J g^{-1}, T_{on}^{ex1} = 99°C, T_p^{ex1} = 109°C, ΔH^2= −270 J g^{-1}, T_{on}^{endo2} = 196°C, T_p^{endo2} = 199°C, ΔH^3= 4 J g^{-1} T_{on}^{endo3} = 248°C, T_p^{endo3} = 250°C, ΔH^4= 8 J g^{-1}, T_{on}^{ex2} = 310°C T_p^{ex2} = 317°C, ΔH^5= −467 J g^{-1}. IR (THF cm^{-1}) ν = 2092vs, 2058s. ^{14}N-NMR (CD_2Cl_2, 29 MHz) δ [ppm] = −136 (N_β) (FWHM: 24 Hz), −207 (N_γ), −263 (N_α) (FWHM: 552 Hz).

9.2.26 Preparation of $(PPh_4)Sn(N_3)_3$ (15). $SnCl_2$ (0.345 g, 1.82 mmol) and PPh_4Cl (0.682 g, 1.82 mmol) were combined in a Schlenk tube and dissolved in THF (20 mL)

and stirred for 1 hr. This solution was transferred *via* a cannula to a new Schlenk tube containing sodium azide (2.180 g, 14.2 mmol) and stirred for 16 hrs before being filtered onto a second batch of sodium azide (2.176 g, 14.1 mmol) and stirred for a further 16 hrs. The white suspension was filtered giving a clear, colourless solution that was concentrated to approximately 2 mL before being treated with diethyl ether (20 mL) giving a turbid solution that was cooled at −28°C for 24 hrs. Colourless needle crystals of **15** were obtained and isolated by filtration and dried under vacuum. (Mass: 0.638 g, 1.10 mmol, 60 % yield with respect to $SnCl_2$. IR (THF cm^{-1}) ν = 2081vs, 2051s. ^{14}N-NMR (CD_3CN, 29 MHz) δ [ppm] = −136 (N_β), −218 (FWHM: 32 Hz) (N_γ), −263 (FWHM: 166 Hz) (N_α). ^{119}Sn-NMR (CD_3CN, 186 MHz) δ [ppm] = −221.

9.2.27 Preparation of bis(2,6-diisopropylphenyl))butaza-1,4-diene. Modified from reference [244]. 2,6-diisopropylphenylamine (49.925 g, 0.27 mol) was dissolved in methanol (50 mL) and acetic acid (0.25 mL) and warmed to 50°C in a 500 mL round bottom flask. Glyoxal (40 % w/w in H_2O, 18.573 g, 0.12 mol) was dissolved in methanol (50 mL) and added to the warm amine solution and stirred for 15 mins giving a clear red solution. The solution was cooled to room temperature and left to stir for 10 hrs and after the first 15 mins a bright yellow precipitate formed. The yellow solid was filtered off and washed with methanol (2 x 100 mL) and dried under high vacuum at 100°C for 16 hrs (Mass: 35.35 g, 0.09 mmol, 67 % yield with respect to glyoxal. ^{1}H NMR ($CDCl_3$, 400 MHz) δ [ppm] = 1.21 (d, 24 H, CH(C*H*$_3$), $^3J_{HH}$ = 6.9 Hz), 2.94 (sept, 4 H, C*H*(CH_3), $^3J_{HH}$ = 6.9 Hz), 7.1 - 7.25 (m, 12 H, aryl-CH), 8.11 (s, 2 H, C*H*).

9.2.28 Preparation of 1,3-bis(2,6-diisopropylphenyl))imidazolium chloride. Modified from ref [244]. Paraformaldehyde (0.807 g, 26.9 mmol) and bis(2,6-diisopropylphenyl))butaza-1,4-diene (9.988 g, 26 mmol) were combined in a 1 L round bottom flask and dissolved in ethyl acetate (250 mL) giving a red solution. This solution was heated in an oil bath at 70°C and treated dropwise with a solution of trimethylsilyl chloride (3.4 mL, 26.7 mmol) in ethyl acetate (5 mL). After 10 mins, a yellow suspension was observed and it was stirred for a further 2 hrs at an oil bath temperature of 70°C. The flask was immersed in an ice bath for 15 mins and the suspension filtered giving a slightly pink solid and a brown solution. The pale pink solid was washed with ethyl acetate (3 x 100 mL) before being dried under high vacuum at

120°C for 48 hrs (Mass: 8.121 g, 19.1 mmol, 73 % yield with respect to bis(2,6-diisopropylphenyl))butaza-1,4-diene. ^{1}H NMR (dmso-d_6, 400 MHz) δ [ppm]: 1.25 (d, 12 H, CH(CH_3), $^{3}J_{HH}$ = 6.9 Hz), 1.36 (d, 12 H, CH(CH_3), $^{3}J_{HH}$ = 6.9 Hz), 3.09 (sept, 4 H, CH(CH$_3$), $^{3}J_{HH}$ = 6.9 Hz), 4.41 (s, 2 H, im- H^{4,5}), 7.3 - 7.6 (m, 6 H, aryl-CH), 9.63 (s, 1 H, im-H^{2}).

9.2.29 Preparation of 1,3-Bis(2,6-diisopropylphenyl)-4,5-dihydro-2H-imidazol-2-ylidene (IPr). Modified from ref [245]. 1,3-bis(2,6-diisopropylphenyl)imidazolium chloride (2.102 g, 4.95 mmol) and lithium bis(trimethylsilyl)amide (0.930 g, 5.56 mmol) were combined in a Schlenk tube and dissolved in THF (30 mL) giving an orange solution and left to stir for 1 hr. The solvent was removed *in vacuo* and the residue was extracted with toluene (2 x 30 mL) and filtered into a new Schlenk tube. The toluene solvent was removed *in vacuo* giving an off-white solid. (Mass: 1.540 g, 3.96 mmol, 80 % yield with respect to 1,3-bis(2,6-diisopropylphenyl)imidazolium chloride. ^{1}H NMR (C_6D_6, 400 MHz) δ [ppm]: 1.19 (d, 12 H, CH(CH_3), $^{3}J_{HH}$ = 6.9 Hz), 1.29 (d, 12 H, CH(CH_3), $^{3}J_{HH}$ = 6.9 Hz), 2.97 (sept, 4 H, CH(CH$_3$), $^{3}J_{HH}$ = 6.9 Hz), 6.62 (s, 2 H, im- H^{4,5}), 7.1 - 7.3 (m, 6 H, aryl-CH).

9.2.30 Preparation of 1,3-Bis(tert-butyl)imidazolium tetrafluoroborate. Modified from ref [246]. Paraformaldehyde (2.161 g, 0.072 mol) was suspended in toluene (20 mL) and cooled to −10°C. ^{t}Butylamine (13.920 g, 0.190 mol) was syringed into the toluene suspension to give an orange suspension. Glyoxal (40 % w/w in H_2O, 13.178 g, 0.091 mol) was added dropwise giving an immediate white precipitate. Still at −10°C, aqueous HCl (35 %, 4.8 mL) was added dropwise with stirring. After addition was complete the suspension was warmed to 40°C and stirred for 16 hrs. The resulting two turbid layers, one orange and one white, were evaporated *in vacuo* on a rotary evaporator to give a thick oily orange residue. Water (50 mL) was added to the residue and any undissolved material was filtered off. HBF_4 (50 % w/w in H_2O, 12.644 g, 0.072 mol) was added to the water solution giving an immediate white precipitate. The suspension was left to stand at ambient temperature for 2 hrs to ensure complete precipitation. The white fluffy solid was filtered, washed with cold water (2 x 10 mL) and dried. (Mass: 5.885 g, 0.023 mol, 32 % yield with respect to paraformaldehyde. ^{1}H

NMR ($CDCl_3$, 400 MHz) δ [ppm]: 1.74 (s, 18 H, (C(CH_3)$_3$), 7.42 (s, 2 H, im- $H^{4,5}$), 8.93 (s, 1 H, im- H^2).

9.2.31 Preparation of 1,3-Bis(tert-butyl)-4,5-dihydro-2H-imidazol-2-ylidene (I^{t}Bu). Modified from ref [245]. 1,3-bis(tert-butyl)imidazolium tetrafluoroborate (1.805 g, 7 mmol) and NaH (0.212 g, 8.8 mmol) were combined in a Schlenk tube and suspended in THF (20 mL). Effervescence was observed immediately and the resulting white suspension was stirred for 24 hrs. The THF solvent was removed *in vacuo* and the residue extracted with toluene (30 mL). The solvent was removed *in vacuo* giving a white, microcrystalline solid. (Mass: 0.748 g, 4.4 mmol, 63 % yield with respect to 1,3-bis(tert-butyl)imidazolium tetrafluroborate. ^{1}H NMR (C_6D_6, 400 MHz) δ [ppm]: 1.50 (s, 18 H, (C(CH_3)$_3$), 6.72 (s, 2 H, im- $H^{4,5}$).

9.2.32 Preparation of IPrSiCl$_2$. Modified from reference 74. A Schlenk tube was charged with IPr (1.768 g, 4.54 mmol) and dissolved in toluene (30 mL). $HSiCl_3$ (0.308 g, 0.23 mL, 2.27 mmol) was added *via* a volumetric pipette giving an immediate white precipitate and yellow solution. The yellow suspension was stirred for 16 hrs, filtered off and evaporated to dryness to give a yellow solid. (Mass: 0.652 g, 1.33 mmol, 59 % yield with respect to $HSiCl_3$. ^{1}H NMR (C_6D_6, 400 MHz) δ [ppm]: 1.01 (d, 12 H, CH(CH_3), $^3J_{HH}$ = 6.9 Hz), 1.43 (d, 12 H, CH(CH_3), $^3J_{HH}$ = 6.9 Hz), 2.79 (sept, 4 H, CH(CH_3), $^3J_{HH}$ = 6.9 Hz), 6.36 (s, 2 H, im- $H^{4,5}$), 7.05 - 7.22 (m, 6 H, aryl-CH).

9.2.33 Addition of sodium azide to IPrSiCl$_2$. $IPrSiCl_2$ (0.652 g, 1.33 mmol) and sodium azide (0.805 g, 12.4 mmol) were combined in a Schlenk tube and suspended in benzene (30 mL). The yellow suspension that formed was heated to reflux, 85°C oil bath temperature, for 5 days. The solution was filtered off to give a yellow solution and colourless filter residue. Concentration of the yellow solution affords a thick yellow oil. (IR (C_6H_6 cm^{-1}) ν = 2154m, 2102w, 2086w, 2014w).

9.2.34 Addition of sodium azide to IPrSiI$_2$. $IPrSiI_2$ (0.117 g, 0.17 mmol) and sodium azide (0.220 g, 3.38 mmol) were combined in a Schlenk tube and suspended in THF (10 mL). The resulting orange suspension was stirred for 16 hrs and filtered off to give a

clear orange solution. Concentration of this solution resulted in an orange oil. (IR (THF cm^{-1}) ν = 2152s).

9.2.35 Preparation of $Si(N_3)_4$. Modified from ref 54. A Schlenk tube was charged with sodium azide (4.002 g, 61.6 mmol) suspended in benzene (30 mL). The suspension was treated with $SiCl_4$ (0.7 mL, 1.036 g, 6.1 mmol) and the Schlenk tube fitted with a condenser and a mercury bubbler before being heated to 80°C and stirred for 5 days. The suspension was filtered onto a further batch of sodium azide (4.012 g, 61.7 mmol) and heated for a further 5 days. The suspension was filtered giving a clear, colourless solution of ca. 0.2 mmol mL^{-1} of $Si(N_3)_4$ in benzene. (IR (C_6H_6) cm^{-1} = 2170vs, 1328m).

9.2.36 Preparation of $Ge(N_3)_4$. The same procedure for $Si(N_3)_4$ was applied using $GeCl_4$. (IR (C_6H_6) cm^{-1} = 2151w, 2133s).

9.2.37 Attempted preparation of $HSi(N_3)_3$. The same procedure for $Si(N_3)_4$ was attempted using $HSiCl_3$ instead of $SiCl_4$. However, $Si(N_3)_4$ was obtained. (IR (C_6H_6) cm^{-1} = 2170vs, 1328m).

9.2.38 Preparation of $IPrSi(N_3)_4$ (16). A Schlenk tube was charged with IPr (116 mg, 0.3 mmol) in a glovebox and treated with $Si(N_3)_4$ in benzene solution (0.3 mmol, 3 mL at 0.1 mmol mL^{-1}) giving a yellow suspension, which on stirring starts to dissolve before precipitating a new white solid. After 1 hr stirring the solvent was evaporated *in vacuo* to give an off-white solid. Crystals of the material can be obtained by storing a concentrated THF solution overnight at −28°C. (Mass: 170 mg, 0.29 mmol, 97 % yield with respect to $Si(N_3)_4$. IR (nujol) cm^{-1} = 3419w, 3390w, 3155m, 3129m, 3084w, 3071w, 3036w, 2150vs, 2137vs, 2121vs, 2101vs, 1596w, 1557w, 1531w, 1476m, 1447m, 1421m, 1386m, 1331m, 1312s, 1273w, 1257w, 1212m, 1183m, 1150w, 1134m, 1125w, 1105w, 1060w, 1044vw, 983vw, 960vw, 951w, 935w, 909w, 902w, 883w, 864w, 802s, 773s, 770s, 757s, 751s, 741m, 732m, 722m, 683s, 670m, 635w, 599s, 586s, 574m, 564s, 541s, 509vs. ^1H NMR (CD_2Cl_2, 400 MHz) δ [ppm]: 1.12 (d, 3 H, CH(C*H*$_3$), $^3J_{HH}$ = 5.4Hz), 1.14 (d, 3 H, CH(C*H*$_3$), $^3J_{HH}$ = 5.2 Hz), 1.42 (d, 3 H, CH(C*H*$_3$), $^3J_{HH}$ = 6.7 Hz), 1.46 (d, 3 H, CH(C*H*$_3$), $^3J_{HH}$ = 6.7 Hz) 2.68 (sept, 2 H,

C*H*(CH_3), $^3J_{HH}$ = 6.9 Hz), 2.76 (sept, 2 H, C*H*(CH_3), $^3J_{HH}$ = 6.9 Hz), 7.18 (s, 1 H, im-H), 7.20(s, 1H, im-H), 7.36-7.64 (m, 6H, aryl-CH). ^{13}C NMR: (CD_2Cl_2) δ: 21.7 (*C*H_3CH), 21.8 (*C*H_3CH), 25.9 (*C*H_3CH), 26.0(*C*H_3CH), 29.1 (*C*HCH$_3$), 29.4 (*C*HCH$_3$), 29.7 (*C*HCH$_3$), 124.3 (H*C*N), 124.5 (H*C*N), 124.6 (m-C_6H_3), 125.4 (m-C_6H_3), 131.4 (p-C_6H_3), 131.7 (p-C_6H_3) 132.8 (o-C_6H_3), 145.0 (ipso-C_6H_3), 146.2 (ipso-C_6H_3) 157.9 (*C*Si). ^{14}N-NMR (CD_2Cl_2, 29 MHz) δ [ppm] = –146 (N_β) (FWHM: 173 Hz), –201 (N_γ) (FWHM: 368 Hz).

9.2.39 Attempted alternative preparation of 16. IPr (2.042 g, 5.25 mmol) was suspended in *n*-hexane (40 mL) in a Schlenk tube and treated with $SiCl_4$ (0.6 mL, 0.892 g, 5.25 mmol). On addition, a voluminous white precipitate had formed and the resulting suspension was stirred for 16 hrs. The hexane solution was filtered off and the solid residue dried. Sodium azide (1.709, 26.3 mmol) was added to the solid and both suspended in THF (30 mL) giving an orange suspension. The suspension was heated to 40°C and stirred for 48 hrs. The suspension was filtered and the resulting orange solution was found to contain $[Si(N_3)_6]^{2-}$. (IR (THF) cm^{-1} ν = 2108)

9.2.40 Preparation of IPrGe(N$_3$)$_4$. The same procedure for IPrSi(N_3)$_4$ was applied to Ge(N_3)$_4$. An off-white solid was obtained. Attempts to crystallise this solid were unsuccessful and on dissolving in THF or CH_2Cl_2 the solution turned purple. (IR (nujol) cm^{-1} = 3351vw, 3150w, 3126w, 3071vw, 2121s, 2107s, 2088vs, 2077vs, 1589w, 1550w, 1528w, 1365m, 1330w, 1292m, 1259m, 1212w, 1199w, 1182w, 1163vw, 1148vw, 1100w, 1060m, 1043w, 951w, 935w, 802s, 778m, 768m, 755s, 721w, 678m, 633w, 583w).

9.2.41 Preparation of bis(1,3-bis(tert-butyl)imidazolin-2-imido)diazidosilane (17). A Schlenk tube was charged with I^{t}Bu (0.435 g, 2.41 mmol) dissolved in benzene (10 mL). Si(N_3)$_4$ in benzene (1.2 mmol, 12 mL at 0.1 mmol mL^{-1}) was added giving an immediate white precipitation and effervescence. After 10 mins the bubbling had stopped and the suspension was stirred for a further 1 hr. The solvent was removed *in vacuo* and the residue dissolved in boiling toluene (5 mL) and after allowing to cool to room temperature was stored in a freezer overnight affording large colourless needle crystals. (Mass: 193 mg, 0.39 mmol, 39 % yield with respect to Si(N_3)$_4$. IR (nujol) ν /

cm^{-1} = 3426w, 3173w, 2144s, 2116s, 1713m, 1646s, 1602m, 1483w, 1416m, 1392w, 1365m, 1321m, 1266m, 1230m, 1203w, 1179w, 1167w, 1127m, 1116m, 1036m, 1009m, 985m, 957m, 824w, 813w, 799w, 730vw, 721vw, 699m, 693m, 672w, 643s, 623m, 592s, 564m, 546s, 536s. ^{1}H NMR ($CDCl_3$, 400 MHz) δ [ppm]: 1.57 (s, 18 H, (C(C*H*$_3$)$_3$), 6.34 (s, 2 H, im- H^{4,5}). ^{13}C NMR ($CDCl_3$, 400 MHz) δ [ppm]: ($CDCl_3$) δ: 28.3 (C(*C*H$_3$)$_3$), 55.2 (*C*(CH$_3$)$_3$), 107.6 (H*C*N), 139.6 (N*C*N). ^{15}N NMR MAS δ [ppm]: 71.4, 113.2, 159.8, 160.6, 168.5, 236.1. ^{29}Si NMR MAS δ [ppm]: −113.4, −114.2, −115.2.

9.2.42 Preparation of IPrP(N$_3$)$_5$ (18). A solution of NaP(N$_3$)$_6$ (ca. 0.08 mmol mL^{-1}, 2.57 mmol, 30 mL) in acetonitrile was transferred *via* a cannula into a Schlenk tube containing IPr (0.959 g, 2.57 mmol) cooled to −50°C. On addition, a yellow precipitate formed and the mixture was warmed to ambient temperature and stirred for 16 hrs. After which the solvent was concentrated *in vacuo* to approximately half volume and the yellow precipitate filtered off. The precipitate was dried and extracted with THF (2 x 20 mL) and the solvent concentrated to approximately 5 mL. Storage of the solution at −28°C for 18 hrs afforded colourless crystals of **18** which were subsequently filtered and washed with cold acetonitrile (10 mL). Yield: 1.275 g (82 %). Elemental Analysis: Calculated: C, 51.50; H, 5.76 N; 37.81%; found: C, 51.57; H, 5.69; N, 37.43%. Melting point (with strong decomposition): 151-154°C. IR (nujol) ν / cm^{-1}: 3386(w), 3350(w), 3185(w), 3156(w), 3119 (vw), (3078(vw), 3070(vw), 3013(vw), 2553(w), 2138(s), 2126(s), 2113(s), 2080(s), 1608(vw), 1595(vw), 1571(w), 1445(s), 1410(m), 1384(m), 1366(m), 1348(w), 1326(m), 1296(s), 1286(s), 1198(w), 1179(w), 1152(vw), 1136(w), 1121(w), 1099(vw), 1057(w), 1043(w), 969(w), 954(w), 957(w), 935(w), 928(w), 904(w), 888(w), 809(w), 800(m), 756(m), 740(m), 726(m), 712(m), 708(m), 696(m),642(w), 634(vw), 597(w), 587(vw), 569(m), 553(w), 539(m), 509(m), 503(m). ^{1}H NMR: (CD_2Cl_2) δ: 1.15 (d, 6.92 Hz, 12H, C*H*$_3$CH), 1.48 (d, 6.75 Hz, 12H, C*H*$_3$CH), 2.58 (sept, 6.76 Hz, 4H, C*H*(CH$_3$)$_2$), 7.04 (d, 1.83 Hz, 2H, *H*C=C*H*), 7.43-7.55, (m, 6H, aromatic protons). ^{13}C NMR: (CD_2Cl_2) δ: 21.9 (*C*H$_3$CH), 25.7 (*C*H$_3$CH), 30.1 (*C*HCH$_3$), 124.3 (H*C*N), 125.4 (m-C$_6$H$_3$), 130.5 (p-C$_6$H$_3$), 132.8 (o-C$_6$H$_3$), 144.9 (ipso-C$_6$H$_3$), 162.8 (*C*P, d, 200 Hz). ^{14}N NMR (CD_2Cl_2) δ: −272 (N(α)), −196 (NHC), −170 (N(γ)), −168 (N(γ)), −144 (N(β)), −142 (N(β)). ^{31}P NMR (CD_2Cl_2) δ: −199.2.

9.2.43 Addition of $(PPh_4)N_3$ to 18. 18 (50 mg, 0.079 mmol) was suspended in acetonitrile (3 mL) in a sample vial in a glove box. $(PPN)N_3$ (30 mg, 0.079 mmol) was added to the suspension resulting in dissolution of the $IPrP(N_3)_5$ and the resulting colourless solution was stirred for 3 hrs. IR analysis of the solution showed the formation of $(PPN)P(N_3)_6$. (IR (MeCN) ν / cm^{-1} = 2118 cm^{-1}).

9.2.44 Addition of HN_3 to 18. 18 (50 mg, 0.08 mmol) was dissolved in THF (3 mL) in a sample vial in a glove box. Ethereal HN_3 (0.025 mL, 3.3 mmol mL^{-1}, 0.083 mmol) was added to the solution and was stirred for 24 hrs to give a solution of $(IPrH)P(N_3)_6$. (IR (MeCN) ν / cm^{-1} = 2112 cm^{-1}.

9.2.45 Addition of HBF_4 to 18. 18 (0.278 g, 0.44 mmol) was dissolved in dichloromethane (5 mL) and treated with ethereal HBF_4 (0.06 mL, 71 mg, 0.44 mmol) and stirred for 1 hr. The solution was stored at −28°C overnight to give large colourless plate crystals of $IPrPF_5$. Yield: 0.120 g (43 %). ^{31}P NMR: ($CDCl_3$) δ: −149 ppm (dquint, 757 Hz, 790 Hz). ^{19}F NMR: ($CDCl_3$) δ: −52 ppm (dd, 56 Hz, 790 Hz, F_{cis}), −76 ppm (dquint, 56 Hz, 757 Hz, F_{trans}).

9.2.46 Attempted preparation of $IPrP(N_3)_3$. A Schlenk tube was charged with sodium azide (0.911 g, 14.2 mmol) and acetonitrile (30 mL). The resulting white suspension was treated with PCl_3 (0.314 g, 2.29 mmol) with stirring and then stirred for a further 48 hrs. The suspension was filtered into a second Schlenk tube containing IPr (0.888 g, 2.29 mmol) giving a red solution. Concentration of this solution afforded a red oil. (IR (MeCN) ν / cm^{-1} = 2152s, 2006m).

9.2.47 Preparation of KC_8. Modified from reference [212]. Potassium (0.808 g, 20.7 mmol) was cut into small pieces and added to a Schlenk tube with a glass stirrer bar. Graphite (1.987 g, 165 mmol) was added to the Schlenk tube and sonicated to ensure all the graphite was at the bottom of the tube. The Schlenk tube was submerged in an oil bath and heated to 200°C and stirred for 2 hrs where the solid turned into a homogenous bronze solid.

9.2.48 Preparation of bis(2,6-diisopropylphenyl)-1,5-*β*-diketimine (^{dipp}NacnacH). Modified from reference [247]. Acetylacetone (11.237 g, 0.112 mol) and

2,6-diisopropylaniline (49.517 g, 0.279 mol) were added to a round bottom flask and dissolved in ethanol (350 mL) and aqueous HCl (35 %, 15 mL) giving a red/brown solution which was heated at 85°C for 72 hrs. A large amount of white precipitate had formed and the solvent was removed *in vacuo*. Hexane (300 mL) was added to the precipitate and the mixture was refluxed for 30 mins after which the suspension was filtered. The solid was dried and dissolved with saturated aqueous Na_2CO_3 solution (500 mL) and dichloromethane (700 mL), stirred for 1 hr and the resulting two layers were separated. The organic layer was dried over $MgSO_4$, filtered and solvent removed *in vacuo* and the resulting solid redissolved in boiling dichloromethane (50 mL) and stored at −28°C overnight affording small fluffy white crystals. (Mass: 35.201 g, 0.084 mol, 75 % yield with respect to acetylacetone. ^{1}H NMR: ($CDCl_3$, 400 MHz) δ [ppm]: 1.14 (d, 12 H, CH(C*H*$_3$)$_2$, $^3J_{HH}$:7.3 Hz), 1.23 (d, 12 H, CH(C*H*$_3$)$_2$, $^3J_{HH}$: 7.1 Hz), 1.74 (s, 6 H, CHC*H*$_3$), 3.14 (sept, 4 H, C*H*(CH$_3$)$_2$, $^3J_{HH}$: 6.9 Hz), 4.89 (s, 1 H, C*H*CH$_3$), 7.14-7.38 (m, 6 H, aryl-H), 12.1 (s, 1 H, N*H*)).

9.2.49 Preparation of (^{mes}Nacnac)MgI. Modified from reference [248]. Magnesium turnings (0.673 g, 27.7 mmol) were suspended in diethyl ether (30 mL) in a Schlenk tube and cooled in ice before treated with MeI (1.85 mL, 4.218 g, 27 mmol). The grey slurry that forms was stirred for 5 hrs before being filtered into a Schlenk tube containing ^{mes}NacnacH (9.024 g, 27 mmol) dissolved in diethyl ether (20 mL) pre-cooled to −30°C. On addition, an immediate white precipitate was observed and the Schlenk tube was connected to a mercury bubbler. The suspension was warmed to room temperature and stirred for 16 hrs. The white solid was collected by filtration, washed with toluene (3 x 10 mL) and dried under vacuum giving a fine white powder. (Mass: 10.951 g, 19.2 mmol, 71 % yield with respect to ^{mes}NacnacH. ^{1}H NMR: (C_6D_6) δ [ppm]: 1.67 (s, 6 H, CHC*H*$_3$), 2.02 (s, 6 H, C$_6$H$_2$-C*H*$_3$), 2.41 (s, 3 H, C$_6$H$_2$-C*H*$_3$), 4.92 (s, 1 H, C*H*CH$_3$), 6.97 (s, 4 H, aryl-H).

(^{dipp}Nacnac)MgI·Et$_2$O can be prepared using the same method. Reference [214]. ^{1}H NMR: (C_6D_6, 400 MHz) δ [ppm]: 1.15-1.166 (m, 36 H, CH(C*H*$_3$)$_2$, (C*H*$_3$CH$_2$)$_2$O, CHC*H*$_3$), 3.38 (q, 4 H, $^3J_{HH}$: 7.1 Hz, (CH$_3$C*H*$_2$)$_2$O), 3.83 (sept, 4 H, $^3J_{HH}$: 6.8 Hz, C*H*(CH$_3$)$_2$.), 4.83 (s, 1 H, C*H*CH$_3$), 7.12-7.15 (m, 6 H, aryl-H).

9.2.50 Preparation of (^{dipp}Nacnac)MgN$_3$ (24). (^{dipp}Nacnac)MgI (1.903 g, 3.3 mmol) and sodium azide (0.234 g, 3.6 mmol) were combined in a Schlenk tube and suspended in THF (30 mL). The white suspension was stirred for 16 hrs before the solvent was filtered and evaporated *in vacuo* to give a white oil. (IR (THF) ν / cm^{-1} = 2120s).

9.2.51 Preparation of [(^{mes}Nacnac)Mg]$_2$. Modified from reference [248]. A Schlenk tube was coated with a sodium mirror (0.685 g, 29.8 mmol) and a glass stirrer bar was added. (^{mes}Nacnac)MgI (1.684 g, 2.9 mmol) was added to the Schlenk tube and suspended in toluene (60 mL) and diethyl ether (2 mL). After 5 days of stirring the black solution that formed was filtered giving a yellow solution and leaving a black solid residue. The yellow solution was concentrated to approximately 10 mL and left at −28°C for 16 hrs resulting in microcrystalline yellow crystals that were isolated by filtration and dried under vacuum. (Mass: 0.795 g, 0.9 mmol, 60 % yield with respect to (^{mes}Nacnac)MgI. ^{1}H NMR: (C_6D_6) δ [ppm]: 1.55 (s, 12 H, CHC*H*$_3$), 1.91 (s, 24 H, C_6H_2-C*H*$_3$), 2.30 (s, 12 H, C_6H_2-C*H*$_3$), 4.80 (s, 2H, C*H*CH$_3$), 6.86 (s, 8 H, aryl-H).
[(^{dipp}Nacnac)Mg]$_2$ can be prepared in the same method.[249] ^{1}H NMR: (C_6D_6, 400 MHz) δ [ppm]: 1.04 (d, 24 H, CH(C*H*$_3$)$_2$, $^3J_{HH}$:6.9 Hz), 1.22 (d, 24 H, CH(C*H*$_3$)$_2$, $^3J_{HH}$: 6.9 Hz), 1.59 (s, 12 H, CHC*H*$_3$), 3.11 (sept, 8 H, C*H*(CH$_3$)$_2$, $^3J_{HH}$: 6.9 Hz), 4.87 (s, 2 H, C*H*CH$_3$), 7.08-7.18 (m, 12 H, aryl-H).

9.2.52 Attempted reduction of 16 with KC$_8$. A Schlenk tube containing KC_8 (230 mg, 1.7 mmol) and **16** (340 mg, 0.58 mmol) was cooled to −50°C. Ambient temperature toluene was added giving a black suspension that was stirred for 2 hrs at ambient temperature before being filtered off to give a yellow solution. Concentration of the solution resulted in a yellow oil. (IR (toluene) ν / cm^{-1} = 2150s, 2103m, 2014m).

9.2.53 Attempted reduction of 16 with [($^{dipp/mes}$Nacnac)Mg]$_2$. A Schlenk tube containing **16** (350 mg, 0.60 mmol) and [($^{dipp/mes}$Nacnac)Mg]$_2$ (0.60 mmol) was cooled to −50°C. Toluene (30 mL) was added to the two solids giving a yellow suspension. The solution was stirred for 16 hrs at ambient temperature giving an orange solution. Concentration of the solution and storing at −28°C overnight afforded small block crystals of ($^{dipp/mes}$Nacnac)MgN$_3$.
(^{dipp}Nacnac)MgN$_3$ (**24**): (IR (toluene) ν / cm^{-1} = 2198s)

(^{mes}Nacnac)MgN_3 (**23**): (IR (toluene) ν / cm^{-1} = 2160s)

9.2.54 Preparation of 1,3-Bis(2,6-diisopropylphenyl)-2-(4-tert-butylphenyl)carbodiimine (^{dipp}NCN)H. Modified from reference 85. Lithium ingots (213 mg, 30.7 mmol) were added to a Schlenk tube, suspended in diethyl ether (30 mL) and treated with 1-bromo-4-^{t}butyl-benzene (3.601 g, 16.9 mmol) under a flow of argon. The mixture was heated in an oil bath at 45°C and stirred for 1 hr giving a grey suspension. This suspension was filtered into a second Schlenk tube containing bis(2,6-diisopropylphenyl)carbodiimide (5.580 g, 15.4 mmol) dissolved in diethyl ether (20 mL) cooled to −20°C, giving a yellow solution. This solution was stirred at room temperature for 1 hr. Water (15 mL) was added slowly to the yellow solution initially producing a white precipitate before dissolving and forming two layers. The layers were separated and the aqueous layer extracted with dichloromethane (2 x 15 mL). All organic layers were combined, dried with $MgSO_4$, filtered and evaporated to dryness resulting in a white precipitate. The precipitate was dissolved in boiling hexane (30 mL) and cooled to −28°C overnight giving colourless plate crystals, which were filtered and dried. (Mass: 5.076 g, 10.2 mmol, 66 % yield with respect to bis(2,6-diisopropylphenyl)carbodiimide. IR (Nujol) ν / cm^{-1}: 3424s, 3360s, 1651s, 1621s, 1587s, 1563m, 1407m, 1326m, 1298m, 1269m, 1105m, 1081m, 936m, 848m, 826m, 780m, 760s. Both the E and Z isomer are present in the ^{1}H NMR spectrum. ^{1}H NMR (C_6D_6, 400 MHz): main isomer, δ 0.89 (d, 6H, CH(C*H*$_3$)$_2$, $^3J_{HH}$ = 6.8 Hz), 0.92 (d, 6H, CH(C*H*$_3$)$_2$, $^3J_{HH}$ = 6.8 Hz), 1.05 (s, 9H, C(C*H*$_3$)$_3$), 1.39 (d, 6H, CH(C*H*$_3$)$_2$, $^3J_{HH}$ = 6.8 Hz), 1.40 (d, 6H, CH(C*H*$_3$)$_2$, $^3J_{HH}$ = 6.8 Hz), 3.30 (sept, 2H, C*H*(CH$_3$)$_2$, $^3J_{HH}$ = 6.8 Hz), 3.50 (sept, 2H, C*H*(CH$_3$)$_2$, $^3J_{HH}$ = 6.8 Hz), 5.92 (s, 1H, N*H*), 6.93 (d, 2H, aryl-H, $^3J_{HH}$ = 8.0 Hz), 6.99-7.30 (m, 6H, aryl-H), 7.64 (d, 2H, aryl-H, $^3J_{HH}$ = 8.0 Hz) ; minor isomer, δ 0.65 (br, 6H, CH(C*H*$_3$)$_2$), 0.97 (br, 6H, CH(C*H*$_3$)$_2$, 1.05 (s, 9H, C(C*H*$_3$)$_3$), 1.11 (br, 6H, CH(C*H*$_3$)$_2$), 1.24 (vbr, 6H, CH(C*H*$_3$)$_2$), 3.31 (vbr, 2H, C*H*(CH$_3$)$_2$), 3.58 (vbr, 2H, CH(CH$_3$)$_2$), 5.68, (s, 1H, N*H*), 7.01-7.31 (m, 10H, aryl-H).

9.2.55 Preparation of (^{dipp}NCN)Si(N$_3$)$_3$ (20). (^{dipp}NCN)H (0.959 g, 1.93 mmol) and lithium bis(trimethylsilyl)amide (0.322 g, 1.93 mmol) were combined in a Schlenk tube and dissolved in diethyl ether (20 mL), giving a yellow solution, and stirred for 1 hr. After which the solvent was evaporated and the residue dried. The material was redissolved in diethyl ether (20 mL) and treated with $SiCl_4$ (0.329 g, 1.93 mmol) which

resulted in an immediate precipitation. After 1 hr stirring, the solution was evaporated to dryness and sodium azide (1.120 g, 17.2 mmol) was added to the residue, suspended in THF (30 mL) and stirred for 24 hrs. The suspension was filtered onto a second batch of sodium azide (1.143 g, 17.5 mmol) and stirred for a further 24 hours. The suspension was filtered and solvent evaporated to give a sticky off-white residue which was extracted with *n*-hexane (2 x 30 mL). The hexane extracts were combined and concentrated to approximately 5 mL and storage of this solution at –28°C overnight affords colourless block crystals of (^{dipp}NCN)Si(N_3)$_3$. (Mass: 0.495 g, 0.76 mmol, 40 % yield with respect to (^{dipp}NCN)H. IR (nujol) ν / cm^{-1}: 3406w, 3060m, 2160vs, 2137vs, 2130vs, 2116vs, 1609s, 1592m, 1588m, 1568s, 1544s, 1514m, 1497s, 1429m, 1395m, 1382s 1349m, 1343m, 1314s, 1299s, 1272w, 1258m, 1227w, 1201m, 1179m, 1173w, 1164w, 1138m, 1131w, 1112m, 1099m, 1055m, 1047w, 1023w, 1016w, 993s, 972w, 955w, 935m, 924w, 862m, 839m, 830w, 816m, 791s, 759s, 749m, 734s, 719m, 703w, 696vw, 681m, 674m, 633w, 617m, 592s, 579s, 556s, 549m, 539m, 522m, 505s).

9.2.56 Preparation of (^{dipp}NCN)Ge(N_3)$_3$. The same procedure for **20** was applied to $GeCl_4$ to prepare (^{dipp}NCN)Ge(N_3)$_3$. (Mass: 0.602 g, 0.88 mmol, 54 % yield with respect to $GeCl_4$. IR (nujol) ν / cm^{-1}: 3338w, 3059w, 2127vs, 2110vs, 2099vs, 2089vs, 1607m, 1590w, 1585w, 1567m, 1532m, 1512w, 1491w, 1425m, 1396m, 1364m, 1337w, 1323w, 1259vs, 1201m, 1098s, 1055m, 1016m, 984m, 955w, 933m, 923m, 906w, 852m, 834w, 827w, 802s, 789m, 783m, 754m, 749m, 723w, 705m, 694m, 684w, 666w, 658w, 632w, 612w, 592w, 580m, 558m).

9.2.57 Preparation of (^{dipp}NCN)GeN$_3$. The same procedure for **20**, up to the *n*-hexane step, was applied to $GeCl_2$(1,4-dioxane) to prepare a THF solution of (^{dipp}NCN)GeN_3. (IR (THF) ν / cm^{-1}: 2070).

9.2.58 Preparation of (^{dipp}NCN)SiHCl$_2$. (^{dipp}NCN)H (2.010 g, 4.05 mmol) and lithium bis(trimethylsilyl)amide (0.680 g, 4.06 mmol) were combined in a Schlenk tube and dissolved in diethyl ether (20 mL), giving a yellow solution, and stirred for 1 hr. After which the solvent was evaporated and the residue dried. The material was redissolved in diethyl ether (20 mL) and treated with $HSiCl_3$ (0.966 g, 7.1 mmol) to give an immediate white precipitate. The suspension was stirred for 1 hr followed by evaporation of all

volatiles under vacuum giving a white residue. The residue was extracted with *n*-hexane (2 x 20 mL) and concentrated to approximately 5 mL. Cooling this solution to −28°C overnight affords colourless crystals of (^{dipp}NCN)SiHCl$_2$. (Mass: 1.134 g, 1.90 mmol, 47 % yield with respect to (^{dipp}NCN)H. ^{1}H NMR (C_6D_6, 400 MHz) δ [ppm]: 0.88 (s, 9 H, C(C*H*$_3$)$_3$), 1.08 (d, 6 H, CH(C*H*$_3$)$_2$, $^3J_{HH}$: 6.9 Hz), 1.51 (d, 6 H, CH(C*H*$_3$)$_2$, $^3J_{HH}$: 6.6 Hz), 3.71 (sept, 4 H, C*H*(CH$_3$)$_2$, $^3J_{HH}$: 6.6 Hz), 6.47 (s, 1 H, Si*H*), 6.90-7.33 (m, 10 H, aryl-H).

9.2.59 Preparation of (^{dipp}NCN)SiH(N$_3$)$_2$ (25). (^{dipp}NCN)SiHCl$_2$ (0.540 g, 0.91 mmol) and sodium azide (0.146 g, 2.25 mmol) were combined in a Schlenk tube and suspended in THF (20 mL) and stirred for 16 hrs before being filtered onto a second batch of sodium azide (0.152 g, 2.33 mmol) and stirred for a further 16 hrs. The suspension was filtered and the solvent removed *in vacuo* to give a white residue. The residue was redissolved in a 1:1 mixture of hexane and toluene (30 mL total) and concentrated to approximately 3 mL and cooled to −28°C overnight to give colourless crystals of **25**. (Mass: 0.100 g, 0.16 mmol 19 % yield with respect to (^{dipp}NCN)SiHCl$_2$. IR (nujol) ν /cm^{-1}: 3449w, 3414w, 3368w, 3176w, 3060m, 2159s, 2148s, 2119s, 1934vw, 1873vw, 1794vw, 1622m, 1608s, 1574s, 1552s, 1505s, 1418s, 1384s, 1365s, 1346s, 1317s, 1294m, 1270m, 1257m, 1229w, 1200m, 1179m, 1135m, 1127m, 1112m, 1100m, 1057m, 1046m, 1027w, 1017w, 991s, 978w, 971w, 951w, 936m, 886w, 845m, 837s, 814m, 791s, 783s, 760s, 746s, 729s, 694s, 670vw, 656w, 634vw, 615vw, 571s, 551s, 529w, 513m. ^{1}H NMR (C_6D_6, 400 MHz) δ [ppm]: 0.76 (s, 9 H, C(C*H*$_3$)$_3$), 0.96 (d, 6 H, CH(C*H*$_3$)$_2$, $^3J_{HH}$: 7.4 Hz), 1.40 (d, 6 H, CH(C*H*$_3$)$_2$, $^3J_{HH}$: 6.93 Hz), 3.50 (sept, 4 H, C*H*(CH$_3$)$_2$, $^3J_{HH}$: 6.7 Hz), 6.13 (s, 1 H, Si*H*), 6.75-7.18 (m, 10 H, aryl-H).)

9.2.60 Preparation of (^{dipp}NCN)P(N$_3$)$_2$ (21). The same procedure for **20** was applied to PCl$_3$ to prepare (^{dipp}NCN)P(N$_3$)$_2$. (Mass: 0.370 g, 0.6 mmol, 26 % yield with respect to PCl$_3$. (IR (nujol) ν / cm^{-1}: 3370w, 3337w, 3058m, 2128s, 2109vs, 1619s, 1602s, 1586s, 1560w, 1515m, 1445m, 1406m, 1382m, 1362m, 1341m, 1319w, 1310w, 1276s, 1245s, 1221m, 1200w, 1174m, 1127m, 1107m, 1091m, 1054m, 1043w, 1025w, 1016w, 977m, 934w, 885w, 868m, 832s, 793s, 768s, 752m, 733m, 718s, 695s, 666vw, 640m, 609m, 591w, 563s, 523vs, 506s).

9.2.61 Preparation of (^{dipp}NCN)P(N_3)$_4$ (22). The same procedure for **20** was applied to PCl_5 to prepare (^{dipp}NCN)P(N_3)$_4$. (Mass: 0.482 g, 0.69 mmol, 33 % yield with respect to PCl_5. Melting point: 148-150°C (decomposes at 180°C). IR (nujol) ν / cm^{-1}: 3369 (w), 3063(w), 2560(w), 2544(w), 2132(sh), 2123(s), 2105(s), 2095(s), 1611(m), 1593(w), 1584(w), 1569(w), 1554(m), 1497(m), 1404(m), 1383(m), 1364(m), 1350(w), 1323(w), 1289(s), 1275(s), 1200(m), 1179(m), 1163(w), 1139(w), 1114(w), 1098(w), 1056(w), 1024(w), 987(w), 933(w), 855(w), 831(m), 816(w), 803(w), 785(s), 754(s), 721(s), 693(m), 669(w), 634(w), 616(w), 594(w), 572(s), 563(s), 539(s), 530(s), 510(s). ^{1}H NMR: (CD_2Cl_2) δ: 0.79 (d, 6.86 Hz, 12H, C*H*$_3$CH), 1.23 (s, 9H C*H*$_3$C), 1.48 (d, 6.60 Hz, 12H, C*H*$_3$CH), 3.64 (sept, 6.77 Hz, 4H, C*H*(CH_3)$_2$), 7.1-7.5, (m, 10H, aromatic protons). ^{14}N NMR (CD_2Cl_2) δ: −297 (N(α)),−254 (N(α)), −169 (N(γ)), −146 (N(β)), −142 (N(β)). ^{31}P NMR (CD_2Cl_2) δ: −159.9.)

9.2.62 Attempted reduction of 20 with KC_8. 20 (1.207 g, 1.86 mmol) and KC_8 (0.553 g, 4.09 mmol) were combined in a Schlenk tube and cooled to −28°C. The solids were suspended in toluene and stirred for two hrs at ambient temperature. The resulting black suspension was filtered to give a yellow solution which was concentrated to give a yellow oil. (IR (toluene) ν / cm^{-1}: 2044m.)

9.2.63 Attempted reduction of 20 with [($^{dipp/mes}$Nacnac)Mg]$_2$. 20 (0.077 g, 0.12 mmol) and [($^{dipp/mes}$Nacnac)Mg]$_2$ (0.12 mmol) were combined in a Schlenk tube, dissolved in toluene (20 mL), to give a yellow solution, and stirred. After 1 hr stirring the solution had changed from yellow to dark green. A FT-IR spectrum of the solution displayed signals for the starting material and **23** or **24**. The solution was transferred to a second Schlenk tube containing [($^{dipp/mes}$Nacnac)Mg]$_2$ (0.06 mmol) and stirred for a further hour where the solution turned dark blue. The toluene solvent was removed *in vacuo* and the residue was dissolved in *n*-hexane (5 mL). After storage for 16 hrs at −28°C small, colourless block crystals of ($^{dipp/mes}$Nacnac)MgN_3 had formed in the solution. The crystals were filtered off and dried under vacuum.

(**24**): (IR (toluene) ν / cm^{-1} = 2198s)

(**23**): (IR (toluene) ν / cm^{-1} = 2160s)

9.2.64 Attempted reduction of (^{dipp}NCN)Ge(N$_3$)$_3$ with [($^{dipp/mes}$Nacnac)Mg]$_2$. (^{dipp}NCN)Ge(N$_3$)$_3$ (0.105 g, 0.19 mmol) and [($^{dipp/mes}$Nacnac)Mg]$_2$ (0.19 mmol) were combined in a Schlenk tube, dissolved in toluene (20 mL), to give a yellow solution, and stirred. After 1 hr stirring the solution had changed from yellow to pink. A FT-IR spectrum of the solution displayed signals for the starting material and **23** or **24**. The solution was transferred to a second Schlenk tube containing [($^{dipp/mes}$Nacnac)Mg]$_2$ (0.095 mmol) and stirred for a further hour where the solution turned red. The toluene solvent was removed *in vacuo* and the residue was dissolved in n-hexane (5 mL). After storage for 16 hrs at −28°C small, colourless block crystals of ($^{dipp/mes}$Nacnac)MgN$_3$ had formed in the solution. The crystals were filtered off and dried under vacuum.
(**24**): (IR (toluene) ν / cm^{-1} = 2198s)
(**23**): (IR (toluene) ν / cm^{-1} = 2160s)

9.2.65 Attempted reduction of 21 with [($^{dipp/mes}$Nacnac)Mg]$_2$. 21 (0.098 g, 0.18 mmol) and [($^{dipp/mes}$Nacnac)Mg]$_2$ (0.09 mmol) were combined in a Schlenk tube, dissolved in toluene (20 mL), to give a yellow solution, and stirred. After 1 hr stirring the solution had changed from yellow to orange. A FT-IR spectrum of the solution displayed signals for the starting material **23** or **24**. The solution was transferred to a second Schlenk tube containing [($^{dipp/mes}$Nacnac)Mg]$_2$ (0.09 mmol)and stirred for a further hour where the solution remained orange. The toluene solvent was removed *in vacuo* and the residue was dissolved in *n*-hexane (5 mL). After storage for 16 hrs at −28°C small, colourless block crystals of ($^{dipp/mes}$Nacnac)MgN$_3$ had formed in the solution. The crystals were filtered off and dried under vacuum.
(**24**): (IR (toluene) ν / cm^{-1} = 2198s)
(**23**): (IR (toluene) ν / cm^{-1} = 2160s)

9.2.66 Attempted reduction of 25 with IPr. 25 (1.166 g, 1.91 mmol) and IPr (0.760 g, 1.96 mmol) were combined in a Schlenk tube and dissolved in toluene (20 mL) giving a pale yellow solution. The solution was stirred for 24 hrs and the solvent removed *in vacuo* to give an off-white residue. The residue was extracted with *n*-hexane (2 x 20 mL) and concentrated to approximately 5 mL. Storage of this solution at −28°C afforded colourless block crystals of (^{dipp}NCN)SiH(N$_3$)$_2$IPr which were filtered off and dried under vacuum. (Mass: 0.308 g, 0.31 mmol, 16 % yield with respect to **25**. IR (nujol / cm^{-1}) ν = 3406w, 3386w, 3150m, 3135m, 3056m, 2163m, 2113vs, 2092vs,

2014vw, 1971vw, 1886vw, 1613m, 1597w, 1570m, 1561w, 1543s, 1496w, 1402w, 1365s, 1352w, 1341w, 1328m, 1313s, 1289w, 1271m, 1253m, 1199m, 1181m, 1138w, 1098w, 1090m, 1078w, 1059m, 1044w, 988m, 959s, 938m, 898vw, 884vw, 849vw, 831m, 818m, 806s, 782s, 770m, 758s, 748w, 728m, 703s, 693m, 686w, 679w, 671m, 658vw, 636vw, 609vw, 594m, 588w, 558m, 543w, 535w, 516s. ^{1}H-NMR (C_6D_6, 400 MHz) δ / [ppm] : 0.91 (d, CH(C*H*$_3$)$_2$, 6 H, $^{3}J_{HH}$ 6.9 Hz), 0.93 (d, CH(C*H*$_3$)$_2$, 6 H, $^{3}J_{HH}$ 7.3 Hz), 1.06 (s, C(C*H*$_3$)$_3$), 1.41 (d, CH(C*H*$_3$)$_2$, 12H, $^{3}J_{HH}$ 6.9 Hz), 3.31 (sept, C*H*(CH$_3$)$_2$, 8H, $^{3}J_{HH}$ 6.7 Hz), 3.53 (sept, CH(C*H*$_3$)$_2$, 8H, $^{3}J_{HH}$ 6.7 Hz), 5.94 (s, Si*H*), 6.93-7.67 (m, aryl-H, 10H).

9.2.67 Attempted reduction of 25 with Li(N(SiMe$_3$)$_2$). 25 (0.477 g, 0.78 mmol) and lithium bis(trimethylsilyl)amide (0.132 g, 0.79 mmol) were combined in a Schlenk tube and suspended in toluene (30 mL). The resulting off-white suspension was stirred for 24 hrs. The suspension was filtered and the residue was identified as LiN_3 by IR spectroscopy. The filtrate was evaporated *in vacuo* and the off-white oily residue was dissolved in *n*-hexane (3 mL). Storage of this solution at −28°C for 16 hrs gives colourless, short needle crystals of (^{dipp}NCN)SiH(N$_3$)(N(SiMe$_3$)$_2$) which were isolated by filtration and dried under vacuum. (IR (nujol) ν / cm^{-1}: 3402vw, 3060m, 2249m, 2222m, 2145vs, 2118s, 1603s, 1583s, 1514w, 1505w, 1439w, 1421m, 1407w, 1364m, 1343w, 1318s, 1306s, 1282w, 1266w, 1254s, 1213w, 1202w, 1176w, 1168w, 1128m, 1110m, 1100w, 1090m, 1055m, 1044m, 1016m, 994s, 978s, 964s, 943s, 935s, 907s, 846vs, 828s, 802w, 793m, 770m, 763m, 748m, 729w, 698m, 676m, 658w, 563m, 549w, 531m. ^{1}H NMR (C_6D_6, 400 MHz) δ [ppm]: 0.1 (s, 9 H, Si(C*H*$_3$)$_3$), 0.40 (s, 9 H, Si(C*H*$_3$)$_3$), 0.72 (d, 6 H, CH(C*H*$_3$)$_2$, $^{3}J_{HH}$: 6.4 Hz), 0.82 (s, 9 H, C(C*H*$_3$)$_3$), 1.25 (d, 6 H, CH(C*H*$_3$)$_2$, $^{3}J_{HH}$: 7.2 Hz), 1.33 (d, 6 H, CH(C*H*$_3$)$_2$, $^{3}J_{HH}$: 7.2 Hz), 1.47 (d, 6 H, CH(C*H*$_3$)$_2$, $^{3}J_{HH}$: 7.2 Hz), 3.34 (sept, 4 H, C*H*(CH$_3$)$_2$, $^{3}J_{HH}$: 6.7 Hz), 3.89 (sept, 4 H, C*H*(CH$_3$)$_2$, $^{3}J_{HH}$: 6.7 Hz), 5.97 (s, 1 H, Si*H*), 6.75-7.24 (m, 10 H, aryl-H).)

9.2.68 Attempted reduction of 25 with Li(^{dipp}Nacnac). 25 (0.485 g, 0.8 mmol) and Li(^{dipp}Nacnac) (0.340 g, 0.8 mmol) were combined in a Schlenk tube and dissolved in toluene (15 mL). After stirring the solution for 1 hr the solution had turned pale yellow. The solution was concentrated to approximately 5 mL and stored at −28°C for 16 hrs. Colourless long needle crystals of (^{dipp}NCN)SiH(N$_3$)$_2$·Li(^{dipp}Nacnac) had formed, which were filtered and dried under vacuum. (Mass: 0.451 g, 0.43 mmol, 55 % yield with

respect to **25**. IR (nujol) ν / cm^{-1}: 3518w, 3449w, 3179w, 3069m, 3057m, 2174vs, 2148vs, 1609m, 1591m, 1574s, 1553s, 1510s, 1429m, 1407s, 1394m, 1383m, 1364m, 1349m, 1318s, 1296m, 1270m, 1255m, 1227m, 1200w, 1174s, 1160w, 1135m, 1129w, 1109m, 1097m, 1057s, 1045m, 1020s, 994s, 980s, 955w, 934s, 912w, 903w, 883w, 854m, 837s, 815m, 803m, 789s, 759s, 753s, 724s, 709w, 695s, 669m, 655m, 634m, 592s, 572s, 550s, 542w, 525w, 514m, 506w. ^{1}H NMR: (C_6D_6) δ [ppm]: 0.87 (s, 9H C*H*$_3$C), 1.05 (d, 7.00 Hz, 12H, C*H*$_3$CH), 1.31 (d, 7.8 Hz, 12H, C*H*$_3$CH), 1.33 (d, 8.1 Hz, 12H, C*H*$_3$CH) 1.47 (d, 6.5 Hz, 12H, C*H*$_3$CH), 3.33 (sept, 6.79 Hz, 4H, C*H*(CH_3)$_2$), 3.56 (sept, 6.79 Hz, 4H, C*H*(CH_3)$_2$), 5.02 (s, 1 H, C*H*CH_3), 6.13 (s, 1 H, Si*H*),6.86-7.31, (m, 16H, aryl-H).

9.2.69 Attempted reduction of 25 with I^{t}Bu. 25 and I^{t}Bu were combined in a Schlenk tube and dissolved in toluene (30 mL). The mixture was warmed up to 35°C and stirred for 24 hrs. An off-white precipitate had formed and after the suspension had cooled to ambient temperature it was filtered off. The filtrate solvent was removed *in vacuo* and the residue was extracted with *n*-hexane (2 x 30 mL). The filter residue from the previous step was redissolved in toluene heated to 50°C and allowed to cool down to ambient temperature slowly before being placed in a freezer overnight. The hexane solution was concentrated to approximately 10 mL and warmed gently to aid dissolution before being stored in a freezer overnight. Both solutions contained small, block crystals which were identified as (I^{t}BuH)(^{dipp}NCN)SiH(N_3)$_3$ by single crystal X-ray diffraction as either a toluene or hexane solvate. (IR (nujol / cm^{-1}) ν = 3392w, 3177w, 3160m, 3131m, 3087w, 3058m, 3026m, 2126vs, 2102vs, 2081s br, 2015d, 1912w, 1859vw, 1795vw, 1652w, 1614s, 1586s, 1573s, 1541s, 1514s, 1403m, 1364s, 1326s, 1309s, 1290m, 1270m, 1256s, 1234s, 1204s, 1181s, 1129s, 1116m, 1099s, 1082m, 1058s, 1045m, 1032w, 1018vw, 995w, 979s, 936s, 882s, 850m, 833s, 803s, 789m, 780s, 754s, 747vs, 729vs, 705vs, 695vs, 682s, 667m, 655s, 634m, 614m, 594m, 559s, 543m, 519s).

9.2.70 Preparation of Li(^{dipp}Nacnac). Modified from reference [247]. A Schlenk tube was charged with ^{dipp}NacnacH (4.258 g, 10.2 mmol) dissolved in *n*-hexane (25 mL), giving a yellow/green solution, and was cooled to −40°C. ^{n}BuLi in hexanes (2.5 M, 4.2 mL, 10.5 mmol) was added to the solution which was stirred for 2 hrs resulting in a white

suspension. The suspension was stored at −28°C for 16 hrs and the white solid was filtered off and dried under vacuum. (Mass: 3.828 g, 9 mmol, 88% yield with respect to ^{dipp}NacnacH. ^{1}H-NMR ($CDCl_3$, 400 MHz) δ / [ppm] : 1.14 (d, CH(C*H*$_3$)$_2$, 8H, $^{3}J_{HH}$ 7.1 Hz), 1.23 (d, CH(C*H*$_3$)$_2$. 8H, $^{3}J_{HH}$ 7.1 Hz), 1.74 (s, CHC*H*$_3$, 6 H), 3.13 (sept, C*H*(CH$_3$)$_2$. 4H, $^{3}J_{HH}$ 7.1 Hz), 4.89 (s, 1H, C*H*CH$_3$), 7.14-7.15 (m, aryl-H, 6H), 12.14 (s, NH, 1H).

9.2.71 Preparation of (^{dipp}Nacnac)SiHCl$_2$ (26). Li(^{dipp}Nacnac) (1.002 g, 2.36 mmol) was added to a Schlenk tube and dissolved in diethyl ether (20 mL) giving a yellow/green solution. To this solution $HSiCl_3$ (0.25 mL, 2.47 mmol) was added dropwise producing an immediate suspension that was stirred at ambient temperature for 1 hr. The suspension was filtered and the solvent was evaporated to dryness giving a colourless solid. (Mass: 0.998 g, 1.9 mmol, 81% yield with respect to Li(^{dipp}Nacnac). IR (nujol / cm^{-1}) ν = 3130m, 3066m, 2658w, 2164m, 2151m, 1967vw, 1945vw, 1864vw, 1853vw, 1792vw, 1781vw, 1728w, 1692w, 1620m, 1592m, 1554s, 1498s, 1440w, 1431w, 1384m, 1365, 1323m, 1293vs, 1257w, 1248w, 1187m, 1146w, 1098w, 1071vs, 1035s, 979w, 960w, 935w, 913m, 824m, 796s, 774m, 760m, 752m, 699w, 660w, 649w, 610w, 563w, 535w. ^{1}H-NMR (C_6D_6, 400 MHz) δ / [ppm]: 1.24 (d, 6 H, CH(C*H*$_3$)$_2$, $^{3}J_{HH}$ 7.2 Hz), 1.30 (d, 6 H, CH(C*H*$_3$)$_2$, $^{3}J_{HH}$ 6.8 Hz), 1.32 (d, 12 H, CH(C*H*$_3$)$_2$, $^{3}J_{HH}$ 6.8 Hz), 1.40 (s, 3 H, CHC*H*$_3$), 3.00 (sept, 2H, C*H*(CH$_3$)$_2$, $^{3}J_{HH}$ 6.8 Hz), 3.17 (s, 3H, CHC*H*$_3$, 3.41 (sept, 2H, C*H*(CH$_3$)$_2$, $^{3}J_{HH}$ 6.8 Hz), 5.03 (s, 1H, C*H*CH$_3$), 5.55 (s, 1H, Si*H*), 7.14-7.29 (m, 6H, aryl-H).

9.2.72 Preparation of (^{dipp}Nacnac)SiH(N$_3$)$_2$ (27). 26 (0.998 g, 1.9 mmol) was combined with sodium azide (0.584 g, 8.9 mmol) and suspended in MeCN (20 mL) and stirred for 20 hrs. After this time, the suspension turned purple. The solvent was removed *in vacuo* and the resultant purple residue was extracted with *n*-hexane (2 x 20 mL). The purple hexane solution was concentrated to approximately 2 mL and stored at −28°C for 24 hrs to give sticky colourless crystals, which were filtered off. (Mass: 0.371 g, 0.7 mmol, 37 % yield with respect to **26**. IR (nujol) cm^{-1} = 3437vw, 3387vw, 3233w, 3179w, 3053m, 2157s, 2144vs, 2123s, 2105s, 1622s, 1588m, 1551vs, 1486s, 1442m, 1361s, 1322s, 1277s, 1254m, 1222w, 1174s, 1161m, 1148w, 1101m, 1058m, 1043w, 1020m, 996vw, 975vw, 964vw, 948w, 935s, 894w, 882w, 857w, 834w, 823m, 804s,

799s, 788vs, 758vs, 733s, 728s, 722s, 701s, 685w, 649vw, 629vw, 613w, 601w, 596vw.)

9.2.73 Preparation of bis(p-tolyl)triazene. p-tolylamine (5.962 g, 55.653 mmol) was suspended in H_2O (20 mL) and treated with aqueous HCl (7.4 mL, 35 %) to give a colourless solution. $NaNO_2$ (2.108 g) was dissolved in H_2O (15 mL) and both solutions were cooled in an ice-water bath. The $NaNO_2$ solution was added dropwise over a period of 5 mins to the amine solution and stirred for a further 5 mins. At which point an ice cooled aqueous solution of NaOAc (3.790 g, 46.2 mmol dissolved in water 15 mL) was added to the reaction solution dropwise and the solution stirred at room temperature. After 1 hr a yellow precipitate had formed. The yellow solid was filtered and washed with H_2O (3 x 20 mL) before it was dissolved in diethyl ether (20 mL) to give a colourless bottom layer and an orange top layer. The layers were separated and the organic layer dried with $MgSO_4$ and evaporated *in vacuo* giving a dry yellow solid. (Mass: 3.784 g, 55 % relative to $NaNO_2$). ^{1}H-NMR (400 MHz; d^6-DMSO) δ / [ppm]: 3.35 (s, 6H, CH3), 7.19 (m, 6H, ArH), 7.40 (d, 2H, ArH), 12.27 (s, 1H, NH). IR (nujol) cm^{-1} = 3199w, 3115w, 3021w, 2924vs, 2855s, 1612w, 1525s, 1495m, 1397m, 1310w, 1245s, 1177m, 1107w, 812s, 656w, 507w).

9.2.74 Preparation of sodium bis(p-toly)triazanate. NaH (0.120 g, 5 mmol) and bis(p-tolyl)triazene (1.044 g, 4.634 mmol) were combined in a Schlenk tube and cooled to −30°C. The solids were suspended in THF (20 mL) giving an immediate effervescence and the solution turned black. A bubbler was attached to the Schlenk tube and the reaction solution was warmed to room temperature and stirred for 1 hr. The solvent was evaporated *in vacuo* giving an orange solid. (Mass: 1.356 g, 92 % yield relative to bis(p-tolyl)triazene. ^{1}H-NMR (400 MHz; CD_3CN) δ / [ppm] = 1.83 (4H, q, RC*H*$_2$), 2.27(6H, s, C*H*$_3$), 3.68 (4H, q, ROC*H*$_2$), 7.01 (4H, d, $^3J_{HH}$ = 8, ArH), 7.21 (4H, d, $^3J_{HH}$ = 9, ArH). IR (nujol) cm^{-1} = 3016w, 2922w, 2854w, 1602w, 1498vs, 1457w, 1407w, 1378w, 1293vs, 1246vs, 1155w, 1034w, 875w, 823m, 654w, 612w, 521m).

9.2.75 Preparation of bis(p-toly)triazanatodichlorosilicon (33). Sodium bis(p-tolylphenyl)triazanate (1.356 g, 4.25 mmol) was dissolved in THF (20 mL) and treated with $SiCl_4$ (0.49 mL, 4.25 mmol) dropwise giving an immediate precipitation. The resultant red suspension was stirred for 2 hrs and filtered. The red filtrate solution

was concentrated to approximately 5 mL and treated with diethyl ether (10 mL) and stored at −28°C for 24 hrs to give red needle crystals. The crystals were filtered and dried under vacuum. (Mass: 1.007 g, 66 % yield relative to sodium bis(p-tolyl)triazenide). ^{1}H-NMR (400 MHz; C_6D_6) δ / [ppm] = 1.98 (6H, s, C*H*$_3$), 2.19 (6H, s, C*H*$_3$), 6.78 (4H, d, $^{3}J_{HH}$ = 8.5, ArH), 7.12 (4H, d, $^{3}J_{HH}$ = 8.5, ArH), 7.41 (4H, d, $^{3}J_{HH}$ = 8.5, ArH), 8.12 (4H, d, $^{3}J_{HH}$ = 8.5, ArH). IR (nujol) cm^{-1} = 3033vw, 2923vs, 2854s, 1581vw, 1507s, 1461m, 1379m, 1314vs, 1248s, 1198m, 1170m, 1109vw, 1017vw, 861vw, 815s, 773w, 650m, 608m, 575w).

9.2.76 Preparation of bis(p-methoxyphenyl)triazanatodichlorosilicon (32). The same procedures for bis(p-tolyl)triazene, sodium bis(p-toly)triazanate and bis(p-toly)triazanatodichlorosilicon were applied using p-methoxyphenylamine to prepare bis(p-methoxyphenyl)triazanatodichlorosilicon. (Mass: 0.825 g, 48 % yield relative to sodium bis(p-methoxyphenyl)triazenide). ^{1}H-NMR (400 MHz; C_6D_6) δ / [ppm] = 3.07 (6H, s, C*H*$_3$), 3.26 (6H, s, C*H*$_3$), 6.49 (4H, d, $^{3}J_{HH}$ = 8.5, ArH), 6.50 (4H, d, $^{3}J_{HH}$ = 8.5, ArH), 7.34 (4H, d, $^{3}J_{HH}$ = 8.5, ArH), 8.00 (4H, d, $^{3}J_{HH}$ = 8.5, ArH).

9.2.77 Preparation of (PPN)bis(1-methyltetrazole)triazanate (34). NaOH (10.261 g, 0.257 mol) and 5-aminotetrazole hydrate (25.156 g, 0.250 mol) were added to a two-necked RB flask and dissolved in H_2O (60 mL) to give a colourless solution. A condenser and a dropping funnel were attached to the RB flask, and the flask heated in an oil bath at a temperature of 95°C. Dimethylsulfate (12.5 mL, 0.132 mol) was added to the dropping funnel and added dropwise to the colourless solution over a period of 20 mins. After addition, the solution was stirred for 1 hr at 95°C at which point the solution was allowed to cool to room temperature. On cooling, small, fluffy, white crystals of 1-methyl-5-aminotetrazole (3.960 g, 40 mmol) had precipitated out of the solution which were filtered, washed with H_2O (2 x 10 mL) and dried. 1-methyl-5-aminotetrazole was suspended in H_2O (60 mL) and cooled in an ice-water bath and treated with aqueous HCl (3.60 mL, 35 %) giving a colourless solution. $NaNO_2$ (1.359 g, 19 mmol) was dissolved in water (40 mL), cooled in an ice-water bath and added dropwise to the acidified 1-methyl-5-aminotetrazole solution giving a pale yellow solution and a fluffy white solid. The suspension was stirred for 15 mins in an ice-water bath and then for 16 hrs at room temperature. After this time, a spongy white

solid floating on a pale yellow solution had formed. The solid was filtered off and treated with a 30°C aqueous solution of NaOH (0.760 g, 19 mmol) giving a clear, yellow solution. To the warm pale yellow solution, a solution of (PPN)Cl (5.453 g, 9.5 mmol) dissolved in water at 60°C was added slowly giving an immediate shiny yellow precipitate. The suspension was stirred for a further 5 hrs and the yellow solid was filtered off. The solid was dissolved in warm acetonitrile and stored at −28°C to give large, yellow, prismatic crystals of (PPN)bis(1-methyltetrazole)triazanate. (Mass: 1.296 g, 29 % relative to (PPN)Cl). Elem. Anal: Calc: C, 64.02; H, 4.99; N, 23.12. Found: C, 63.96; H, 5.01; N, 23.01). ^{1}H-NMR (400 MHz; $CDCl_3$) δ / [ppm] = 2.02 (3H, s, C*H*$_3$CN), 4.05 (6H, s, NC*H*$_3$), 7.41-7.52 (26H, m, ArH), 7.66 (7H, m, ArH). IR (nujol) cm^{-1} = 3061vw, 2925vs, 2854s, 2245vw, 2052vw, 1831vw, 1588w, 1438m, 1287s, 1190vw, 1112w, 1042vw, 997w, 868vw, 749s, 724s, 606vw, 535s).

9.2.78 Attempted preparation of bis(1-methyltetrazole)triazantotrichlorostanane. A Schlenk tube was charged with **34** and suspended in acetonitrile giving a yellow suspension. $SnCl_4$ was added to the suspension dropwise and the solid material dissolved. The solution was stirred for 16 hrs and then the solvent was evaporated in *vacuo* to give a sticky yellow residue. The residue was dissolved in THF and treated with an equal volume of diethyl ether precipitating a white solid. This solid was filtered off and discarded and the solution evaporated to give a yellow oil.

9.2.79 Preparation of 1-(phenylmethylene)aminotetrazole (35). Hydrazine hydrate (17.5 mL, 0.36 mol) was dissolved in EtOH (100 mL) in a RB flask fitted with a condenser. The flask was heated in an oil bath at 85°C and benzaldehyde (12.760 g, 0.120 mol) was added dropwise to the solution over a period of 20 mins. The oil bath temperature was increased by a further 10°C and the solution was stirred for 90 mins. After which, the solution was cooled to room temperature and added to water (200 mL) and dichloromethane (350 mL). The two layers that formed were separated and the aqueous layer extracted with dichlormethane (1 x 100 mL and 1 x 50 mL). The organic layers were combined and dried with $MgSO_4$ and evaporated *in vacuo* to give benzylhydrazone as a yellow oil. Benzylhydrazone, sodium azide (9.395 g, 0.144 mol) and triethylorthoformate (36 mL, 0.22 mol) were combined in a RB flask. Acetic acid (140 mL) was added to the mixture and the flask was heated in an oil bath at 85°C. The suspension was stirred and after 15 mins of stirring the sodium azide had dissolved and

the solution turned red. After a further 16 hrs of stirring the red solution was allowed to cool to room temperature inducing the precipitation of a thick sticky solid. The mixture was slowly added to water giving an immediate yellow precipitate. This new suspension was stirred for 1 hr and the yellow solid was filtered and washed with H_2O (3 x 50 mL). The yellow solid was dissolved in diethyl ether (250 mL) and dried with $MgSO_4$. The solvent was removed *in vacuo* and the resultant yellow solid was recrystallized in ethyl acetate. (Mass: 7.709 g, 0.045 mol, 38 % yield with respect to benzaldehyde. ^{1}H-NMR (400 MHz; $CDCl_3$) δ / [ppm] = 7.49-7.66 (3H, m, ArH), 7.86-7.97 (2H, m, ArH), 8.91 (1H, s, NCH) 9.33 (1H, s, NH). IR (nujol) cm^{-1} = 3141w, 1601m, 1576w, 1449m, 1314w, 1218m, 1150w, 1071m, 991m, 876w, 755m, 690m, 593w).

9.2.80 Preparation of 1-(phenylmethylene)amino-5-methyltetrazole (36). The same procedure for 1-(phenylmethylene)aminotetrazole was applied using triethylorthoacetate to prepare 1-(phenylmethylene)amino-5-methyltetrazole. (Mass = 13.928 g, 74.4 mmol, 16 % yield with respect to benzaldehyde. ^{1}H-NMR (400 MHz; $CDCl_3$) δ / [ppm] = 2.73 (3H, s, C*H*$_3$), 7.51-7.66 (3H, m, ArH), 7.91-7.99 (2H, m, ArH), 9.33 (1H, s, N=C*H*). IR (nujol) cm^{-1} = 3050vw, 1610m, 1538w, 1246vw, 1207w, 1114m, 1072vw, 997m, 758vs, 691vs, 601m).

9.2.81 Preparation of 1-aminotetrazole (37). 1-(phenylmethylene)aminotetrazole (5.868 g, 33.9 mmol) was suspended in H_2O (90 mL) and treated with HCl (45 mL, 35 %). The suspension was heated in an oil bath at 105°C and stirred for 1 hr. Vacuum distillation apparatus was attached to the reaction vessel and the mixture was distilled under vacuum. The mixture distilled at a head temperature of 46°C and a pressure of 0.11 bar. When the solvent had been distilled off, water (100 mL) and HCl (50 mL, 35 %) were added to the distillation sump and the distillation repeated. After distillation was complete further water (100 mL) and HCl (50 mL) were added to the distillation sump and the distillation repeated. The distillation sump, a thick, orange oil, was dissolved in water giving a turbid solution. The solution was filtered to give a clear yellow solution which was neutralised with aqueous ammonia. The solution was evaporated *in vacuo* and the residue was dissolved in dichloromethane (50 mL) and water (50 mL) and separated. The orange organic layer was dried with $MgSO_4$ and evaporated to give a yellow oil. (Mass: 0.298 g, 11 % relative to 1-

benzylideneaminotetrazole). ^{1}H-NMR (400 MHz; d^{6}-DMSO) δ / [ppm] 7.13 (2H, s, N*H*$_2$), 9.27 (1H, s, C*H*); IR (thin film) cm^{-1} = 3568vw, br, 3448vw, br, 3332vs, 3199s, 3146s, 1628m, 1390vw, 1430w, 1272w, 1186s, 1100vs, 966m, 874w, 799vw, 723w, 645s).

9.2.82 Preparation of 1-amino-5-methyltetrazole (38). The same procedure for 1-aminotetrazole was applied using 1-(phenylmethylene)amino-5-methyltetrazole. However, on storage of a concentrated dichloromethane solution at −28°C overnight afford small, colourless block crystals. (Mass: 0.125 g, 6 % relative to 1-benzylideneamino(5-methyl)tetrazole); ^{1}H-NMR (400 MHz; d^{6}-DMSO) 2.42 (3H, s, C*H*$_3$), 6.85 (2H, s, N*H*$_2$). IR (nujol) cm^{-1} = 3307m, br, 3224m, br, 1581vw, 1264m, 1161w, 1014w, 926w, 800w, 740m, 665m).

10. REFERENCES

1 W. Jensen, *J. Chem. Educ.*, 2006, **83**, 1751–1752.

2 G. N. Lewis, *Valence and the Structure of Atoms and Molecules*, The Chemical Catolgue Company, New York, NY, 1923.

3 I. Langmuir, *Science*, 1921, **54**, 59–67.

4 R. E. Rundle, *J. Am. Chem. Soc.*, 1947, **69**, 1327–1331.

5 G. Pimentel, *J. Chem. Phys.*, 1951, **19**, 446–448.

6 J. I. Musher, *Angew. Chem. Int. Ed.*, 1969, **8**, 54–68.

7 R. J. Gillespie and B. Silvi, *Coord. Chem. Rev.*, 2002, **233**, 53–62.

8 N. V. Sidgwick, *The Electronic Theory of Valence*, Oxford: Clarendon, 1927.

9 A. F. Holleman and E. Wiberg, *Inorganic Chemistry*, Academic Press: San Diego, 2001.

10 R. S. Drago, *J. Chem. Phys.*, 1958, **62**, 353–357.

11 P. Schwerdtfeger, G. A. Heath, M. Dolg and M. A. Bennet, *J. Am. Chem. Soc.*, 1992, **114**, 7518–7527.

12 T. M. Klapötke, *Chemistry of High-Energy Materials*, De Gruyter, 3rd edn., 2015.

13 A. K. Sikder and N. Sikder, *J. Hazard. Mater.*, 2004, **112**, 1–15.

14 P. F. Pagoria, G. S. Lee, A. R. Mitchell and R. D. Schmidt, *Thermochim. Acta*, 2002, **384**, 187–204.

15 S. Zhang, Q. Yang, X. Liu, X. Qu, Q. Wei, G. Xie, S. Chen and S. Gao, *Coord. Chem. Rev.*, 2015, **307**, 292–312.

16 R. P. Singh, R. D. Verma, D. T. Meshri and J. M. Shreeve, *Angew. Chem. Int. Ed.*, 2006, **45**, 3584–3601.

17 C. Ye, J. Xiao, B. Twamley and J. M. Shreeve, *Chem. Commun.*, 2005, **21**, 2750–2752.

18 T. M. Klapötke, P. Mayer, J. Stierstorfer and J. J. Weigand, *J. Mater. Chem.*, 2008, **18**, 5248–5258.

19 M. Göbel, K. Karaghiosoff and T. M. Klapötke, *Angew. Chem. Int. Ed.*, 2006, **45**, 6037–6040.

20 K. C. Patil, C. Nesamani and V. R. Verneker, *Synth. React. Inorg. Met. Chem.*, 1982, **12**, 383.

21 K. K. Narang, M. K. Singh, K. B. Singh and R. A. Lal, *Synth. React. Inorg. Met. Chem.*, 1996, **26**, 573.

22 B. D. Wu, L. Yang, S. W. Wang, T. L. Zhang, J. G. Zhang, Z. N. Zhou and K. B. Yu, *Zeitschrift fur Anorg. Allg. Chem.*, 2011, **637**, 450–455.

23 J. A. Ladd and W. J. Orville-Thomas, *Spectrochim. Acta*, 1966, **22**, 919.

24 T. Curtius, *Berichte der Dtsch. Chem. Gesellschaft*, 1890, **23**, 2023.

25 US: 858904 19070702, 1907.

26 E. H. Eyster, *J. Chem. Phys.*, 1940, **8**, 135.

27 V. R. Schomaker and A. Spurr, *J. Am. Chem. Soc.*, 1942, **64**, 1184.

28 J. Evers, M. Göbel, B. Krumm, F. Martin, S. Medvedyev, G. Oehlinger, F. X. Steemann, I. Troyan, T. M. Klapötke and M. I. Eremets, *J. Am. Chem. Soc.*, 2011, **133**, 12100–12105.

29 W. Beck, W. Becker, K. F. Chew, W. Derbyshire, N. Logan, D. M. Revitt and D. B. Sowerby, *J. Chem. Soc., Dalton. Trans.*, 1972, 245–247.

30 V. Luzzati, *Acta Crystallogr.*, 1951, **4**, 120.

31 D. R. Allan, W. G. Marshall, D. J. Francis, I. D. H. Oswald, C. R. Pulham and C. Spanswick, *Dalton. Trans.*, 2010, **39**, 3736–43.

32 I. J. Dagley and R. J. Spear, *Organic Energetic Compounds*, Nova Science Publishers Inc., 1996.

33 W. P. Fehlhammer and W. Beck, *Z. Anorg. Allg. Chem.*, 2013, **639**, 1053–1082.

34 P. Portius and M. Davis, *Coord. Chem. Rev.*, 2013, **257**, 1011–1025.

35 C. C. Addison, N. Logan, S. C. Wallwork and C. D. Garner, *Q. Rev. Chem. Soc.*, 1971, **25**, 289–322.

36 H. Ostmark, S. Wallin, T. Brinck, P. Carlqvist, R. Claridge, E. Hedlund and L. Yudina,

Chem. Phys. Lett., 2003, **379**, 539–546.

37 I. Kobrsi, W. Zheng, J. E. Knox, M. J. Heeg, H. B. Schlegel and C. H. Winter, *Inorg. Chem.*, 2006, **45**, 8700–8710.

38 E. S. Andreiadis, R. Demadrille, D. Imbert, J. Pecaut and M. Mazzanti, *Chem. Eur. J.*, 2009, **15**, 9458–9476.

39 M. Seredyuk, L. Pineiro-Lopez, M. C. Munoz, F. J. Martinez-Casado, G. Molnar, J. A. Rodriguez-Velamazan, A. Bousseksou and J. A. Real, *Inorg. Chem.*, 2015, **54**, 7424–7432.

40 Z. Du, Y. Zhang, Z. Han and Q. Yao, *Propellants, Explos. Pyrotech.*, 2015, **40**, 954–959.

41 K. O. Christe, *Propellants, Explos. Pyrotech.*, 2007, **32**, 194–204.

42 E. W. Abel and I. D. H. Towle, *J. Organomet. Chem.*, 1978, **155**, 299–306.

43 D. Mackay and D. D. McIntyre, *Can. J. Chem.*, 1982, **60**, 990–999.

44 D. Mackay, D. D. Mcintyre and N. J. Taylor, *J. Org. Chem.*, 1982, **442**, 532–535.

45 J. Beck and J. Strähle, *Angew. Chem. Int. Ed.*, 1985, **24**, 409–410.

46 J. Beck and J. Strähle, *Angew. Chem. Int. Ed.*, 1988, **27**, 896–901.

47 J. Leman, A. Barron, J. Ziller and R. Kren, *Polyhedron*, 1989, **8**, 1909–1912.

48 J. Braddock-Wilking, J. T. Leman, C. T. Farrar, S. C. Larsen, D. J. Singel and A. R. Barren, *J. Am. Chem. Soc.*, 1995, **117**, 1736–1745.

49 R. E. Cowley, J. Elhaïk, N. A. Eckert, W. W. Brennessel, E. Bill and P. L. Holland, *J. Am. Chem. Soc.*, 2008, **130**, 6074–6075.

50 S. J. Bonyhady, S. P. Green, C. Jones, S. Nembenna and A. Stasch, *Angew. Chem. Int. Ed.*, 2009, **48**, 2973–2977.

51 S. Gondzik, S. Schulz, D. Bläser, C. Wölper, R. Haack and G. Jansen, *Chem. Commun.* , 2014, **50**, 927–9.

52 J. A. Bellow, P. D. Martin, R. L. Lord and S. Groysman, *Inorg. Chem.*, 2013, **52**, 12335–12337.

53 T. M. Klapoetke, N. K. Minar and J. Stierstorfer, *Polyhedron*, 2009, **28**, 13–26.

54 P. Portius, A. C. Filippou, G. Schnakenburg, M. Davis and K.-D. Wehrstedt, *Angew. Chem. Int. Ed.*, 2010, **49**, 8013–6.

55 A. C. Filippou, P. Portius and G. Schnakenburg, *J. Am. Chem. Soc.*, 2002, **124**, 12396–7.

56 B. Lyhs, D. Blaser, C. Wolper, S. Schulz and G. Jansen, *Inorg. Chem.*, 2012, **51**, 5897–5902.

57 B. Lyhs, G. Jansen, D. Bläser, C. Wölper and S. Schulz, *Chem. Eur. J.*, 2011, **17**, 11394–11398.

58 R. A. Fischer, A. Miehr, H. Sussek, H. Pritzkow, E. Herdtweck, J. Muller, O. Ambacher and T. Metzger, *Chem. Commun.*, 1996, **2**, 2685–2686.

59 U. Müller and H. Bärnighausen, *Acta Crystallogr. Sect. B Struct. Crystallogr. Cryst. Chem.*, 1970, **26**, 1671–1679.

60 U. Muller and W. Kolitsch, *Spectrochim. Acta*, 1975, **31**, 1455–1461.

61 C. C. Addison and N. Logan, *Adv. Inorg. Radiochem.*, 1964, 71–142.

62 J. Muller, *J. Organomet. Chem.*, 1973, **51**, 119.

63 W. Beck, W. Becker, K. F. Chew, W. Derbyshire, N. Logan, D. M. Revitt and D. B. Sowerby, *J. Chem. Soc., Dalton. Trans.*, 1973, 119.

64 M. A. Healy and A. Morris, *Spectrochim. Acta*, 1975, **31A**, 1695–1697.

65 A. J. Arduengo, M. Kline and R. L. Harlow, *J. Am. Chem. Soc.*, 1991, **113**, 361–363.

66 M. Denk, R. K. Hayashi and R. West, *J. Am. Chem. Soc.*, 1994, **116**, 10813–10814.

67 A. J. Arduengo III, H. Bock, H. Chen, M. Denk, D. a Dixon, J. C. Green, W. a Herrmann, N. L. Jones, M. Wagner, R. West, J. A. C. Soc, A. J. Arduengo, M. De, W. a Herrmanrql, R. Westa and X. J. W. Gocthe-universitbt, *J. Am. Chem. Soc.*, 1994, **116**, 6641–6649.

68 A. J. Arduengo, F. Davidson, H. V. R. Dias, J. R. Goerlich, D. Khasnis, W. J. Marshall and T. K. Prakasha, *J. Am. Chem. Soc.*, 1997, **119**, 12742–12749.

69 B. Gehrhus, P. B. Hitchcock and M. F. Lappert, *Z. Anorg. Allg. Chem.*, 2001, **627**, 1048–1054.

70 F. Antolini, B. Gehrhus, P. B. Hitchcock and M. F. Lappert, *Chem. Commun.*, 2005,

5112–5114.

71 S. Nagendran and H. W. Roesky, *Organometallics*, 2008, **27**, 457–492.

72 Y. Wang, Y. Xie, P. Wei, R. B. King, H. F. Schaefer, P. V. R. Schleyer and G. H. Robinson, *J. Am. Chem. Soc.*, 2008, **130**, 14970–14971.

73 P. V. R. Schleyer and G. H. Robinson, *Science*, 2008, **321**, 1069–1071.

74 R. S. Ghadwal, H. W. Roesky, S. Merkel, J. Henn and D. Stalke, *Angew. Chem. Int.Ed.*, 2009, **48**, 5683–5686.

75 H. Cui, Y. Shao, X. Li, L. Kong and C. Cui, *Organometallics*, 2009, **28**, 5191–5195.

76 A. C. Filippou, O. Chernov and G. Schnakenburg, *Angew. Chem. Int. Ed.*, 2009, **2**, 5687–5690.

77 Y. Wang and G. H. Robinson, *Chem. Commun.*, 2009, **32**, 5201–5213.

78 Y. Mizuhata, T. Sasamori and N. Tokitoh, *Chem. Rev.*, 2010, **110**, 3850.

79 S. S. Sen, H. W. Roesky, D. Stern, J. Henn and D. Stalke, *J. Am. Chem. Soc.*, 2010, **132**, 1123–1126.

80 R. S. Ghadwal, H. W. Roesky, M. Granitzka and D. Stalke, *J. Am. Chem. Soc.*, 2010, **132**, 10018–10020.

81 Y. Wang and G. H. Robinson, *Inorg. Chem.*, 2011, **50**, 12326–12337.

82 Y. Wang and G. H. Robinson, *Dalton. Trans.*, 2012, **41**, 337–345.

83 H. W. Roesky, *J. Organomet. Chem.*, 2013, **730**, 57–62.

84 A. C. Filippou, Y. N. Lebedev, O. Chernov, M. Straßmann and G. Schnakenburg, *Angew. Chem. Int. Ed.*, 2013, **52**, 6974–6978.

85 C. Jones, S. J. Bonyhady, N. Holzmann, G. Frenking and A. Stasch, *Inorg. Chem.*, 2011, **50**, 12315–12325.

86 M. Asay, C. Jones and M. Driess, *Chem. Rev.*, 2011, **111**, 354–396.

87 R. Azhakar, R. S. Ghadwal, H. W. Roesky, H. Wolf and D. Stalke, *Organometallics*, 2012, **31**, 4588–4592.

88 C. C. Addison, *Coord. Chem. Rev.*, 1966, **1**, 58–65.

89 B. M. Gatehouse, S. E. Livingstone and R. S. Nyholm, *J. Chem. Soc*., 1957, 4222–4225.

90 F. A. Miller and C. H. Wilkins, *Anal. Chem.*, 1952, **24**, 1253–1294.

91 S. Mizushima and J. V. Quagliano, *J. Chem. Soc.*, 1953, **75**, 4870–4870.

92 C. C. Addison and W. B. Simpson, *J. Chem. Soc. Dalton. Trans.*, 1961, 598–602.

93 C. D. Garner, D. Sutton and S. C. Wallwork, *J. Chem. Soc.*, 1966, **111**, 1949–1957.

94 C. D. Garner and S. C. Wallwork, *J. Chem. Soc.*, 1966, 1496–1500.

95 C. C. Addison, J. Lewis and R. Thompson, *J. Chem. Soc.*, 1951, 2829–2833.

96 K. O. Christe, C. J. Schack and R. D. Wilson, *Inorg. Chem.*, 1974, **13**, 2811–2815.

97 O. A. Dyachenko, L. O. Atovmyan, N. Shirokova and Y. A. Rosolovskii, *J. Chem. Soc. Chem. Commun.*, 1973, **16**, 595–596.

98 D. Bowler and N. Logan, *J. Chem. Soc. D Chem. Commun.*, 1971, 582–583.

99 G. S. Brownlee, A. Walker, S. C. Nyburg and J. T. Szymanski, *J. Chem. Soc. D., Chem. Commun.*, 1971, 1073.

100 C. R. Guibert and M. D. Marshall, *J. Am. Chem. Soc.*, 1966, **483**, 189–190.

101 B. Field and C. J. Hardy, *J. Chem. Soc.*, 1964, 4428–4434.

102 B. B. M. Gatehouse and R. S. Nyholm, *J. Chem. Soc.*, 1956, 4222–4225.

103 B. B. Field and C. J. Hardy, *J. Chem. Soc.*, 1956, 5278–5281.

104 K. V. Titova and V. Y. Rosolovskii, *Russ. J. Inorg. Chem.*, 1971, **16**, 767–768.

105 G. N. Shirokova and V. Y. Rosolovskii, *Russ. J. Inorg. Chem.*, 1971, **16**, 1106–1109.

106 G. N. Shirokova and V. Y. Rosolovskii, *Russ. J. Inorg. Chem.*, 1971, **16**, 808–811.

107 G. N. Shirokova, S. Zhuk and V. Y. Rosolovskii, *Russ. J. Inorg. Chem.*, 1975, 856–859.

108 B. N. Ivanov-Emin, Z. K. Odinets, S. F. Yushchenko, B. E. Zaitsev and A. I. Ezhov, *Russ. J. Inorg. Chem.*, 1975, **20**, 843–846.

109 O. A. D'yachenko and L. O. Atovmyan, *J. Struct. Chem.*, 1975, **16**, 73–78.

110 G. N. Shirokova, S. Zhuk and V. Y. Rosolovskii, *Russ. J. Inorg. Chem.*, 1976, **21**, 527–529.

111 N. V. Krivtsov, G. N. Shirokova, S. Zhuk and Y. A. Rosolovskii, *Russ. J. Inorg. Chem.*, 1976, **21**, 1409–1410.

112 G. N. Shirokova, S. Zhuk and V. Y. Rosolovskii, *Russ. J. Inorg. Chem.*, 1976, **21**, 1459–1461.

113 A. Guntz and M. Martin, *Bull. Soc. Chim. Fr.*, 1910, **7**, 313.

114 H. H. Morgan, *J. Chem. Soc.*, 1923, **123**, 2901–2907.

115 B. J. Hathaway, D. G. Holah and J. D. Postlethwaite, *J. Chem. Soc.*, 1961, 3215–3218.

116 K. Leschewski, *Chem. Ber.*, 1939, **72**, 1763–1766.

117 C. J. Hardy and B. Field, *J. Chem. Soc. Dalton. Trans.*, 1963, 5130–5134.

118 K. V. Titova and V. Y. Rosolovskii, *Russ. Chem. Bull*, 1970, **19**, 2515–2519.

119 J. D. Archambault, H. H. Sisler and G. E. Ryschkewitsch, *J. Inorg. Nucl. Chem.*, 1961, **17**, 130–134.

120 C. C. Addison, P. M. Boorman and N. J. Logan, *J. Chem. Soc.*, 1966, 1434–1437.

121 M. Schmeisser and K. Braendle, *Angew. Chem.*, 1961, **73**, 388–393.

122 D. Potts, H. D. Sharma, A. J. Carty and A. Walker, *Inorg. Chem.*, 1974, **13**, 1205–1211.

123 J. E. Drake and H. E. Henderson, *J. Inorg. Nucl. Chem.*, 1978, **40**, 137–139.

124 K. W. Bagnall, D. Brown and J. G. H. Du Preez, *J. Chem. Soc.*, 1964, 5523–5525.

125 D. Potts and A. Walker, *Can. J. Chem.*, 1971, **49**, 202–206.

126 D. Potts and A. Walker, *Can. J. Chem.*, 1969, **47**, 1621–1626.

127 S. Metz, C. Burschka and R. Tacke, *Organometallics*, 2008, **27**, 6032–6034.

128 I. R. Beattie and G. J. Leigh, *J. Chem. Soc.*, 1961, 4249–4250.

129 C. Eaborn, P. B. Hitchcock, P. D. Lickiss, A. Pidcock and K. D. Safa, *J. Chem. Soc., Dalton. Trans.*, 1984.

130 M. S. Wickleder, F. Gerlach, S. Gagelmann, J. Bruns, M. Fenske and K. Al-Shamery, *Angew. Chem. Int. Ed.*, 2012, **51**, 2199–2203.

131 K. C. Patil, C. Nesamani and V. R. P. A. I. Verneker, *Polyhedron*, 1982, **1**, 421–422.

132 O. S. Bushuyev, G. R. Peterson, P. Brown, A. Maiti, R. H. Gee, B. L. Weeks and L. J. Hope-Weeks, *Chem. Eur. J.*, 2013, **19**, 1706–1711.

133 O. S. Bushuyev, P. Brown, A. Maiti, R. H. Gee, G. R. Peterson, B. L. Weeks and L. J. Hope-Weeks, *J. Am. Chem. Soc.*, 2012, **134**, 1422–1425.

134 S. Li, Y. Wang, C. Qi, X. Zhao, J. Zhang, S. Zhang and S. Pang, *Angew. Chem. Int. Ed.*, 2013, **52**, 14031–14035.

135 J. Zhang and J. M. Shreeve, *Dalton. Trans.*, 2016, 2363–2368.

136 L. C. Gilday, S. W. Robinson, T. A. Barendt, M. J. Langton, B. R. Mullaney and P. D. Beer, *Chem. Rev.*, 2015, **115**, 7118–7195.

137 G. R. Desiraju, *J. Am. Chem. Soc.*, 2013, **135**, 9952–9967.

138 G. R. Desiraju, *J. Chem. Sci.*, 2010, **122**, 667–675.

139 L. Brammer, G. Mínguez Espallargas and S. Libri, *CrystEngComm*, 2008, **10**, 1712.

140 T. Clark, M. Hennemann, J. S. Murray and P. Politzer, *J. Mol. Model.*, 2007, **13**, 291–296.

141 L. Brammer, *Chem. Soc. Rev.*, 2004, **33**, 476–489.

142 D. Braga, L. Brammer and N. R. Champness, *CrystEngComm*, 2005, **7**, 1.

143 E. Corradi, S. V. Meille, M. T. Messina, P. Metrangolo and G. Resnati, *Angew. Chem. Int. Ed.*, 2000, **39**, 1782–1786.

144 E. Wiberg and H. Michaud, *Zeitschrift fur Naturforsch. - Sect. B J. Chem. Sci.*, 1954, **9**, 500–501.

145 K. Hensen, R. Mayr-Stein, B. Spangenberg and M. Bolte, *Acta Crystallogr. Sect. C Cryst. Struct. Commun.*, 2000, **56**, 610–613.

146 M. Bolte and K. Hensen, *J. Chem. Cryst.*, 2000, **30**, 1–5.

147 O. Bechstein, B. Ziemer and D. Hass, *Z. Anorg. Allg. Chem.*, 1990, **582**, 211–216.

148 S. S. Zigler, K. J. Hailer, R. West and M. S. Gordon, *Organometallics*, 1989, **8**, 1656–1660.

149 C. Janiak, *Dalton. Trans.*, 2000, 3885–3896.

150 S. Alvarez, *Dalton. Trans.*, 2013, **42**, 8617–8636.

151 P. V. Simpson, K. Radacki, H. Braunschweig and U. Schatzschneider, *J. Organomet. Chem.*, 2015, **782**, 116–123.

152 G. Cavallo, P. Metrangolo, R. Milani, T. Pilati, A. Priimägi, G. Resnati and G. Terraneo, *Chem. Rev.*, 2016, **116**, 2478–2601.

153 E. V. Lider, O. L. Krivenko, E. V. Peresypkina, A. I. Smolentsev, Y. G. Shvedenkov, S. F. Vasilevskii and L. G. Lavrenova, *Russ. J. Coord. Chem.*, 2007, **33**, 896–907.

154 E. V. Lider, E. V. Peresypkina, L. G. Lavrenova, O. L. Krivenko, E. G. Boguslavskii, A. I. Smolentsev, L. A. Sheludyakova and S. F. Vasilevskii, *Russ. J. Coord. Chem.* , 2009, **35**, 442–453.

155 J. M. Leger, J. Haines and A. Atouf, *J. Phys. Chem. Solids*, 1996, **57**, 7–16.

156 C. W. Moulton and J. G. Miller, *J. Am. Chem. Soc.*, 1956, **78**, 2702–2704.

157 V. I. Kulishov, N. G. Bokii, Y. T. Struchkov, O. M. Nefedov, S. P. Kolesnikov and B. L. Perl'mutter, *J. Struct. Chem.*, 1970, **11**, 61–64.

158 B. Lyhs, D. Blaser, C. Wolper, S. Schulz, R. Haack and G. Jansen, *Inorg. Chem.*, 2013, **52**, 7236–7241.

159 A. C. Filippou, P. Portius, G. Kociok-köhn, A. Chemie, H. Berlin and H. Str, *Chem. Commun.*, 1998, **34**, 2327–2328.

160 A. C. Filippou, R. Steck and G. Kociok-köhn, *Dalton. Communcation*, 1999, **225**, 2267–2268.

161 A. C. Filippou, P. Portius, G. Kociok-Köhn and V. Albrecht, *J. Chem. Soc. Dalton. Trans.*, 2000, 1759–1768.

162 A. E. Ayers, D. S. Marynick and H. V Dias, *Inorg. Chem.*, 2000, **39**, 4147–51.

163 A. E. Ayers, T. M. Klapötke and H. V. R. Dias, *Inorg. Chem.*, 2001, **40**, 1000–1005.

164 V. N. Khrustalev, I. a. Portnyagin, N. N. Zemlyansky, I. V. Borisova, Y. a. Ustynyuk and M. Y. Antipin, *J. Organomet. Chem.*, 2005, **690**, 1056–1062.

165 Y. Xiong, S. Yao and M. Driess, *Chem. Commun.*, 2013, **50**, 418–20.

166 B. Kamenar, *J. Inorg. Nucl. Chem.*, 1962, **24**, 1039–1045.

167 U. Müller, N. Mronga and C. Schumacher, *Zeitschrift fur Naturforsch.*, 1982, **37B**, 1122–1126.

168 U. M. Tripathi, G. L. Wegner, A. Schier, A. Jockisch and H. Schmidbaur, *Zeitschrift fur Naturforsch.*, 1998, **53**, 939–945.

169 Y. Ding, H. Hao, H. W. Roesky, M. Noltemeyer and H. G. Schmidt, *Organometallics*, 2001, **20**, 4806–4811.

170 N. Delhi, K. Rao, M. Kimura, K. Kajita, N. Onoda and S. Morosawa, *J. Org. Chem.*, 1990, **93**, 93–98.

171 R. Campbell, M. F. Davis, M. Fazakerley and P. Portius, *Chem. Eur. J.*, 2015, **21**, 18690–18698.

172 T. G. Müller, F. Karau, W. Schnick and F. Kraus, *Angew. Chem. Int. Ed.*, 2014, **53**, 13695–13697.

173 A. C. Filippou, P. Portius, D. U. Neumann and K. Wehrstedt, *Angew. Chem. Int. Ed.*, 2000, **39**, 4333–4336.

174 T. Ochiai, D. Franz, X.-N. Wu and S. Inoue, *Dalton. Trans.*, 2015, **44**, 10952–10956.

175 K. B. Dillon and A. Marshall, *J. Chem. Soc., Dalton. Trans.*, 1987, 315–317.

176 M. Currie, J. Estager, P. Licence, S. Men, P. Nockemann, K. R. Seddon, M. Swadźba-Kwaśny and C. Terrade, *Inorg. Chem.*, 2013, **52**, 1710–21.

177 H.-W. Fruhauf, *Chem. Rev.*, 1997, **97**, 523–596.

178 V. Aureggi and G. Sedelmeier, *Angew. Chem. Int. Ed.*, 2007, **46**, 8440–8444.

179 P. Portius and M. Davis, *Dalton. Trans.*, 2016, **45**, 17141–17152.

180 B. Gehrhus and M. F. Lappert, *Polyhedron*, 1998, **17**, 999–1000.

181 N. J. Hill, D. F. Moser, I. a. Guzei and R. West, *Organometallics*, 2005, **24**, 3346–3349.

182 A. C. Tomasik, A. Mitra and R. West, *Organometallics*, 2009, **28**, 378–381.

183 R. S. Ghadwal, H. W. Roesky, C. Schulzke and M. Granitzka, *Organometallics*, 2010, **29**, 6329–6333.

184 W. Fraenk, T. Habereder, A. Hammerl, T. M. Klapötke, B. Krumm, P. Mayer, H. Noeth and M. Warchhold, *Inorg. Chem.*, 2001, **40**, 1334–1340.

185 D. M. Khramov and C. W. Bielawski, *Chem. Commun.*, 2005, **10**, 4958–4960.

186 M. Tamm, S. Randoll, T. Bannenberg and E. Herdtweck, *Chem. Commun.*, 2004, **49**, 876–877.

187 M. Tamm, S. Randoll, E. Herdtweck, N. Kleigrewe, G. Kehr, G. Erker and B. Rieger, *Dalton. Trans.*, 2006, **2**, 459–467.

188 D. M. Khramov and C. W. Bielawski, *J. Org. Chem.*, 2007, **72**, 9407–9417.

189 M. Tamm, D. Petrovic, S. Randoll, S. Beer, T. Bannenberg, P. G. Jones and J. Grunenberg, *Org. Biomol. Chem.*, 2007, **5**, 523–530.

190 R. S. Ghadwal, S. S. Sen, H. W. Roesky, G. Tavcar, S. Merkel and D. Stalke, *Organometallics*, 2009, **28**, 6374–6377.

191 H. Staudinger and J. Meyer, *Helv. Chim. Acta*, 1919, **2**, 612–618.

192 R. D. Kroshefsky and J. G. Verkade, *Inorg. Chem.*, 1975, **14**, 3090–3095.

193 H. R. Allcock, *Chemistry and Applications of Polyphosphazenes*, John Wiley & Sons, 2003.

194 H. R. Allcock and R. L. Kugel, *Inorg. Chem.*, 1966, **5**, 1716–1718.

195 H. R. Allcock, R. L. Kugel and K. J. Valan, *Inorg. Chem.*, 1966, **5**, 1709–1715.

196 H. R. Allcock and R. L. Kugel, *J. Am. Chem. Soc.*, 1965, **87**, 4216–4217.

197 W. Buder and A. Schmidt, *Z. Anorg. Allg. Chem.*, 1975, **415**, 263–267.

198 F. D. Henne, A. T. Dickschat, F. Hennersdorf, K. O. Feldmann and J. J. Weigand, *Inorg. Chem.*, 2015, **54**, 6849–6861.

199 P. Portius, P. W. Fowler, H. Adams and T. Z. Todorova, *Inorg. Chem.*, 2008, **47**, 12004–12009.

200 C. Aubauer, T. M. Klapötke, H. Noth, A. Schulz, M. Suter and J. Weigand, *Chem. Commun.*, 2000, **13**, 2491–2492.

201 K. B. Dillon, A. W. G. Platt and T. C. Waddington, *J. Chem. Soc.*, 1981, 2292–2295.

202 K. C. Mondal, S. Roy, B. Maity, D. Koley and H. W. Roesky, *Inorg. Chem.*, 2016, **55**, 163–169.

203 H.-J. Cheng, K. Lippe, E. Kroke, J. Wagler, G. W. Fester, Y.-L. Li, M. R. Schwarz, T. Saplinova, S. Herkenhoff, V. Ischenko and J. Woltersdorf, *Appl. Organomet. Chem.*, 2011, **25**, 735–747.

204 V. Amo, R. Andres, E. de Jesus, J. de la Mata, J. C. Flore, R. Gomez, M. P. Gomez-Sal and J. F. C. Turner, *Organometallics*, 2005, **24**, 2331–2338.

205 A. Kienzle, J. Weidlein, R. Riedel, A. Obermeyer and A. Simon, *Z. Anorg. Allg. Chem.*, 1994, **620**, 1357–1363.

206 G. M. Sheldrick and R. Taylor, *J. Organomet. Chem.*, 1975, **101**, 19–25.

207 C. Aubauer, K. Karaghiosoff, T. M. Klapo, G. Kramer, A. Schulz, J. Weigand and C. Kristallstruktur, *Z. Anorg. Allg. Chem.*, 2001, 2547–2552.

208 H. Sussek, F. Stowasser, H. Pritzkow and R. A. Fischer, *Eur. J. Inorg. Chem.*, 2000, 455–461.

209 W. Honeise, W. Schwarz, G. Heckmann and A. Schmidt, *Z. Anorg. Allg. Chem.*, 1986, **533**, 55–64.

210 M. Seidl, C. Kuntz, M. Bodensteiner, A. Y. Timoshkin and M. Scheer, *Angew. Chem. Int. Ed.*, 2015, **54**, 2771–2775.

211 K. Muralidharan, B. a Omotowa, B. Twamley, C. Piekarski and J. N. M. Shreeve, *Chem. Commun.*, 2005, 5193–5.

212 D. E. Bergbreiter and J. M. Killough, *J. Am. Chem. Soc.*, 1978, **100**, 2126–2134.

213 C. W. So, H. W. Roesky, J. Magull and R. B. Oswald, *Angew. Chem. Int. Ed.*, 2006, **45**, 3948–3950.

214 S. J. Bonyhady, C. Jones, S. Nembenna, A. Stasch, A. J. Edwards and G. J. Mcintyre, *Chem. Eur. J.*, 2010, **9**, 938–955.

215 B. L. Tran, J. Krzystek, A. Ozarowski, C. H. Chen, M. Pink, J. A. Karty, J. Telser, K. Meyer and D. J. Mindiola, *Eur. J. Inorg. Chem.*, 2013, 3916–3929.

216 K.-M. Lin, P.-Y. Wang, Y.-J. Shieh, H.-Z. Chen, T.-S. Kuo and Y.-C. Tsai, *New J. Chem.*, 2010, **34**, 1737.

217 Y. Yu, A. R. Sadique, J. M. Smith, T. R. Dugan, R. E. Cowley, W. W. Brennessel, C. J. Flaschenriem, E. Bill, T. R. Cundari and P. L. Holland, *J. Am. Chem. Soc.*, 2008, **21**,

6624–6638.

218 T. Böttcher, S. Steinhauer, B. Neumann, G. Stammler, G.-V. Röschenthaler and B. Hoge, *Chem. Commun.*, 2014, 6204–6207.

219 M. Driess, S. Yao, M. Brym, C. Van Wüllen and D. Lentz, *J. Am. Chem. Soc.*, 2006, **128**, 9628–9629.

220 O. Schuster, L. Yang, H. G. Raubenheimer and M. Albrecht, *Chem. Rev.*, 2009, **109**, 3445–3478.

221 Y. Tang, H. Yang, J. Shen, B. Wu, X. Ju, C. Lu and G. Cheng, *New J. Chem.*, 2012, **36**, 2447.

222 Y. Tang, H. Yang, B. Wu, X. Ju, C. Lu and G. Cheng, *Angew. Chem. Int. Ed.*, 2013, **52**, 4875–4877.

223 Q. Zhang and J. M. Shreeve, *Angew. Chem. Int. Ed.*, 2013, **52**, 8792–8794.

224 C. M. Fitchett, C. Richardson and P. J. Steel, *Org. Biomol. Chem.*, 2005, **3**, 498–502.

225 P. Portius, M. Davis, R. Campbell, F. Hartl, Q. Zeng, A. J. H. M. Meijer and M. Towrie, *J. Phys. Chem. A*, 2013, **117**, 12759–12769.

226 T. Schroer, R. Haiges, S. Schneider and K. O. Christe, *Chem. Commun.*, 2005.

227 H. Ostmark, S. Wallin, T. Brinck, P. Carlquist, R. Claridge, E. Hedlund and L. Yudina, *Chem. Phys. Lett.*, 2003, **379**, 539–546.

228 A. Vij, J. G. Pavlovich, W. W. Wilson, V. Vij and K. O. Christe, *Angew. Chem. Int. Ed.*, 2002, **41**, 3051–3054.

229 A. S. Lyakhov, P. N. Gaponik, D. S. Pytleva, S. V. Voitekhovich and L. S. Ivashkevich, *Acta Crystallogr. C*, 2004, **60**, 421–422.

230 T. V. Serebryanskaya, L. S. Ivashkevich, A. S. Lyakhov, O. Gaponik and L. S. Ivashkevich, *Polyhedron*, 2010, **29**, 2844–2850.

231 Martius, *Zeit. fur. Chem.*, 1866, 381.

232 K. Vrieze and G. van Koten, *Comprehensive Coordination Chemistry*, Pergamon Press, 1987.

233 P. N. Gaponik and V. P. Karavai, *Chem. Heterocyl. Compd.*, 1983, **19**, 681–682.

234 I. Hagedorm and H. D. Winkelmann, *Eur. J. Inorg. Chem.*, 1965, **13**, 850–855.

235 R. Raap, *Can. J. Chem.*, 1969, **47**, 3677–3681.

236 T. M. Klapötke and D. G. Piercey, *Inorg. Chem.*, 2011, **50**, 2732–2734.

237 Y. X. Tang, H. W. Yang, B. Wu, X. H. Ju, C. X. Lu and G. Bin Cheng, *Angew. Chem. Int. Ed.*, 2013, **52**, 4875–4877.

238 G. R. Fulmer, A. J. M. Miller, N. H. Sherden, H. E. Gottlieb, A. Nudelman, B. M. Stoltz, J. E. Bercaw and K. I. Goldberg, *Organometallics*, 2010, **29**, 2176–2179.

239 L. M. T. Frija, E. C. B. A. Alegria, M. Sutradhar, M. L. S. Cristiano, A. Ismael, M. N. Kopylovich and A. J. L. Pombeiro, *J. Mol. Catal. A Chem.*, 2016, **425**, 283–290.

240 G. M. Sheldrick, *Acta Crystallogr. A*, 2008, **64**, 112–122.

241 G. M. Sheldrick, *Acta Crystallogr. C*, 2015, **71**, 3–8.

242 A. Martinsen, J. Songstad, R. Larsson, M. Pouchard, P. Hagenmuller and A. F. Andresen, *Acta Chem. Scand.*, 1977, 31a, 645–650.

243 O. M. Nefedov, S. P. Kolesnikov and I. S. Rogozhin, *Russ. Chem. Bull*, 1973, **22**, 2762–2762.

244 L. Hintermann, *Beilstein J. Org. Chem.*, 2007, **3**, 1–5.

245 A. J. Arduengo III, R. Krafczyk, R. Schmutzler, H. A. Craig, J. R. Goerlich, W. J. Marshall and M. Unverzagt, *Tetrahedron*, 1999, **55**, 14523–14534.

246 W. A. Herrmann, V. P. W. Bohm, C. W. K. Gstottmayr, M. Grosche, C.-P. Reisinger and T. Weskamp, *J. Organomet. Chem.*, 2001, **617**, 616–628.

247 J. Prust, K. Most, I. Muller, E. Alexopoulos, A. Stasch, I. Uson and H. W. Roesky, *Zeitschrift fur Anorg. Allg. Chem.*, 2001, **627**, 2032–2037.

248 S. J. Bonyhady, C. Jones, S. Nembenna, A. Stasch, A. J. Edwards and G. J. McIntyre, *Chem. Eur. J.*, 2010, **16**, 938–955.

249 S. P. Green, C. Jones and A. Stasch, *Science*, 2007, **318**, 1754–1757.

11. APPENDIX

11.1 Abbreviations

2c-2e	Two centre-two electron
4c-3e	Four centre-three electron
2c-1e	Two centre-one electron
MO	Molecular orbital
SALCs	Symmetry adapted linear combinations
IPs	Ionisation potentials
IR	Infrared
FT-IR	Fourier Transform Infrared
NMR	Nuclear Magnetic Resonance
WCC	Weakly coordinating cation
PPN	$((Ph_3P)_2N)^+$
py	pyridine
bpy	2,2'-bipyridine
phen	1,10-phenanthroline
FWHM	full width half maximum
NHC	N-heterocyclic carbene
DTA	Differential thermal analysis
TGA	Thermal gravimetric analysis
MOFs	Metal-organic frameworks
CSD	Cambridge Structural Database
DSC	Differential scanning calorimetry
Ad	adamantyl
BPR	Berry pseudo-rotation
DFT	Density functional theory
ATI	*N*-(n-propyl)-2-(n-propylamino)-troponiminate
IPr	1,3-bis(2,6-diisopropylphenyl)imidazol-2-ylidene
(^{dipp}NCN)	1,3-bis(2,6-diisopropylphenyl)-2-(*para*-t-butylphenyl)-amidinate
Nacnac	1,5-β-diketiminate

Np	$CH_2{}^tBu$
dipp	2,6-diisopropylphenyl
mes	2,4,6-trimethylphenyl
I^tBu	1,3-t-butyl-imidazol-2-ylidene
p-dmap	*para*-dimethylaminopyridine
TMEDA	tetramethylethylenediamine
aIPr	abnormal bound IPr
b1mtt	1,3-bis(1-methyltetrazol-5-yl)triazenide
b5mtt	1,3-bis(5-methyltetrazol-1-yl)triazenide
bptt	1,3-bis(*para*-toluidine)triazenide
bpat	1,3-bis(*para*-anisidine)triazenide

11.2 Compound Numbers

1	$Si(NO_3)_4$
2	$(PPN)_2Si(NO_3)_6$
3	$As(NO_3)_3$
4	$AsCl_2(NO_3)$
5	$(PPN)AsCl_2(NO_3)_2$
6	$(3\text{-fluoropyridine})_2Si(N_3)_4$
7	$(3\text{-chloropyridine})_2Si(N_3)_4$
8	$(3\text{-bromopyridine})_2Si(N_3)_4$
9	$(3\text{-iodopyridine})_2Si(N_3)_4$
10	$(1\text{-methyl-3-iodopyridinium})(NO_3)$
11	$(1\text{-methyl-3-bromopyridinium})(NO_3)$
12	$(1\text{-methyl-3-bromopyridinium})_2Ge(NO_3)_6$
13	$(1\text{-methyl-3-bromopyridinium})_2Sn(NO_3)_6$
14a	$(PPh_4)Ge(N_3)_3$
14b	$(PPN)Ge(N_3)_3$
14c	$(AsPh_4)Ge(N_3)_3$
15	$(PPh_4)Ge(N_3)_3$
16	$IPrSi(N_3)_4$
17	$(I^tBuN)_2Si(N_3)_2$

18 $IPrP(N_3)_5$

19 $NaP(N_3)_6 \cdot 6py$

20 $(^{dipp}NCN)Si(N_3)_3$

21 $(^{dipp}NCN)P(N_3)_2$

22 $(^{dipp}NCN)P(N_3)_4$

23 $(^{mes}Nacnac)MgN_3$

24 $(^{dipp}Nacnac)MgN_3$

25 $(^{dipp}NCN)SiH(N_3)_2$

26 $(^{dipp}Nacnac)SiHCl2$

27 $(^{dipp}Nacnac)SiH(N_3)_2$

28 $(^{dipp}NCN)SiH(N_3)_2 \cdot Li(^{dipp}Nacnac)$

29 $(^{dipp}NCN)SiH(N_3)(N(SiMe_3)_2)$

30 $(^{dipp}NCN)SiH(N_3)$(*ab*-IPr)

31 $(IPrH)[(^{dipp}NCN)SiH(N_3)_3]$

32 $(bpat)_2SiCl_2$

33 $(bptt)_2SiCl_2$

34 (PPN)(b1mtt)

35 1-(phenylmethylene)aminotetrazole

36 1-(phenylmethylene)amino-5-methyltetrazole

37 1-aminotetrazole

38 1-amino-5-methyltetrazole

11.3 FT-IR and NMR spectra

Figure 1. FT-IR spectrum of a THF solution containing $IPrSiI_2$ and sodium azide. 262
Figure 2. FT-IR spectrum of a benzene solution containing $IPrSiCl_2$ and sodium azide. 262
Figure 3. FT-IR spectrum of a THF solution containing $IPrSi(N_3)_4$ and KC_8. 263
Figure 4. FT-IR spectrum of a toluene solution containing $(NCN)Si(N_3)_3$ and KC_8....263
Figure 5. FT-IR spectrum of a THF solution containing $IPrP(N_3)_5$ and $(PPh_4)N_3$.....264
Figure 6. IR spectral series of $IPrP(N_3)_5$ and ethereal HN_3 in THF. Black line is before HN_3 addition and red line is after HN_3 addition.....264
Figure 7. FT-IR spectrum of $NaP(N_3)_6 \cdot 6py$ as a nujol mull.....265

Figure 8. FT-IR spectrum of $(PPN)_2Si(NO_3)_6$ as a nujol mull. 265
Figure 9. FT-IR spectrum of $(PPN)AsCl_2(NO_3)_2$ as a nujol mull. 266
Figure 10. FT-IR spectrum of $IPrSi(N_3)_4$ as a nujol mull. 266
Figure 11. FT-IR spectrum of $(^{dipp}NCN)Si(N_3)_3$ as a nujol mull. 267
Figure 12. FT-IR spectrum of oil obtained between the reaction of $(^{dipp}NCN)Si(N_3)_3$ and two equivalents of KC_8 as a nujol mull. 267
Figure 13. FT-IR spectrum of $IPrSi(N_3)_4$ dissolved in acetonitrile. 268
Figure 14. ^{1}H-NMR spectrum of $(NCN)SiH(N_3)_2$ in C_6D_6. 268
Figure 15. ^{1}H-NMR spectrum of $(^{dipp}Nacnac)SiHCl_2$ in $CDCl_3$. 269
Figure 16. ^{1}H-NMR spectrum of $(^{dipp}Nacnac)SiH(N_3)_2$ in $CDCl_3$. 269
Figure 17. ^{1}H-NMR spectrum of $(NCN)SiH(N_3)(N(SiMe_3)_2)$ in C_6D_6. 270
Figure 18. ^{1}H-NMR spectrum of $(NCN)SiH(N_3)_2$(ab-IPr) in C_6D_6. 270
Figure 19. ^{1}H-NMR spectrum of $(NCN)SiH(N_3)_2$·Li(dippNacnac) in C_6D_6. 271

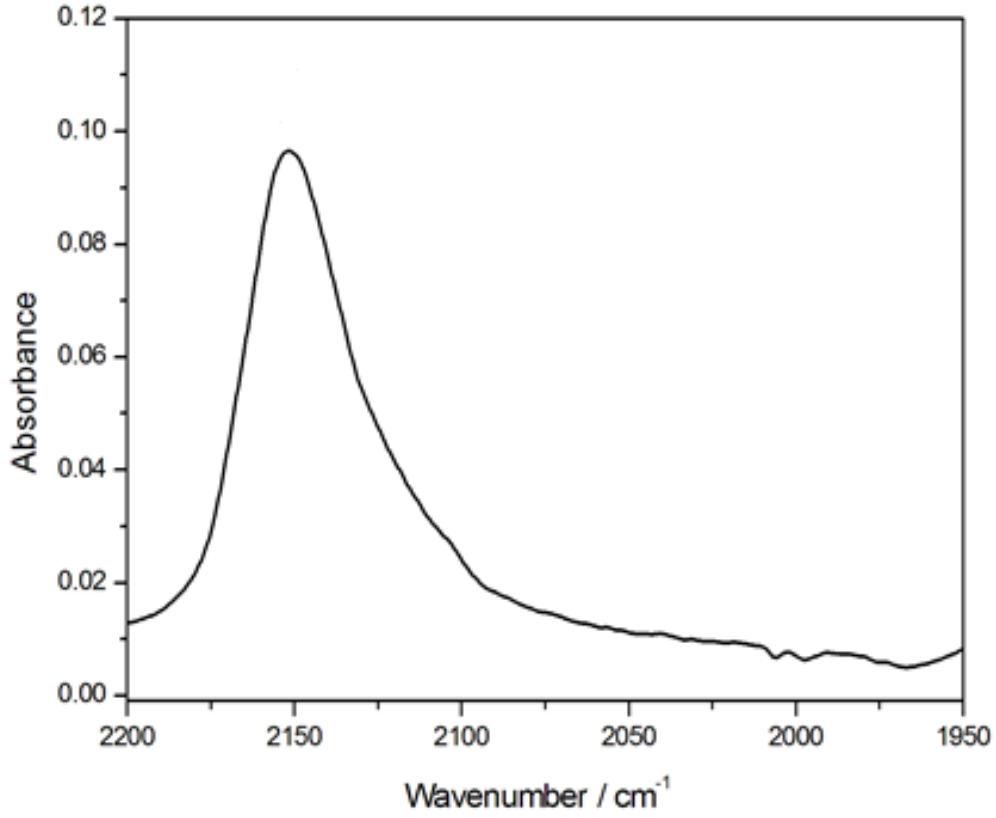

Figure 1. FT-IR spectrum of a THF solution containing $IPrSiI_2$ and sodium azide.

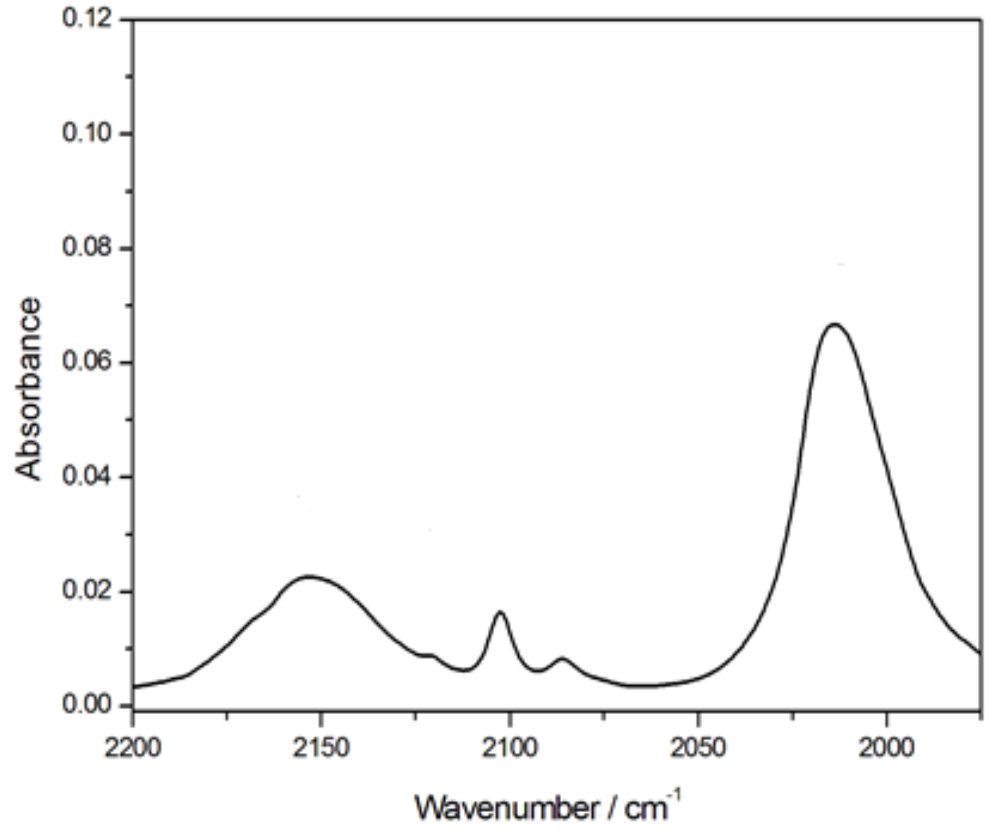

Figure 2. FT-IR spectrum of a benzene solution containing $IPrSiCl_2$ and sodium azide.

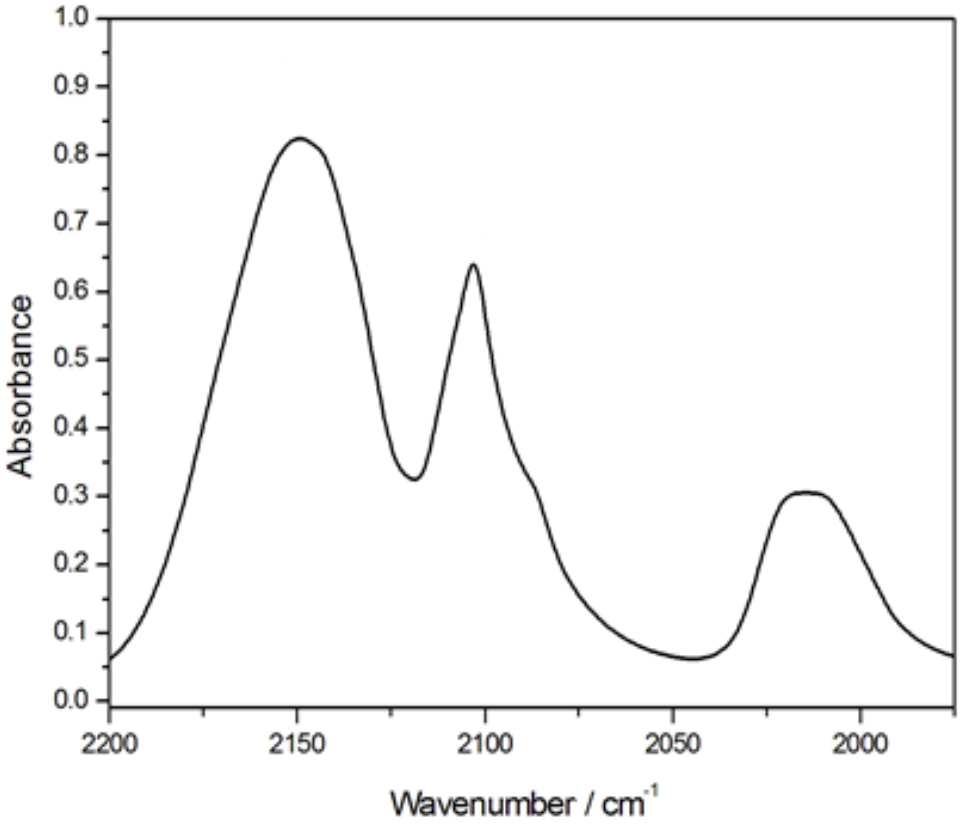

Figure 3. FT-IR spectrum of a THF solution containing $IPrSi(N_3)_4$ and KC_8.

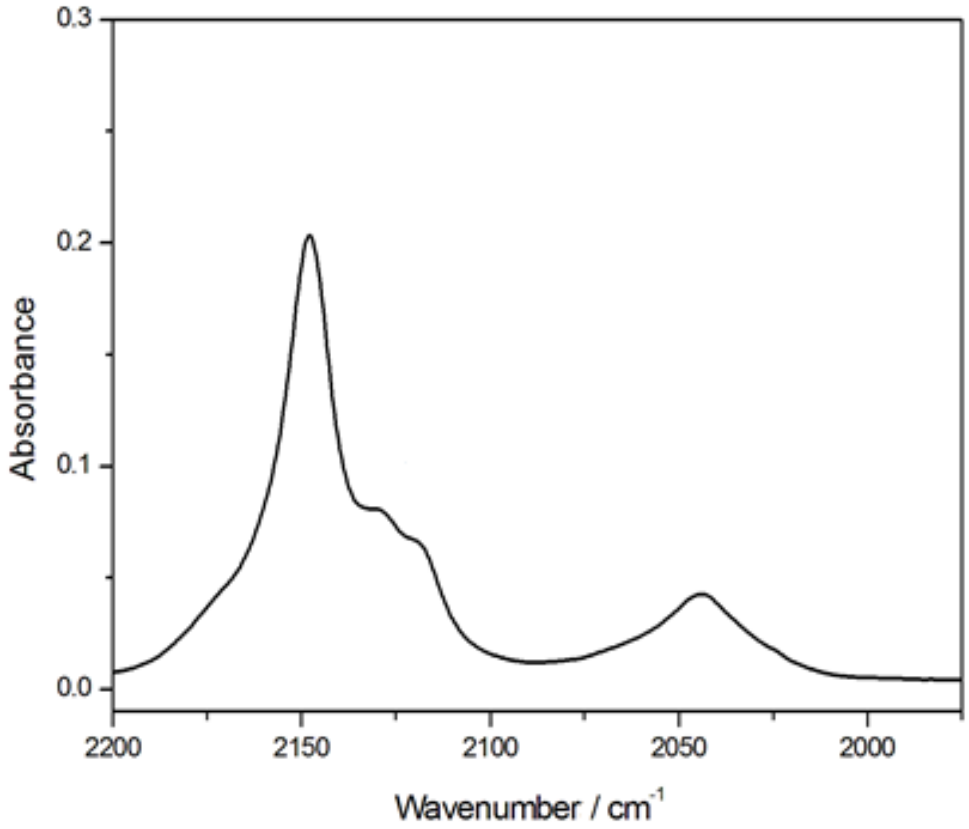

Figure 4. FT-IR spectrum of a toluene solution containing $(NCN)Si(N_3)_3$ and KC_8.

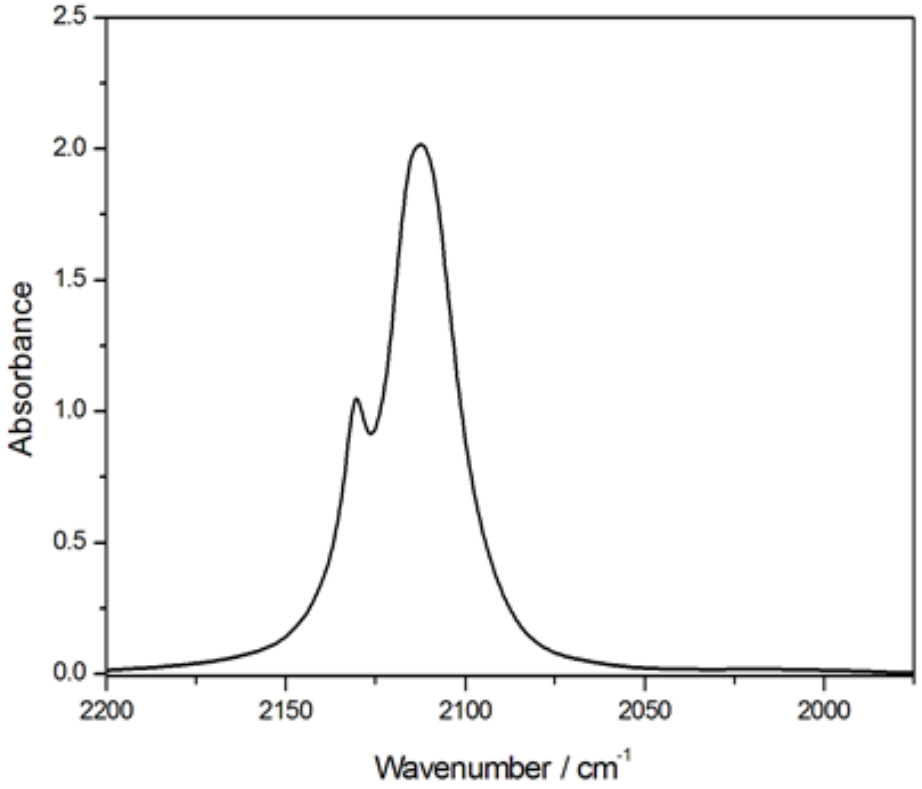

Figure 5. FT-IR spectrum of a THF solution containing $IPrP(N_3)_5$ and $(PPh_4)N_3$.

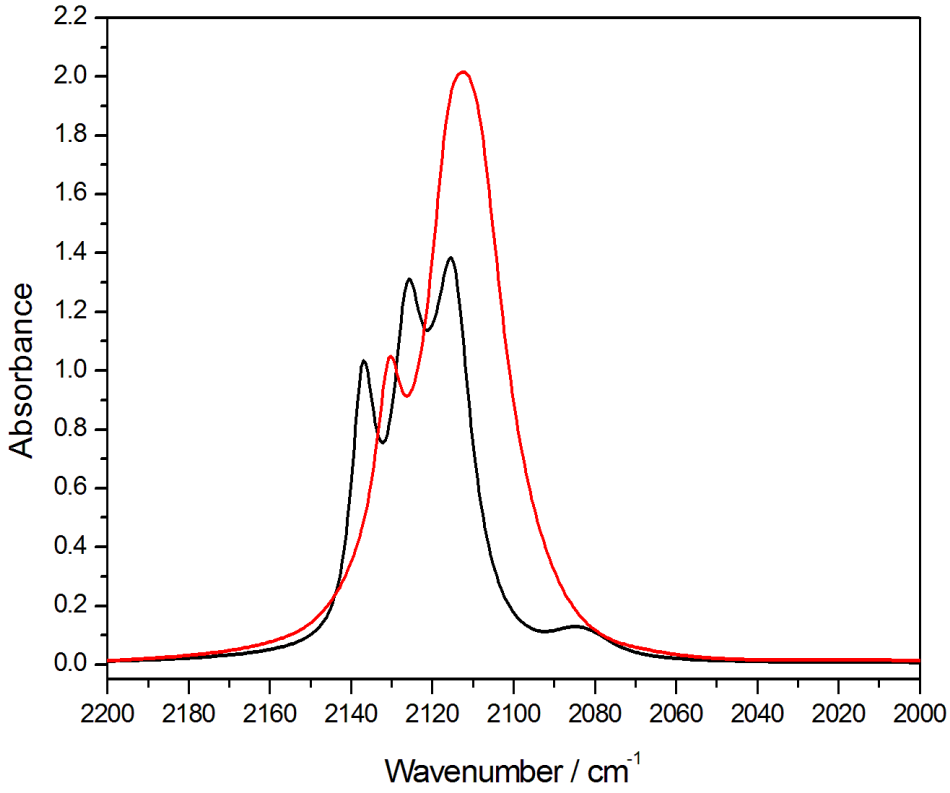

Figure 6. IR spectral series of $IPrP(N_3)_5$ and ethereal HN_3 in THF. Black line is before HN_3 addition and red line is after HN_3 addition.

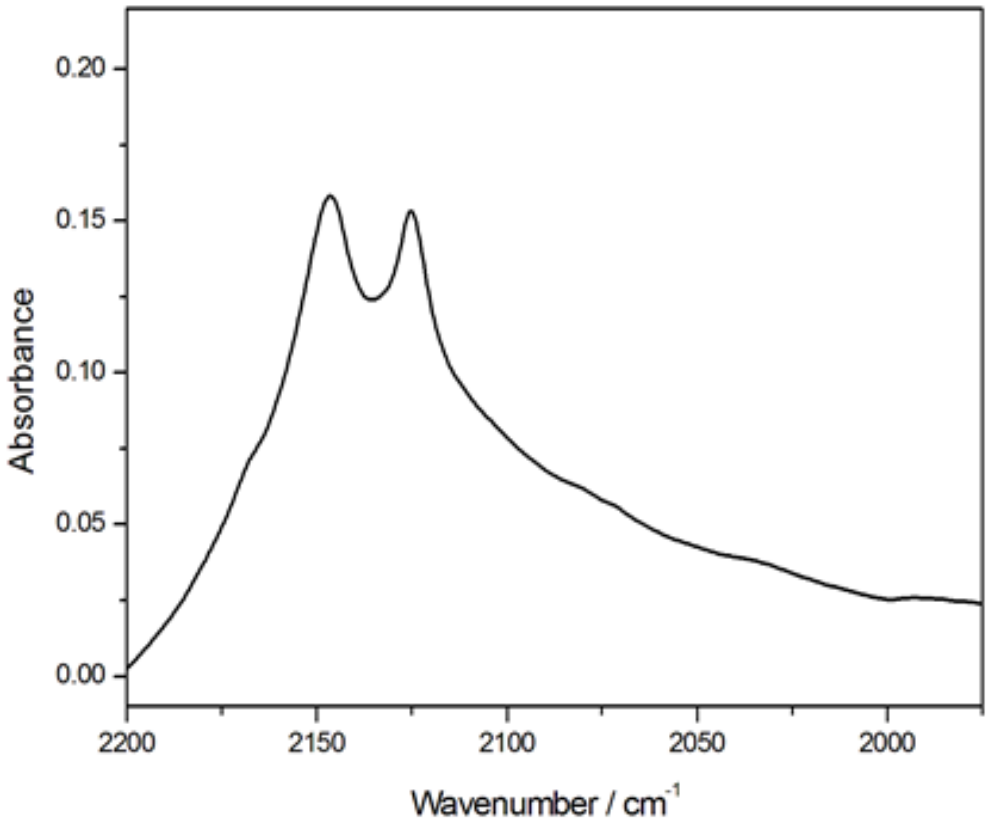

Figure 7. FT-IR spectrum of $NaP(N_3)_6 \cdot 6py$ as a nujol mull.

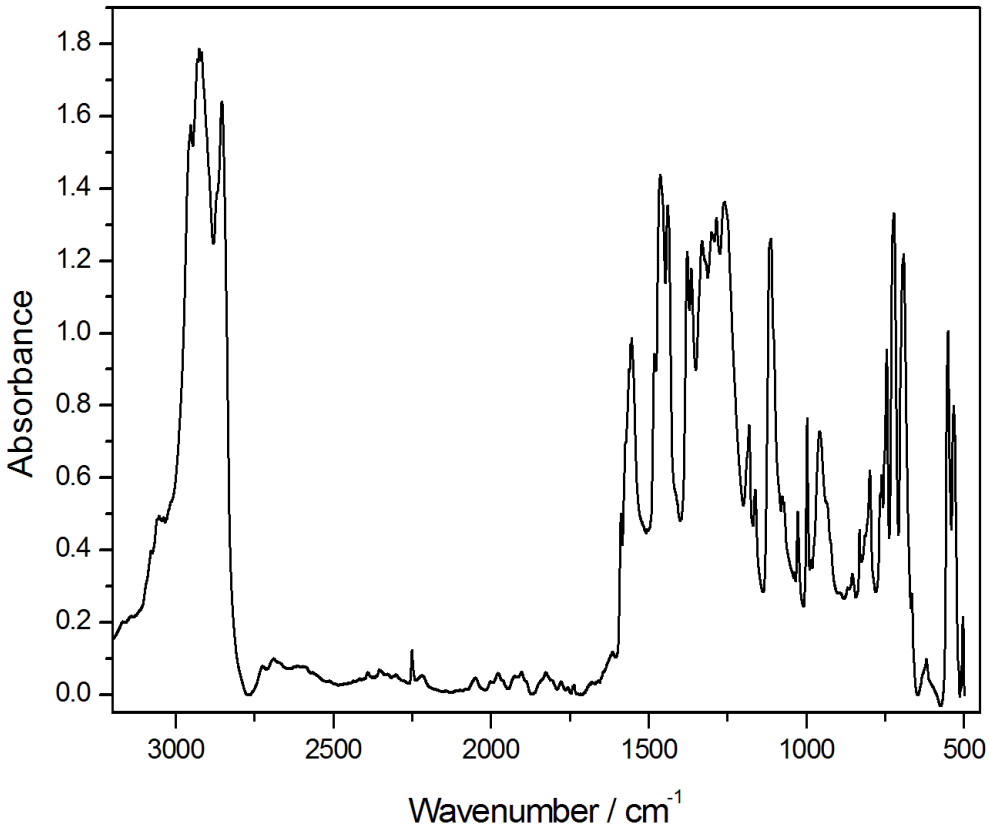

Figure 8. FT-IR spectrum of $(PPN)_2Si(NO_3)_6$ as a nujol mull.

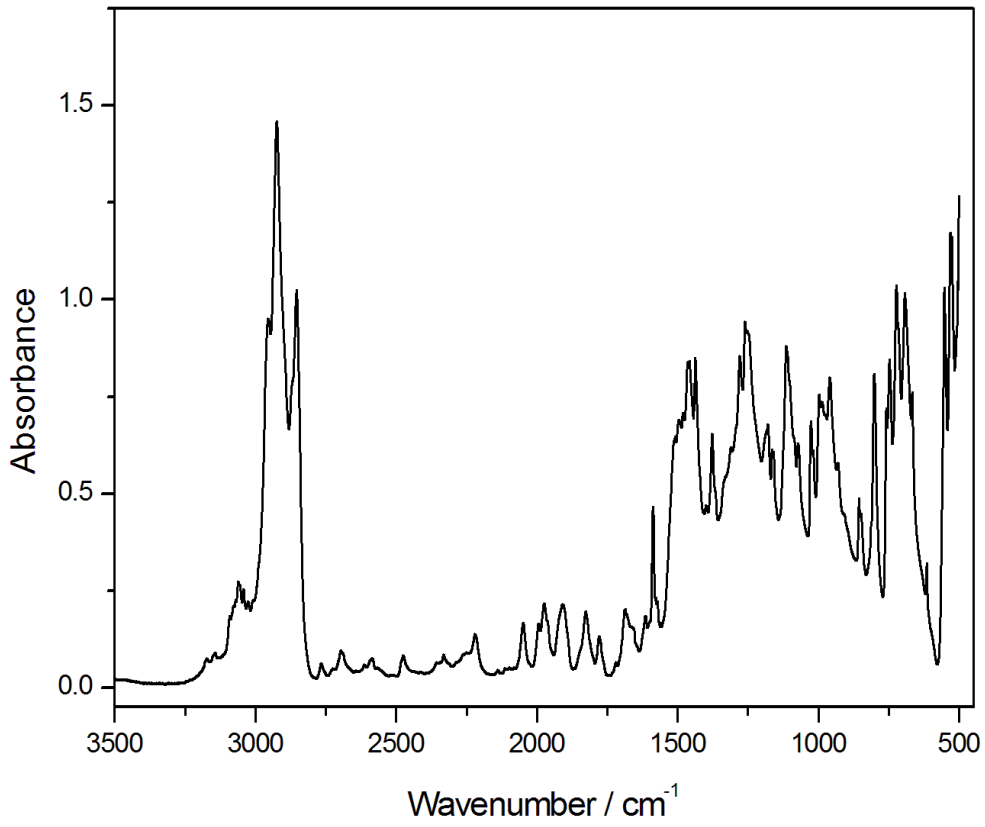

Figure 9. FT-IR spectrum of (PPN)$AsCl_2(NO_3)_2$ as a nujol mull.

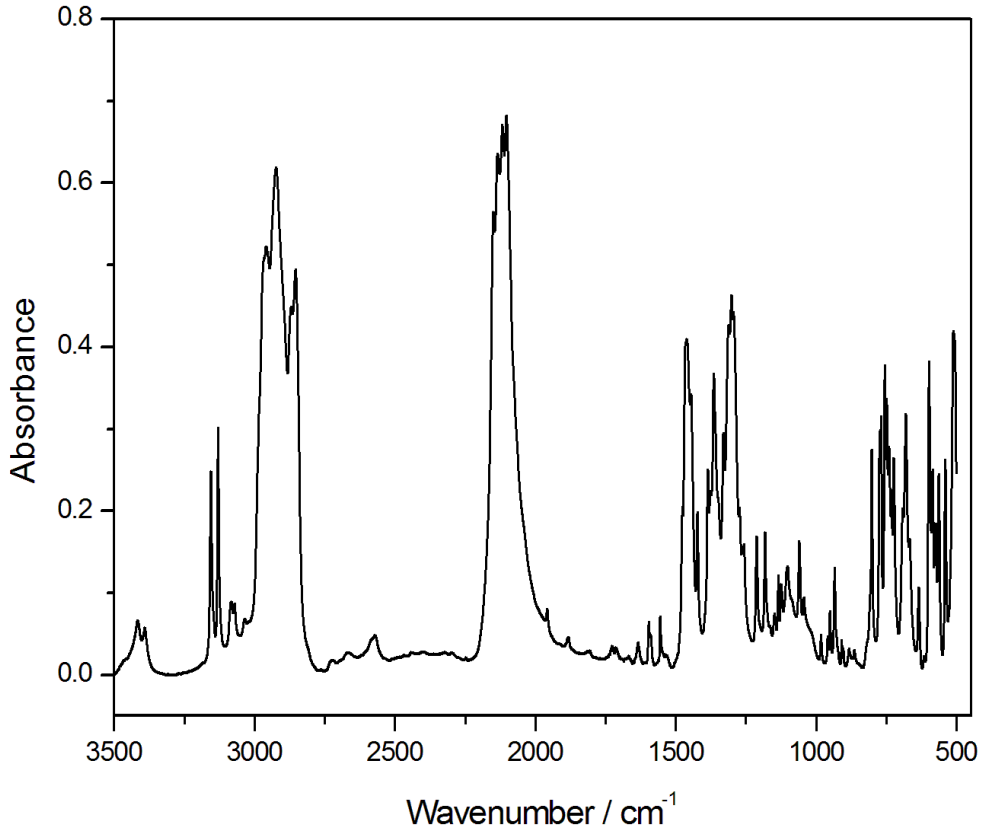

Figure 10. FT-IR spectrum of $IPrSi(N_3)_4$ as a nujol mull.

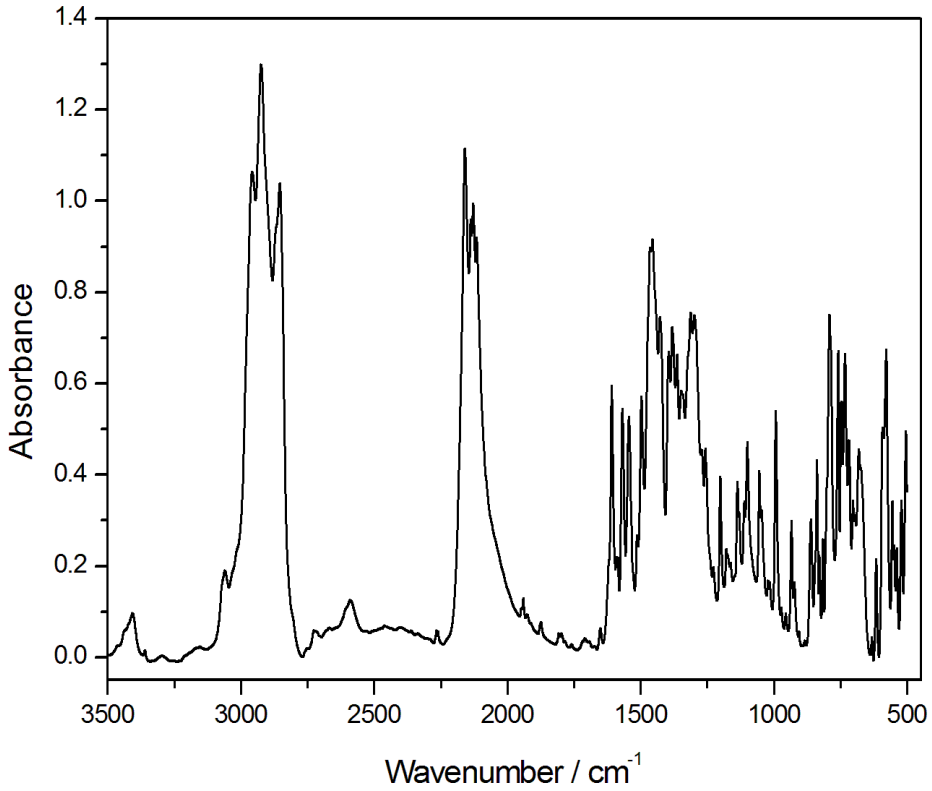

Figure 11. FT-IR spectrum of (^{dipp}NCN)Si(N_3)$_3$ as a nujol mull.

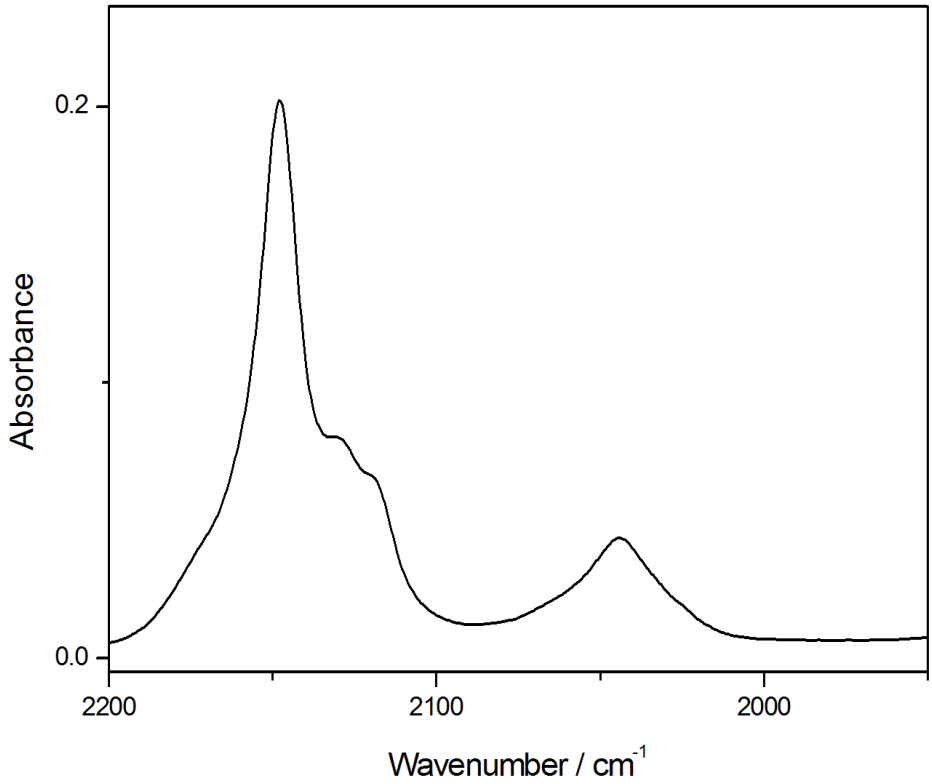

Figure 12. FT-IR spectrum of oil obtained between the reaction of (^{dipp}NCN)Si(N_3)$_3$ and two equivalents of KC_8 as a nujol mull.

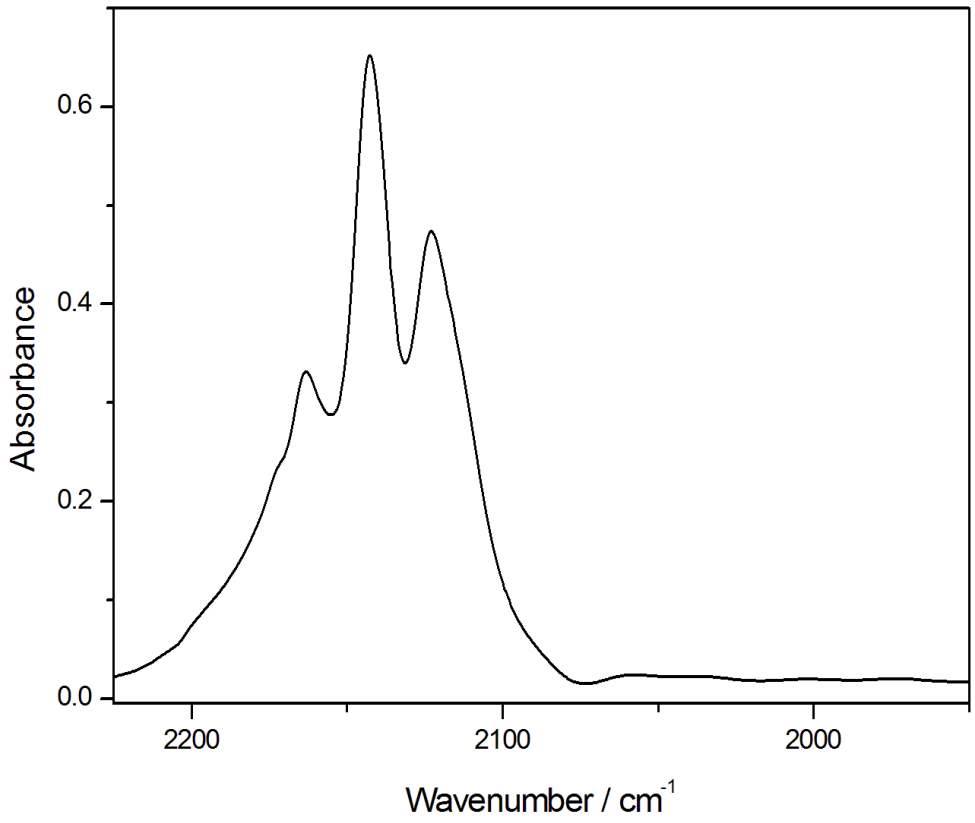

Figure 13. FT-IR spectrum of $IPrSi(N_3)_4$ dissolved in acetonitrile.

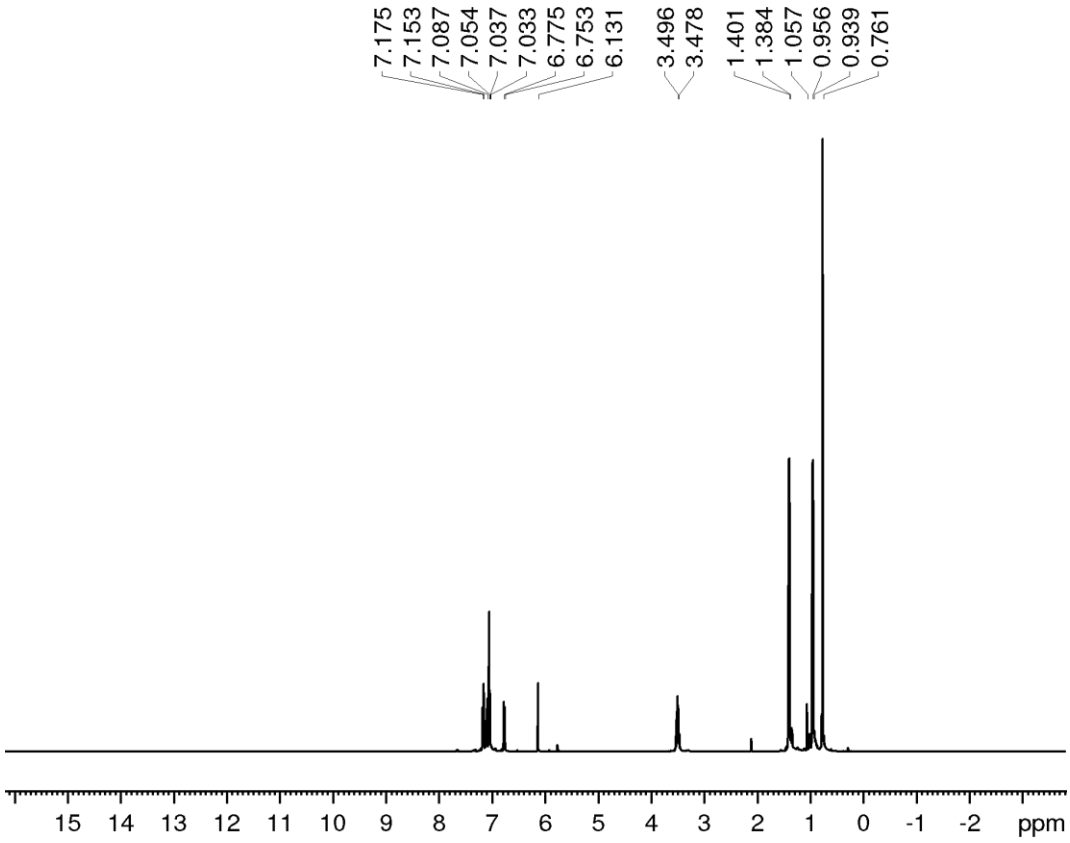

Figure 14. ^{1}H-NMR spectrum of $(NCN)SiH(N_3)_2$ in C_6D_6.

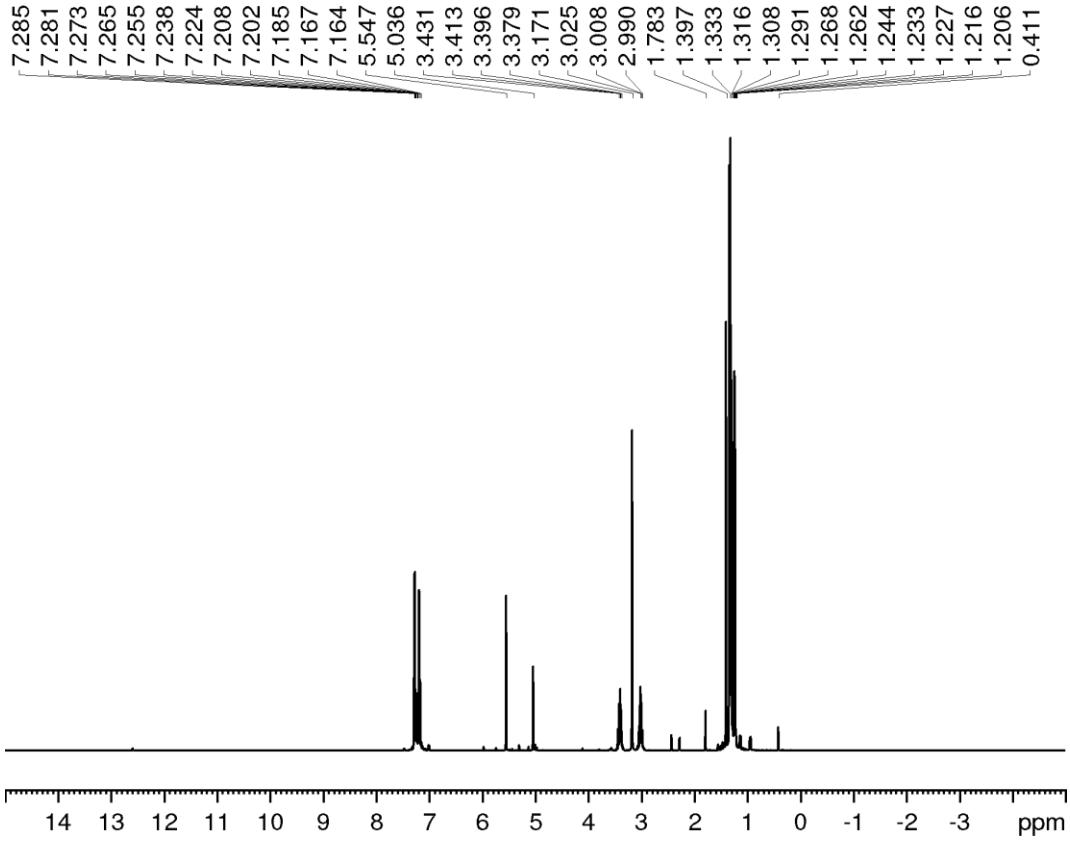

Figure 15. ^{1}H-NMR spectrum of (^{dipp}Nacnac)SiHCl$_2$ in CDCl$_3$.

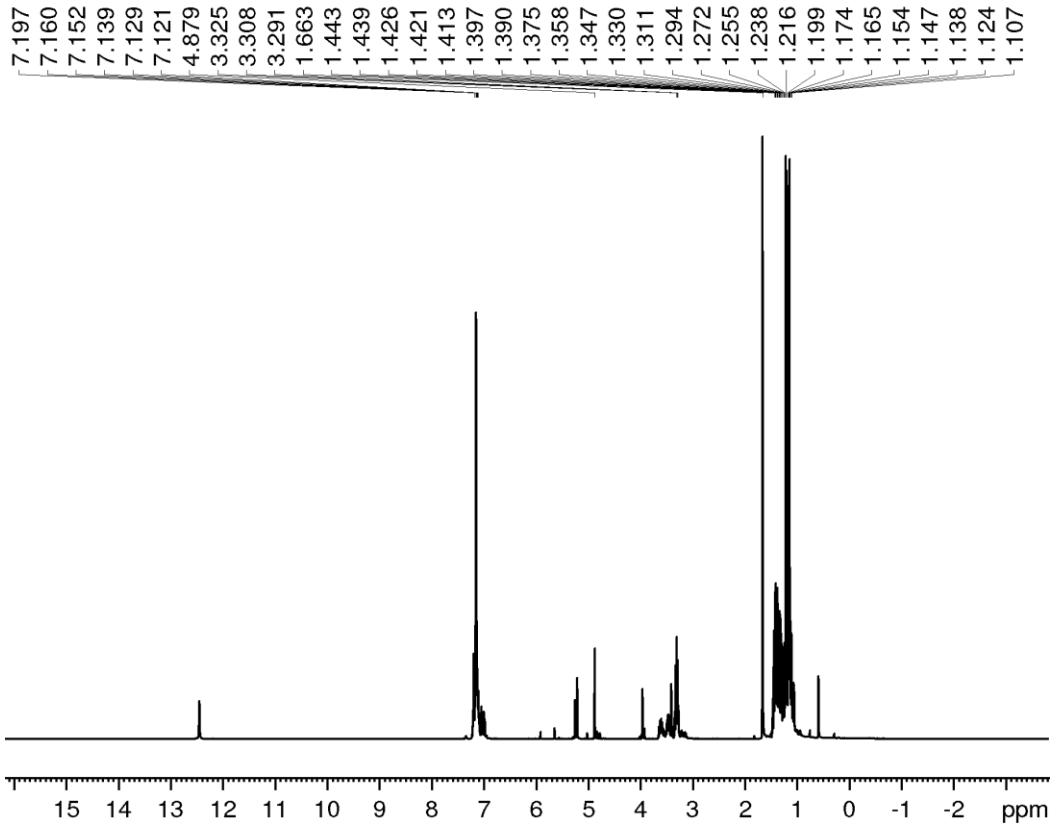

Figure 16. ^{1}H-NMR spectrum of (^{dipp}Nacnac)SiH(N$_3$)$_2$ in CDCl$_3$.

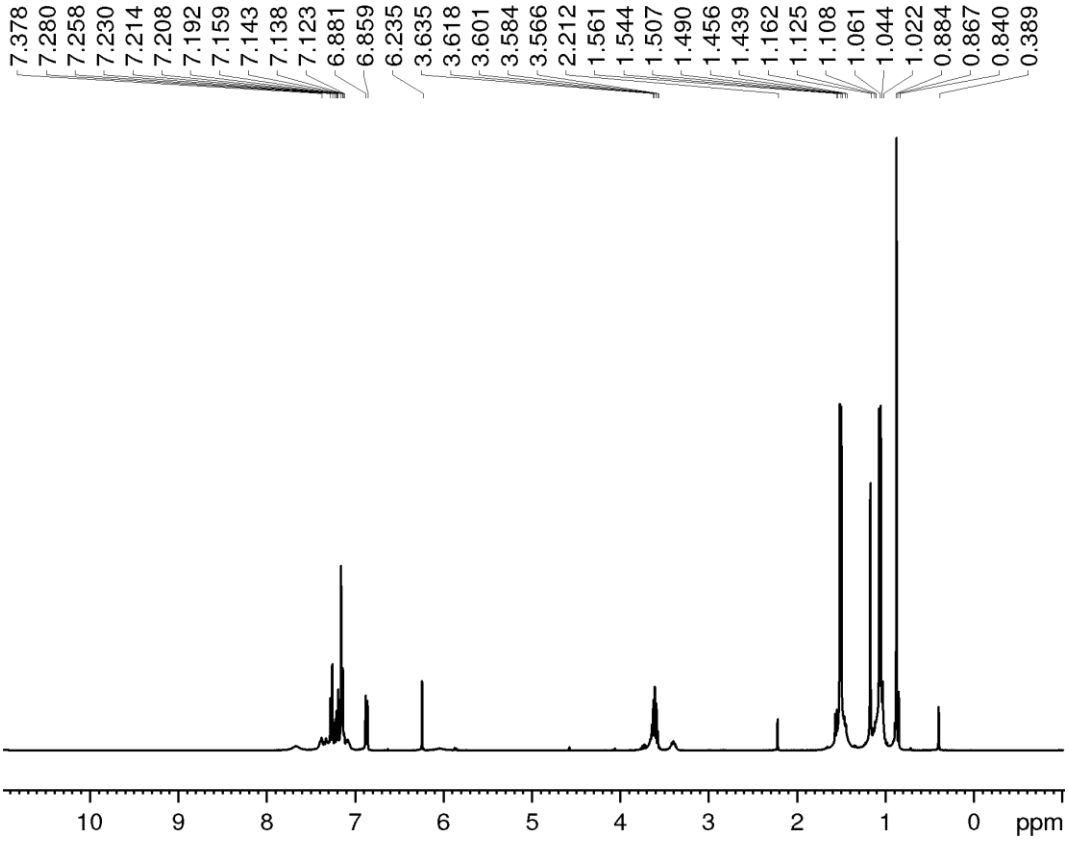

Figure 17. ^{1}H-NMR spectrum of (NCN)SiH(N_3)(N($SiMe_3$)$_2$) in C_6D_6.

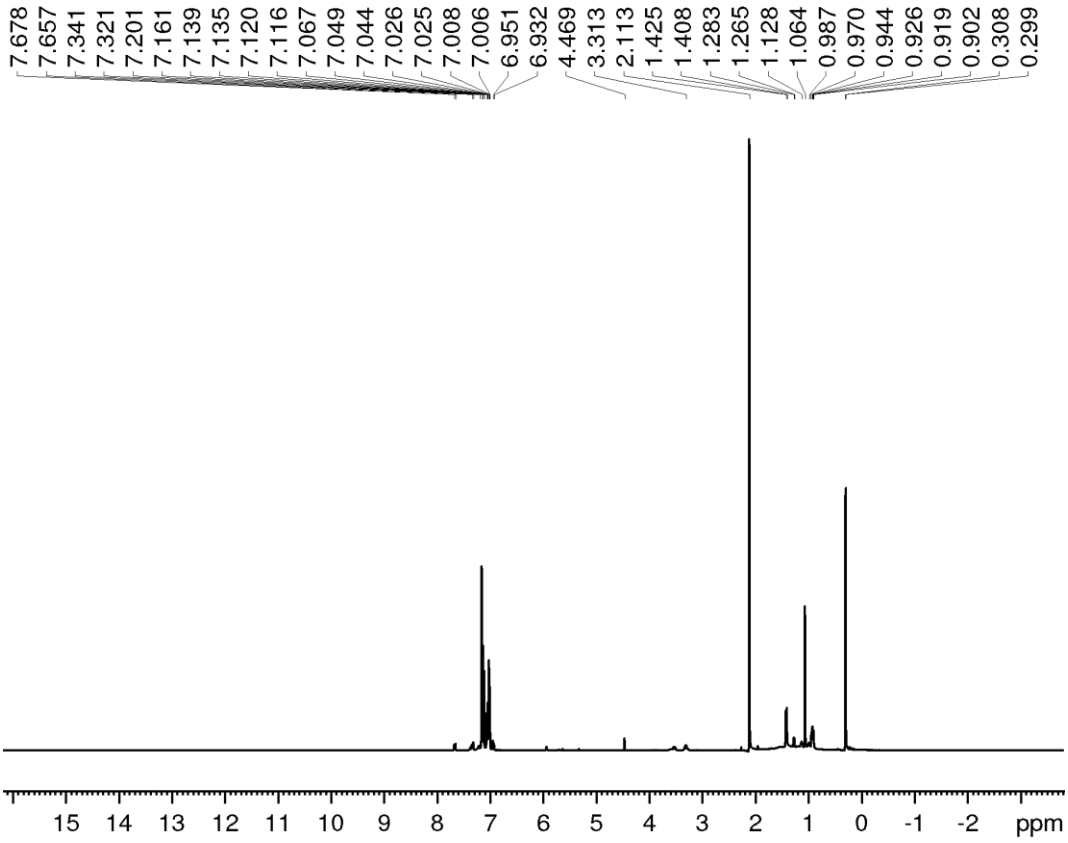

Figure 18. ^{1}H-NMR spectrum of (NCN)SiH(N_3)$_2$(*ab*-IPr) in C_6D_6.

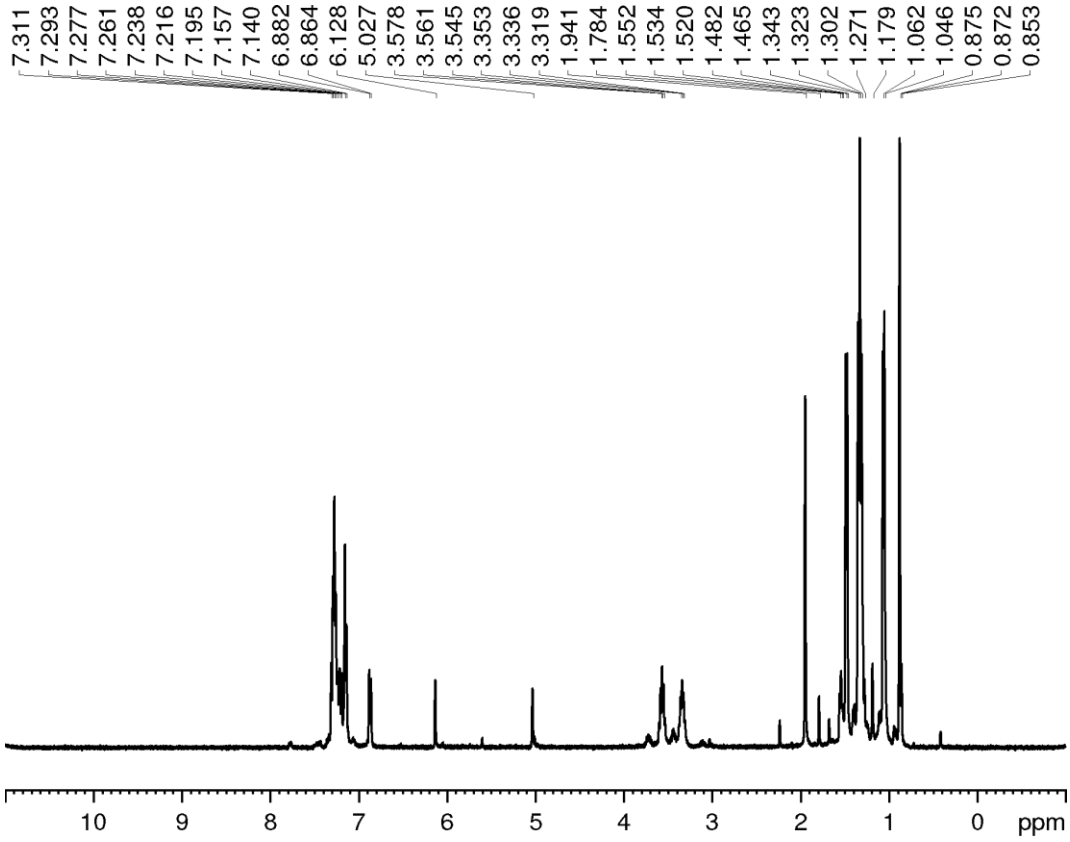

Figure 19. ^{1}H-NMR spectrum of (NCN)SiH(N_3)$_2$·Li(dippNacnac) in C_6D_6.

11.4 Crystal data and structure refinement tables

Table 1. Crystal data and structure refinement for $(PPN)_2Si(NO_3)_6$……273
Table 2. Crystal data and structure refinement for $(PPN)AsCl_2(NO_3)_2$……274
Table 3. Crystal data and structure refinement for $(PPh_4)Ge(N_3)_3$……275
Table 4. Crystal data and structure refinement for $(PPh_4)Sn(N_3)_3$……276
Table 5. Crystal data and structure refinement for $(PPN)Ge(NO_3)Cl_2/GeCl_3$……...277
Table 6. Crystal data and structure refinement for $(3\text{-iodopyrindine})_2Si(N_3)_4$……..278
Table 7. Crystal data and structure refinement for $(3\text{-bromopyridine})_2Si(N_3)_4$.....279
Table 8. Crystal data and structure refinement for $(3\text{-chloropyridine})_2Si(N_3)_4$……280
Table 9. Crystal data and structure refinement for $(3\text{-fluoropyridine})_2Si(N_3)_4$……281
Table 10. Crystal data and structure refinement for 1-methyl-3-bromo-pyridinium nitrate……282
Table 11. Crystal data and structure refinement of 1-methyl-3-iodopyridinium nitrate……283
Table 12. Crystal data and structure refinement for $(1\text{-methyl-3-bromopyridinum})_2Sn(NO_3)_6$……..284
Table 13. Crystal data and structure refinement for $(1\text{-methyl-bromopyridinium})_2Ge(NO_3)_6$……285
Table 14. Crystal data and structure refinement for $IPrSi(N_3)_4$……286
Table 15. Crystal data and structure refinement for $(I^tBu{=}N)_2Si(N_3)_2$……..287
Table 16. Crystal data and structure refinement for $(^{dipp}NCN)Si(N_3)_3$……..288
Table 17. Crystal data and structure refinement for $(^{dipp}Nacnac)SiHCl_2$……..289
Table 18. Crystal data and structure refinement for $(^{dipp}Nacnac)SiH(N_3)_2$……...290
Table 19. Crystal data and structure refinement for $(^{dipp}NCN)SiH(N_3)$……291
Table 20. Crystal data and structure refinement for $(^{dipp}NCN)SiH(N_3)(N(SiMe_3)_2)_2$...292
Table 21. Crystal data and structure refinement for $(^{dipp}NCN)SiH(N_3)_2{\cdot}Li(^{dipp}Nacnac)$……293
Table 22. Crystal data and structure refinement for $(^{dipp}NCN)SiH(N_3)_2$(*ab*-IPr)……..294
Table 23. Crystal data and structure refinement for $(ItBuH)(^{dipp}NCN)SiH(N_3)_3{\cdot}C_7H_8$.295
Table 24. Crystal data and structure refinement for $(ItBuH)(^{dipp}NCN)SiH(N_3)_3{\cdot}C_6H_{14}$……..296
Table 25. Crystal data and structure refinement for $(^{mes}Nacnac)MgN_3{\cdot}0.33C_6H_{14}$…...297
Table 26. Crystal data and structure refinement for $NaP(N_3)_6{\cdot}6py$……...298
Table 27. Crystal data and structure refinement for $IPrP(N_3)_5$……..299
Table 28. Crystal data and structure refinement for $(^{dipp}NCN)P(N_3)_4$……...300
Table 29. Crystal data and structure refinement for $(^{dipp}NCN)P(N_3)_2$……...301
Table 30. Crystal data and structure refinement for $(anisNNNanis)_2SiCl_2$……...302
Table 31. Crystal data and structure refinement for $(tolylNNNtolyl)_2SiCl_2$……303
Table 32. Crystal data and structure refinement for (PPN)bis(1-methyltetrazol-5-yl)triazenide……...304
Table 33. Crystal data and structure refinement for 1-amino-5-methyltetrazole……..305

Empirical formula	C72 H60 N8 O18 P4 Si	
Formula weight	1477.25	
Temperature	100(2) K	
Wavelength	0.71073 Å	
Crystal system	Triclinic	
Space group	P-1	
Unit cell dimensions	a = 13.1566(5) Å	α= 85.964(2)°.
	b = 15.5873(6) Å	β= 77.737(2)°.
	c = 17.2414(8) Å	γ = 83.246(2)°.
Volume	3427.4(2) $Å^3$	
Z	2	
Density (calculated)	1.431 Mg/m^3	
Absorption coefficient	0.208 mm^{-1}	
F(000)	1532	
Crystal size	0.310 x 0.300 x 0.220 mm^3	
Theta range for data collection	1.957 to 27.555°.	
Index ranges	-17<=h<=17, -20<=k<=20, -22<=l<=22	
Reflections collected	47638	
Independent reflections	15364 [R(int) = 0.0827]	
Completeness to theta = 25.000°	98.4 %	
Refinement method	Full-matrix least-squares on F^2	
Data / restraints / parameters	15364 / 4 / 927	
Goodness-of-fit on F^2	0.963	
Final R indices [I>2sigma(I)]	R1 = 0.0525, wR2 = 0.0973	
R indices (all data)	R1 = 0.1019, wR2 = 0.1157	
Extinction coefficient	n/a	
Largest diff. peak and hole	0.472 and -0.403 $e.Å^{-3}$	

Table 1. Crystal data and structure refinement for $(PPN)_2Si(NO_3)_6$

Empirical formula	C36 H30 As Cl2 N5 O12 P2	
Formula weight	932.41	
Temperature	100(2) K	
Wavelength	0.71073 Å	
Crystal system	Monoclinic	
Space group	$P2_1/c$	
Unit cell dimensions	a = 10.6196(2) Å	α= 90°.
	b = 12.8483(2) Å	β= 98.3550(10)°.
	c = 26.0484(5) Å	γ = 90°.
Volume	3516.42(11) $Å^3$	
Z	4	
Density (calculated)	1.761 Mg/m^3	
Absorption coefficient	1.287 mm^{-1}	
F(000)	1896	
Crystal size	0.450 x 0.250 x 0.200 mm^3	
Theta range for data collection	1.580 to 27.516°.	
Index ranges	-13<=h<=13, -16<=k<=16, -33<=l<=33	
Reflections collected	71973	
Independent reflections	8097 [R(int) = 0.0467]	
Completeness to theta = 25.242°	100.0 %	
Refinement method	Full-matrix least-squares on F^2	
Data / restraints / parameters	8097 / 23 / 470	
Goodness-of-fit on F^2	1.064	
Final R indices [I>2sigma(I)]	R1 = 0.0460, wR2 = 0.1152	
R indices (all data)	R1 = 0.0694, wR2 = 0.1314	
Extinction coefficient	n/a	
Largest diff. peak and hole	1.403 and -1.178 $e.Å^{-3}$	

Table 2. Crystal data and structure refinement for $(PPN)AsCl_2(NO_3)_2$

Empirical formula	C24 H20 Ge N9 P	
Formula weight	538.05	
Temperature	120(2) K	
Wavelength	0.71073 Å	
Crystal system	Triclinic	
Space group	P-1	
Unit cell dimensions	a = 7.7712(2) Å	α= 93.278(2)°.
	b = 11.4711(4) Å	β= 99.357(2)°.
	c = 14.2003(4) Å	γ = 100.865(2)°.
Volume	1221.59(6) $Å^3$	
Z	2	
Density (calculated)	1.463 Mg/m^3	
Absorption coefficient	1.351 mm^{-1}	
F(000)	548	
Crystal size	0.27 x 0.27 x 0.06 mm^3	
Theta range for data collection	1.46 to 27.57°.	
Index ranges	-10<=h<=10, -14<=k<=14, -18<=l<=18	
Reflections collected	24417	
Independent reflections	5614 [R(int) = 0.0598]	
Completeness to theta = 25.00°	99.9 %	
Absorption correction	Semi-empirical from equivalents	
Max. and min. transmission	0.9233 and 0.7117	
Refinement method	Full-matrix least-squares on F^2	
Data / restraints / parameters	5614 / 0 / 316	
Goodness-of-fit on F^2	1.277	
Final R indices [I>2sigma(I)]	R1 = 0.0379, wR2 = 0.0740	
R indices (all data)	R1 = 0.0652, wR2 = 0.0945	
Largest diff. peak and hole	0.338 and -0.467 e.$Å^{-3}$	

Table 3. Crystal data and structure refinement for $(PPh_4)Ge(N_3)_3$

Empirical formula	C24 H20 N9 P Sn	
Formula weight	584.15	
Temperature	100(2) K	
Wavelength	0.71073 Å	
Crystal system	Triclinic	
Space group	P1	
Unit cell dimensions	a = 10.7554(6) Å	α= 91.674(3)°.
	b = 11.0597(6) Å	β= 108.388(3)°.
	c = 12.3539(6) Å	γ = 116.535(3)°.
Volume	1222.28(11) $Å^3$	
Z	1	
Density (calculated)	0.794 Mg/m^3	
Absorption coefficient	0.571 mm^{-1}	
F(000)	292	
Crystal size	0.27 x 0.17 x 0.14 mm^3	
Theta range for data collection	2.10 to 29.16°.	
Index ranges	-14<=h<=14, -14<=k<=15, -16<=l<=16	
Reflections collected	49474	
Independent reflections	6417 [R(int) = 0.0533]	
Completeness to theta = 29.16°	97.3 %	
Absorption correction	None	
Max. and min. transmission	0.9243 and 0.8610	
Refinement method	Full-matrix least-squares on F^2	
Data / restraints / parameters	6417 / 0 / 316	
Goodness-of-fit on F^2	1.016	
Final R indices [I>2sigma(I)]	R1 = 0.0542, wR2 = 0.1380	
R indices (all data)	R1 = 0.0683, wR2 = 0.1517	
Largest diff. peak and hole	3.389 and -1.921 $e.Å^{-3}$	

Table 4. Crystal data and structure refinement for $(PPh_4)Sn(N_3)_3$

Empirical formula	C72 H60 Cl3 Ge2 N5 O3 P4	
Formula weight	832.62	
Temperature	296(2) K	
Wavelength	0.71073 Å	
Crystal system	Triclinic	
Space group	P-1	
Unit cell dimensions	a = 9.9690(5) Å	α= 104.030(2)°.
	b = 10.0617(4) Å	β= 100.589(3)°.
	c = 17.7650(8) Å	γ = 94.907(2)°.
Volume	1683.44(13) $Å^3$	
Z	1	
Density (calculated)	1.643 Mg/m^3	
Absorption coefficient	1.150 mm^{-1}	
F(000)	850	
Crystal size	0.280 x 0.200 x 0.200 mm^3	
Theta range for data collection	1.209 to 27.573°.	
Index ranges	-12<=h<=12, -13<=k<=12, -23<=l<=23	
Reflections collected	31101	
Independent reflections	7710 [R(int) = 0.0689]	
Completeness to theta = 25.242°	99.8 %	
Refinement method	Full-matrix least-squares on F^2	
Data / restraints / parameters	7710 / 3 / 428	
Goodness-of-fit on F^2	1.054	
Final R indices [I>2sigma(I)]	R1 = 0.0537, wR2 = 0.1204	
R indices (all data)	R1 = 0.1040, wR2 = 0.1416	
Extinction coefficient	n/a	
Largest diff. peak and hole	1.232 and -1.163 $e.Å^{-3}$	

Table 5. Crystal data and structure refinement for (PPN)Ge(NO_3)Cl_2/$GeCl_3$

Empirical formula	C10 H8 I2 N14 Si	
Formula weight	606.19	
Temperature	100(2) K	
Wavelength	1.54178 Å	
Crystal system	Monoclinic	
Space group	C2/c	
Unit cell dimensions	a = 9.7045(3) Å	α= 90°.
	b = 13.7502(4) Å	β= 99.3026(15)°.
	c = 14.0669(4) Å	γ = 90°.
Volume	1852.38(9) $Å^3$	
Z	4	
Density (calculated)	2.174 Mg/m^3	
Absorption coefficient	27.574 mm^{-1}	
F(000)	1144	
Crystal size	0.300 x 0.250 x 0.250 mm^3	
Theta range for data collection	5.629 to 66.646°.	
Index ranges	-9<=h<=11, -16<=k<=16, -16<=l<=16	
Reflections collected	6308	
Independent reflections	1617 [R(int) = 0.0408]	
Completeness to theta = 66.646°	98.8 %	
Refinement method	Full-matrix least-squares on F^2	
Data / restraints / parameters	1617 / 30 / 125	
Goodness-of-fit on F^2	1.220	
Final R indices [I>2sigma(I)]	R1 = 0.0248, wR2 = 0.0652	
R indices (all data)	R1 = 0.0331, wR2 = 0.0996	
Extinction coefficient	0.00021(4)	
Largest diff. peak and hole	0.839 and -0.920 $e.Å^{-3}$	

Table 6. Crystal data and structure refinement for (3-iodopyrindine)$_2$Si(N_3)$_4$

Empirical formula	C10 H8 Br2 N14 Si	
Formula weight	512.21	
Temperature	100(2) K	
Wavelength	1.54178 Å	
Crystal system	Monoclinic	
Space group	C2/c	
Unit cell dimensions	a = 9.4733(3) Å	α= 90°.
	b = 13.5754(4) Å	β= 98.7713(15)°.
	c = 13.9066(4) Å	γ = 90°.
Volume	1767.53(9) $Å^3$	
Z	4	
Density (calculated)	1.925 Mg/m^3	
Absorption coefficient	6.766 mm^{-1}	
F(000)	1000	
Crystal size	0.200 x 0.150 x 0.150 mm^3	
Theta range for data collection	5.740 to 66.557°.	
Index ranges	-11<=h<=10, -14<=k<=16, -16<=l<=16	
Reflections collected	6298	
Independent reflections	1557 [R(int) = 0.0285]	
Completeness to theta = 66.557°	99.5 %	
Refinement method	Full-matrix least-squares on F^2	
Data / restraints / parameters	1557 / 0 / 124	
Goodness-of-fit on F^2	1.167	
Final R indices [I>2sigma(I)]	R1 = 0.0209, wR2 = 0.0443	
R indices (all data)	R1 = 0.0265, wR2 = 0.0460	
Extinction coefficient	n/a	
Largest diff. peak and hole	0.293 and -0.334 $e.Å^{-3}$	

Table 7. Crystal data and structure refinement for (3-bromopyridine)$_2$Si(N_3)$_4$

Empirical formula	C10 H8 Cl2 N14 Si	
Formula weight	423.29	
Temperature	296(2) K	
Wavelength	0.71073 Å	
Crystal system	Triclinic	
Space group	P-1	
Unit cell dimensions	a = 7.3532(4) Å	α= 92.809(4)°.
	b = 7.5239(4) Å	β= 106.111(3)°.
	c = 8.1834(5) Å	γ = 103.158(3)°.
Volume	420.49(4) $Å^3$	
Z	1	
Density (calculated)	1.672 Mg/m^3	
Absorption coefficient	0.490 mm^{-1}	
F(000)	214	
Crystal size	0.300 x 0.280 x 0.250 mm^3	
Theta range for data collection	2.610 to 27.586°.	
Index ranges	-9<=h<=9, -9<=k<=9, -10<=l<=10	
Reflections collected	6225	
Independent reflections	1921 [R(int) = 0.0523]	
Completeness to theta = 25.242°	99.9 %	
Refinement method	Full-matrix least-squares on F^2	
Data / restraints / parameters	1921 / 0 / 124	
Goodness-of-fit on F^2	2.022	
Final R indices [I>2sigma(I)]	R1 = 0.0516, wR2 = 0.1232	
R indices (all data)	R1 = 0.0615, wR2 = 0.1360	
Extinction coefficient	n/a	
Largest diff. peak and hole	0.656 and -0.460 $e.Å^{-3}$	

Table 8. Crystal data and structure refinement for (3-chloropyridine)$_2$Si(N_3)$_4$

Empirical formula	C5 H4 F N13 Si	
Formula weight	293.30	
Temperature	296(2) K	
Wavelength	0.71073 Å	
Crystal system	Triclinic	
Space group	P-1	
Unit cell dimensions	a = 6.9432(4) Å	α= 113.373(3)°.
	b = 7.9976(4) Å	β= 94.115(4)°.
	c = 7.9989(4) Å	γ = 106.350(3)°.
Volume	382.66(4) $Å^3$	
Z	1	
Density (calculated)	1.273 Mg/m^3	
Absorption coefficient	0.177 mm^{-1}	
F(000)	148	
Crystal size	0.250 x 0.200 x 0.200 mm^3	
Theta range for data collection	2.836 to 27.620°.	
Index ranges	-7<=h<=9, -10<=k<=10, -10<=l<=10	
Reflections collected	6137	
Independent reflections	1771 [R(int) = 0.0419]	
Completeness to theta = 25.242°	99.6 %	
Refinement method	Full-matrix least-squares on F^2	
Data / restraints / parameters	1771 / 0 / 124	
Goodness-of-fit on F^2	2.081	
Final R indices [I>2sigma(I)]	R1 = 0.0528, wR2 = 0.0734	
R indices (all data)	R1 = 0.0711, wR2 = 0.0842	
Extinction coefficient	n/a	
Largest diff. peak and hole	0.715 and -0.672 $e.Å^{-3}$	

Table 9. Crystal data and structure refinement for $(3\text{-fluoropyridine})_2Si(N_3)_4$

Empirical formula	C7 H7 Br N2 O3	
Formula weight	247.06	
Temperature	296(2) K	
Wavelength	0.71073 Å	
Crystal system	Monoclinic	
Space group	$P2_1/n$	
Unit cell dimensions	a = 4.2858(2) Å	α= 90°.
	b = 13.8481(8) Å	β= 91.481(4)°.
	c = 13.7397(8) Å	γ = 90°.
Volume	815.18(8) $Å^3$	
Z	4	
Density (calculated)	2.013 Mg/m^3	
Absorption coefficient	5.016 mm^{-1}	
F(000)	488	
Crystal size	? x ? x ? mm^3	
Theta range for data collection	2.088 to 27.536°.	
Index ranges	-5<=h<=4, -17<=k<=18, -17<=l<=14	
Reflections collected	6439	
Independent reflections	1869 [R(int) = 0.0804]	
Completeness to theta = 25.242°	99.5 %	
Refinement method	Full-matrix least-squares on F^2	
Data / restraints / parameters	1869 / 0 / 110	
Goodness-of-fit on F^2	1.084	
Final R indices [I>2sigma(I)]	R1 = 0.0629, wR2 = 0.1728	
R indices (all data)	R1 = 0.0890, wR2 = 0.1965	
Extinction coefficient	n/a	
Largest diff. peak and hole	1.456 and -0.873 $e.Å^{-3}$	

Table 10. Crystal data and structure refinement for 1-methyl-3-bromo-pyridinium nitrate

Empirical formula	C6 H7 I N2 O3	
Formula weight	282.04	
Temperature	296(2) K	
Wavelength	0.71073 Å	
Crystal system	Monoclinic	
Space group	$P2_1/c$	
Unit cell dimensions	a = 7.5499(10) Å	α= 90°.
	b = 15.328(2) Å	β= 113.955(7)°.
	c = 8.0347(10) Å	γ = 90°.
Volume	849.75(19) $Å^3$	
Z	4	
Density (calculated)	2.205 Mg/m^3	
Absorption coefficient	3.738 mm^{-1}	
F(000)	536	
Crystal size	? x ? x ? mm^3	
Theta range for data collection	2.658 to 27.606°.	
Index ranges	-9<=h<=9, -19<=k<=19, -10<=l<=10	
Reflections collected	9459	
Independent reflections	1807 [R(int) = 0.0325]	
Completeness to theta = 25.242°	93.0 %	
Refinement method	Full-matrix least-squares on F^2	
Data / restraints / parameters	1807 / 31 / 110	
Goodness-of-fit on F^2	1.210	
Final R indices [I>2sigma(I)]	R1 = 0.0715, wR2 = 0.2289	
R indices (all data)	R1 = 0.0882, wR2 = 0.2761	
Extinction coefficient	n/a	
Largest diff. peak and hole	2.854 and -3.392 $e.Å^{-3}$	

Table 11. Crystal data and structure refinement of 1-methyl-3-iodopyridinium nitrate

Empirical formula	C12 H14 Br2 N8 O18 Sn	
Formula weight	836.82	
Temperature	296(2) K	
Wavelength	0.71073 Å	
Crystal system	Orthorhombic	
Space group	Pbca	
Unit cell dimensions	a = 13.5302(10) Å	α= 90°.
	b = 13.4676(11) Å	β= 90°.
	c = 14.1901(13) Å	γ = 90°.
Volume	2585.7(4) $Å^3$	
Z	4	
Density (calculated)	2.150 Mg/m^3	
Absorption coefficient	4.177 mm^{-1}	
F(000)	1624	
Crystal size	0.200 x 0.200 x 0.100 mm^3	
Theta range for data collection	2.572 to 27.673°.	
Index ranges	-17<=h<=15, -17<=k<=17, -18<=l<=18	
Reflections collected	22273	
Independent reflections	3013 [R(int) = 0.0916]	
Completeness to theta = 25.242°	100.0 %	
Refinement method	Full-matrix least-squares on F^2	
Data / restraints / parameters	3013 / 0 / 188	
Goodness-of-fit on F^2	1.443	
Final R indices [I>2sigma(I)]	R1 = 0.0434, wR2 = 0.0470	
R indices (all data)	R1 = 0.0853, wR2 = 0.0598	
Extinction coefficient	n/a	
Largest diff. peak and hole	1.208 and -1.059 $e.Å^{-3}$	

Table 12. Crystal data and structure refinement for (1-methyl-3-bromopyridinum)$_2$Sn(NO$_3$)$_6$

Empirical formula	C12 H14 Br2 Ge N8 O18	
Formula weight	790.72	
Temperature	100(2) K	
Wavelength	1.54178 Å	
Crystal system	Orthorhombic	
Space group	Pbca	
Unit cell dimensions	a = 13.4340(3) Å	α= 90°.
	b = 13.3067(3) Å	β= 90°.
	c = 14.1096(3) Å	γ = 90°.
Volume	2522.26(10) $Å^3$	
Z	4	
Density (calculated)	2.082 Mg/m^3	
Absorption coefficient	6.301 mm^{-1}	
F(000)	1552	
Crystal size	? x ? x ? mm^3	
Theta range for data collection	5.633 to 66.746°.	
Index ranges	-15<=h<=16, -15<=k<=15, -16<=l<=16	
Reflections collected	32798	
Independent reflections	2230 [R(int) = 0.0549]	
Completeness to theta = 66.746°	99.9 %	
Refinement method	Full-matrix least-squares on F^2	
Data / restraints / parameters	2230 / 0 / 188	
Goodness-of-fit on F^2	0.976	
Final R indices [I>2sigma(I)]	R1 = 0.0227, wR2 = 0.0524	
R indices (all data)	R1 = 0.0288, wR2 = 0.0549	
Extinction coefficient	n/a	
Largest diff. peak and hole	0.234 and -0.494 $e.Å^{-3}$	

Table 13. Crystal data and structure refinement for (1-methyl-bromopyridinium)$_2$Ge(NO_3)$_6$

Empirical formula	C27 H36 N14 Si	
Formula weight	584.79	
Temperature	296(2) K	
Wavelength	0.71073 Å	
Crystal system	Monoclinic	
Space group	$P2_1$	
Unit cell dimensions	a = 8.6717(2) Å	α= 90°.
	b = 16.1932(4) Å	β= 109.2286(15)°.
	c = 11.6539(3) Å	γ = 90°.
Volume	1545.18(7) $Å^3$	
Z	2	
Density (calculated)	1.257 Mg/m^3	
Absorption coefficient	0.119 mm^{-1}	
F(000)	620	
Crystal size	0.24 x 0.18 x 0.14 mm^3	
Theta range for data collection	2.238 to 27.494°.	
Index ranges	-11<=h<=11, -21<=k<=16, -15<=l<=13	
Reflections collected	17055	
Independent reflections	5984 [R(int) = 0.0506]	
Completeness to theta = 25.242°	100.0 %	
Absorption correction	Semi-empirical from equivalents	
Max. and min. transmission	0.7456 and 0.6725	
Refinement method	Full-matrix least-squares on F^2	
Data / restraints / parameters	5984 / 1 / 387	
Goodness-of-fit on F^2	1.005	
Final R indices [I>2sigma(I)]	R1 = 0.0477, wR2 = 0.0690	
R indices (all data)	R1 = 0.0811, wR2 = 0.0785	
Absolute structure parameter	-0.02(8)	
Extinction coefficient	n/a	
Largest diff. peak and hole	0.285 and -0.228 e.$Å^{-3}$	

Table 14. Crystal data and structure refinement for $IPrSi(N_3)_4$

Empirical formula	C22 H40 N12 Si	
Formula weight	500.75	
Temperature	100(2) K	
Wavelength	1.54178 Å	
Crystal system	Monoclinic	
Space group	C2/c	
Unit cell dimensions	a = 15.2310(5) Å	α= 90°.
	b = 12.8424(4) Å	β= 106.1843(14)°.
	c = 14.5306(5) Å	γ = 90°.
Volume	2729.59(16) $Å^3$	
Z	4	
Density (calculated)	1.219 Mg/m^3	
Absorption coefficient	1.033 mm^{-1}	
F(000)	1080	
Crystal size	0.280 x 0.200 x 0.180 mm^3	
Theta range for data collection	4.582 to 77.106°.	
Index ranges	-19<=h<=19, -16<=k<=16, -18<=l<=18	
Reflections collected	17377	
Independent reflections	2854 [R(int) = 0.0486]	
Completeness to theta = 67.679°	99.9 %	
Absorption correction	Semi-empirical from equivalents	
Max. and min. transmission	0.7541 and 0.6547	
Refinement method	Full-matrix least-squares on F^2	
Data / restraints / parameters	2854 / 0 / 165	
Goodness-of-fit on F^2	1.032	
Final R indices [I>2sigma(I)]	R1 = 0.0341, wR2 = 0.0806	
R indices (all data)	R1 = 0.0434, wR2 = 0.0861	
Extinction coefficient	n/a	
Largest diff. peak and hole	0.238 and -0.334 $e.Å^{-3}$	

Table 15. Crystal data and structure refinement for $(I^tBu{=}N)_2Si(N_3)_2$

Empirical formula	C35 H47 N11 Si	
Formula weight	649.92	
Temperature	100(2) K	
Wavelength	0.71073 Å	
Crystal system	Monoclinic	
Space group	$P2_1/c$	
Unit cell dimensions	a = 20.1529(9) Å	α= 90°.
	b = 18.3091(7) Å	β= 99.734(3)°.
	c = 20.3300(9) Å	γ = 90°.
Volume	7393.4(5) $Å^3$	
Z	8	
Density (calculated)	1.168 Mg/m^3	
Absorption coefficient	0.104 mm^{-1}	
F(000)	2784	
Crystal size	0.300 x 0.300 x 0.200 mm^3	
Theta range for data collection	1.025 to 27.546°.	
Index ranges	-26<=h<=22, -23<=k<=14, -26<=l<=26	
Reflections collected	66803	
Independent reflections	17026 [R(int) = 0.1645]	
Completeness to theta = 25.242°	100.0 %	
Refinement method	Full-matrix least-squares on F^2	
Data / restraints / parameters	17026 / 3 / 863	
Goodness-of-fit on F^2	0.946	
Final R indices [I>2sigma(I)]	R1 = 0.0868, wR2 = 0.1830	
R indices (all data)	R1 = 0.2706, wR2 = 0.2678	
Extinction coefficient	n/a	
Largest diff. peak and hole	0.667 and -0.330 $e.Å^{-3}$	

Table 16. Crystal data and structure refinement for $(^{dipp}NCN)Si(N_3)_3$

Empirical formula	C32 H49 Cl2 N2 Si	
Formula weight	560.72	
Temperature	296(2) K	
Wavelength	0.71073 Å	
Crystal system	Triclinic	
Space group	P-1	
Unit cell dimensions	a = 11.1096(13) Å	α= 80.496(4)°.
	b = 12.9167(14) Å	β= 65.257(4)°.
	c = 13.1956(15) Å	γ = 68.608(4)°.
Volume	1601.1(3) $Å^3$	
Z	2	
Density (calculated)	1.163 Mg/m^3	
Absorption coefficient	0.263 mm^{-1}	
F(000)	606	
Crystal size	0.450 x 0.400 x 0.370 mm^3	
Theta range for data collection	2.382 to 27.668°.	
Index ranges	-14<=h<=14, -16<=k<=15, -16<=l<=17	
Reflections collected	23227	
Independent reflections	7141 [R(int) = 0.0921]	
Completeness to theta = 25.000°	97.5 %	
Refinement method	Full-matrix least-squares on F^2	
Data / restraints / parameters	7141 / 6 / 345	
Goodness-of-fit on F^2	1.061	
Final R indices [I>2sigma(I)]	R1 = 0.0860, wR2 = 0.1520	
R indices (all data)	R1 = 0.1375, wR2 = 0.1700	
Extinction coefficient	n/a	
Largest diff. peak and hole	0.677 and -0.601 $e.Å^{-3}$	

Table 17. Crystal data and structure refinement for (^{dipp}Nacnac)$SiHCl_2$

Empirical formula	C29 H42 N6 Si	
Formula weight	502.77	
Temperature	296(2) K	
Wavelength	0.71073 Å	
Crystal system	Monoclinic	
Space group	$P2_1/c$	
Unit cell dimensions	a = 16.6641(11) Å	α= 90°.
	b = 11.3295(7) Å	β= 109.176(2)°.
	c = 16.7894(10) Å	γ = 90°.
Volume	2993.9(3) $Å^3$	
Z	4	
Density (calculated)	1.115 Mg/m^3	
Absorption coefficient	0.105 mm^{-1}	
F(000)	1088	
Crystal size	0.380 x 0.350 x 0.250 mm^3	
Theta range for data collection	1.294 to 27.514°.	
Index ranges	-21<=h<=21, -14<=k<=11, -21<=l<=21	
Reflections collected	44379	
Independent reflections	6869 [R(int) = 0.1022]	
Completeness to theta = 25.242°	99.9 %	
Refinement method	Full-matrix least-squares on F^2	
Data / restraints / parameters	6869 / 0 / 353	
Goodness-of-fit on F^2	1.017	
Final R indices [I>2sigma(I)]	R1 = 0.0573, wR2 = 0.1112	
R indices (all data)	R1 = 0.1202, wR2 = 0.1492	
Extinction coefficient	n/a	
Largest diff. peak and hole	0.312 and -0.295 $e.Å^{-3}$	

Table 18. Crystal data and structure refinement for (^{dipp}Nacnac)SiH(N_3)$_2$

Empirical formula	C35 H42 N8 Si	
Formula weight	602.85	
Temperature	296(2) K	
Wavelength	0.71073 Å	
Crystal system	Orthorhombic	
Space group	Pbca	
Unit cell dimensions	a = 19.7525(12) Å	α= 90°.
	b = 14.9757(9) Å	β= 90°.
	c = 23.7323(14) Å	γ = 90°.
Volume	7020.2(7) $Å^3$	
Z	8	
Density (calculated)	1.141 Mg/m^3	
Absorption coefficient	0.102 mm^{-1}	
F(000)	2576	
Crystal size	0.350 x 0.280 x 0.230 mm^3	
Theta range for data collection	1.716 to 27.535°.	
Index ranges	-25<=h<=25, -19<=k<=19, -30<=l<=30	
Reflections collected	101481	
Independent reflections	8080 [R(int) = 0.1485]	
Completeness to theta = 25.242°	100.0 %	
Refinement method	Full-matrix least-squares on F^2	
Data / restraints / parameters	8080 / 2 / 413	
Goodness-of-fit on F^2	1.125	
Final R indices [I>2sigma(I)]	R1 = 0.1042, wR2 = 0.2639	
R indices (all data)	R1 = 0.1863, wR2 = 0.3718	
Extinction coefficient	0.0027(8)	
Largest diff. peak and hole	0.656 and -0.853 $e.Å^{-3}$	

Table 19. Crystal data and structure refinement for (^{dipp}NCN)SiH(N_3)$_2$

Empirical formula	C41 H66 N6 Si3	
Formula weight	727.26	
Temperature	296(2) K	
Wavelength	0.71073 Å	
Crystal system	Triclinic	
Space group	P-1	
Unit cell dimensions	a = 11.4192(9) Å	α= 90.389(3)°.
	b = 19.4416(16) Å	β= 103.542(3)°.
	c = 20.7547(17) Å	γ = 105.170(3)°.
Volume	4312.1(6) $Å^3$	
Z	4	
Density (calculated)	1.120 Mg/m^3	
Absorption coefficient	0.145 mm^{-1}	
F(000)	1584	
Crystal size	? x ? x ? mm^3	
Theta range for data collection	1.012 to 26.837°.	
Index ranges	-8<=h<=14, -24<=k<=24, -25<=l<=26	
Reflections collected	57552	
Independent reflections	16294 [R(int) = 0.0649]	
Completeness to theta = 25.242°	98.3 %	
Refinement method	Full-matrix least-squares on F^2	
Data / restraints / parameters	16294 / 0 / 943	
Goodness-of-fit on F^2	1.039	
Final R indices [I>2sigma(I)]	R1 = 0.0526, wR2 = 0.1289	
R indices (all data)	R1 = 0.0950, wR2 = 0.1683	
Extinction coefficient	n/a	
Largest diff. peak and hole	0.543 and -0.592 $e.Å^{-3}$	

Table 20. Crystal data and structure refinement for (^{dipp}NCN)SiH(N_3)(N($SiMe_3$)$_2$)

Empirical formula	C29 H45 Li N5 Si	
Formula weight	498.73	
Temperature	100(2) K	
Wavelength	1.54178 Å	
Crystal system	Monoclinic	
Space group	$P2_1$	
Unit cell dimensions	a = 11.9152(5) Å	α= 90°.
	b = 17.4107(7) Å	β= 93.143(2)°.
	c = 15.4977(6) Å	γ = 90°.
Volume	3210.2(2) $Å^3$	
Z	4	
Density (calculated)	1.032 Mg/m^3	
Absorption coefficient	0.807 mm^{-1}	
F(000)	1084	
Crystal size	? x ? x ? mm^3	
Theta range for data collection	2.855 to 66.795°.	
Index ranges	-14<=h<=14, -20<=k<=20, -18<=l<=18	
Reflections collected	50143	
Independent reflections	11186 [R(int) = 0.0603]	
Completeness to theta = 66.795°	99.7 %	
Refinement method	Full-matrix least-squares on F^2	
Data / restraints / parameters	11186 / 1 / 710	
Goodness-of-fit on F^2	1.013	
Final R indices [I>2sigma(I)]	R1 = 0.0360, wR2 = 0.0879	
R indices (all data)	R1 = 0.0421, wR2 = 0.0919	
Absolute structure parameter	0.027(12)	
Extinction coefficient	n/a	
Largest diff. peak and hole	0.147 and -0.263 $e.Å^{-3}$	

Table 21. Crystal data and structure refinement for (^{dipp}NCN)SiH(N_3)$_2$·Li(^{dipp}Nacnac)

Empirical formula	C62 H84 N10 Si	
Formula weight	997.48	
Temperature	296(2) K	
Wavelength	0.71073 Å	
Crystal system	Triclinic	
Space group	P-1	
Unit cell dimensions	a = 10.5178(7) Å	α= 90.916(3)°.
	b = 12.5471(9) Å	β= 94.128(3)°.
	c = 25.5648(16) Å	γ = 109.612(3)°.
Volume	3166.9(4) $Å^3$	
Z	2	
Density (calculated)	1.046 Mg/m^3	
Absorption coefficient	0.080 mm^{-1}	
F(000)	1080	
Crystal size	? x ? x ? mm^3	
Theta range for data collection	0.799 to 27.625°.	
Index ranges	-13<=h<=12, -16<=k<=16, -32<=l<=33	
Reflections collected	59187	
Independent reflections	14655 [R(int) = 0.0569]	
Completeness to theta = 25.242°	99.9 %	
Refinement method	Full-matrix least-squares on F^2	
Data / restraints / parameters	14655 / 0 / 769	
Goodness-of-fit on F^2	1.051	
Final R indices [I>2sigma(I)]	R1 = 0.0614, wR2 = 0.1656	
R indices (all data)	R1 = 0.1006, wR2 = 0.1975	
Extinction coefficient	n/a	
Largest diff. peak and hole	0.708 and -0.626 $e.Å^{-3}$	

Table 22. Crystal data and structure refinement for (^{dipp}NCN)SiH(N_3)$_2$(*ab*-IPr)

Empirical formula	C46 H68 N10 Si	
Formula weight	789.19	
Temperature	100(2) K	
Wavelength	1.54178 Å	
Crystal system	Triclinic	
Space group	P-1	
Unit cell dimensions	a = 10.4703(4) Å	α= 84.0750(18)°.
	b = 12.1974(5) Å	β= 76.9772(18)°.
	c = 22.7935(9) Å	γ = 71.2094(17)°.
Volume	2683.46(19) $Å^3$	
Z	4	
Density (calculated)	1.953 Mg/m^3	
Absorption coefficient	1.324 mm^{-1}	
F(000)	1712	
Crystal size	0.300 x 0.280 x 0.250 mm^3	
Theta range for data collection	3.830 to 66.801°.	
Index ranges	-12<=h<=12, -14<=k<=14, -27<=l<=27	
Reflections collected	38570	
Independent reflections	9432 [R(int) = 0.0560]	
Completeness to theta = 66.801°	98.8 %	
Refinement method	Full-matrix least-squares on F^2	
Data / restraints / parameters	9432 / 117 / 672	
Goodness-of-fit on F^2	1.033	
Final R indices [I>2sigma(I)]	R1 = 0.0800, wR2 = 0.1987	
R indices (all data)	R1 = 0.0961, wR2 = 0.2103	
Extinction coefficient	n/a	
Largest diff. peak and hole	0.900 and -0.420 $e.Å^{-3}$	

Table 23. Crystal data and structure refinement for (ItBuH)(^{dipp}NCN)SiH(N_3)$_3$·C_7H_8

Empirical formula	C47 H65 N10 Si	
Formula weight	798.18	
Temperature	100(2) K	
Wavelength	1.54178 Å	
Crystal system	Triclinic	
Space group	P-1	
Unit cell dimensions	a = 10.4124(4) Å	α= 88.369(3)°.
	b = 12.1081(5) Å	β= 77.069(3)°.
	c = 22.4864(9) Å	γ = 71.666(3)°.
Volume	2620.11(19) $Å^3$	
Z	2	
Density (calculated)	1.012 Mg/m^3	
Absorption coefficient	0.685 mm^{-1}	
F(000)	862	
Crystal size	0.200 x 0.100 x 0.030 mm^3	
Theta range for data collection	2.018 to 66.773°.	
Index ranges	-12<=h<=12, -13<=k<=14, -26<=l<=26	
Reflections collected	33718	
Independent reflections	9180 [R(int) = 0.1047]	
Completeness to theta = 66.773°	98.8 %	
Refinement method	Full-matrix least-squares on F^2	
Data / restraints / parameters	9180 / 141 / 645	
Goodness-of-fit on F^2	1.025	
Final R indices [I>2sigma(I)]	R1 = 0.0761, wR2 = 0.1927	
R indices (all data)	R1 = 0.1241, wR2 = 0.2206	
Extinction coefficient	n/a	
Largest diff. peak and hole	0.689 and -0.699 $e.Å^{-3}$	

Table 24. Crystal data and structure refinement for (ItBuH)(^{dipp}NCN)SiH$(N_3)_3 \cdot C_6H_{14}$

Empirical formula	C162 H230 Mg6 N30	
Formula weight	2743.61	
Temperature	296(2) K	
Wavelength	0.71073 Å	
Crystal system	Triclinic	
Space group	P-1	
Unit cell dimensions	a = 14.4763(9) Å	α= 66.438(3)°.
	b = 16.6040(10) Å	β= 87.947(3)°.
	c = 19.7982(12) Å	γ = 72.692(3)°.
Volume	4145.7(5) $Å^3$	
Z	1	
Density (calculated)	1.099 Mg/m^3	
Absorption coefficient	0.086 mm^{-1}	
F(000)	1484	
Crystal size	0.3 x 0.27 x 0.25 mm^3	
Theta range for data collection	1.399 to 27.559°.	
Index ranges	-18<=h<=18, -21<=k<=21, -25<=l<=25	
Reflections collected	58106	
Independent reflections	18967 [R(int) = 0.0655]	
Completeness to theta = 25.242°	99.5 %	
Refinement method	Full-matrix least-squares on F^2	
Data / restraints / parameters	18967 / 0 / 920	
Goodness-of-fit on F^2	1.720	
Final R indices [I>2sigma(I)]	R1 = 0.1170, wR2 = 0.2863	
R indices (all data)	R1 = 0.1667, wR2 = 0.3378	
Extinction coefficient	n/a	
Largest diff. peak and hole	1.017 and -0.611 $e.Å^{-3}$	

Table 25. Crystal data and structure refinement for (^{mes}Nacnac)$MgN_3 \cdot 0.33C_6H_{14}$

Empirical formula	C30 H30 N24 Na P	
Formula weight	780.74	
Temperature	100(2) K	
Wavelength	1.54178 Å	
Crystal system	Trigonal	
Space group	R-3	
Unit cell dimensions	a = 15.6739(8) Å	α= 90°.
	b = 15.6739(8) Å	β= 90°.
	c = 13.2642(7) Å	γ = 120°.
Volume	2822.1(3) $Å^3$	
Z	3	
Density (calculated)	1.378 Mg/m^3	
Absorption coefficient	1.264 mm^{-1}	
F(000)	1212	
Crystal size	0.200 x 0.180 x 0.180 mm^3	
Theta range for data collection	4.661 to 76.925°.	
Index ranges	-19<=h<=19, -19<=k<=19, -16<=l<=15	
Reflections collected	13686	
Independent reflections	1317 [R(int) = 0.0356]	
Completeness to theta = 67.679°	99.6 %	
Absorption correction	Semi-empirical from equivalents	
Max. and min. transmission	0.7541 and 0.6805	
Refinement method	Full-matrix least-squares on F^2	
Data / restraints / parameters	1317 / 0 / 86	
Goodness-of-fit on F^2	1.085	
Final R indices [I>2sigma(I)]	R1 = 0.0293, wR2 = 0.0726	
R indices (all data)	R1 = 0.0311, wR2 = 0.0737	
Extinction coefficient	n/a	
Largest diff. peak and hole	0.235 and -0.369 $e.Å^{-3}$	

Table 26. Crystal data and structure refinement for $NaP(N_3)_6 \cdot 6py$

Empirical formula	C27 H36 N17 P	
Formula weight	629.70	
Temperature	100(2) K	
Wavelength	0.71073 Å	
Crystal system	Monoclinic	
Space group	$P2_1/m$	
Unit cell dimensions	a = 9.0687(3) Å	α= 90°.
	b = 20.0385(7) Å	β= 107.3039(17)°.
	c = 9.2869(3) Å	γ = 90°.
Volume	1611.26(9) $Å^3$	
Z	2	
Density (calculated)	1.298 Mg/m^3	
Absorption coefficient	0.134 mm^{-1}	
F(000)	664	
Crystal size	0.300 x 0.250 x 0.200 mm^3	
Theta range for data collection	2.033 to 27.515°.	
Index ranges	-11<=h<=11, -25<=k<=26, -12<=l<=12	
Reflections collected	27494	
Independent reflections	3803 [R(int) = 0.0462]	
Completeness to theta = 25.242°	99.9 %	
Absorption correction	Semi-empirical from equivalents	
Max. and min. transmission	0.7456 and 0.6870	
Refinement method	Full-matrix least-squares on F^2	
Data / restraints / parameters	3803 / 0 / 254	
Goodness-of-fit on F^2	1.044	
Final R indices [I>2sigma(I)]	R1 = 0.0365, wR2 = 0.0855	
R indices (all data)	R1 = 0.0516, wR2 = 0.0948	
Extinction coefficient	n/a	
Largest diff. peak and hole	0.396 and -0.305 $e.Å^{-3}$	

Table 27. Crystal data and structure refinement for $IPrP(N_3)_5$

Empirical formula	C41 H61 N14 P	
Formula weight	781.00	
Temperature	100(2) K	
Wavelength	1.54178 Å	
Crystal system	Monoclinic	
Space group	$P2_1/c$	
Unit cell dimensions	a = 16.2128(3) Å	α= 90°.
	b = 13.3430(3) Å	β= 111.4990(10)°.
	c = 21.6297(4) Å	γ = 90°.
Volume	4353.54(15) $Å^3$	
Z	4	
Density (calculated)	1.192 Mg/m^3	
Absorption coefficient	0.921 mm^{-1}	
F(000)	1680	
Crystal size	0.25 x 0.20 x 0.19 mm^3	
Theta range for data collection	2.929 to 66.700°.	
Index ranges	-19<=h<=19, -15<=k<=15, -25<=l<=25	
Reflections collected	63969	
Independent reflections	7657 [R(int) = 0.0743]	
Completeness to theta = 66.700°	99.4 %	
Absorption correction	Semi-empirical from equivalents	
Max. and min. transmission	0.7528 and 0.6623	
Refinement method	Full-matrix least-squares on F^2	
Data / restraints / parameters	7657 / 0 / 518	
Goodness-of-fit on F^2	2.048	
Final R indices [I>2sigma(I)]	R1 = 0.0430, wR2 = 0.0640	
R indices (all data)	R1 = 0.0618, wR2 = 0.0657	
Extinction coefficient	n/a	
Largest diff. peak and hole	0.492 and -0.364 $e.Å^{-3}$	

Table 28. Crystal data and structure refinement for $(^{dipp}NCN)P(N_3)_4$

Empirical formula	C35 H36 N8 P	
Formula weight	599.69	
Temperature	100(2) K	
Wavelength	0.71073 Å	
Crystal system	Monoclinic	
Space group	$P2_1/n$	
Unit cell dimensions	a = 9.346(2) Å	α= 90°.
	b = 24.200(6) Å	β= 90.056(4)°.
	c = 15.580(4) Å	γ = 90°.
Volume	3524.0(15) $Å^3$	
Z	4	
Density (calculated)	1.130 Mg/m^3	
Absorption coefficient	0.113 mm^{-1}	
F(000)	1268	
Crystal size	0.300 x 0.300 x 0.250 mm^3	
Theta range for data collection	2.131 to 27.473°.	
Index ranges	-12<=h<=12, -25<=k<=24, -18<=l<=20	
Reflections collected	14328	
Independent reflections	6801 [R(int) = 0.0787]	
Completeness to theta = 25.242°	87.7 %	
Refinement method	Full-matrix least-squares on F^2	
Data / restraints / parameters	6801 / 140 / 473	
Goodness-of-fit on F^2	1.003	
Final R indices [I>2sigma(I)]	R1 = 0.0693, wR2 = 0.1220	
R indices (all data)	R1 = 0.1567, wR2 = 0.1558	
Extinction coefficient	n/a	
Largest diff. peak and hole	0.272 and -0.451 $e.Å^{-3}$	

Table 29. Crystal data and structure refinement for $(^{dipp}NCN)P(N_3)_2$

Empirical formula	C28 H28 Cl2 N6 O4 Si1	
Formula weight	407.70	
Temperature	100(2) K	
Wavelength	1.54178 Å	
Crystal system	Monoclinic	
Space group	$P2_1/n$	
Unit cell dimensions	a = 11.8261(3) Å	α= 90°.
	b = 17.9705(4) Å	β= 104.8486(12)°.
	c = 13.8396(3) Å	γ = 90°.
Volume	2842.99(12) $Å^3$	
Z	6	
Density (calculated)	1.429 Mg/m^3	
Absorption coefficient	2.848 mm^{-1}	
F(000)	1272	
Crystal size	0.250 x 0.100 x 0.050 mm^3	
Theta range for data collection	4.120 to 66.681°.	
Index ranges	-14<=h<=13, -21<=k<=21, -16<=l<=16	
Reflections collected	37412	
Independent reflections	5028 [R(int) = 0.0970]	
Completeness to theta = 66.681°	99.8 %	
Refinement method	Full-matrix least-squares on F^2	
Data / restraints / parameters	5028 / 0 / 374	
Goodness-of-fit on F^2	1.580	
Final R indices [I>2sigma(I)]	R1 = 0.0426, wR2 = 0.0628	
R indices (all data)	R1 = 0.0685, wR2 = 0.0657	
Extinction coefficient	n/a	
Largest diff. peak and hole	0.348 and -0.302 $e.Å^{-3}$	

Table 30. Crystal data and structure refinement for $(anisNNNanis)_2SiCl_2$

Empirical formula	C18 H24 Cl2 N6 O Si	
Formula weight	439.42	
Temperature	296(2) K	
Wavelength	0.71073 Å	
Crystal system	Monoclinic	
Space group	$P2_1/c$	
Unit cell dimensions	a = 10.9145(8) Å	α= 90°.
	b = 19.1426(14) Å	β= 91.058(5)°.
	c = 14.4708(10) Å	γ = 90°.
Volume	3022.9(4) $Å^3$	
Z	6	
Density (calculated)	1.448 Mg/m^3	
Absorption coefficient	0.405 mm^{-1}	
F(000)	1380	
Crystal size	? x ? x ? mm^3	
Theta range for data collection	1.764 to 27.544°.	
Index ranges	-14<=h<=14, -24<=k<=24, -16<=l<=18	
Reflections collected	38524	
Independent reflections	6932 [R(int) = 0.0990]	
Completeness to theta = 25.242°	99.9 %	
Refinement method	Full-matrix least-squares on F^2	
Data / restraints / parameters	6932 / 0 / 365	
Goodness-of-fit on F^2	1.056	
Final R indices [I>2sigma(I)]	R1 = 0.0664, wR2 = 0.1789	
R indices (all data)	R1 = 0.1340, wR2 = 0.2336	
Extinction coefficient	n/a	
Largest diff. peak and hole	1.064 and -0.704 $e.Å^{-3}$	

Table 31. Crystal data and structure refinement for $(tolylNNNtolyl)_2SiCl_2$

Empirical formula	C42 H39 N13 P2	
Formula weight	787.80	
Temperature	100(2) K	
Wavelength	1.54178 Å	
Crystal system	Triclinic	
Space group	P-1	
Unit cell dimensions	a = 9.8510(2) Å	α= 67.1078(8)°.
	b = 14.8564(3) Å	β= 77.7106(9)°.
	c = 15.4893(3) Å	γ = 80.3530(8)°.
Volume	2031.40(7) $Å^3$	
Z	2	
Density (calculated)	1.288 Mg/m^3	
Absorption coefficient	1.360 mm^{-1}	
F(000)	824	
Crystal size	? x ? x ? mm^3	
Theta range for data collection	3.139 to 66.643°.	
Index ranges	-11<=h<=11, -17<=k<=17, -16<=l<=18	
Reflections collected	32813	
Independent reflections	7123 [R(int) = 0.0321]	
Completeness to theta = 66.643°	98.9 %	
Refinement method	Full-matrix least-squares on F^2	
Data / restraints / parameters	7123 / 0 / 517	
Goodness-of-fit on F^2	1.047	
Final R indices [I>2sigma(I)]	R1 = 0.0331, wR2 = 0.0793	
R indices (all data)	R1 = 0.0401, wR2 = 0.0839	
Extinction coefficient	n/a	
Largest diff. peak and hole	0.307 and -0.326 $e.Å^{-3}$	

Table 32. Crystal data and structure refinement for (PPN)bis(1-methyltetrazol-5-yl)triazenide

Empirical formula	C2 H5 N5	
Formula weight	99.11	
Temperature	100(2) K	
Wavelength	0.71073 Å	
Crystal system	Tetragonal	
Space group	$I4_1/a$	
Unit cell dimensions	a = 16.8311(16) Å	α= 90°.
	b = 16.8311(16) Å	β= 90°.
	c = 6.4348(7) Å	γ = 90°.
Volume	1822.9(4) $Å^3$	
Z	16	
Density (calculated)	1.445 Mg/m^3	
Absorption coefficient	0.109 mm^{-1}	
F(000)	832	
Crystal size	? x ? x ? mm^3	
Theta range for data collection	3.390 to 27.500°.	
Index ranges	-21<=h<=21, -16<=k<=21, -4<=l<=8	
Reflections collected	5531	
Independent reflections	1040 [R(int) = 0.0316]	
Completeness to theta = 25.242°	99.9 %	
Refinement method	Full-matrix least-squares on F^2	
Data / restraints / parameters	1040 / 0 / 84	
Goodness-of-fit on F^2	1.055	
Final R indices [I>2sigma(I)]	R1 = 0.0330, wR2 = 0.0849	
R indices (all data)	R1 = 0.0422, wR2 = 0.0919	
Extinction coefficient	n/a	
Largest diff. peak and hole	0.177 and -0.241 $e.Å^{-3}$	

Table 33. Crystal data and structure refinement for 1-amino-5-methyltetrazole